6-4-2009

Comparison of the Focal Properties of Selected Magnetic and Electrostatic Lenses and Tests of Their Theoretical Models

Luis Thomas Almarez
Portland State University

COMPARISON OF THE FOCAL PROPERTIES OF SELECTED MAGNETIC AND ELECTROSTATIC LENSES AND TESTS OF THEIR THEORETICAL MODELS

by

LUIS THOMAS ALMARAZ

A dissertation submitted in partial fulfillment of the
requirements for the degree of

DOCTOR OF PHILOSOPHY
in
ENVIRONMENTAL SCIENCES AND RESOURCES:
PHYSICS

Portland State University
2009

DISSERTATION APPROVAL

The abstract and dissertation of Luis Thomas Almaraz for the Doctor of Philosophy in Environmental Sciences and Resources: Physics were presented June 4, 2009, and accepted by the dissertation committee and the doctoral program.

COMMITTEE APPROVALS:

[redacted]
Erik Bollegom, Chair

[redacted]
Gertrude Rempfer

[redacted]
Jun Jiao

[redacted]
Rolf Koenenkamp

[redacted]
Carl Wamser
Representative of the Office of Graduate Studies

DOCTORAL PROGRAM APPROVAL:

[redacted]
Aslam Khalil, Director
Environmental Sciences and Resources
Ph.D. Program

ABSTRACT

An abstract of the dissertation of Luis Thomas Almaraz for the Doctor of Philosophy in Environmental Sciences and Resources: Physics presented June 4, 2009.

Title: Comparison of the Focal Properties of Selected Magnetic and Electrostatic Lenses and Tests of Their Theoretical Models.

The main goal of the present research is to determine whether there is a significant difference between the aberrations of magnetic and electrostatic electron lenses when they are used in the same way. Comparison of the lenses was done in an electron-optical bench, set up to resemble a scanning electron microscope (SEM).

Five different lenses, two magnetic and three electrostatic, were compared. Each group included two lenses with different lens-field lengths (pole-face spacing in magnetic lenses and interior length in electrostatic lenses). The lenses were used in turn to focus the electron beam into a demagnified image, or probe. The shadowgraph method was used to determine the paraxial properties and the spherical aberration coefficients C_S' of the probes. Graphs of C_S' versus working distance (*WD*) were used to compare the spherical aberrations of the probes focused by the different lenses. The main difference was shown to be not the type of lens, but rather differences in the lengths of the lens fields. For the same *WD*, lenses of either type, with shorter lens fields, had higher values of C_S' than did lenses with longer lens fields. An exception

occurs when the focal length f_o goes through a minimum, causing C_S to be lower for a short-field lens.

Theoretical models with the same physical basis for focusing as the respective lens types, but with analytical solutions for the paraxial image and lens properties, were introduced for comparison with the experimental lenses. Lowering the activation of the models brought the curves of model properties into agreement with the corresponding lens graphs. The reduction in model activation needed for agreement was greater for short-field than for long-field lenses, showing that short-field lenses had weaker paraxial fields and higher spherical aberration coefficients.

The analytical curves of lens properties obtained from the reduced activation models were used to evaluate the chromatic coefficients C_C' of the probes. Curves of C_C' vs. *WD* show that C_C' is higher for the electrostatic lenses than for the magnetic lenses.

ACKNOWLEDGMENTS

I would like to thank Dr. Erik Bodegom for his guidance and support in helping me to finish this thesis. I very much appreciate the valuable time he took away from his position as Head of the Physics Department to review the paper with me and make suggestions for improvements. His patience and sense of humor was very much appreciated in the final frantic days before my defense.

Several of Dr.Gertrude Rempfer's protégés deserve a special thank you for all their support and words of wisdom through my educational journey. Michael Mauck was my advisor for my Masters Degree in Physics and has continued to support me through the years as I worked on this Ph.D. I would also like to thank Todd Dixon who has been a great friend and supporter during this period.

Finally, my appreciation goes to Dr. Gertrude Rempfer for letting me share her world of electron optics. Her breath and knowledge of the field is simply amazing. I've often wished we could have met and worked together sooner. I value her display of warmth but especially her patience in my struggle at times to understand a point or two. But most of all, I appreciate her friendship and support.

This research was partially supported by DOE and NSF under grant numbers DE-FG02-07ER46406 and DBI-0352224, respectively.

TABLE OF CONTENTS

LIST OF TABLES

LIST OF FIGURES

Chapter 1. Background and Introduction

Background

The use of magnetic and electrostatic lenses to focus electrons in a microscope began in the early 1930's. As the name implies, magnetic lenses use a magnetic field to focus the electrons and the electrostatic lenses uses an electric field to do the focusing. Not much was known of the physics and technology of these types of microscopes at the time. Early research concentrated more on magnetic lenses than the electrostatic lenses, even though focusing by magnetic lenses was less well understood. The reason for this earlier start was that images could be demonstrated with less-advanced and more-available apparatus than was needed for electrostatic focusing. Modern reconstructions resembling the early beam tubes still delight and fascinate viewers because of the low-tech apparatus which can be used to form electron images of a specimen. (Ref. 1)

As the physics and technology improved, higher magnifications could be achieved if the specimen were placed closer to the center of the lens in magnetic lenses. This meant that placement of the specimen could be internal to the lens and this helped the aberrations of the lens to be smaller. The electrostatic lenses could not have the specimen inside the lens as this would distort the electric field.

The electrostatic lenses are more commonly used where the target or specimen is outside the lens as in the Scanning Electron Microscope (SEM). The SEM uses a beam of electrons that are focused to a very fine point outside the lens and used as a probe on a specimen, scanning it in the manner of a television camera. Secondary or

reflected electrons produced by the specimen are picked up by a suitable detector; the signal is amplified and displayed on a television monitor which is synchronized with the deflection system. The use of electrostatic lenses in the SEM permits the use of other types of beam sources that have a charge-to-mass ratio different from the electron. The focal properties of an electrostatic lens are not dependent on the charge-to-mass ratio as the magnetic lens is. If a beam of protons for example were used as a probe in an SEM using magnetic lenses, the focal length would be impractically long.

In present chapter, a novel way to describe the focusing process in a magnetic lens is presented. By means of diagrams and geometry, the electron's coordinates and velocity components relative to the axis about which electron spirals are translated into coordinates and velocity components relative to the lens axis. The focal properties of the magnetic lens are found from the trajectory of the electron relative to the lens system. This chapter also describes the physical basics for focusing by the electrostatic lens. This study also describes the two most important aberrations, spherical and chromatic. A plan is presented for the comparison of the two types of lenses including the development of models to help with the comparisons and facilitate analytical solutions for the paraxial focal properties.

Introduction

The schematic diagrams in Figures 1.1a and 1.1b illustrate the arrangement of the pole-pieces in a magnetic lens and the electrodes in an electrostatic lens.

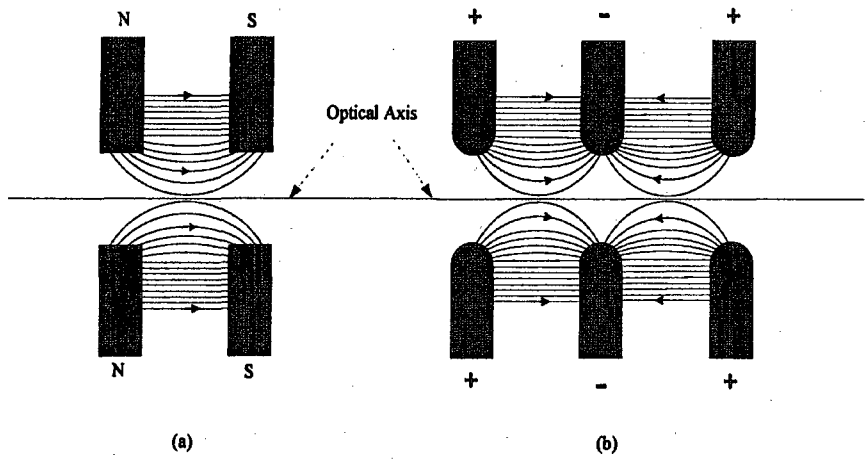

Figure 1.1. Schematic diagram of (a) a magnetic lens and (b) an electrostatic lens. The lenses are rotationally symmetric about the optical axis. Meridional sections illustrate the arrangement of the pole-pieces in (a) and the electrodes in (b).

Magnetic Lenses

A magnetic lens has a rotation-symmetric magnetic field, produced either by permanent magnets or by current-carrying coils. In the usual arrangement, two magnetic pole-pieces, centered on the optical axis, face each other across a short gap, as in Figure 1.1a. Central openings (bores) in the pole-pieces enable passage of electrons through the lens. The pole-pieces create a magnetic field between them, one pole-piece acting as a north pole and the other as a south pole. Magnetic flux enters the lens radially inward through the wall of the north bore, passes parallel to the lens axis through the gap between the bores, and leaves the lens radially outward through the wall of the south bore. The magnetic circuit is completed through an external low-reluctance path consisting of the pole-pieces and the lens housing (not shown).

The physical process by which the magnetic-field arrangement in Figure 1.1(a) focuses electrons is not obvious. The uniform-field model (Ref. 2) is used to

approximate the magnetic field in the gap between the bores. A partly qualitative paraxial description of the focusing process is presented here as a four-step process. We assume that an electron is incident parallel to the lens axis with velocity $\dot{z}$, and it enters the lens at height r_i off the lens axis.

STEP ONE: The radial component B_r of the magnetic field in the entrance bore exerts a rotary force on the electron given by

$$F_{rot} = \dot{z} q B_r \ . \tag{1.1}$$

By the time the electron has traveled through the entrance bore and enters the gap between the bores the electron has acquired a rotary velocity component

$$v_{rot} = \frac{q}{m} \int_{\text{length}}^{\text{Entrance bore}} \dot{z} |B_r| dt = \frac{q}{m} \int_{\text{length}}^{\text{Entrance bore}} |B_r| dz = \frac{q}{m} \int_{\text{length}}^{\text{Entrance bore}} \left| -\frac{r_i}{2} \frac{dB_z}{dz} \right| dz = \frac{qB}{m} \frac{r_i}{2}, \tag{1.2}$$

where B is the magnetic field in the gap, and $q = -e$ and *Gauss's law for magnetism* is used to obtain the final expression. In this process, a small part of the electron's incident kinetic energy is converted to the rotary kinetic energy associated with v_{rot}. This loss of axial energy by the electron is proportional to r_i^2 and is a source of spherical aberration. The aberration can be ignored in the present paraxial treatment.

STEP TWO: In the gap between the bores the magnetic field is uniform, and being parallel to $\dot{z}$, does not affect $\dot{z}$. The field does, however, affect the electron's motion in a plane at right angles to the lens axis, by exerting a force on the electron

$$\vec{F}_c = q \vec{v}_{rot} \times \vec{B} \tag{1.3}$$

since v_{rot} is perpendicular to B. F_c is a centripetal force and it preserves the rotary motion in the gap. Equating F_c/m to the electron's centripetal acceleration in an orbit of radius r_c, gives $(qv_{rot}B/m) = v_{rot}^2/r_c$, or

$$\frac{qB}{m} = \frac{v_{rot}}{r_c} = \omega_c \tag{1.4}$$

where ω_c is the angular frequency (cyclotron frequency) of the electron in its orbit. Expressing v_{rot} as $(qB/m)r_i/2$ as in Eq. (1.2), and solving for r_c gives

$$r_c = \frac{r_i}{2} \tag{1.5}$$

The combination of rotary and axial velocity components results in a spiral path for the electron as it moves through the gap. The spiral axis is parallel to the lens axis, but displaced from it in the r_i azimuth by the spiral radius $r_c = r_i/2$. The spiral diameter in the r_i azimuth has one end at $r = r_i$ and the other end at $r = 0$ (the lens axis). Figure 1.2 is a rear-view of the spiral, projected onto a plane at right angles to the lens axis. The spiral axis C is directed into the page at the center of the projected circle, and the lens axis O at the bottom of the circle is likewise directed into the page. The electron is incident with velocity $\dot{z}$ parallel to the lens axis and is directed into the page at I at the top of the spiral circle. After having rotated through an angle $\omega_c(t - t_i)$ around the spiral axis from its initial position I in the r_i azimuth, the electron is shown at E. The meridional plane $\mathcal{M}_c$ (shown edgewise) extends axially into the page. $\mathcal{M}_c$ contains the C-axis and the electron, and rotates about the C-axis at the ω_c rate.

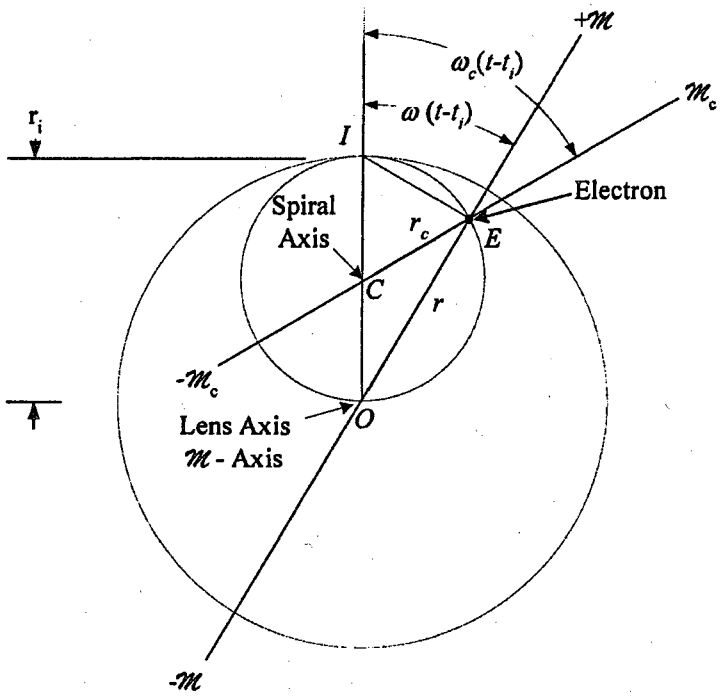

Figure 1.2 A rear-view of the spiral, projected onto a plane at right angles to the lens axis.

Relative to $\mathcal{M}_c$, the electron's angular velocity is zero, and its radial velocity is also zero, since r_C is constant in magnitude. The axial velocity component is $\dot{z}$, and the axial coordinate is $z = \dot{z}\left(t - t_i\right)$.

STEP THREE: Please refer again to Figure 1.2 to see how the *C*-coordinates r_c and $\omega_c(t - t_i)$ relate to the lens coordinates r and $\omega(t - t_i)$ in describing the location of the electron. The initial lens coordinates of the electron as it enters the lens gap are $r = r_i$, $z = z_i$, and $\phi = \phi_i$, and the time is $t = t_i$. As the electron moves around the spiral axis *C*, it also moves toward and away from the lens axis *0*, so its motion relative to the lens axis is partly radial and partly rotational. The electron's distance r from the lens axis is *OE* in Figure 1.2, and it lies in the meridional plane $\mathcal{M}$ (shown edgewise).

$\mathcal{M}$, like $\mathcal{M}_c$, contains the electron, but unlike $\mathcal{M}_c$, $\mathcal{M}$ contains the lens axis *0*, rather than the spiral axis *C*. The angle between the initial and rotated azimuths of the electron and the $\mathcal{M}_c$ plane in Figure 1.2 is $\omega_c(t - t_i)$, measured at the spiral axis *C*, whereas the angle between the initial and rotated azimuths of the electron and the $\mathcal{M}$ plane is $\omega(t - t_i)$, measured at the lens axis *O*. Since *C* is at the center of the spiral diameter *OI*, and *O* is at the lens-axis end of the diameter, from geometry $\omega(t - t_i) = \omega_c(t - t_i)/2$, or

$$\omega = \frac{\omega_c}{2} = \frac{qB}{2m} \tag{1.6}$$

Also from geometry, the triangle *IEO* has a right angle at *E*, so the distance from the lens axis to the electron is

$$r = r_i \cos\omega(t - t_i), \tag{1.7}$$

where t_i is the time at which the electron entered the gap between the bores.

The radial velocity component is

$$\dot{r} = -\omega r_i \sin\omega(t - t_i). \tag{1.8}$$

Since the $\mathcal{M}$ plane rotates with the electron about the lens axis at the ω rate, the electron's rotational motion relative to the $\mathcal{M}$-plane is zero. However, the electron moves radially in the $\mathcal{M}$ plane according to Equations (1.7) and (1.8). In a given time, the electron executes the same fraction of its cosine cycle as the $\mathcal{M}$ plane does of its rotational cycle. The combined effect of the electron's radial motion and the $\mathcal{M}$ plane's

rotational motion is to keep the lens's radial and rotational lens coordinates (Equations (1.7) and (1.8) in step with the coordinates on the spiral circle, ($r_C = r_i/2$ = constant, $\phi_C = \omega_C(t - t_i)$. In Figure 1.3, six diagrams (a) to (f) show the angular positions E of the electron in the axial spiral projection, and the orientations of the $\mathcal{M}$ and $\mathcal{M}_c$ planes, at different times after the electron has left the starting point I in the r_i-azimuth.

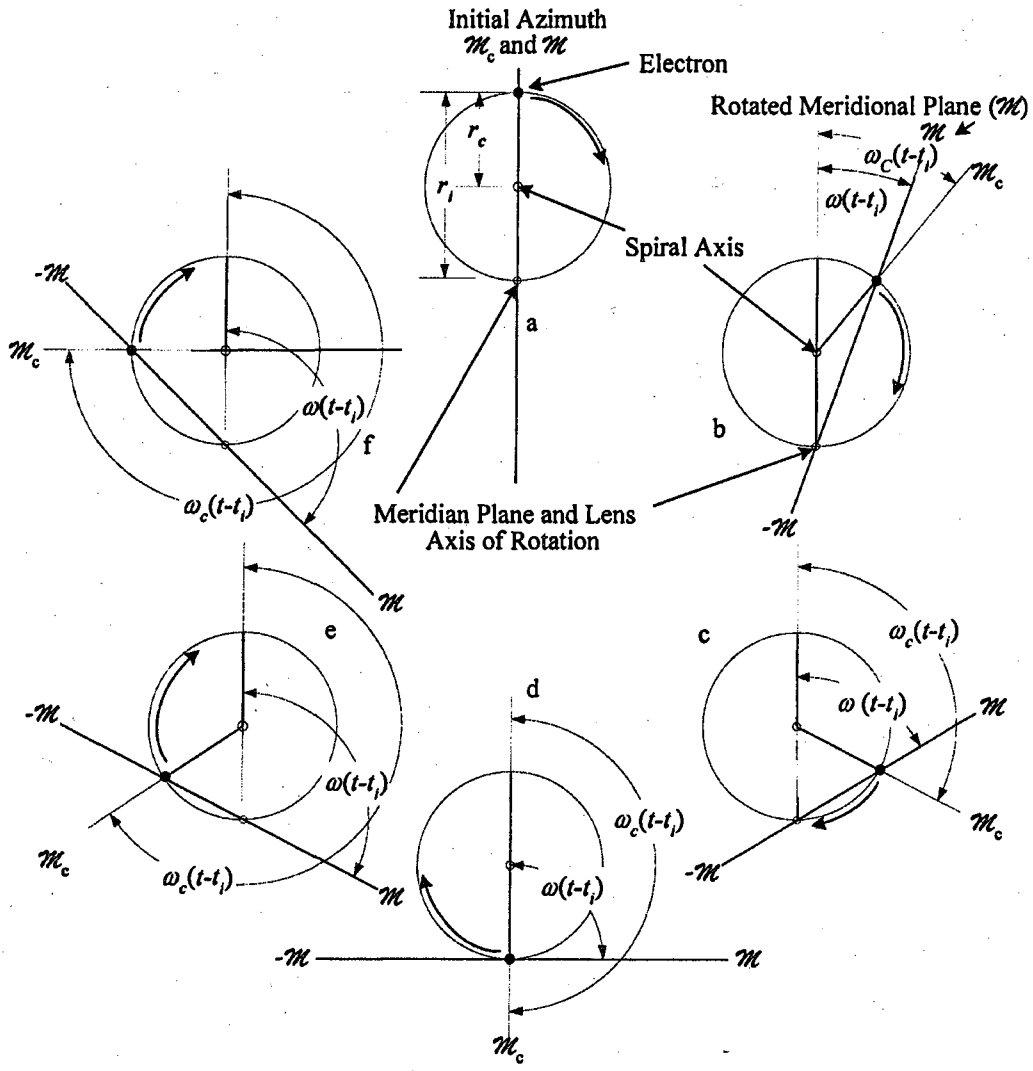

Figure 1.3. Six diagrams (a) to (f) show the angular positions of the electron in the axial spiral projection and the orientations of the $\mathcal{M}$ and $\mathcal{M}_c$ planes at different times after the electron has left the starting point in the ri-azimuth.

As the angles $\omega_C(t-t_i)$ and $\omega(t-t_i)$ increase with time in the lens gap, the distance r between the electron and the lens axis decreases until in Figure 1.3(d) the electron is at the lens axis (which is also the axis of the rotating plane $\mathcal{M}$). That location has the C-axis coordinates $r_C = r_i/2$, $\omega_C(t-t_i) = 180°$ (relative to the initial azimuth at I. In the mean-time, $\mathcal{M}$ has rotated by 90° (1/4 cycle) from its vertical orientation at I to a horizontal orientation, and the electron has executed 1/4 of a cosine cycle in the $\mathcal{M}$ plane, so the lens system coordinates are $r = r_i \cos(90°) = 0$, $\phi = 90°$, which places the electron on the lens axis in agreement with the location specified by the C coordinates above. With a further increase in $\omega(t - t_i)$ the electron crosses the $\mathcal{M}$ axis and enters the negative half of the $\mathcal{M}$-plane. (Note: In the stationary coordinate system associated with the lens, the electron touches the lens axis but does not cross into the negative half of the plane). Diagrams (e) and (f) show the electron penetrating more deeply into the negative half of the $\mathcal{M}$ plane. In diagram (f) the $\mathcal{M}$ plane and the electron have rotated by 135° around the lens axis. In addition the electron's radial coordinate r has changed from r_i to $r_i \cos 135°$, so the distance of the electron from the $\mathcal{M}$ axis is now $r = -0.707 r_i$. Relative to the non-rotating lens system, the rotation $\omega(t - t_i) = 135°$ of the $\mathcal{M}$ plane and the electron, plus the radial coordinate $r = -0.707 r_i$ of the electron in the $\mathcal{M}$ plane, places the electron on the spiral circle at

$\omega_c(t - t_i) = 270°$, as shown in Figure 1.3(f). This location agrees with the coordinates $\omega_c(t - t_i) = 270°$, $r_C = r_i/2$ on the spiral circle. At $\omega(t - t_i) = 180°$ (not shown) the $\mathcal{M}$-plane has turned through a half cycle around the lens axis, and the electron has executed half of a cosine cycle in the $\mathcal{M}$-plane. The electron is now at $r = -r_i$ in the negative half of the $\mathcal{M}$ plane, putting it back at the initial azimuth I, after half a turn around the lens axis. At the same time $\omega_c(t - t_i) = 360°$, and the electron and $\mathcal{M}_c$-plane are back at the initial azimuth, having made a complete turn around the spiral axis. Another turn around the spiral axis in the C-system would enable the electron to complete a full cycle in the lens system.

STEP FOUR: The electron reaches the exit end of the gap at $t = t_f$. The electron's final radial and axial coordinates, relative to the $\mathcal{M}$ plane, at the exit end of the gap are

$$r_f = r_i \cos\omega\left(t_f - t_i\right) \text{ and} \tag{1.9a}$$

$$z_f - z_i = \dot{z}\left(t_f - t_i\right) = S, \tag{1.9b}$$

and the azimuth of the $\mathcal{M}$ plane is

$$\phi_f = \phi_i + \omega\left(t_f - t_i\right) \tag{1.9c}$$

As the electron enters the exit bore, the radial component of the magnetic field in the bore cancels the rotational motion of the $\mathcal{M}$ plane. For $t > t_f$ the final velocity components are,

$$\dot{r}_f = -\omega r_i \sin\omega\left(t_f - t_i\right), \text{ and} \tag{1.10a}$$

$$\dot{z}_f = \dot{z} \tag{1.10b}$$

The $\mathcal{M}$ rotation rate is

$$\dot{\phi}_f = \omega = 0 \tag{1.10c}$$

The final coordinates, r_f and z_f, and velocity components, $\dot{r}_f$ and $\dot{z}_f$, are the initial point and slope of a straight line path in the now-stationary $\mathcal{M}$ plane. The electron follows this path to the image-side focal point F'_0 on the lens axis. In the case, as here, of a symmetric lens, it is convenient to use the center plane as the reference plane from which to measure distances and times. With $t = 0$ at the midpoint of the gap S, then at the gap exit $t_i = -t_f$, and the total length of time in the gap is $t_S = t_f - t_i = \frac{S}{\dot{z}}$. Likewise with $z = 0$ at gap center, and $z = z_f$ at gap exit, z_i at gap entrance = $-z_f$, and the total length of the gap is $z_f - (-z_f) = 2z_f = S$. Equations (1.9a) and (1.10a) can then be written

$$r_f = r_i \cos(\omega t_S) \text{ and} \tag{1.9a)'}$$

$$\dot{r}_f = -\omega r_i \sin(\omega t_S). \tag{1.10a)'}$$

The paraxial distance to the focal point F_0' from the center of the lens is g_0. From Figure 1.4

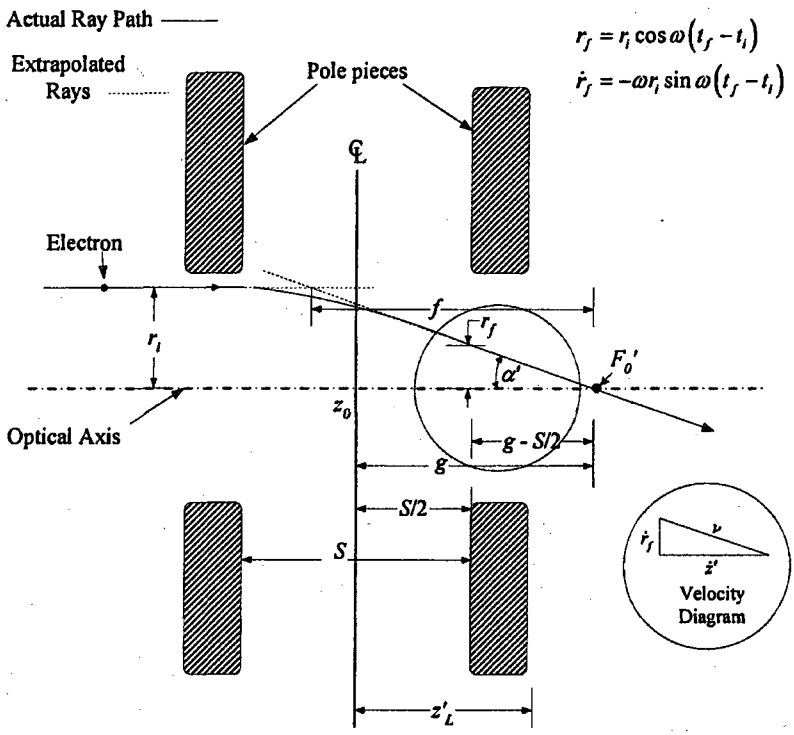

Figure 1.4 Exiting of electron from a magnetic lens without showing rotation for clarity. Upper circle shows length parameters of exiting electron and insert circle shows where velocity parameters.

$$\frac{g_0 - S/2}{r_f} = \frac{\dot{z}'}{-\dot{r}_f} = \frac{1}{\tan(\alpha')} = \frac{1}{\alpha'} \text{ so}$$

$$\alpha' = \frac{\omega r_i \sin(\omega t_s)}{\dot{z}'} \quad . \tag{1.11a}$$

Also

$$g_0 - \frac{S}{2} = \frac{r_f}{\alpha'} = \frac{\dot{z}'}{\omega \tan(\omega t_s)} = \frac{S}{\omega t_s \tan(\omega t_s)} \tag{1.11b}$$

and

$$f_0 = \frac{r_i}{r_f}\left(g_0 - \frac{S}{2}\right) = \frac{S}{\omega t_s \sin(\omega t_s)} \tag{1.11c}$$

Focusing can be done by changing ωt_f through changes in NI (which changes ω) or changes in V (which changes $\dot{z}$ and thus t_f).

The above-described trajectory of the electron through the lens is representative of initially parallel trajectories with different incident radii and azimuths (Ref. 3). In the paraxial approximation, for a given activation, all of the electrons converge to the same focal point on the lens axis. Further analysis of the magnetic lens models is carried on in Chapter 9.

The designs of the magnetic lenses selected for the experiments are discussed in Chapter 2. Experimentally obtained lens properties are provided in Chapter 7 and are compared with experimental results obtained from electrostatic lenses in Chapter 8, and from theoretical models in Chapter 9.

Electrostatic Lenses

Electron lenses, which use electric fields for focusing, are called electrostatic lenses. In the simplest case (see Figure 1.1(b)), an electrostatic lens can be made by using three rotation-symmetric coaxial electrodes, with central openings for passage of electrons, spaced along the optical axis. The electrodes are made of metal and are separated by insulating spacers which isolate the center electrode from the outer electrodes and the lens housing. The lens is activated by applying a potential difference, V_A - V_L, between the outer electrodes (usually grounded) and the center electrode (usually negative). The lens power increases as V_A - V_L increases, and decreases as the electron beam voltage $V_A - V_C$ increases. The physics of focusing by electrostatic lenses is more readily understandable than it is for magnetic lenses. The

electric field between the electrodes exerts forces on electrons passing through the lens. The radial field component near the negative center electrode exerts a converging force on the electrons, and the radial field components near the grounded outer electrodes exert a diverging force on the electrons. The axial field component on the left side of center in Figure 1.1(b) is opposite to the axial component on the right side. An electron incident from the left, after entering the lens, experiences a decelerating force on the left side of center and an accelerating force on the right side of center. As a result the electrons travel more slowly in the converging parts of the field than in the diverging parts. The lower speed in the converging part of the field gives the converging forces more time than the diverging forces to act on the electrons, so the lens has a net converging action.

The designs of the electrostatic lenses selected for this research are described in Chapter 2. Their properties, determined experimentally, are given in Chapter 7, and are compared with the experimentally determined properties of the magnetic lenses in Chapter 8, and with the properties of a theoretical electrostatic model in Chapter 9.

Aberrations

In electron optics, as in light optics, lenses suffer from a number of imaging errors, in particular, spherical and chromatic aberrations. Spherical aberration has the same meaning in electron optics as in light optics; it refers to the variation in focal properties with height off-axis at which the ray goes through the lens. Chromatic aberration in light optics historically referred to the variation in focal properties with the color of the light, but can be more accurately expressed today in terms of the

frequency of the light. In electron optics chromatic aberration refers to the variation in focal properties with electron energy. Chromatic aberration in electron optics gets its name because it behaves analogously to chromatic aberration in light optics. The spherical and chromatic aberrations, along with the diffraction limit due to the wave nature of the radiation, limit the resolution in the image formed by the lens.

Applications and Limitations

Electron lenses are applied widely in science and industry. Magnetic lenses are preferred for some applications, and electrostatic lenses for other applications. For example, magnetic lenses are preferred for ultra-high-resolution transmission electron microscopes (TEMs). This is because most specimens can be placed inside the magnetic lens field (magnetic specimens excepted). This enables shorter focal lengths to be achieved and lower aberrations, and thus better resolution in the image. In contrast, in electrostatic optics, specimens must be exterior to the lens to avoid disturbing the electrostatic field inside. Electrostatic lenses have an advantage when it comes to focusing charged particles other than electrons (i.e., protons, and other ions). This is because particle trajectories in electrostatic fields are independent of the charge-to-mass ratio q/m (except for relativistic effects). This means that, for the same electric fields and appropriate polarity, protons or other ions would follow the same trajectories as electrons do; only the speed along the trajectory would depend on q/m. In contrast, trajectories in magnetic lenses are not independent of q/m. Focal lengths are proportional approximately to (m/q) for very small angles (paraxial rays) and

proportional to $(m/q)^{1/2}$ for larger angles. The focal lengths are impractically long for ions other than electrons.

There are many applications where neither of the above limitations applies. For example, in photoelectron microscopy (PEM) and scanning electron microscopy (SEM) the charged particles which are being focused are electrons, and the specimen or target is external to the lens. The choice of which type of lens to use then depends on other considerations, one of the most important being the resolution limit imposed by aberrations. Knowledge of the aberrations of candidate lenses in a given application could aid in optimizing the design of the instruments and could avoid mistakes which otherwise would cost time, and resources.

Experimental Plan for Comparing Lenses

It is commonly thought that the spherical and chromatic aberrations of magnetic lenses are much smaller than those of electrostatic lenses. A major aim of the present research has been to determine whether there is in fact a great difference between the aberrations of the two types of lenses when used in the same way. The spherical and chromatic image aberration coefficients C_s and C_c depend strongly on the working distance (WD) and magnification of the image, so a comparison of the performances of different lenses needs to be carried out under closely similar conditions. In the present research five different lenses, two magnetic and three electrostatic, were studied. The lenses were selected so that the lens-field lengths and paraxial focal lengths of the electrostatic lenses at least partially overlapped those of the magnetic lenses. Performance measurements were carried out experimentally in a

vacuum electron-optical bench. The electron-optical system was set up to resemble a scanning electron microscope with the test lenses serving in turn as the objective lens. The spherical aberration coefficients of the images and the lenses were determined by the shadowgraph method described in Chapter 3, over a range of lens excitations. Graphs of the spherical aberration coefficients C_s' and chromatic aberration coefficients C_c' versus working distance are used to compare the performances of the different lenses.

The Theoretical Models

A theoretical aspect of this research involved theoretical models of the magnetic and electrostatic lenses being studied. These models enabled analytical solutions for the paraxial focal properties. Comparisons with the results obtained experimentally show how these theoretical models can be helpful in determining paraxial focal properties and in indicating trends as a function of lens activation. It is shown that adjustments of the activations of the models can bring their paraxial properties into remarkable agreement with the paraxial properties of the lenses studied experimentally. At the same time, these comparisons provide information as to the effective strength of the focusing fields in the experimental lenses.

Overview of Following Chapters

In Chapter 2 drawings and descriptions of the lenses used in this study are presented. In Chapter 3 the shadowgraph method of obtaining image and lens properties is explained (Ref. 4). In Chapter 4 the equipment and supplies for the experiments are described. In Chapter 5 the experimental procedures used in

operating the test bench and recording shadowgraphs are provided. In Chapter 6 a numerical example is used to illustrate the procedure for finding the image and lens properties by analysis of the shadowgraphs. In Chapter 7 the paraxial values z_o' and m_o of image distance z' and magnification m, and their spherical and chromatic aberration coefficients, C_s' and μ_s, and C_c' and μ_c, are (assembled in Tables and displayed in graphs as functions of lens activation for each test lens. Likewise the paraxial lens properties f_0 and g_0 of focal length f and focal distance g and their spherical and chromatic aberration coefficients S_f and S_g and C_f and C_g are assembled in Tables and displayed in graphs. Determination of C_f and C_g is aided by results from the lens models in Chapter 9. In Chapter 8 the performances of the five lenses acting as would-be objectives in an SEM are compared by means of graphs of the spherical and chromatic aberration coefficients C_s' and C_c' versus working distance (*WD*). The results bring to light an unexpected effect of lens length on C_S', triggering a broadening of our research. In Chapter 9 the theoretical models of magnetic and electrostatic lenses are presented. The paraxial model properties are derived, evaluated, and compared with the paraxial properties of the experimental lenses as a function of lens activation. It is found that the paraxial properties of the models can be brought into agreement with those of the corresponding test lenses in each case through adjustment of a factor applied to the model's activation parameter. Chapter 10 contains a summary of the findings of the research accomplished for this dissertation. References to related work by other investigators are included and commented on. The different chapters of this dissertation emphasize different aspects of the research.

Reviewing the findings leads to a number of interesting connections and conclusions as well as suggestions for further work.

Chapter 2. Descriptions of the Lenses Compared in This Study

The five test lenses are described with the aid of engineering drawings; the voltage and current parameters used for activating the lenses are introduced; and the focal properties characterizing the lenses and the images are defined. Lenses L_1 and L_2 are magnetic lenses which were designed and constructed for this study. Lenses L_3, L_4, and L_5 are electrostatic lenses; these lenses were chosen from existing electrostatic lenses to achieve as close a match as feasible between the lens-field lengths and paraxial focal properties of the two types of lenses.

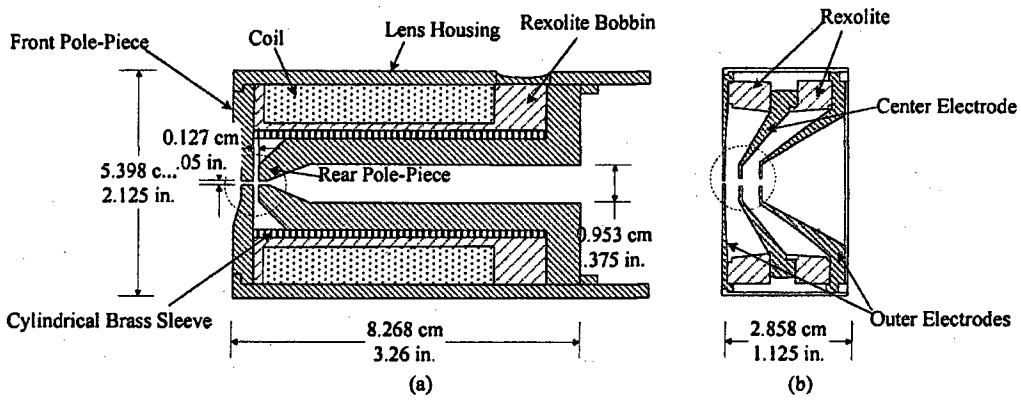

Figure 2.1. Engineering drawings of (a) magnetic lens L_1 and (b) electrostatic lens L_3.

Lens Design: Magnetic Lenses L_1 and L_2

The pole-piece arrangements of lenses L_1 and L_2 resemble the arrangement depicted schematically in Chapter 1, Figure 1.1a. A scale drawing of lens L_1 is shown in Figure 2.1a. The electron-optically (e.o.)-important part of L_1 is encircled. The inner faces of the pole pieces are flat and are separated by a gap of 0.050 in. (1.27 mm). The bore diameters are 0.050 in. (1.27 mm) and the bore lengths are 0.100 in. (2.54 mm). The outer parts of the lens are asymmetric to enable a close approach to

the optical center (o.c.) at one end of the lens, by meshes used in the shadowgraph method of analysis. The outside diameter of the lens is restricted to 2.125 in. (5.40 cm) by the need to fit the dimensions of the vee-way in the electron bench. The coil which carries the magnetizing current is shown in cross-section, wound on a plastic bobbin. The coil extends in the axial direction enough to make room for the number of turns (3235) on the bobbin. A grounded brass sleeve lines the bobbin to shield the electron beam from any charge which might build up on the bobbin. The housing and pole pieces are made of ultra-low-carbon iron (CMI-C) from Cold Metals Products, Inc.) to provide a low-reluctance external path for the magnetic flux. The overall length of the lens body is 3.256 in. (8.27 cm).

Our design for the magnetic lenses includes the option of changing the pole-piece gap length. The gap is adjustable between 0.050 in. and 0.250 in. (1.27 mm and 6.35mm). The adjustment is accomplished by sliding the rear pole-piece along the axis and fastening it in place with the appropriate spacer and a retaining ring. Lens L_2 differs from L_1 only in the length of the gap between the pole-pieces, 0.050 in. for L_1, 0.100 in. for L_2. Thus, L_1 can be converted to L_2 simply by increasing the pole-piece gap from 0.050 in. to 0.100 in. Except for this difference, the lens description given above applies to both L_1 and L_2.

Lens Design: Electrostatic Lenses L_3, L_4, and L_5

Our choice for L_3 was an electrostatic TEM objective, which normally operates with a short working distance. A drawing of L_3 is shown in Figure 2.1(b). The e.o-important part of the lens is encircled. This is a simple three-plate lens, such as is

shown in the schematic illustration in Figure 1.1(b). The lens is unipotential, meaning that the object and image spaces outside the lens are at the same electrical potential. In the present studies the outer electrodes and external space are at ground potential, and the center electrode is negative. The central openings in the front, center, and rear electrodes are respectively: 0.050, 0.115, and 0.075 in. (1.27, 2.92, and 1.905 mm); the thickness of each electrode near the axis is 0.025 in. (0.63 mm); and the spacing between electrodes is 0.100 in. (2.54 mm). Although the openings in the outer (grounded) electrodes are somewhat different, the optical center of the lens can be assumed to be at the center plane of the opening in the center electrode to within an experimental error of 0.05 mm. The outer parts of the electrodes have a larger spacing (0.350 in.) to allow sufficient length for the insulating spacers to standoff voltages of up to 40 *kV*. The lens electrodes are made from lead-free naval brass, and the housing is made from free-machining brass. The insulators are made of cross-linked polystyrene (Rexolite). The outer part of the lens body is asymmetric along the axis to allow a close approach to the optical center (o.c.) at one end, by a specimen or target or analyzing mesh. The choice for lens L_4 was the objective lens for a photoelectron microscope (PEM), with a relatively long working distance. The e.o.-important electrode structure is identical to that of lens L_3, except for the size of the opening in the center electrode, which has a diameter of 0.154 in. (3.91 mm), rather than 0.115 in. (2.92 mm) as in L_3. The choice for L_5 was an interface lens designed for use with an electron mirror. This lens has a working distance intermediate between those of the other two electrostatic lenses. In the e.o.-important region, L_5 has the same type of

three-plate structure as is used in the other electrostatic lenses, but in this case the diameter of the central opening is 0.200 in. (5.08 mm), the thickness of the center electrode is 0.050 in. (1.27 mm), and the spacing between electrodes is 0.125 in. (3.18 mm). The half-length of L_5 from the center plane of the center electrode to the outside face of the front electrode is 0.175 in. (4.44 mm), whereas it is 0.138 in. (3.50 mm) for L_3 and L_4. For comparison, the half-lengths of the magnetic lenses are 0.125 in. (3.175mm) for L_1, and 0.150 in. (3.81mm) for L_2.

Activation Parameters: Magnetic Lenses

Figure 1.2 of Chapter 1 is a rear view of the electron moving through the gap between the bores of the magnetic lens on a spiral path of radius r_c = (*radius of incident* r_i)/ 2. The axis *C* of the spiral is displaced from the optical axis *O* of the lens in the r_i azimuth by the radius of the spiral, so in this azimuth the diameter of the spiral has one end on the lens axis at $r = 0$, and the other end at $r = r_i$.

The electron is maintained in its circular orbit by a centripetal force $F_C = -qv_{rot}B$ (Eq 1.3) exerted by the axial magnetic field *B* in the gap. F_C is directed toward the spiral axis and its direction rotates with the electron at the angular rate $\omega_c = qB/m$. Substituting the expression for v_{rot} from Eq (1.2) into Eq (1.3) gives $F_C = \frac{(qB)^2}{m}\frac{r_i}{2}$, showing that F_C depends on B^2.

The spiral angle which the electron turns through in its trip through the gap is $\phi_C = \omega_C\left(t_f - t_i\right)$, where t_f is the time marker at which the electron reaches the exit end of the gap and t_i is the time marker at the beginning of the gap. The radius of the

spiral is constant at $r_c = r_i/2$. The corresponding lens-system coordinates are $\phi_f = \omega(t_f - t_i)$ and $r_f = r_i \cos(\omega(t_f - t_i))$, where $\omega = \frac{\omega_c}{2}$. For a given value of t_f, an increase in B^2 increases ω and ϕ_f, which decreases r_f and increases $\dot{r}_f = -\omega r_i \sin(\omega(t_f - t_i))$, making the focal distance shorter, the slope of the ray coming out of the lens steeper, and the lens stronger. A decrease in B^2 would have the opposite effect. B^2 or B (or the NI which produces B) are appropriate activation parameters for a magnetic lens. On the other hand if B^2 were fixed and $\dot{z}$ were increased, that would decrease $(t_f - t_i)$, increase r_f, and decrease $\dot{r}_f$ which would weaken the lens. The lens is further weakened by a second effect of $\dot{z}$, the reduced slope of the ray as it leaves the lens due to the increase in $\dot{z}$. So $\dot{z}^2$, or a better choice, the accelerating voltage V, is another activation parameter for controlling the lens power. The above parameters can be used separately, or in combination as in the compound parameter $\frac{(NI)^2}{V}$, as activation parameters. The square-root $\frac{NI}{\sqrt{V}}$ is also used as a compound activation parameter. A useful and efficient method of graphing data on magnetic lens properties is to plot versus $\frac{(NI)^2}{V}$ or $\frac{NI}{\sqrt{V}}$. Several sets of data for a given lens property, taken under various voltage and current conditions, can be plotted on one graph. If NI and V change in such a way that $\frac{(NI)^2}{V}$ remains the same, the lens properties are not affected.

Activation Parameters: Electrostatic Lenses

The focusing power of electrostatic lenses increases with the voltage V_A - V_L between the center electrode and the grounded outer electrodes, and decreases with increasing accelerating voltage V_A - V_C between the cathode and the grounded outer electrodes. The increasing strength of the lens with increasing lens voltage is due to the increasing force exerted on the electron by the electric fields between the electrodes. The decreasing strength of the lens with increasing accelerating voltage is due, as in magnetic lenses, to the decrease in time for a deflecting force to act and to decrease the deflection angle as the beam velocity increases. If the voltage ratio $\frac{V_A - V_L}{V_A - V_C}$ (= $\mathcal{V}_{LC}$ for short) remains the same the focusing power does not change with changes in cathode and lens voltage (except for a small relativistic effect). Lens voltages can be conveniently provided at constant voltage ratios from taps on a voltage divider connected between cathode and ground. The voltage ratio $\mathcal{V}_{LC}$ is the preferred activation parameter for electrostatic lenses.

Focal Properties and Image Properties: Definitions and Relationships

Definitions

The focal properties of a lens can be characterized in terms of a focal distance *g* and a focal length *f*. These properties are illustrated in Figure 2.2 for a symmetrical electron lens. The dashed box represents a space containing the lens. The object space (real, as opposed to virtual) is on the left, exterior to the lens. The object is at a

distance z from the center plane of the lens (the reference plane). The image space is on the right with a real image point shown at a distance z' from the reference plane. In Figure 2.2(a), a ray, parallel to the lens axis, enters the lens from the left. The ray emerges on the right, after being deflected by the lens.

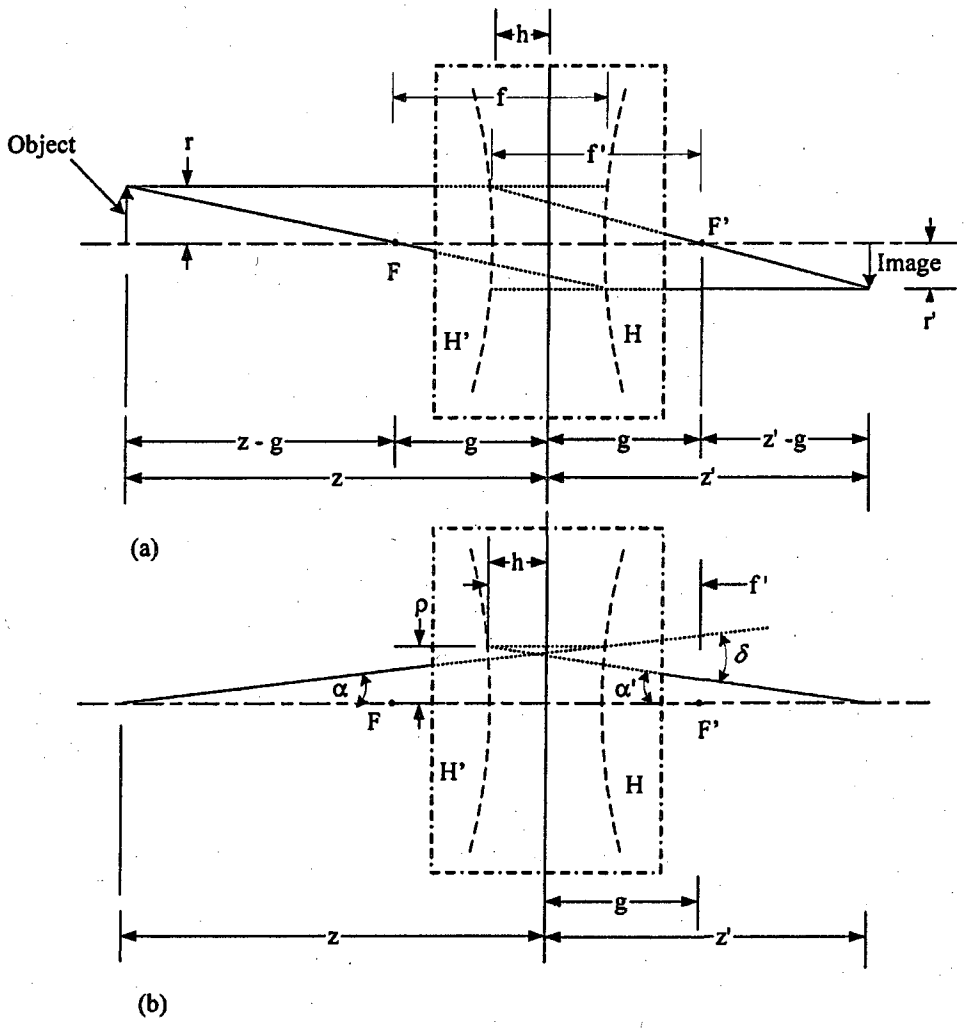

Figure 2.2 (a and b). Ray diagrams illustrating the definitions of lens and image properties and the relationships between them. In (a) the lens properties f (focal length) and g (focal distance are emphasized, and the diagram is used in deriving equations relating z and z'. In (b) the diagram emphasizes f ($\delta = \rho / f$) and h, and leads to alternative relations between z and z'.

The point at which the deflected ray crosses the lens axis is the focal point F' in image space. The object and image parts of the ray, when extrapolated to their intersection define a point (usually virtual) on the principal surface H' in image space.
The axial distance from this point on H' to the focal point F' is the focal length f' in image space. The distance from the reference plane to the focal point is the focal distance g' in image space. The difference in length $(g' - f') = h'$ is the axial distance of the intersection point on H' from the reference plane (negative, in this diagram). The corresponding diagram for a ray parallel to the axis in image space defines the focal point F and principal surface H, and the distances f, g, and h in object space. (Since the lens is symmetrical, the primes on the lens properties f', g', and h' in image space are usually omitted). The angle between two rays through the object point at z is denoted α, and through the image point at z' is denoted α'.

Figure 2.2b illustrates the use of principal surfaces in drawing rays between object and image points (Ref. 5). In this diagram the object and image points are on the axis, and one ray between object and image is on the lens axis. Another ray leaves the object at a random angle α, and is drawn as a straight line to a point at height ρ off-axis on the object-side principal surface H. (The part of the ray inside the lens is virtual.) The image ray is drawn from a point at the same height ρ on H' to the image point on the axis. As in (a), the angle between the two rays (one axial, in this diagram) through the object point at z is denoted α, and through the image point at z' is denoted α'. This method of constructing rays can be used for rays between off-axis object and

image points as well. Angles should be small enough to avoid unacceptable errors due to aberrations.

In (a) and (b) of Figure 2.2 the principal surfaces H and H' are shown as curved surfaces to illustrate the fact that in general these surfaces are not flat. The curvature of H and H' is an aberration of h (equal to the difference between the aberrations of g and f). The aberrations of the other lens properties f and g, and the image aberrations are not shown, to avoid further complexity. In the paraxial range the angles are small enough that aberrations can be ignored, and the principal surfaces can be replaced by planes H_0 and H_o', tangent to H and H' at the lens axis. If the lens is "thin", the principal surfaces coincide at the center plane, $h = 0$, and f and g are equal.

Relationships Between Lens Properties and Image Properties

Figure 2.2(a) emphasizes the relationships between lens properties, f and g, and the image distance z' and magnification m for a given object distance z. Newton's relationships

$$z' - g = fm \tag{2.1}$$

$$z - g = \frac{f}{m} \tag{2.2}$$

are readily derivable from the diagram. Equations (2.1) and (2.2) lead to the Newtonian lens equations relating z and z',

$$(z' - g)(z - g) = f^2 \tag{2.3}$$

$$\frac{(z' - g)}{(z - g)} = m^2 \tag{2.4}$$

These equations show that, when $(z - g)$ or $(z' - g)$ are small, the value of g is especially critical and aberrations of g play the major role in limiting the geometrical resolution in an image or a probe.

Figure 2.2b emphasizes the relationship between focal properties f and h and the object and image properties z, z', and m. From geometry the deflection angle δ produced by the lens is equal to $\alpha + \alpha'$. Under paraxial conditions δ can be written ρ/f, and $(\alpha + \alpha')$ can be written $\rho/(z - h) + \rho/(z' - h)$. Equating these two expressions and dividing by ρ gives the well-known lens formula

$$\frac{1}{z-h}+\frac{1}{z'-h}=\frac{1}{f} \tag{2.5}$$

and dividing α by α' gives

$$\frac{\alpha}{\alpha'}=\frac{z'-h}{z-h}=m \tag{2.6}$$

(Note: in Figures 2.2a and 2.2b, h has a negative value.)

If the lens is "thin" $h = 0$, $g = f$, and the above equations reduce to

$$\frac{1}{z}+\frac{1}{z'}=\frac{1}{f} \tag{2.5'}$$

$$\frac{z'}{z}=m\,. \tag{2.6'}$$

Chapter 3. Principle of the Shadowgraph Method of Measuring Lens Properties

In the shadowgraph method, the lens being studied is used to form a de-magnified image of a "point" source of rays (in these case electrons). Fine meshes placed separately before and after the lens, cast shadows which are used to trace the rays in object and image space (Ref. 4 and 7). The arrangement is shown schematically in Figure 3.1. [The symbol () used in light optics to represent a lens is used also in electron optics.]

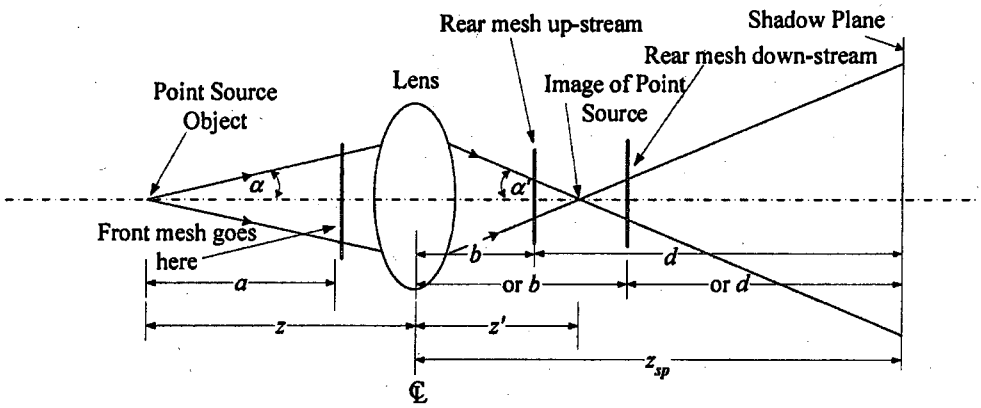

Figure. 3.1. Schematic diagram of the optical setup used in the shadowgraph method for measuring lens properties.

The distance z of the object (pinhole source) and z_{SP} of the shadow plane are known with respect to the optical center (o.c.) of the test lens. The locations where the front mesh and the rear mesh are to be inserted are indicated. The rear mesh can be placed either up-stream or down-stream from the image. The first step is to determine the image distance z' from the lens o.c by means of the shadow cast by the rear mesh.

The second step is to determine the image magnification m with the help of the shadow cast by the front mesh. The focal properties f and g of the test lens can then be calculated from the image properties z' and m. The lens and image properties are each presented in the form of a paraxial value and a spherical aberration coefficient. Chromatic aberration is taken up in a separate section and is followed by a brief description of the principal surfaces.

Ray-Tracing with the Rear Mesh

Ray-tracing in image space is illustrated in Figure 3.1(a) below.

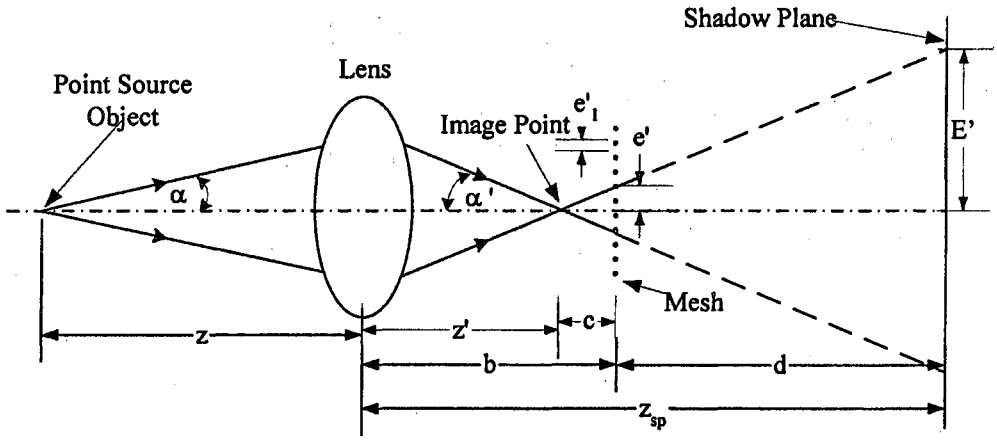

Figure 3.1(a). Schematic arrangement for finding the image distance z' by means of the shadowgraph cast by the rear mesh. The rear mesh is downstream from the image. The front mesh is not used in this part of the experiment.

The rear mesh is at a distance c (to be determined) downstream from the image, and a know distance b downstream from the lens o.c. The rear mesh unit spacing is e_1'. A ray is shown crossing the axis at the image point z'. After passing through the image, the ray is blocked by a bar of the mesh, and the bar shadow is cast on the shadow plane, a distance d from the mesh. The distances b and d and the mesh

bar height e' are known, and the height E' of the shadow can be measured. From similar triangles,

$$\frac{(c+d)}{c} = \frac{E'}{e'} = M' \text{ (the shadow magnification)}. \tag{3.1}$$

where c is the distance to the mesh from the point at which the ray crosses the axis. Solving for c gives

$$c = \frac{d}{M'-1}\,. \tag{3.2}$$

The image distance is

$$z' = b - c\,, \tag{3.3}$$

and the angle α' of the ray crossing the axis at z' is given by

$$\tan\alpha' = \frac{e'}{c} = \frac{E'}{z_{sp} - z'}. \tag{3.4}$$

If the working distance between the lens and the image is sufficient, the rear mesh can be placed upstream from the image (but still downstream from the lens), as shown in Figure 3.1(b). This arrangement enables additional rear-mesh data to be acquired. Equations (3.1) to (3.4) apply in this case also, but c and M' are now negative.

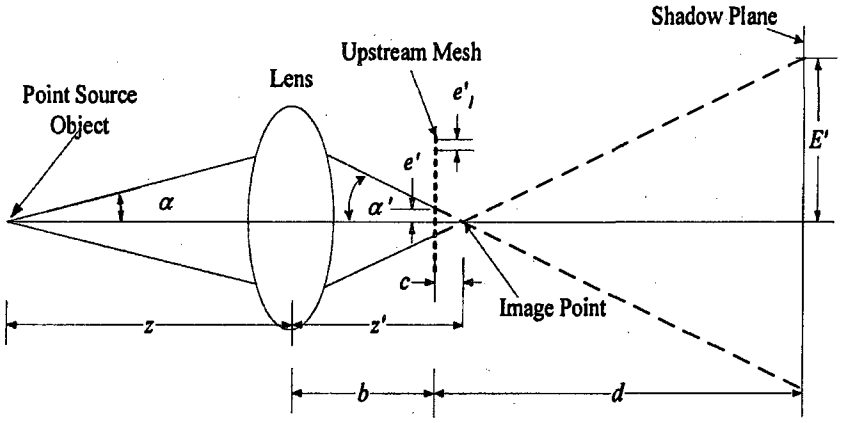

Figure 3.1(b). Schematic diagram for determining the image distance z' with the rear mesh upstream from the image but downstream from the lens, i.e. between the lens and the image.

Spherical Aberration of the Image Distance z'

There are many mesh bar shadows in each shadowgraph, with α' ranging from paraxial to marginal. Because of spherical aberration, the value of c, z' and M' depart from their paraxial values c_0, z_0', and M_0', as the ray angles get larger. The longitudinal spherical aberration coefficient C_s' of the image distance is defined to second order in α' by

$$z' = z_0' - C_s'\alpha'^2. \tag{3.5}$$

Plotting z' versus α'^2 gives a straight line. The intercept on the z' axis is the paraxial value z_0', and the slope of the graph is the negative of the spherical aberration coefficient C_s' of the image distance z'. (The sign of C_s' was established by convention). For angles larger than the range considered here, higher-order

aberrations become noticeable and the graph diverges upwardly away from the straight line.

The primary use of the rear-mesh data is to provide the graph of z' versus α'^2, used to evaluate C_S'. However, a graph of E' vs z', also from rear-mesh data, is a convenient aid in finding z' for given values of E' or E in between data points. This graph is especially handy when the rear-mesh pitch is changed, or when the bar-shadow height is determined by the front mesh rather than the rear mesh.

Ray-Tracing with the Front Mesh

The reason for needing the front-mesh data is that, in general, real lenses are not "thin", and the locations of the principal surfaces are not known. What we are seeking in this part of the experiment is the magnification m of the image of the pinhole object, which is given by

$$m = \frac{\tan\alpha}{\tan\alpha'} \tag{3.6}$$

This will provide the additional information needed to calculate the focal length f and focal distance g of the lens and the location of the principal surfaces.
Ray tracing with the front mesh is illustrated in Figure 3.1(c).

The front mesh is at a distance a from the object (pinhole source); its unit spacing is e_1. A ray from the object, making an angle α with the axis, is blocked by a bar of the mesh at height e from the axis. The shadow cast by the bar (shown dashed) corresponds to the path, which the unblocked ray would have taken.

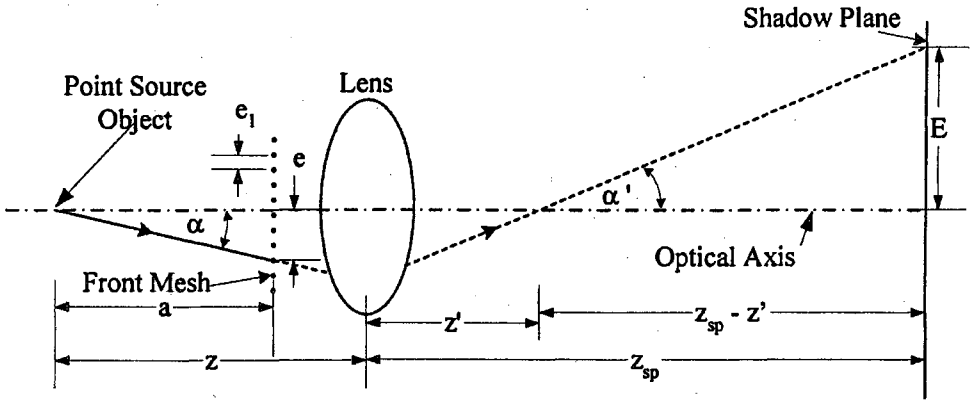

Figure 3.1(c). The optical arrangement using the front mesh for determining the ray angles α and α' and the magnification of the image. The rear mesh has been removed.

The ray angle in object space is given by

$$\tan\alpha = \frac{e}{a} \tag{3.7}$$

After deflection by the lens the shadow ray crosses the axis at z' and falls on the shadow plane, a distance (z_{SP} - z') away, at height E (generally different from E'). The angle, which the ray makes with the axis in image space, is given by

$$\tan\alpha' = \frac{E}{z_{SP} - z'} \tag{3.8}$$

The value of z' can be found from rear-mesh data by graphing z' versus E', and setting E' equal to E, the front-mesh shadow height. Then Eq. (3.8) can be used to find α'.

From Equations (3.7) and (3.8)

$$m = \left(\frac{\tan\alpha}{\tan\alpha'}\right) = \frac{e/a}{[E/(z_{SP} - z')]}. \tag{3.9}$$

Setting $E/e = M$ (the shadow magnification of the front mesh) and z_{SP} - z' = $c + d$ = M'_C, the image magnification m can be expressed as

$$m = \frac{M_c'}{M_a}. \tag{3.10}$$

The paraxial magnification is

$$m_0 = \frac{e/a}{\left[E/(z_{SP} - z_0')\right]} = \frac{M_0' c_0}{M_0 a} \tag{3.10}'$$

where M_0' and M_0 are the shadow magnifications for paraxial rays, and c_0 is the paraxial value of c.

Spherical Aberrations of Magnification

The spherical aberration coefficient μ_s of magnification and the paraxial value m_0, for either magnetic or electrostatic lenses, are determined experimentally from graphs of m vs α'^2 plotted according to the equation

$$m = m_0(1 + \mu_s \alpha'^2) \tag{3.11}$$

Here fractional changes in magnification are related to α'^2 by the aberration coefficient μ_s. The graph is a straight line to second order in α'. The intercept on the m-axis is the paraxial magnification m_0, and the slope is equal to μ_s.

Calculation of Focal Length and Focal Distance

The focal length of a lens can be calculated from the values of z, z', and m. (Spangenberg and Field; Rempfer, Fyfield, and Griffith) Starting from the Newtonian relations, Equations (2.1) and (2.2) of Chapter 2

$$\frac{z-g}{f} = \frac{r}{r'} = \frac{1}{m}, \text{ and}$$
$$\frac{z'-g}{f} = \frac{r'}{r} = m,$$

and subtracting the second expression from the first gives

$$\frac{z-z'}{f}=\frac{1}{m}-m, \quad \text{or}$$

$$f=\frac{z-z'}{\frac{1}{m}-m}. \tag{3.12a}$$

Then from Eq. (2.2)

$$g=z'-fm \tag{3.12b}$$

The paraxial expressions for f and g are

$$f_0=\frac{z-z_0'}{\frac{1}{m_0}-m_0}. \tag{3.12a)'}$$

$$g_0=z_0'-f_0m_0 \tag{3.12b)'}$$

Experimentally measured values of the image properties z' and m as a function of α'^2 can be used via Equations (3.12a and b) to find the corresponding values of f and g.

Spherical Aberration of f and g

The longitudinal spherical aberrations Δf and Δg are defined to second order by the following equations,

$$\Delta f=f-f_0=f_0S_f\left(\frac{\rho}{f_0}\right)^2=f_0S_f\delta^2 \tag{3.13a}$$

$$\Delta g = g - g_0 = f_0 S_g \left(\frac{\rho}{f_0}\right)^2 = f_0 S_g \delta^2 . \qquad (3.13b)$$

where ρ is the height of the ray at the principal surfaces, and δ is the angle through which the ray is deflected by the lens. The angle $\delta = (\alpha + \alpha') = (1 + m_0)\alpha'$, and so includes object-space, as well as image-space, aberration. The paraxial values f_o and g_o and spherical aberration coefficients S_f and S_g of f and g can be found from graphs of f and g versus δ^2. The intercepts of the graphs on the f or g axis are the paraxial values f_o or g_o, and the slopes divided by f_0 are the aberration coefficients S_f or S_g. Since the graphs are influenced by all of the plotted points, the values of f_o and g_o obtained from the intercepts, may differ slightly from the single values given in Equations (3.12a)' and (3.12b)'.

From geometry, the deflection δ is equal to the sum of the object and image ray angles, $\alpha + \alpha'$, and to first order, $\rho/f_0 = \tan(\delta) = \delta$. Thus, to first order, δ does not vary with magnification $m_0 = \alpha/\alpha'$ at a given height ρ. As a result the aberration coefficients S_f and S_g avoid the large variations with magnification such as occur, for example, with the spherical aberration coefficient C_S'. Coefficients S_f and S_g are lens aberrations, as distinct from image aberrations. The image aberration coefficient C_S', expressed in terms of S_f and S_g and the image magnification m_0, is given by

$$C_S' = - \{(1 + m_0^2)S_g + 2m_0 S_f\}(1 + m_0)^2 f_0. \qquad (3.14)$$

Please see Ref. 3.3 (1985 paper) or Appendix E for a derivation of Eq (3.14). For very small magnifications, and for very large magnifications (referred to object space), Equation (3.14) reduces to $C_S' = - S_g f_0$.

Chromatic Aberration

The focusing power of an electron lens depends on a pair of activation parameters. For a magnetic lens these parameters are the magnetizing current I for the magnetic field and the accelerating voltage V for the electrons. For electrostatic lenses the parameters are the lens-field voltage V_A - V_L and the electron-accelerating voltage V_A - V_C. Adjustment of one or both of the activation parameters of a lens enables the lens to focus the image at the desired distance z'. The activators for either electrostatic or magnetic lenses can be combined in a compound activator in such a way that the lens power is a function of the compound activator alone. The combination $P = \frac{(NI)^2}{V}$ is a compound activator for magnetic lenses, where N is the number of turns in the magnetizing coil. Likewise the combination $\frac{(V_A - V_L)}{(V_A - V_C)} = \mathcal{V}_{LC}$ is a compound activator for electrostatic lenses. With $V_A = 0$, $\mathcal{V}_{LC}$ can be expressed as $\frac{V_L}{V_C}$.

There are four different properties (two image properties, z_0' and m_0, and two lens properties, f_0 and g_0, whose chromatic aberrations are to be related to changes in the compound activators P (for the magnetic lens) and $\mathcal{V}_{LC}$ (for the electrostatic lens). Thus there are eight relationships, four for magnetic lenses and four for electrostatic lenses to be set up. There is a lot of duplication in major parts of the equations, and in the accompanying commentary. To avoid some of the duplication, the details of the relations between only one of the aberrations, $\Delta z_0'$, and the activators P and $\mathcal{V}_{LC}$ are

carried out, and the remaining relations are summarized without descriptive comments.

Chromatic Aberration of the Paraxial Image Distance z_0'

Since the position z' of the focused image depends on the values of P or $\mathcal{V}_{LC}$, small residual fluctuations in these parameters in general cause fluctuations in the focused image, creating chromatic aberration. The amount of aberration is measured by the span of $\Delta z_0'$, over which the paraxial image distance fluctuates. The chromatic aberration coefficient C_C' of the lens relates $\Delta z_0'$ to the fractional change in P or $\mathcal{V}_{LC}$. In the case of magnetic lenses the relation is

$$\Delta z_0' = C_C' \frac{(-\Delta P)}{P} = C_C' \left(\frac{-\Delta \left(\frac{NI}{V} \right)^2}{\left(\frac{NI}{V} \right)^2} \right) \tag{3.15a}$$

For small fluctuations, expanding Equation (3.15a) gives

$$\Delta z_0' = C_C' \left\{ -\frac{2\Delta I}{I} + \frac{\Delta V}{V} \right\} \tag{3.15b}$$

Equation (3.15b) shows that changes of the same sign in I and V (i.e. ΔI and ΔV both positive or both negative) tend to cancel each other's effects on the aberration $\Delta z_0'$. In particular, if the fluctuations in I and V have the same form, and if the fractional change in I is 1/2 the fractional change in V, ΔP and the aberration $\Delta z_0'$ are 0. If $\Delta I = 0$, Equation (3.15b) reduces to

$$\Delta z_0' = C_C' \frac{\Delta V}{V}. \tag{3.15c}$$

In electrostatic lenses the chromatic aberration is

$$\Delta z_0' = C_C' \frac{(-\Delta v_{LC})}{v_{LC}} = C_C' \frac{-\Delta(V_L / V_C)}{V_L / V_C} \tag{3.16a}$$

Expanding (3.16a) gives

$$\Delta z_0' = C_C' \left(\frac{-\Delta V_L}{V_L} + \frac{\Delta V_C}{V_C} \right). \tag{3.16b}$$

This equation shows that aberrations due to fluctuations of the same sign in V_L and V_C tend to cancel. Also, if the fluctuations have the same form, and the fractional changes in V_L and V_C are the same, the chromatic aberration goes to zero. This feature of electrostatic lenses is applied when the accelerating voltage for the electrons is used also to power a voltage divider from which the lens voltage is tapped. This approach to avoiding chromatic aberration is practical because an electrostatic lens is a capacitor and not a current-drawing load. If $\Delta V_L = 0$, (3.16b) reduces to

$$\Delta z_0' = C_C' \frac{\Delta V_C}{V_C}. \tag{3.16c}$$

Solving for C_C' from Equations (3.15c) or (3.16c) provides a formula, $C_C' = \frac{\Delta z_0'}{(\Delta V / V)}$ or $\frac{\Delta z_0'}{(\Delta V_C / V_C)}$, for evaluating C_C'. Using this approach, one can determine the paraxial focus for a series of accelerating-voltage steps, and the value of C_C' can be calculated for each voltage step. This process leads to C_C' as a function of accelerating voltage V or $V_A - V_C'$. A refinement of this procedure is to use curves of already-found experimental values of z_0' as a function of accelerating

potential, determine the slopes at a series of accelerating-voltage steps, and evaluate to find C_C' as a function of V or V_C. If an analytical expression is found which fits the experimental graph of z_0' .vs. V or V_C, then one can use derivatives of z_0' with respect to V or V_C to determine C_C'.

Summary of Equations Linking Chromatic Aberration to Changes in P and $\mathcal{V}_{LC}$

Magnetic Lenses

$$\Delta z_0' = C_C' \frac{-\Delta P}{P}, \tag{3.17a}$$

$$\Delta m_0 = m_0 \mu_C \frac{-\Delta P}{P}, \tag{3.17b}$$

$$\Delta f_0 = f_0 C_f \frac{-\Delta P}{P}, \tag{3.17c}$$

$$\Delta g_0 = f_0 C_g \frac{-\Delta P}{P}, \tag{3.17d}$$

where $P = \frac{(NI)^2}{V}$, and $\frac{-\Delta P}{P} = \frac{-2\Delta I}{I} + \frac{\Delta V}{V}$.

Electrostatic Lenses

$$\Delta z_0' = C_C' \frac{-\Delta \mathcal{V}_{LC}}{\mathcal{V}_{LC}}, \tag{3.18a}$$

$$\Delta m_0 = m_0 \mu_C \frac{-\Delta \mathcal{V}_{LC}}{\mathcal{V}_{LC}}, \tag{3.18b}$$

$$\Delta f_0 = f_0 C_f \frac{-\Delta \mathcal{V}_{LC}}{\mathcal{V}_{LC}}, \tag{3.18c}$$

$$\Delta g_0 = f_0 C_g \frac{-\Delta \mathcal{V}_{LC}}{\mathcal{V}_{LC}}, \tag{3.18d}$$

where $\mathcal{V}_{LC} = \frac{V_A - V_L}{V_A - V_C} = \frac{V_L}{V_C}$ with $V_A = 0$, and $\frac{-\Delta\mathcal{V}_{LC}}{\mathcal{V}_{LC}} = \frac{-\Delta V_L}{V_L} + \frac{\Delta V_C}{V_C}$.

The image chromatic coefficient C_c' is related the lens chromatic coefficients C_f and C_g by the equation

$$C_c' = [(1 + m_0^2)\, C_g + 2m_0 C_f] f_0. \tag{3.19}$$

Please see (Ref. 6) or Appendix E for a derivation of Eq (3.19).

Chromatic Aberration Due to Energy Distribution in the Electron Beam

Another source of chromatic aberration is energy distribution (*ED*) in the electron beam, either from a range of emission energies or from energy losses due to collisions on the way to the lens. For example, an electron is emitted from the electron source with an initial beam voltage V_{ED} in the axial direction. After acceleration this electron has a beam voltage of $V_{ED} + V$ (or $(V_A - V_C)$) = V_B at the lens, and will be focused as if V_B were the accelerating voltage. To include the *ED* effect on aberration, V_{ED} should be added to V in Equation (3.15a), and to $|V_C|$ in Equation (3.16a). Also ΔV_{ED} (a measure of the range of energies in the beam) should be added to ΔV in Equation (3.15b) and to $\Delta|V_C|$ in Equation (3.16b). These additions are included below in Equations (3.20a) and (3.20b) for magnetic lenses and Equations (3.21a) and (3.21b) for electrostatic lenses:

Chromatic Aberration of Magnetic Lenses (Including *ED*)

$$\Delta z_0' = C_C' \left(\frac{-\Delta\left[\frac{(NI)^2}{V+V_{ED}}\right]}{\frac{(NI)^2}{V+V_{ED}}} \right). \tag{3.20a}$$

Expanding Equation (3.20a) gives

$$\Delta z_0' = C_C' \left\{ \frac{-2\Delta I}{I} + \frac{\Delta V}{V} + \frac{\Delta V_{ED}}{V} \right\}. \tag{3.20b}$$

$$\Delta z_0' = C_C' \frac{-\Delta\left(\frac{V_L}{|V_C|+V_{ED}}\right)}{\frac{V_L}{|V_C|+V_{ED}}}. \tag{3.21a}$$

Expanding (3.21a) gives

$$\Delta z_0' = C_C' \left(\frac{-\Delta V_L}{V_L} + \frac{\Delta V_C}{V_C} + \frac{\Delta V_{ED}}{|V_C|} \right). \tag{3.21b}$$

In Equations (3.20b) and (3.21b) the first two terms in the parentheses cause shifts in position of the image along the axis as a function of time due to unsteadiness in the lens-field or accelerating-voltage supplies. The third term ΔV_{ED} causes a spread in position of the paraxial image distance at which electrons of different energies simultaneously focus. This range $(\Delta z_o')_{ED}$ does not change in time, except for moving along the axis with any uncompensated aberration due to the first two terms. If the aberrations due to the first two terms in Equations (3.20b) and (3.21) cancel each other, or are zero, Equations (3.20b) and (3.21b) reduce to

$$\Delta z_0' = (\Delta z_0')_{ED} = C_C' \frac{\Delta V_{ED}}{V \text{ or } |V_C|}. \qquad (3.22)$$

As the width of the energy distribution in the electron beam is reduced, the chromatic aberration due to *ED* is also reduced. The electron beams used in the present experimental work are nearly monochromatic, so the chromatic aberration due to the energy distribution is small and will be ignored for the rest of this dissertation.

Properties of the Principal Surfaces

The principal surfaces, H in object space and H' in image space, are virtual constructs which are involved in defining the focal length of a lens. Please see Figure 2.2(a), of Chapter 2. The virtual intersection point of the image ray and the parallel incident ray defines one end of the focal length; the axial distance of this point to the focal point is the focal length f. The intersection point also defines a point on the principal surface. The principal surface is the locus of such points. The principal surfaces are useful also in drawing rays and providing a measure of the height ρ at which a ray goes through the lens. For example, in Figure 2.2(b) a ray leaves an object point on the axis at a random angle. The ray is extrapolated along a straight line into the lens and intersects H at height ρ. The image ray is drawn backward in a straight line from the image point to the same height ρ on H'. In symmetric lenses H and H' are spaced away from the center plane at equal distances h and h' in opposite directions. In light-optics, in symmetric double-convex glass lenses, each principal surface is on the same side of the center plane as its respective focal point; i.e., h is positive. In electron optics, h is negative for the types of lenses which we are

studying, and the principal surfaces are on opposite sides of the center plane from their respective focal points (crossed principal surfaces). In an ideal thin lens, H and H' reduce to a single plane at the center of the lens, and the intersection points for the object and image rays coincide. The focal length f is defined as the axial distance from the intersection point at height ρ on H' to the focal point F'. For symmetric lenses, g is defined as the distance from the center plane to the focal point. The axial distance h from the center plane to the intersection point at ρ on H' or H is therefore

$$h = g - f. \tag{3.23}$$

In general, the spherical aberrations of f and g result in spherical aberration in h. The spherical aberration coefficient of h is

$$S_h = S_g - S_f, \tag{3.24}$$

where S_h is defined by $\frac{\Delta h}{f_0} = S_h\left(\frac{\rho}{f_0}\right)^2$ or $S_h\delta^2$. Also, in general, h_0 suffers from chromatic aberration. The chromatic coefficient of h_0 is

$$C_h = C_g - C_f. \tag{3.25}$$

C_h relates to shifts of the principal surfaces toward, or away from, the center plane, with changes in lens activation. S_h relates to curvature of the principal surfaces with height ρ of the ray off axis.

Chapter 4. Equipment and Supplies

Test bench

The mainstay of our equipment is the electron-optical test bench Figure 4.1.

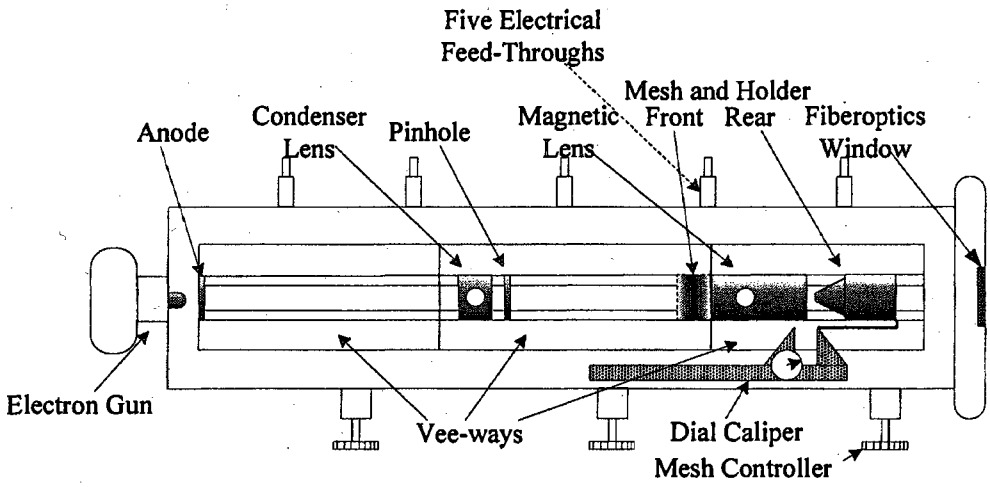

Figure 4.1. Schematic diagram of the electron-optical bench.

The bench is a vacuum enclosure containing a horizontal vee-way for supporting lenses and other parts of the optical system in alignment. Manual actuators on the front wall enable one to move lenses and other components along the vee-way while setting up and during the experiment. Feed-throughs along the back wall enable voltages and currents to be fed to the components in the vacuum. A thermionic triode electron gun is mounted at one end of the bench, and a phosphor-coated fiber-optics window is mounted at the other end. The bench has a hinged top of thick glass which can be opened for access to the experiment, and through which one can observe the experiment in progress. The bench is mounted on a Veeco vacuum system which can

provide sufficiently low pressure (<10^{-4} torr) for the electron-optics experiments. A photograph of the optical bench is shown in Figure 4.2.

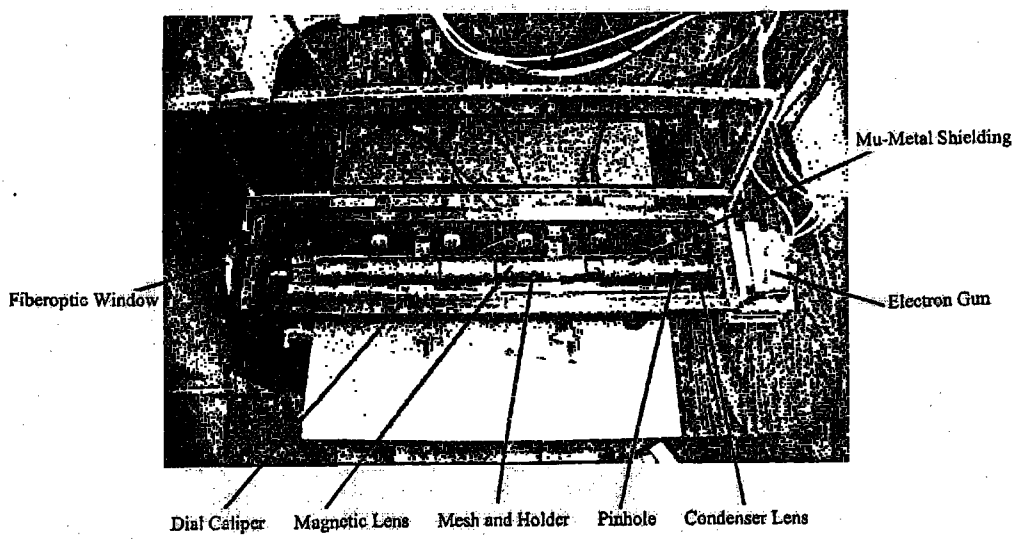

Figure 4.2. Experimental setup for measuring lens properties in the electron optical bench.

Vacuum System

In order to avoid undue scattering of electrons by air molecules, the pressure in the test bench is reduced below 10^{-4} torr by means of the pumping system on which the bench is mounted. This system is oil-pumped, and has a typical pumping arrangement with a diffusion pump backed by a mechanical pump, and a parallel roughing line. See Figure 4.3. There are three valves, one between the high-vacuum end of the diffusion pump and the vacuum bench (hi-vac valve), another between the foreline end of the diffusion pump and the mechanical pump (foreline valve), and a third valve in the roughing line between the mechanical pump and the bench (roughing valve). A fourth valve (relief valve) between atmosphere and the bench vacuum is for

letting air into the bench. There are two thermocouple pressure gauges, one reading the foreline pressure of the diffusion pump, and one reading the pressure in the roughing line.

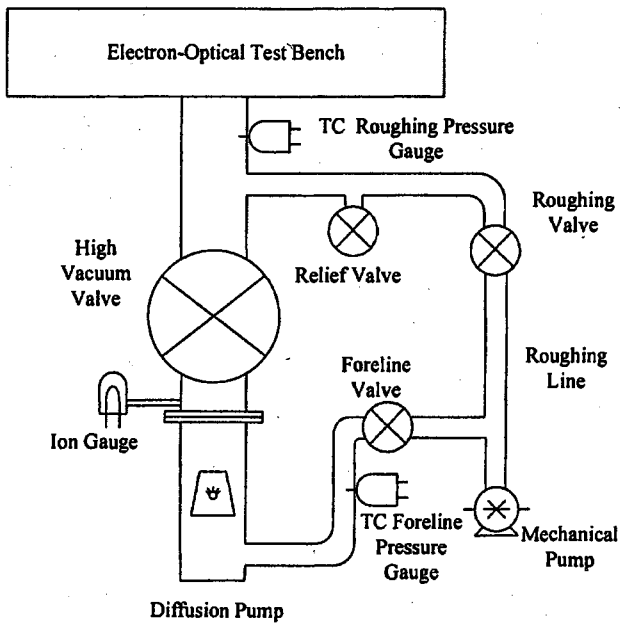

Figure. 4.3. Schematic drawing of the vacuum system.

An ion gauge is used to read the pressure at the high-vacuum end of the diffusion pump. Instruction sheets explain how to carry out various procedures, such as pumping down and letting the system up to air, without damage to the pumping system.

Voltage and Current Sources

A current supply, adjustable from 0 to1 ampere, is used for activating the magnetic test lenses. A high voltage supply, adjustable up to -30kV is used for

accelerating the electron beam from the electron gun filament (at negative potential) to the anode (at ground potential). This power supply also provides the high voltage for the voltage divider. The voltage divider is a string of precision resistors (twenty 20-Meg resistors in series); a 2200 *pf* capacitor is connected across each resistor to filter out high frequency fluctuation. The negative end of the divider is at the potential of the gun filament, and the positive end is at ground potential. Taps along the divider provide fractions of the accelerating voltage for the electrostatic lenses. A low voltage power supply, isolated from ground, is used to operate the electron gun. This power supply is described in connection with the description of the electron gun.

Electron Gun

The electron gun provides the electron beam for the shadowgraph experiments. The electrons are emitted thermionically from the pointed bend of a vee-shaped filament, made from 4 mil thoriated tungsten wire. The filament is connected electrically to the negative high-voltage end of the voltage divider, and is heated by the low-voltage power supply, isolated from ground. A cup-shaped control electrode (Wehnelt) with a central opening for passage of electrons is maintained at a negative potential relative to the filament. The negative bias for the Wehnelt is derived from a dropping resistor between the negative lead from the high-voltage power supply and negative end of the voltage divider. See Figure 4.4.

A potentiometer connected across the resistor provides a negative bias to the Wehnelt. A switch in series with the potentiometer, as shown, can be used to abruptly turn the electron beam off and on as needed, e.g., as when shadowgraphs are being

recorded. The anode of the gun is a grounded electrode with a central opening for passage of electrons. The potential difference between the filament and the anode accelerates the electrons into a high-energy beam centered on the optical axis.

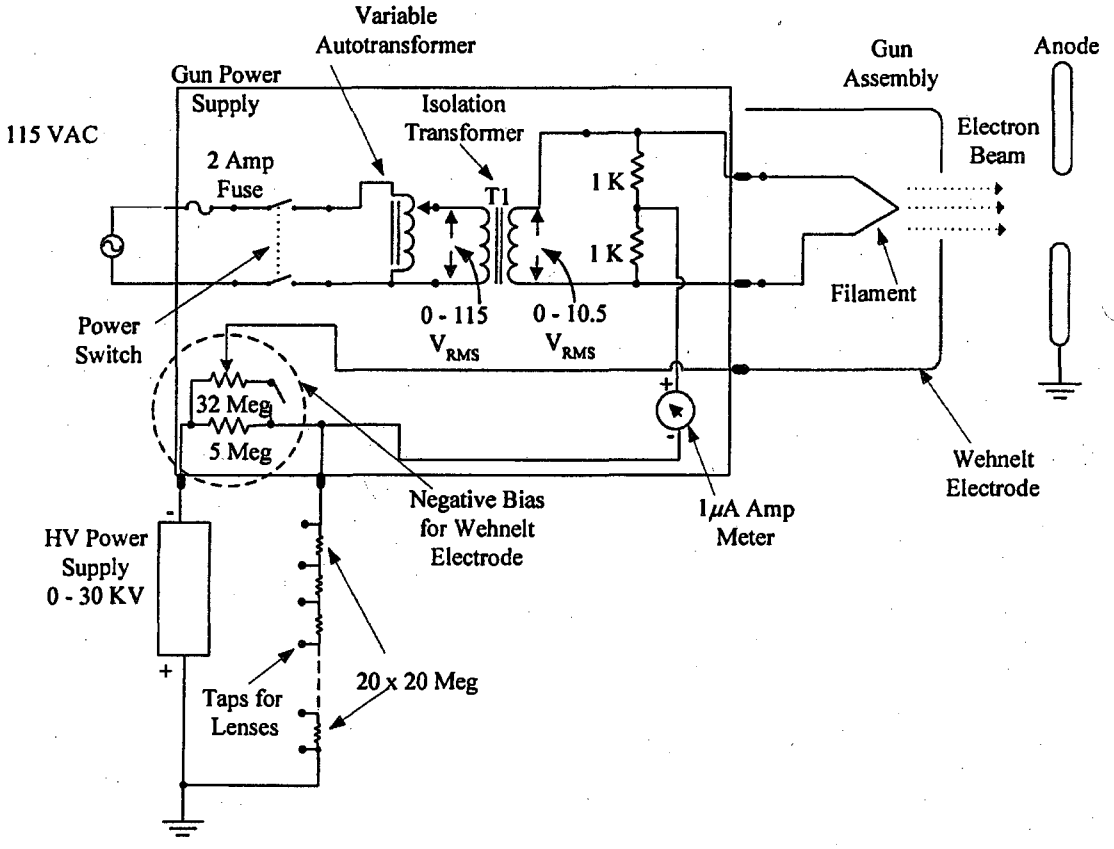

Figure 4.4. Schematic diagram of the filament power supply and Wehnelt biasing arrangement with HV connection and voltage divider.

The gun anode is supported on the vee-way at the gun end of the bench. X and Y controls on the gun can be used to center the Wehnelt with respect to the anode during operation, and X, Y, and Z controls can adjust the centering and spacing of the

filament relative to the Wehnelt. Instruction sheets explain how to operate the electron gun to best advantage.

The Condenser Electron Lens and Pinhole Stop

The condenser lens is placed so as to form a demagnified image of the electron source at the pinhole stop, thus creating a "point" source of electrons which serves as the object for the test lens. In the present set-up the condenser is an electrostatic lens, and its voltage is obtained from a tap on the voltage divider.

Test Lens

Five lenses were tested, two magnetic and three electrostatic. The test lenses are described in Chapter 2. In the tests, the lens is supported and aligned by the vee-way. Magnetic lenses are activated by the magnetizing current from the current power supply. Their focal properties depend on both activation current and the beam voltage of the electrons. Electrostatic lenses are activated by voltages from taps on the voltage divider. Their focal properties depend on the ratio of the lens voltage to the accelerating voltage.

Meshes and Mesh Holders

A rear mesh with 2000 openings per inch (787.4/cm) is used for shadow casting over most of the ranges of current and voltage settings used in finding the image location z'. If the shadow magnification is low, and the bar shadows are inconveniently close together, a coarser mesh is used. The holder supporting the rear mesh is attached to a slide, which can be moved along the axis by an external actuator, enabling the mesh to be placed optimally during an experiment. The movable arm of

a dial caliper is attached to the slide. The caliper reading is used to determine the position of the mesh.

A mesh with 600 openings per inch (236.2/cm) is used as the front-mesh for most of the voltage and current settings. If the magnification of the 600-mesh shadow pattern is so high that only a few bar shadows are included in the field of view, a finer mess is used. There is no need to move the front mesh during the front-mesh experiments.

Mu-metal Shields

Mu-metal shields are placed between the components on the vee way to shield the electron beam from electric and magnetic fields. Also, the bench is lined with mu-metal.

Phosphor-Coated Fiber-Optics Window

A fiber-optics window seals the opening in the end of the test bench opposite to the gun-end. The inside face of the window is coated with a phosphor screen. The impact of electrons striking the screen causes the phosphor to emit light. Part of the light is transmitted through the fibers to the outside face of the window. In this way patterns projected onto the phosphor coating on the inside of the fiber-optics window can be recorded by pressing a photographic film against the outer face of the window.

Photographic Film

The photographic film used in our experiments has a slow speed (25) and can be handled under red light. The film (Kodalith 2556), and the developer and fixer for processing it, are available at local photographic supply stores.

Densitometer

The densitometer consists of an LED light source, a focusing lens, a moving table, and a sensor array, as shown in Figure 4.5. The densitometer measures the spacing of the bar shadows in the shadowgraph by scanning the shadowgraph on the translating table. The densitometer is connected to a computer both for recording shadow spacing and for controlling movement of the translating table via a stepper motor.

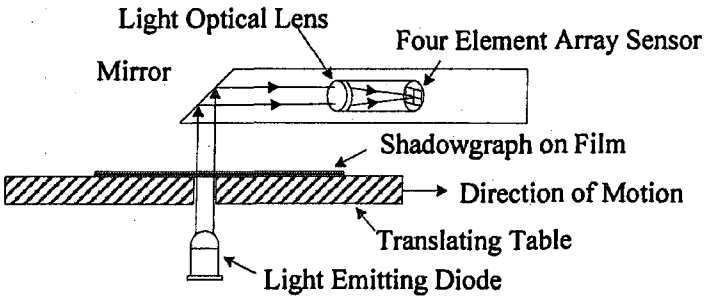

Figure 4.5. Densitometer used to scan shadowgraphs.

Computer

A computer with a spreadsheet like Microsoft Excel is used to work up the shadowgraph data and present the results in the form of tables and graphs of the numerical values of the paraxial and aberration properties of the image distance and magnification. Lens properties from the image properties are also found, and displayed in Tables and graphs. The computer and spreadsheet are further used in

calculating the properties of the theoretical models of the magnetic and electrostatic lenses.

Chapter 5. Experimental Procedure

Brief Review of Shadowgraph Method and Apparatus

The shadowgraph experiments were carried out according to the description of the shadowgraph method given in Chapter 3. To summarize: the test lens forms a demagnified image of a small ("point") source of electrons. The rays in image space are traced by means of the shadow cast by a fine mesh placed between the lens and the shadow plane (rear mesh). A mesh placed between the electron source and the lens (front mesh) is used to trace the rays in object space and the corresponding ray in image space. The shadow patterns of the front and rear meshes are analyzed to obtain the paraxial values and spherical and chromatic aberration coefficients of the image distance and the image magnification. The focal properties of the lens itself can then be calculated from the image properties.

The "point" source for this experiment is the pinhole source created by the combination of condenser lens and pinhole stop. The pinhole source is the object for the test lens. The test lens is placed on the vee way of the electron bench, between the pinhole source and the phosphor-coated window (the shadow plane). The distance from the pinhole to the optical center (o.c.) of the lens is the object distance z, and the distance from the lens o.c. to the phosphor screen is the shadow-plane distance z_{SP}. It is desirable that both z and z_{SP} be relatively large. A large z allows a high demagnification of the paraxial image at z_o'. This results in sharper mesh shadows and

enables image aberrations to be more easily detected and more accurately measured. A large z_{SP} enables a large magnification of the shadow patterns.

In the first part of the experiment, the rear mesh is placed between the lens and the phosphor screen and is used to trace the rays in image space. In the second part of the experiment, the rear mesh is removed, and the front mesh is placed between the pinhole electron-source and the lens to trace the corresponding rays in object space as well as image space. The lens position and activation are the same as for tracing the rays in image space.

Recording the Rear-Mesh Shadowgraphs

The test lens is oriented on the vee-way of the bench so that the end which allows closest approach to the lens o.c. faces the shadow plane. The other end of the lens is backed against a stop on the vee-way to avoid accidentally bumping the lens out of place during rear-mesh manipulation.

The rear mesh in its moveable carrier is placed between the lens and the shadow plane. An external actuator is used to move the mesh holder into contact with the lens, and the dial reading (D_0) is recorded. At this setting, the rear mesh is at its minimum distance b_0 from the lens o.c. This distance (b_0) can be found from the drawings of the lens and the mesh holder. For other settings of the mesh holder, the mesh distance b can found by adding the change in dial reading ($D - D_0$) to b_0. NOTE: To avoid errors due to back-lash in the mechanism, the mesh holder should be moved into position from the far side.

The internal voltage and current leads are connected to the condenser lens and test lens, and the mu-metal shields are set in place. The bench is closed and pumped down to a pressure of less than 10^{-4} Torr. The external leads are connected to the lens feedthroughs, and the desired voltage or current settings selected.

The electron gun, at one end of the test bench, is isolated from ground potential for up to 30 *kV*. A current of up to about 1.5 ampere is sufficient to heat the *V*-filament in the gun to electron emission temperatures. A center-tap between the filament leads puts the filament tip at the same potential as the negative end of the voltage divider, and taps on the divider provide voltages for the electrostatic lenses. The divider current ($50\mu A$ at $20kV$) through a 2 Meg resistor in the lead from the high voltage power supply provides a $100V$ source of negative bias for the control electrode (Wehnelt) in the gun relative to the filament. This bias is made adjustable by a high-resistance potentiometer across the dropping resistor.

To run the experiment, turn on the high-voltage supply and (for magnetic lenses) also the current supply. Since the high-voltage end of the voltage divider and the electron gun filament are connected together electrically, the voltages supplied to the electrostatic lenses by the divider taps are constant fractions of the accelerating voltage, and changes in lens power are accomplished by changing the tap supplying the lens voltage. In contrast, the magnetizing currents for magnetic lenses are independent of the accelerating voltage, and several different voltages (15, 20, or 25 kV) and currents (100 ma to 400 ma) are used in the present magnetic lens tests.

Turn on the electron gun supply. (The heated filament will emit a warm white light). In order to avoid undue shortening of the filament life, the setting of the variac, which (in the present apparatus) regulates the heating current in the filament, should not exceed 20 on its indicator. The bias electrode, or Wehnelt, controls the flow of electrons emitted from the hot filament. One can cut off the beam gradually by turning the bias knob until the negative bias is high enough to prevent the electrons from leaving the gun. The optimum beam occurs at the brightness maximum just before cutoff. There are several phosphor screens with central openings along the optical axis, which are helpful in monitoring the electron beam alignment and focus.

Adjust the focusing power of the condenser lens so that it focuses the electron beam to a small spot at the pinhole stop. The rays coming from the pinhole are refocused to a demagnified image by the test lens, activated by the chosen lens voltage or current and accelerating voltage. The rear mesh casts shadows in the beam of electrons diverging from the image, and the enlarged shadow pattern is projected onto the phosphor-coated window. The closer the mesh is to the image spot, the higher the shadow magnification is, and the more sensitive the shadows are to aberration in the image distance z'. In recording patterns for analysis optimum conditions occur when the mesh is close enough to the image for good sensitivity to aberrations, but far enough away to include enough bar shadows to average out mesh or reading errors. The rear mesh can be placed upstream as well as downstream from the image if there is sufficient clearance between the lens and the image. As mentioned earlier, the shadow patterns can be recorded by pressing a photographic film against the exterior

face of the fiber-optics window, and exposing the film to the shadow pattern for the required amount of time by means of the beam cut-off switch. The rear-mesh shadow patterns for a given test lens operating under a series of lens activations and beam voltages can be recorded without breaking vacuum. After the rear-mesh recordings have been completed, the gun supply and the high voltage and current supplies are turned off. The bench is then isolated from the pumps and brought up to atmosphere to prepare for recording the front-mesh shadowgraphs.

Recording the Front-Mesh Shadowgraphs

The front-mesh is installed in front of the test lens at a known distance *a* from the pinhole, and the rear mesh is removed. Any mu-metal shields or screens removed for this operation are re-installed, where needed. No other changes are made.

The bench is again closed and pumped down to below 10^{-4} Torr. Power supplies are turned on, and front mesh shadowgraphs are recorded for the same series of voltage and current conditions as was used for the rear-mesh shadowgraphs. When recording of the front-mesh shadowgraphs has been completed, the power supplies are turned off, and the bench isolated from the pumps and brought up to atmosphere. The bench is opened, the test lens and the front mesh are removed. The bench is ready for the next test lens to be studied, and the photographic film, which was exposed to the shadowgraph patterns, is ready to be processed into negatives.

Densitometer Readings and Computer Processing

The positions of the bar shadows in the shadowgraph negatives are read automatically by a computer controlled scanning densitometer and the data then fed

directly into a computer with the spreadsheet. The spreadsheet presents the results of the rear-mesh shadowgraphs in the form of graphs and numerical values of the image distance z' as a function of α'^2, from which the paraxial image distance z_o' and the spherical aberration coefficient of the image C_s' are found. These results along with the data from the front-mesh shadowgraphs enable the magnification m of the image to be found as a function of α'^2, and from there the paraxial value m_o and the spherical aberration coefficient μ_s of the image magnification are determined. The image properties are then used to calculate the lens properties f and g and their paraxial values f_o and g_o and the spherical aberration coefficients S_f and S_g. The chromatic aberration coefficients for the image properties z' and m, and the lens properties f and g, are found experimentally from changes in the paraxial values with changes in activation. Graphs of z'_0 vs lens activation are constructed from experimental data, and C_C' is found from the slopes of these curves (Eq. 3.8)

Examples of shadowgraphs are shown in Figure 6.1(a, b, and c) in Chapter 6. These shadowgraphs were obtained with lens L_1 operating at $V = 15kV$ and $I = 100mA$ and are (c) front mesh, (b) upstream rear mesh, and (a) downstream rear mesh shadowgraphs. Data from these shadowgraphs are used in Chapter 6. to illustrate the process of obtaining the image properties and lens properties from the shadow- graphs.

Chapter 6. Analysis of Shadowgraphs: A Numerical Example

The procedure for obtaining the properties of the test lens from the shadowgraph patterns is illustrated with data taken from the shadowgraphs in Figure 6.1 below. (Ref. 4 and 7)

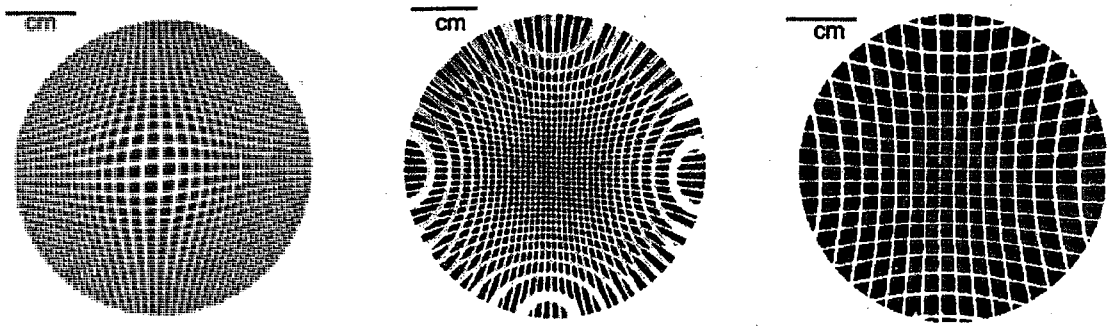

(a) (b) (c)

Figure 6.1 (a, b, and c). Examples of shadowgraphs: (a) and (b) are rear-mesh shadowgraphs; (c) is a front-mesh shadowgraph. In (a) the mesh was downstream from the lens and downstream from the image; in (b) the mesh was downstream from the lens, but upstream from the image, (i.e., between the lens and the image); in (c) the mesh was upstream from the lens.

These patterns were obtained during testing of lens L_1 (magnetic lens with 0.050 in. (1.27 mm) pole-piece gap). In (a) the mesh was downstream from the image; in (b) the mesh was upstream from the image, but still downstream from the lens (i.e., between the lens and the image); in (c) the mesh was placed between the electron source and the lens. The magnetizing current was 100 milliamps, and the accelerating voltage for the electrons was 15 kV. The positions of the object ("pinhole source") and the shadow plane (phosphor-coated window), relative to the optical center (o.c.) of this lens were z = 9.87 in. (25.08 cm) on the front side, and z_{sp} = 10.58 in. (26.88 cm) on the rear side. In (a) the mesh was at a distance downstream from the lens o.c. of b

= 0.395 in. (1.003 cm) and was downstream from the image by a distance c to be determined. In (b) the mesh was downstream from the lens by a distance $b = 0.170$ in. (0.432 cm) and was upstream from the image. Figure 6.1 (c) is a front-mesh shadowgraph with the mesh at a distance from the pinhole of $a = 6.13$ in. (15.57 cm). The front mesh had 600 bars per inch (236.2/cm), and a unit spacing e_1 of 0.004233 cm. The rear mesh had 2000 bars per inch, (787.4/cm), and a unit spacing (e_1') of 0.00127 cm.

In practice, where possible, all of the rear-mesh data sets (X and Y, and upstream and downstream from image) are used in determining the paraxial image distance z_o' and the spherical aberration coefficient C_s' of the image. Both the X and Y front-mesh data sets are used in finding the paraxial magnification m_o and its spherical aberration coefficient μ_s. However, for the purpose of illustrating the procedure, the numerical steps are carried through for only a small fraction of the data available: a single line (bolded) of each of the Tables of data for the three shadowgraphs in Figure 6.1. For a review of ray drawings, nomenclature, and equations please refer back to Chapter 3 and Figures 3.1 - 3.4.

The primary shadowgraph information is obtained by recording the positions of the bar shadows along a diameter at right angles to one or the other set of bar shadows. The center of the pattern is determined from the symmetry of the shadow spacing. The difference between corresponding readings on opposite sides of the optical axis is divided by 2 to obtain sets of average distances E' (rear-mesh shadow) or E (front-mesh shadow) from the axis. The actual mesh-bar distances from the axis,

e' or e, are considered to be multiples (n) or half-multiples ($n - ½$) of the mesh unit e_1' or e_1, depending on whether the shadow pattern is more nearly centered on a shadow or on a space between shadows.

The magnification M' of the rear-mesh shadow is E'/e' for the mesh downstream from the image, and $-E'/e'$ for the mesh upstream from the image. The magnification of the front-mesh shadow is $M = E/e$. When focal length and focal point aberrations are present, the shadow magnifications vary with distance from the axis, as is evident in Figure 6.1(a) (b) and (c). Focal length aberration (Δf) is mainly responsible for distortion of front-mesh shadows, whereas focal point aberration (Δg) is mainly responsible for rear-mesh shadow distortion. The rear-mesh distortion is accentuated by positioning the mesh close to the image.

Analysis of Rear-Mesh Data

Table 6.1(a) shows the X-readings for the bar shadows in Figure 6.1(a) (rear mesh downstream from the image). The pattern center in this case is between mesh bars, and is better represented by a half bar position than by an integral bar position. The distances e' of the n^{th} mesh bar from the axis is (n -1/2) times the mesh unit e_1' = 0.00127 cm. For example, the average distance e' of the 4th mesh bar on each side of the axis is 3.5 mesh units, or (3.5)*(0.00127cm) = 0.004445 cm (see bold data line in Table 6.1(a). The average distance of the shadow of the 4th bar from the axis is E' = 0.715 cm. The shadow magnification M' is then 0.715/0.004445 = 160.86. The distance $d = z_{sp} - b$ from the mesh to the shadow plane is 25.87 cm (see data line at top of Table 6.1(a)).

Mesh/inch	I/milliamps	Mesh	e'_1/cm	d/cm	b/cm		Beam	Voltage	15 kV
2000	100	Rear	0.00127	25.87	1.003	DS			
Bar location/ units	Shadow Reading X/cm	Spacing Δ/cm	E'/cm	M'	c/cm	$\alpha' \times 10^2$	$\alpha'^2 \times 10^4$	z'/cm	
5.5	1.745		0.972	139.10	0.187	3.728	13.901	0.816	
4.5	1.865	0.120	0.851	148.86	0.175	3.266	10.668	0.828	
3.5	2.001	0.136	0.715	160.90	0.162	2.747	7.547	0.842	
2.5	2.160	0.159	0.558	175.81	0.148	2.145	4.602	0.855	
1.5	2.352	0.192	0.366	191.86	0.136	1.405	1.975	0.868	
0.5	2.591	0.238	0.127	200.74	0.130	0.490	0.240	0.874	
-0.5	2.846	0.255							
-1.5	3.083	0.238			Slope	z_0'/cm	C_z'/cm		
-2.5	3.276	0.193		0.000056	-0.0052	0.878	52.44		
-3.5	3.432	0.155							
-4.5	3.566	0.135							
-5.5	3.688	0.122							

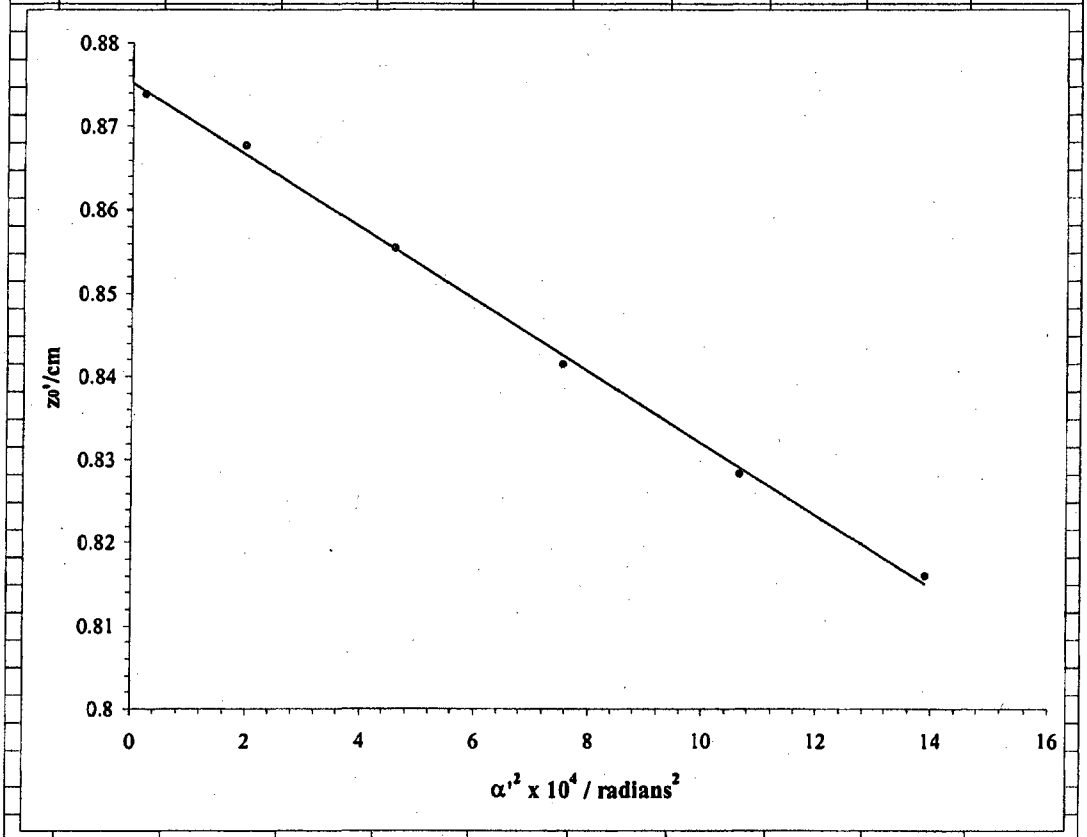

Table 6.1(a) Table and graph for a rear mesh shadowgraph with mesh down stream from the image. The data point 4th from left in the graph was obtained from the bold line in the data table.

From similar triangles, or from Eq.(3.2) of Chapter 3, the distance from the image to the mesh is $c = 0.162$ cm. The distance of the image from the lens o.c. is then $z' = b - c = (1.003\text{-}0.162)\text{cm} = 0.841$ cm, and the tangent of the angle α' at which the ray crosses the lens axis is $e/c = 0.004445/0.162 = 0.02747$

In the graph accompanying Table 6.1(a), the values of z' for the different X-bar heights (including the z' value just calculated) are plotted versus $\alpha'^2 \text{x} 10^4$ rad^2 up to $\alpha' \cong 0.03728$ radians. The straight-line character of the graph shows that z' can be represented by Eq.(3.5): $z' = z_o' - C_s'\alpha'^2$. The intercept of this graph on the z' axis is the paraxial value $z_o' = 0.878$ cm. The spherical aberration coefficient of z' (the slope times -10^4) is $C_s' = 52.4$ cm. The sample data point ($z' =$ 0.842 cm and $\alpha'^2 = (0.02747\text{rad})^2 = 7.546x10^{-4}$ rad^2 calculated above is highlighted in the graph in Figure 6.1(a).

The shadowgraph in Figure 6.1(b) for the rear mesh downstream from the lens, but upstream from the image (i.e. between the lens and the image), is processed in the same way as for the downstream location. The parameters are the same as in Table 6.1(a) except for b and d, which now correspond to the upstream location. Also, the shadow magnification M' and image-to-mesh distance c are now negative.

Table 6.1(b) shows the work-up of the X - shadowgraph data for the rear mesh upstream from the image. See the graph (accompanying Table 6.1(b)) of z' vs. $\alpha'^2 X10^4$ with $z_o' = 0.879$ cm and $C_s' = 45.2$ cm. For comparison, the values of z_o' and C_s' obtained from rear mesh downstream X-data in Table 6.1(a) were

Mesh/inch	I/milliamps	Mesh	e'_1/cm	d/cm	b/cm		Beam	Voltage	15 kV
2000	100	Rear	0.00127	26.44	0.432	US			

Bar location/ units	Shadow Reading X/cm	Spacing Δ/cm	E'/cm	M'	c/cm	$\alpha' \times 10^2$	$\alpha'^2 \times 10^4$	z'/cm
10.5	1.965		0.869	-65.19	-0.400	3.34	11.14	0.831
9.5	2.062	0.097	0.765	-63.42	-0.411	2.94	8.64	0.842
8.5	2.153	0.091	0.672	-62.22	-0.418	2.58	6.66	0.850
7.5	2.238	0.085	0.583	-61.25	-0.425	2.24	5.03	0.857
6.5	2.322	0.083	0.498	-60.36	-0.431	1.92	3.67	0.863
5.5	2.404	0.082	0.416	-59.58	-0.437	1.60	2.56	0.868
4.5	2.480	0.076	0.338	-59.19	-0.439	1.30	1.69	0.871
3.5	2.557	0.077	0.261	-58.74	-0.443	1.00	1.01	0.874
2.5	2.633	0.076	0.185	-58.33	-0.446	0.71	0.51	0.878
1.5	2.706	0.073	0.111	-58.24	-0.446	0.43	0.18	0.878
0.5	2.782	0.076	0.036	-56.92	-0.457	0.14	0.02	0.888
-0.5	2.854	0.072						
-1.5	2.928	0.074			Slope	z_0'/cm	C_s'/cm	
-2.5	3.004	0.076		2.21E-05	-0.00452	0.879	45.2	
-3.5	3.079	0.076						
-4.5	3.157	0.077						
-5.5	3.236	0.080						
-6.5	3.318	0.082						
-7.5	3.405	0.087						
-8.5	3.497	0.092						
-9.5	3.592	0.095						
-10.5	3.703	0.111						

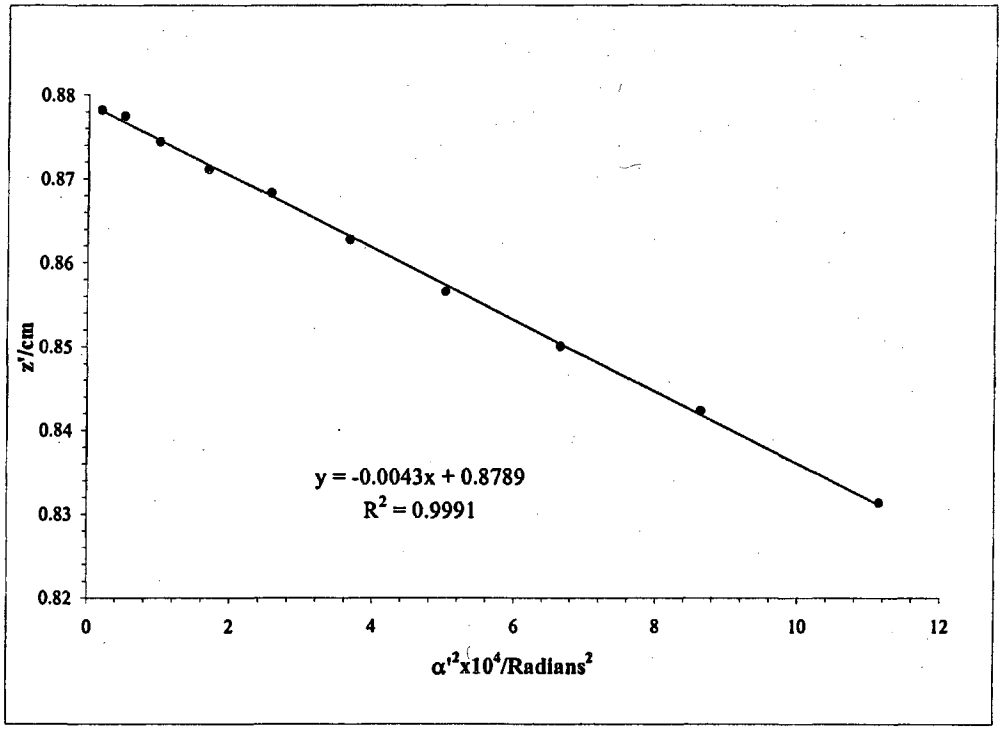

Table 6.1(b). Table and graph for rear mesh shadowgraph with mesh up-stream from image.

z_o'= 0.878 cm and 52.44 cm. The complete set of experimental data for the numerical sample including the *y*-bar data gives z_o = 0.878 cm and C_s' = 48.50 cm.

Analyses of the Front Mesh Data

As pointed out in Chapter 3, since real lenses cannot in general be treated as "thin" lenses, further data is needed to calculate the focal properties, *f* and *g*. The front-mesh shadowgraph results are used in combination with the rear-mesh results to determine the needed information, namely, the magnification of the image $m = \tan \alpha / \tan \alpha'$, ($\alpha$ is the angle which the ray from the axial object point makes with the axis in object space, and α' is the angle which the same ray makes with the axis in image space).

Table 6.1(c) shows the *X*-readings and processing for the front mesh shadowgraph in Figure 6.1(c). The distance from the pinhole object to the front mesh is a = 15.56 cm. The pattern center is on a mesh bar, so the distances of the mesh bars from the axis are integers times the mesh spacing e_1 = 0.004233 cm. For example, the distance of the third mesh bar from the axis is e = 3 mesh units, or (3) (0.004233) cm = 0.01270 cm. (See bold data line in Table 6.1(c).) The average distance of the shadow of the third bar from the axis is E = 0.603 cm, and the shadow magnification is M = 0.603/0.01270 = 47.48. The object ray angle is given by $\tan \alpha = e/a$ = 0.01270cm/15.56cm = 0.0008162. The image ray angle is given by $\tan \alpha' = E/(z_{SP} - z')$ = (0.603 cm)/(26.88 cm - z'). The missing value of z' is obtained from Figure 6.1(d) a graph of z' vs. E' from Table 6.1(a) data. Setting E' equal to E = 0.594 cm gives

Mesh/inch	I/milliamps	Mesh	z/cm	e_1/cm	a/cm	z_{sp}/cm	z_0'/cm	C_s'/cm	$z_{sp}-z_0'$/cm
600	100	Front	25.08	0.004233	15.56	26.88	0.878	48.50	26.00

Bar location/ units	Shadow Reading X/cm	Spacing Δ/cm	E/cm	$\alpha \times 10^4$	$\alpha' \times 10^2$	$\alpha'^2 \times 10^4$	m	z'/cm
6	1.559		1.296	16.324	4.960	24.605	0.03291	0.758
5	1.830	0.270	1.049	13.603	4.023	16.181	0.03382	0.799
4	2.079	0.249	0.819	10.883	3.145	9.889	0.03461	0.830
3	2.310	0.231	0.603	8.162	2.316	5.362	0.03525	0.852
2	2.527	0.217	0.396	5.441	1.523	2.320	0.03572	0.866
1	2.733	0.206	0.196	2.721	0.755	0.571	0.03602	0.875
0	2.932	0.199						
-1	3.126	0.194			Slope	m_0	μ_s	
-2	3.320	0.193		1.45E-06	-0.0002	0.036103	-45.82	
-3	3.515	0.196						
-4	3.717	0.201						
-5	3.927	0.211						
-6	4.151	0.223						

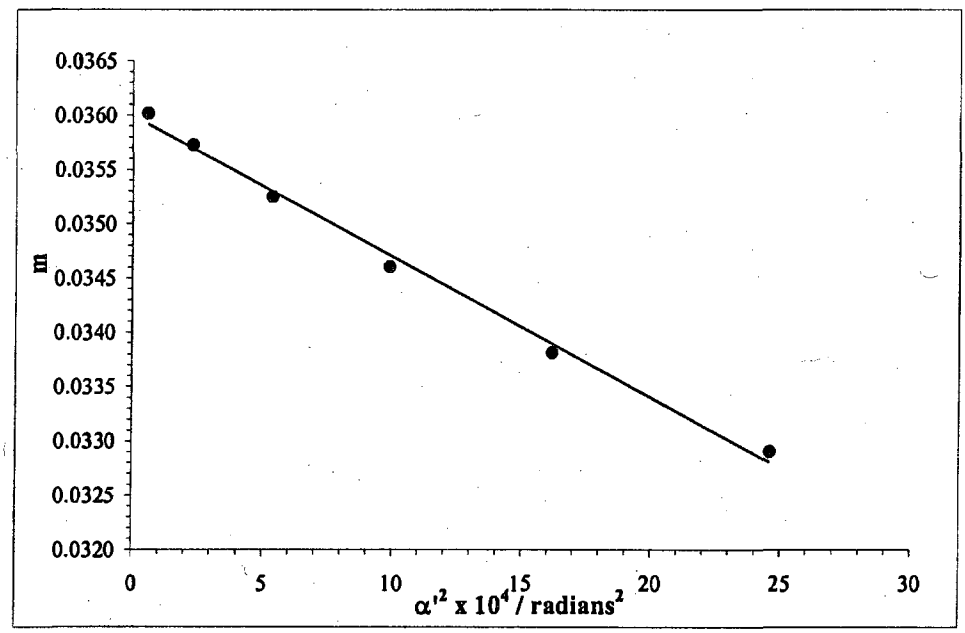

Table 6.1(c). Sample of a table and graph for a front shadowgraph analysis.

$z' = 0.853$ cm. The $tan\ \alpha' = 0.594/(26.873 - 0.853) = 0.594/26.02 = 0.02283$. The image magnification from $tan\ \alpha / tan\ \alpha'$ is $m = 0.0008162/0.02283 = 0.03575$. Figure 6.1(c) is a graph of the magnification m for the different X-bar-shadow heights as a function of the corresponding values of α'^2. The graph is a straight line showing that m can be represented by Eq (3.15), with the paraxial value $m_o = 0.036103$, and the spherical aberration coefficient is $\mu_s = -45.8$. The complete data set including the y-bar readings give $m_o = 0.03560$ and $\mu_s = -46.4$.

E /cm	z'/cm
0.972	0.816
0.851	0.828
0.715	0.842
0.558	0.855
0.366	0.868
0.127	0.874

Table (6.1d)

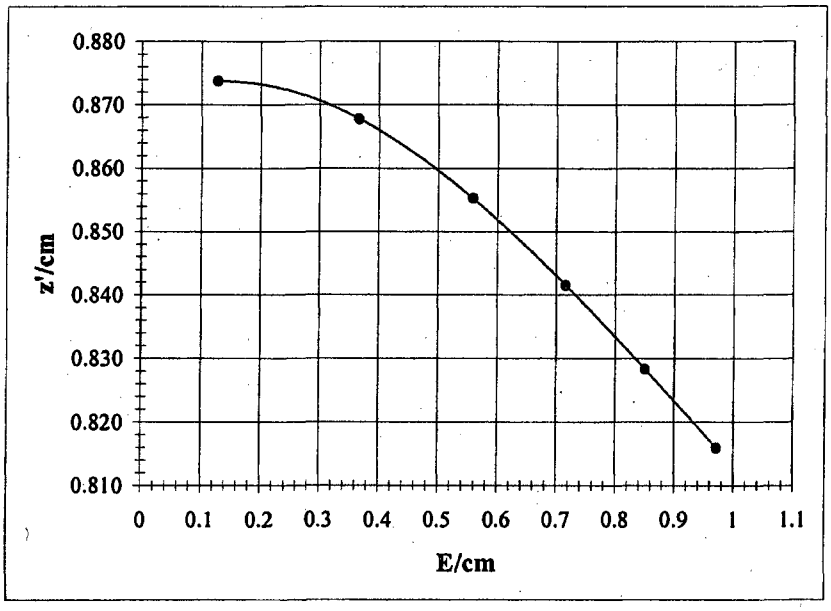

Figure 6.1(d). Plot of z' vs. E from Table 6.1(a) data. See Table 6.1(d) above.

Focal Length, Focal Distance, and Principal Surface Locations

The values $z' = 0.852$ cm and $m = 0.03525$, used in illustrating the numerical steps in data line 3 of Table (6.1c), and the given value $z = 25.08$ cm for the object distance, are used to illustrate the calculation of f and g, and from their values, h. From Eq (3.18), $f = (z - z')/(1/m - m)$ = (25.08 - 0.852)/(28.369 - 0.03525) cm = 0.855 cm. From Eq ((3.19)), $g = z' - fm$ = 0.852 cm - (0.855 x 0.03525) cm = 0.821 cm. Using $h = g - f$ = 0.821 cm - 0.855 cm gives h = - 0.034 cm.

The values of z', m, α', and ρ/f_o [$= \alpha + \alpha' = \delta$] are listed in Table 6.2 for the different X-bar heights, along with the resulting values for f, g, and h. Graphs accompanying Table (6.2), show f and g versus $(\rho/f)^2$ with $f_o = 0.875$ cm and g_o = 0.846 cm and $h_o = g_o - f_o = 0.029$ cm. The slopes of the graphs give the spherical aberration coefficients as S_f = -40.95, S_g = -48.65, and S_h = -7.70. The values, obtained from the full body of data, for the paraxial quantities, are $f_o = 0.863$ cm, g_o = 0.847 cm, and $h = 0.016$ cm; and the spherical aberration coefficients are S_f = -41.52, S_g =-49.44, and S_h = -7.92.

Chromatic Aberration

The chromatic aberration coefficients C_C' of z_o', and C_f and C_g of f_o and g_o were determined from the variation of the paraxial properties of the image and the lens with change in lens activation. The numerical values of the coefficients were obtained from a combination of experimental measurements and the chromatic aberration equations derived from the theoretical models. The full-data results for the entire test

lenses, over the range of activation parameters studied, are shown in Tables and graphs in Chapter 7.

Beam Voltage	I/milliamp	Mesh	z/cm	z_0'/cm	m_o	C_z'/cm
15 kV	100	Front	25.08	0.878	0.036103194	48.50

Bar location/ units	$\alpha' \times 10^2$	$\alpha'^2 \times 10^4$	m	z'/cm	$(\rho/f)^2 = (m+1)^2 \alpha'^2$	f/cm	g/cm	h/cm
6	4.960	24.605	0.032909	0.758	26.414	0.801	0.732	-0.069
5	4.023	16.18081	0.033818	0.799	17.370	0.822	0.771	-0.051
4	3.145	9.889348	0.034606	0.830	10.616	0.840	0.801	-0.040
3	2.316	5.361709	0.035249	0.852	5.756	0.855	0.821	-0.034
2	1.523	2.319898	0.035725	0.866	2.490	0.866	0.835	-0.031
1	0.755	0.570588	0.036017	0.875	0.613	0.873	0.843	-0.030

	$slope_f$	f_o/cm	S_f
0.000	-0.00358	0.875	-40.95

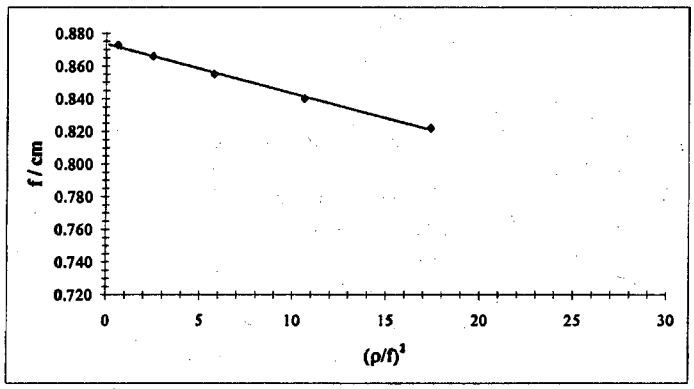

	$slope_g$	g_o/cm	S_g
-2.428E-06	-0.00426	0.846	-48.65

$S_g - S_f = S_h = -7.70$

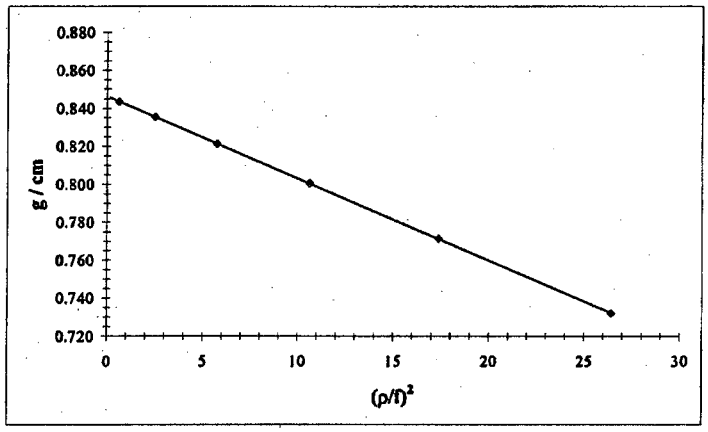

Table 6.2 Sample of data and its graphs to find f_0, g_0, S_f, S_g, and S_h.

Chapter 7. Tabulated and Graphical Results

In this chapter, the full complement of experimental data is used in determining the image properties z' and m, and from there the focal properties f and g of the lens. Both X- and Y-readings of the rear-mesh shadowgraphs are used in finding z' and, if there is sufficient clearance between the lens and the image, readings from the upstream location of the rear mesh as well as the downstream location are included. Both X- and Y-readings of the front mesh shadowgraph are used in finding the image magnification m. Please see Chapter 3 for a review of the shadowgraph nomenclature and method.

For each voltage and current combination applied to the lens the quantities z' and m are plotted versus α'^2, and the best-fit straight lines and their equations are generated. The straight-line character of the graph extends over a range of α', from zero to around 35 millirad (mr) depending on the magnification of the (pin-hole) image. The paraxial image properties z_o' and m_o are obtained from the intercepts of the best-fit lines on the z' or m axes. The spherical aberration coefficients C_s' of the image distance z' and the spherical aberration coefficient μ_s of the magnification are obtained from the slopes of the graphs. The paraxial values, z_0' and m_0, and the spherical aberration coefficients C_s' and μ_s, are listed in Tables and presented in graphs for each lens as functions of the lens activation.

The focal properties, f and g, of the lens are calculated from the image properties z' and m, and the given distance z of the pinhole-object from the lens. The

values of f and g are plotted versus δ^2, where δ is the angle through which the ray is deflected in passing through the lens. See Figures 2.7(a) and (b) in Chapter 2. From geometry $\delta = \alpha + \alpha'$, the sum of the object and image ray angles. To 1st order δ does not depend on magnification $m = \alpha / \alpha'$ for a given height ρ at which the ray goes through the lens. As a result, the spherical aberration coefficients S_f and S_g of f and g avoid the strong dependence on magnification, which occurs, for example, in the image aberration coefficient C_s'. The square of the ratio ρ/f_o (= tan δ) can also be used for plotting graphs of f and g, but the meaning conveyed by δ^2 is more readily recognizable. The paraxial values, f_0 and g_0, are obtained from the intercepts of the best-fit lines generated from graphs of f and g vs δ^2. The spherical aberration coefficients S_f and S_g are obtained from the slopes of the best-fit lines. The paraxial values and spherical aberration coefficients of the lens and image properties are listed in Tables and presented in graphs for each lens, as functions of lens activation. The smooth curves which over-lie the experimental graphs of paraxial properties were generated from analytical equations. These equations were derived in Chapter 9 from theoretical models for the magnetic and electrostatic lenses.

The chromatic aberration coefficients C_c' and μ_c of the image are obtained from changes in the paraxial z_0' and m_0 with lens activation. Likewise, the chromatic aberration coefficients C_f and C_g of f_0 and g_0 are obtained from the changes in f_0 and g_0 with lens activation. The theoretical lens models proved useful in determining the chromatic aberration coefficients and in shaping the graphs versus lens activation, as described in Chapter 9. The chromatic coefficients for the two magnetic lenses and

three static lenses are listed in tables and shown in graphs as function of lens activation. The models of the magnetic and electrostatic lenses are described in Chapter 9.

Five different lenses are included in the present experiments. Lenses L_1 and L_2 are magnetic lenses designed for this study: please refer to Figure 2.1 (a). L_1 has a 0.05 in. (1.27 mm) gap between pole-pieces. L_2 has a 0.10 in. (2.54 mm) gap, but is otherwise identical to L_1. Lenses L_3, L_4, and L_5 are pre-existing electrostatic lenses, designed for different purposes and chosen for comparison with the magnetic lenses. L_3 is a transmission electron microscope (TEM) objective lens with a short working distance (see Figure 2.1 (b)). L_4 is a photoelectron microscope (PEM) objective lens with a relatively long working distance. L_5 is an interface lens for use with an electron mirror and has an intermediate working distance.

A consideration in choosing the electrostatic lenses was to have their geometries overlap the geometries of the magnetic lenses as much as possible, especially as to the lengths of their respective fields. The half-lengths of the electrostatic lenses, from optical center to the outer faces of the lens, are 0.1375 in. (3.50 mm) for L_3 and L_4, and 0.175 in. (4.445 mm) for L_5. The half-lengths for the magnetic lenses are 0.125 in. (3.175 mm) for L_1 and 0.150 in. (3.81 mm) for L_2.

The focusing power of the electrostatic lenses increases as the ratio $\frac{V_A - V_L}{V_A - V_C} = \mathcal{V}_{LC}$ increases. V_L and V_C are the potentials of the center electrode and the electron source (cathode) relative to the potential V_A of the outer electrodes. In the

present case $V_A = zero$, and $\mathcal{V}_{LC}$ can be written V_L/V_C. This ratio is the usual choice for the activation parameter of electrostatic lenses.

The focusing power of the magnetic lenses increases with the square of the magnetic field $\boldsymbol{B}$ in the lens, and decreases with increasing beam voltage V. The field $\boldsymbol{B}$, or the ampere-turns NI creating $\boldsymbol{B}$, and the beam voltage V can be used separately or in combination as activation parameters for the magnetic lenses. For instance, lens properties can be shown as functions of NI in separate graphs for different voltages, or shown as a function of the compound parameter $P = \frac{(NI)^2}{V}$ in a single graph. The square root $\frac{NI}{\sqrt{V}}$ of P is also used as a magnetic activation parameter. Separate graphs of lens properties vs. magnetizing current for different voltages are more readily understood, but graphs vs. $\frac{(NI)^2}{V}$ or $\frac{NI}{\sqrt{V}}$ are more compact.

The pinhole-source of electrons for the experiments is the object for the lenses. The object distance z is large and the paraxial image of the pinhole is strongly demagnified. This arrangement has several advantages. The imaging rays are spread into larger angles making the shadow patterns cast by the analyzing meshes easier to measure accurately. At the same time, the paraxial image of the pinhole is greatly reduced, resulting in sharper mesh shadows. In addition, the aberrations of the image in this set-up are automatically referred to the low-magnification side of the lens.

In assembling our results of this research we discovered that some of the measurements were made with object distance $z = 30$ cm rather than 25 cm as planned. This difference affected the image properties, especially the magnification. The image distance and aberrations were not strongly affected because the image is highly demagnified, [for example, the change in image distance $(z_2' - z_1') = - m_1 m_2 (z_2 - z_1)$], but the results still required correction. Since the lens properties f_0 and g_0 and their aberration coefficients were not affected, it was possible to recalculate the image properties corresponding to z = 25 cm where needed. The properties of the lenses and images, including the modifications, are presented in Tables and graphs in the main text. The unmodified image properties are listed in Tables in the Appendix A.

Experimental Results for Magnetic Lenses L_1 and L_2

Image and Lens Properties of L_1

Lens L_1 was studied as a function of magnetizing current I for three accelerating voltages $V = 15\ kV$, $20\ kV$, and $25\ kV$. The procedures described in Chapter 3 were used to determine the properties of the image and the lens. The rear-mesh shadowgraph readings were used to find z' and α', and graphs of z' vs α'^2 provided the paraxial value z_o' and the spherical aberration coefficient C_s'. Front mesh readings combined with results from the rear-mesh readings enabled the values of m (the pinhole image magnification) and the corresponding values of α' to be found. The values of z' vs. α'^2 and m vs. α'^2 are listed for each accelerating voltage and magnetizing current in Tables of Appendix A with accompanying graphs of z' and m vs. α'^2. The paraxial properties z_0' and m_0 and the spherical aberration coefficients C_s'

and μ_s are listed in Tables 7.1 (a), 7.1 (b), and 7.1 (c) as functions of current I for the three accelerating voltages. The four image properties z_0', m_0, C_S', and μ_S are shown separately for the three voltages in graphs vs. I in Figures 7.1 (a), 7.1 (b), 7.1 (c), and 7.1 (d), respectively.

Magnetic Lens L_1					
Table 7.1a		**15000**	**Volts**		
Current	**Activation**				
milliamps	**$(NI)^2/V$**	**z_0'/cm**	**$m_0 \times 10^2$**	**C_s/cm**	**μs**
350	85.5	0.098	0.466	0.261	-1.22
250	43.6	0.177	0.752	0.624	-2.93
200	27.9	0.261	1.08	1.620	-5.53
180	22.6	0.304	1.32	2.660	-7.01
150	15.7	0.404	1.75	5.39	-11.4
130	11.8	0.543	2.36	11.9	-18.1
100	6.98	0.878	3.57	48.6	-46.4
Table 7.1b		**20000**	**Volts**		
Current	**Activation**				
milliamps	**$(NI)^2/V$**	**z_0'/cm**	**$m_0 \times 10^2$**	**C_s/cm**	**μs**
400	83.7	0.094	0.462	0.213	-1.08
350	64.1	0.123	0.531	0.265	-1.44
250	32.7	0.224	0.907	1.10	-3.78
200	20.9	0.330	1.39	3.14	-8.93
180	17.0	0.410	1.69	5.29	-11.9
150	11.8	0.578	2.35	16.0	-26.3
130	8.84	0.747	3.29	33.8	-39.9
Table 7.1c		**25000**	**Volts**		
Current	**Activation**				
milliamps	**$(NI)^2/V$**	**z_0'/cm**	**$m_0 \times 10^2$**	**C_s/cm**	**μs**
400	67.0	0.121	0.544	0.260	-1.68
350	51.3	0.150	0.659	0.353	-1.81
250	26.2	0.271	1.14	1.48	-5.06
200	16.7	0.395	1.70	5.30	-11.9
180	13.6	0.467	2.03	8.07	-14.8
150	9.42	0.666	2.70	21.9	-28.7
130	7.07	0.855	3.56	49.0	-52.5
100	4.19	1.389	5.91	182	-117

Table 7.1(a), (b), and (c). Paraxial images properties z_0' and m_0 with their spherical aberrations coefficients Cs' and μ_s at 3 accelerating voltages, 15 kV, 20 kV, and 25 kV for the magnetic lens L_1 and the lens activation $(NI)^2/V$.

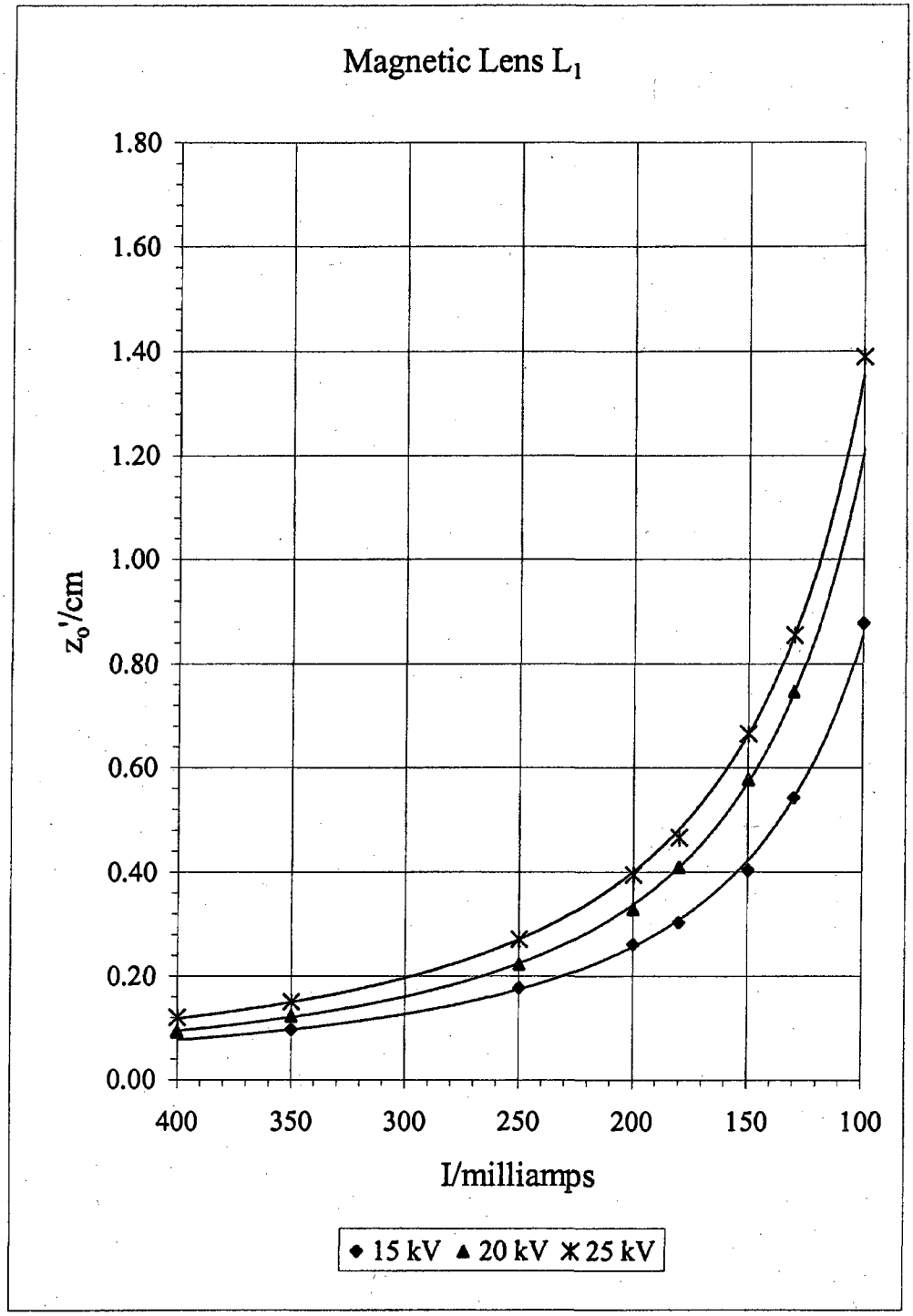

Figure 7.1(a). Graphs of the paraxial image distance z_0' data points vs. Current (I), at three accelerating voltages, 15 kV, 20 kV, and 25 kV for the magnetic lens L_1 with best fit power series curves.

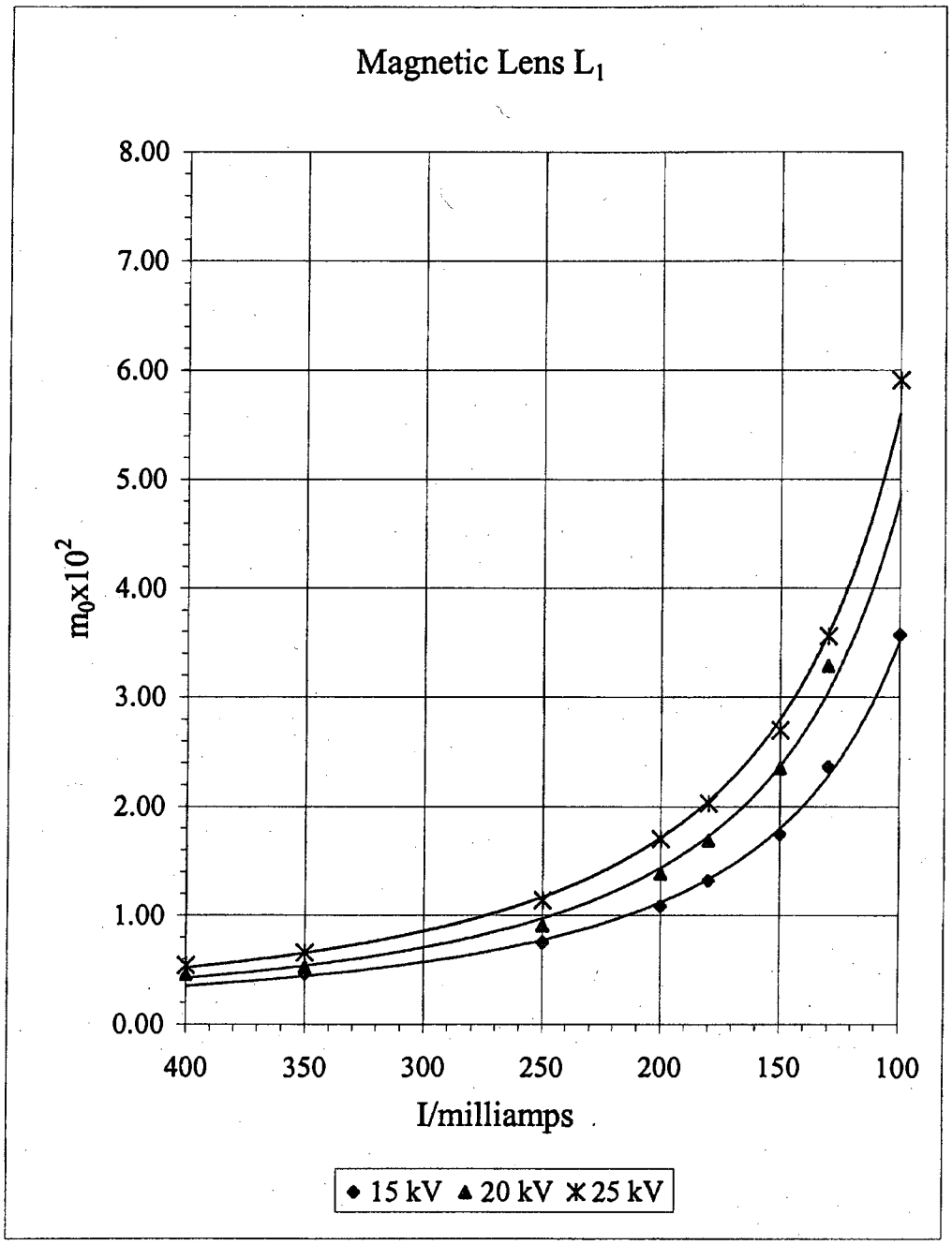

Figure 7.1(b). Plot of paraxial magnification m_0 versus activation current I at the three accelerating voltages 15 kV, 20 kV, and 25 kV for the magnetic lens L_1 with best fit power series curves.

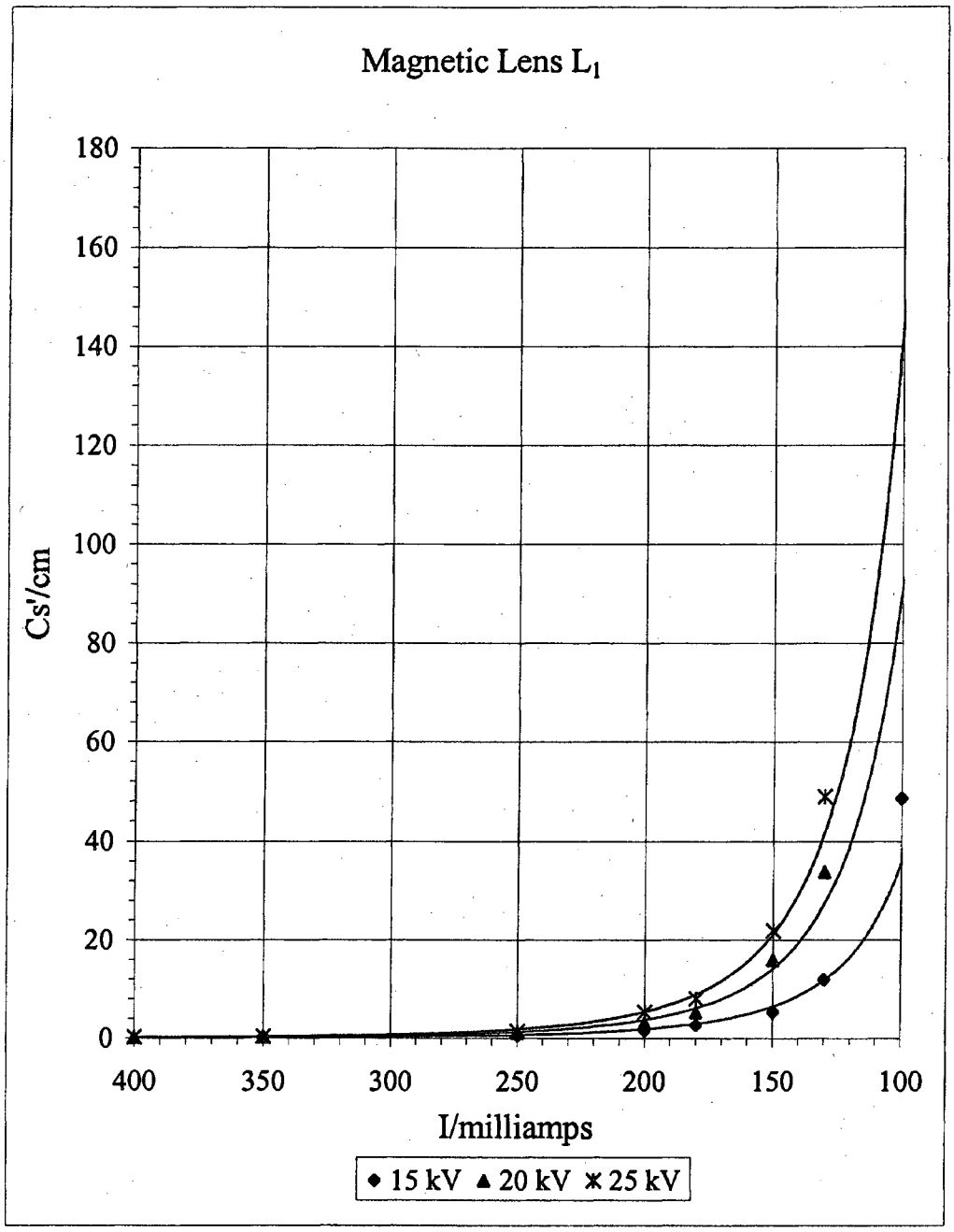

Figure 7.1(c). Plot of spherical aberration Cs' versus activation current I at the three accelerating voltages 15 kV, 20 kV, and 25 kV for the magnetic lens L_1 with best fit power series curves.

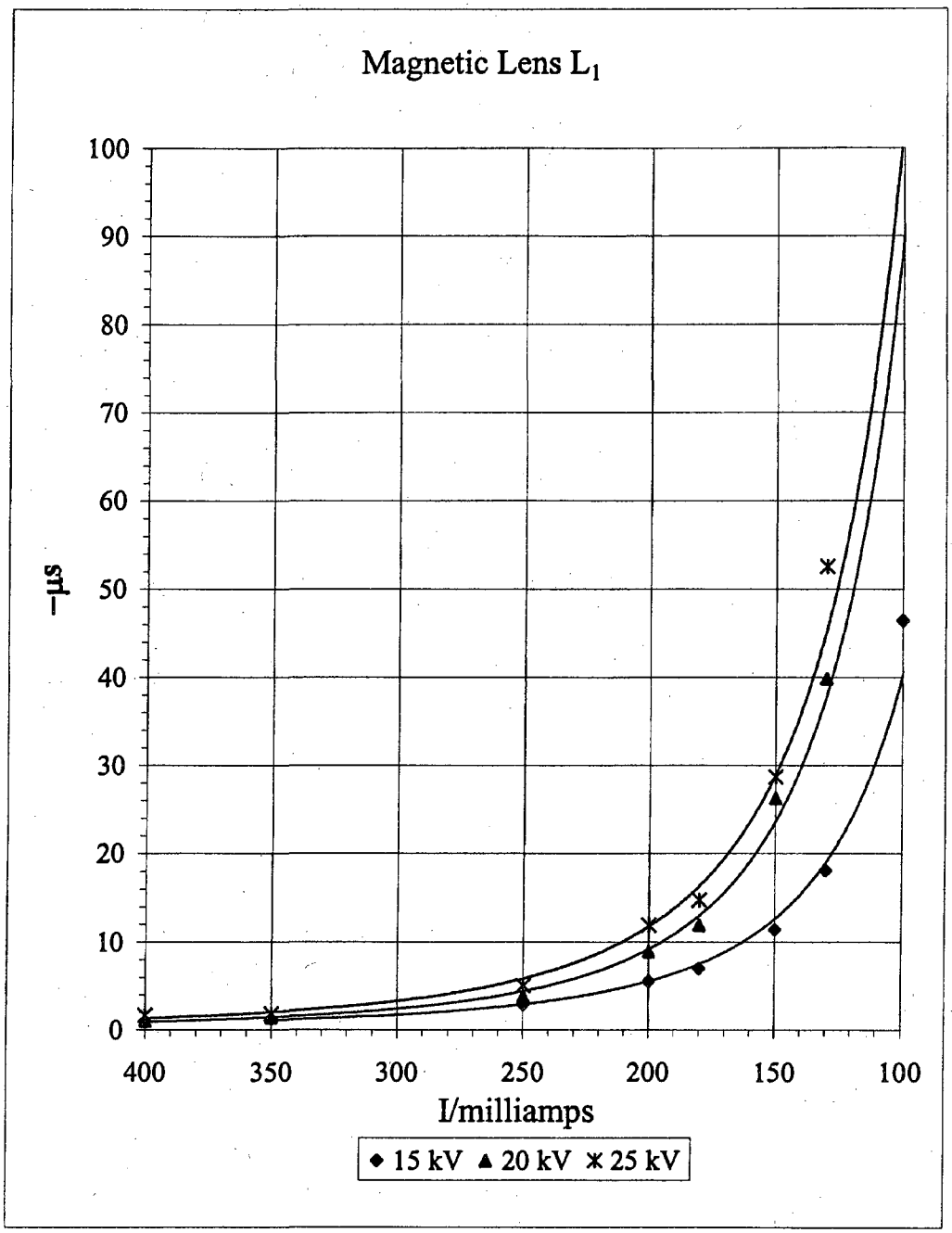

Figure 7.1(d). Plot of the spherical aberration coefficient of magnification μ_s' versus activation current I at the three accelerating voltages 15 kV, 20 kV, and 25 kV for the magnetic lens L_1 with best fit power series curves.

The lens properties f and g of L_1, were calculated by means of Equation (3.17) from the image properties z' and m and the known object distance $z = 25$ cm. These lens properties are listed as functions of δ^2 (where $\delta = \alpha + \alpha'$) for the three voltages in Tables of the Front data sheets for each corresponding current activation of the lenses, in Appendix A. Accompanying graphs of f and g vs δ^2 illustrate the determination of the paraxial values f_0 and g_o, and the spherical aberration coefficients S_f and S_g, of the lens. The four lens properties f_0, g_0, S_f, and S_g of lens L_1 are listed together as functions of current I in Tables 7.2 (a), 7.2 (b), and 7.2 (c) for the three voltages $15kV$, $20kV$, and $25kV$. The four L_1 lens properties are plotted separately vs magnetizing current I for the three accelerating voltages, as shown in Figures 7.2 (a), 7.2 (b), 7.2 (c), and 7.2 (d).

Magnetic Lens L_1						
			Lens Properties			
(a)			15000	Volts		
	Current					
	milliamps	$(NI)^2/V$	f_o/cm	g_o/cm	S_f	S_g
	350	85.5	0.116	0.097	-1.20	-2.22
	250	43.6	0.187	0.176	-2.86	-3.25
	200	27.9	0.268	0.258	-5.35	-5.79
	180	22.6	0.326	0.299	-6.72	-7.77
	150	15.7	0.430	0.396	-10.79	-11.73
	130	11.8	0.578	0.529	-16.85	-18.90
	100	6.98	0.863	0.847	-41.52	-49.44
(b)			20000	Volts		
	Current					
	milliamps	$(NI)^2/V$	f_o/cm	g_o/cm	S_f	S_g
	400	83.7	0.115	0.094	-1.06	-1.83
	350	64.1	0.132	0.123	-1.41	-1.97
	250	32.7	0.225	0.222	-3.67	-4.73
	200	20.9	0.342	0.325	-8.57	-8.70
	180	17.0	0.416	0.403	-11.35	-11.92
	150	11.8	0.575	0.564	-24.50	-25.37
	130	8.8	0.799	0.721	-36.18	-37.26
(c)			25000	Volts		
	Current					
	milliamps	$(NI)^2/V$	f_o/cm	g_o/cm	S_f	S_g
	400	66.98	0.135	0.120	-1.65	-1.88
	350	51.28	0.164	0.149	-1.77	-2.10
	250	26.16	0.282	0.268	-4.89	-5.03
	200	16.74	0.418	0.388	-11.33	-11.86
	180	13.56	0.498	0.457	-13.87	-15.02
	150	9.42	0.657	0.648	-26.39	-30.21
	130	7.07	0.861	0.824	-47.23	-49.64
	100	4.19	1.400	1.306	-98.28	-103.77

Table 7.2 (a), (b), and (c). Paraxial focal properties f_0 and g_0 with their spherical aberration coefficients S_f and S_g for magnetic lens L_1 at different electron beam accelerations and lens activation $(NI)^2/V$.

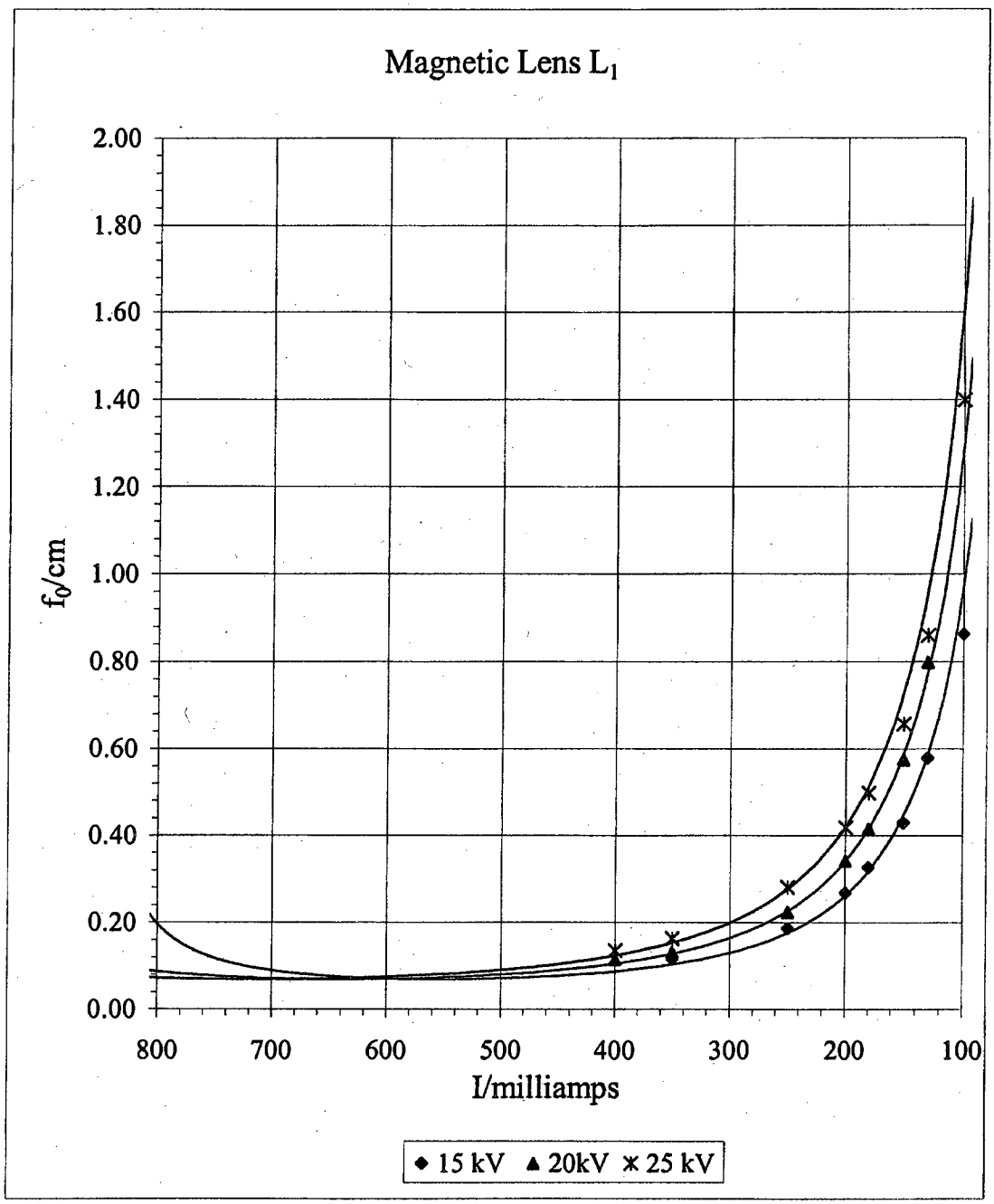

Figure 7.2(a). Plot of the paraxial focal length f_0 versus activation current I at the three accelerating voltages 15 kV, 20 kV, and 25 kV for magnetic lens L_1 with their close fitting respective model curves.

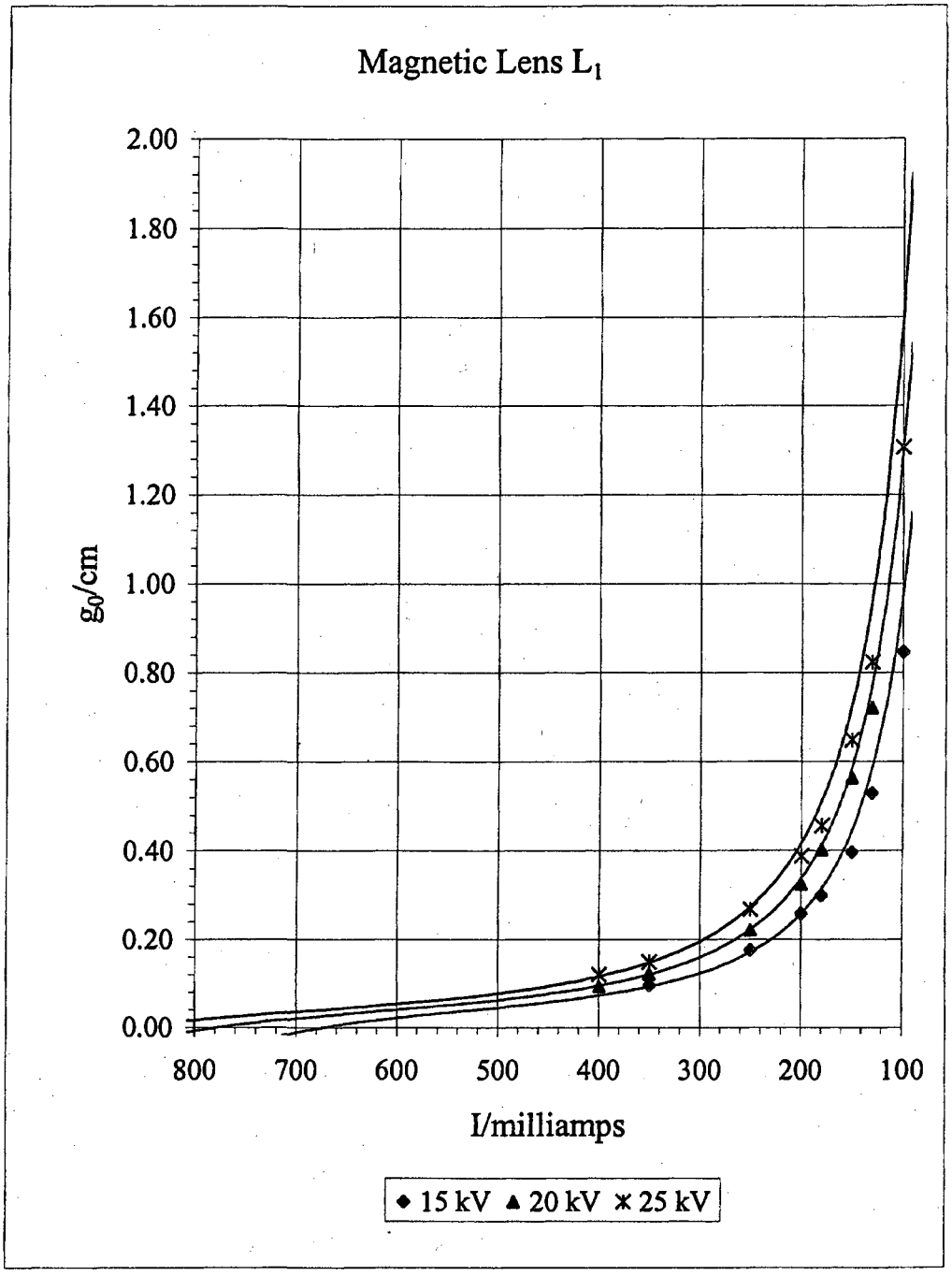

Figure 7.2(b). Plot of the paraxial focal distance g_0 versus activation current I at the three accelerating voltages 15 kV, 20 kV, and 25 kV for magnetic lens L_1 with their close fitting respective model curves.

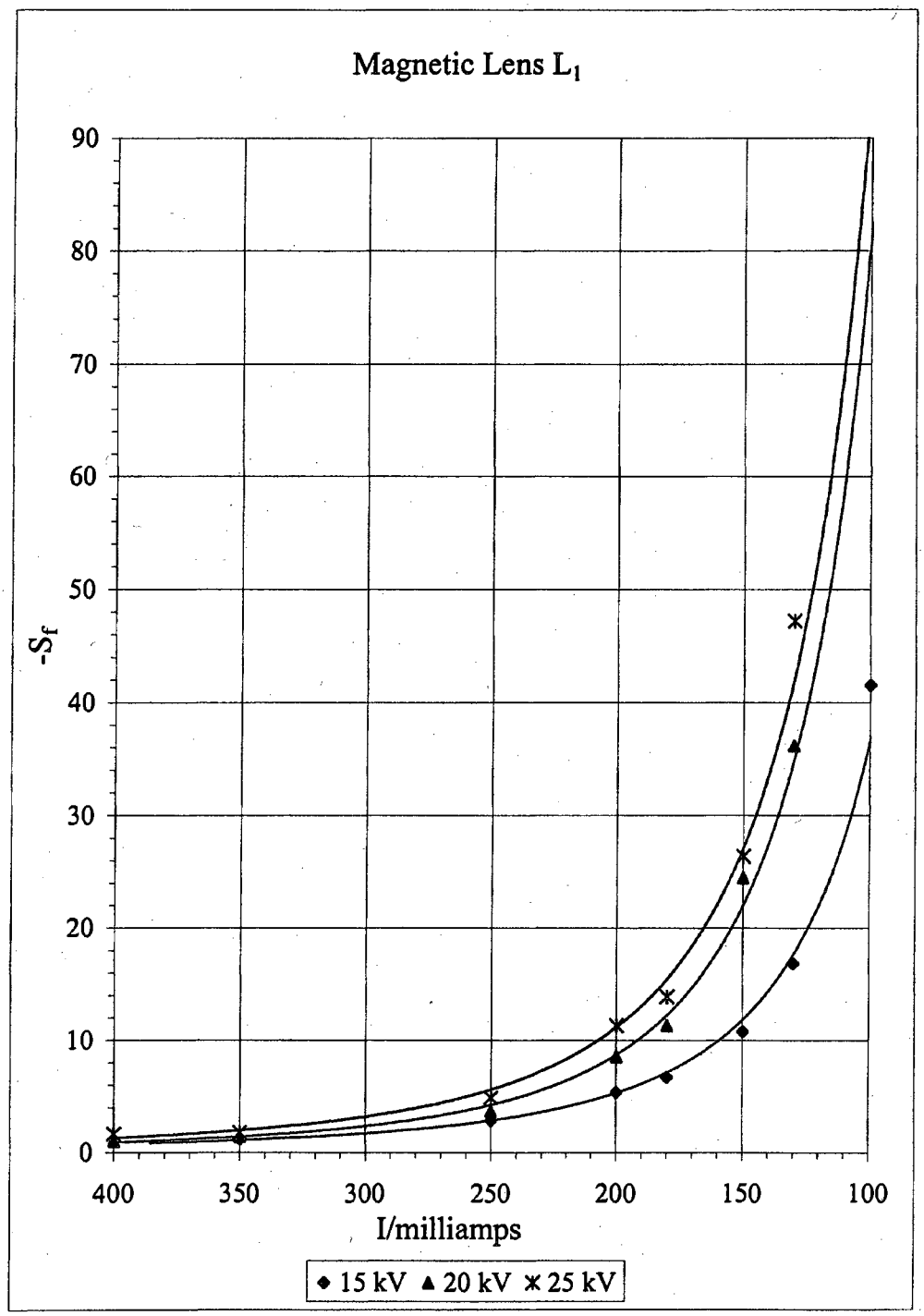

Figure 7.2(c). Plot of the spherical aberration coefficient Sf of focal length *f* versus the activation current *I* at the three accelerating voltages 15 kV, 20 kV, and 25 kV for magnetic lens L_1 with their respective close power series fitting curves .

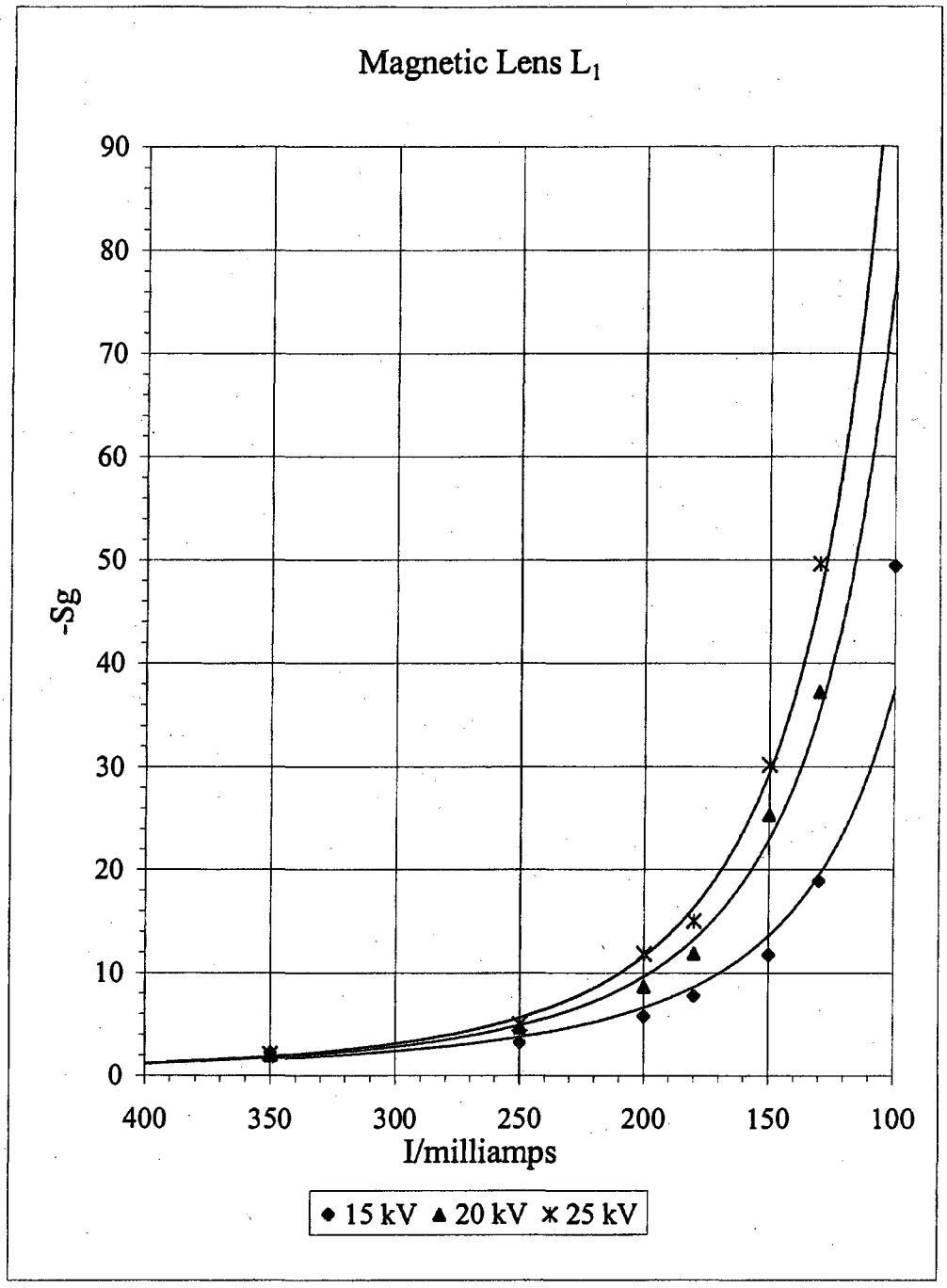

Figure 7.2(d). Plot of the spherical aberration coefficient characteristic Sg of the lenses versus the activation current I at the three accelerating voltages 15 kV, 20 kV, and 25 kV for the magnetic lens L_1 with the 15 kV, 20kV and 25 kV fitted with power series curves.

Image and Lens Properties of L_2

Lens L_2 was studied as a function of magnetizing current I for an accelerating voltage of 20 kV. The measurements of z' and m are listed in tables of Appendix A and plotted in graphs as functions of α'^2. The L_2 paraxial image properties z_o' and m_o and the image aberration coefficients C_s' and μ_s obtained from the z' and m graphs are listed in Table 7.3 as functions of magnetizing current for $V = 20$ kV. They are shown separately as graphs vs. current in Figures 7.3 (a), (b), (c), and (d), respectively for the single accelerating voltage.

Current milliamps	Activation $(NI)^2/V$	z_0'/cm	m_0 x10^2	C_s/cm	μ_s
350	64.1	0.166	0.859	0.37	-1.12
300	47.1	0.229	1.083	0.70	-1.80
250	32.7	0.300	1.455	1.32	-3.09
200	20.9	0.480	2.158	4.27	-7.03
180	17.0	0.562	2.558	6.71	-10.24
150	11.8	0.868	3.613	23.26	-22.36
130	8.84	1.164	4.678	53.22	-41.94
100	5.23	1.789	7.231	179.466	-92.21

Table 7.3. Paraxial properties z_0' and m_o with their spherical aberration coefficients Cs' and $\mu s'$ for the magnetic lens L_2 at the electron beam acceleration of 20 kV and lens activation $(NI)^2/V$.

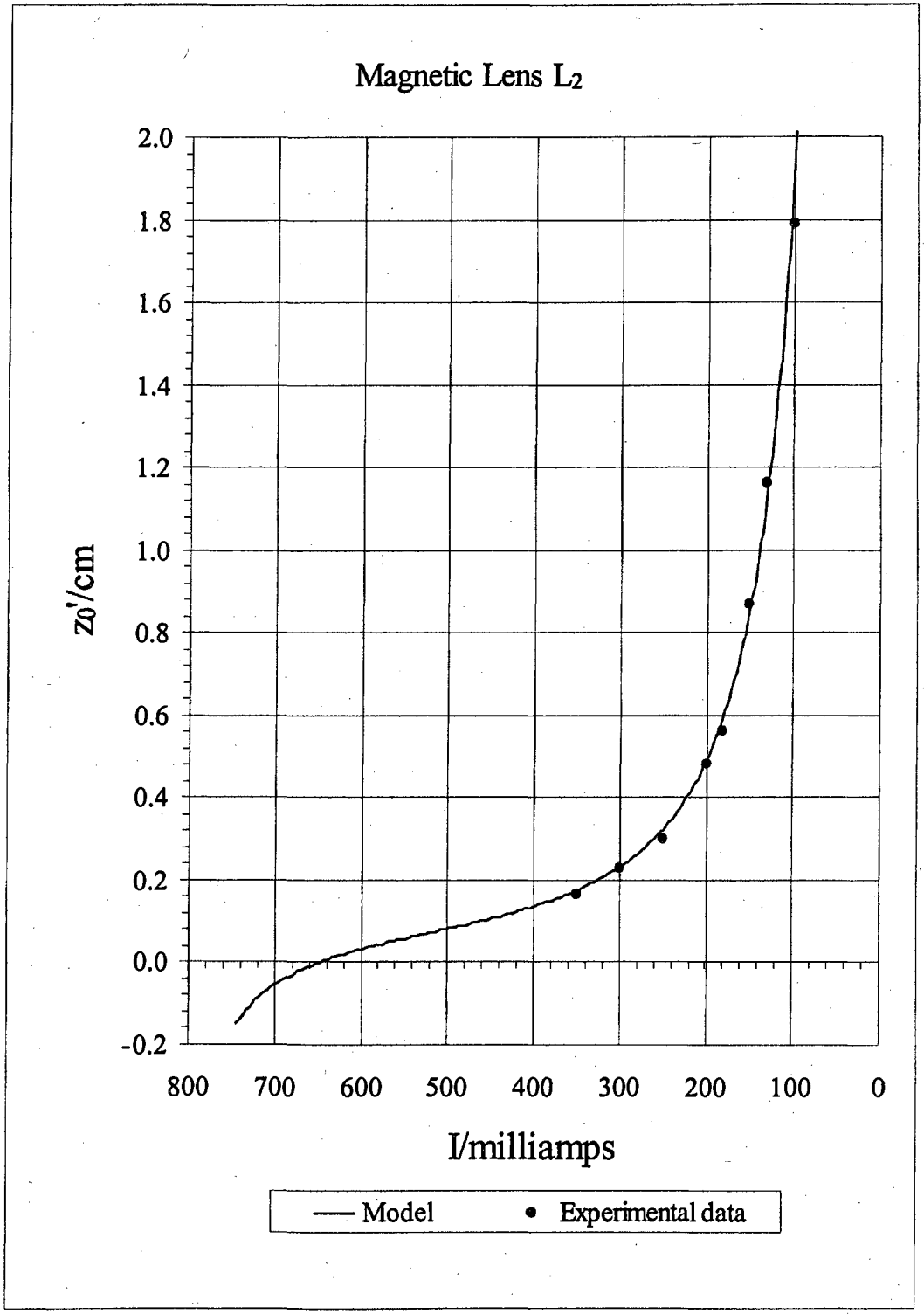

Figure 7.3(a). Paraxial image distance z_0' versus Current (I), for the magnetic lens L_2 at acceleration voltage 20kV and its model curve.

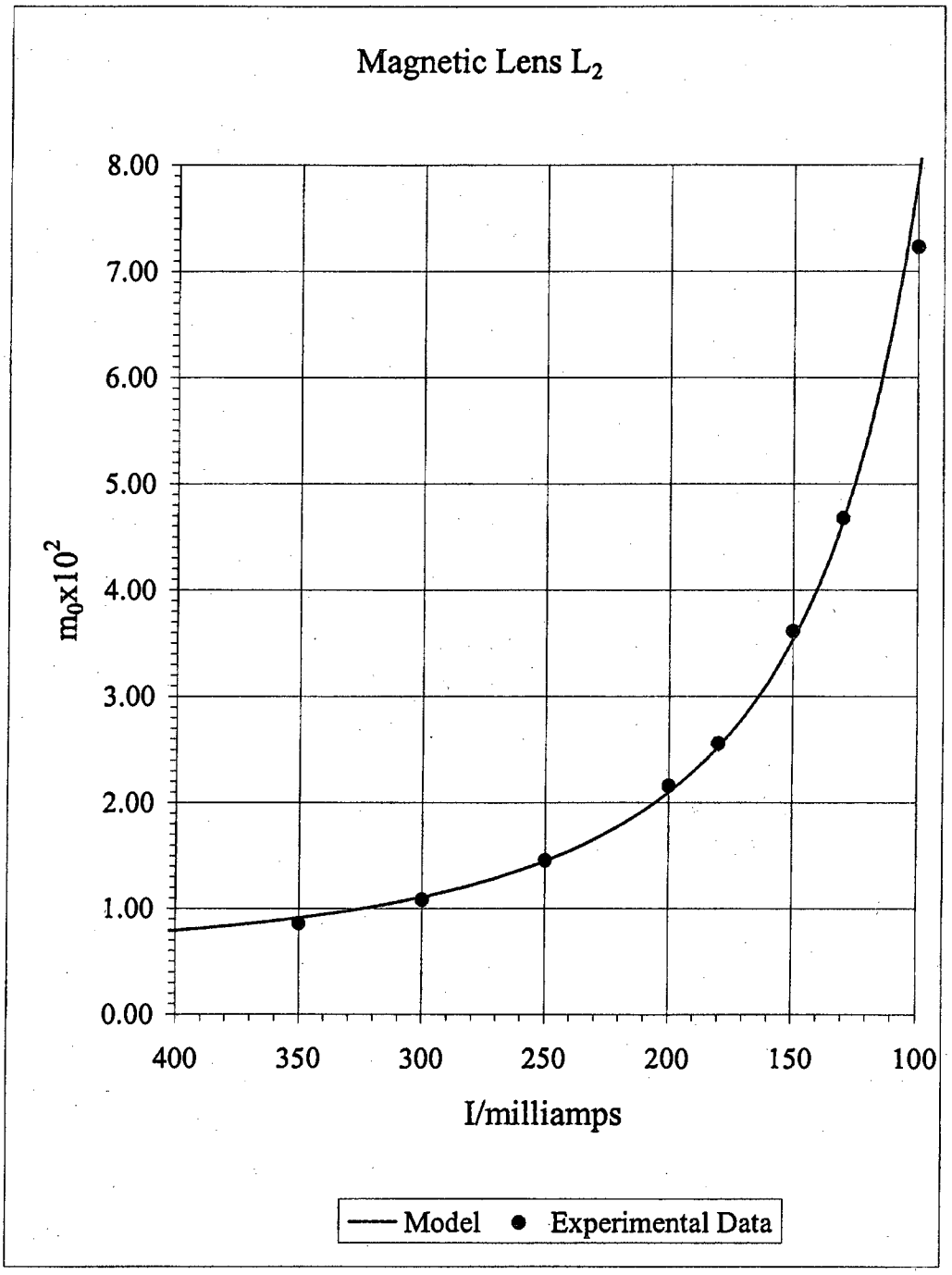

Figure 7.3(b). Paraxial magnification m_0 versus activation current I for the magnetic lens L_2 at acceleration voltage 20kVwith its model curve.

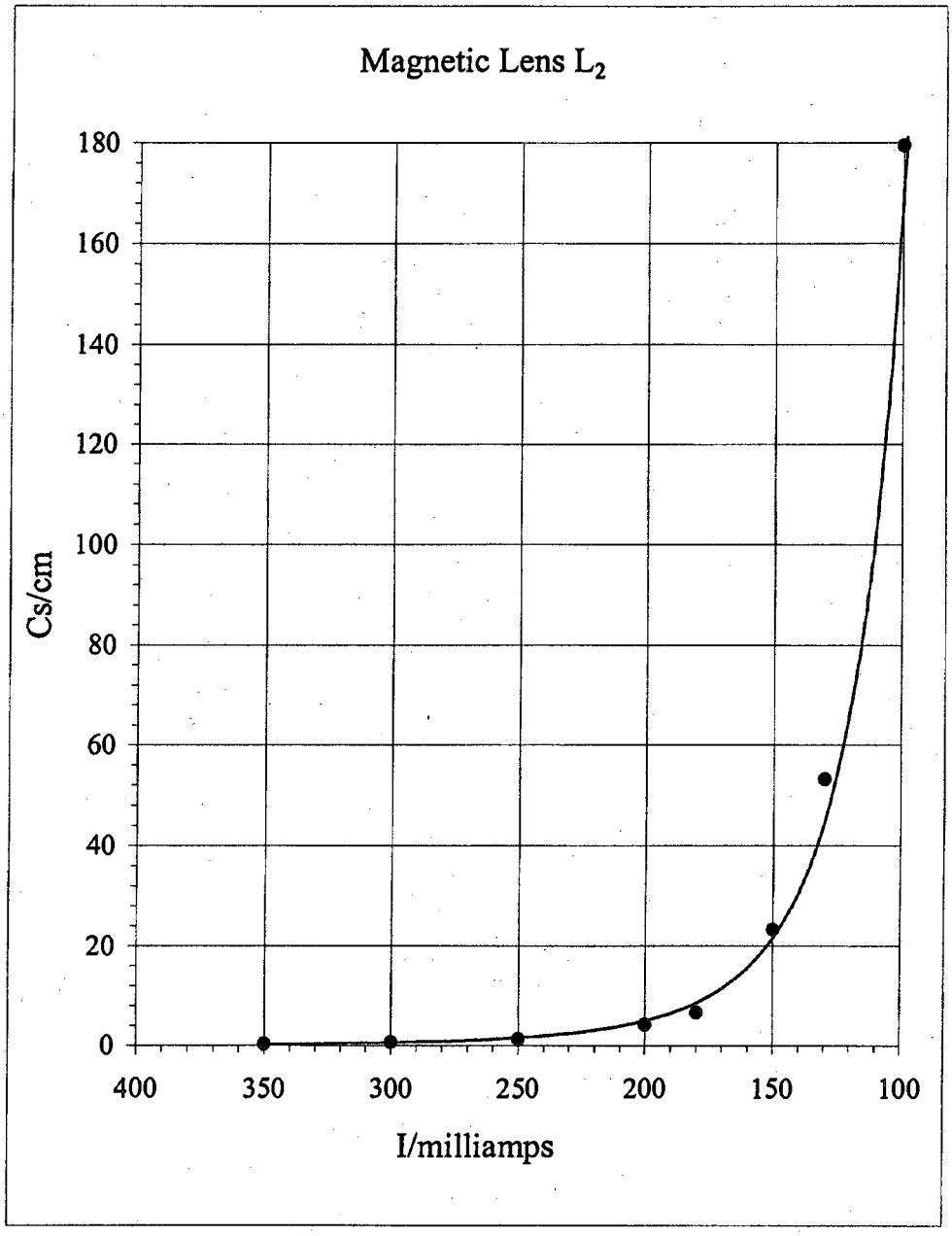

Figure 7.3(c). Spherical aberration C_s' versus activation current I for the magnetic lens L_2 at acceleration voltage 20kVwith a power series fitting curve.

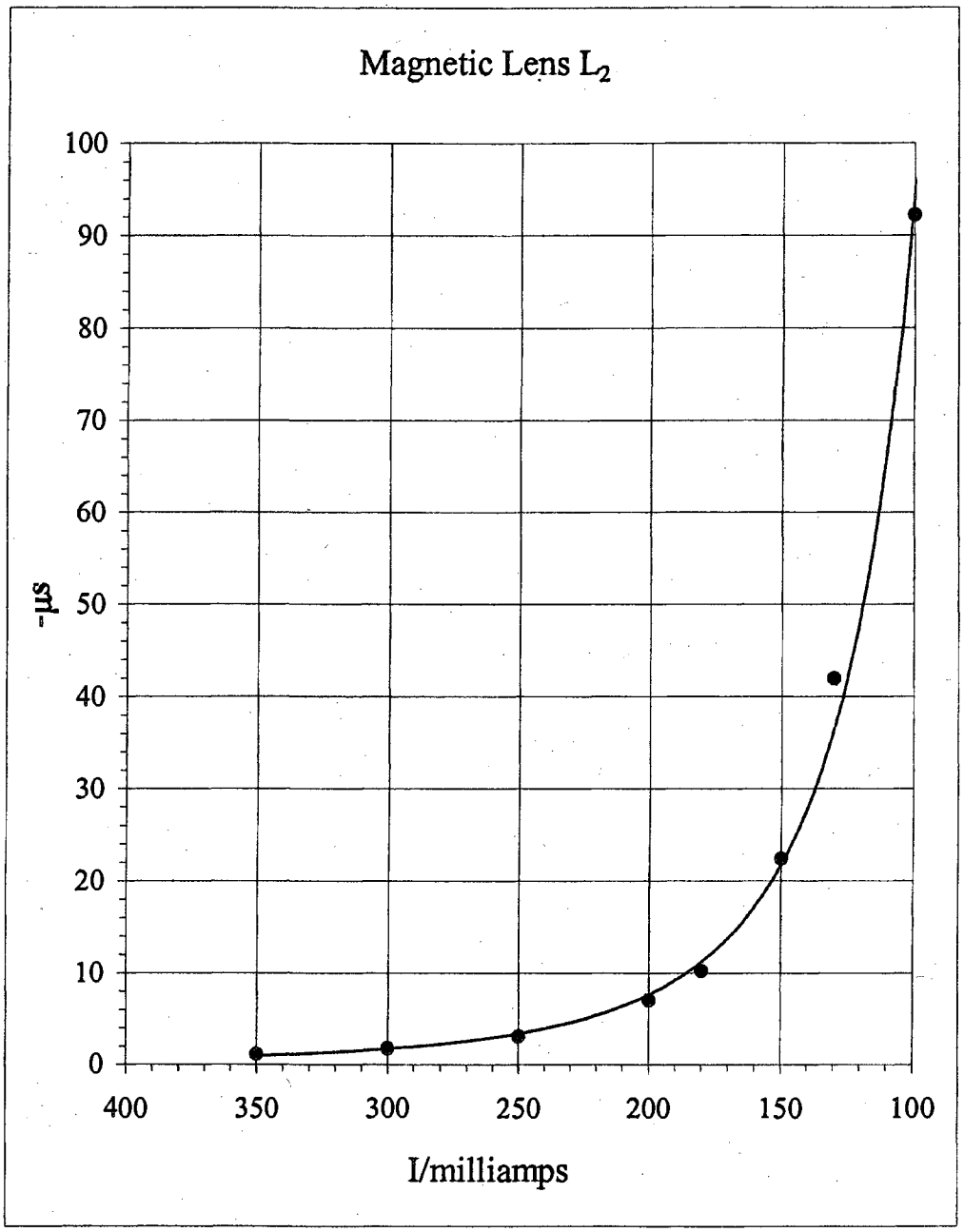

Figure 7.3(d). Spherical aberration coefficient of magnification $\mu s'$ versus activation current I for the magnetic lens L_2 at acceleration voltage 20 kV with a power series fitting curve.

The lens properties f and g of L_2, calculated from z, z', and m, are listed as functions of $(\delta)^2$ in the Front sheets of L_2 data in Tables in Appendix A. Graphs of f and g vs δ^2 illustrate how the paraxial lens properties f_o and g_o and the spherical aberration coefficients S_f and S_g are determined. The four focal properties f_o, g_o, S_f, and S_g of L_2 are listed as functions of magnetizing current I in Table 7.4 for $V = 20\ kV$. The four lens properties are shown separately in graphs vs. magnetizing current in Figures 7.4 (a), 7.4(b), 7.4 (c), and 7.4 (d) for 20 kV.

Current milliamps	Activation $(NI)^2/V$	f_o/cm	g_o/cm	S_f	S_g
350	64.1	0.2133	0.164	-1.08	-1.70
300	47.1	0.2684	0.226	-1.73	-2.51
250	32.7	0.3594	0.295	-2.96	-3.48
200	20.9	0.5294	0.469	-6.58	-7.45
180	17.0	0.6254	0.546	-9.49	-9.70
150	11.8	0.8731	0.837	-19.98	-23.34
130	8.84	1.1175	1.112	-36.41	-39.97
100	5.23	1.6872	1.667	-74.31	-81.34

Table 7.4. Paraxial focal properties f_o and g_o with their spherical aberration coefficients Sf and Sg for the magnetic lens L_2 at 20 kV for the electron beam acceleration and their corresponding lens activation (NI)2/V.

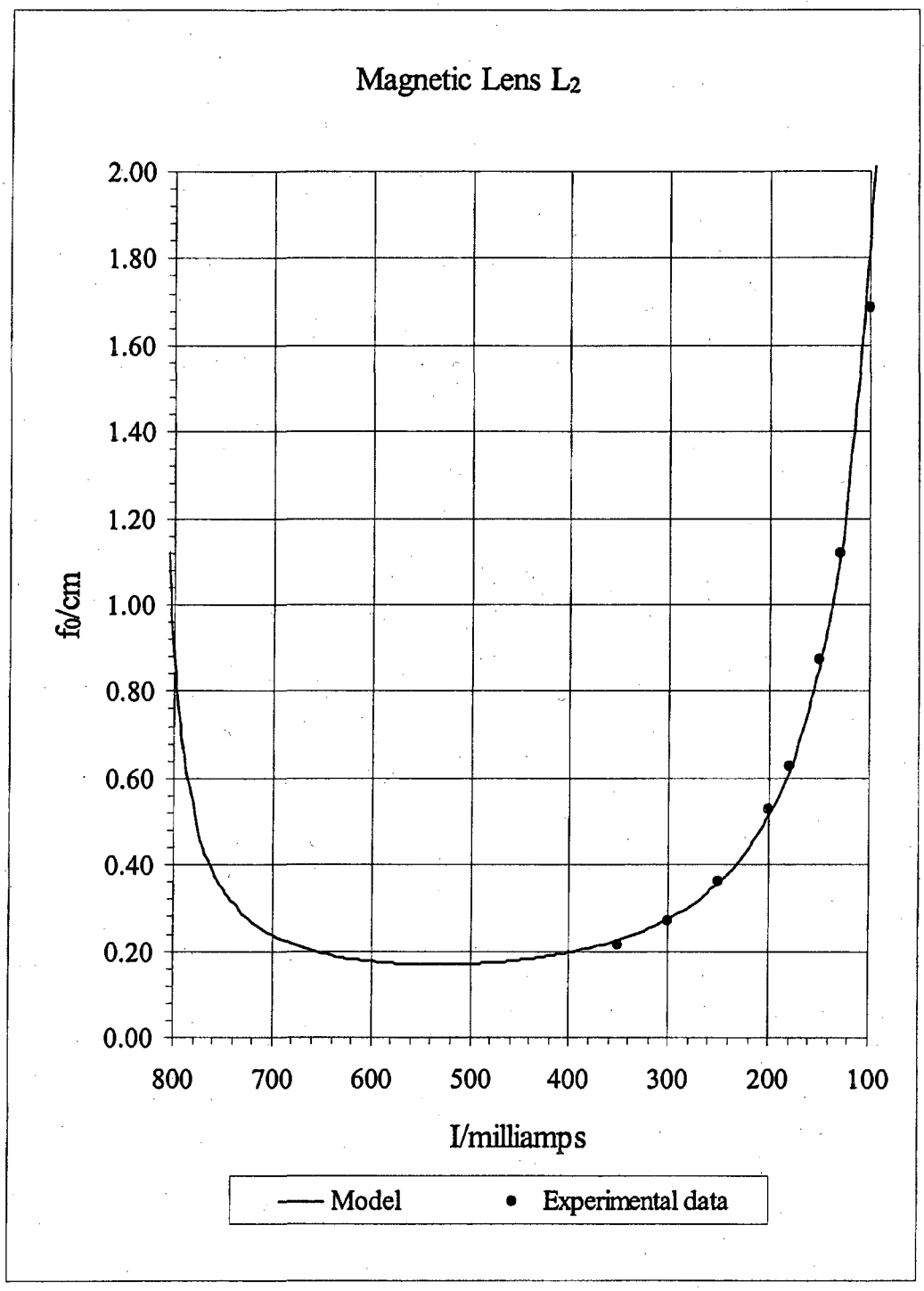

Figure 7.4(a). Paraxial focal length f_0 versus activation current I for the magnetic lens L_2 at acceleration voltage 20kV with its model curve.

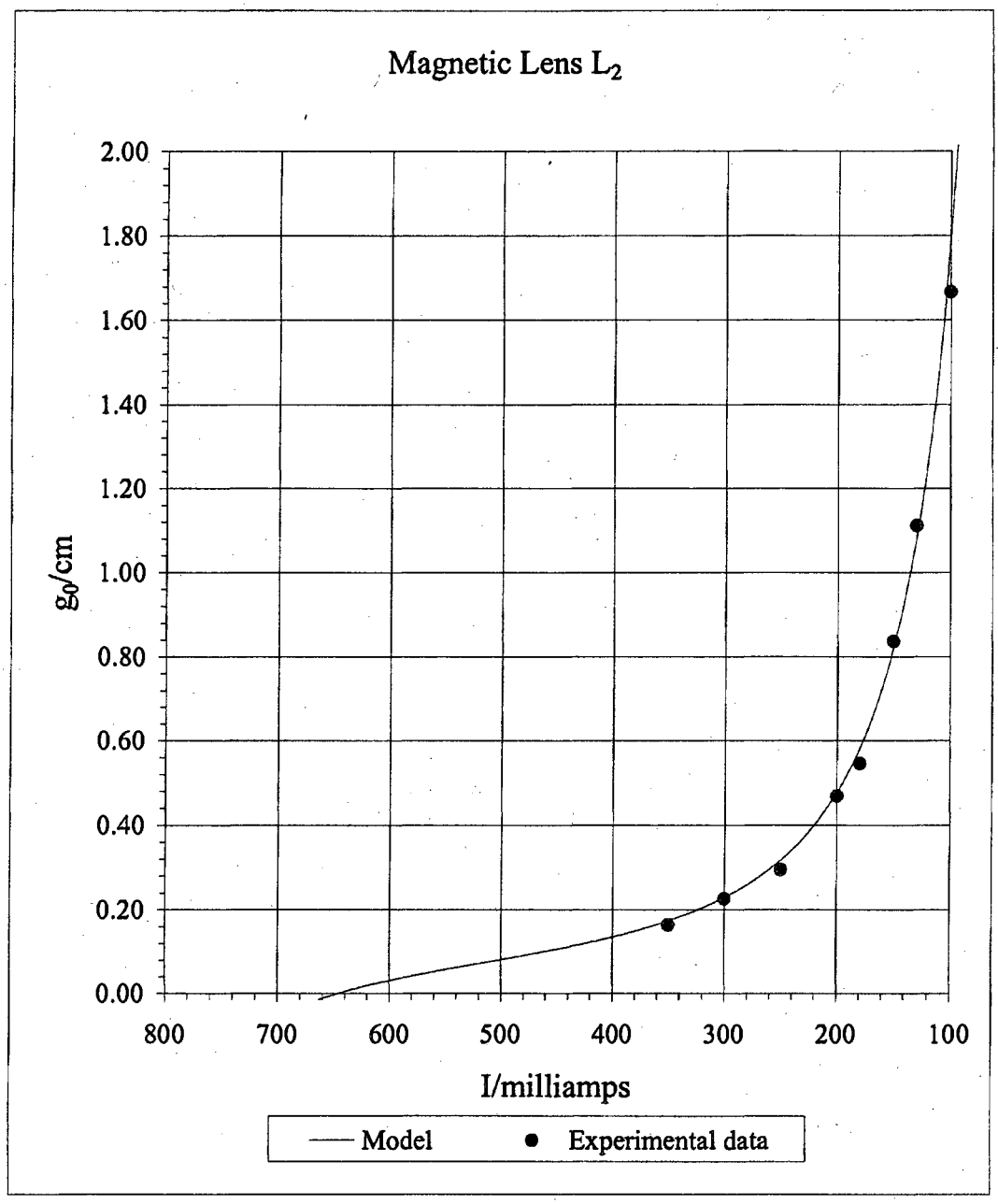

Figure 7.4(b). Paraxial focal distance g_0 versus activation current I for the magnetic lens L_2 at acceleration voltage 20 kV.

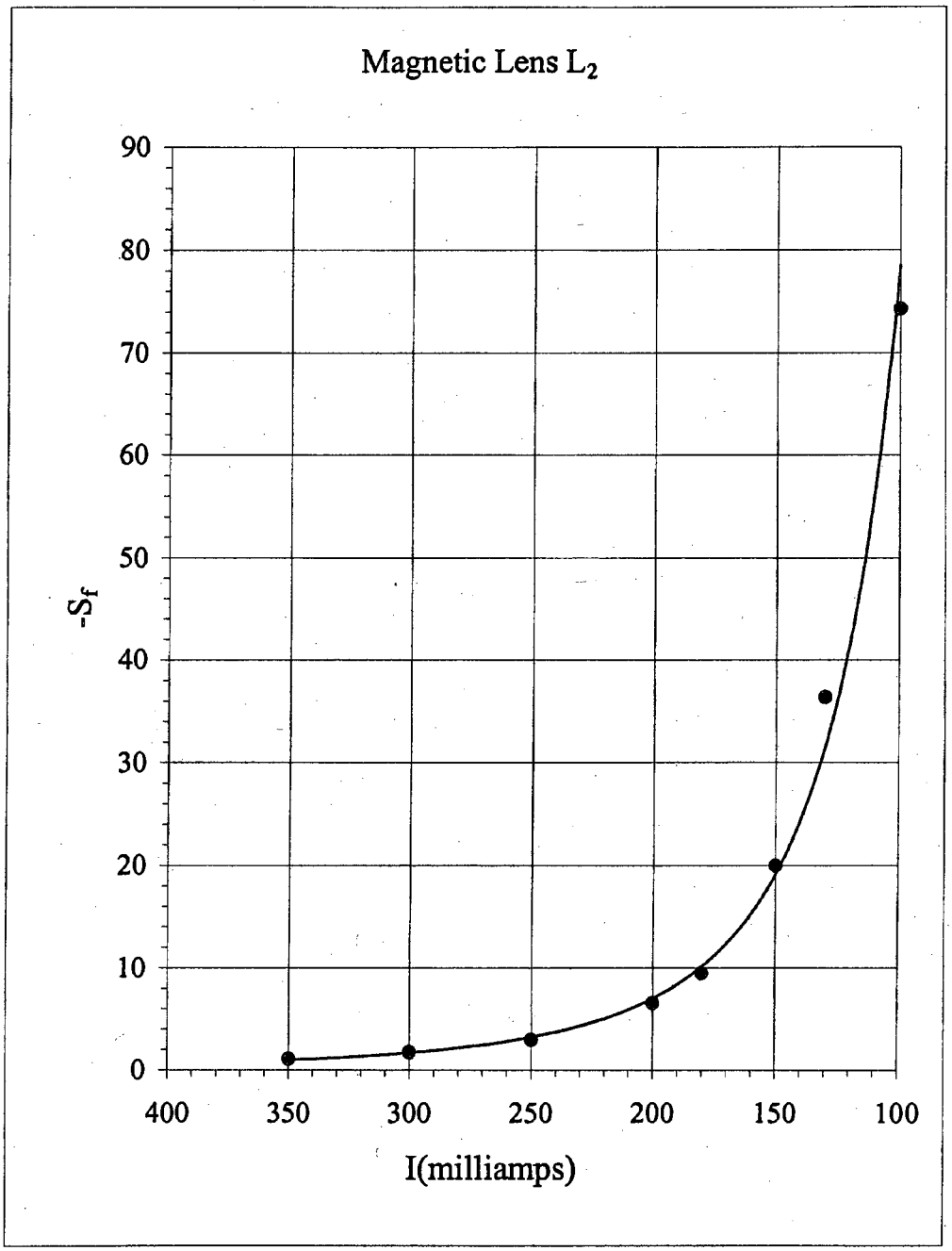

Figure 7.4(c). Spherical aberration coefficient S_f of the focal length f versus the activation current I for the magnetic lens L_2 at acceleration voltage 20 kV with its power series best-fit curve.

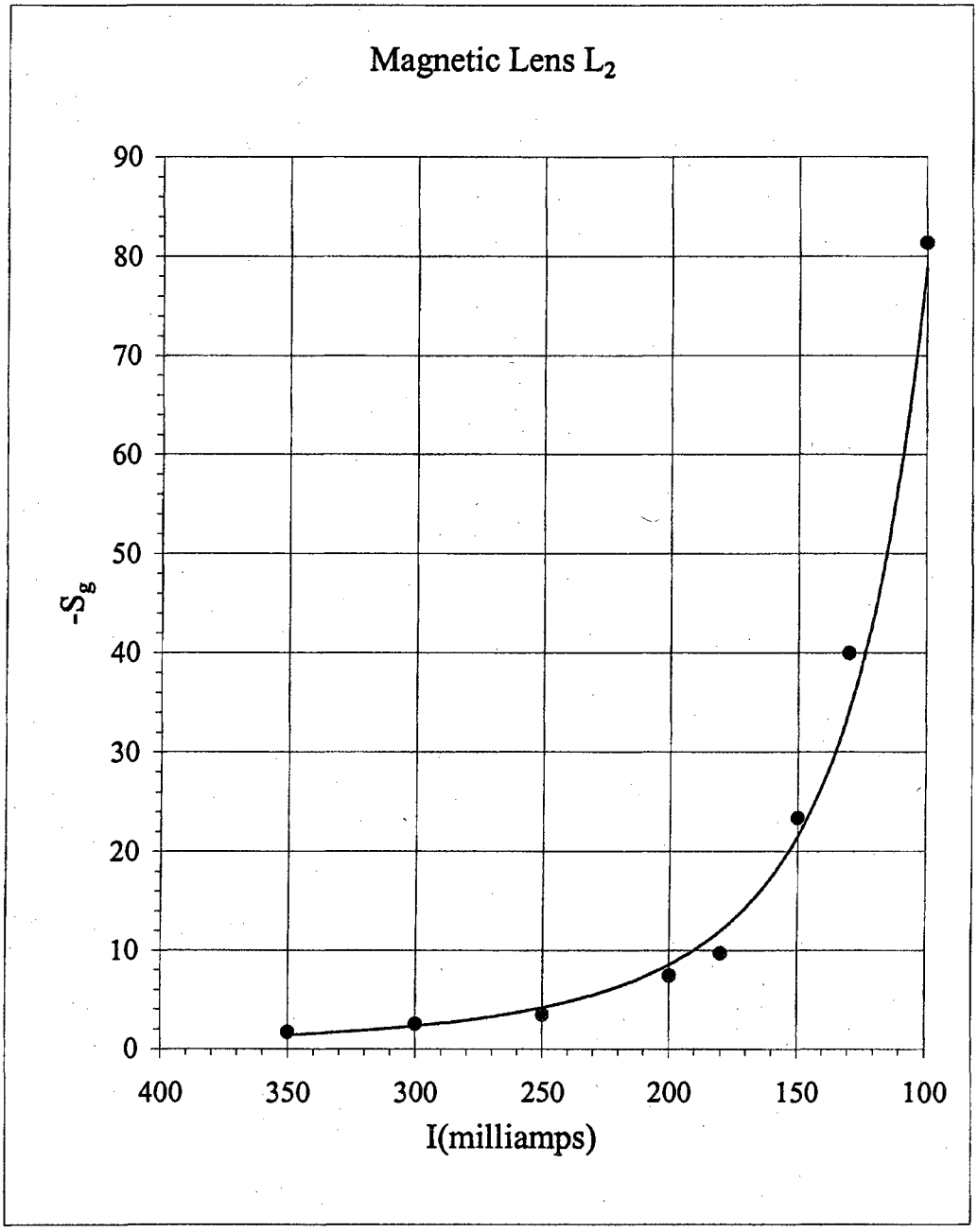

Figure 7.4(d). Spherical aberration coefficient S_g of focal distance g versus the activation current I for magnetic lens L_2 with its power series best-fit curve.

Image and Lens Properties of L_1 and L_2 vs. $(NI)^2/V$

Lens L_1

The paraxial image properties z_0' and m_0 and aberration coefficient C_s', and μ_s, listed in the L_1 image Tables 7.1(a), (b), and (c) were shown separately in Figures 7.1(a), (b), (c) and (d) as functions of magnetizing current for three voltages 15 kV, 20 kV, and 25 kV. The same information is shown in a more compact form in Figures 7.5 (a), 7.5 (b), 7.5 (c), and 7.5 (d) where the properties have been plotted versus the compound activation parameter $\frac{(NI)^2}{V}$. For example, the three curves showing z_0' vs. I, for three different voltages in Figure 7.1(a), reduce to the single curve in Figure 7.5(a). The red, green, and blue data points correspond to accelerating voltages of 15, 20, and 25 kV. The results for the other three image properties m_0, C_s', and μ_s can also be represented compactly by plotting versus $\frac{(NI)^2}{V}$, as shown in Figures 7.5 (b), 7.5 (c), and 7.5 (d).

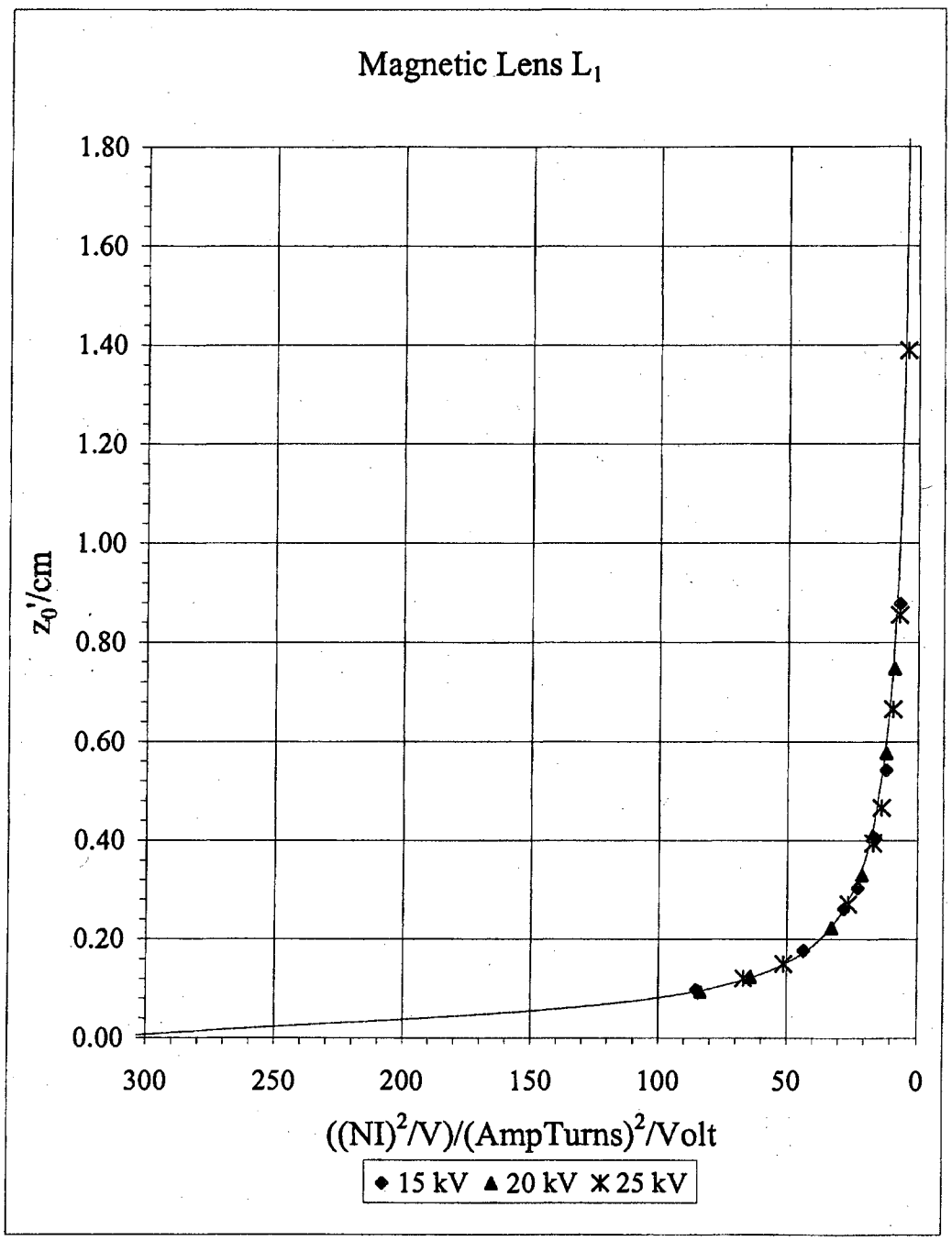

Figure 7.5(a). z_0' vs. $(NI)^2/V$ for all three accelerating voltages for lens L_1 showing the very close fit with their corresponding model curves .

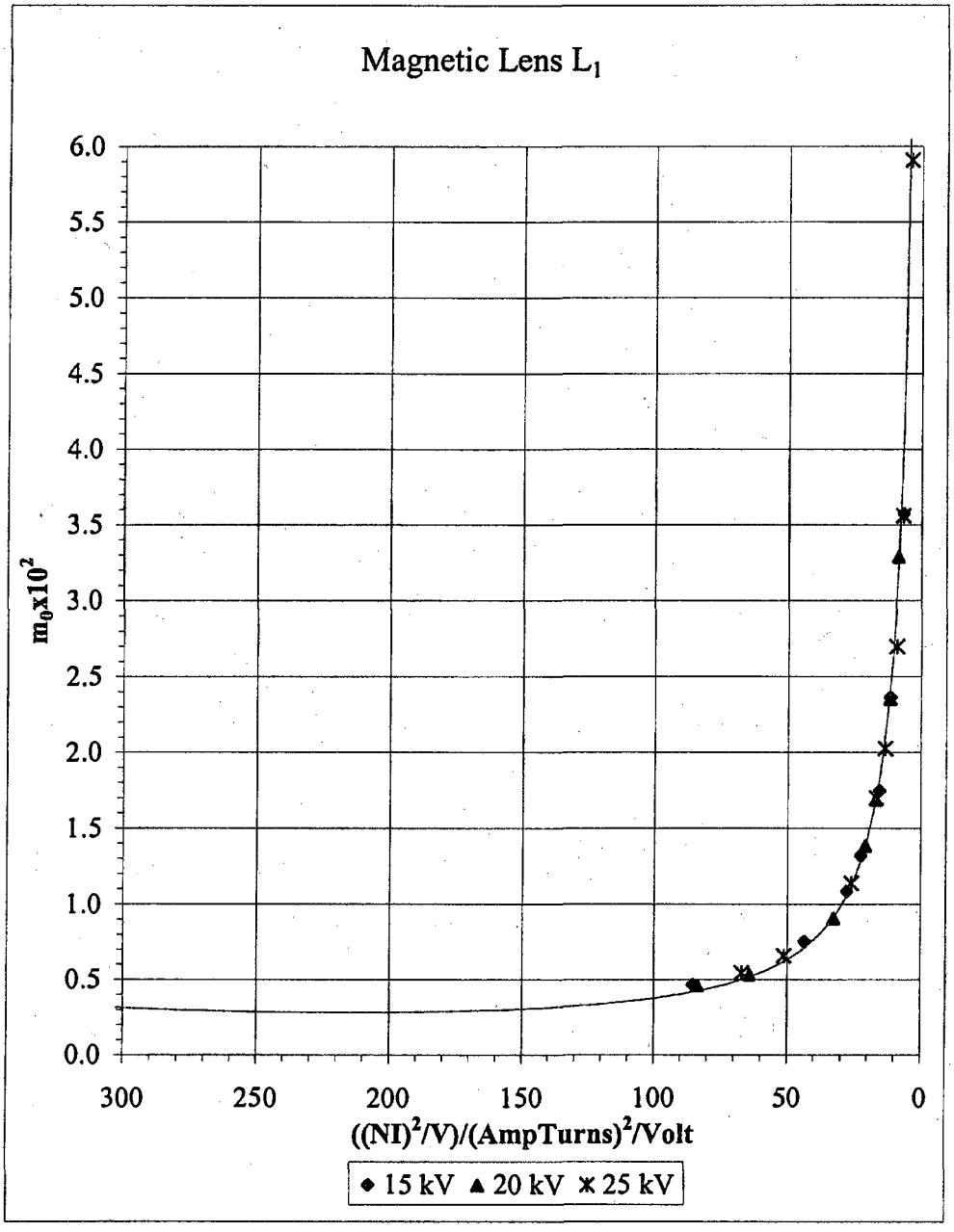

Figure 7.5(b). m_0' vs. $(NI)^2/V$ for all three accelerating voltages for magnetic lens L_1 showing very close fit with their corresponding model curves.

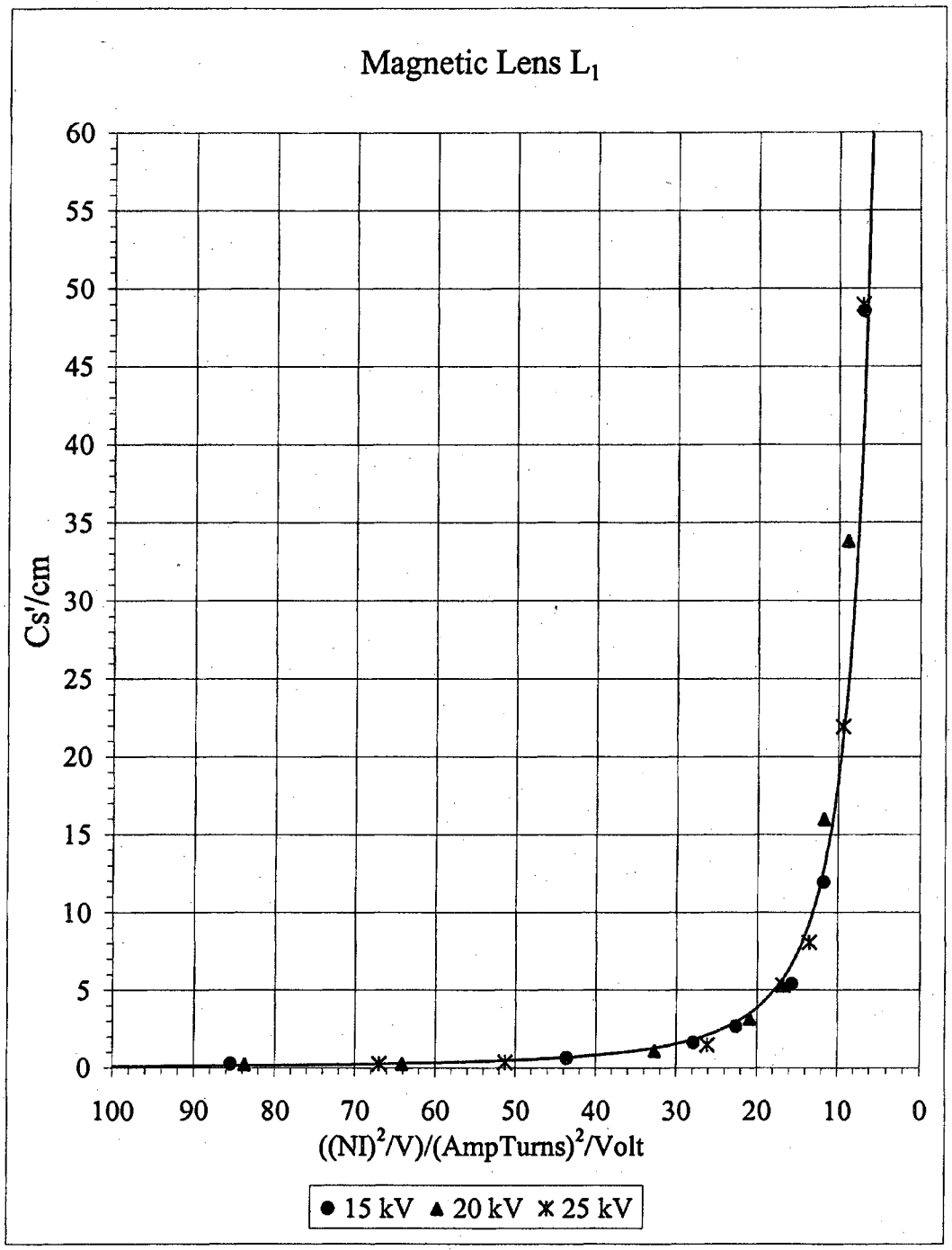

Figure 7.5(c). *Cs'* vs. $(NI)^2/V$ for all three accelerating voltages for magnetic lens L_1. Curve is a best fit power series curve for the data.

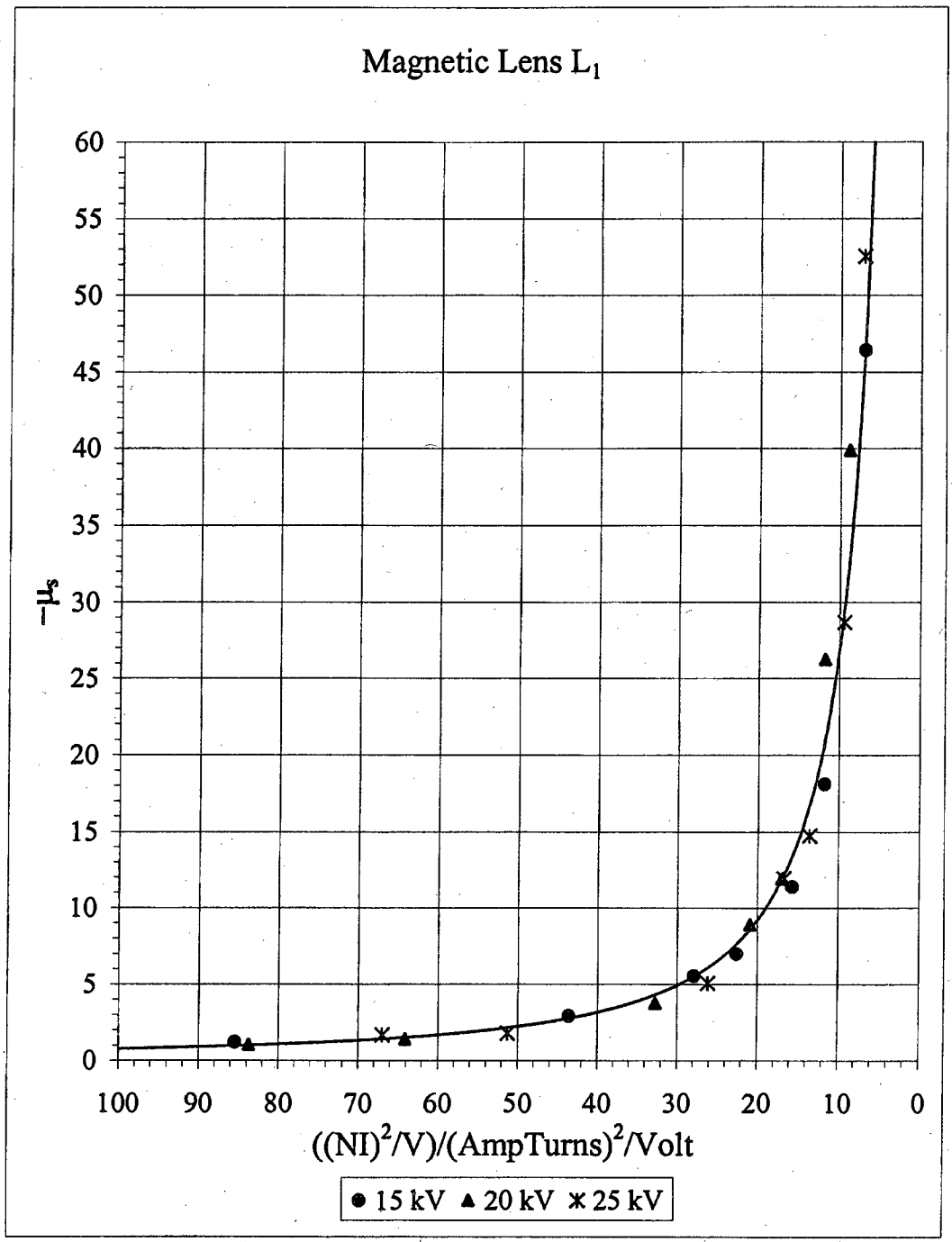

Figure 7.5(d). $\mu s'$ vs $(NI)^2/V$ for all three accelerating voltages for the magnetic lens L_1. Curve is a best fit power series curve for the data.

The L_1 paraxial focal properties f_0 and g_0 and the spherical aberration coefficients S_f and S_g, listed earlier in the L_1 Tables 7.2 (a), (b), and (c), were shown separately as functions of I in Figures 7.2 (a), (b), (c), and (d), for the three acceleration voltages. This information is shown more compactly vs $(NI)^2/V$ in Table 7.6, and in graphs of the four lens properties, Figures 7.6a - 7.6d.

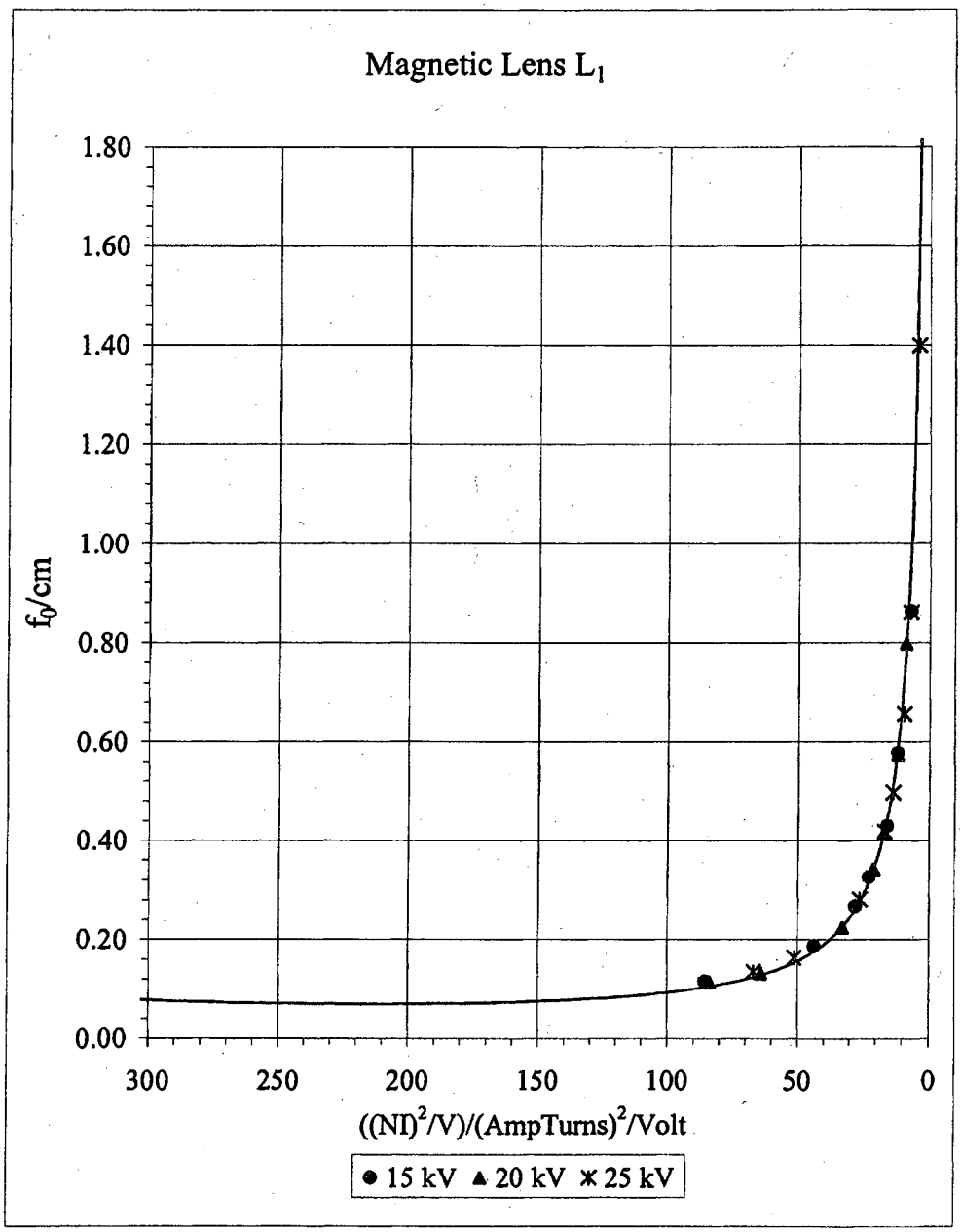

Figures 7.6(a). Paraxial focal length f_0 versus $(NI)^2/V$ for all three accelerating voltages of magnetic lens L_1 showing very close fit with their corresponding model curves.

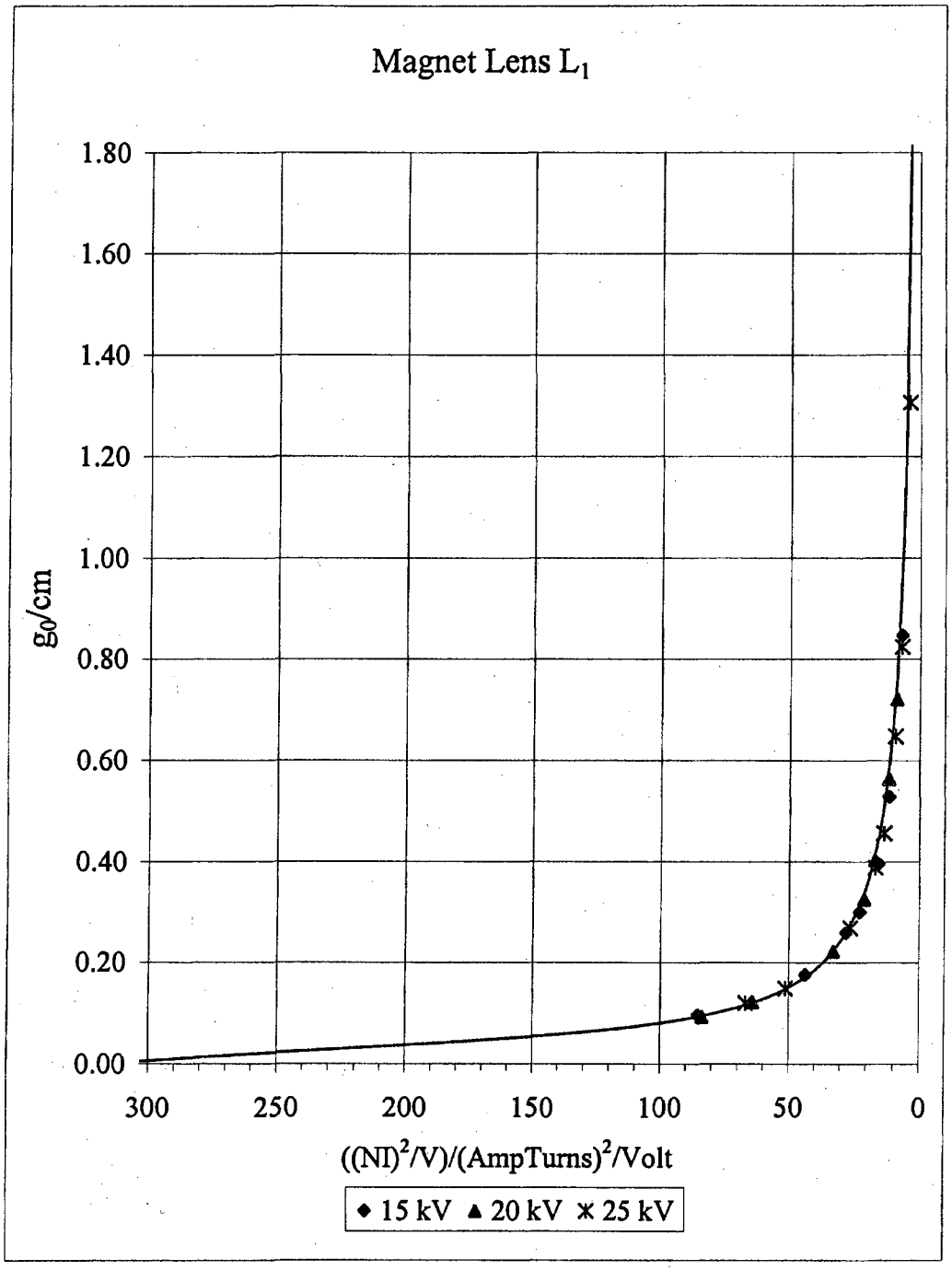

Figure 7.6(b). Paraxial focal distance g_0 versus $(NI)^2/V$ for all three accelerating voltages of magnetic lens L_1 showing very close fit with their corresponding model curves.

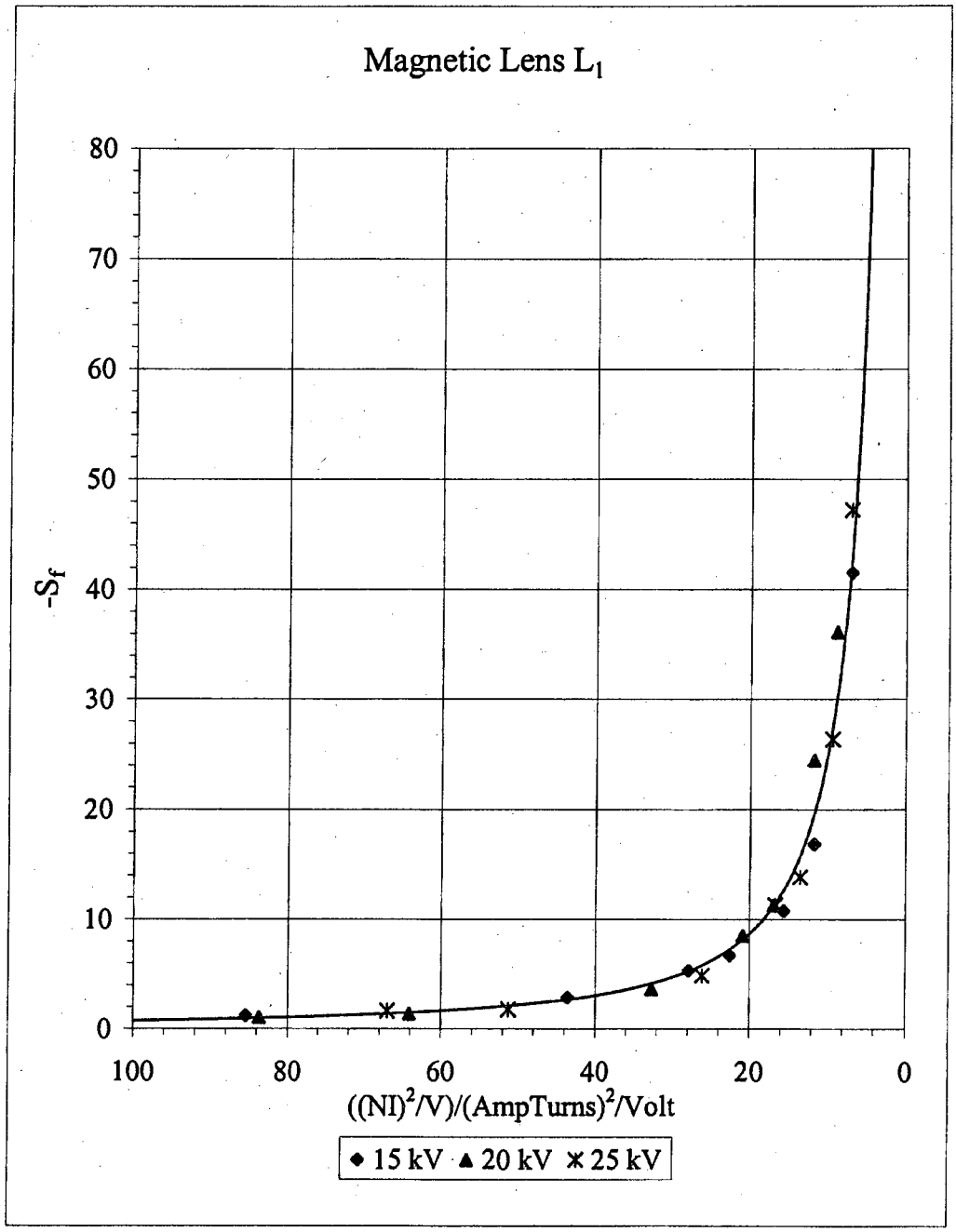

Figure 7.6(c). Spherical aberration coefficient S_f versus $(NI)^2/V$ for all three accelerating voltages of magnetic lens L_1 with best fit power series curve.

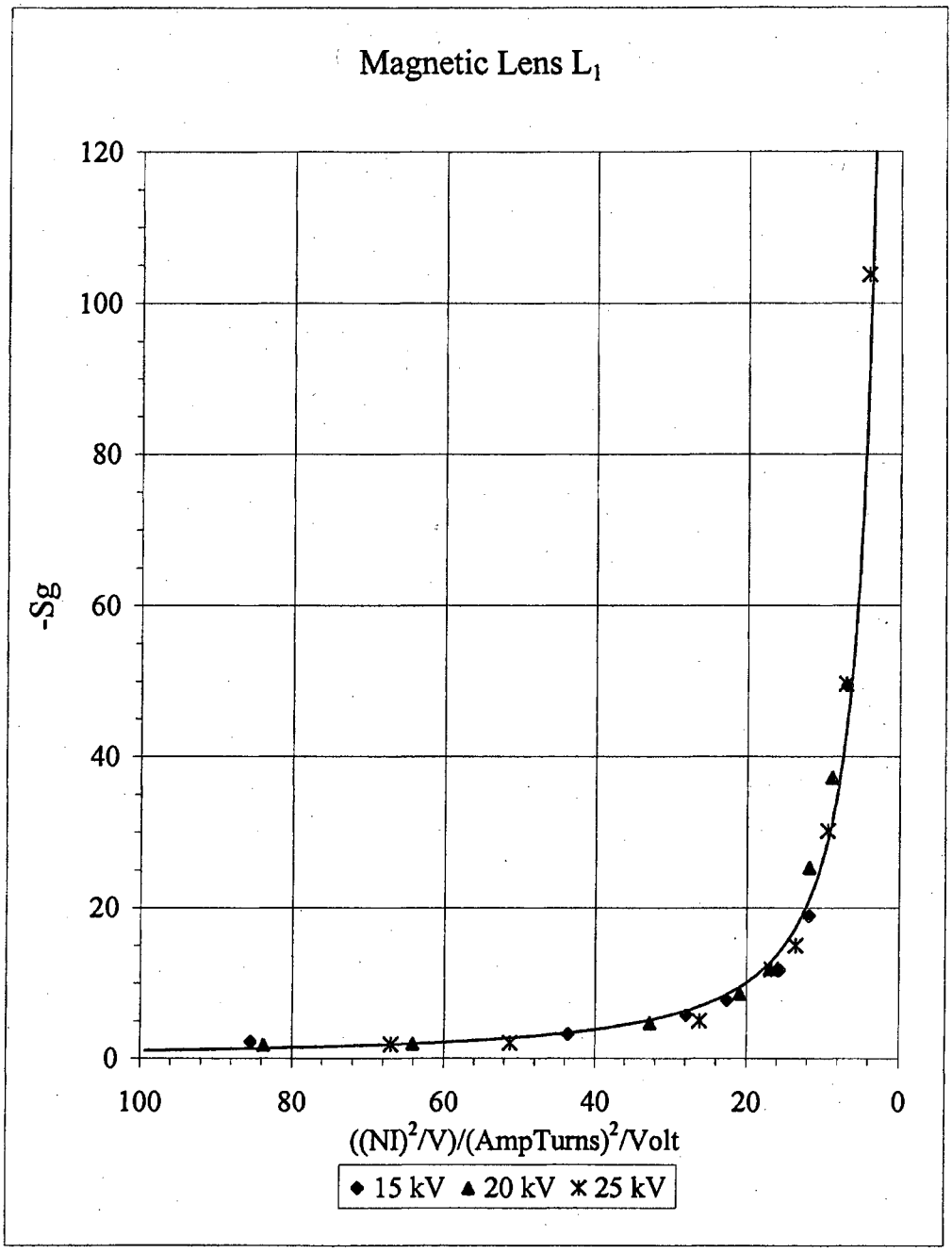

Figure 7.6(d). Spherical aberration coefficient S_g versus $(NI)^2/V$ for all three accelerating voltages of magnetic lens L_1 with best fit power series curve.

Lens L_2

The L_2 image properties z_0', m_0, C_s', and μ_s listed in Table 7.3 were shown earlier as graphs versus current I in Figures 7.3 (a), (b), (c), and (d), and for the single voltage $V = 20$ kV. For uniformity with the L_1 curves in Figures 7.5 (a), (b), (c), and (d), the L_2 image properties are plotted vs. $(NI)^2/V$ in Figures 7.7 (a-d) for z_o', m_o, C_s', and μ_s.

Current milliamps	Activation $(NI)^2/V$	z_0'/cm	m_0 x10^2	C_s/cm	m_s
350	64.1	0.166	0.859	0.37	-1.12
300	47.1	0.229	1.08	0.70	-1.80
250	32.7	0.300	1.45	1.32	-3.09
200	20.9	0.480	2.16	4.27	-7.03
180	17.0	0.562	2.56	6.71	-10.2
150	11.8	0.868	3.61	23.3	-22.4
130	8.84	1.16	4.68	53.2	-41.9
100	5.23	1.79	7.23	179	-92.2

Copy of Table 7.3. The image properties of Lens L_2 with lens activation $(NI)^2/V$.

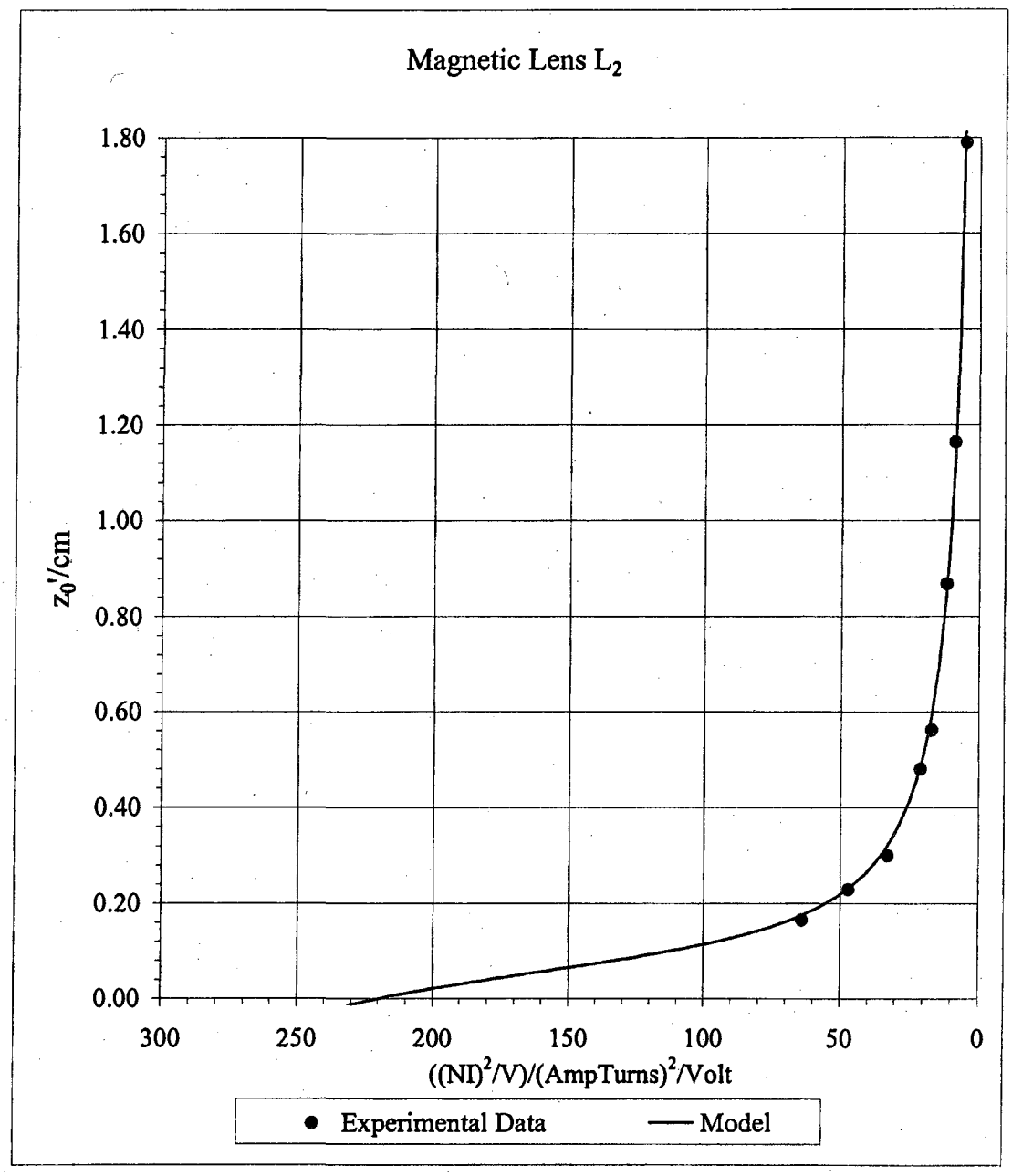

Figure 7.7(a). z_0' vs. $(NI)^2/V$ for magnetic lens L_2 at the accelerating voltage of 20 kV with its model curve.

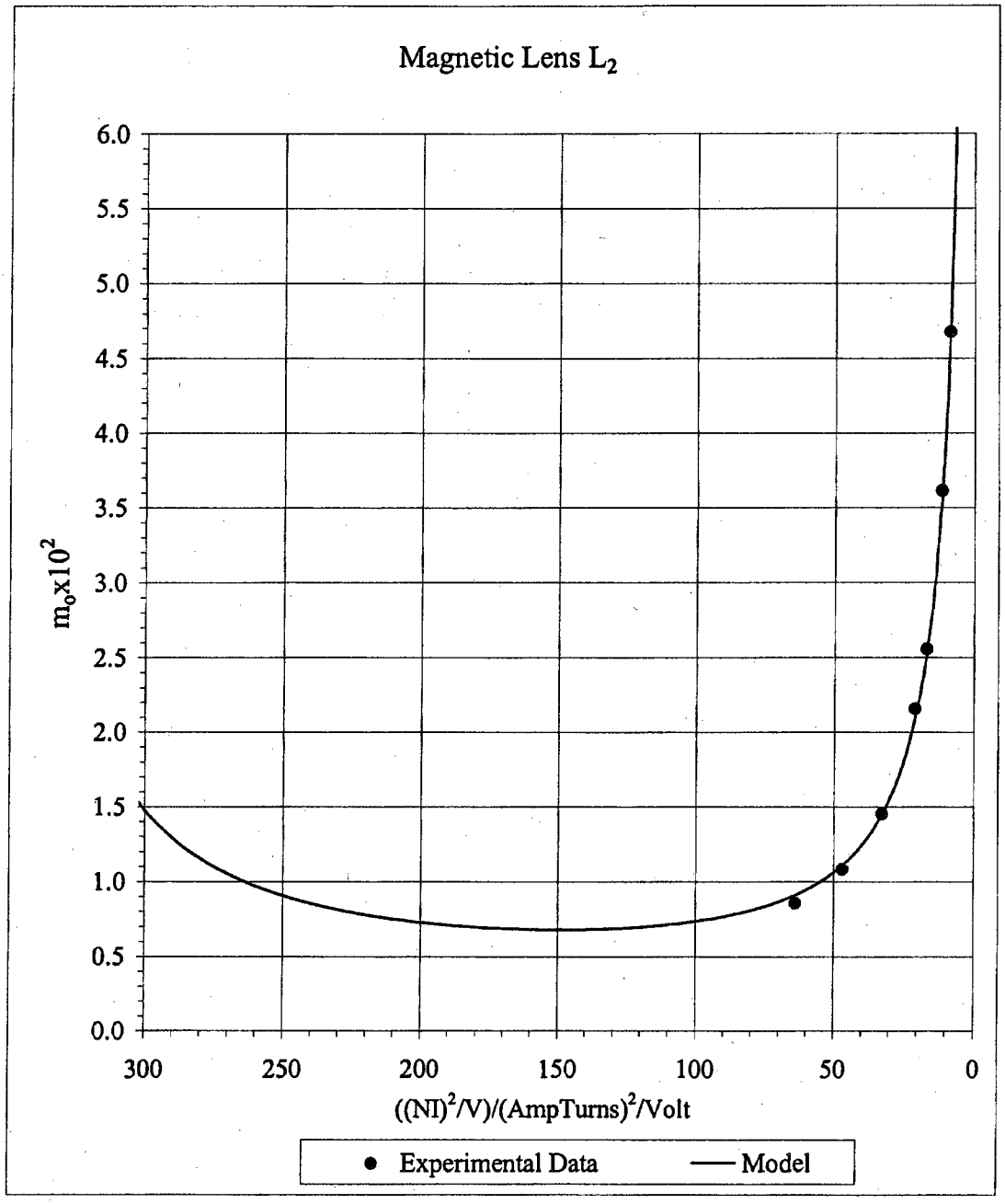

Figure 7.7(b). m_0 vs. $(NI)^2/V$ for magnetic lens L_2 at the accelerating voltage of 20 kV with its model curve.

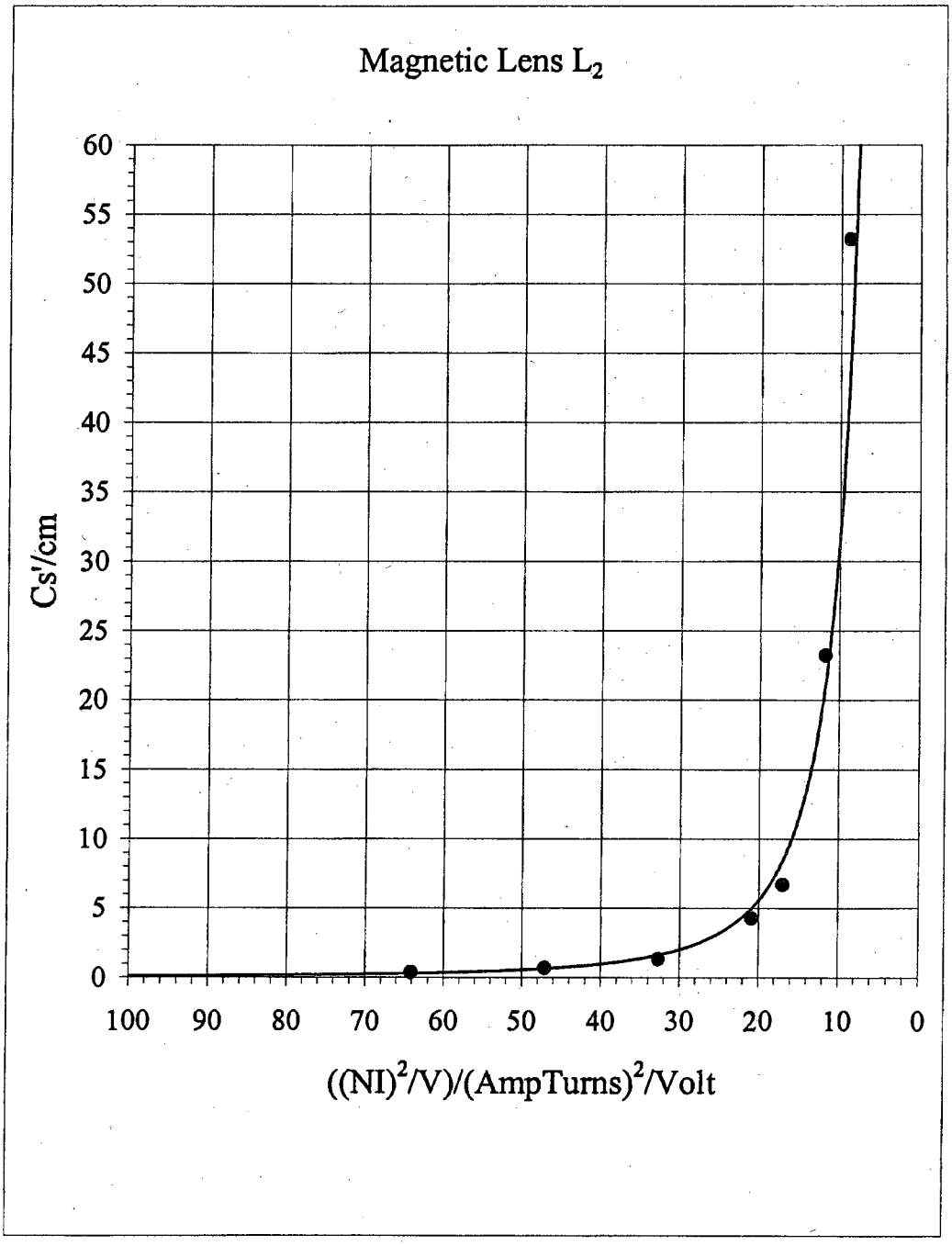

Figure 7.7(c). *Cs'* vs. $(NI)^2/V$ for magnetic lens L_2 at the accelerating voltage of 20 kV with a power series curve.

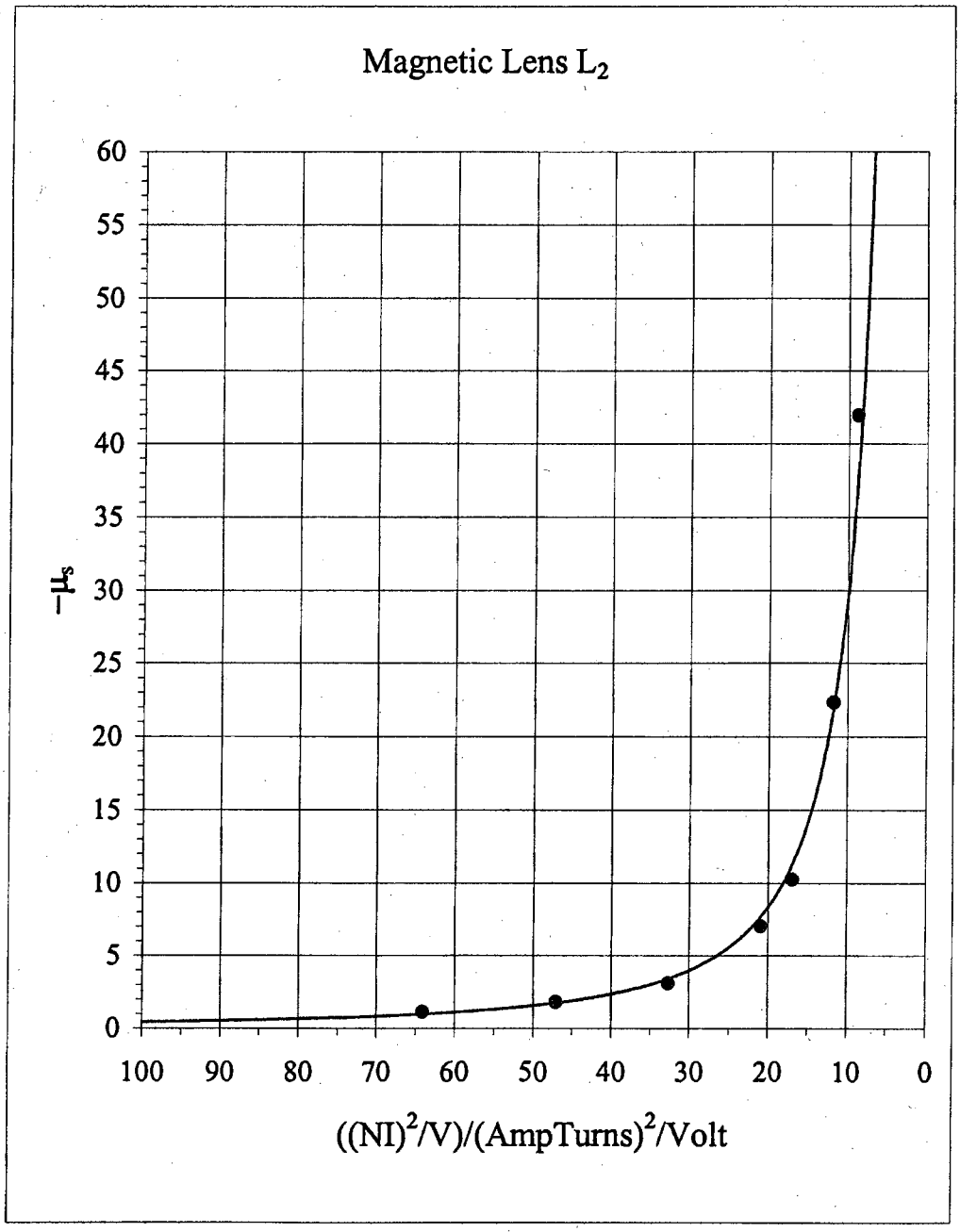

Figure 7.7(d). μ_s vs $(NI)^2/V$ for magnetic lens L_2 at the accelerating voltage of 20 kV with a power series curve.

The paraxial focal properties f_0 and g_0 of L_2 and the spherical aberration coefficients S_f and S_g, listed in L_2 Table 7.4 were shown in Figures 7.4 (a), (b), (c), and (d) as functions of current I for the single voltage 20 kV. For uniformity with the L_1 graphs in Figures 7.6 (a), (b), (c), and (d), the L_2 lens properties are plotted vs. $(NI)^2/V$ in Figures 7.8(a), (b), (c), and (d).

Current milliamps	Activation $(NI)^2/V$	f_o/cm	g_o/cm	S_f	S_g
350	64.1	0.213	0.164	-1.08	-1.70
300	47.1	0.268	0.226	-2.18	-2.51
250	32.7	0.359	0.295	-2.87	-3.48
200	20.9	0.529	0.469	-6.58	-7.45
180	17.0	0.627	0.546	-7.09	-9.74
150	11.8	0.884	0.836	-15.7	-22.6
130	8.84	1.12	1.11	-36.4	-40.0
100	5.23	1.69	1.67	-74.3	-81.3

Copy of Table 7.4. The lens properties of L_2 with lens activation $(NI)^2/V$

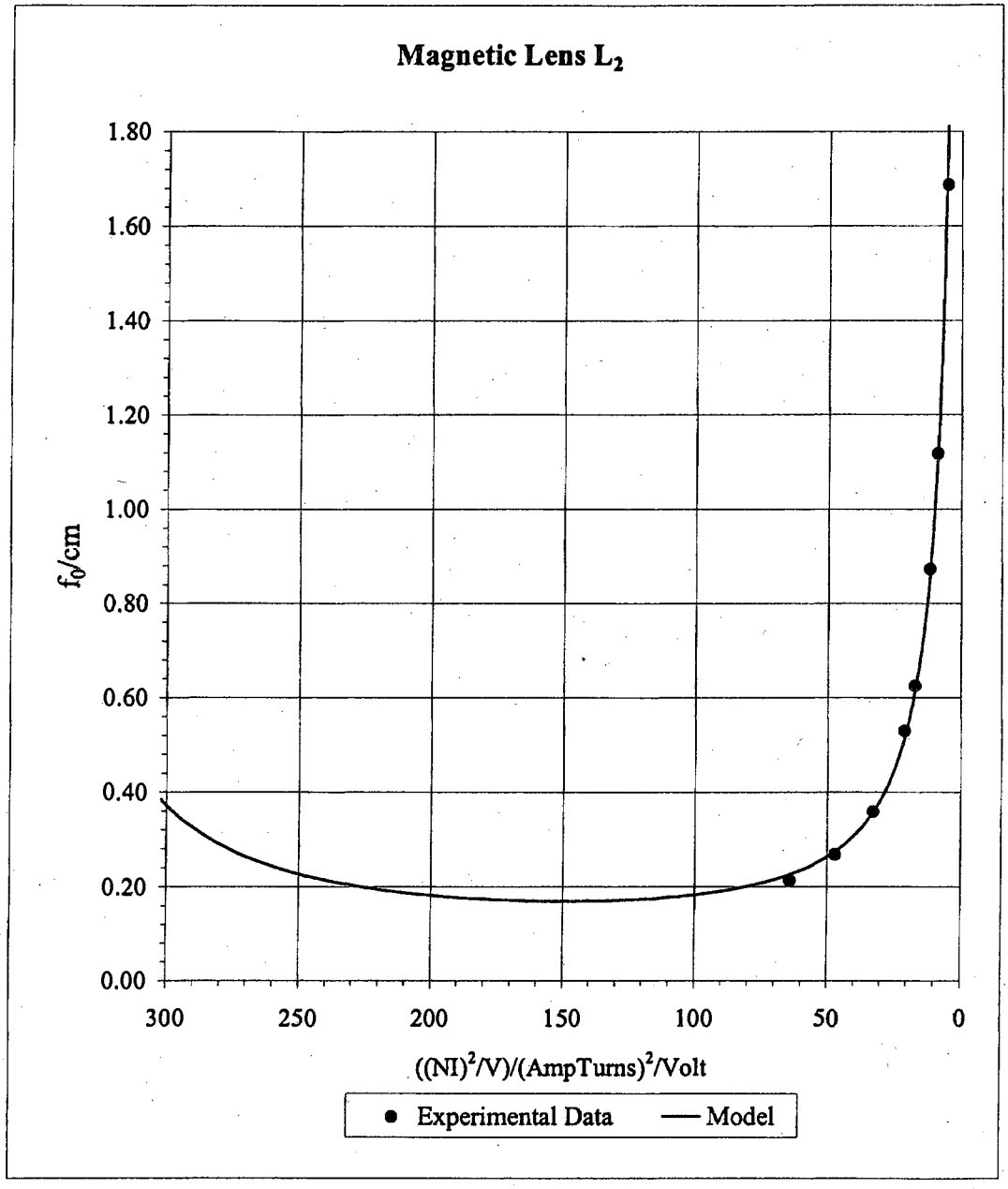

Figure 7.8(a). f_0 vs. $(NI)^2/V$ for magnetic lens L_2 at the accelerating voltage of 20 kV with its model fit curve.

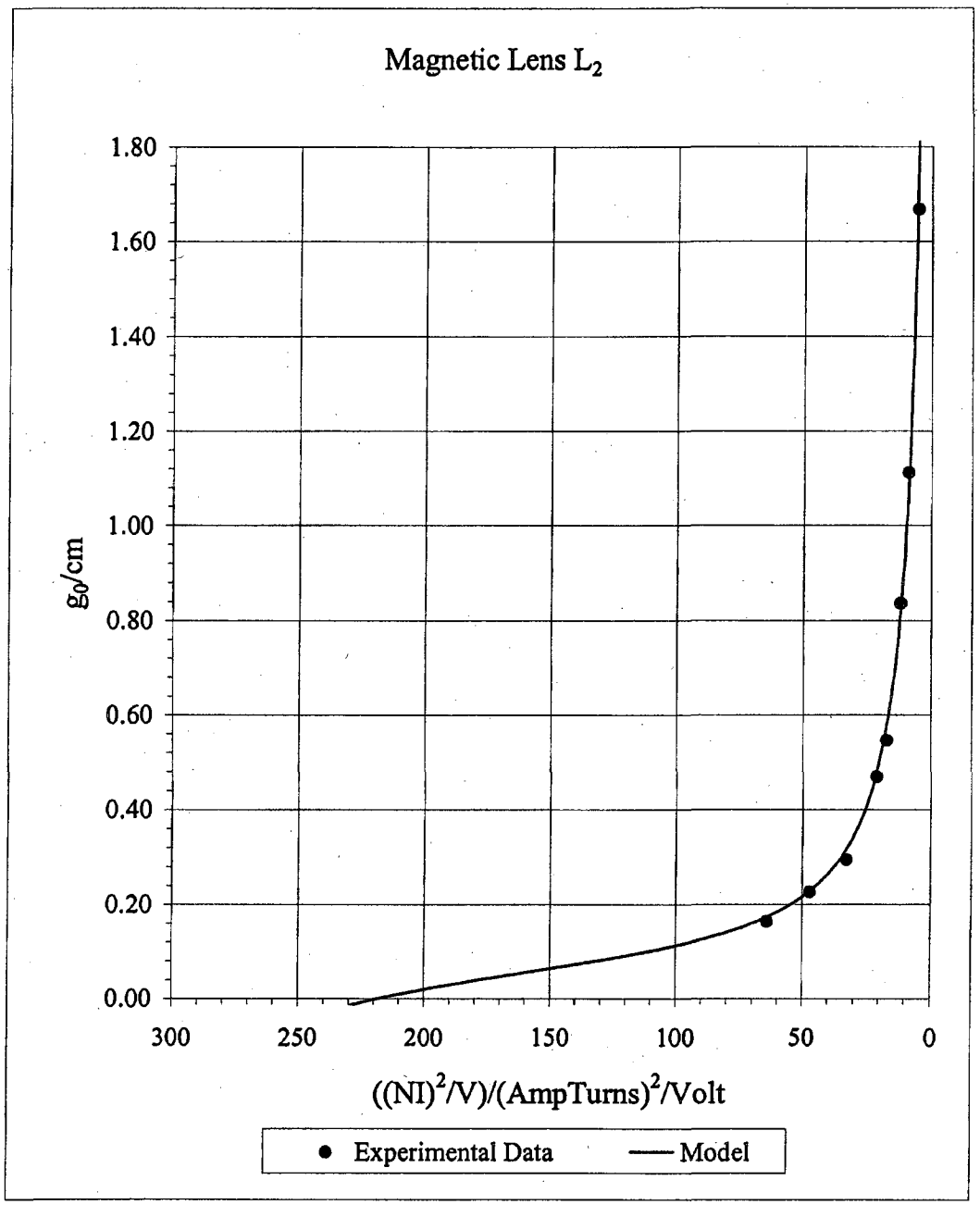

Figure 7.8(b). g_0 vs. $(NI)^2/V$ for magnetic lens L_2 at the accelerating voltage of 20 kV with its model fit curve.

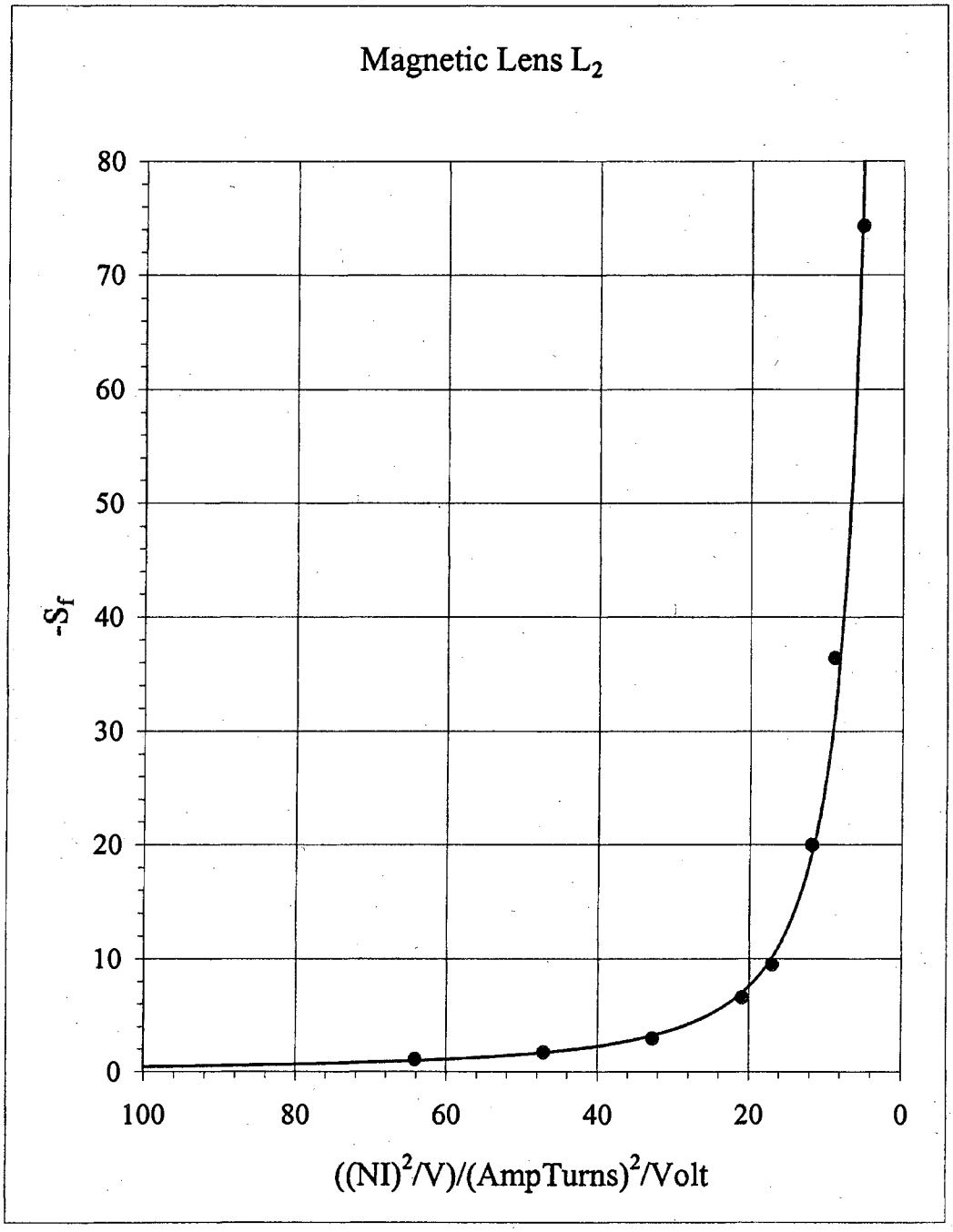

Figure 7.8(c). S_f vs. $(NI)^2/V$ for magnetic lens L_2 at the accelerating voltage of 20 kV with its power series curve.

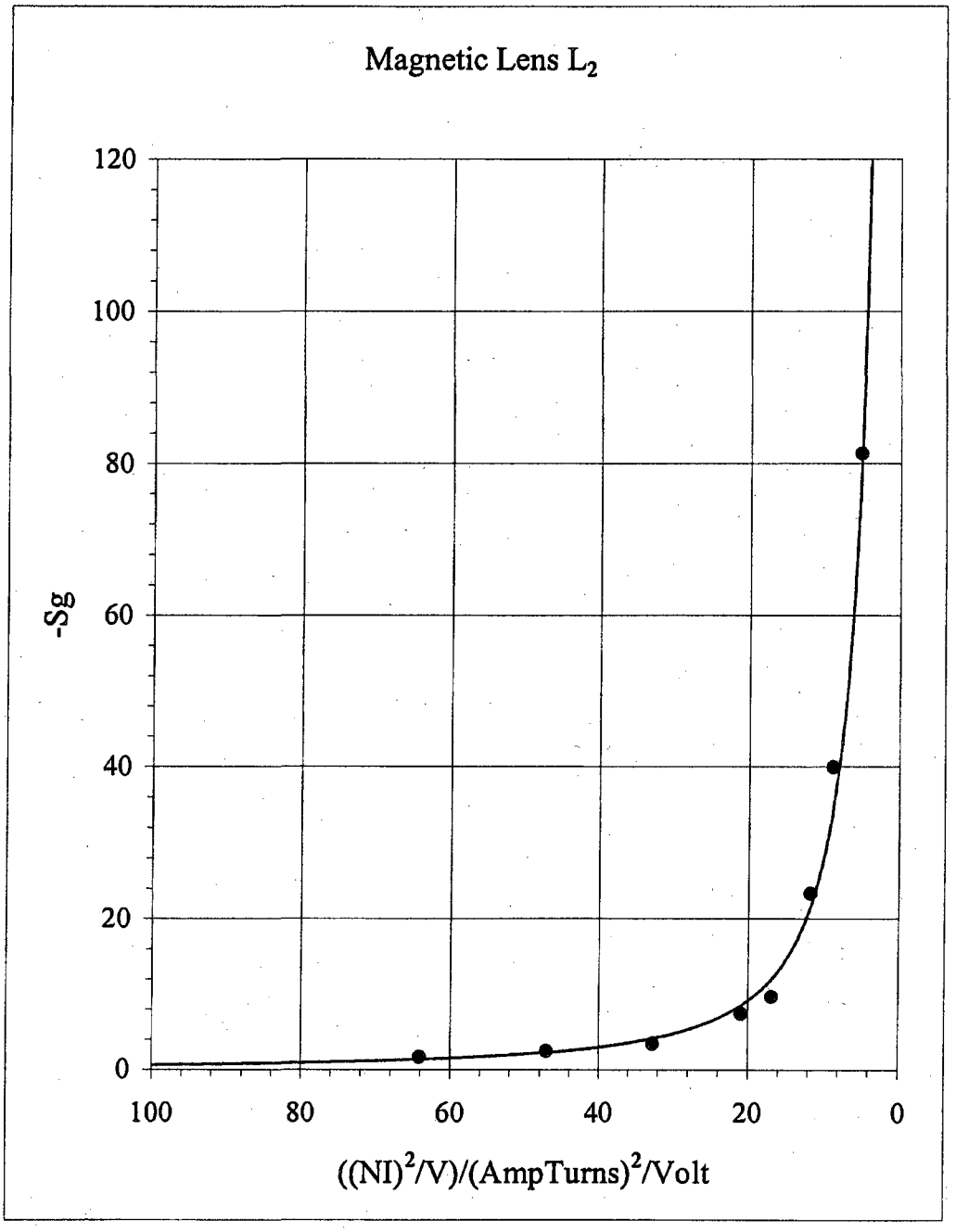

Figure 7.8(d). S_g vs. $(NI)^2/V$ for magnetic lens L_2 at the accelerating voltage of 20 kV with its power series curve.

Experimental Results for Electrostatic Lenses L_3, L_4, and L_5

Shadowgraphs were recorded for the electrostatic lenses at accelerating voltages of 20 kV and voltage ratios V_L/V_C from 1.0 down to 0.6. The shadowgraphs were recorded and analyzed in the same way as they were for the magnetic lenses. The measurements leading to z' and m were carried out for each lens at each voltage ratio.

L_3, L_4, L_5: Image and Lens Properties

The values for z' and m obtained from the shadow measurements are listed as functions of α'^2 for L_3, L_4, and L_5 in Tables in Appendix A for each lens and each voltage ratio. Accompanying graphs of z' vs α'^2, and m vs α'^2 are used to determine the paraxial image properties z_o' and m_o and the spherical aberration coefficients C_s' and μ_s for the lenses. These properties are listed as functions of V_L/V_C in Tables 7.9 (a), 7.9 (b), and 7.9 (c). The four image properties z_o', m_o, C_S', and μ_S are each shown vs V_L/V_C for the three lenses in separate Figures 7.9 (a), 7.9 (b), 7.9 (c), and 7.9 (d).

Table 7.9(a)	L_3				
	V_L/V_C	z_0'/cm	$m_0 x10^2$	C_s/cm	μ_s
	1.00	0.451	1.92090	6.44	-15.31
	0.95	0.579	2.42546	11.77	-21.50
	0.90	0.748	3.06822	22.15	-28.91
	0.80	1.094	4.45164	68.02	-58.44
	0.70	1.744	7.04597	263.79	-117.55
	0.60	2.926	11.87312	1090.41	-313.56
Table 7.9(b)	L_4				
	V_L/V_C	z_0'/cm	$m_0 x10^2$	C_s/cm	μ_s
	1.00	0.824	3.38416	32.04	-23.57
	0.95	0.969	3.91716	42.87	-32.91
	0.90	1.152	4.66440	71.82	-44.42
	0.85	1.348	5.46981	111.40	-62.39
	0.80	1.646	6.60213	183.48	-96.96
	0.70	2.414	9.69818	500.32	-168.13
Table 7.9(c)	L_5				
	V_L/V_C	z_0'/cm	$m_0 x10^2$	C_s/cm	μ_s
	1.00	0.661	2.91176	9.52	-10.99
	0.95	0.797	3.40620	14.56	-13.53
	0.90	0.975	4.09125	21.96	-18.49
	0.80	1.447	5.85863	60.83	-39.00
	0.70	2.045	8.59533	198.13	-84.76

Table 7.9(a), (b), and (c). Paraxial image properties z_0' and m_0, with their spherical aberrations coefficients, Cs' and μs , for the electrostatic lenses, L_3, L_4, and L_5.

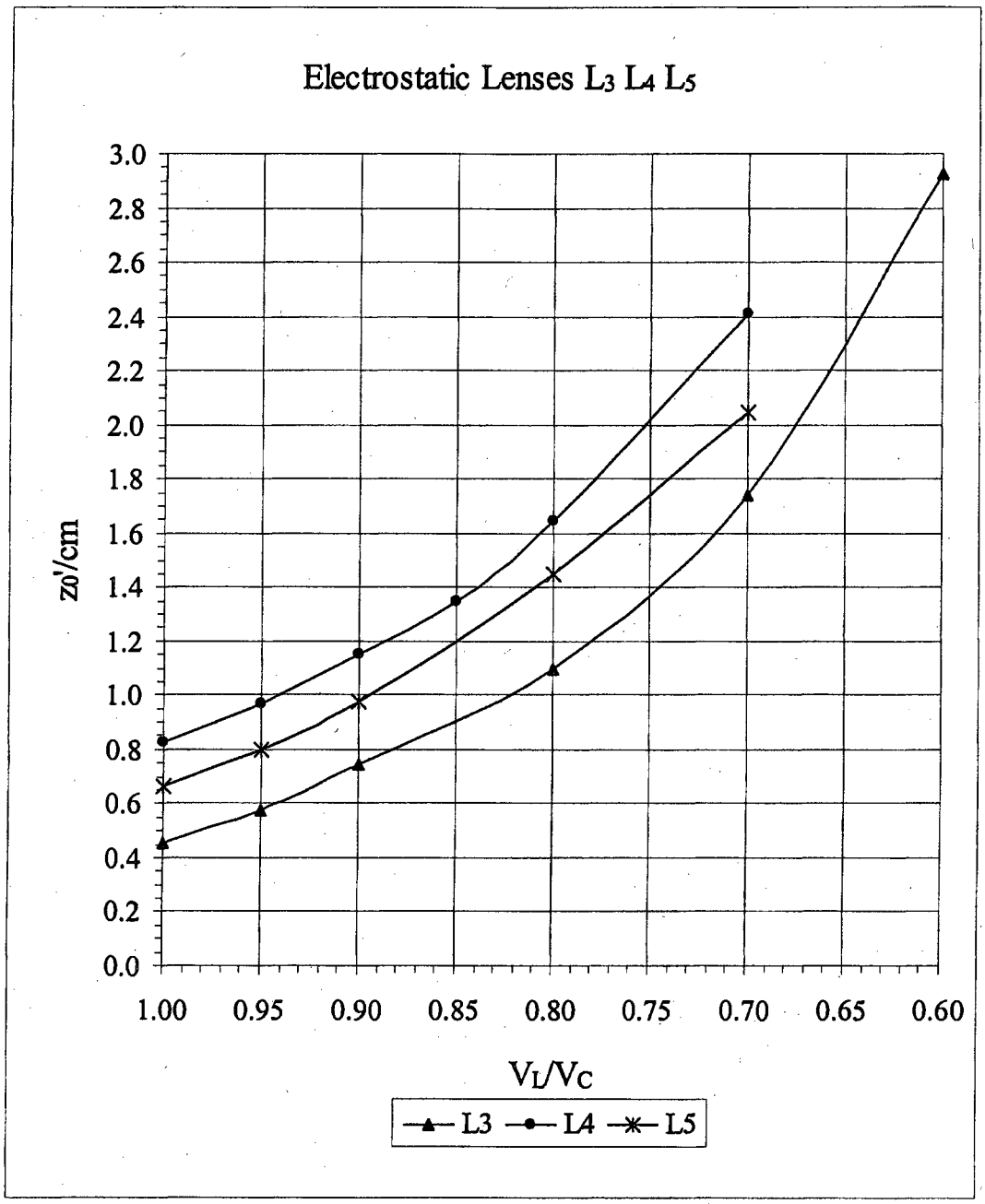

Figure 7.9(a). z_0' versus V_L/V_C for the three electrostatic lenses L_3, L_4, and L_5 with smooth line connecting data points

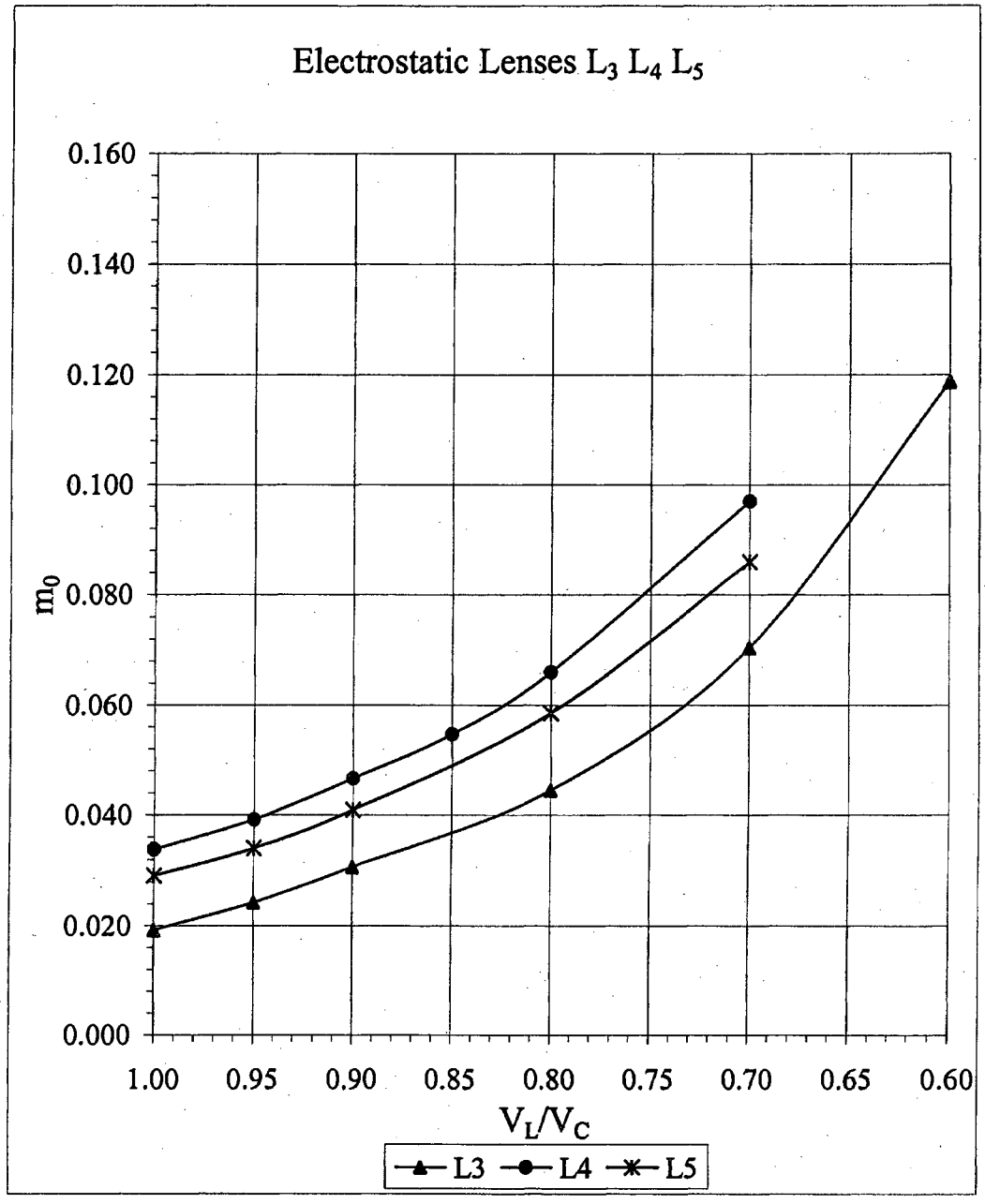

Figure 7.9(b). m_0 versus V_L/V_C for the three electrostatic lenses L_3, L_4, and L_5 with smooth line connecting data points.

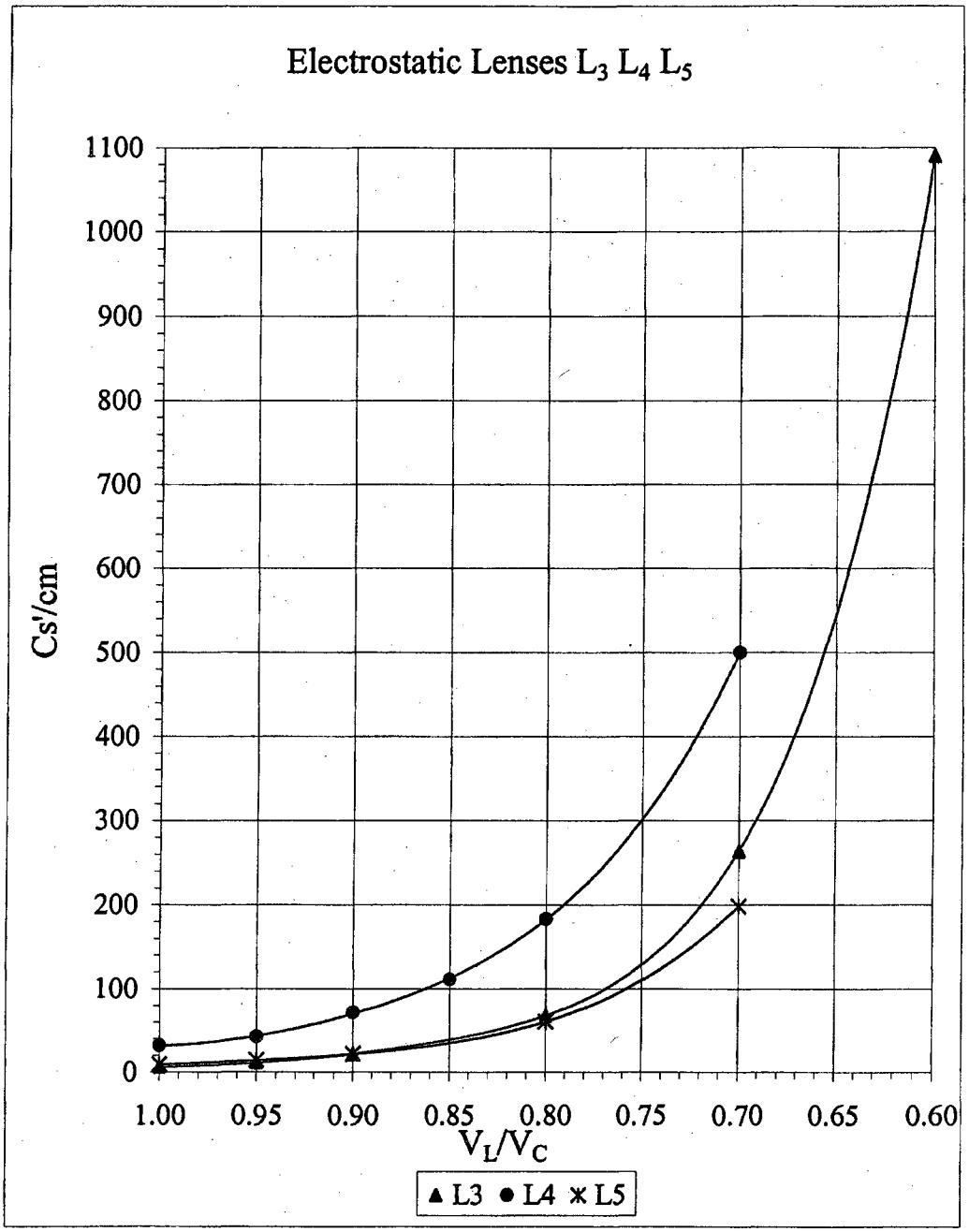

Figure 7.9(c). *Cs'* versus V_L/V_C for the three electrostatic lenses L_3, L_4, and L_5 with least square polynomial fit curves. Look at Figure 7.9 (c) ' for a closer look at the higher activation cross-over of the C'_S versus V_L/V_C graph.

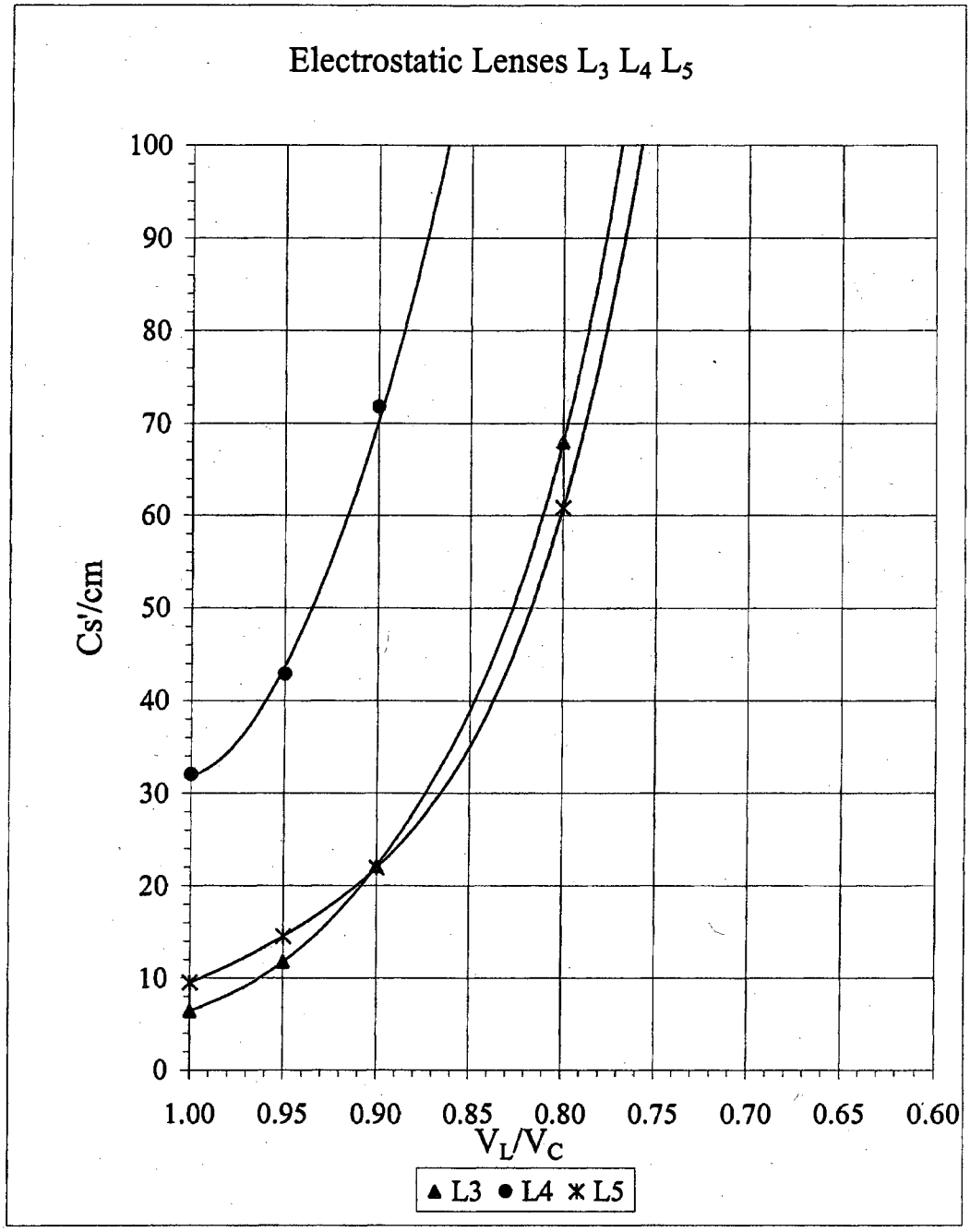

Figure 7.9(c)'. A closer look at the higher activation crossover of the C_S' versus V_L/V_C graph.

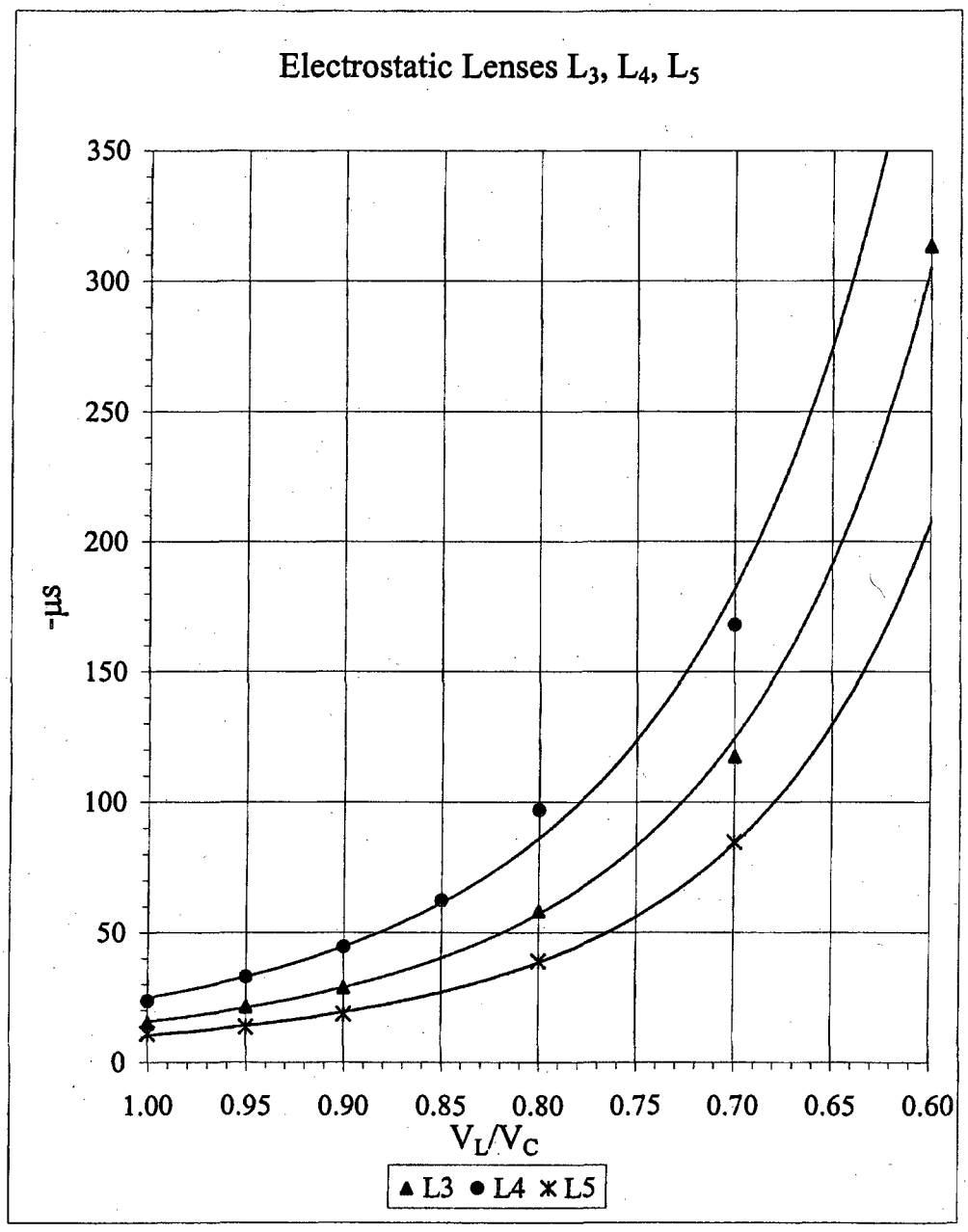

Figure 7.9(d). $-\mu_s'$ versus V_L/V_C for the three electrostatic lenses L_3, L_4, and L_5 with power series fit curves.

The lens properties f and g, of L_3, L_4, and L_5, calculated from the values of z, z', and m for the respective lenses, are listed in Appendix-A as functions of $(\delta)^2$ for each voltage ratio. The paraxial lens properties f_0 and g_0 and the spherical aberration coefficients S_f and S_g obtained from graphs of f and g vs. δ^2 are listed for each lens as functions of V_L/V_C in Tables 7.10(a), (b), and (c). The four lens properties f_o, g_o, S_f, and S_g are shown separately vs V_L/V_C for the three lenses, in Figures 7.10 (a), 7.10 (b), 7.10 (c), and 7.10 (d).

Table 7.10(a) L_3

V_L/V_C	f_0/cm	g_0/cm	S_f	S_g
1.00	0.472	0.442	-14.500	-12.579
0.95	0.593	0.564	-20.065	-17.952
0.90	0.745	0.725	-26.409	-26.359
0.80	1.066	1.046	-51.189	-53.848
0.70	1.647	1.628	-93.842	-126.155
0.60	2.658	2.610	-218.965	-273.270

Table 7.10(b) L_4

V_L/V_C	f_0/cm	g_0/cm	S_f	S_g
1.00	0.819	0.797	-20.859	-35.144
0.95	0.943	0.932	-28.916	-39.780
0.90	1.115	1.100	-37.972	-55.146
0.85	1.298	1.277	-52.189	-71.252
0.80	1.549	1.544	-79.157	-93.403
0.70	2.211	2.199	-123.962	-162.454

Table 7.10(c) L_5

V_L/V_C	f_0/cm	g_0/cm	S_f	S_g
1.00	0.709	0.640	-10.03	-12.08
0.95	0.825	0.769	-12.12	-15.65
0.90	0.985	0.934	-16.28	-19.22
0.80	1.385	1.366	-32.74	-35.24
0.70	1.988	1.874	-65.63	-72.70

Table 7.10(a), (b), and (c). The paraxial focal properties f_0 and g_0 with the spherical aberration coefficients S_f and S_g, for the electrostatic lenses L_3, L_4, and L_5.

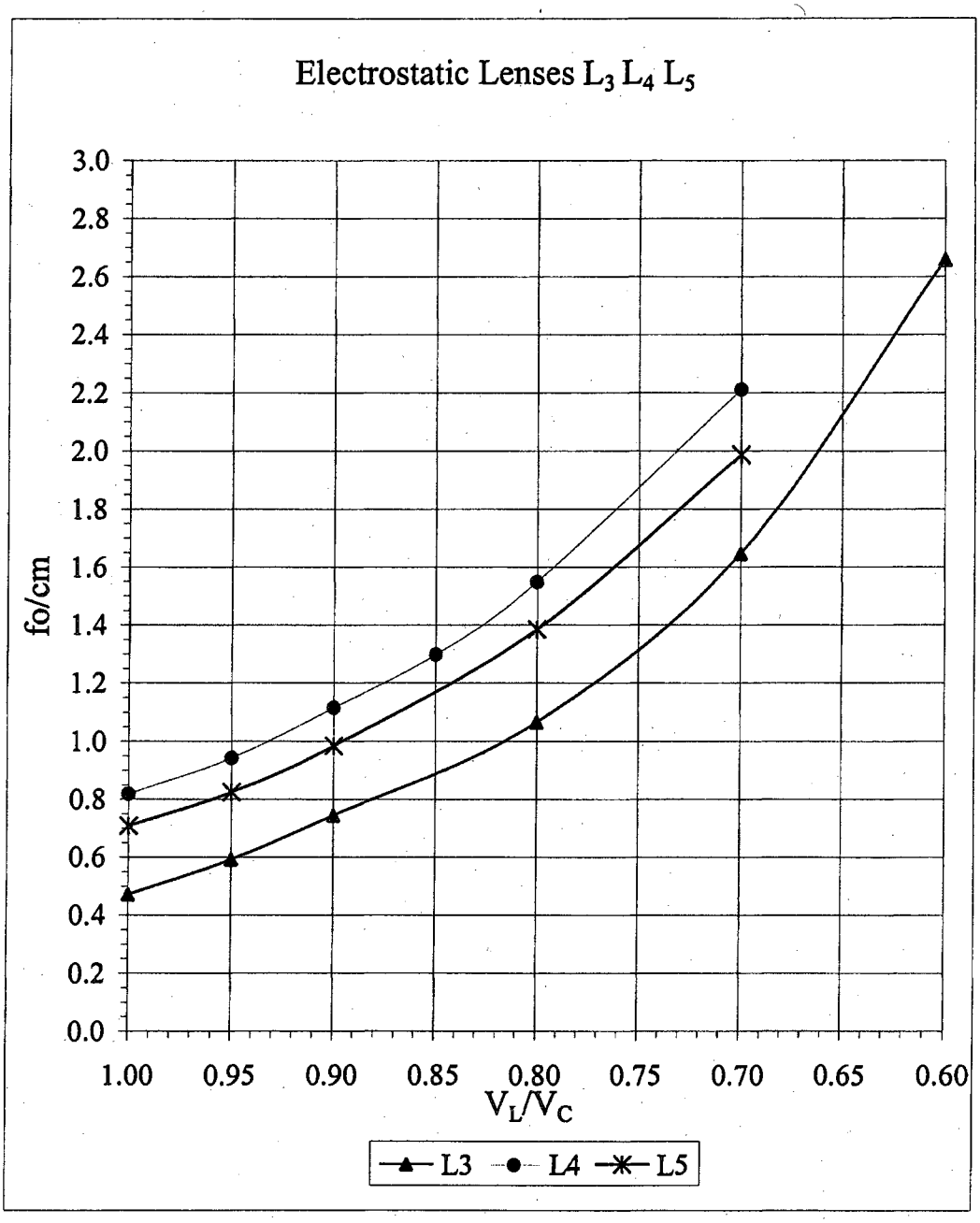

Figure 7.10 (a). f_0 versus V_L/V_C for the three electrostatic lenses L_3, L_4, and L_5 with smooth line connecting data.

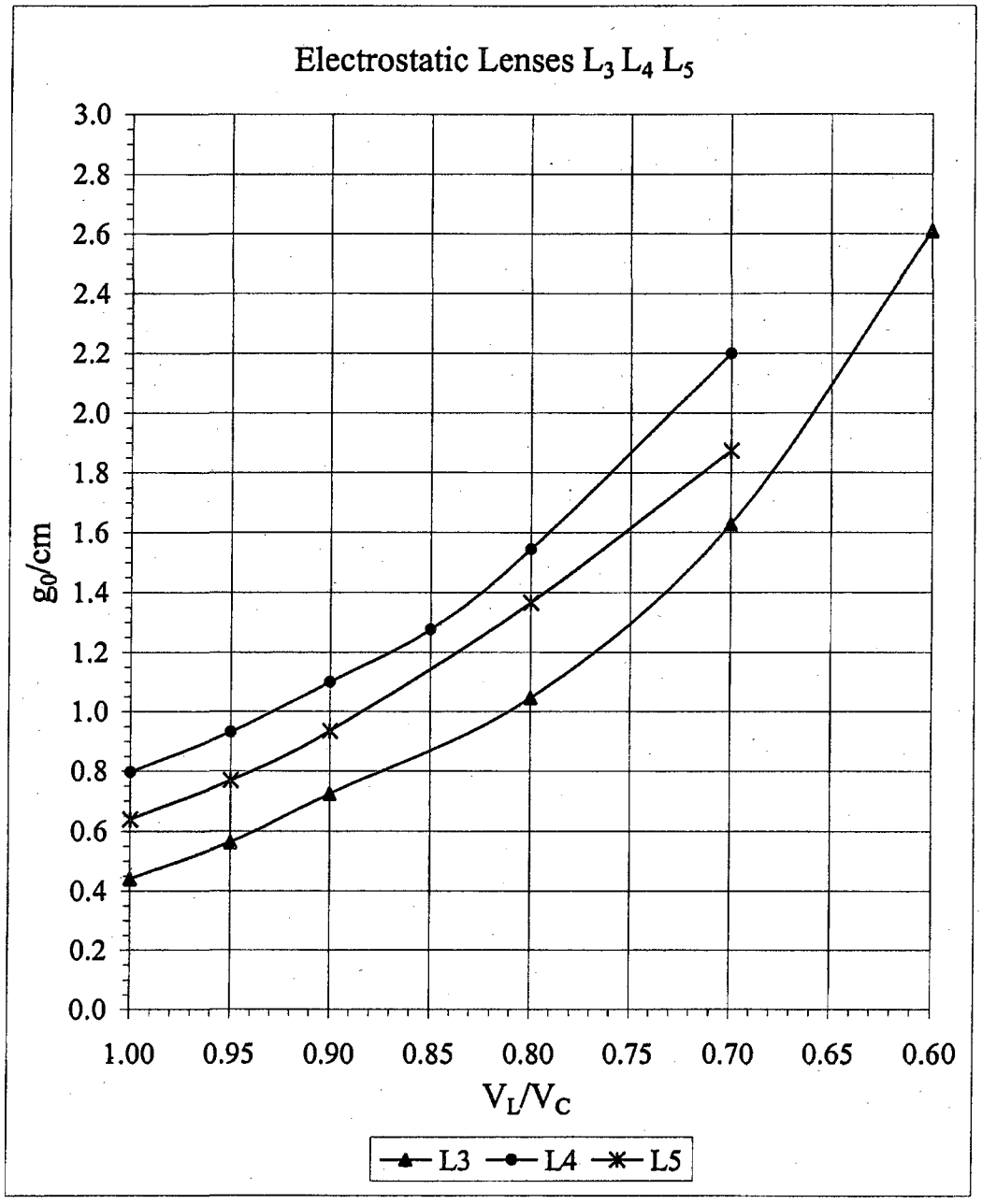

Figure 7.10 (b). g_0 versus V_L/V_C for the three electrostatic lenses L_3, L_4, and L_5 with smooth line connecting data.

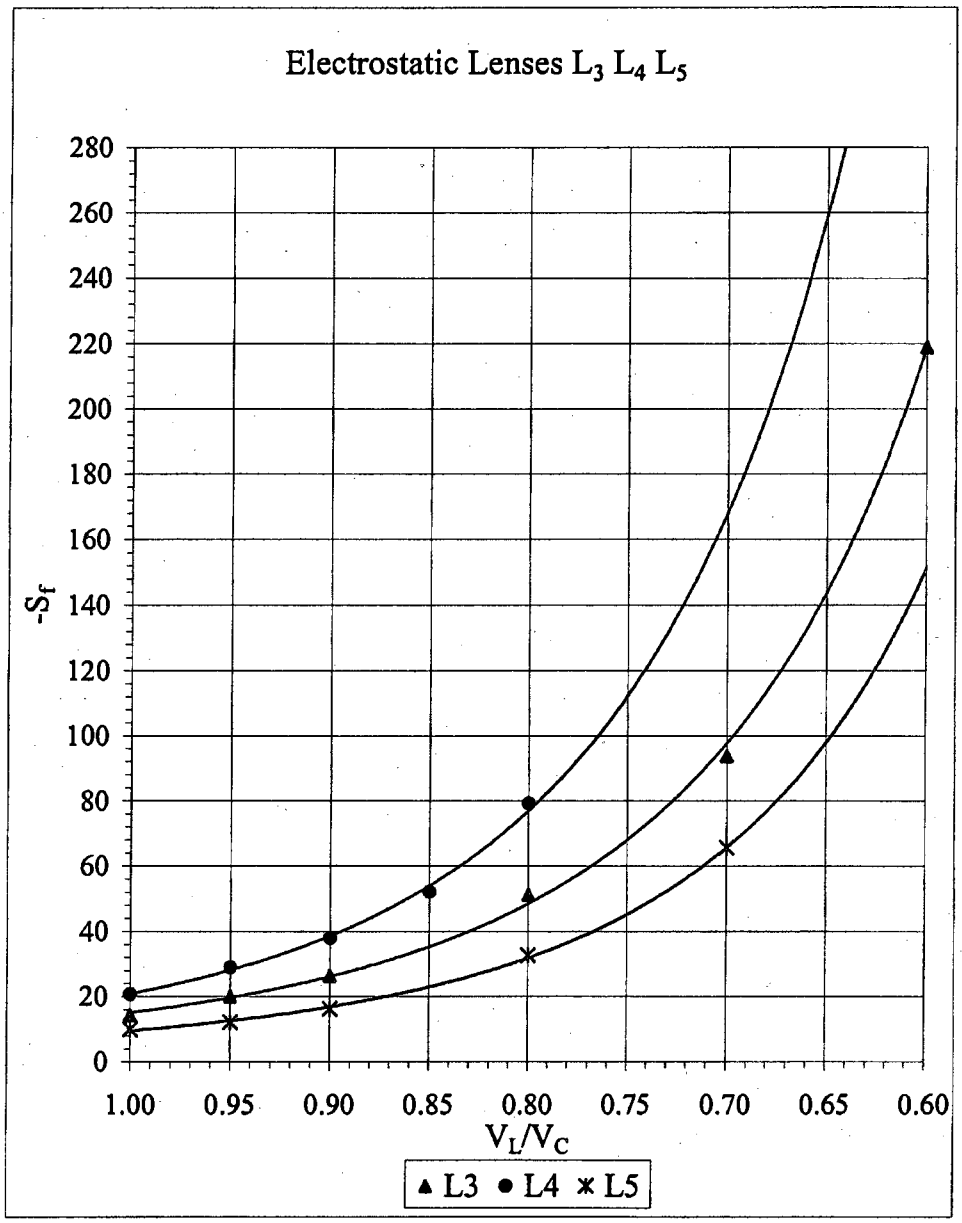

Figure 7.10 (c). *-Sf* versus V_L/V_C for the three electrostatic lenses L_3, L_4, and L_5 with their respective power series curve fits.

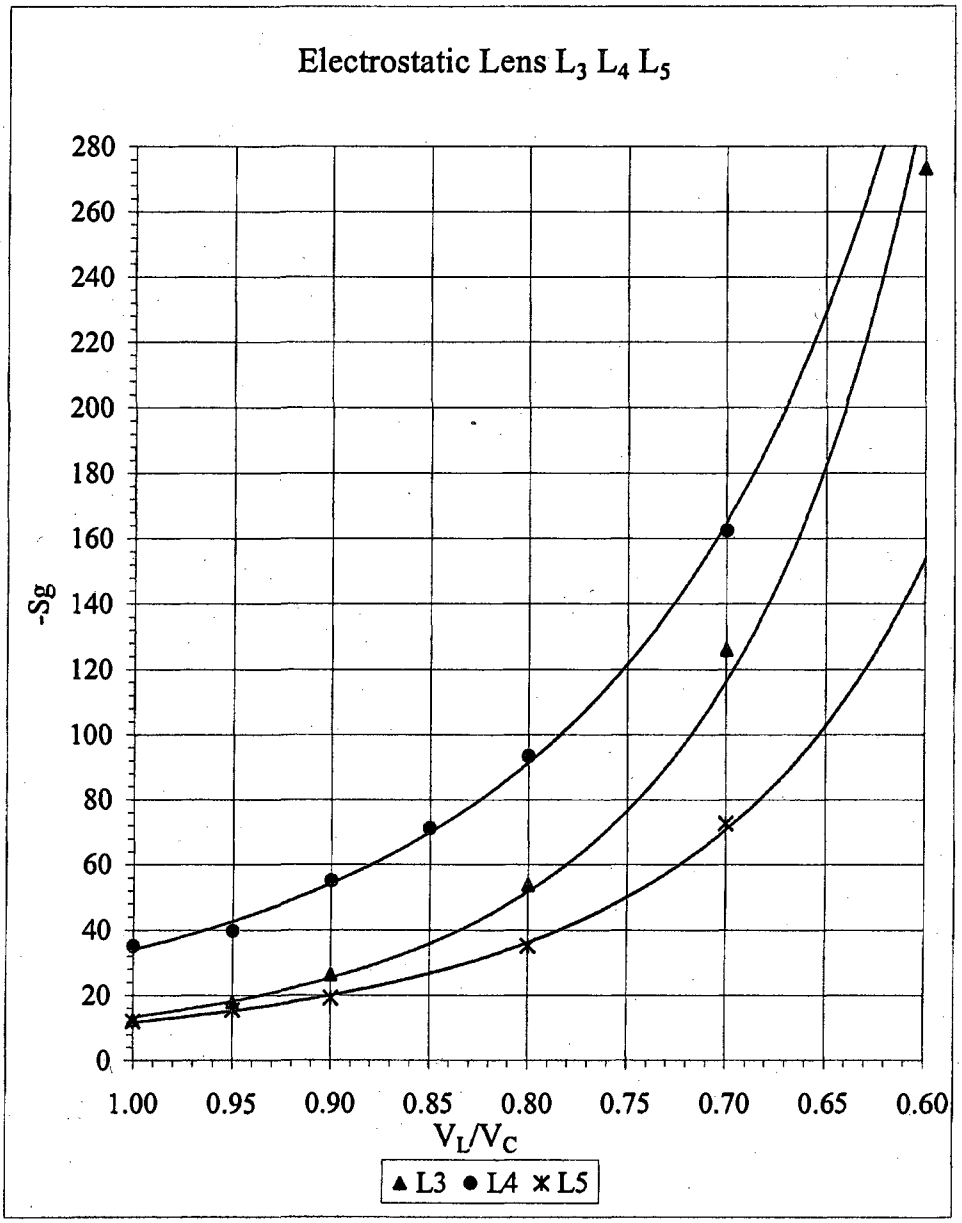

Figure 7.10 (d). $-S_g$ versus V_L/V_C for the three electrostatic lenses L_3, L_4, and L_5 and their respective power series curve fits.

Determination of Chromatic Aberration Coefficients

Chromatic aberration in electron optics has to do with fluctuations in image properties due to unsteadiness of current or voltage sources or to energy distributions in the electron beam. In particular, such disturbances lead to a range of image distances z_o' and magnifications m_o for a given object point, and this results in blurring and smearing of the image. Energy distribution (ED) in electronic beams was considered in Chapter 3. It was decided that the EDs in the beams in the present research were narrow enough to be ignored. So we omit the ED effect here and go on to discuss the effects of voltage and current instabilities on chromatic aberrations.

The properties of magnetic lenses depend on the ratio $(NI)^2/V = P$, where I is the magnetizing current and V is the accelerating voltage. In general the lens properties do not change with changes in I and V. However, if I and V change in such a way that the ratio $\frac{(NI)^2}{V}$ remains unchanged, the lens properties are also unchanged. Since the current and voltage come from two different sources, it may not be possible to synchronize current and voltage fluctuations in the way needed to cancel chromatic aberrations, and highly-regulated supplies may be needed to avoid contributing to chromatic aberration.

The properties of electrostatic lenses depend on the voltage ratio $\frac{V_A - V_L}{V_A - V_C} = \mathcal{V}_{LC}$, where V_A -V_L is the voltage between the grounded outer electrodes and center electrode and, V_A - V_C is the voltage between the ground outer electrode and

cathode. (V_C for electrostatic lenses, and V for magnetic lenses, has the same function, which is to accelerate the electrons.) If the ratio $\frac{V_A - V_L}{V_A - V_C} = \mathcal{V}_{LC}$ remains the same, the lens properties are not affected by changes in V_L and V_C. (Small relativistic effects are being ignored here in both magnetic and electrostatic focusing.) In principle, chromatic aberration due to fluctuations in V_L or V_C can be avoided by deriving V_L from V_C by means of a voltage divider, where fractional changes in V_C are automatically compensated by equal fractional changes in V_L. To compensate fluctuations in magnetic lenses the fractional changes in I should be one-half the fractional changes in V.

Chromatic aberration due to changes in $P = \frac{(NI)^2}{V}$ or $\mathcal{V}_{LC}$ is illustrated for z_0' in Equation (7.1) for magnetic lenses, and in Equation (7.2) for electrostatic lenses:

$$\Delta z_0' = -C_C' \frac{\Delta P}{P} = -C_C' \frac{\Delta\left[(NI)^2/V\right]}{\left[(NI)^2/V\right]} \qquad (7.1)$$

$$= C_C'\left(\frac{\Delta V}{V} - \frac{2\Delta I}{I}\right),$$

$$\Delta z_0' = -C_C' \frac{\Delta \mathcal{V}_{LC}}{\mathcal{V}_{LC}} = -C_C' \frac{\Delta(V_L/V_C)}{V_L/V_C} \qquad (7.2)$$

$$= C_C'\left(\frac{\Delta V_C}{V_C} - \frac{\Delta V_L}{V_L}\right)$$

Equation (7.1) shows that, for small fluctuations, ΔP and $\Delta z_0' = 0$ when $\Delta V/V = 2\Delta I/I$ (the factor 2 is because the focusing force depends on I^2). An analogous

compensation applies to Equation (7.2) with $\Delta V_C/V_C = \Delta V_L/V_L$. Solving for C_C' under these conditions would give a $\frac{0}{0}$ result. C_C' can be determined most directly by measuring z_0' vs. accelerating voltage at constant lens current ($\Delta I = 0$) or constant lens voltage ($\Delta V_L = 0$), and using the slope of the graph to determine $\Delta z_0'$ for a given voltage increment. This corresponds to the usual way of defining C_C' in terms of $\Delta V/V$ or $\Delta V_C/V_C$. However, in making experimental measurements it is often more convenient to change the lens activation by changing I or V_L, with constant accelerating voltage V or V_C, rather than vice versa as above. In the case of magnetic lenses, the equivalent increment $\Delta V/V$ which would produce the same fractional change in $(NI)^2/V$ as is produced by $2\Delta I/I$ can be used to calculate C_C'. For small increments $-2\Delta I/I$ is equivalent to $\Delta V/V$. For electrostatic lenses, the equivalent increment for $\Delta V_C/V_C$ is $-\Delta V_L/V_L$.

In equations (7.7a) and (7.8a) C_C' relates changes in z_o' to fractional changes in the lens activation, so C_C' has the dimensions of z_o'. In the remaining equations, the aberration coefficients relate fractional changes in the properties to fractional changes in the activations, and the coefficients are dimensionless.

Numerical Values of C_c', μ_c, C_f, and C_g

Magnetic Lenses L_1 and L_2

The chromatic coefficients C_c' and μ_C of the image were obtained from graphs of z_0' and m_0 vs. $P = (NI)^2/V$ in Figures 7.5(a) and (b) for L_1 and Figures 7.7(a) and (b) for L_2. The chromatic coefficients C_f and C_g of the lenses were derived from graphs of

f_0 and g_0 vs. P in Figures 7.6(a) and (b) for L_1 and Figures 7.8(a) and (b) for L_2. The four chromatic coefficients C_c', μ_C, C_f, and C_g for magnetic lenses L_1 and L_2 are listed versus P in Tables 7.11 and 7.12, and are shown as graphs vs. P in Figures 7.11(a), 7.11(b), 7.11(c), and 7.11(d) for L_1 and Figures 7.12(a), 7.12(b), 7.12(c), and 7.12(d) L_2.

Current (AmpTurns)^2/ milliamps	Volt	C_f	C_g	μ_c'	Cc'/cm
400	83.7	0.700	0.814	0.704	0.086
350	64.1	0.777	0.843	0.782	0.109
250	32.7	0.891	0.908	0.900	0.209
200	20.9	0.932	0.938	0.945	0.328
180	17.0	0.945	0.949	0.961	0.407
150	11.8	0.962	0.964	0.985	0.593
130	8.8	0.972	0.973	1.003	0.802

Table 7.11. Table for L_1 with selected data points from tables generated from the chromatic aberration equations for C_f, C_g, $\mu c'$, and C_C'.

Current (AmpTurns)^2/ milliamps	Volt	C_f	C_g	μ_c'	Cc'/cm
400	83.7	0.537	0.786	0.543	0.157
350	64.1	0.662	0.804	0.670	0.185
250	32.7	0.839	0.875	0.852	0.322
200	20.9	0.900	0.914	0.919	0.489
180	17.0	0.919	0.929	0.943	0.601
150	11.8	0.944	0.949	0.978	0.868
130	8.8	0.959	0.961	1.003	1.170

Table 7.12. Table for L_2 with selected data points from tables generated from the chromatic aberration equations for C_f, C_g, $\mu c'$, and C_C'.

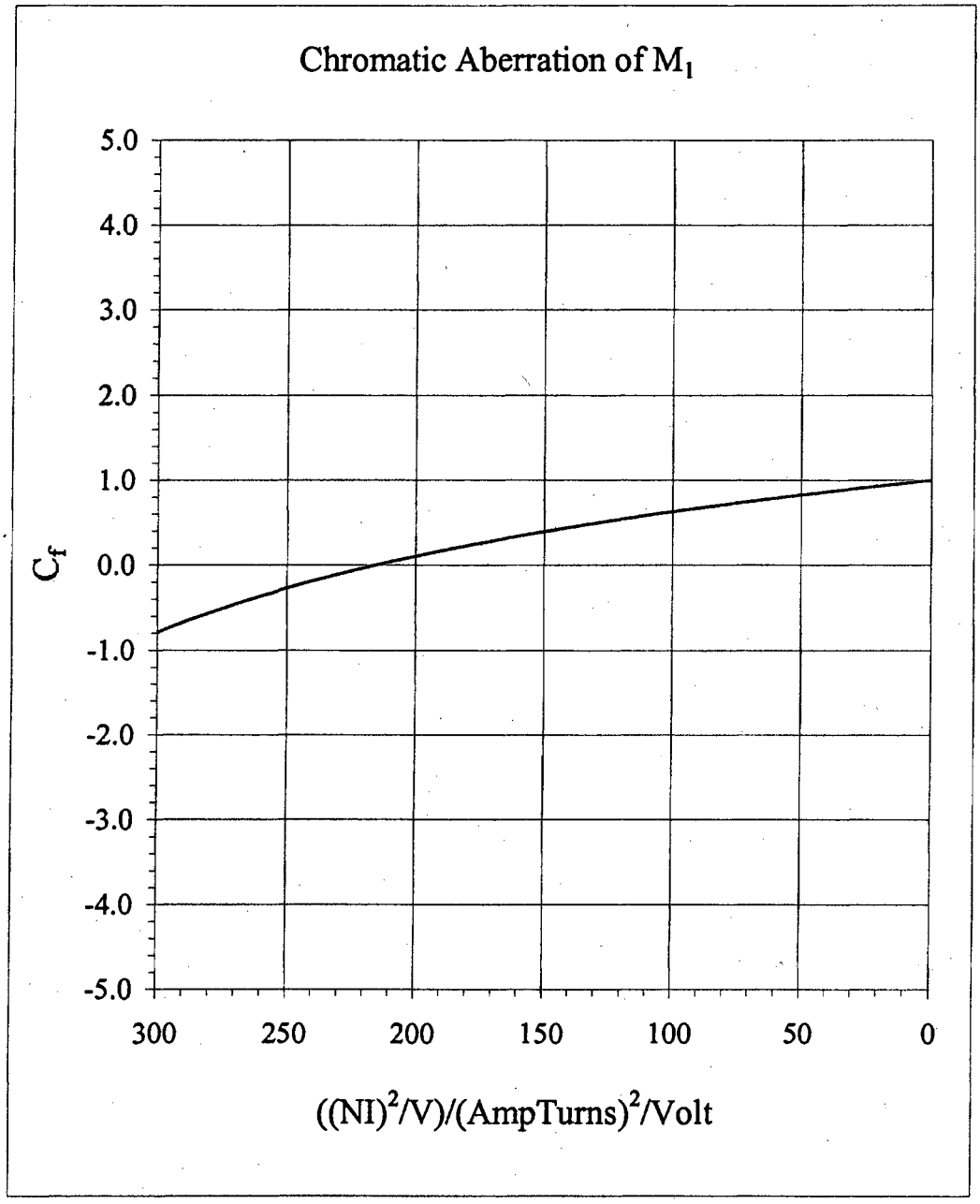

Figure 7.11(a). C_f versus $(NI)^2/V$ for M_1.

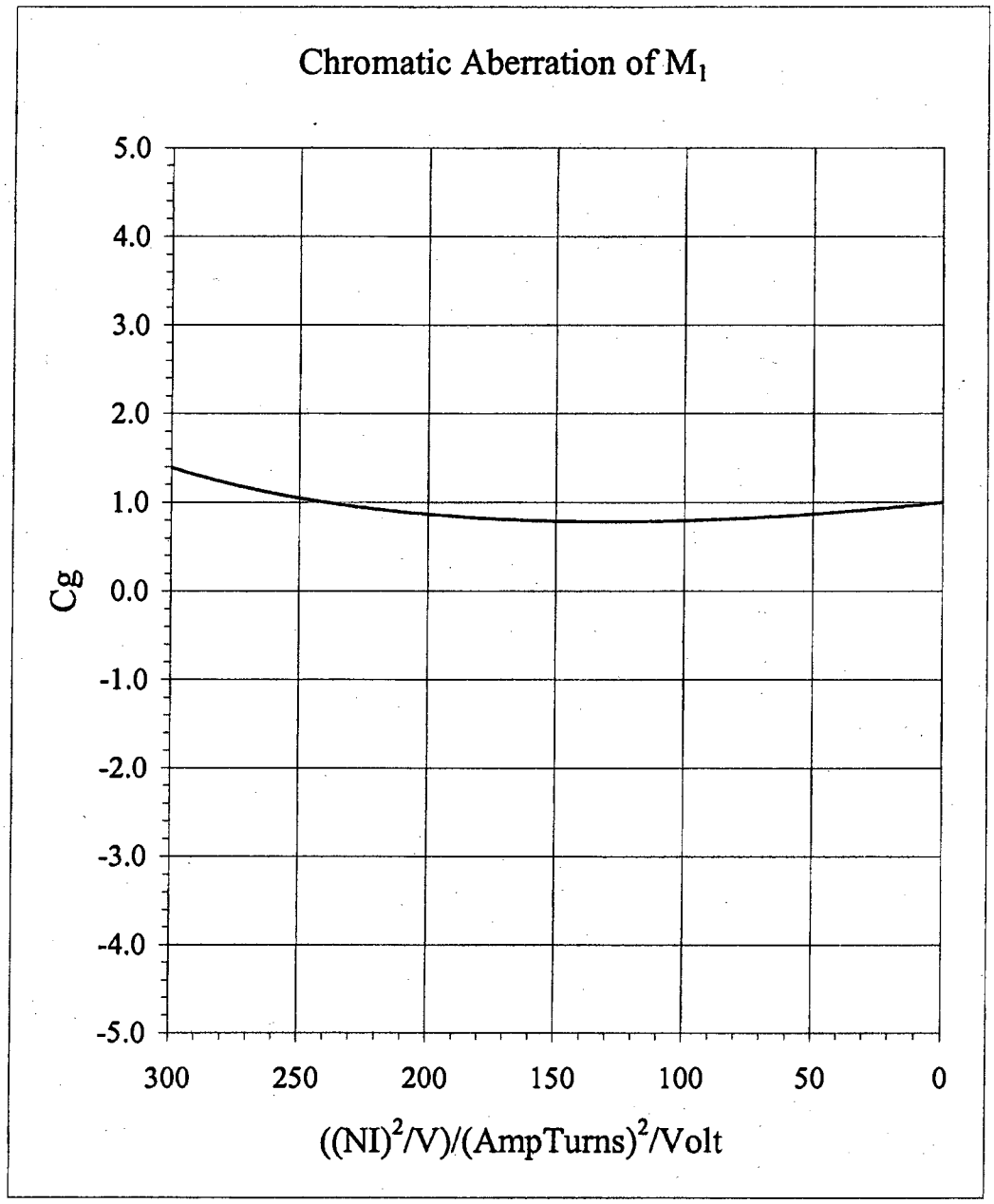

Figure 7.11(b). C_g versus $(NI)^2/V$ for M_1.

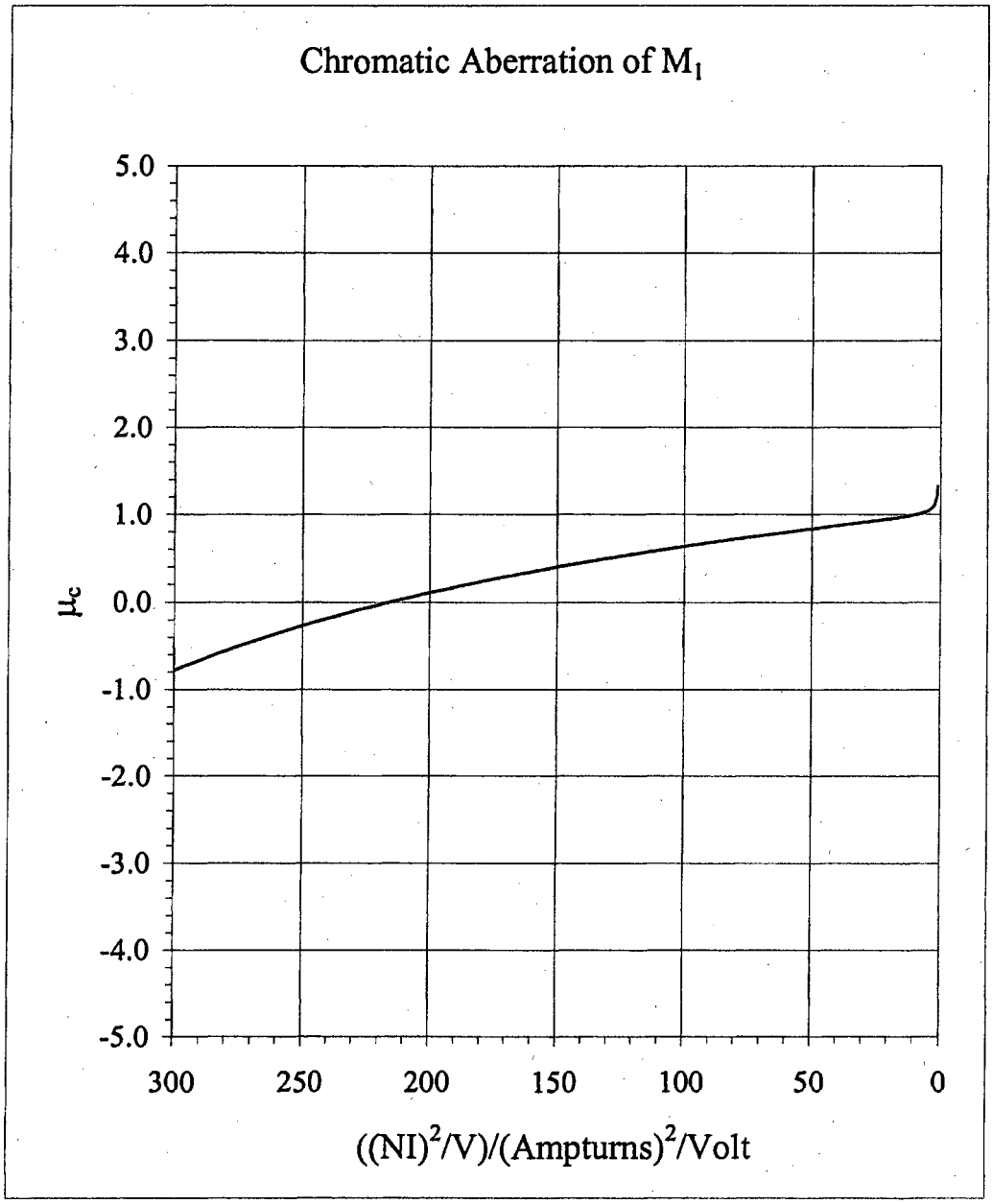

Figure 7.11(c). μ_C versus $(NI)^2/V$ for M_1.

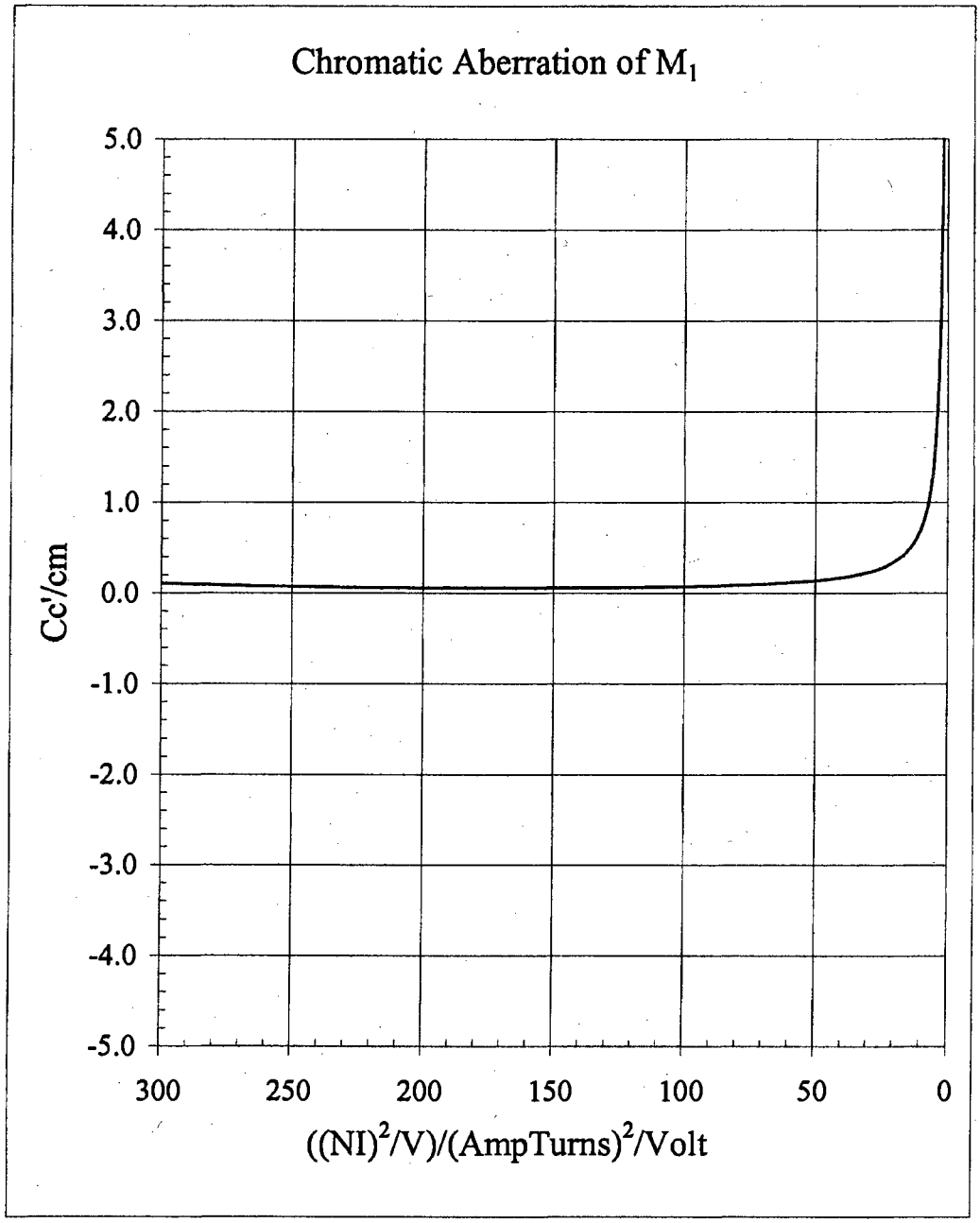

Figure 7.11(d). C_C ' versus $(NI)^2/V$ for M_1.

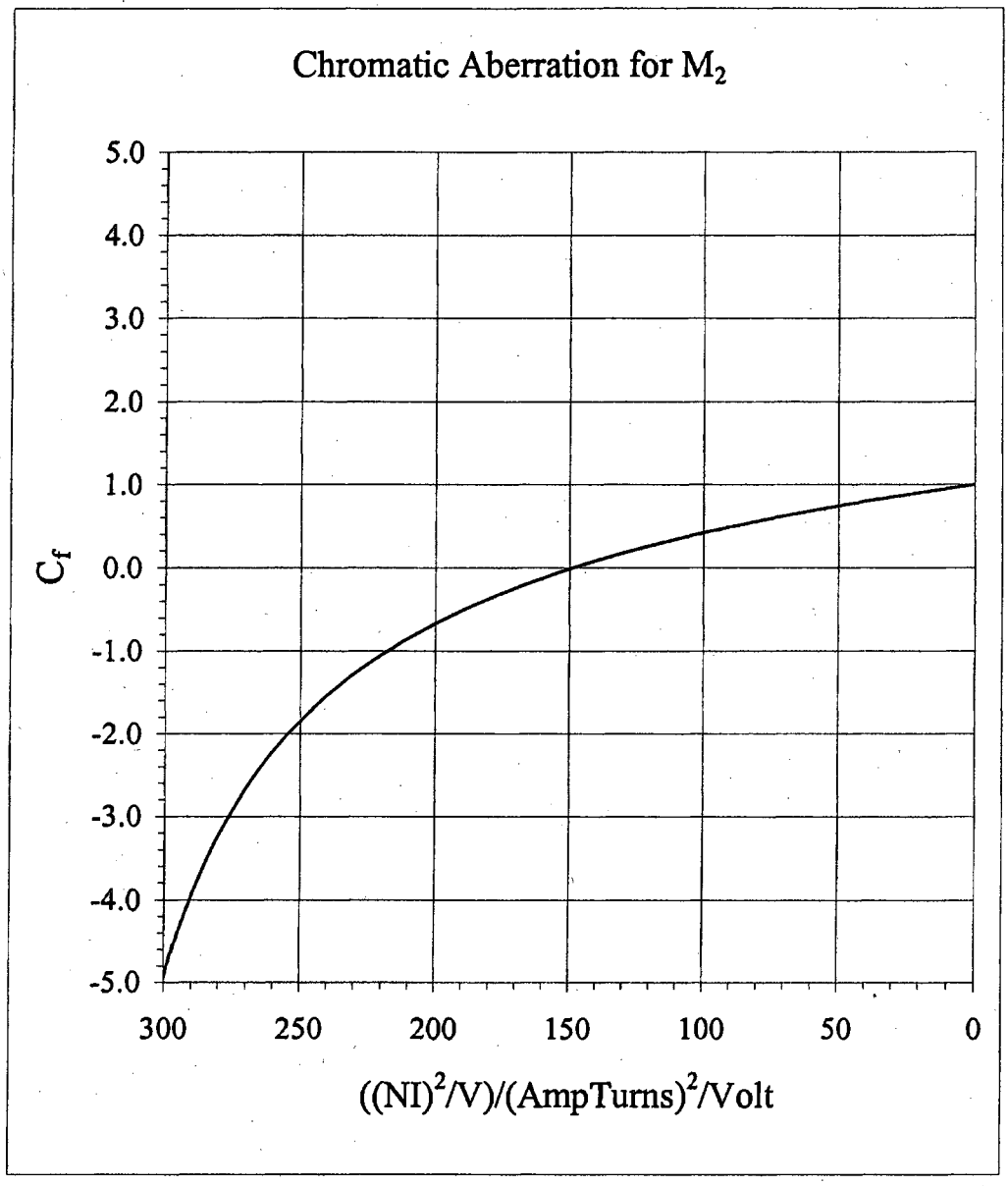

Figure 7.12(a). C_f versus $(NI)^2/V$ for M_2.

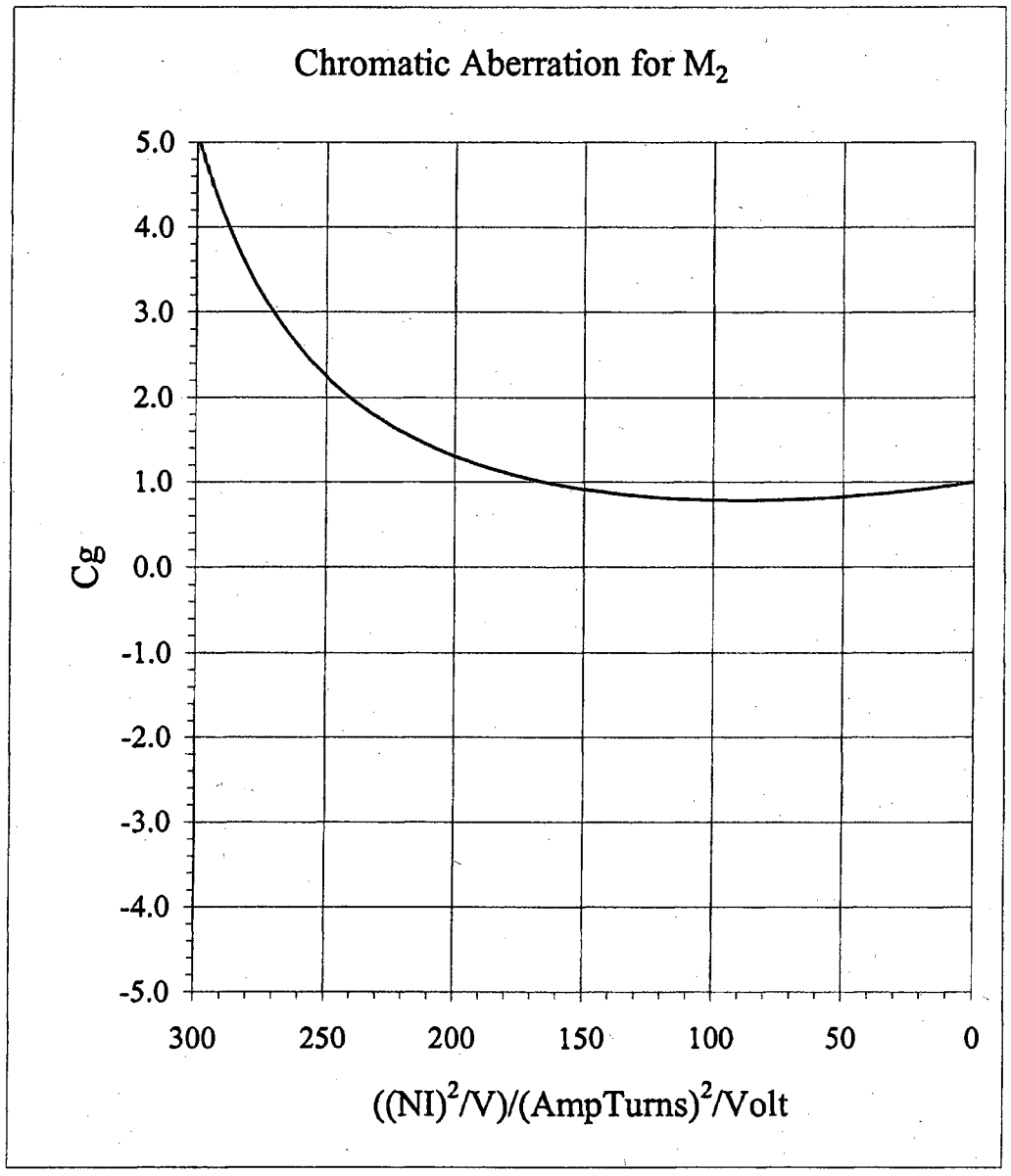

Figure 7.12(b). C_g versus $(NI)^2/V$ for M_2.

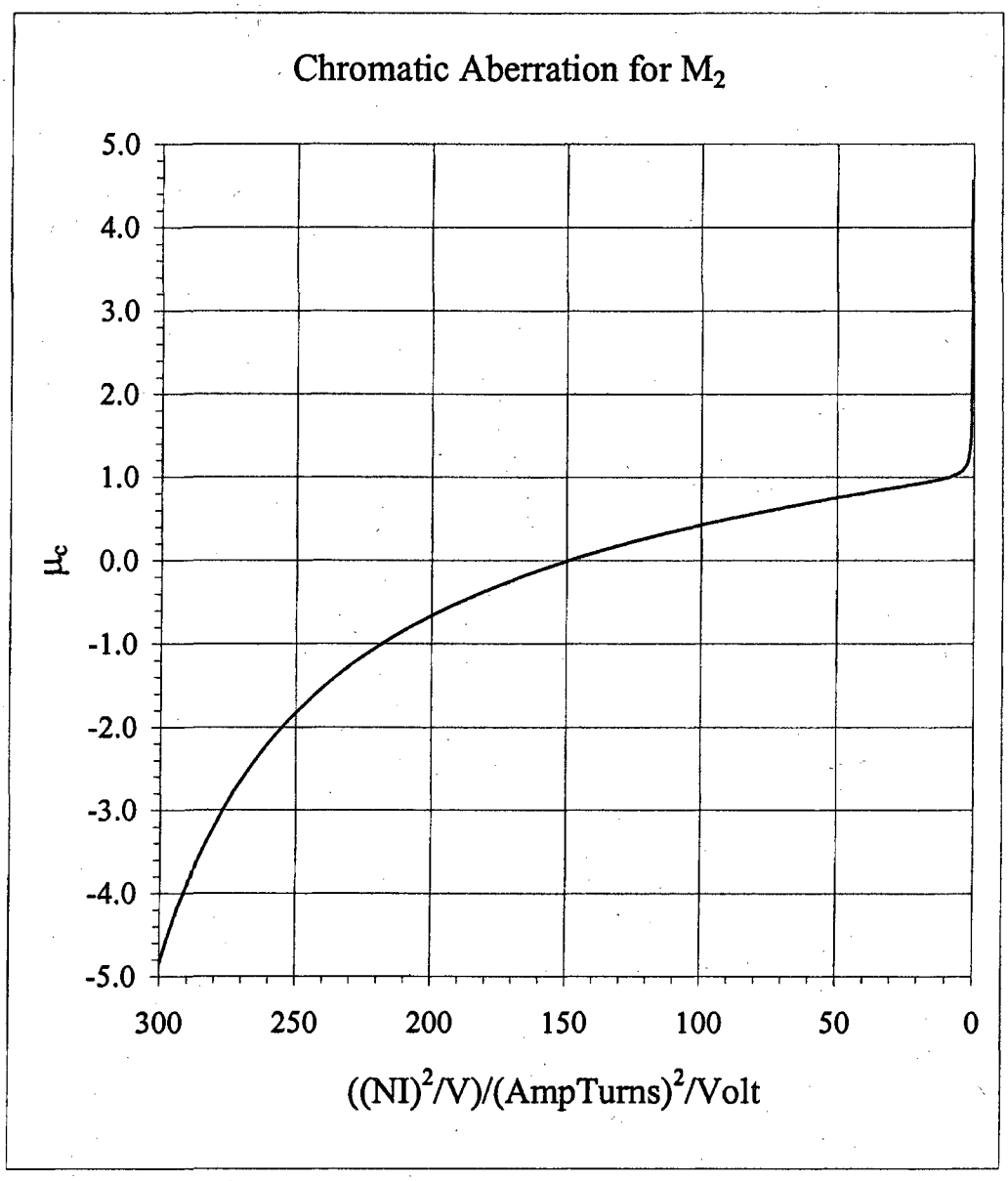

Figure 7.12(c). μ_C versus $(NI)^2/V$ for M_2.

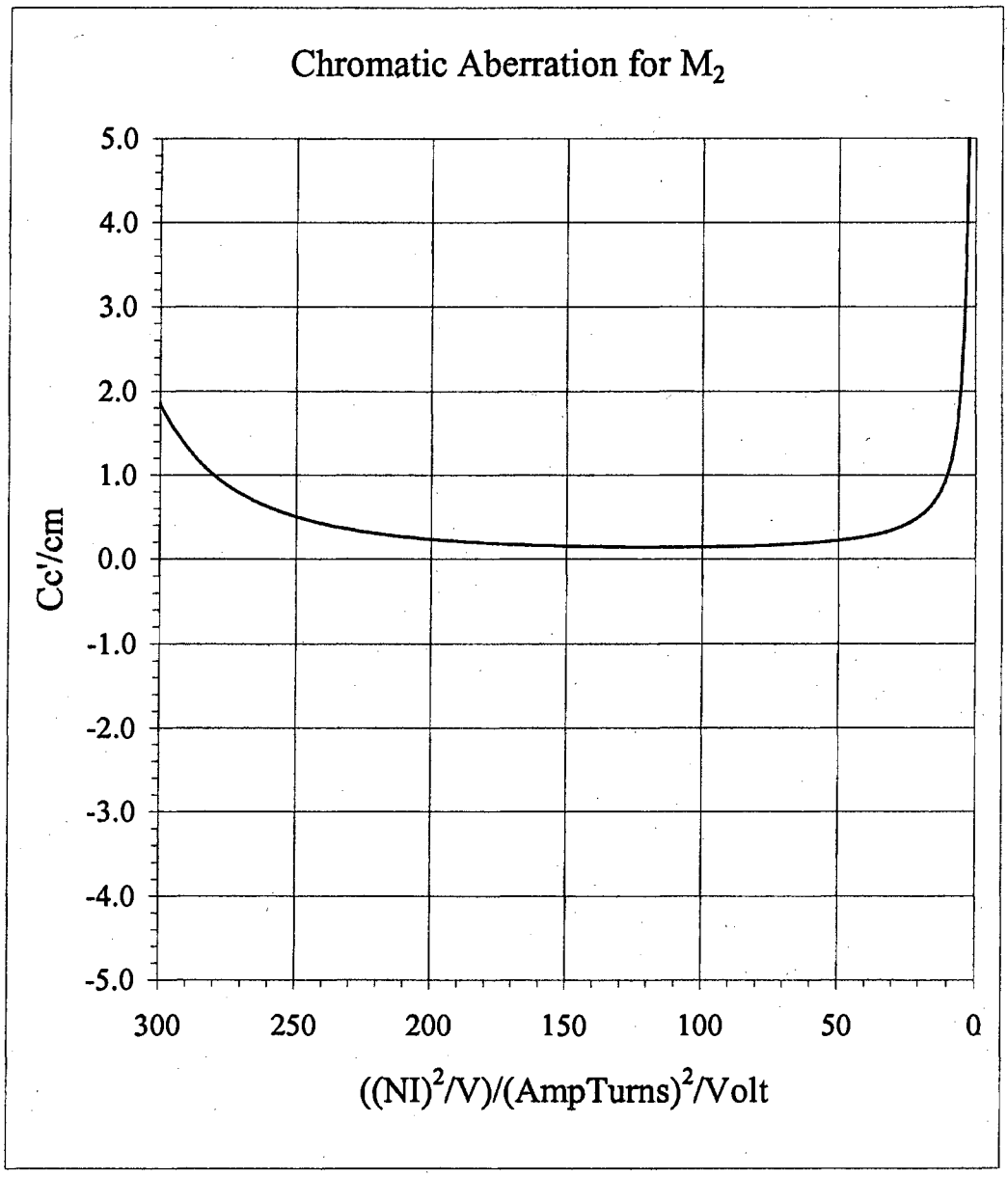

Figure 7.12(d). C_C ' versus (NI)^2/V for M_2.

Electrostatic Lenses L_3, L_4, and L_5

The chromatic coefficients C_c' and μ_C for the electrostatic lenses L_3, L_4, and L_5 were derived from the L_3, L_4, and L_5 graphs of z_0' and m_0 vs. $\mathcal{V}_{LC}$ in Figures 7.9(a) and (b). The chromatic coefficients C_f and C_g of the lenses were derived from the L_3, L_4, and L_5 graphs of f_o and g_o vs $\mathcal{V}_{LC}$ in Figures 7.10(a) and 7.10(b). The values of the four chromatic aberration coefficients C_f, C_g, μ_C, and C_c' for electrostatic lenses M_3, M_4, and M_5 are listed vs $\mathcal{V}_{LC}$ in Tables 7.13(a), 7.13(b), and 7.13(c) for the three model lenses. Each of the four chromatic aberration coefficients is shown in graphs vs. $\mathcal{V}_{LC}$ for the three lenses in Figures 7.13a, 7.13b, 7.13c, and 7.13d.

Table 7.13 (a) M_3

V_L/V_C	C_f	C_g	μ_c'	Cc'/cm
1.00	3.38	3.68	3.46	1.86
0.95	3.35	3.53	3.43	2.13
0.90	3.31	3.42	3.41	2.49
0.80	3.27	3.29	3.41	3.62
0.70	3.28	3.25	3.50	5.77
0.60	3.39	3.32	3.78	10.69

Table 7.13 (b) M_4

V_L/V_C	C_f	C_g	μ_c'	Cc'/cm
1.00	2.87	2.97	2.97	2.63
0.95	2.83	2.90	2.95	3.01
0.90	2.79	2.84	2.92	3.48
0.85	2.76	2.79	2.91	4.07
0.80	2.72	2.75	2.90	4.83
0.70	2.67	2.68	2.93	7.16

Table 7.13 (c) M_5

V_L/V_C	C_f	C_g	μ_c'	Cc'/cm
1.00	3.04	3.24	3.14	2.45
0.95	3.00	3.08	3.10	2.72
0.90	2.95	2.95	3.07	3.08
0.80	2.85	2.76	3.01	4.12
0.70	2.78	2.62	2.99	5.88

Tables 7.13(a)-(c). Chromatic aberrations and V_L/V_C for Lenses L_3, L_4, and L_5. These are selected data points from the corresponding equation models

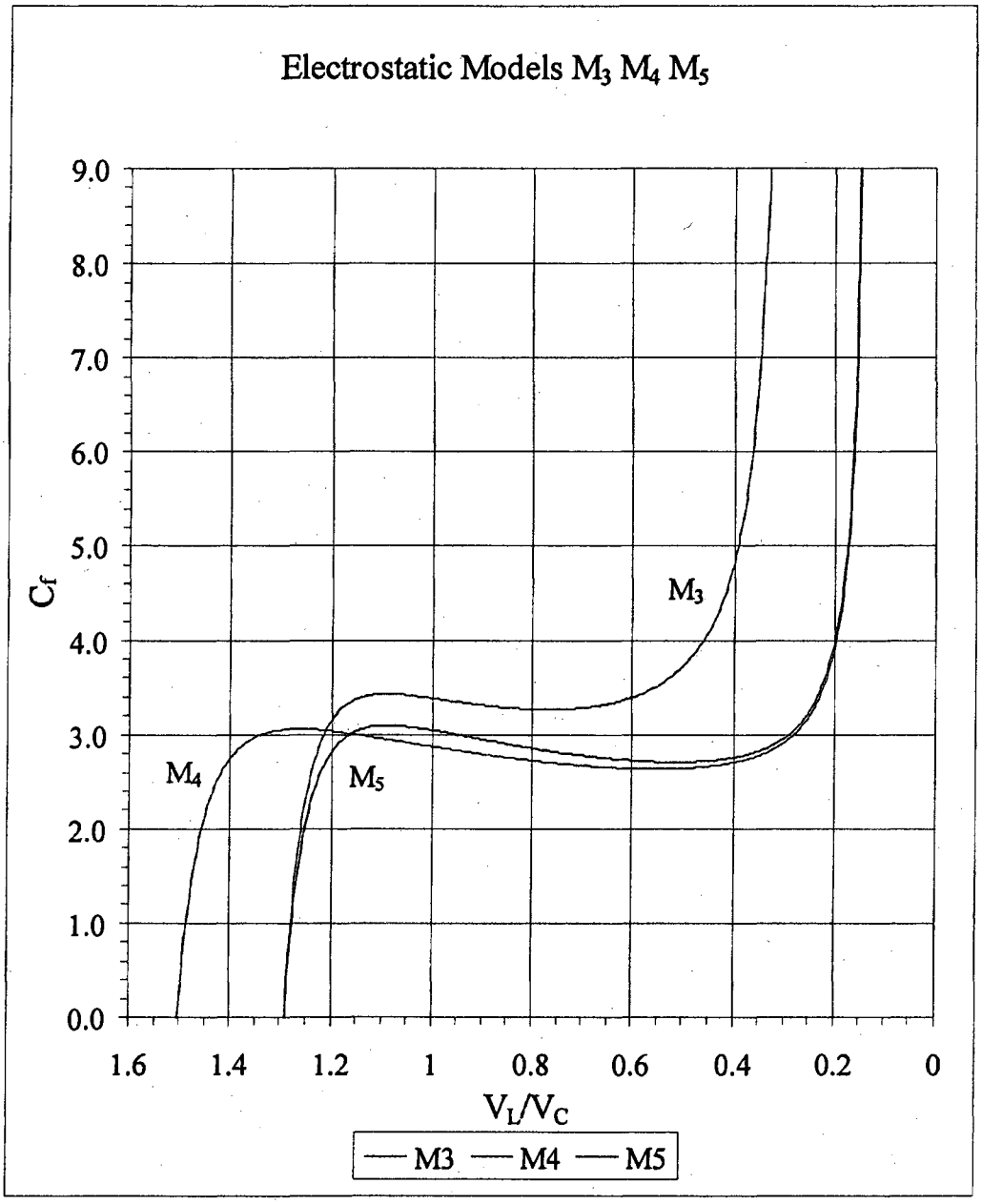

Figure 7.13(a). Chromatic C_f versus V_L/V_C model curves M_3, M_4 and M_5

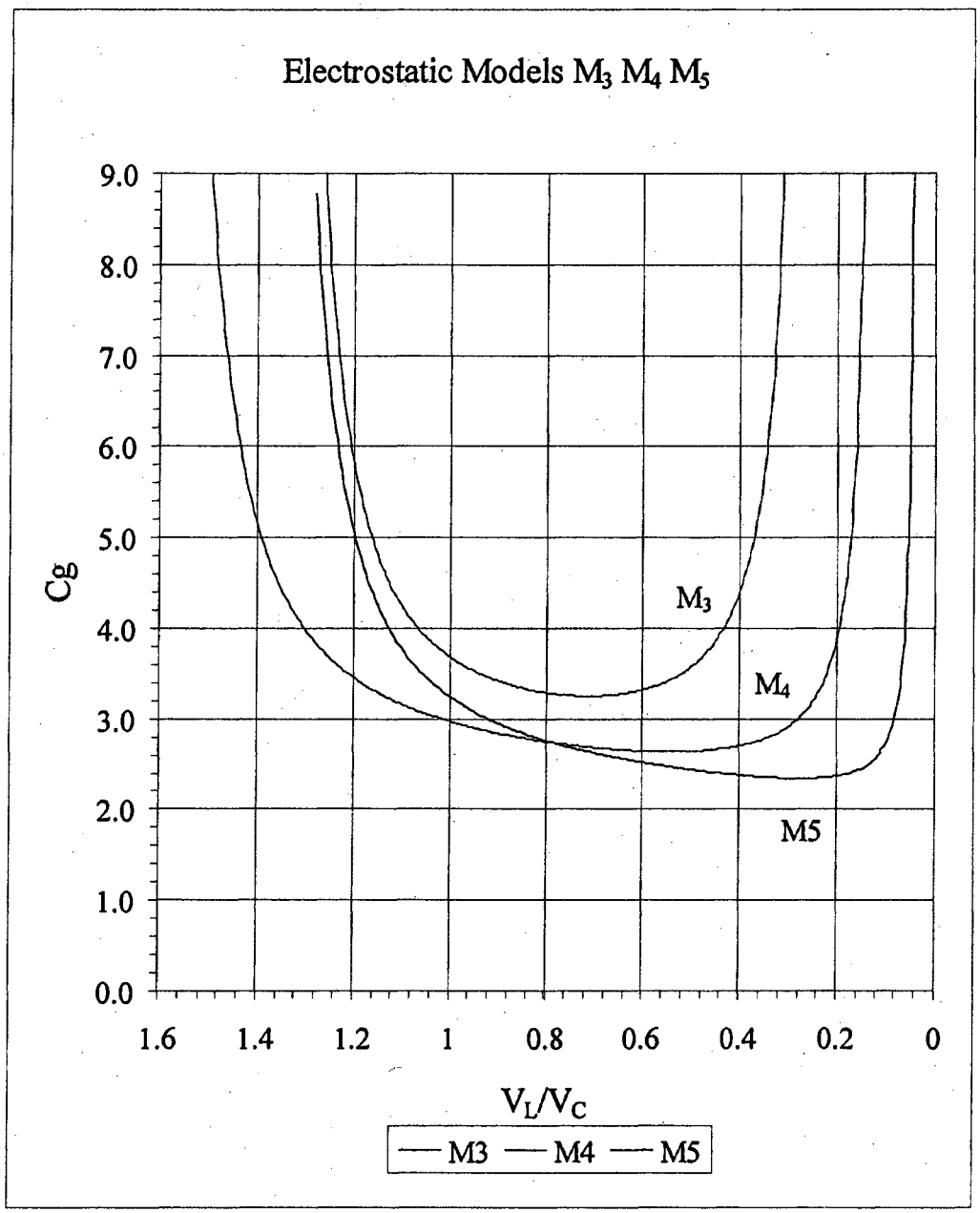

Figure 7.13(b). Chromatic C_g versus V_L/V_C model curves M_3, M_4 and M_5

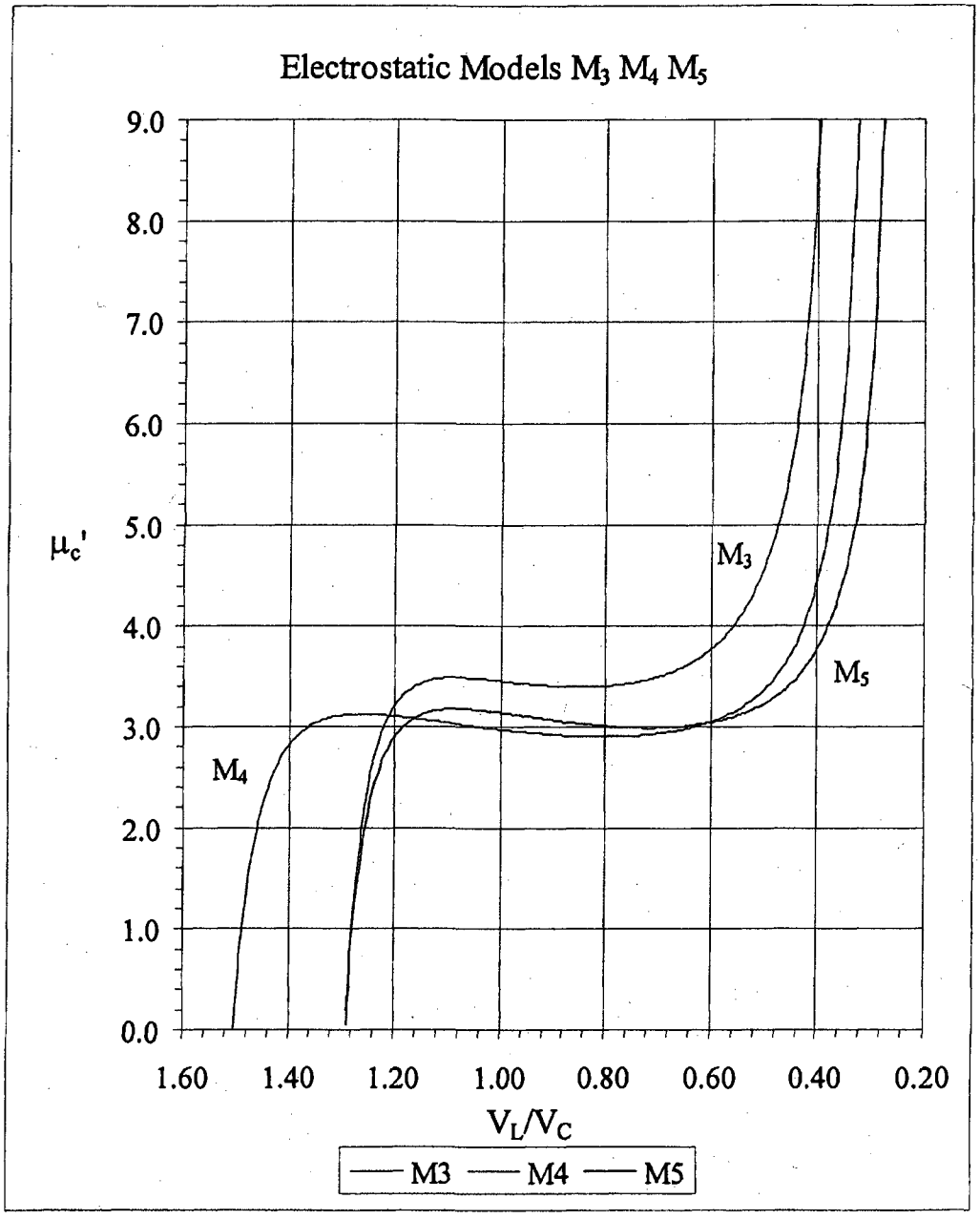

Figure 7.13(c). Chromatic μ_C versus V_L/V_C model curves M_3, M_4 and M_5.

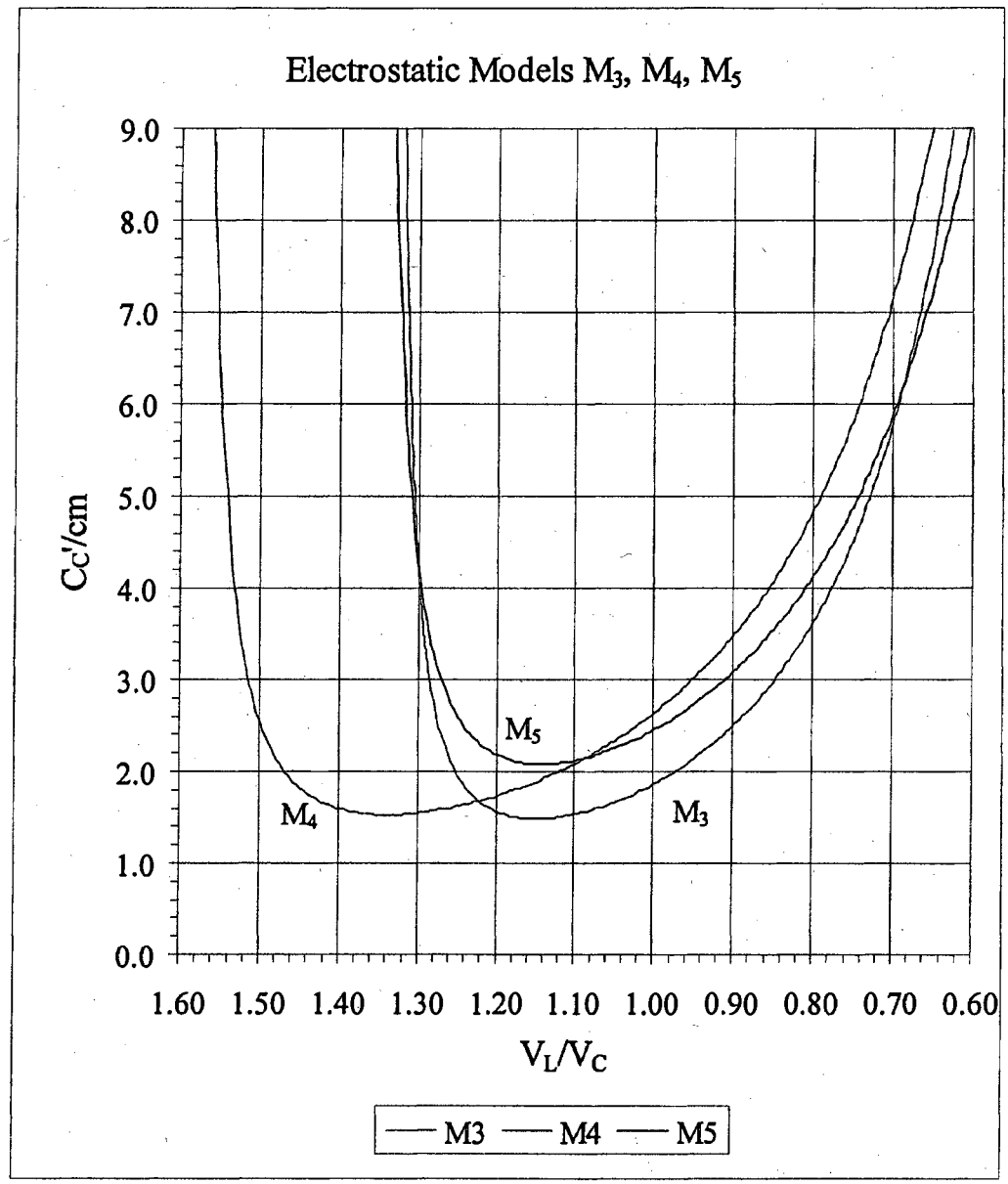

Figure 7.13(d). Chromatic C_C' versus V_L/V_C model curves M_3, M_4 and M_5.

Chapter 8. Magnetic and Electrostatic Lenses as Objectives in a Scanning Electron Microscope

The scanning electron microscope (SEM) is the most appropriate instrument in which to compare the aberrations of magnetic and electrostatic lenses (See Chapter 1). Electrostatic and magnetic lenses differ in two respects, which affect the capability of some instruments to compare the lenses equally. One difference is that electrostatic objective lenses require the specimen to be external to the lens, whereas magnetic objective lenses can accept most specimens inside the lens field. This difference makes possible shorter focal lengths and lower aberration coefficients for magnetic than for electrostatic lenses in high-resolution transmission electron microscopes (TEMs). Under these conditions, the TEM cannot compare electrostatic and magnetic lenses equally.

Another difference between the two types of lenses is that the focal properties of magnetic lenses depend on the charge-to-mass ratio of the charged particles being focused, whereas the focal properties of electrostatic lenses are independent of the charge-to-mass ratio (except for small relativistic effects). Thus, aside from the impractically long focal lengths, which magnetic lenses have for ions, a comparison in an ion-focusing system, such as a focused-ion-beam (FIB) instrument, is not suitable for magnetic lenses.

The forgoing limitations discussed do not affect the comparison of electrostatic and magnetic lenses in SEMs where the specimen is external to the lenses and the charged particles are electrons. In SEM the objective lens focuses the electron beam

into a fine probe which is used to scan the surface of a sample. The electron probe creates secondary electrons or other effects, which act as signals, enabling an image to be constructed, based on the position and intensity of the signal as the probe scans. The resolution in the image is limited by the aberrations of the probe. The paraxial and aberration properties of the probe can be found experimentally by the shadowgraph method described in Chapter 3.

Alternatives to SEM for comparing the aberrations of magnetic and electrostatic lenses are photoelectron microscopy (PEM) and other forms of emission microscopy. However, in emission microscopy it is usually not feasible to test for aberrations in the probe mode (where the direction of the electron beam through the optical system is reversed) because the electron velocities after deceleration are close to zero. Instead, the focal properties and aberrations of the objective lens can be found separately and then combine the found aberrations of the objective lens with the aberrations calculated for the field that accelerates the electrons emitted from the specimen.

In SEM, a decelerating field between the lens and the sample can be used because it leaves the electrons with sufficient kinetic energy to create an effective probe. The shadowgraph method in this case includes the aberrations of the field as well as those of the lens. The required experimental set-up is more complicated with a field between the lens and the sample than it is without a field. We have chosen the simpler arrangement for studying the aberrations of the probe, with the sample in field-free space.

In our experiments, the object for the objective lens is a small source of electrons at a relatively large distance from the lens. Each test lens in turn serves as the objective lens, and is used to form a demagnified image of the source. Please refer to Figure 3.1(a) or (b) in Chapter 3. The imaging properties determined for the lenses represent the way the lenses would focus the un-deflected electron beam if incorporated in an SEM having the same object distance (i.e, pinhole source distance) z. The pin-hole source distances were measured to the optical centers (o.c.)s of the lenses. The tests were carried out for a range of lens activations. The electrostatic lenses were selected so that the electron-optical geometries and paraxial properties of the electrostatic lenses at least partially overlapped those of the magnetic lenses.

Graphs of the image aberration coefficients C_s' and C_C' versus working distances (WD) are used to compare the performances of the different lenses. The specimen surface is assumed to be in the paraxial image plane at z_0'. The working distance is the difference between the paraxial image distance z_0', measured from the lens o.c., and the lens half-length z_L' from the lens o.c. to the outside face of the lens on the specimen side; i.e., $WD = z_0' - z_L'$.

Experimental Graphs of C_s' vs. WD

Sets of image properties z_0' and C_s' versus lens activation, along with the values of z_L', were used in constructing the C_s' vs. WD graphs. Using the curves of z_0' versus lens activation the values of z_0' corresponding to selected values of WD were used to determine the corresponding lens activation. C_s' for magnetic lenses L_1 and L_2 were found from graphs of z' vs α^2 found in the data sheets in the Appendix-A for

those lenses. Values for z_0' and C'_S from the upstream and downstream data sheets for each activation were found and averaged to give the z_0' and C'_S for that activation. In some cases, only the down stream data was available. This data was assembled in Tables 7.1(a-c). L_1 and L_2 were compared at the acceleration voltage of 20 kV. The tables for L_1 include the data for the 15 kV and 25 kV acceleration voltages, as a check on the accuracy with which the three sets of data with different accelerating voltages would fall on the same curve plotted versus $(NI)^2/V$.

The z_0' and C'_S data for L_1 are plotted in graphs vs. activation parameter $P = (NI)^2/V$ in Figures 7.5(a) and 7.5(c) of Chapter 7 and Table 7.7 provided the values for the magnetic lens L_2 and plotted in Figures 7.7(a) and 7.7(c). The values of z_0' and C_s' for the electrostatic lenses L_3, L_4, and L_5 were found the same way as the magnetic lenses and placed in Tables 7.9 (a-c) and graphed vs. the electrostatic activation $\mathcal{V}_{LC} = \frac{V_L}{V_C}$ shown in Figures 7.9(a) and 7.9(c) of Chapter 7.

The working distance (WD) between the lens and the specimen was obtained from the difference $z'_0 - z'_L$. The data points for the C_s' vs. WD graphs are given in Table 8.1(a), along with the values of z'_0 for lenses L_1 and L_2. The distances z'_L is given on the side of each data set. The data points for the C_s' vs WD graphs are given in Table 8.1(b) for the Lenses L_3, L_4, and L_5 with their half-lengths z'_L.

L1 Magnetic Lens with 0.05 inch gap @ 20 kV.

Center of lens to out side of lens 3.175 mm

20000 kV Turns 3235

Activation $(NI)^2/V$	Current milliamps	z_0' cm	Working Dist. /mm	C_s/cm
83.7	400	0.094	-2.231	0.213
64.1	350	0.123	-1.942	0.265
32.7	250	0.224	-0.936	1.097
20.9	200	0.330	0.125	3.14
17.0	180	0.410	0.930	5.29
11.8	150	0.578	2.602	16.0
8.8	130	0.747	4.299	33.8

z_L' = 0.3175 cm

$z_t = z_L' - 0.254$cm

z_t = 0.0635 cm

L2 Magnetic Lens with 0.1 inch gap @ 20 kV.

Center of lens to out side of lens 3.81 mm

20000 kV Turns 3235

Activation $(NI)^2/V$	Current milliamps	z_0' cm	Working Dist. /mm	C_s/cm
64.1	350	0.166	-2.153	0.373
47.1	300	0.229	-1.518	0.700
32.7	250	0.300	-0.807	1.32
20.9	200	0.480	0.994	4.27
17.0	180	0.562	1.812	6.71
11.8	150	0.868	4.872	23.26
8.8	130	1.164	7.831	53.22
5.2	100	1.789	14.082	179

z_L' = 0.381 cm

$z_t = z_L' - 0.254$cm

z_t = 0.127 cm

Table 8.1(a). WD and half-lengths distance for the lenses L_1 and L_2.

L3 Elektros Objective Lens			TEM	
Center of lens to out side of lens			3.5052 mm	z_L' = 0.35052 cm
Voltage ratio	z_0' cm	Working Dist. /mm	C_s/cm	$z_t = z_L' - 0.0635$ cm
1.00	0.451	1.003	6.44	z_t = 0.28702 cm
0.95	0.579	2.280	11.8	
0.90	0.748	3.971	22.2	
0.80	1.094	7.434	68.0	
0.70	1.744	13.931	264	
0.60	2.926	25.754	1090	

L4 Pem II Objective Lens			PEM	
Center of lens to out side of lens			3.5052 mm	z_L' = 0.35052 cm
Voltage ratio	z_0' cm	Working Dist. /mm	C_s/cm	$z_t = z_L' - 0.0635$ cm
1.00	0.819	4.680	24.51	z_t = 0.28702 cm
0.95	0.960	6.091	38.07	
0.90	1.143	7.926	61.33	
0.85	1.337	9.864	95.97	
0.80	1.633	12.823	188.25	
0.70	2.378	20.278	462.41	

L5 Swept back Interface Lens				
Center of lens to out side of lens			4.445 mm	z_L' = 0.4445 cm
Voltage ratio	z_0' cm	Working Dist. /mm	C_s/cm	$z_t = z_L' - 0.0635$ cm
1.00	0.661	2.161	9.52	z_t = 0.381 cm
0.95	0.797	3.529	14.56	
0.90	0.975	5.302	21.96	
0.80	1.447	10.028	60.83	
0.70	2.045	16.001	198.13	

Table 8.1(b). WD and half-lengths distance for the lenses L_3, L_4, and L_5.

Graphs of C_s' vs. *WD* for the five lenses are shown together in Figure 8.1(a). The C_s' curves for the magnetic lenses range from long *WD*s of about 6 mm to negative *WDs*, as the activation parameter $\frac{(NI)^2}{V}$ is increased. At the high-activation ends of the curves, the values of z_0' are virtual. They were obtained by extrapolating

the tangent of field-free electron trajectory into the lens to obtain its crossing point with the axis.

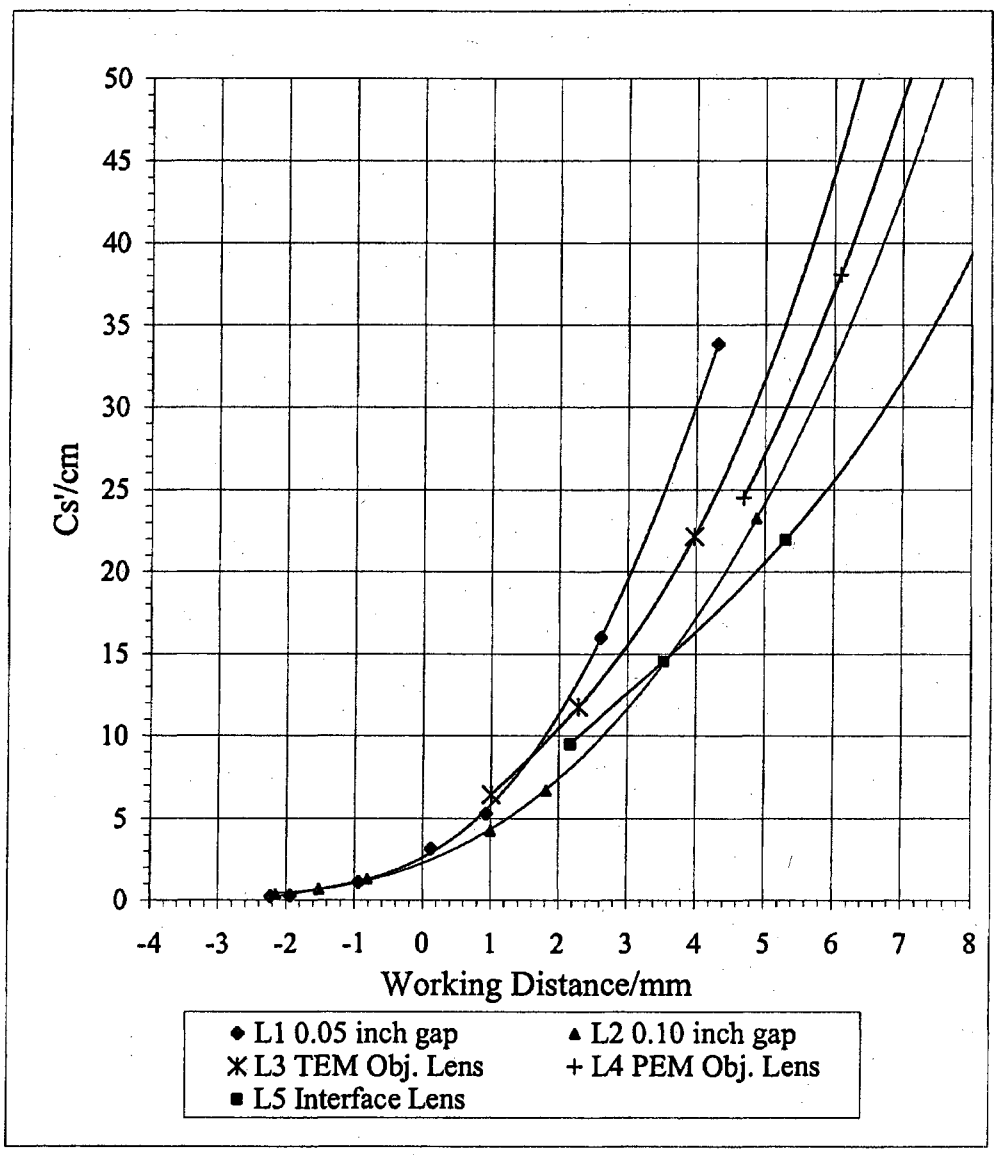

Figure 8.1(a). Graphs of Cs' vs Working Distance (WD) for the five lenses for comparison

The electrostatic lenses are activated from a voltage divider, and their C_s' curves are shown ranging from about 6 mm at the long *WD* end to the values of their

working distances for $V_L/V_C = 1$. (The behavior of the electrostatic lenses at smaller or negative WDs could be explored by using voltage ratios greater than 1, or by using smaller openings in the center electrodes.)

As expected C_s' rises rapidly as *WD* increases and Figure 8.1(a) shows that the C_s' curves for the electrostatic lenses intermingle with those for the magnetic lenses. This result indicates that the spherical aberration properties of the lenses used in this study do not differ appreciably as to type (electrostatic or magnetic). What we found surprising were the large differences in C_s' values for lenses of the same type at given *WD*s, and the crossing over of some curves as *WD* increased. Examples are discussed in the next paragraphs.

For clarity, the curves for the magnetic lenses are shown, separately from the electrostatic curves, in Figure 8.1(b). The shorter-gap magnetic lens L_1 has a smaller C_s' than does the larger-gap magnetic lens L_2 at smaller (in this case, negative) *WD*s (see the magnified insert where the L_1 curve dips under the L_2 curve). The two C_s' curves cross each other at about *WD* = -0.8mm; and at *WD* = 4mm C_s' is larger for L_1 than for L_2 by a difference of (30mm – 17mm =) 13mm (See Insert of Figure 8.1(b) below). In other words, lenses which have the lowest C_s's at short *WD*s are not necessarily the ones with the lowest C_s's at long WDs. The only difference between L_1 and L_2 is the gap length (0.05in. in L_1 and 0.10in. in L_2). Please see Figure 2.1a and the descriptions of L_1 and L_2 in Chapter 2.

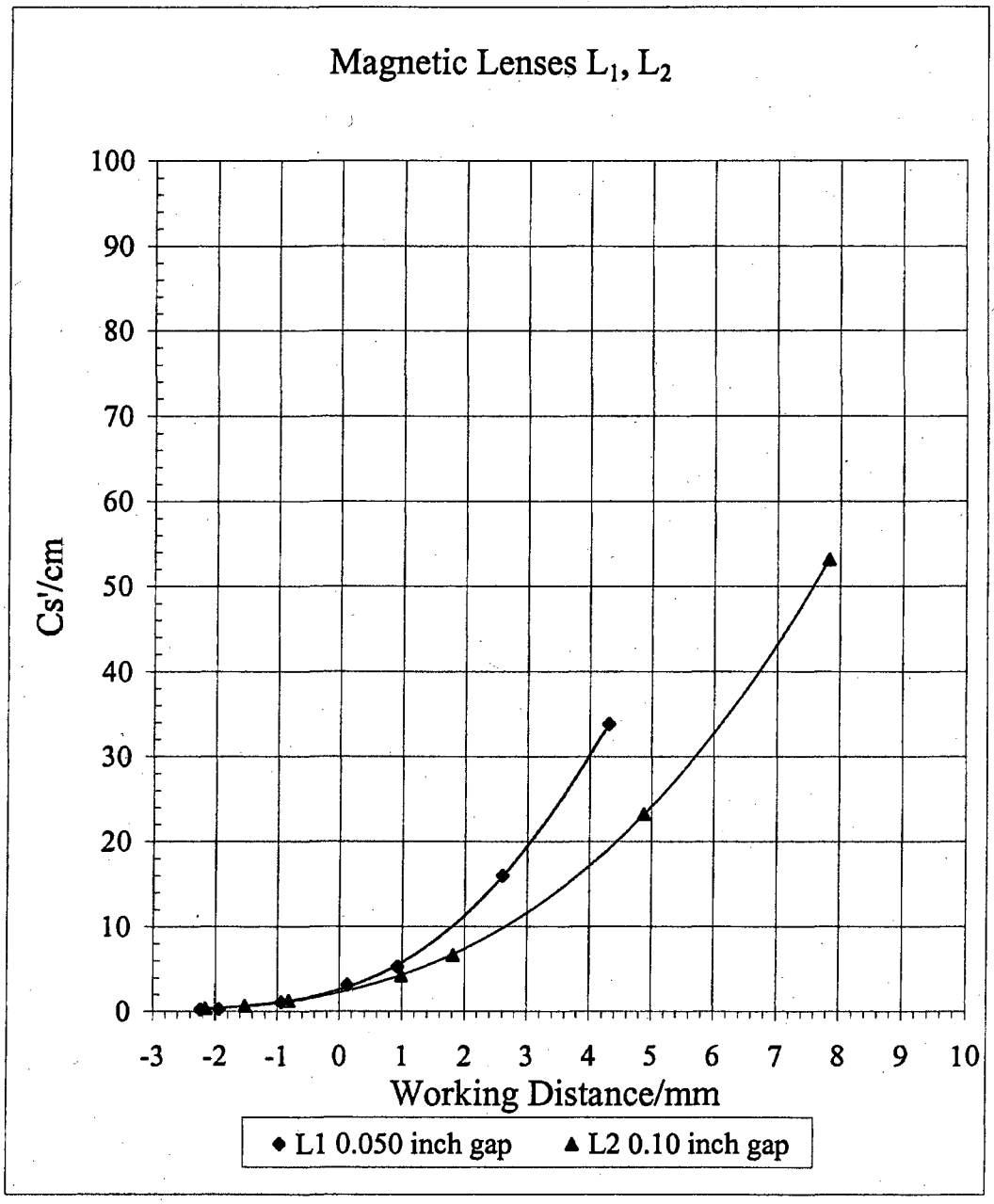

Figure 8.1(b). Cs' .vs. Working Distance (WD) for the two magnetic lenses L_1 with a 0.05-inch gap and L_2 with a 0.10 inch gap between their poles.

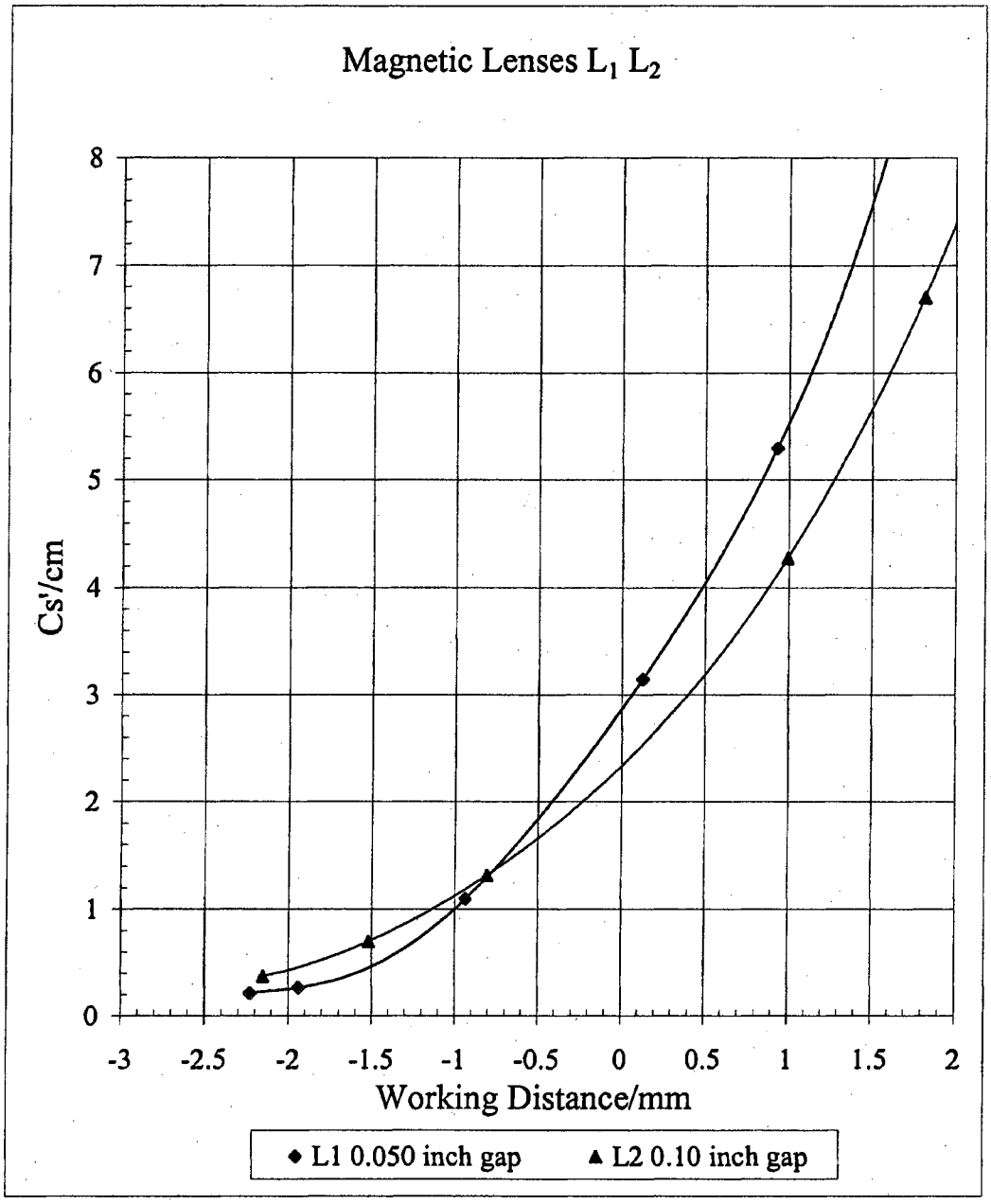

Magnified insert of Figure 8.1(b). A closer look of the magnetic lenses L_1 and L_2 curves to see the crossover.

The comparison between L_1 and L_2 shows that the length of the lens field is an important parameter to take into account in designing an objective lens with the smallest C_s' at the desired working distance.

The three electrostatic lenses L_3, L_4, and L_5 are shown together in a table of their paraxial properties in Figure 7.3. These lenses all have the same type of electrode structure: three parallel electrodes separated by insulating spacers. The center electrode, of thickness t has a central opening of diameter D. Please refer to Figure 2.1b. The sizes of the openings in the outer electrodes, if not too large, have a minor effect on the lens properties. The outer electrodes are grounded and the center electrode is at a negative potential. The only difference between L_3 and L_4 is that D = 0.115in. in L_3, and 0.154 in. in L_4. As a result, for the same voltage ratio, L_4 has a longer WD than does L_3, but the C_s' values for L_4 still fall close to (and slightly under) the extension of the C_s' curve for L_3. This indicates that the diameter of the opening in the center electrode is not very important in changing the course of the C_s' curve; it changes mainly the *WD*-position along the curve. The dimensions of L_5 differ from those of L_3 in several respects: in L_5 D = 0.200in., t = 0.050in., and s = 0.125in., whereas in L_3 D = 0.115 in., t = 0.025in., and s = 0.100in.. The length z_L' from o.c. to outside face of L_5 is 0.175in. compared with 0.138in. for L_3 and L_4. Part of the extra length of L_5 comes from the thicker center electrode. The C_s' vs WD curves in Figure 8.1(c) again show that at longer WDs the lens with the longer field length has a lower C_s'. At WD = 5mm, C_s' for L_3 compared with C_s' for L_5 the difference is about (34mm

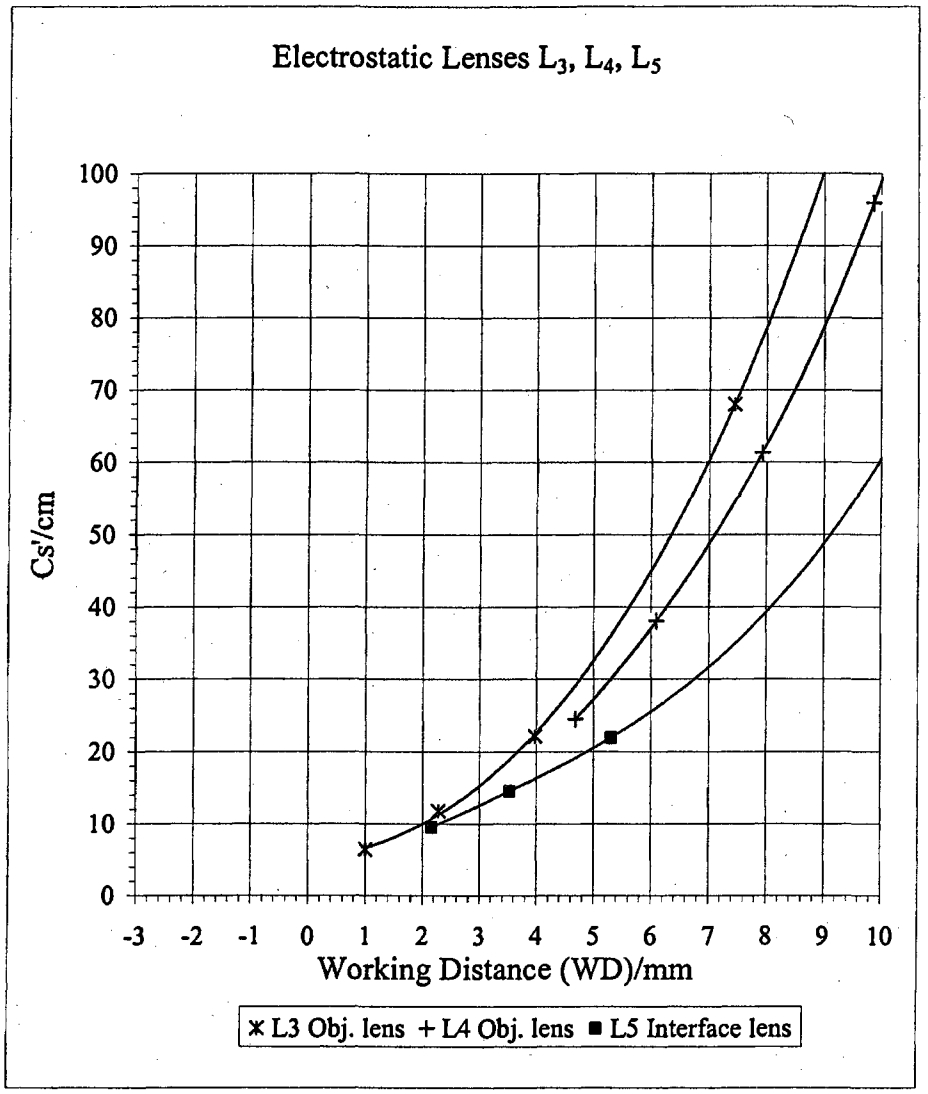

Figure 8.1(c). The Electrostatic Lenses L_3, L_4, and L_5 plots of Cs' vs. Working Distance.

– 22mm =) 12mm. and affirms the conclusion that the field length is an important parameter to consider in designing a lens for a given *WD*.

The finding that C_s' at larger *WDs* is smaller for lenses with longer field lengths is counter-intuitive from one aspect. The reason for this is that lenses with longer field lengths must have longer image distances to achieve a given working distance, and this reasoning, by itself, should lead to a larger, rather than a smaller, C_s'. Another aspect argues in the opposite direction: the longer field length enables the rays going through the lens to be less strongly curved, and to subtract less kinetic energy from the axial motion, and these effects should lead to smaller values of C_s'. The findings of the present experiments indicate that the second aspect has the stronger effect and the net result is a lowering of C_s'. However, such a large dependence on lens-field length was unexpected.

In view of what we have learned about the effects of the lens length on the spherical aberration coefficient, we can say that a fair comparison of magnetic and electrostatic lenses requires not only that the object distance and working distance be the same, but also that each lens length be optimized for the minimum value of C_s' at the chosen working distance. The present work did not extend far enough to find the optimum lens-field lengths as a function of working distance, but the C_s' curves in Figures 8.1(a) to 8.1(b) alerted us to how important the field length is. The curves also show how an erroneous conclusion could be reached about the relative merits of the two types of lenses. If only one example of each type, say L_1 and L_5, were compared at *WD* = 4mm; this could lead to the conclusion that electrostatic lenses have

substantially lower C_s's than do magnetic lenses. On the other hand, comparing L_2 with L_3 could lead to the opposite conclusion. Our research, thus far, indicates that when the lens-field lengths are taken into account the spherical aberration coefficients C_s' are essentially the same. Some consideration of the reason for the strong lens-field effect is given in Chapter 9 in connection with the theoretical lens models.

Experimental Graphs of C_c' vs. *WD*

After the surprises provided by the C_s' vs *WD* graphs, the C_c' vs *WD* graphs are somewhat anticlimactic in that nothing surprising showed up. Sets of image properties z'_0 and C_c', along with the values of z'_L, were used in constructing the C_c' vs. *WD* graphs. The values of z'_0 for the magnetic lenses were taken from graphs of z'_0 vs. $P = (NI)^2/V$ shown in Figure 7.5(a) for L_1 and in Figure 7.7(a) for L_2. The values of z'_0 for the electrostatic lenses L_3, L_4, and L_5 were obtained from graphs vs. the activation parameter $\mathcal{V}_{LC} = V_L / V_C$, shown for the three lenses in Figure 7.9(a) of Chapter 7. The corresponding values of C_c' were obtained from the slopes of the graphs as indicated in Equation (7.-) in Chapter 7. The working distance *WD* is obtained by subtracting z_L' from z_o'. The values of *WD*, z_o', and C_c' for L_1 and L_2 are listed in Table 8.2(a). The values of *WD*, z_o', and C_c' for L_3, L_4, and L_5 are listed in Table 8.2(b). The values of z_L' and z are given in the data bars at the top.

Graphs of C_C' vs. *WD* for the five lenses are shown together in Figure 8.2(a). The high activation ends of the magnetic C_c' graphs extend into the negative *WD* range. The extension of the electrostatic curves into the negative *WD* values was shown only for comparison with the magnetic C_C' vs. WD curves. The highest

activation for the electrostatic lenses in the experimental data was to $\mathcal{V}_{LC} = 1.0$. This corresponded to values of $C_C' = 1.86$ cm at WD = 1.43 mm for L_3, $C_C' = 2.63$ cm at WD = 4.95 mm for L_4, and a $C_C' = 2.45$ at WD = 2.33mm for L_5. The most noticeable result in the range where both sets of graphs are shown is that the chromatic aberration coefficient C_c' is larger for electrostatic lenses than for magnetic lenses. One reason for this difference is that most of the focusing in these "saddle-field" electrostatic lenses takes place near the saddle point, where the beam's voltage is lowest.

L1 Magnetic Lens with 0.05 inch gap @ 20 kV.

Center of lens to out side of lens 3.175 mm

20000 kV Turns 3235

Activation $(NI)^2/V$	Current milliamps	z_0' cm	Working Dist. /mm	C_c/cm
83.7	400	0.096	-2.217	0.086
64.1	350	0.122	-1.957	0.109
32.7	250	0.225	-0.926	0.209
20.9	200	0.343	0.252	0.328
17.0	180	0.420	1.023	0.407
11.8	150	0.600	2.825	0.593
8.8	130	0.798	4.806	0.802

z_L' = 0.3175 cm

$z_t = z_L' - 0.254$cm

z_t = 0.0635 cm

L2 Magnetic Lens with 0.1 inch gap @ 20 kV.

Center of lens to out side of lens 3.81 mm

20000 kV Turns 3235

Activation $(NI)^2/V$	Current milliamps	z_0' cm	Working Dist. /mm	C_c/cm
64.1	350	0.176	-2.055	0.185
47.1	300	0.232	-1.491	0.234
32.7	250	0.323	-0.584	0.322
20.9	200	0.488	1.073	0.489
17.0	180	0.597	2.156	0.601
11.8	150	0.850	4.693	0.868
8.8	130	1.131	7.497	1.170
5.2	100	1.940	15.589	2.076

z_L' = 0.381 cm

$z_t = z_L' - 0.254$cm

z_t = 0.127 cm

Table 8.2(a). The chromatic Cc' with WD and half-lengths distance for the lenses L_1 and L_2. The Cc' values were selected from the analytical models.

L3	Elektros Objective Lens			TEM
	Center of lens to out side of lens			3.5052 mm
	Voltage ratio	z_0' cm	Working Dist. /mm	C_c/cm
	1.00	0.494	1.431	1.86
	0.95	0.596	2.451	2.13
	0.90	0.720	3.698	2.49
	0.80	1.075	7.242	3.62
	0.70	1.687	13.368	5.77
	0.60	2.904	25.532	10.69

z_L' = 0.35052 cm

$z_\ell = z_L' - 0.0635$ cm

z_ℓ = 0.28702 cm

L4	Pem II Objective Lens			PEM
	Center of lens to out side of lens			3.5052 mm
	Voltage ratio	z_0' cm	Working Dist. /mm	C_c/cm
	1.00	0.845	4.950	2.63
	0.95	0.990	6.394	3.01
	0.90	1.165	8.144	3.48
	0.85	1.380	10.295	4.07
	0.80	1.649	12.983	4.83
	0.70	2.437	20.868	7.16

z_L' = 0.35052 cm

$z_\ell = z_L' - 0.0635$ cm

z_ℓ = 0.28702 cm

L5	Swept back Interface Lens			
	Center of lens to out side of lens			4.445 mm
	Voltage ratio	z_0' cm	Working Dist. /mm	C_c/cm
	1.00	0.677	2.328	2.45
	0.95	0.809	3.649	2.72
	0.90	0.965	5.210	3.08
	0.80	1.384	9.392	4.12
	0.70	2.038	15.934	5.88

z_L' = 0.4445 cm

$z_\ell = z_L' - 0.0635$ cm

z_ℓ = 0.381 cm

Table 8.2(b). The chromatic Cc' with WD and half-lengths distance for the lenses L_3, L_4 and L_5. The Cc' values were selected from the analytical models.

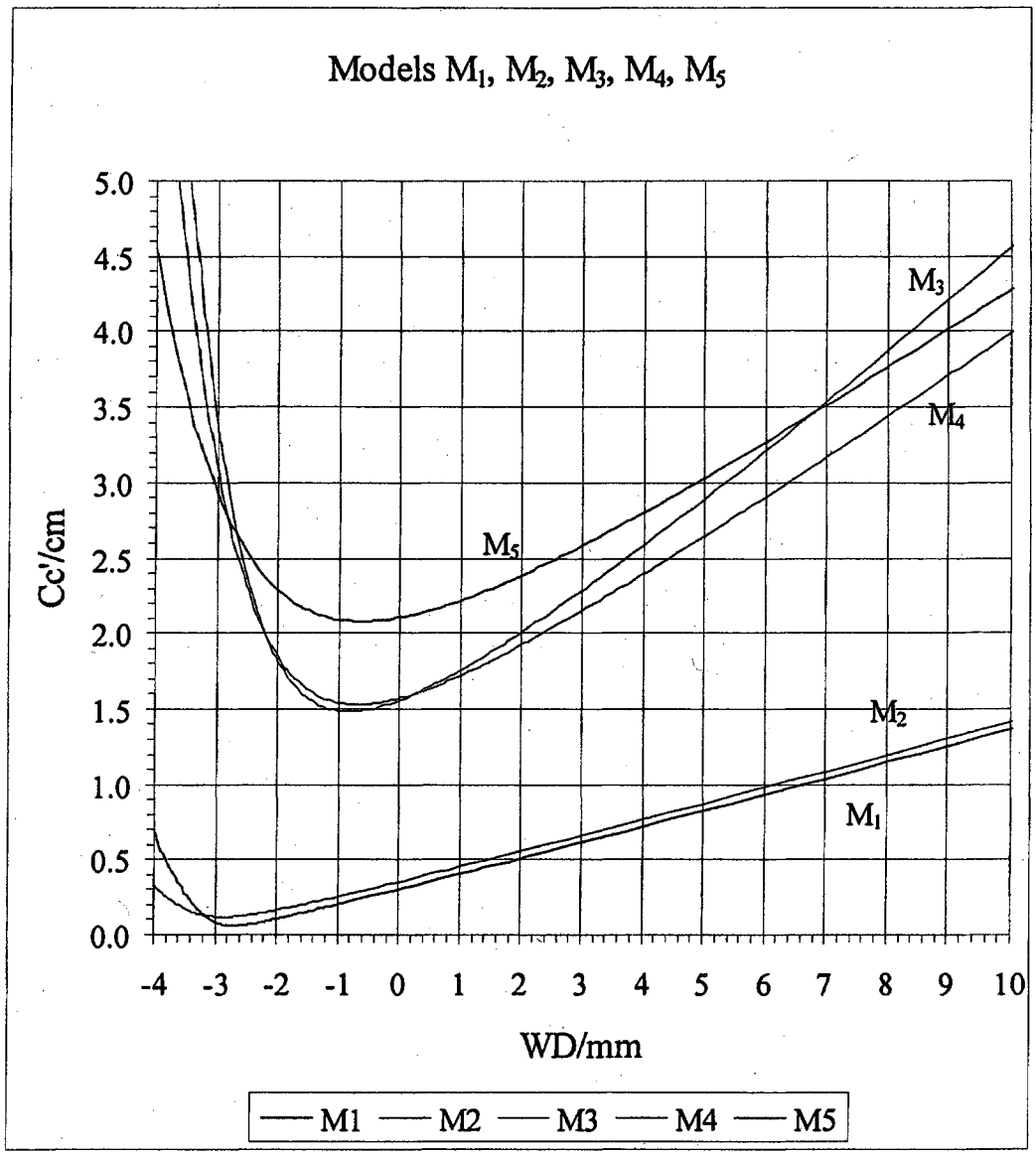

Figure 8.2(a). Chromatic *Cc'* plot of Models M_1-M_5 versus Working Distance shown for comparison.

Chapter 9. Theoretical Models of the Magnetic and Electrostatic Lenses

The designs of the lens models are described, and the theoretical expressions for their focal paraxial properties are determined. Graphs of the paraxial focal properties of the models and of the corresponding lenses are compared under conditions where the effective magnetic field on the axis (in magnetic lenses), or the electric potential at the saddle point (in electrostatic lenses), are the same for the model as for the lens. A number of interesting corollary results of this comparison are discussed and illustrated. The magnetic lens models are discussed in part A; the electrostatic models are discussed in part B.

A. Magnetic Lens Models M_1 and M_2

The geometry of the theoretical magnetic lens models M_1 and M_2 is patterned after magnetic lenses L_1 and L_2 described in Chapter 2. The magnetic models are "Uniform-field" Models, in which the magnetic field in the gap between the bores is assumed to be axial and uniform and to have the same intensity as the field between the surrounding pole-faces. (Ref. 2). The magnetic flux enters the lens through the wall of the entrance bore and leaves the lens through the wall of the exit bore, creating oppositely directed radial components of the magnetic field in the two bores. The model field differs from the field in the actual lens, where the intensity in the gap has a minimum with respect to r on the axis, due to the presence of the bores in the pole-pieces.

A paraxial calculation of an electron trajectory in a magnetic model is presented in Chapter 1 to aid in explaining how magnetic lenses focus charged particles. In brief, a parallel-incident electron acquires a rotary velocity v_{rot} through interaction with the radial field in the entrance bore. At the juncture between the bore and the gap, the field changes from radial to axial. In the gap, the rotary motion is preserved by the centripetal force of the now axial field. The radius of curvature of the circular motion is $r_c = (incident\ radius)\, r_i / 2$, and the angular frequency of rotation is $\omega_c = \frac{qB}{m}$ (the cyclotron frequency). The center of curvature C of the circular path is displaced from the lens axis in the r_i azimuth by an amount equal to r_c, (See Figure 1.2 of Chapter 1). The rotational velocity v_{rot} and the axial velocity $\dot{z}$ combine to create a spiral path for the electron. The spiral axis is normal to the page at C and parallel to the lens axis through *0*. The coordinates of the electron in the spiral, measured from: the spiral axis C, the incident end of the gap z_i, and the incident azimuth r_i) are

$$r_c = \text{constant} = r_i / 2, \quad z = \dot{z}(t - t_i), \quad \text{and} \quad \phi_c = \omega_c (t - t_i). \quad (9.1\text{a,b,c})$$

The electron and its radial and axial coordinates define a meridional plane $\mathcal{M}_c$ containing the electron and the spiral axis. $\mathcal{M}_c$ rotates with the electron about the spiral axis at the ω_c angular rate. In the $\mathcal{M}_c$ plane the electron traces a straight line as a function of time at a distance r_c from the spiral axis. This line becomes the spiral described above in the non-rotating coordinate system.

Another set of coordinates is used to describe the electron's location in a meridional plane $\mathcal{M}$ which contains the electron and the lens axis and rotates about the lens axis at the angular rate $\omega = \frac{\omega_c}{2}$. The electron's coordinates in the $\mathcal{M}$-plane are

$$r = r_i \cos\omega(t - t_i), \qquad z - z_i = \dot{z}(t - t_i), \tag{9.2a,b}$$

and the $\mathcal{M}$-plane's rotation angle is

$$\phi - \phi_i = \omega(t - t_i) \tag{9.2c}$$

. Please see Figure 1.2 of Chapter 1. In the $\mathcal{M}$-plane, the electron traces out a cosine curve as a function of time, as per Equations (9.2a) and (9.2b).

At time $t = t_f$ the electron leaves the gap and enters the exit bore. Two effects of this change are: first, the centripetal force due to the axial field is no longer present to preserve the spiral; and second, the radial component of the magnetic field in the bore cancels the rotational motion of the electron and the $\mathcal{M}$-plane. The final coordinates in the gap, given by Equations (9.3a, 9.3b, and 9.3c), are the initial coordinates for the exit bore,

$$r_f = r_i \cos\omega(t_f - t_i), \tag{9.3a}$$

$$z_f - z_i = \dot{z}(t_f - t_i) = S, \tag{9.3b}$$

$$\phi_f - \phi_i = \omega(t_f - t_i). \tag{9.3c}$$

Also, the final r and z velocities on leaving the gap are the initial velocities for the bore,

$$\dot{r}_f = -\omega r_i \sin\omega\left(t_f - t_i\right) \tag{9.4a}$$

$$\dot{z}_f = \dot{z}' \tag{9.4b}$$

These velocities are now constant, and the angular velocity is zero, since ω is zero for $t > t_f$,

$$\dot{\phi}_f = \omega = 0. \tag{9.4c}$$

The electron, starting at $\left(r_f, z_f\right)$ with slope $\left(-\frac{r_f}{z_f}\right)$, follows a straight line to the focal point F_o' on the axis. See Figure 9.1. The angle at which the electron crosses the axis

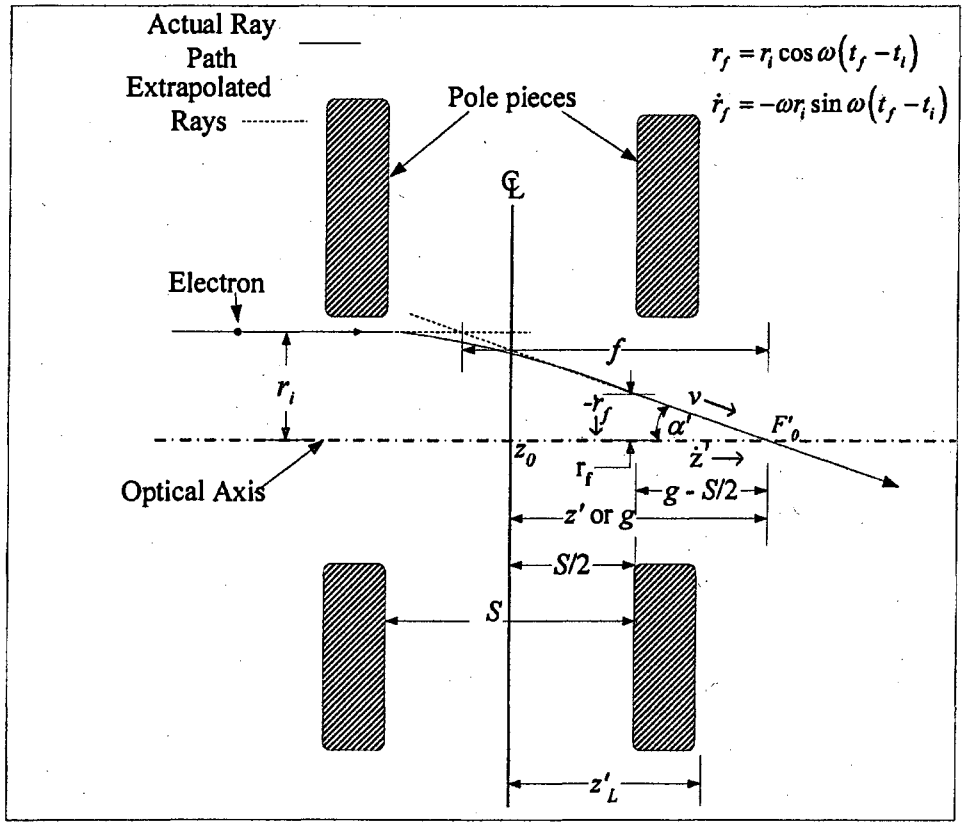

Figure 9.1. Electron exiting from a magnetic lens. For clarity, rotation about the spiral axis is not shown.

is $\alpha' = -\frac{\dot{r}_f}{\dot{z}'}$. The axial distance from the end of the gap at z_f to the focal point is $\frac{r_f}{\alpha'}$.

Paraxial Focal Properties of the Magnetic Models

The straight-line trajectory through F_0', extrapolated backward, intersects the principal surface H' at the height r_i of the incident ray (but in the rotated azimuth ϕ_f). See Figure 9.1. The axial distance from this intersection point to F_0' is $r_i/\alpha' = f_0$, the focal length of the lens. The distance from the center of the lens to the focal point is $\frac{S}{2} + \frac{r_f}{\alpha'} = g_0$, the focal distance. The difference $g_0 - f_0$ is the axial distance h_0 of the intersection point on H' from the center plane of the lens.

Substituting the expressions in Equations 9.3(a-c) and 9.4(a-c) for the coordinates and velocities into the above relationships yields the following equations for the lens properties. Letting $t_S = t_f - t_i$, where $S = z_f - z_i$ is the gap spacing between pole-faces,

$$\alpha' = -\frac{\dot{r}_f}{\dot{z}'} = \frac{\omega r_i \sin(\omega t_S)}{\dot{z}'} = \omega t_S \sin(\omega t_S)\left(\frac{r_i}{S}\right), \tag{9.5a}$$

$$\frac{f_0}{S} = \frac{(r_i/S)}{\alpha'} = \frac{1}{\omega t_S \sin(\omega t_S)} \tag{9.5b}$$

$$\frac{g_0}{S} - \frac{1}{2} = \frac{(r_f/S)}{\alpha'} = \frac{(r_i/S)\cos(\omega t_S)}{(r_i/S)\omega t_S \sin(\omega t_S)}, \text{ or}$$

$$\frac{g_0}{S} = \frac{1}{2} + \frac{1}{\omega t_s \tan(\omega t_s)} \tag{9.5c}$$

$$\frac{h_0}{S} = \frac{g_0}{S} - \frac{f_0}{S} = \frac{1}{2} - \frac{1-\cos(\omega t_s)}{\omega t_s \sin(\omega t_s)} \tag{9.5d}$$

An alternative way of expressing Equations (9.5a to 9.5d) is obtained by replacing t_S with $\frac{S}{\dot{z}_f}$, and writing $\tilde{\omega}S$ in place of ωt_S, where

$$\tilde{\omega} = \frac{qB/2m}{\sqrt{2qV/m}} = \sqrt{\frac{q}{8mV}}B \text{ and} \tag{9.6a}$$

$$\tilde{\omega}S = \omega t_s = \phi_f - \phi_i \tag{9.6b}$$

Equations (9.5a) to (9.5d), rewritten in terms of B and S are

$$\alpha' = (\tilde{\omega}S\sin\tilde{\omega}S)\frac{r_i}{S} = \frac{r_i}{S}\left(\sqrt{\frac{q}{8mV}}BS\right)\sin\left(\sqrt{\frac{q}{8mV}}BS\right), \tag{9.7a}$$

$$\frac{f_0}{S} = \frac{1}{\tilde{\omega}S\sin(\tilde{\omega}S)} = \frac{1}{\left(\sqrt{\frac{q}{8mV}}BS\right)\sin\left(\sqrt{\frac{q}{8mV}}BS\right)}, \tag{9.7b}$$

$$\frac{g_0}{S} - \frac{1}{2} = \frac{1}{\tilde{\omega}S\tan(\tilde{\omega}S)} = \frac{1}{\left(\sqrt{\frac{q}{8mV}}BS\right)\tan\left(\sqrt{\frac{q}{8mV}}BS\right)}, \tag{9.7c}$$

$$\frac{h_0}{S} = \frac{1}{2} - \frac{1-\cos(\tilde{\omega}S)}{\tilde{\omega}S\sin(\tilde{\omega}S)} = \frac{1}{2} - \frac{1-\cos\left(\sqrt{\frac{q}{8mV}}BS\right)}{\left(\sqrt{\frac{q}{8mV}}BS\right)\sin\left(\sqrt{\frac{q}{8mV}}BS\right)}. \tag{9.7d}$$

Finally, Equations (9.5) to (9.7) can be expressed in terms of $NI/V^{1/2}$ by replacing BS with $\mu_0 NI$ where $\mu_0 = 4\pi \times 10^{-7}\,\text{Tesla}\,\frac{\text{meter}}{\text{AmpTurns}}$, as illustrated for $\alpha', f_0, g_0, \text{and}\, h_0'$ below:

$$\alpha' = \frac{r_i}{S}\left(\sqrt{\frac{q\mu_0^2}{8m}}\sqrt{\frac{(NI)^2}{V}}\right)\sin\left(\sqrt{\frac{q\mu_0^2}{8m}}\sqrt{\frac{(NI)^2}{V}}\right), \qquad (9.8a)$$

$$= \frac{r_i}{S}\kappa\sqrt{P}\sin\left(\kappa\sqrt{P}\right)$$

where $\kappa = (\mu_0{}^2 q/8m)^{1/2}$ and $P = \frac{(NI)^2}{V}$, the compound magnetic lens activator.

Likewise,

$$\frac{f_0}{S} = \frac{1}{\left(\kappa\sqrt{P}\right)\sin\left(\kappa\sqrt{P}\right)}, \qquad (9.8b)$$

$$\frac{g_0}{S} - \frac{1}{2} = \frac{1}{\left(\kappa\sqrt{P}\right)\tan\left(\kappa\sqrt{P}\right)}, \qquad (9.8c)$$

$$\frac{h_0}{S} = \frac{1}{2} - \frac{1-\cos\left(\kappa\sqrt{P}\right)}{\left(\kappa\sqrt{P}\right)\sin\left(\kappa\sqrt{P}\right)}. \qquad (9.8d)$$

Comparison with the Experimental Magnetic Lenses L_1 and L_2

The experimental magnetic lenses are described in Chapter 2, and their measured properties are assembled in Chapter 7. The geometry of the bores and gaps in the actual lenses is the same as that of the corresponding models, but the actual magnetic fields in the gaps between the bores are weakened by the presence of the

bores, and thus differ from the uniform fields assumed for the models. As a result, not only is the actual field non-uniform, but also its intensity on the axis is lower than in the uniform model for the same activation. However, in the paraxial region the actual field approximates a uniform field because of the minimum with respect to r at the axis. Thus if the field intensity in the model were adjusted to match the paraxial field in the lens, one could expect the paraxial properties of the model and the lens to agree reasonably well as a function of lens activation. We explored this approach by changing NI in the equations for the Model properties (but not for the lens properties) by a factor η and adjusting it for best fit to the experimental graphs. The experimental graphs of z_o', f_o, and g_o versus $(NI)^2/V$ for magnetic lens L_1 are shown in Figure 7.5(a), and Figures 7.6(a) and (b), of Chapter 7. The corresponding graphs for lens L_2 are shown in Figure 7.7(a) and Figures 7.8(a) and (b). The over-lying best-fit model curves demonstrate the remarkably close fit between the theoretical curves and the experimental graphs. The curves for f_o and g_o were generated from Equations (9.8b and 9.8c) modified by replacing NI by ηNI in the expressions for the model properties, where $\eta_1 = 0.74$ (for M_1) and $\eta_2 = 0.89$ (for M_2). The model curve for z_o' was obtained from the relation $z_o' = g_o + f_o m_o$, with object distance $z = 25$ cm. The fit is excellent over the entire activation range used in acquiring the experimental data. The large range of agreement promotes confidence in the accuracy of the theoretical equations and curves, beyond the present experimental range.

Having analytical expressions for the paraxial lens properties makes available continuous and more accurate values of the lens properties, and enables manipulations

such as determining slopes and deriving analytic expressions for chromatic aberrations. For example, Equations (9.9a to 9.9c) below describe the dimensionless chromatic coefficients C_f and C_g of f_o and g_o and, for a known object distance z, the dimensional coefficient C_c' of z_o'.

$$C_f = \frac{1}{2}\left(1 + \frac{\tilde{\omega} S}{\tan(\tilde{\omega} S)}\right) \tag{9.9a}$$

$$C_g = \frac{1}{2}\left(\cos(\tilde{\omega} S) + \frac{\tilde{\omega} S}{\sin(\tilde{\omega} S)}\right) \tag{9.9b}$$

$$C_C' = \left[\left(1 + m_0^2\right) C_g + 2 m_0 C_f\right] f_0 \tag{9.9c}$$

where $m_0 = f_0/(z - g_0)$.

Equations (9.9 a to c)' written in terms of $\eta\ (NI)/V^{1/2} = \eta\, P^{1/2}$, and including the η-factor, are:

$$C_f = \frac{1}{2}\left[1 + \frac{\eta\kappa\sqrt{P}}{\tan\left(\eta\kappa\sqrt{P}\right)}\right] \tag{9.9a)'}$$

$$C_g = \frac{1}{2}\left(\cos(\eta\kappa\sqrt{P}) + \frac{\eta\kappa\sqrt{P}}{\sin(\eta\kappa\sqrt{P})}\right) \tag{9.9b)'}$$

$$C_C' = \left[\left(1 + m_0^2\right) C_g + 2 m_0 C_f\right] f_0 \tag{9.9c)'}$$

Equations 9.9(a)' and (b)', evaluated for M_1 and M_2, and modified by η_1 and η_2, were used to generate the chromatic aberration curves for C_f and C_g shown vs. $(NI)^2/V$ in

Figures 7.11(a-d) for M_1, and in Figure 7.12(a-d) for M_2. The individual points (shown separately from the curves) were obtained by fitting, respectively, 4th and 5th degree polynomials in $(NI)^2/V$ to the experimental graphs of f_0 and g_0, and then using the polynomial expressions to calculate the chromatic coefficients. The activation range was relatively short, and the points are shown mainly as checks on the theoretical curves. The points obtained from the polynomial fit, as far as they go, agree well enough to serve as a satisfactory check.

The values of the η-factors which achieve agreement between the modified model curves and experimental graphs for f_0, g_0, and z_0' at the same time provided quantitative information as to the effective magnetic field on the axis of the actual lenses relative the field between the surrounding pole-faces. The ratio for L_1 was $\eta_1 =$ 0.74, and for L_2 was $\eta_2 = 0.89$. Starting with $\eta = 1$ (full-strength NI) between the pole faces and moving radially inward to the lens axis the L_1 field decreased by 26 % to 74% of full strength, and the L_2 field decreased by 11%. Thus the field decreased at a faster rate with r in L_1 than in L_2, causing greater over-focusing of the non-paraxial rays and a higher spherical aberration coefficient for L_1 than for L_2. Graphs of C_S'/f_0 versus WD for L_1 and L_2 in Figure 9.3 show that C_S'/f_0 is smaller for L_2 than for L_1 over the entire experimental WD range. The ratio of C_{S2}'/f_{20} to C_{S1}'/f_{10} is about 0.90 at WD = -1.5 mm, and about 0.46 at WD = 8.0 mm. See Figure 9.4. Multiplying the ratio C_{S2}'/f_{20} to C_{S1}'/f_{10} by f_{02}/f_{01}, brings back the C_{S2}'/C_{S1}' ratio. The ratio f_{02}/f_{01}, shown in Figure 9.2 vs WD, has a strong peak where f_{01} is near its minimum. This

peak brings the C_{S2}'/C_{S1}' ratio above the 1.0 level, as shown in Figure 9.5, indicating that C_{S1}' is now smaller than C_{S2}. These results agree with the

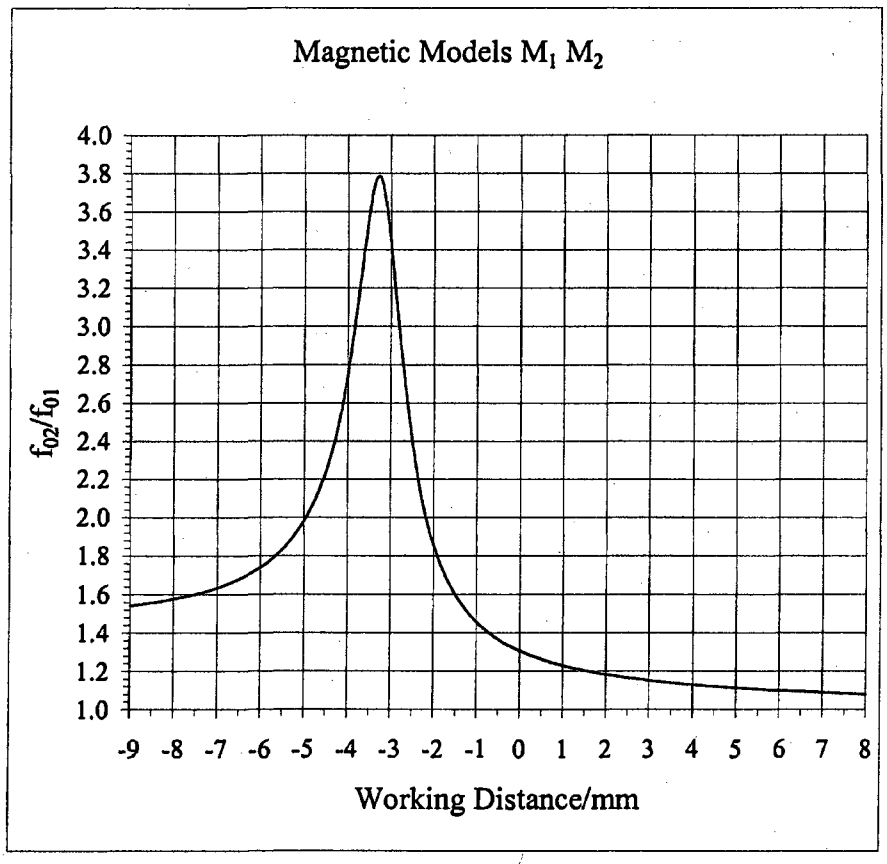

Figure 9.2. Plot of ratio f_{o2}/f_{o1} versus Working Distance from models M_1 and M_2..

experimental findings reported earlier in Chapter 8, where experimental graphs of C_S' versus *WD* for L_1 and L_2 in Figure 8.1(b) show that C_S' is significantly lower for L_2 than for L_1 for the same *WD*, except near the *WD* at which L_1 has its minimum focal length and the C_{S1}' curve dips under the C_{S2}' curve. See enlarged insert. The graph of C_{S2}'/C_{S1}' vs *WD* in Figure 9.5 shows the range over which C_{S2}'/C_{S1}' is > 1, and where

C_{S2}'/C_{S1}' is < 1; that is, where L_1 would provide better resolution, and where L_2 would provide better resolution in an SEM. .

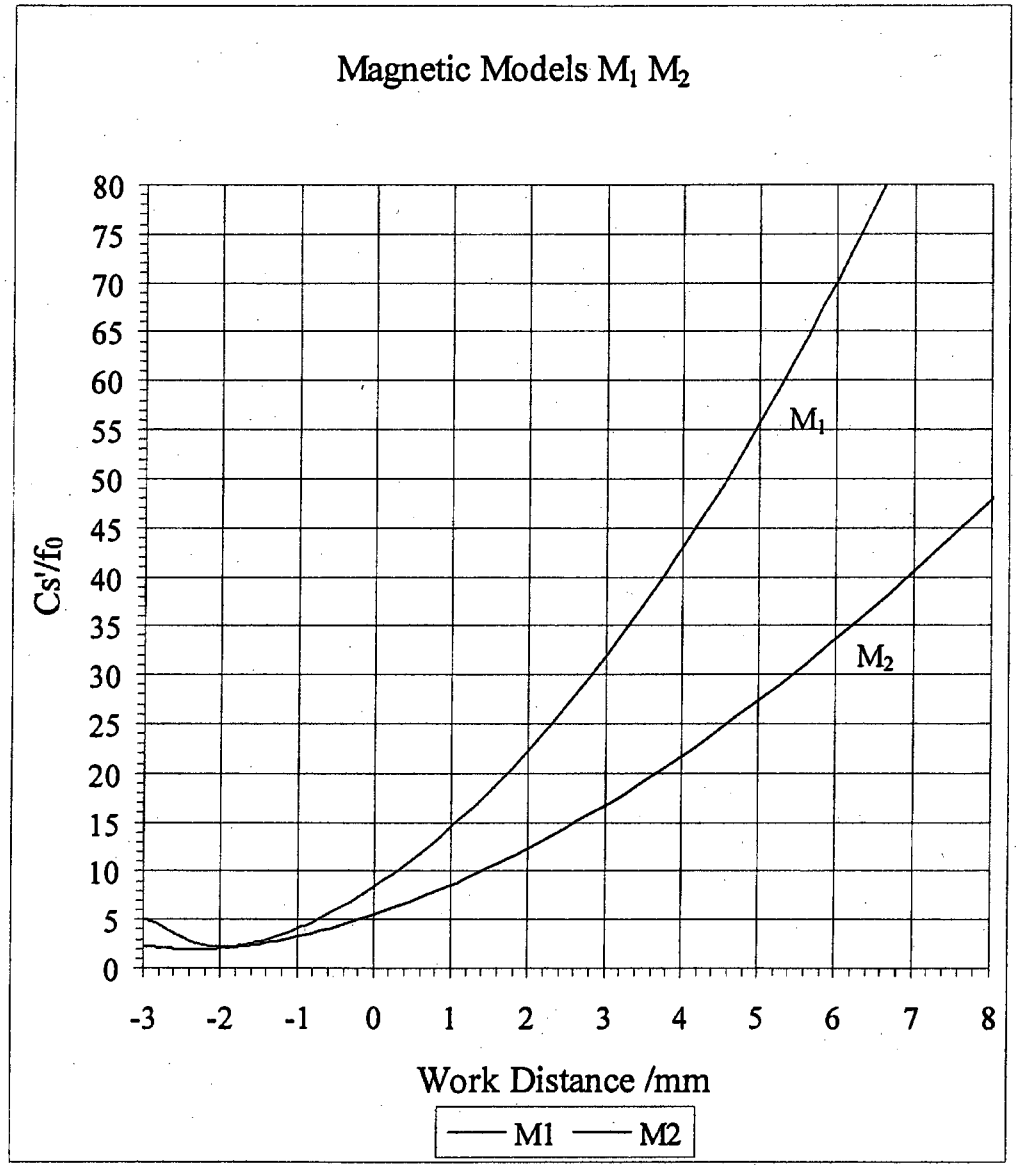

Figure 9.3. Plot of C_S'/f_0 versus Working Distance for Model Lenses M_1 and M_2 .

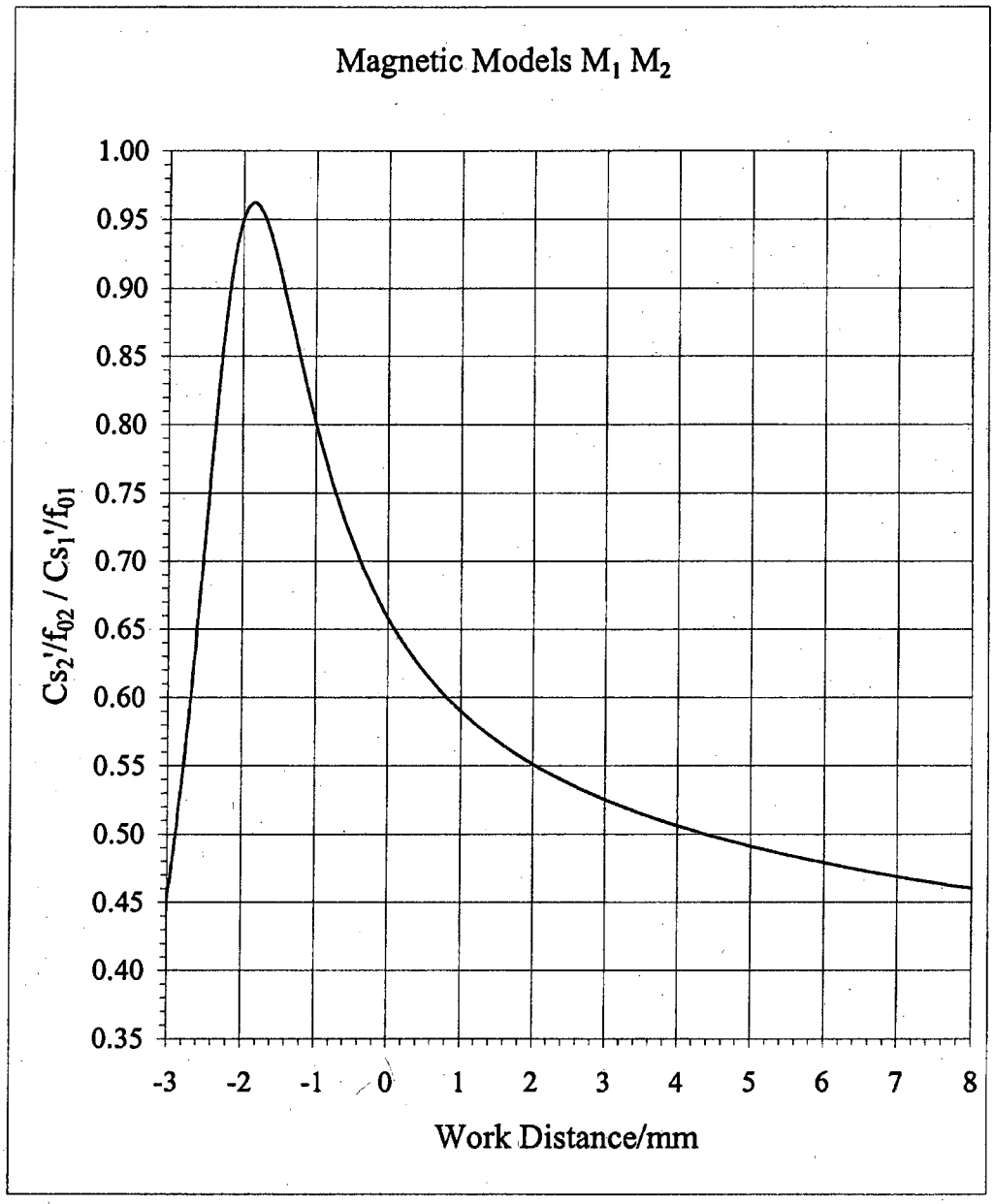

Figure 9.4. Plot of C'_{s2}/f_{02} / C'_{s1}/f_{01} versus Working Distance

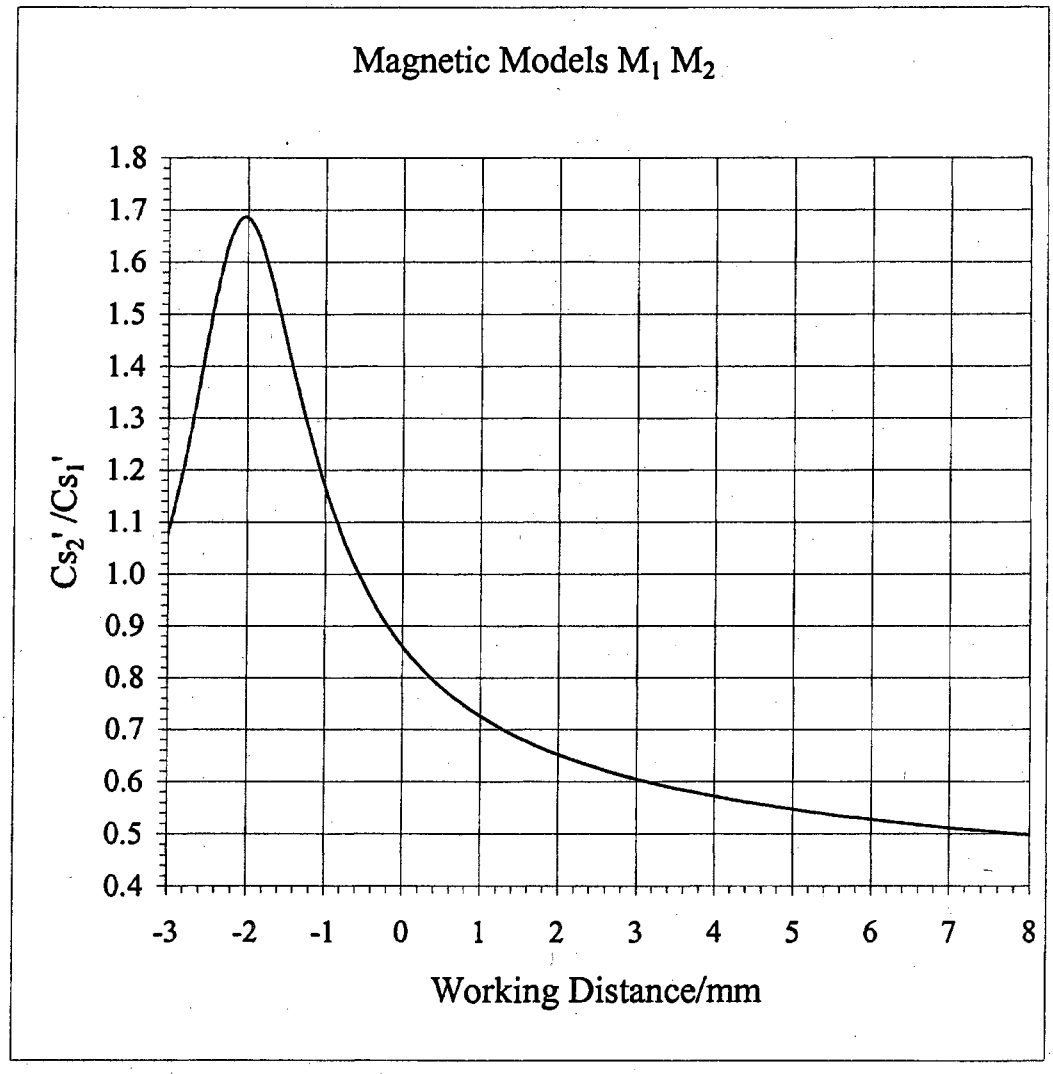

Figure 9.5. Plot of Cs'_2/Cs'_1 versus Working Distance.

B. Electrostatic Lens Models M_3, M_4, and M_5

The electrostatic lens models resemble the actual electrostatic lenses in having three electrodes with axial openings for passage of electrons, and in operating with the center electrode at a negative potential with respect to the end electrodes, which are at

ground potential. Like the actual lenses, the models have saddle-type potential fields. The shapes of the electrodes in the models are based on the shapes of equipotential surfaces in a hyperbolic potential field.

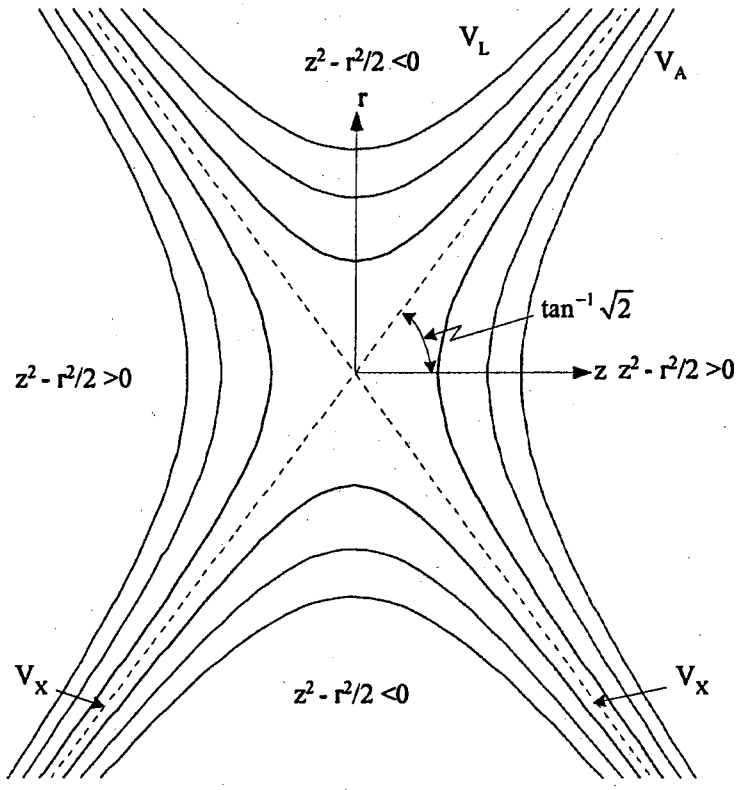

Figure 9.6. Meridional section of the hyperbolic field showing the intersections of various equipotential surfaces with the meridional plane.

Figure 9.6 is a meridional section of the hyperbolic field showing the intersections of various equipotential surfaces with the meridional plane. The more-negative surfaces are annular hyperboloids of revolution around the lens axis. The less-negative surfaces are pairs of curved hyperboloid sheets crossing the axis at right angles. (The models require axial openings in the end electrodes. The effect of these openings will be taken into account later.) The interface between the two types of equipotential

surfaces is a pair of asymptotic cones with vertices at lens center and opening in opposite directions around the lens axis. The intersection of these cones with the meridional plane produces the pair of straight lines crossing at lens center and labeled V_X. The angles, which these lines make with the lens axis, have tangents of $\pm\sqrt{2}$.

The rotation-symmetric hyperbolic potential field is described by the equation

$$V(r,z)-V_x = k\left(z^2-\frac{r^2}{2}\right), \tag{9.10}$$

where $k=\frac{(V_A-V_X)}{z_A^2}$. V_A is the potential of the end electrodes (ground in this case) and V_X is the potential of the asymptotic cones. z_A is the axial distance from the center plane of the lens to the end electrodes. The potential along the axis has a maximum (negative) value at the saddle point in the center of the lens. In the radial direction the negative potential goes through a minimum at this point. Throughout the volume of the hyperbolic field, the radial force component acting on an electron is proportional to r and is directed toward the axis. In effect, the field acts as a distributed converging lens for electrons.

Lenses

In the models, the axial openings in the end electrodes cause the potential field to differ locally from the hyperbolic form. The result is that fields around the end apertures in the hyperbolic models (and in the actual lenses) become thin diverging lenses for electrons. Thus, the hyperbolic lens with end apertures is a composite of

three lenses: the incident-side aperture lens at $z = -z_A$ (diverging), the hyperbolic-field lens between $-z_A$ and $+z_A'$ (converging), and the exit aperture lens at $+z_A'$ (diverging).

Paraxial Focal Properties of the Electrostatic Models M_3, M_4, and M_5

A schematic diagram of a hyperbolic model lens is shown in Figure 9.7.

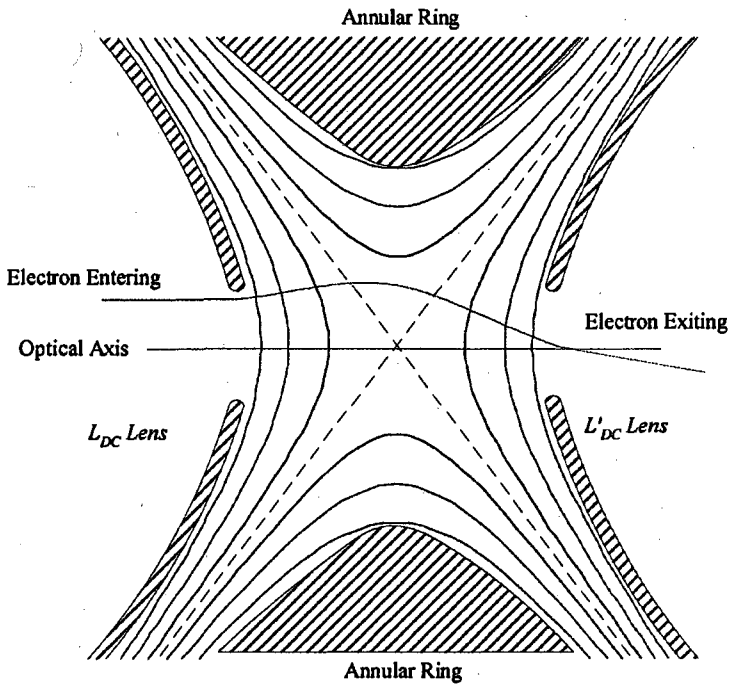

Figure 9.7. Schematic diagram of a hyperbolic model lens with an electron traversing through the model.

An electron, traveling parallel to the lens axis at height r_i, is incident from the left on the model. The electron trajectory is traced through the composite lens, one component at a time, to the focal point on the axis. From there the effective paraxial

focal properties g_o, f_o, and h_o of the model, and its chromatic aberrations, can be calculated. The z-coordinates are measured from the origin at lens center.

Incident Aperture Lens: Focal Length and Angular Deflection.

The paraxial focal length of an aperture lens is given by the Davisson-Calbick formula (Ref. 8),

$$f_0 = \frac{4V_B}{\left(\frac{dV}{dz}\right)_2 - \left(\frac{dV}{dz}\right)_1} \tag{9.11}$$

where V_B is the beam voltage of the electron (V_A - V_C), V_A is the potential of the aperture electrode, V_C is the potential of the electron source, and 1 and 2, refer to the order in which the electron encounters the fields on the two faces of the aperture. dz is positive in the direction of the electron's motion. The beam voltage V_B and gradients are calculated as if the aperture were not there. In the present example the axial gradient dV/dz at face 1, equals zero, and the axial gradient at face 2, evaluated at - z_A, is $-\frac{d\left(k z^2\right)}{dz} = -2k z_A$. Then the focal length of the entrance electrode is given by

$$f_{DC} = \frac{4\left(V_A - V_C\right)}{-2kz_A} = -\frac{2z_A\left(V_A - V_C\right)}{\left(V_A - V_X\right)}$$
$$f_{DC} = -\frac{2z_A}{v_{XC}}, \tag{9.12}$$

where $k = \frac{V_A - V_X}{z_A^2}$ and $v_{XC} = \frac{\left(V_A - V_X\right)}{\left(V_A - V_C\right)}$. [Note: In the usual application of the DC formula, the potential changes in a linear manner as the aperture is approached, rather

than in a quadratic manner as in the hyperbolic field. In the usual case, $f_{DC} = -\frac{4z_A}{\mathcal{V}_{XC}}$.]

The deflection produced by the aperture lens is directed away from the lens axis and its magnitude is

$$\delta_{DC} = \frac{r_i}{-f_{DC}} = \left(\frac{r_i}{z_A}\right)\frac{\mathcal{V}_{XC}}{2}. \tag{9.13}$$

Focusing Properties of the Hyperbolic Field

The paraxial *r*- and *z*-equations of the electron motion in the hyperbolic field are separable as functions of *t*, and can be obtained from the potential energy Equation (9.10), and Newton's law. The hyperbolic field begins immediately at the inside face of the entrance aperture lens L_{DC} (assumed to be ideally "thin"). The electron trajectory in the hyperbolic field makes an initial angle of $\delta_{DC} = r_i/-f_{DC}$ to the axis as a result of the diverging action of L_{DC}. The initial height r_A of the ray in the hyperbolic field is the same as that of the incident ray r_i, but the radial velocity is increased abruptly, from $\dot{r}_i = 0$ to $\dot{r}_A = \delta_{DC}\dot{z}$ as the electron passes through the aperture.

Radial Motion in the Hyperbolic Field

From Newton's second law, the radial motion in the hyperbolic field is

$$\begin{aligned} F_r &= m\ddot{r} = qE_r = -q\frac{\partial V}{\partial r} = qkr \\ \ddot{r} &= \frac{kq}{m}r = -\frac{ke}{m}r = -\omega^2 r \end{aligned} \tag{9.14}$$

where $\omega^2 = ke/m$ (not the same as $\omega = qB/2m$ in magnetic lens formulas) and

$k = \frac{V_A - V_X}{z_A^2}$. The paraxial solutions of Equation (9.14) for r and $\dot{r}$ can be written in the following form with the entrance aperture lens taken into consideration

$$r = \frac{r_A \cos\left(-\phi_{DC} + \omega\left(t - t_A\right)\right)}{\cos\phi_{DC}}, \tag{9.15a}$$

$$\dot{r} = -\frac{\omega r_A \sin\left(-\phi_{DC} + \omega\left(t - t_A\right)\right)}{\cos\phi_{DC}}. \tag{9.15b}$$

The time derivative of Eq. (9.15a) is taken with respect to t to obtain the velocity, Eq.(9.15b), and not t_A which is a constant. The derivations of these equations are found in Appendix C. With the initial values of r, $\dot{r}$, and z at $t = t_A$ given as $r = r_i = r_A$, $\dot{r} = \dot{r}_A$ and $z = -z_A$, the ratio of Equation (9.13b) to Equation (9.13a) is

$$\frac{\dot{r}_A}{r_A} = \frac{-\frac{\omega r_i}{\cos\phi_{DC}}\sin\left(-\phi_{DC} + \omega\left(t - t_A\right)\right)}{\frac{r_i}{\cos\phi_{DC}}\cos\left(-\phi_{DC} + \omega\left(t - t_A\right)\right)} = -\omega\tan\left(-\phi_{DC} + \omega\left(t - t_A\right)\right). \tag{9.15c}$$

At the initial time $t = -t_A$, Equation (9.15c) provides the following relationship for ϕ_{DC},

$$\frac{\dot{r}_A}{\omega r_A} = \tan\left(\phi_{DC}\right). \tag{9.15d}$$

This ratio $\frac{\dot{r}_A}{\omega r_A}$ can also be written as the product of $\left(\frac{\dot{r}_A}{\dot{z}_A}\right)\left(\frac{\dot{z}_A}{\omega r_A}\right)$.

The first factor becomes $\frac{\dot{r}_A}{\dot{z}_A} = \delta_{DC} = \frac{r_{i(A)}}{-f_{DC}} = r_{i(A)} \frac{\mathcal{V}_{XC}}{2z_A}$ where $f_{DC} = -\frac{2z_A}{\mathcal{V}_{XC}}$; the second factor becomes $\sqrt{\frac{2(V_A - V_C)}{(V_A - V_X)}} \left(\frac{z_A}{r_A}\right) = \left(\frac{z_A}{r_A}\right) \sqrt{\frac{2}{\mathcal{V}_{XC}}}$; and the product of the two gives

$$\left(\frac{\mathcal{V}_{XC}}{2z_A}\right)\left(\frac{z_A}{r_A}\right)\sqrt{\frac{2}{\mathcal{V}_{XC}}} = \sqrt{\frac{\mathcal{V}_{XC}}{2}} = \tan(\phi_{DC}). \qquad (9.15d)'$$

Equation (9.15a) shows that the effect of L_{DC} is to add a negative initial phase angle ϕ_{DC}, given by Eq. (9.15d), to the cosine angle, and change the amplitude of the cosine curve from r_A to $\frac{r_A}{\cos\phi_{DC}}$.

Axial Motion in the Hyperbolic Field

The axial equation of motion in the hyperbolic field is given by

$$\ddot{z} = 2\frac{ke}{m} z = 2\omega^2 z, \qquad (9.16)$$

where z is measured from lens center, and again $\omega^2 = ek/m$. The solutions of Eq. (9.16) for z and $\dot{z}$ are

$$z = \frac{\dot{z}(0)}{\sqrt{2}\omega} \sinh\left(\sqrt{2}\omega t\right), \qquad (9.17a)$$

$$\dot{z} = \dot{z}(0) \cosh\left(\sqrt{2}\omega t\right), \qquad (9.17b)$$

where $\dot{z}(0)$ is the axial velocity of the electron at lens center where z and t are zero. The derivations of these equations are found in Appendix C.

The ratio of Eq.'s (9.17b) to (9.17a) above gives

$$\sqrt{2}\omega\frac{z}{\dot{z}} = \tanh\left(\sqrt{2}\omega t\right). \tag{9.17c}$$

At the exit edge of the hyperbolic field $t = t_A'$ and Equation (9.17c) becomes

$$\tanh\left(\sqrt{2}\omega t_A'\right) = \sqrt{2}z_A'\left(\frac{\omega}{\dot{z}_A'}\right) = \frac{\sqrt{2}z_A'}{1}\frac{\sqrt{\frac{e}{m}\frac{(V_A - V_X)}{z_A'^2}}}{\sqrt{\frac{2e}{m}(V_A - V_C)}} = \frac{\sqrt{V_A - V_X}}{\sqrt{V_A - V_C}} \tag{9.17d}$$

$$\tanh\left(\sqrt{2}\omega t_A'\right) = \sqrt{v_{XC}}.$$

The time t_A' represents the time it takes for the electron to g_0 from the center of the lens at $z = 0$ to the exit at $z = z_A'$, while t_A is the time from the entrance at $-z_A$ to the center of the lens at $z = 0$. The total time during which the electron executes its radial cosine motion is $t_A' + t_A' = 2t_A'$. During this time the cosine angle increases by $\phi_{HF} = \omega\left(t_A' + t_A'\right)$. Solving Equation (9.17d) for $\omega t_A'$ and multiplying by 2 gives

$$2\omega t_A' = \sqrt{2}\tanh^{-1}\left(\sqrt{v_{XC}}\right). \tag{9.17e}$$

and then letting $2\omega t_A' = \phi_{HF}$

At the exit edge of the hyperbolic field $r = r_A'$, the radial Equations (9.15a), (9.15b), and (9.15c) become

$$r_A' = \frac{r_A}{\cos\phi_{DC}}\cos\left(-\phi_{DC} + \phi_{HF}\right) \tag{9.18a}$$

$$\dot{r}_A' = \frac{-\omega r_A}{\cos\phi_{DC}}\sin\left(-\phi_{DC} + \phi_{HF}\right), \text{ and} \tag{9.18b}$$

$$\frac{\dot{r}'_A}{\omega r_A} = -\tan\left(-\phi_{DC} + \phi_{HF}\right) \tag{9.18c}$$

At this point the electron has reached the exit aperture-lens L'_{DC}, but has not yet passed through it.

Effect of the Exit Aperture Lens L'_{DC}

As the electron passes through the exit aperture the direction of its velocity vector is altered by the deflection δ'_{DC} produced by the aperture lens. As with the incident-side aperture lens L_{DC}, where $r_i = r_A$, but $\dot{r}_i \neq \dot{r}_A$, the height r at the exit lens is not changed, i.e., $r'_A = r_f$, but the radial component of the velocity is increased by $\dot{r}'_{DC} = \delta'_{DC}\,\dot{z}'_A$, where $\delta'_{DC} = \dfrac{r'_A}{-f'_{DC}}$. The sum of the radial velocity components becomes

$$\dot{r}_f = \dot{r}'_A + \dot{r}'_{DC}. \tag{9.19}$$

In addition, $z'_A = z_f$ and, in the paraxial range, $\dot{z}'_A = \dot{z}_f$.

Equations (9.20a - c) below reflect the change due to $\dot{r}'_{DC}$ in the radial component of the electron's velocity due to exit lens L'_{DC}.

$$r_f = r'_A = \frac{r_A}{\cos\left(\phi_{DC}\right)}\cos\left(-\phi_{DC} + \phi_{HF}\right) \tag{9.20a}$$

$$\dot{r}_f = -\frac{\omega r_A}{\cos\left(\phi_{DC}\right)}\sin\left(-\phi_{DC} + \phi_{HF}\right) + \dot{r}'_{DC} \text{ and} \tag{9.20b}$$

$$\frac{-\dot{r}_f}{\omega r_f} = \tan\left(-\phi_{DC} + \phi_{HF}\right) - \frac{\dot{r}'_{DC}}{\omega r_f} \tag{9.20c}$$

Rewriting $\frac{\dot{r}'_{DC}}{\omega r_f}$

$$\frac{\delta'_{DC}\dot{z}_f}{\omega r_f} = \frac{\cancel{r_f}}{-f'_{DC}}\frac{\dot{z}_f}{\omega}\frac{1}{\cancel{r_f}} = \left(\frac{1}{-f'_{DC}}\right)\left(\frac{\dot{z}_f}{\omega}\right) = \left(\frac{v_{XC}}{2\cancel{z_A}}\right)\left(\frac{\cancel{z_A}}{1}\sqrt{\frac{2}{v_{XC}}}\right) = \sqrt{\frac{v_{XC}}{2}} = \tan\left(\phi'_{DC}\right)$$

and then inserting into Eq. (9.20c) gives

$$\frac{-\dot{r}_f}{\omega r_f} = \tan\left(-\phi_{DC}+\phi_{HF}\right) - \tan\left(\phi'_{DC}\right). \tag{9.20d}$$

After leaving the exit lens L_{DC}', the electron follows a straight path of slope $\frac{r_f}{z_f}$

passing through the paraxial focal point F_0' on the axis. The ray angle is

$$\alpha' = \frac{-\dot{r}_f}{\dot{z}_f} = r_f\left(\frac{\omega}{\dot{z}_f}\right)\left(\frac{-\dot{r}_f}{\omega r_f}\right)$$
$$\alpha' = \frac{r_f}{z_f}\sqrt{\frac{v_{XC}}{2}}\left\{\tan\left(-\phi_{DC}+\phi_{HF}\right)+\tan\left(-\phi'_{DC}\right)\right\} \tag{9.20e}$$

The distance of the focal point from the exit lens is

$$z'_{F_0} - z_f = \frac{r_f}{\alpha'} = \frac{\cancel{r_f}}{\frac{\cancel{r_f}}{z_f}\sqrt{\frac{v_{XC}}{2}}\left\{\tan\left(-\phi_{DC}+\phi_{HF}\right)+\tan\left(-\phi'_{DC}\right)\right\}}$$
$$\frac{r_f}{\alpha'} = \frac{z_f}{\sqrt{\frac{v_{XC}}{2}}\left\{\tan\left(-\phi_{DC}+\phi_{HF}\right)+\tan\left(-\phi'_{DC}\right)\right\}} \tag{9.20f}$$

Effective Focal Properties of the Electrostatic Models

Lens Properties f_0 and g_o

The effective focal lengths of the compound electrostatic model lens can be found by extrapolating the parallel object ray forward and the corresponding image

ray backward to their intersection point. The axial distance from the intersection point to the focal point F_0' in image space is the focal length of the lens. See the diagram in Figure 9.1. The intersection point defines a point on the image-space principal surface H'. The effective paraxial focal length is given by

$$
\begin{aligned}
f_0 &= \frac{r_i}{\alpha'} = \frac{r_A}{\alpha'} = \frac{z_f}{\frac{r_f}{r_A}\sqrt{\frac{v_{XC}}{2}}\left\{\tan\left(-\phi_{DC}+\phi_{HF}\right)+\tan\left(-\phi'_{DC}\right)\right\}} \\
f_0 &= \frac{z_f}{\sqrt{\frac{v_{XC}}{2}}\left\{\frac{r_f}{r_A}\tan\left(-\phi_{DC}+\phi_{HF}\right)+\frac{r_f}{r_A}\frac{\sin\left(-\phi'_{DC}\right)}{\cos\left(-\phi_{DC}\right)}\right\}} \\
f_0 &= \frac{z_f}{\sqrt{\frac{v_{XC}}{2}}\left\{\frac{\cancel{r_A}\cos\left(-\phi_{DC}+\phi_{HF}\right)}{\cancel{r_A}\cos\left(-\phi_{DC}\right)}\tan\left(-\phi_{DC}+\phi_{HF}\right)+\frac{r_f}{r_A}\frac{\sin\left(-\phi'_{DC}\right)}{\cos\left(-\phi_{DC}\right)}\right\}} \\
f_0 &= \frac{z_f\cos\left(-\phi_{DC}\right)}{\sqrt{\frac{v_{XC}}{2}}\left\{\sin\left(-\phi_{DC}+\phi_{HF}\right)+\frac{r_f}{r_A}\sin\left(-\phi'_{DC}\right)\right\}}
\end{aligned}
\tag{9.21}
$$

where $\phi_{DC}=\phi'_{DC}$ and $\cos\left(\phi_{DC}\right)=\cos\left(-\phi_{DC}\right)$. Substitute r_f from Equation (9.20a) to give

$$
f_0 = \frac{z_f\cos\left(-\phi_{DC}\right)}{\sqrt{\frac{v_{XC}}{2}}\left\{\sin\left(-\phi_{DC}+\phi_{HF}\right)+\cos\left(-\phi_{DC}+\phi_{HF}\right)\tan\left(-\phi'_{DC}\right)\right\}}. \tag{9.22a}
$$

Multiply the top and bottom of the above equation by $\cos\left(-\phi'_{DC}\right)$ to get

$$
f_0 = \frac{z_f\cos\left(-\phi_{DC}\right)\cos\left(-\phi'_{DC}\right)}{\left[\sqrt{\frac{v_{XC}}{2}}\left\{\sin\left(-\phi_{DC}+\phi_{HF}\right)\cos\left(-\phi'_{DC}\right)+\cos\left(-\phi_{DC}+\phi_{HF}\right)\sin\left(-\phi'_{DC}\right)\right\}\right]} \tag{9.22b}
$$

Using the trigonometry identity: $\sin(x+y) = \sin x \cos y + \cos x \sin y$ on the denominator of Eq.(9.22b), simplifies the equation to

$$f_0 = \frac{z_f \cos(-\phi_{DC}) \cos(-\phi'_{DC})}{\sqrt{\frac{\mathcal{V}_{XC}}{2}} \sin(-\phi_{DC} + \phi_{HF} - \phi'_{DC})} \tag{9.22c}$$

The effective paraxial focal distance g_0 is the distance from the center of the lens to the focal point, and is given by

$$g_0 = z_f + \frac{z_f}{\sqrt{\frac{\mathcal{V}_{XC}}{2}} \left\{ \tan(-\phi_{DC} + \phi_{HF}) + \tan(-\phi'_{DC}) \right\}} \tag{9.23}$$

where $-\phi_{DC}$ and $-\phi'_{DC} = \tan^{-1}\left(\sqrt{\frac{\mathcal{V}_{XC}}{2}}\right)$ and $\phi_{HF} = \sqrt{2}\tanh^{-1}\left(\sqrt{\mathcal{V}_{XC}}\right)$.

It is interesting those Equations (9.22c) and (9.23) for f_0 and g_0 depend on only one parameter, namely $\sqrt{\mathcal{V}_{XC}}$, aside from the model's half-length z_f. Ordinarily $\mathcal{V}_{XC}$ in electrostatic lenses are not known, and the focal properties are plotted versus the known activation parameter $\mathcal{V}_{LC}$. In hyperbolic lenses however, the ratio $\frac{\mathcal{V}_{XC}}{\mathcal{V}_{LC}}$ [which reduces to $\frac{V_A - V_X}{V_A - V_L} = \mathcal{V}_{XL}$] can be found from the geometry of the hyperbolic lens electrodes. The relationship is

$$\frac{V_A - V_X}{V_A - V_L} = \frac{1}{1 + \frac{D^2}{8z_f^2}} \tag{9.24}$$

where D is the diameter of the opening in the hyperbolic center-electrode. The hyperbolic models, which we are using, have D to z_f ratios of 0.80, which results in the relationship

$$\mathcal{V}_{XC} = \frac{\mathcal{V}_{LC}}{1.08}. \tag{9.25}$$

Substituting the expression, $\frac{\mathcal{V}_{LC}}{1.08}$ for $\mathcal{V}_{XC}$ in Eqs. (9.22b) and (9.23b), enables model curves of f_0 and g_0 to be generated versus $\mathcal{V}_{LC}$, thus making it easier to compare the model curves with corresponding experimental graphs.

The f_0 and g_0 Equations (9.22c) and (9.23) are modified by best-fit factors η shown below.

$$f_0 = \frac{z_f \cos(-\phi_{DC})\cos(-\phi'_{DC})}{\eta\sqrt{\frac{\mathcal{V}_{XC}}{2}}\sin(-\phi_{DC}+\phi_{HF}-\phi'_{DC})}$$

$$g_0 = z_f + \frac{z_f}{\eta\sqrt{\frac{\mathcal{V}_{XC}}{2}}\left\{\tan(-\phi_{DC}+\phi_{HF})+\tan(-\phi'_{DC})\right\}}$$

These were used to generate the best-fit curves in Figure 9.7 and 9.8.

The curves show how f_0 and g_0 vary with $\frac{V_A - V_L}{V_A - V_C}(\mathcal{V}_{LC})$ for a hyperbolic-model lens with center-electrode opening of diameter $D = 0.160$ in. (4.06mm) and $z_f = 0.200$ in. (5.08mm). The ratio $\frac{\mathcal{V}_{XC}}{\mathcal{V}_{LC}} = \frac{1}{1+\frac{D^2}{8z_A^2}}$ equals $\frac{1}{1.08}$ for a hyperbolic lens of these dimensions.

Image Properties z_0' and m_0

In the usual case neither the object distance z nor the image distance z' is infinite. It is convenient to find z' and z from the Newtonian relations, Eq. (3.20) and (3.21) of Chapter 3. Solving these equations for z_o' and z_o gives

$$z_0' = g_0' + f_0' m_0, \text{and} \tag{9.26a}$$

$$z_0 = g_0 + \frac{f_0}{m_0}, \tag{9.26b}$$

where $m_o = \alpha/\alpha'$ is the image magnification. The magnitudes of the focal distance and the focal length are the same in object space as in image space. The primes (') on f_0 and g_0 in the above equations are used to identify the image side equation. In the usual case, the object distance z is known, as well as $f_0$and g_0. Then m_o can be found from Equation (9.26b) and used to solve Equation (9.26a) for z_o'. The curves for z_o' and m_o versus $\mathcal{V}_{LC}$ in Figures (7.9(a) and b) were generated from Equations (9.26(b) and a) along with the numerical values of f_0 and g_0 from the previous section and with $z = 25$ cm. In this example m_o is small, and the z_o' curve does not differ greatly from the curve for g_o.

Comparison of the Paraxial Properties of the Electrostatic Lens Models with the Properties Determined Experimentally

The designs of the electrostatic lenses are illustrated and described in Chapter 2. In the electron-optically important region around the axis the electrodes of the lenses are simply plates with central openings, as illustrated for L_3 in Figure 2.1b of

Chapter 2. The spacing s between electrodes, the thickness t of the electrodes, and the diameter D of the central openings are, respectively:

Lens	Spacing of Electrode	Thickness of Center Electrode	Diameter of Central Electrode
L_3	0.100" (2.54mm)	0.025" (0.635mm)	0.115"(2.921 mm)
L_4	0.100" (2.54mm)	0.025" (0.635mm)	0.154" (3.917 mm)
L_5	0.125" (3.175mm)	0.050" (1.27mm)	0.200" (5.08mm)

The openings in the end electrodes are the same for all three lenses: 0.050 inches (1.27 mm) for the front electrode and 0.075inches (1.905 mm) for the rear electrode. A negative voltage is applied to the middle electrode.

The electrodes in the actual lenses are obviously much different from those in the hyperbolic models, which invites the question, what is the basis for using hyperbolic models for comparison. A redeeming feature for this comparison is that the lenses are saddle-type lenses, and the potential distribution approaches the hyperbolic form as the saddle point is approached. For paraxial rays the electrons near the saddle can be considered to be in a hyperbolic field. Furthermore, the electrons have their lowest beam potential at the saddle, so the effect of the hyperbolic field is enhanced by the extra time to act. However, the actual voltage ratio $\frac{V_A - V_X}{V_A - V_C} = \mathcal{V}_{XC}$ at the saddle point is not expected to be the same as that in the models at the same activation $\frac{V_A - V_L}{V_A - V_C} = \mathcal{V}_{LC}$. As in the magnetic models, where η-factors were applied to $\frac{NI}{\sqrt{V}}$ to adjust the model field to the strength of the axial field in the lens, a set of η

and β-factors where applied to $\sqrt{\frac{\mathcal{V}_{XC}}{2}}$ and $\sqrt{\mathcal{V}_{XC}}$ respectively to each electrostatic models to bring the voltage ratios at the saddle point $\mathcal{V}_{XC}$ into agreement with the saddle-point voltage ratios of the lenses. Since the latter ratios are not known *a priori*, best fit of the model curves with the experimental graphs was used as a criterion for agreement between the voltage ratios. The extra factor β is included to allow for a small corrections to the power of the model's entrance and exit lenses, L_{DC} and L_{DC}'. Best fit is expected when the effective saddle-point voltage in the model is the same as that in the lens.

The experimentally measured properties of the electrostatic lenses L_3, L_4, L_5 are assembled in Chapter 7. The paraxial properties z_o', f_o, and g_o, of L_3, L_4, and L_5 are given as functions of lens activation in Tables 7.9(a), (b), and(c) and Tables 7.10 (a), (b), and (c). The properties are also shown plotted as functions of the activation parameter $\frac{V_L}{V_C}\left(=\frac{V_A-V_L}{V_A-V_C}=\mathcal{V}_{LC}\right)$ for all three electrostatic lenses in Figures 9.7, 9.8, and 9.10 below. The smooth curves superimposed on the experimental graphs are the model curves with η and β adjusted for best fit. The best-fit η and β factors for the M_3, M_4, and M_5 curves are shown below in Table 9.1.

L_3

Experimenntal				Model		
				η	η	
				1.000	1.000	
				β	β	
Voltage Ratio				0.89	0.89	
V_L/V_C	f_o/cm	g_o/cm	z_0'/cm	f_o/cm	g_o/cm	z_0'/cm
1.00	0.472	0.442	0.451	0.498	0.480	0.490
0.95	0.593	0.564	0.579	0.591	0.577	0.591
0.90	0.745	0.725	0.748	0.707	0.695	0.715
0.80	1.066	1.046	1.094	1.040	1.023	1.068
0.70	1.647	1.628	1.744	1.605	1.568	1.678
0.60	2.658	2.610	2.926	2.670	2.577	2.895

L_4

Experimenntal				Model		
				η	η	
				0.86	0.86	
				β	β	
Voltage Ratio				0.82	0.820	
V_L/V_C	f_o/cm	g_o/cm	z_0'/cm	f_o/cm	g_o/cm	z_0'/cm
1.00	0.819	0.795	0.823	0.830	0.817	0.845
0.95	0.947	0.928	0.965	0.961	0.952	0.990
0.90	1.137	1.096	1.150	1.119	1.113	1.165
0.85	1.298	1.277	1.348	1.311	1.308	1.380
0.80	1.561	1.545	1.649	1.547	1.547	1.649
0.70	2.214	2.197	2.412	2.218	2.221	2.437

L_5

Experimenntal				Model		
				η	η	
				0.93	0.898	
				β	β	
Voltage Ratio				0.885	0.885	
V_L/V_C	f_o/cm	g_o/cm	z_0'/cm	f_o/cm	g_o/cm	z_0'/cm
1.00	0.709	0.640	0.661	0.705	0.656	0.677
0.95	0.825	0.769	0.797	0.823	0.781	0.809
0.90	0.987	0.941	0.982	0.966	0.927	0.966
0.80	1.390	1.356	1.438	1.359	1.309	1.387
0.70	1.986	1.874	2.045	1.979	1.882	2.052

Table 9.1. Table of Experimental Data and Model's smooth curve values, with their η and β factors, for the parameters f_0, g_0, and z'_0 for the Electrostatic Lenses L_3, L_4, and L_5 .

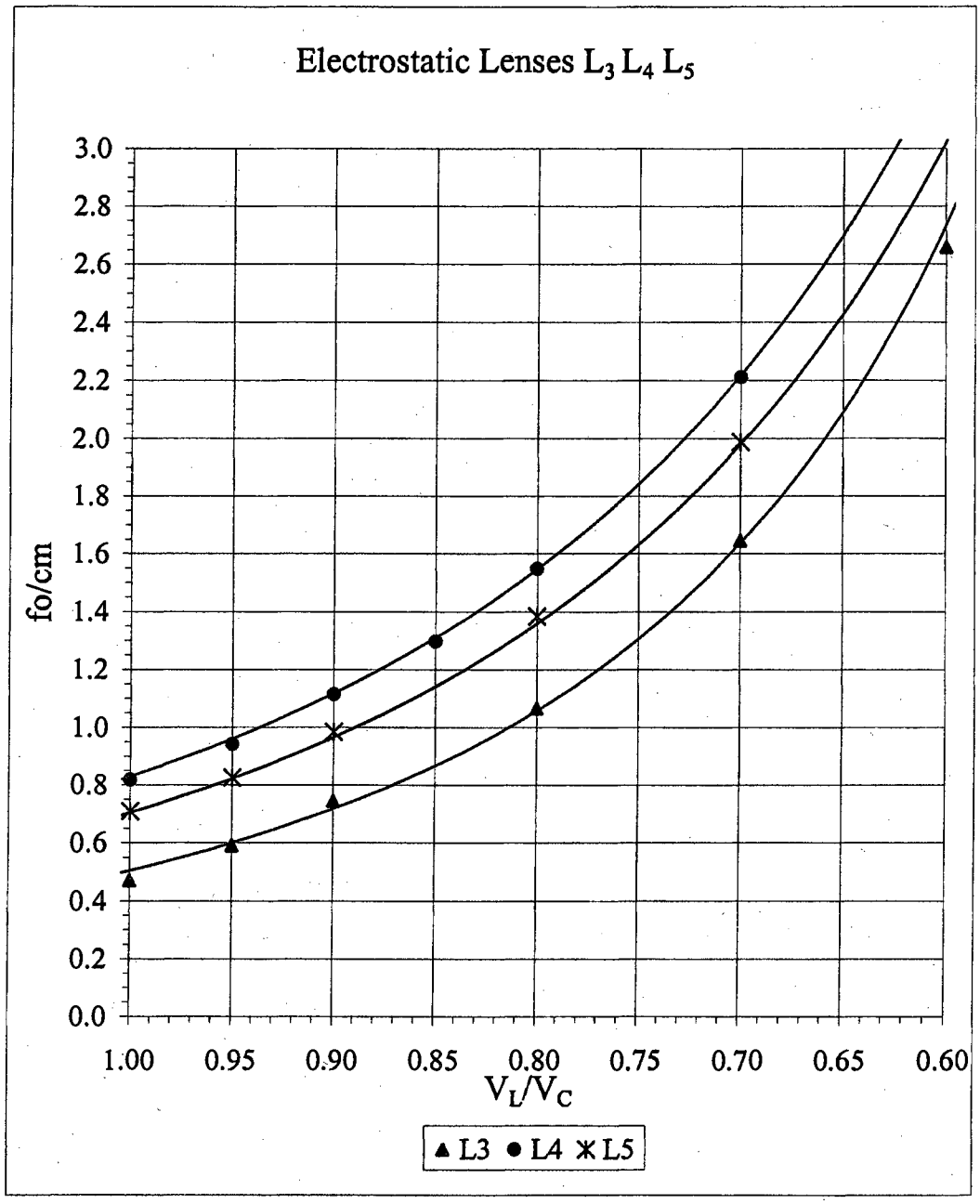

Figure 9.8. Graphs of f_0 versus V_L/V_C for the three electrostatic lenses L_3, L_4, and L_5. The points are the Experimental Data and the smooth curves are the Model data with the η and β factors that best fit the Experimental Data points.

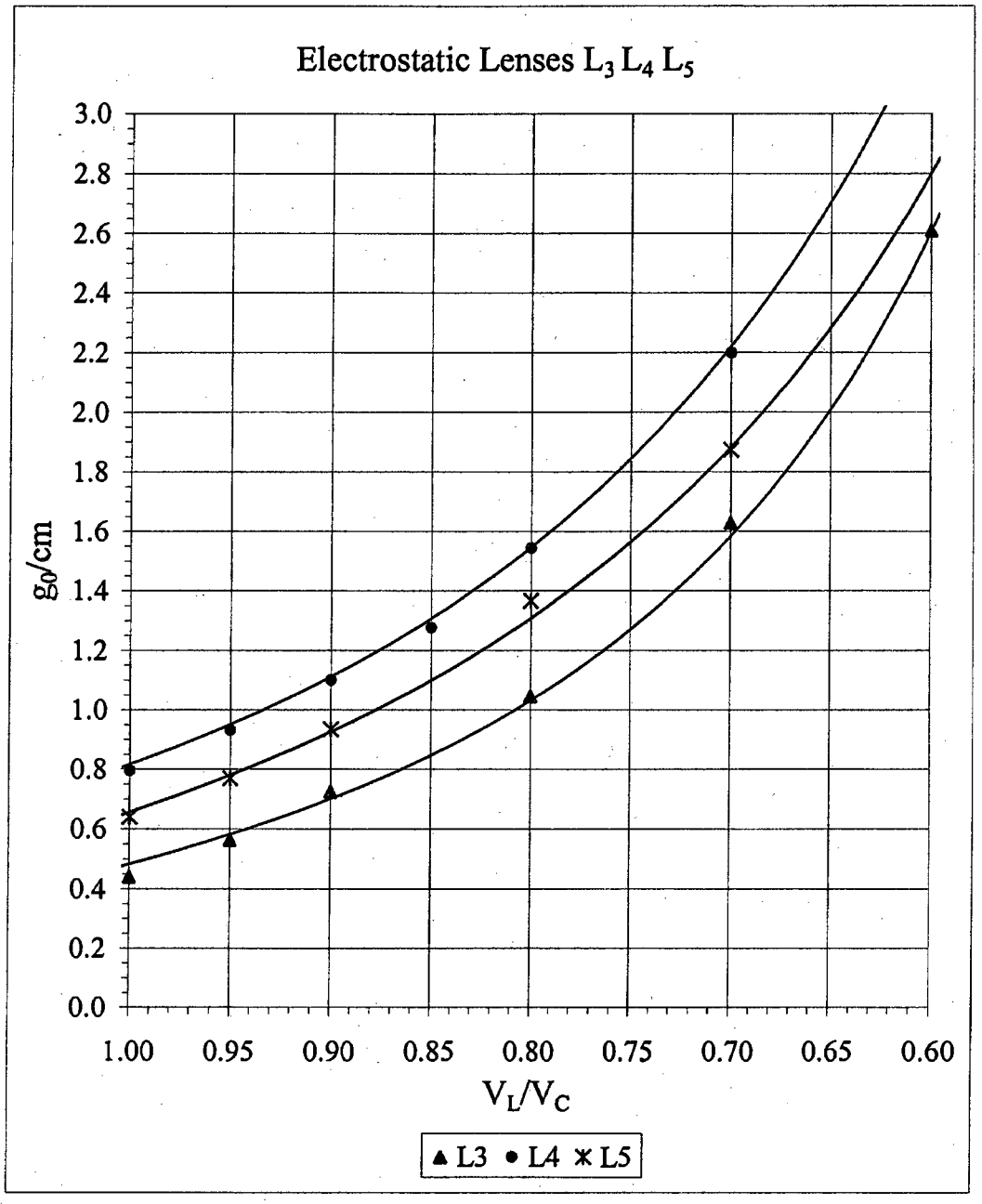

Figure 9.9. Graphs of g_0 versus V_L/V_C for the three electrostatic lenses L_3, L_4, and L_5. The points are the Experimental Data and the smooth curves are the Model data with the η and β factors that best fit the Experimental Data points.

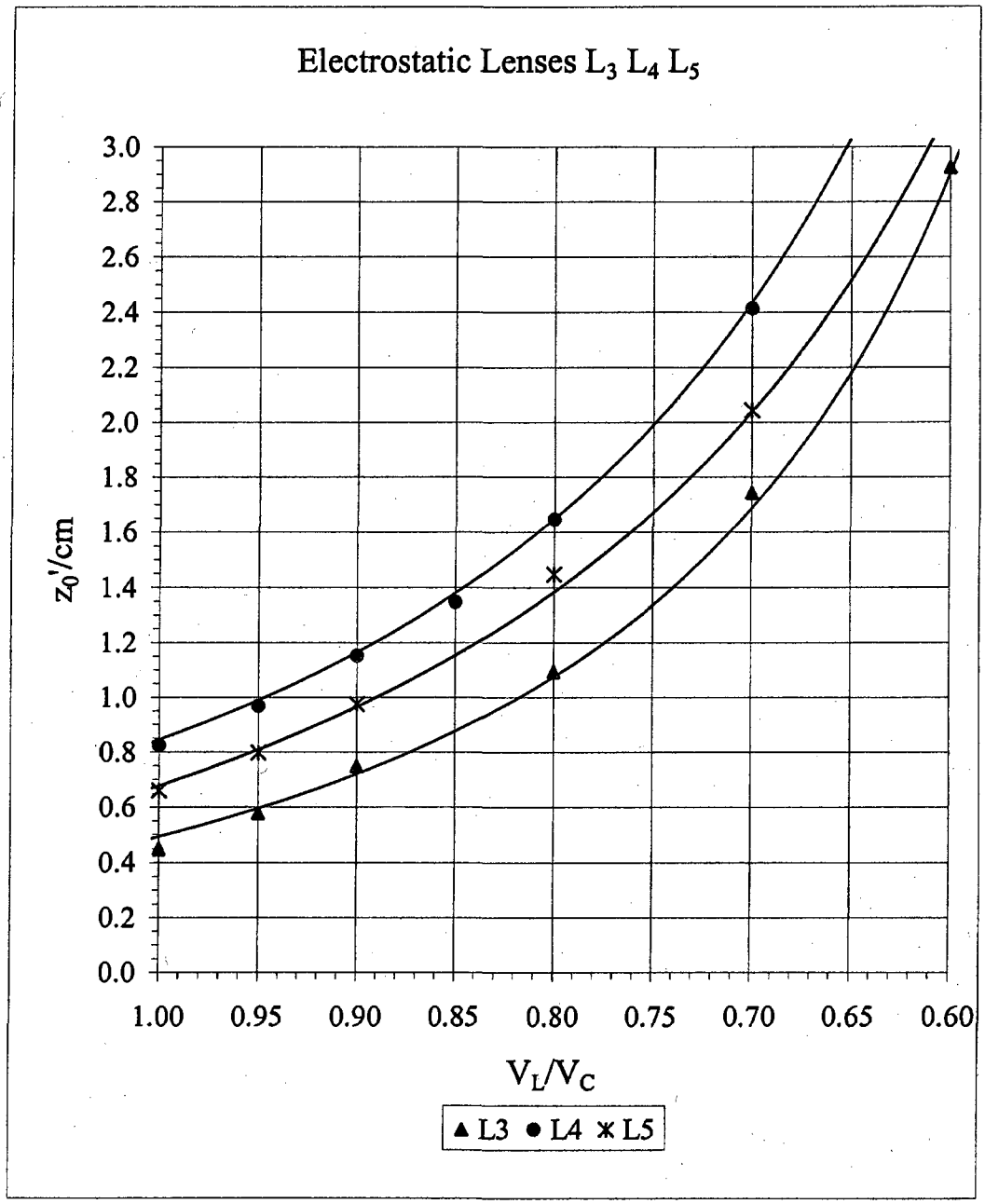

Figure 9.10 Graphs of z'_0 versus V_L/V_C for the three electrostatic lenses L_3, L_4, and L_5. The points are the Experimental Data and the smooth curves are the Model data with the η and β factors that best fit the Experimental Data points.

The excellent agreement between the theoretical curves and the experimental graphs over the whole range of experimental values, as for the magnetic models, builds confidence in the validity of the equations beyond the present experimental range.

Chromatic Aberration

Having equations for the lens properties f_0 and g_0 enables improved accuracy, and access to a continuous range of values. It also makes possible operations such as calculation of the chromatic aberration coefficients. Equations for chromatic coefficients C_f and C_g, derived from model Equations (9.22b and 9.23b) for f_0 and g_0 and modified by best-fit η and β values are given below,

$$C_f = \tfrac{1}{2} + \left[\tan\phi + \cot\left(-\phi_{DC} + \phi_{HF} - \phi'_{DC}\right)\left(\frac{\beta\left(1+\eta^2\frac{v_{XC}}{2}\right)}{\eta\left(1-\beta^2 v_{XC}\right)} - 1\right)\right]\left(\frac{\eta\sqrt{\frac{v_{XC}}{2}}}{1+\eta^2\frac{v_{XC}}{2}}\right) \qquad (9.27a)$$

$$C_g = \frac{1}{2}\left\{\frac{\cos\left(-\phi_{DC}+\phi_{HF}\right)}{\cos\left(-\phi_{DC}\right)} + \eta\sqrt{\frac{v_{XC}}{2}}\left(\frac{\left(\frac{2\beta}{\eta\left(1-\beta^2 v_{XC}\right)} - \frac{1}{1+\eta^2\left(\frac{v_{XC}}{2}\right)}\right) - \cos^2\left(-\phi_{DC}+\phi_{HF}\right)}{\sin\left(-\phi_{DC}+\phi_{HF}-\phi'_{DC}\right)}\right)\right\} \qquad (9.27b)$$

Details of the derivations are provided in Appendix D. The model equation for chromatic coefficient C_C' of z_o' can be obtained by means of Equation (3.19) of Chapter 3 (repeated here);

$$C_c' = ([1 + m_o^2]C_g + 2m_o C_f)f_o.$$

Curves of C_f and C_g for Models M_3, M_4, and M_5 are shown in Figures 7.13(a) and (b) of Chapter 7. Model curves of C_C' with $z = 25$ cm are shown for M_3, M_4, and M_5 in

Figure 7.13(c). The points were included as checks on the theoretical curves. The checks show satisfactory agreement with theory over the range of the experimental points. In Part A (Magnetic Lenses) the values of the η-factors gave information as to the effective strength of the magnetic field on the axis. Analogously in Part B, knowing the η-factors for the electrostatic lenses gives information as to the value of $\mathcal{V}_{XC}$ at the saddle point. When the theoretical curves of $\frac{f_0}{z_A}$ and $\frac{g_0}{z_A}$ agree with the corresponding experimental graphs, the theoretical quantity $\eta\sqrt{\frac{\mathcal{V}_{LC}}{1.08}}$ in the model equation equals $\sqrt{\mathcal{V}_{XC}}$ in the lens, or

$$\mathcal{V}_{XC} = \eta^2\left(\frac{\mathcal{V}_{LC}}{1.08}\right). \tag{9.28a}$$

Since η is, a known parameter applied to the model, and $\mathcal{V}_{LC}$ is the known activation parameter applied to the lens, the value of $\mathcal{V}_{XC}$ can be found from Equation (9.28a). The value of η is not the same for the three electrostatic lenses. The values of η, and a tweak factor β for the entrance and exit aperture lenses L_{DC} and L_{DC}', are shown in Table (9.1). Multiplying Eq (9.28a) by the factor $V_A - V_C$ leaves

$$V_A - V_X = \eta^2\frac{V_A - V_L}{1.08}. \tag{9.28b}$$

Comparison of the paraxial properties of the magnetic lens models with the properties determined experimentally

Results for Magnetic Lenses L_1 and L_2

The theoretical models, whose properties are to be compared with those of the corresponding experimental lenses, are based on the uniform field model described in Chapter 1, and earlier in this Chapter. The experimental magnetic lenses are described in Chapter 2. The geometry of the actual lenses is the same as that of the corresponding models, but the actual magnetic fields in the gaps between the bores differ from the uniform fields assumed for the models. The difference is due to the presence of the bores in the pole-pieces, which is ignored in the models, but which causes the field intensity in the actual lenses to have a minimum on the axis. As a result, not only is the actual field non-uniform, but also its intensity on the the axis is lower than in the uniform model for the same activation. Regardless of the difference in the fields, the actual field near the axis approximates a uniform field because $'B/'r = 0$ at the minimum. Thus if the field intensity in the model were adjusted to match the paraxial field in the lens, one could expect the paraxial properties of the model and the lens to agree reasonably well as a function of lens activation. We explored this approach by changing NI for the Model (but not for the lens) by a factor η and adjusting it for best fit to the experimental curves in Chapter 7.

Figures 7.5(a), 7.6(a), and 7.6(b) show the experimental graphs of z_o', f_o, and g_o versus $(NI)^2/V$ for magnetic lens L_1, and Figures 7.7(a),7.8(a), and 7.8(b) show the corresponding graphs for lens L_2. For convenience, these Figures are copied here.

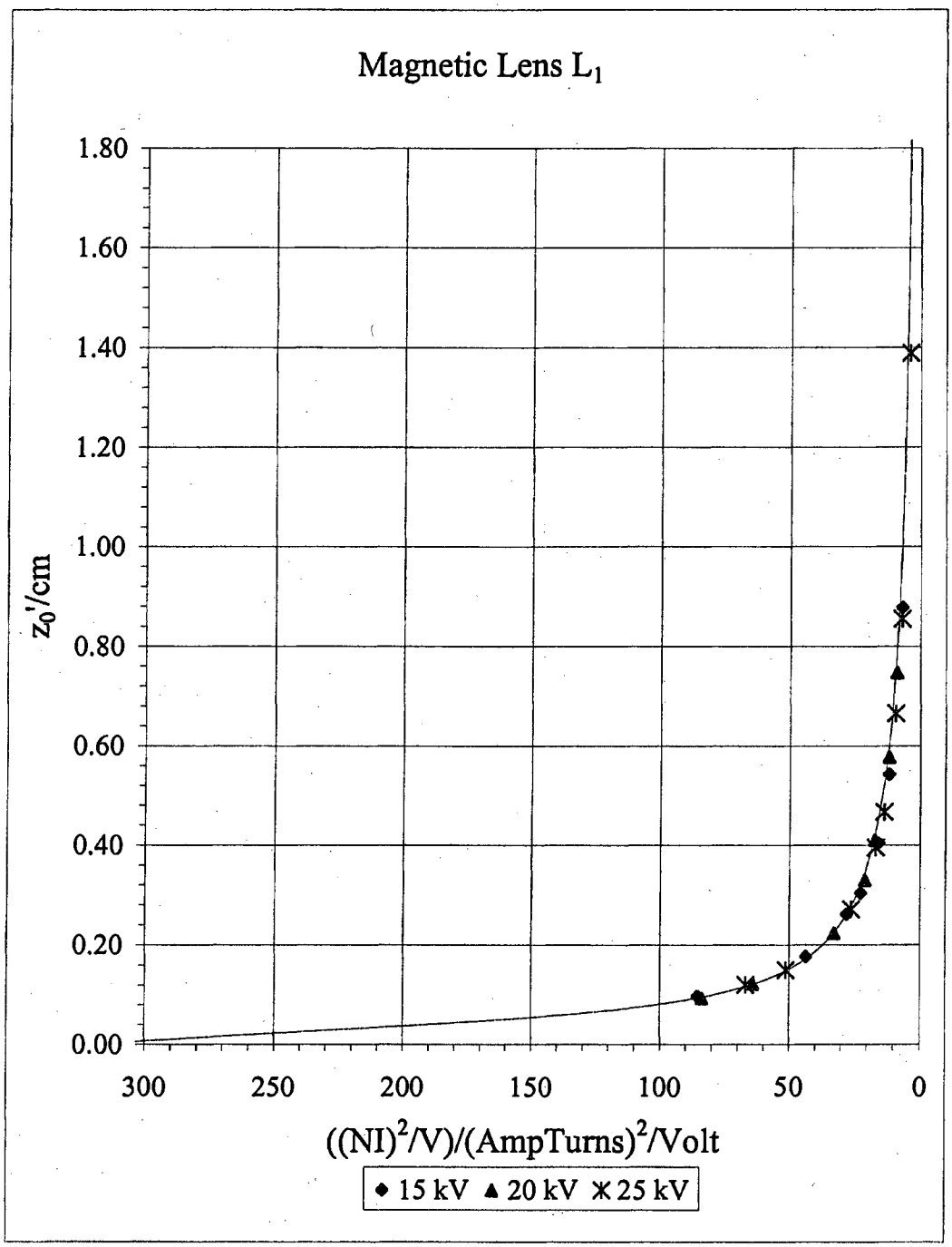

Figure 9.11. Copied graph of z'_0 versus $(NI)^2/V$ from Figure 7.6(a).

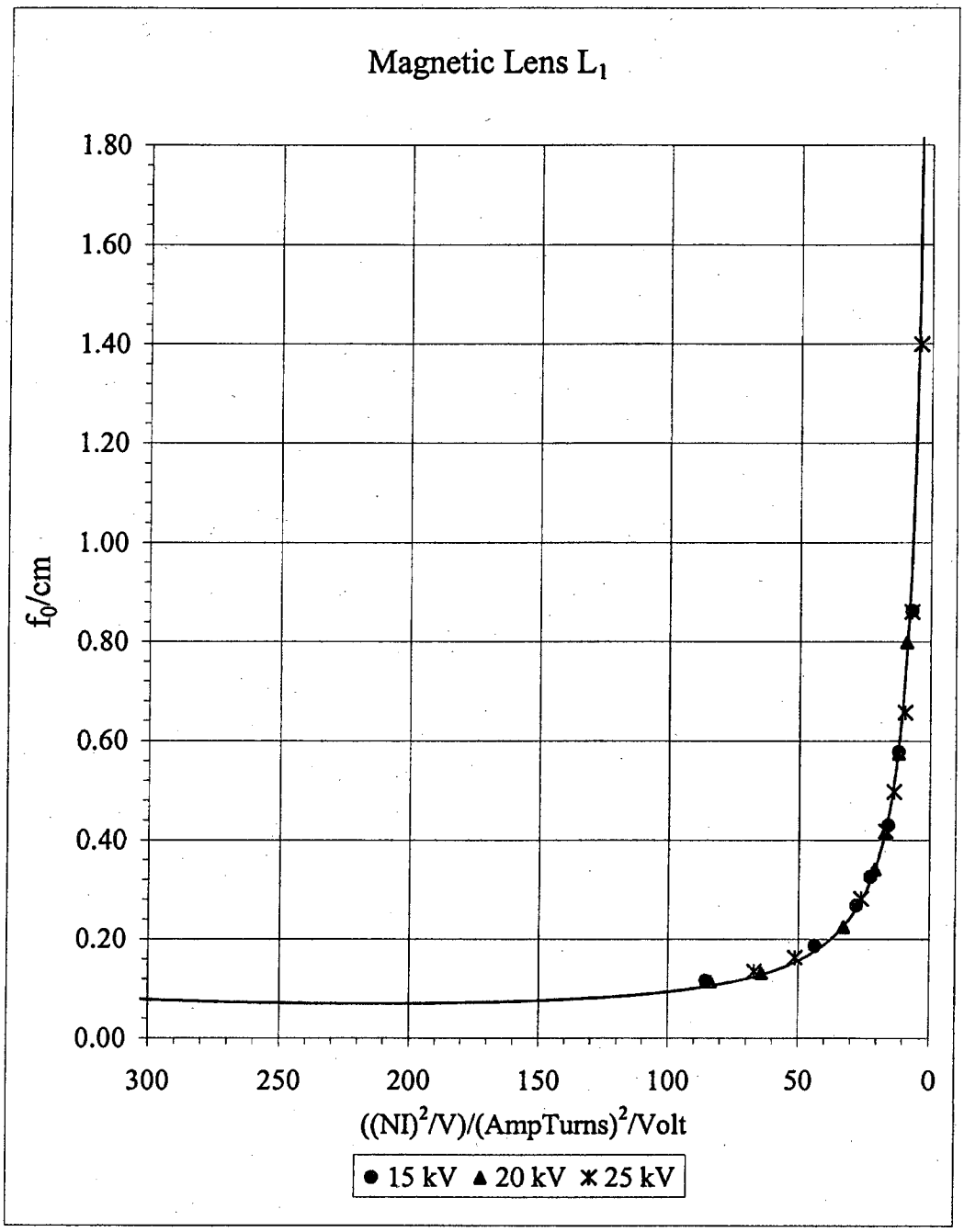

Figure 9.12. Copied graph of f_0 versus $(NI)^2/V$ from Figure 7.6(b).

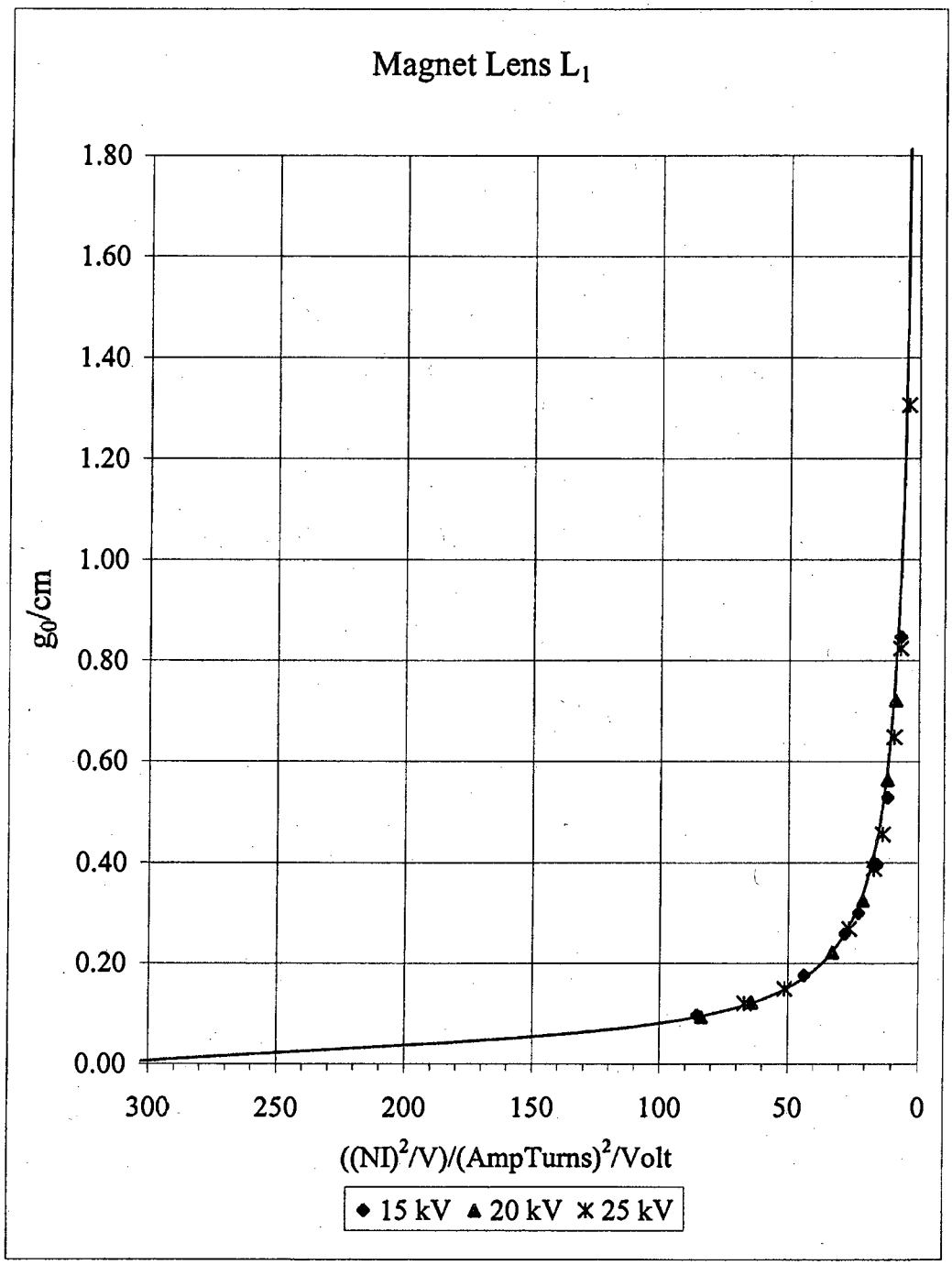

Figure 9.13. Copied graph of g_0 versus $(NI)^2/V$ from Figure 7.6(c).

The graphs, over-laid with best-fit Model curves, demonstrate the remarkably close fit between the experimental graphs and the theoretical curves, generated by Equations(9.5b) for f_0, (9.5c) for g_0, and (9.26a) for z_o'. The fit is excellent over the entire activation range used in acquiring the experimental data. The large range of agreement promotes confidence in the accuracy of the theoretical curves and equations beyond the present experimental range. The best-fit value of η was 0.74 for L_1 and 0.87 for L_2. Agreement would also provide a measure of the effective field on the axis of the actual lens.

The paraxial properties z_o', f_o, and g_o, of the experimental lens L_1 are given as a function of lens activation in Tables 7.1(b) and 7.2(b) and for L_2 are in Tables 7.3 and 7.4 of Chapter 7. These properties are also shown plotted as functions of activation parameter $(NI)^2/V$ in Figures 7.5(a), 7.6(a), and 7.6(b) for L_1 and Figures 7.7(a), 7.8(a), and 7.8(b) for L_2. The smooth curves superimposed on the experimental graphs are the model curves with η adjusted for best fit. The best fit η value for the M_1 curves was 0.74, and for the M_2 curves was 0.87. In the actual lens the paraxial magnetic field approximates a uniform field to first order in r since $dB/dr = 0$ on the axis. In this respect the field is comparable to the uniform field of the model lens.

Chapter 10. Summary, Discussion, and Conclusions

Summary

The initial goal of this research was to compare the performances of magnetic and electrostatic lenses in an application in which neither type of lens is at a disadvantage. This requirement is satisfied in a scanning electron microscope (*SEM*) in which the specimen is exterior to the objective lens. Tests were carried out in an electron-optical bench, set up to resemble an *SEM*. Two magnetic and three electrostatic lenses were used as test objective lenses. The first three chapters of this dissertation serve as a foundation for the experimental and theoretical work which follows.

In Chapter 1, the physical basis for focusing by magnetic and electrostatic lenses is discussed. The uniform magnetic-field model was used to illustrate how focusing occurs in magnetic lenses. The experimental plan for comparing the performances of the test lenses is described. The rationale for using an *SEM*-like arrangement for this purpose is explained.

Chapter 2 contains the designs and descriptions of the magnetic and electrostatic test lenses. Two different lens-field lengths were included in the choices for each type of lens. Activation parameters for the lenses were introduced. Diagrams are used to illustrate the definitions of the lens properties f and g, and the relationships between the lens properties and the image properties.

In Chapter 3, the shadowgraph method for determining the paraxial properties and aberrations of the lenses and images is presented.

Chapters 4 and 5 contain the descriptions of the experimental apparatus used in the shadowgraph method, and the operating instructions for acquiring the imaging data.

In Chapter 6, a sample of experimental data from lens L_1 shadowgraphs was used to illustrate the process of obtaining the properties (z' and m) of the image. Graphs of z' and m versus α'^2 were used to find the paraxial values z_0' and m_0, and the spherical aberration coefficients C_S' and μ_S of the image. Graphs of f and g plotted vs. $\delta^2 = (\alpha + \alpha')^2$ yielded the paraxial values f_0 and g_0, and the spherical aberration coefficients, S_f and S_g of the lens.

In Chapter 7, the procedures in Chapter 6 were carried through for all five test lenses over a range of activations. Use was made of the full body of experimental data. Results are listed in tables and plotted in graphs as functions of the parameter $P = (NI)^2/V$ for magnetic lenses L_1 and L_2, and as functions of $\mathcal{V}_{LC} = \frac{V_L}{V_C}$ for electrostatic lenses L_3, L_4, and L_5. Analytic curves of paraxial properties, obtained from the theoretical models of Chapter 9 were brought into agreement with corresponding experimental graphs by adjusting the activation of the model properties, as illustrated by the smooth analytical curves overlying the experimental graphs in Figures 7.5(a-d) and 7.6(a-d) for L_1, and in Figures 7.7(a-d) and 7.8(a-d) for L_2, and for the three electrostatic lenses in Figures 7.9(a-d) and 7.10(a-d). Derivatives of the adjusted analytical expressions were used in finding expressions for the chromatic coefficients C_C' of the image distance z_o', and C_f, and C_g, of focal length and focal

distance f_o and g_o. In Chapter 8, the tables and graphs from Chapter 7 were used to construct the graphs of C_s' vs working distance *WD* for the five test lenses. These graphs, shown together in Figure 8.1(a), were used to compare the performance of the five lenses. In the positive *WD* range, the C_s' graphs for the electrostatic lenses fall mostly between the graphs of the two magnetic lenses, short-field L_1 and long-field L_2. Lens L_5 differed from the other electrostatic lenses in having not only a longer focusing-field length, but also other dimensional changes. These graphs show that on average the spherical aberration properties of the two types of lenses are about the same. The largest differences between C_s' graphs were for lenses of the same type, but with different lens-field lengths. In the positive *WD* range, lenses with longer lens-fields had significantly lower values of C_S' than did lenses with shorter fields. In the negative *WD* range (i.e., inside the lens) the C_S' curves for short-field L_1 and long-field L_2 crossover each other, as illustrated in Figure 8.1b, where C_{S1}' dips under C_{S2}' in a part of the negative *WD* range. The dimensionless ratio C_S'/f_0 is smaller for L_2 than for L_1 over the entire experimental range. These results were unexpected, and they called for an explanation.

Graphs of the chromatic aberration coefficient C_C' vs. *WD* were also constructed from tables in Chapter 7 and modified analytical expressions from Chapter 9. These graphs show that, for the same *WD*, C_C' is about three times as large for the electrostatic lenses as for the magnetic lenses, but they did not show the strong effect of lens-field length on C_C' that was found for C_S'.

In Chapter 9, theoretical models for the magnetic and electrostatic lenses were introduced for comparison with the experimental lenses. The models have the same physical basis for focusing as the corresponding lenses do, with the advantage of having analytical paraxial expressions for the focal properties.

A. Magnetic models

The magnetic models have the same geometry of the bores and gaps as do the corresponding lenses, but they differ in that the models are assumed to have uniform fields in the gap between the bores, whereas the lenses have magnetic fields which are weakened by the presence of the bores and have a minimum, with respect to r, on the axis. The paraxial field near the minimum approximates a uniform field, as assumed for the models, but the field is weaker in magnitude, by an unknown amount. To match the magnetic field in the model to the unknown axial field in the lens, a factor η was attached to NI where it appeared in the model properties. The η-factor was reduced until the modified model curve was brought into agreement with the experimental graph, signifying that the magnetic field in the modified model agreed with the paraxial field in the lens. This comparison yielded several useful results: (i) the value of η at agreement provided a quantitative value of the effective magnetic field on the axis of the lens relative to the field between the surrounding pole faces and in the unmodified model, (ii) the axial field in the short-field lens L_1 was weaker than in the long-field lens L_2, a result which supports the experimental finding that dimensionless ratio C_{S1}/f_{01} is larger than C_{S2}/f_{02}, (iii) the good fit between the modified analytical curves and the experimental graphs enables the analytical expressions to be

used to advantage in combination with graphs, or in place of the graphs, as for instance, in calculating the chromatic coefficients C_S', C_f, and C_g. Having analytical expressions for the focal properties also makes it possible to avoid the gaps between data points and the scatter in experimental graphs, and to extend the range over which the properties can be obtained.

B. Electrostatic models

The models for the electrostatic lenses are based on the rotation-symmetric hyperbolic field. A meridional section of the hyperbolic field is shown in Figure 9.6. The curved lines are the intercepts of the equipotential surfaces with the meridional plane. In the models, the center electrode is shaped like an annular potential surface with a central opening, and is at a negative potential. The dashed lines crossing at the center are the intersections of two asymptotic cones which open in opposite directions around the *Z*-axis. The crossing point at the center is the saddle-point. The end electrodes are at ground potential, and are shaped like the equipotential surfaces crossing the axis, at the left and right in Figure 9.6, except for the axial openings needed for passage of the electrons. These openings modify the potential locally, creating thin diverging aperture lenses. The electrostatic model thus becomes a three-component lens consisting of a distributed converging hyperbolic field in the middle, terminated by a thin diverging aperture lens at each end. Analytical expressions were derived for the paraxial focal properties of the model. A surprising result was that aside from the length of the lens, the model properties depended on only a single parameter,

$$\sqrt{\frac{V_A - V_X}{V_A - V_C}} = \sqrt{v_{XC}}\,.$$

The center electrode designs in the actual lenses are very different from the hyperbolic design in the models. On the encouraging side, the models and the lenses are both three-component compound lenses and both are saddle-point lenses with negative annular center electrodes and grounded outer electrodes with centered openings. Furthermore, near the saddle point in rotation-symmetric lenses of the present type, the potential field approaches a hyperbolic-type field as in the model, except for the magnitude of the negative potential at the saddle point. The saddle-point potential depends on the design of the electrodes in the lenses. Again, adjusting the activation of the model by applying a η-factor to $\sqrt{v_{LC}}$, and a slight tweaking of the aperture-lens power, brings the theoretical curves into a match with the experimental graphs of the focal properties. From the geometry of the model electrodes, the saddle point voltage in the model is $V_A - V_X = \frac{V_A - V_L}{1.08}$; that is, the saddle point potential is not as high (negatively) as the potential of the center electrode is. The saddle-point potential in the lenses is not known, but can be found from the values of η for which the experimental graphs and theoretical curves agree. After η-adjustment for agreement between the analytical curves from the model and the experimental graphs, then

$$(V_A - V_X)_{Lens} = \eta^2 (V_A - V_X)_{\text{model}} = \eta^2 \left(\frac{V_A - V_L}{1.08} \right)_{\text{model}} \qquad 9.28(a)$$

These equations enable a quantitative value of the saddle-point potential V_X to be obtained and compared for different test lenses relative to the model value. The capability of obtaining good agreement between the analytic curves and the experimental graphs is important in a number of ways where the curves can be used in collaboration with the experimental graphs or in place of the graphs, as noted previously in this chapter.

Discussion

We experienced some luck and some surprises in our investigation of the aberrations of magnetic and electrostatic lenses. The choice of lenses for this project was originally based on the desire to have some overlap in the dimensions of the two types of lenses which were to be compared. Two different lens-field lengths were included in each category. The two magnetic lenses L_1 and L_2 differed only in focusing-field length (gap between pole-faces). This turned out to be lucky in that later analysis was simplified. Among the electrostatic lenses, the field lengths in lenses L_3 and L_4 were the same, and in L_5 the field was longer, but was accompanied by an increase in the thickness of the center electrode and the size of its axial opening. This introduced complications in analyzing the effect of field length, since the effects of the other changes were not known. Nevertheless, in the positive *WD* range, Figure 8.1(a) shows that long-field lens L_5 along with long-field magnetic lens L_2, have considerably smaller values of C_S' than do the shorter-field lenses. As *WD* increases C_S' values for L_5 crosses over L_2, going from larger to smaller values, than for L_2, indicates that the larger opening in the L_5 center electrode and increased electrode

thickness added to the effect of the longer field length. Comparison of L_4 with L_3 supports the additional effect of the larger opening. Except for this crossover, the C_S' graphs for the electrostatic lenses are contained between the graphs for the two magnetic lenses L_1 and L_2. The differences between the graphs are due, not to the different lens types, but to differences between the lengths of the focusing fields.

We were not aware of the effect on C_S' of focusing-field length until it showed up in Chapter 8. Before that, our graphs had been plotted vs. activation, rather than working distance and these graphs do not require a given image distance. When different lenses are being considered for use in an instrument, they need to be compared at the desired *WD*. In general the different lenses will require different activations, which occur at different positions along the activation axis. *WD* is the independent variable, and $z_0' = WD + z_L'$, where z_L' is the half-length of the lens, on the specimen side. The lens activation is found from graphs of z_0' vs. activation. This activation is used to find C_S', for the same lens, from graphs of C_S' vs. activation. Graphs of C_S' vs. *WD* can be built in this way. Graphs of z_0' and C_S' vs. activation are shown in Chapter 7 for all five lenses. C_S' vs. *WD* graphs are shown for the five lenses in Figure 8.1(a).

As noted above, the C_s' values were considerably lower for lenses having longer fields than for those with shorter field, whether the lenses were of the same type or of different types. An exception occurred when the magnetic lenses were operated as strong lenses, bringing the electrons to a focus within the lens boundary (negative *WD*). For part of the negative *WD* range C_{S1}' was smaller than C_{S2}'. See

insert in Figure 8.1(b) where the C_{S1}' graph dips under the C_{S2}' graph. Theoretical models were invoked for help in explaining this behavior of the C_S' vs. *WD* graphs.

Magnetic Models

Magnetic models M_1 and M_2 are uniform-field models, meaning that in the gap region between the bores the magnetic field is parallel to the lens axis and is uniform and equal to the field between the surrounding pole-pieces. The dimensions of the gaps and bores in the models are the same as those of the corresponding lenses, L_1 and L_2. The models have paraxial analytical solutions for their properties, which are functions of $NI/V^{1/2}$.

For comparison, it is known that the field on the axis of actual lens is weakened by the presence of the bores, but by how much is not known. The paraxial field in the lens approximates a uniform field because of the minimum at the axis. To find the strength of the magnetic field on the lens axis, the analytical curve for a given model property is monitored while the activation of the model is reduced. A match between the analytical curve and the experimental graph signifies a match between the axial field strengths in the model and in the lens. Reducing the model activation was accomplished by attaching a factor η to *NI* where it occurred in the expressions for the model properties, and lowering it, from 1.00 at full-strength *NI* to the matching value at the lens axis. The matched graphs and analytical curves are shown versus $(NI)^2/V$ in Chapter 7. This approach led to values of $\eta = 0.74$ and 0.89 for the effective field strength on the axes of L_1 and L_2, respectively. Between the surrounding pole-faces in each case $\eta = 1.00$. η drops by 26%, to 74% at the L_1 axis, and by 11%, to 89% at the

L_2 axis. As the gap-length increases, the field distribution approaches the uniform field of our simple lens model. From Figure 8.1(b), the C_s' values for L_1 and L_2 at *WD* = 4 mm, are about 28 cm and 16.5 cm, respectively, and for the uniform field C_s' is very small, and will be neglected here. The additional aberrations due to the non-uniform fields of L_1 and L_2 then are simply $C_S'_1 = 28$ cm and $C_s'_2 = 16.5$ cm. The ratio of $C_s'_2$ to $C_s'_1$ is 0.58; this is not far from the ratio $\frac{11\%}{26\%} = 0.46$ for the amounts by which the axial fields are weakened in the two lenses. This example illustrates the connections between the longer field length and lower C_s' for positive *WD*s. Analogous reasoning can be used for electrostatic lenses.

The dimension-less ratio C_S'/f_0 is smaller for L_2 than for L_1 over the whole experimental range investigated. C_S', by itself, is also smaller for L_2 than for L_1, except in the negative *WD* range where f_{01} has its minimum. See Figure 9.5 where the ratio C_{S2}/C_{S1} is shown vs. *WD*. L_2 would provide better resolution where the curve is less than 1.0, and L_1 would be better where the curve is greater than 1.0.

Conclusions

At the beginning of this project the main goals were to compare the spherical and chromatic aberrations, C_S' and C_C', of magnetic and electrostatic lenses, used in the same way. Analysis of the graphs of C_S' versus working distance *WD* in Chapter 8 showed that the spherical aberration coefficients were about the same for the two types of lenses used in the experiments. The graphs showed also that C_S was smaller for lenses with longer focusing fields than for lenses with shorter fields, a variable

dimension whose effect on C_S' had not been recognized in the beginning, but which luckily was included in the experiments. With respect to chromatic aberration, graphs of C_C' vs.WD showed that C_C' was about three times as large for electrostatic lenses as for magnetic lenses, but were not dependent on focusing-field length.

The finding that C_S' depends on field length changed the course of our research, and involved the aid of theoretical models in an effort to better understand the focusing fields of the lenses. Comparison of analytic curves derived from the model properties with corresponding experimental graphs enabled quantitative values to be found for the strength of the paraxial magnetic field in magnetic lenses, and showed that the paraxial field was weaker in short-field lenses than in long-field lenses. This information supports the experimental results (above) showing that C_S' is smaller for lenses with longer fields. For strong magnetic lenses, with focal points inside the lens (negative *WD*s), C_S' becomes smaller for L_1 than for L_2 as shown in Figure 9.5. The comparison of electrostatic models with the corresponding lenses follows an analogous process, with the saddle-point potential being a key parameter, but the electrostatic lenses were not operated in negative *WD* range.

The final conclusion is that this is an unfinished project. A more suitable choice of electrostatic test lenses is needed, with only one dimension at a time different between the lenses being compared. Also a series of tests to determine the optimum *WD* for a given focusing-field or vice versa would be useful. To go a little farther, testing dimensions other than the focusing-field length would be useful.

REFERENCES

(1) Panitz, J. A., Rempfer, Gertrude, 2006, Am. J. Phys. 74 (11) (953-956)

(2) Hall, Cecil E., 1966, Introduction to Electron Microscopy, 2nd (96-112)

(3) Klemperer O., Barnett M., E., Electron Optics, 3rd ed. Cambridge at the University Press (1971).

(4) Rempfer, G. F., Fyfield, M. S., and Griffith, O. H., 1997, Microscopy and Microanalysis 4, (1998).

(5) Liebmann, G., 1949, Proceedings of the Physical Society Vol. 62 Part 4 (213-228).

(6) Rempfer, G. F., J. Appl. Phys 57 (7), April (1985)

(7) Almaraz, Luis, 1997, Measurement of the Focal Properties of a Magnetic Electron Lens Using the Shadowgraph Method. Master Thesis, Portland State University.

(8) Davisson C. J., Calbick C. J., Physics Rev. 42, 580 (1932)

Additional Reading:

Jenkins F. A., White H. E., Fundamentals of Optics, 4th ed. New York, McGraw-Hill (1973).

Zworykin,V. K., Morton G. a., Ramberg E. G., Hillier, J., and Vance, A. W., 1945, Electron Optics and the Electron Microscope (11-32).

Cosslett, V. E., 1950, Introduction to Electron Optics 77-86.

Glaser W., Grundlagen der Elektoenoptik. Vienna, Springer-Verlag (1952).

Grivet P., Electron Optics, 2nd ed. New York, Pergammon Press (1972).

Hawkes, P. W., Edited, 1982, Magnetic Electron Lenses (211-216).

Munro, E., 1971, Proc. 25th Anniversary Meeting of Emag. Inst. Physics (84-87).

Rempfer, G. F., 1992, Ultramicroscopy, 47, (241-255).

Spangenberg, K, and Field, L. M., 1942, Proc Inst Radio Eng 30, 138-144.

Appendix A

Magnetic Lens L_1 Data.
Acceleration Voltage 15 kV
Gap size 0.050 inches

Mesh/inch	I/milliamps	Mesh	e'_1/cm	d/cm	b/cm		Beam	Voltage
2000	100	Rear	0.00127	26.44	0.432	US		15 kV

Bar location/ units	Shadow Reading X/cm	Spacing Δ/cm	E'/cm	M'	c/cm	$\alpha' \times 10^2$	$\alpha'^2 \times 10^4$	z'/cm
11	1.866		0.919	-65.77	-0.396	3.53	12.44	0.828
10	1.965	0.099	0.814	-64.07	-0.406	3.12	9.76	0.838
9	2.062	0.097	0.717	-62.76	-0.415	2.76	7.60	0.847
8	2.153	0.091	0.626	-61.61	-0.422	2.41	5.79	0.854
7	2.238	0.085	0.540	-60.73	-0.428	2.08	4.31	0.860
6	2.322	0.083	0.457	-60.00	-0.433	1.76	3.09	0.865
5	2.404	0.082	0.376	-59.28	-0.439	1.45	2.10	0.871
4	2.480	0.076	0.300	-58.99	-0.441	1.15	1.33	0.873
3	**2.557**	**0.077**	**0.223**	**-58.60**	**-0.444**	**0.86**	**0.74**	**0.875**
2	2.633	0.076	0.147	-57.99	-0.448	0.57	0.32	0.880
1	2.706	0.073	0.074	-58.23	-0.446	0.28	0.08	0.878
0	2.782	0.076						
-1	2.854	0.072			Slope	z_o'/cm	C_s'/cm	
-2	2.928	0.074		4.11E-05	-0.0047	0.880	46.56	
-3	3.004	0.076						
-4	3.079	0.076						
-5	3.157	0.077						
-6	3.236	0.080						
-7	3.318	0.082						
-8	3.405	0.087						
-9	3.497	0.092						
-10	3.592	0.095						
-11	3.703	0.111						

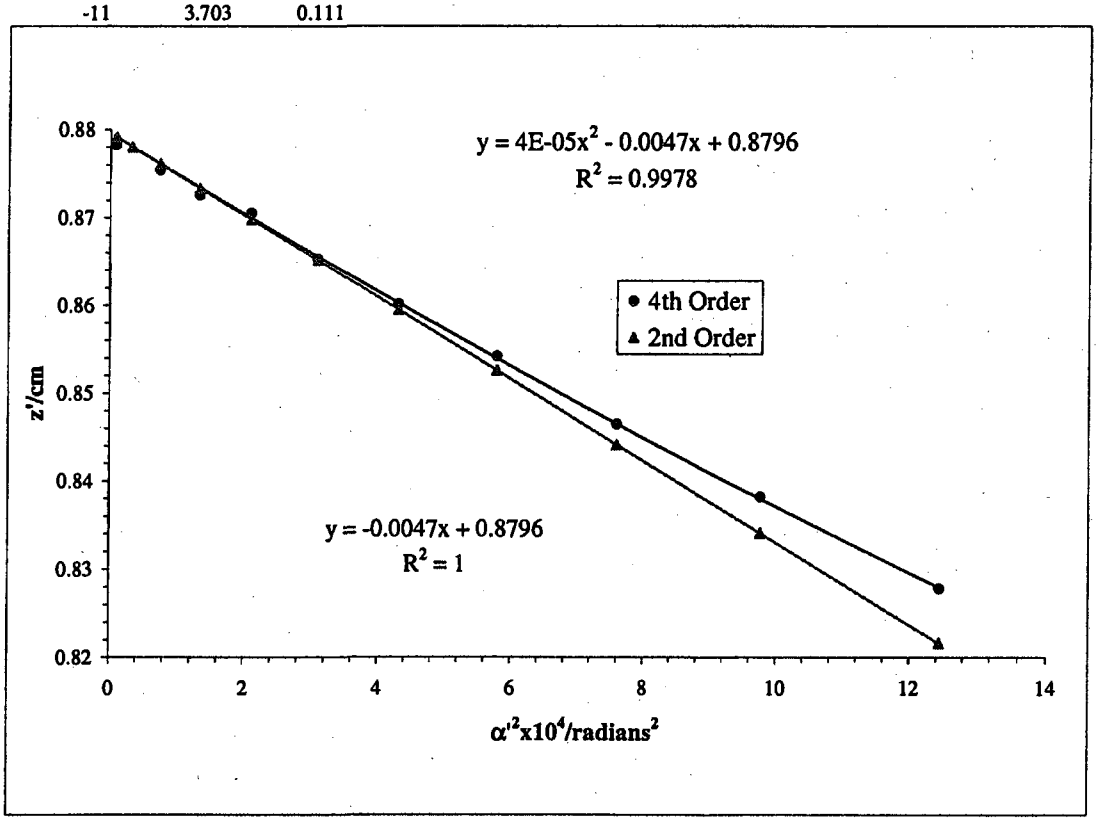

Mesh/inch	I/milliamps	Mesh	e'_1/cm	d/cm	b/cm		Beam	Voltage	15 kV
2000	100	Rear	0.00127	26.4439	0.4318	US			

Bar location/ units	Shadow Reading X/cm	Spacing Δ/cm	E'/cm	M'	c/cm	α' x 10^2	α'^2 x 10^4	z'/cm
10.5	2.240		0.868	-65.08	-0.400	3.3321	11.1027	0.832
9.5	2.335	0.0950	0.767	-63.60	-0.409	2.9473	8.6864	0.841
8.5	2.427	0.0917	0.673	-62.36	-0.417	2.5867	6.6909	0.849
7.5	2.515	0.0876	0.584	-61.33	-0.424	2.2450	5.0399	0.856
6.5	2.599	0.0845	0.501	-60.63	-0.429	1.9240	3.7017	0.861
5.5	2.681	0.0817	0.418	-59.91	-0.434	1.6088	2.5884	0.866
4.5	2.761	0.0806	0.339	-59.23	-0.439	1.3017	1.6944	0.871
3.5	2.839	0.0773	0.261	-58.81	-0.442	1.0054	1.0108	0.874
2.5	2.914	0.0751	0.186	-58.60	-0.444	0.7156	0.5120	0.876
1.5	2.988	0.0744	0.111	-58.28	-0.446	0.4271	0.1824	0.878
0.5	3.063	0.0747	0.037	-57.52	-0.452	0.1405	0.0197	0.884
-0.5	3.136	0.0731						
-1.5	3.210	0.0743			Slope	z_o'/cm	C_3'/cm	
-2.5	3.286	0.0756		6.E-05	-0.0048	0.8784	47.80	
-3.5	3.362	0.0756						
-4.5	3.438	0.0768						
-5.5	3.518	0.0793						
-6.5	3.600	0.0824						
-7.5	3.683	0.0827						
-8.5	3.774	0.0906						
-9.5	3.870	0.0965						
-10.5	3.976	0.1060						

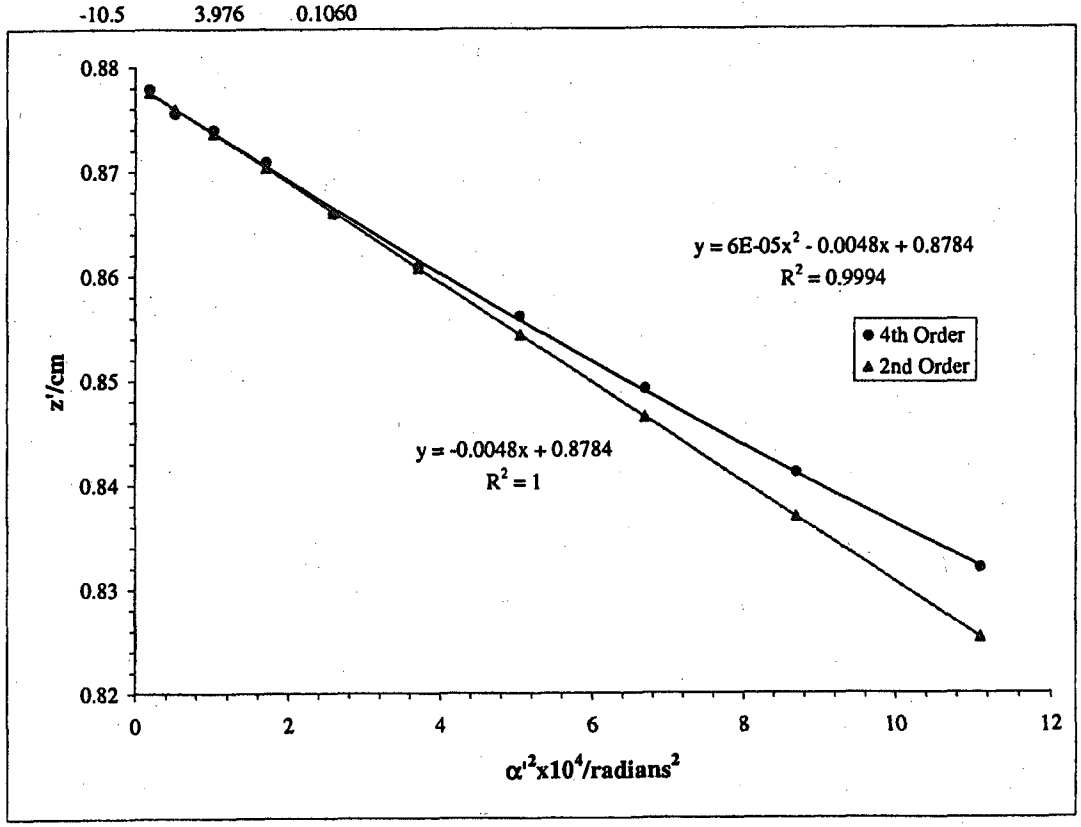

Mesh/inch	I/milliamps	Mesh	e'_1/cm	d/cm	b/cm		Beam	Voltage	15 kV
2000	100	Rear	0.00127	25.87	1.003	DS			

Bar location/ units	Shadow Reading X/cm	Spacing Δ/cm	E'/cm	M'	c/cm	$\alpha' \times 10^2$	$\alpha'^2 \times 10^4$	z'/cm
10.5	1.277		1.436	107.712	0.242	5.500	30.251	0.761
9.5	1.356	0.079	1.355	112.268	0.233	5.189	26.923	0.771
8.5	1.443	0.087	1.268	117.465	0.222	4.859	23.614	0.781
7.5	1.532	0.089	1.177	123.622	0.211	4.514	20.379	0.792
6.5	1.634	0.101	1.080	130.773	0.199	4.141	17.145	0.804
5.5	1.745	0.111	0.972	139.098	0.187	3.728	13.901	0.816
4.5	1.865	0.120	0.851	148.864	0.175	3.266	10.668	0.828
3.5	**2.001**	**0.136**	**0.715**	**160.905**	**0.162**	**2.747**	**7.547**	**0.842**
2.5	2.160	0.159	0.558	175.813	0.148	2.145	4.602	0.855
1.5	2.352	0.192	0.366	191.864	0.136	1.405	1.975	0.868
0.5	2.591	0.238	0.127	200.740	0.130	0.490	0.240	0.874
-0.5	2.846	0.255						
-1.5	3.083	0.238						
-2.5	3.276	0.193			Slope	z_o'/cm	C_z'/cm	
-3.5	3.432	0.155		0.000031	-0.0047	0.875892	47.40	
-4.5	3.566	0.135						
-5.5	3.688	0.122						
-6.5	3.793	0.105						
-7.5	3.887	0.094						
-8.5	3.979	0.092						
-9.5	4.065	0.086						
-10.5	4.149	0.084						

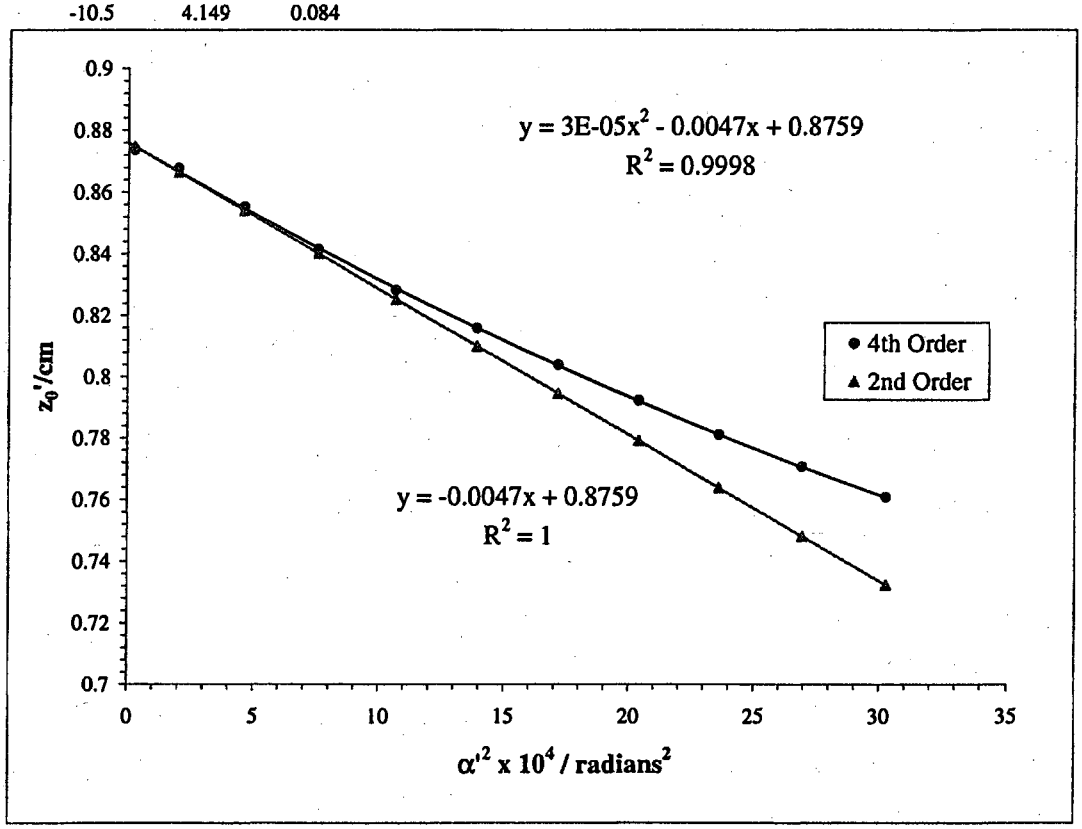

Mesh/inch	I/milliamps	Mesh	e'1/cm	d/cm	b/cm		Beam	Voltage	15 kV
2000	100	Rear	0.00127	25.87	1.003	DS			
Bar location/ units	Shadow Reading Y/cm	Spacing Δ/cm	E'/cm	M'	c/cm	α' x 10^2	α'^{2} x 10^4	z'/cm	
5.5	1.8220		0.966	138.330	0.188	3.708	13.746	0.815	
4.5	1.9418	0.120	0.846	147.987	0.176	3.247	10.542	0.827	
3.5	2.0767	0.135	0.711	160.011	0.163	2.732	7.463	0.841	
2.5	2.2332	0.156	0.552	173.992	0.150	2.123	4.507	0.854	
1.5	2.4239	0.191	0.360	189.114	0.138	1.385	1.918	0.866	
0.5	2.6568	0.233	0.127	200.286	0.130	0.489	0.239	0.873	
-0.5	2.9112	0.254							
-1.5	3.1444	0.233							
-2.5	3.3380	0.194			Slope	z_o'/cm	C_s'/cm		
-3.5	3.4992	0.161		0.000035	-0.0049	0.874793	48.53		
-4.5	3.6333	0.134							
-5.5	3.7545	0.121							

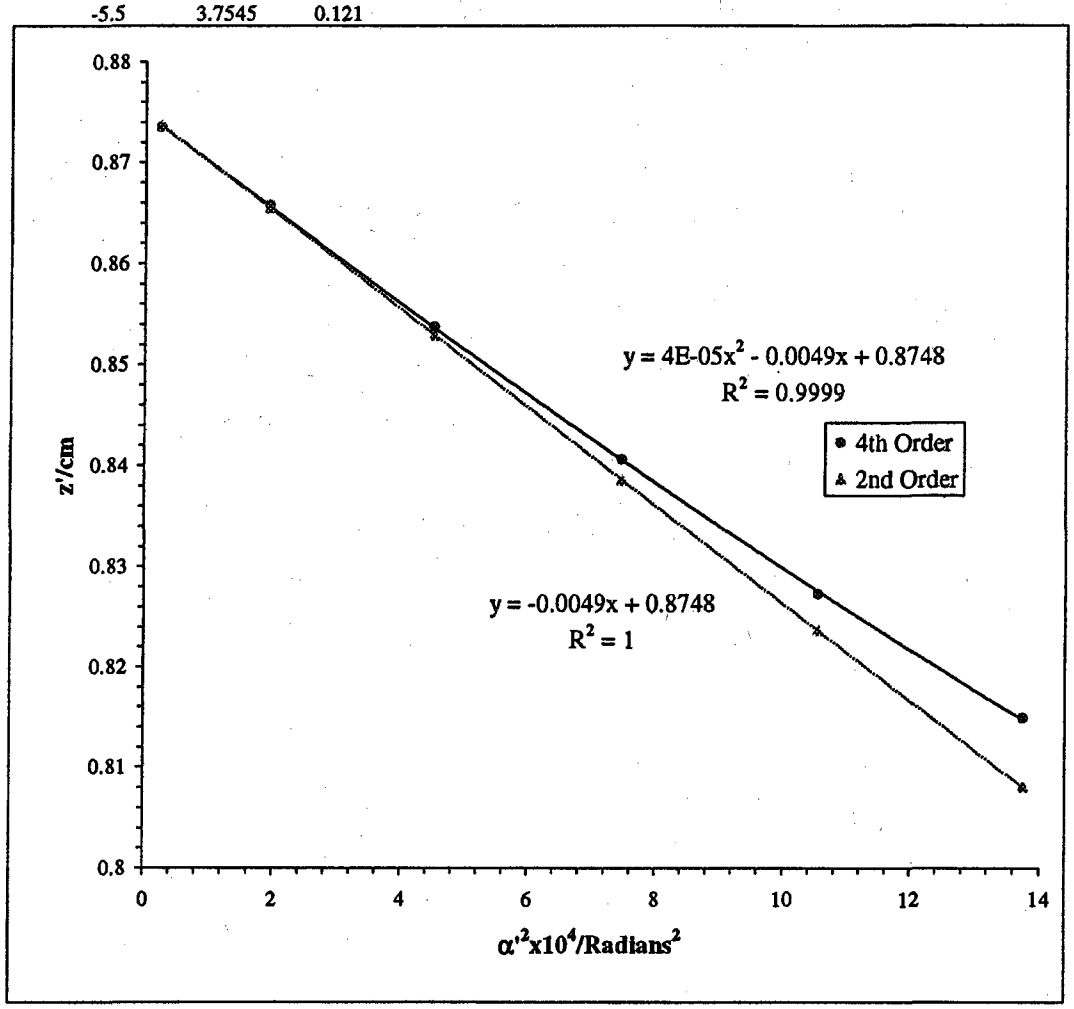

Mesh/Inch	I/milliamps	Mesh	z/cm	e_1/cm	a/cm	z_{sp}/cm	Beam z_0'/cm	Voltage C_s'/cm	15 kV $z_{sp}-z_o'$/cm
600	100	Front	25.08	0.00423	15.56	26.88	0.877	47.58	26.00

Bar location/ units	Shadow Reading X/cm	Spacing Δ/cm	E/cm	$\alpha \times 10^4$	$\alpha' \times 10^2$	$\alpha'^2 \times 10^4$	m	z'/cm	f/cm
6	1.615		1.293	16.324	4.950	24.501	0.03298	0.761	0.803
5	1.876	0.261	1.040	13.603	3.987	15.898	0.03412	0.802	0.829
4	2.113	0.236	0.809	10.883	3.106	9.649	0.03503	0.831	0.851
3	2.332	0.219	0.594	8.162	2.284	5.217	0.03573	0.852	0.867
2	2.538	0.206	0.391	5.441	1.502	2.256	0.03622	0.866	0.878
1	2.737	0.198	0.194	2.721	0.745	0.555	0.03651	0.875	0.885
0	2.931	0.194							
-1	3.124	0.193							
-2	3.319	0.195							
-3	3.520	0.201							
-4	3.731	0.211							
-5	3.956	0.225							
-6	4.201	0.245							

g/cm	$(\rho/f_0)^2 = \delta^2 = (m_0 + 1)^2 \alpha'^2$
0.734	26.328
0.773	17.083
0.801	10.368
0.821	5.606
0.835	2.425
0.842	0.597

	Slope	m_o	μ_s
1.00E-06	-0.0002	0.03661	-47.17

f vs $(\delta)^2$ $S_f = slope_f / f_0$				g vs $(\delta)^2$ $S_g = slope_g / f_0$			
	$slope_f$	fo/cm	S_f		$slope_g$	go/cm	S_g
2.057E-05	-0.003744	0.887	-42.20	-1.88E-06	-0.00415	0.845	-46.78

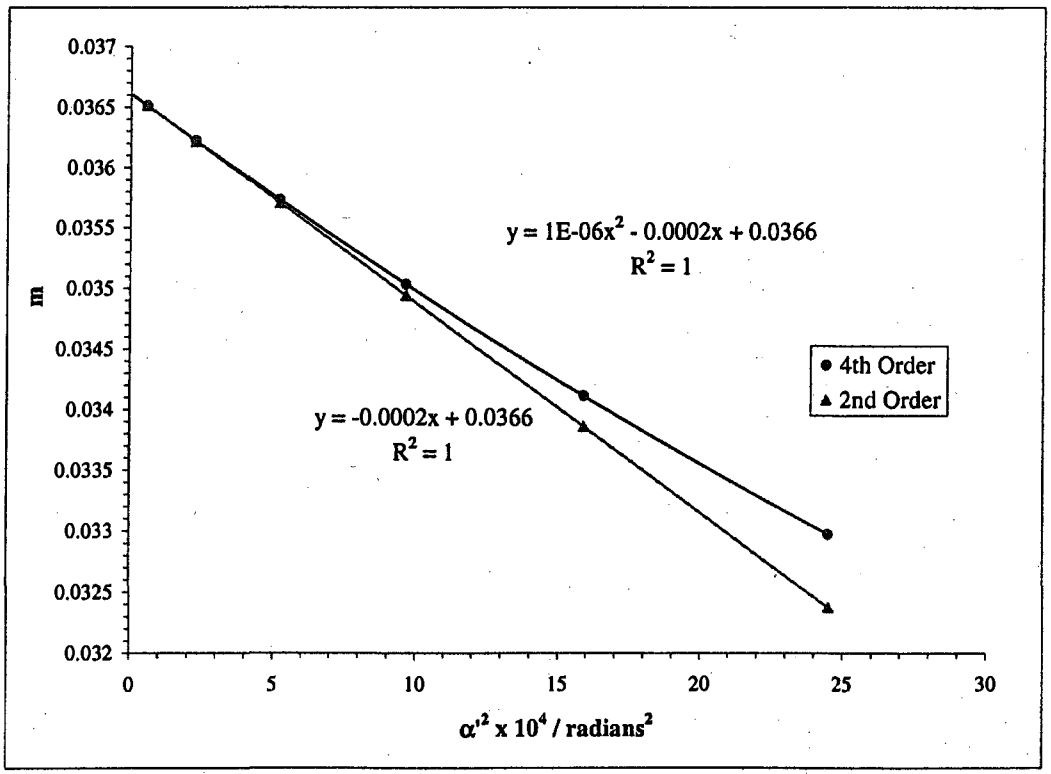

							Beam	Voltage	15 kV
Mesh/inch	I/milliamps	Mesh	z/cm	e_1/cm	a/cm	z_{ap}/cm	z_0'/cm	C_a'/cm	z_{ap}-z_0'/cm
600	100	Front	25.08	0.00423	15.56	26.88	0.877	47.58	26.00

Bar location/ units	Shadow Reading Y/cm	Spacing Δ/cm	E/cm	$\alpha \times 10^4$	$\alpha' \times 10^2$	$\alpha'^2 \times 10^4$	m	z'/cm	f/cm
5.5	1.647		1.238	14.964	4.740	22.471	0.03157	0.770	0.768
4.5	1.905	0.258	0.977	12.243	3.748	14.045	0.03267	0.810	0.794
3.5	2.142	0.237	0.739	9.522	2.839	8.057	0.03355	0.839	0.814
2.5	2.363	0.222	0.517	6.802	1.989	3.955	0.03420	0.858	0.829
1.5	2.575	0.211	0.306	4.081	1.178	1.389	0.03463	0.871	0.839
0.5	2.780	0.205	0.101	1.360	0.390	0.152	0.03485	0.876	0.844
-0.5	2.983	0.203							
-1.5	3.187	0.205					g/cm	$(\rho/f_0)^2 = \delta =$	
-2.5	3.398	0.211						$(m_0 + 1)^2 \alpha'^2$	
-3.5	3.620	0.222					0.746	24.066	
-4.5	3.859	0.239					0.784	15.042	
-5.5	4.122	0.263					0.812	8.629	
							0.830	4.236	
			Slope	m_o	μ_a		0.841	1.487	
		1.19E-06	-0.0002	0.03487	-49.81		0.847	0.163	

f vs $(\delta)^2$				g vs $(\delta)^2$			
	S_f = slope$_f$ / f_0				S_g = slope$_g$ / f_0		
	slope$_f$	fo/cm	S_f		slope$_g$	go/cm	S_g
2.46E-05	-0.0037856	0.845	-44.80	-2.09E-06	-0.00418	0.848	-49.41

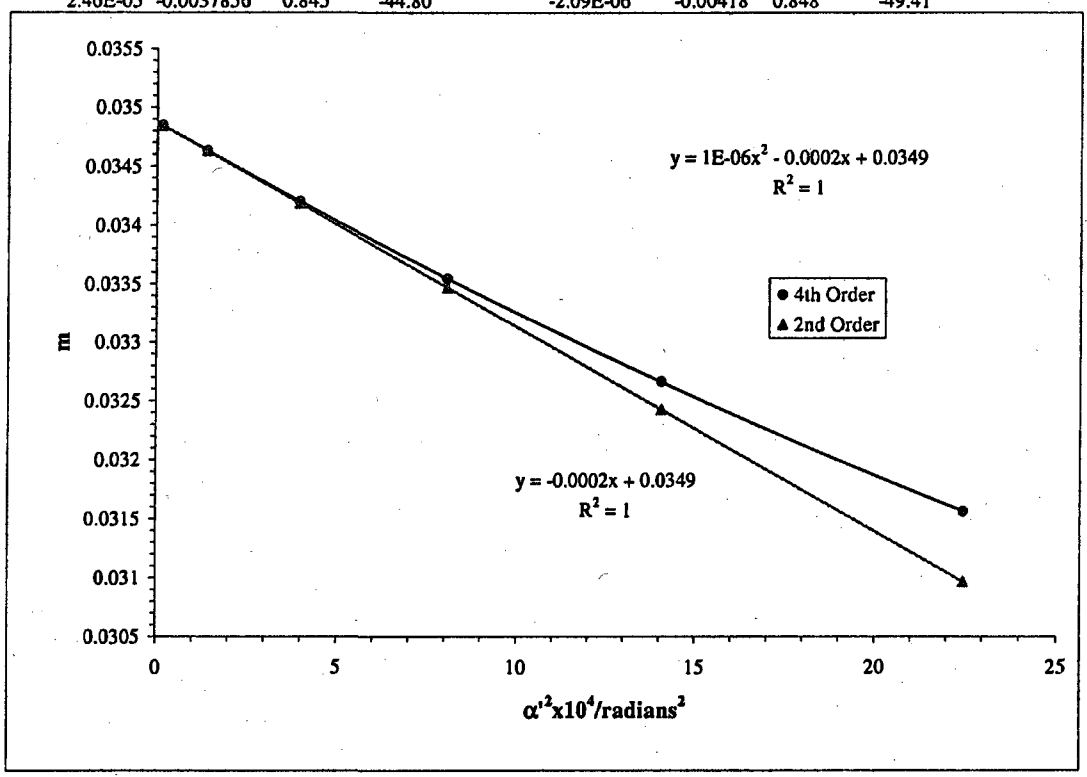

Beam Voltage	I/milliamps	z/cm	z_0'/cm	Cs'/cm
15 kV	100	25.08	0.877	47.58

Average of m_o = 0.0357

Average of μ_s = -48.49

Paraxial properties :

f_o = 0.866 cm

g_o = 0.846 cm

S_f = -43.50

S_g = -48.10

Mesh/Inch	I/milliamps	Mesh	e'1/cm	d/cm	b/cm		Beam	Voltage	15 kV
2000	130	Rear	0.00127	26.44	0.432	US			

Bar location/ units	Shadow Reading X/cm	Spacing Δ/cm	E'/cm	M'	c/cm	α' x 10^2	α'^2 x 10^4	z'/cm
3.5	0.362		1.325	-298.2	-0.088	5.03	25.29	0.520
2.5	0.843	0.481	0.853	-268.7	-0.098	3.24	10.48	0.530
1.5	1.228	0.385	0.474	-249.0	-0.106	1.80	3.24	0.538
0.5	1.553	0.325	0.152	-239.1	-0.110	0.58	0.33	0.542
-0.5	1.857	0.304						
-1.5	2.176	0.320						
-2.5	2.549	0.373			Slope	z_o'/cm	C_s'/cm	
-3.5	3.013	0.464		0.0000	-0.0014	0.542	14.16	

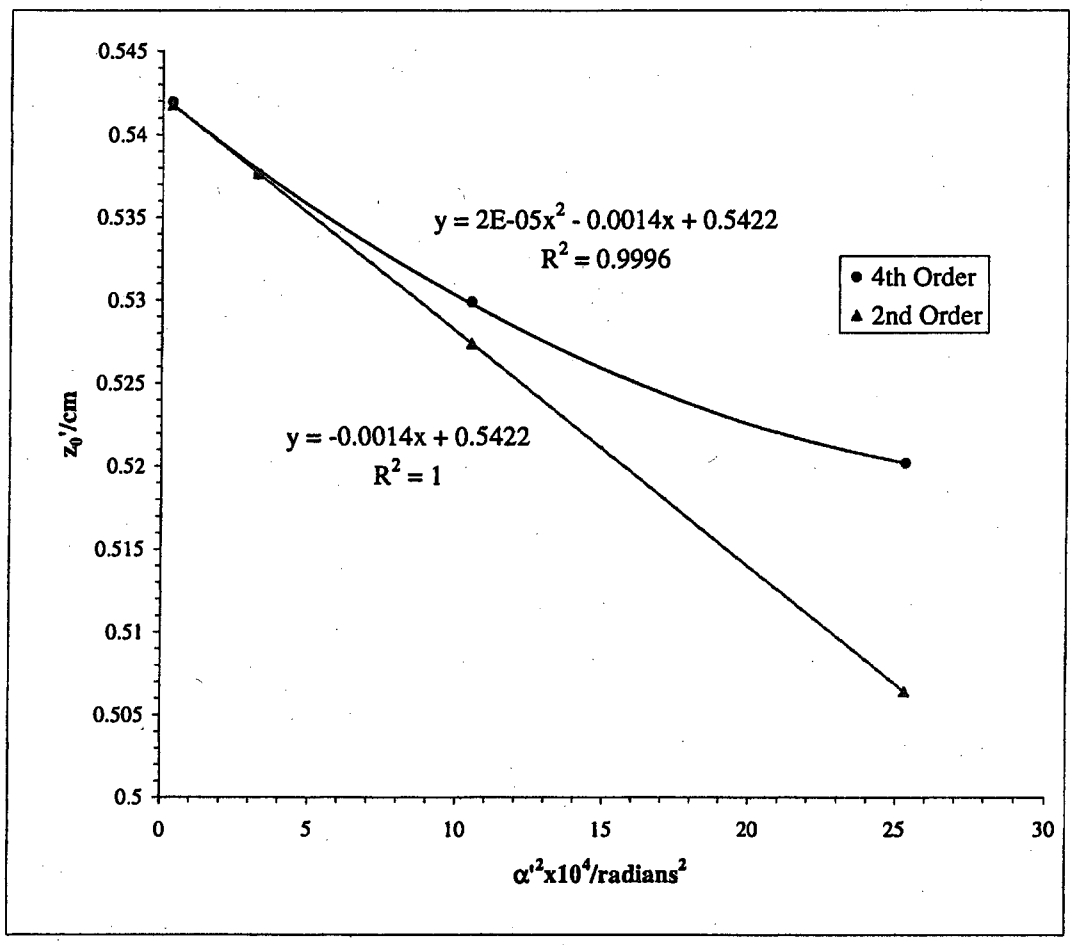

Mesh/inch	I/milliamps	Mesh	e'1/cm	d/cm	b/cm		Beam	Voltage	15 kV
2000	130	Rear	0.00127	26.4439	0.4318	US			

Bar location/ units	Shadow Reading Y/cm	Spacing Δ/cm	E'/cm	M'	c/cm	α' x 10^2	α'^2 x 10^4	z'/cm
3.5	0.1605		1.2997	-292.3984	-0.0901	4.9318	24.3225	0.5219
2.5	0.6317	0.4712	0.8398	-264.4964	-0.0996	3.1877	10.1614	0.5314
1.5	1.0105	0.3788	0.4684	-245.8951	-0.1071	1.7786	3.1635	0.5389
0.5	1.3325	0.3219	0.1502	-236.5944	-0.1113	0.5705	0.3255	0.5431
-0.5	1.6329	0.3005						
-1.5	1.9474	0.3144						
-2.5	2.3112	0.3639			Slope	z_0'/cm	C_s'/cm	
-3.5	2.7599	0.4487		2.18E-05	-0.0014	0.543	14.13	

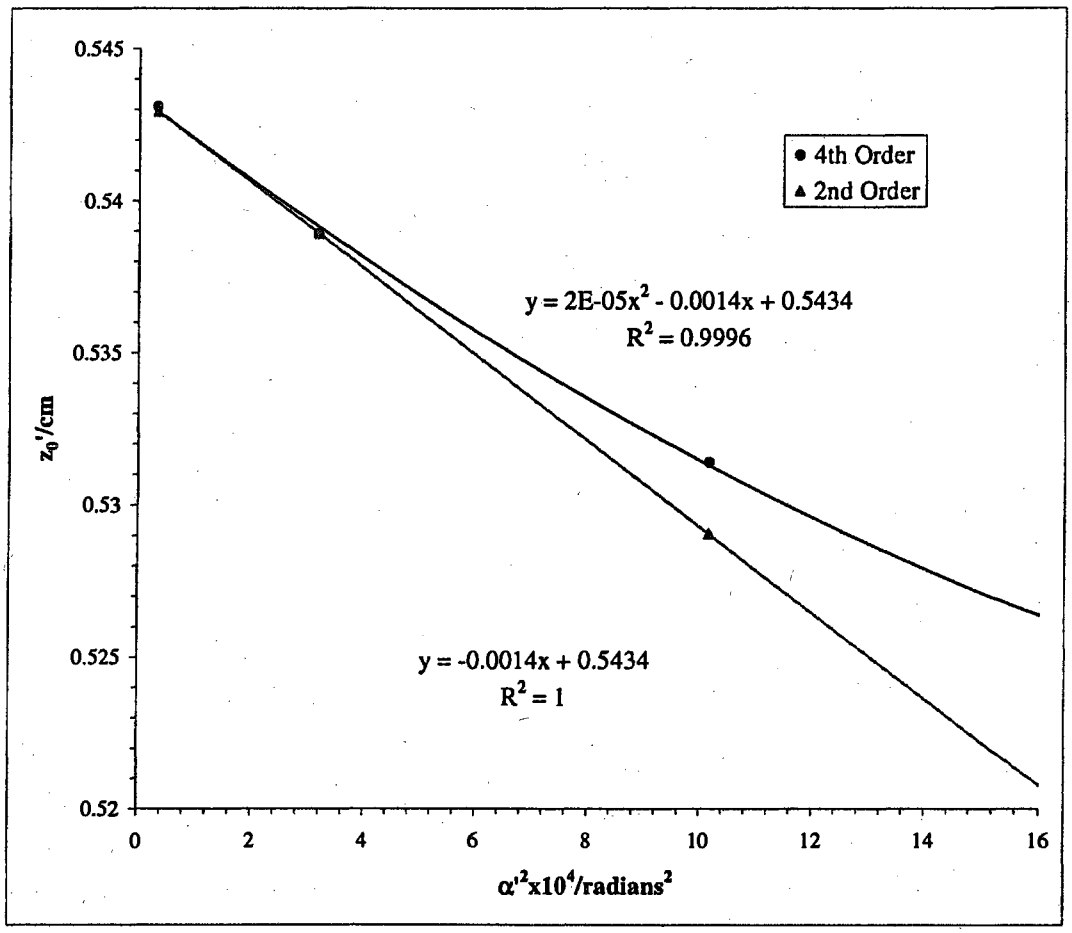

Mesh/Inch	I/milliamps	Mesh	e'1/cm	d/cm	b/cm		Beam	Voltage	15 kV
2000	130	Rear	0.00127	26.1772	0.6985	DS			

Bar location/ units	Shadow Reading X/cm	Spacing Δ/cm	E'/cm	M'	c/cm	α' x 10^2	α'^2 x 10^4	z'/cm
4.5	1.821		0.990	173.289	0.152	3.761	14.148	0.547
3.5	2.010	0.188	0.802	180.537	0.146	3.049	9.294	0.553
2.5	2.214	0.205	0.596	187.804	0.140	2.266	5.133	0.558
1.5	2.445	0.231	0.369	193.541	0.136	1.401	1.963	0.563
0.5	2.685	0.241	0.125	196.104	0.134	0.473	0.224	0.564
-0.5	2.934	0.249						
-1.5	3.182	0.248			Slope	z_o'/cm	C_s'/cm	
-2.5	3.407	0.225		0.000005	-0.0014	0.565	13.90	
-3.5	3.615	0.208						
-4.5	3.802	0.188						

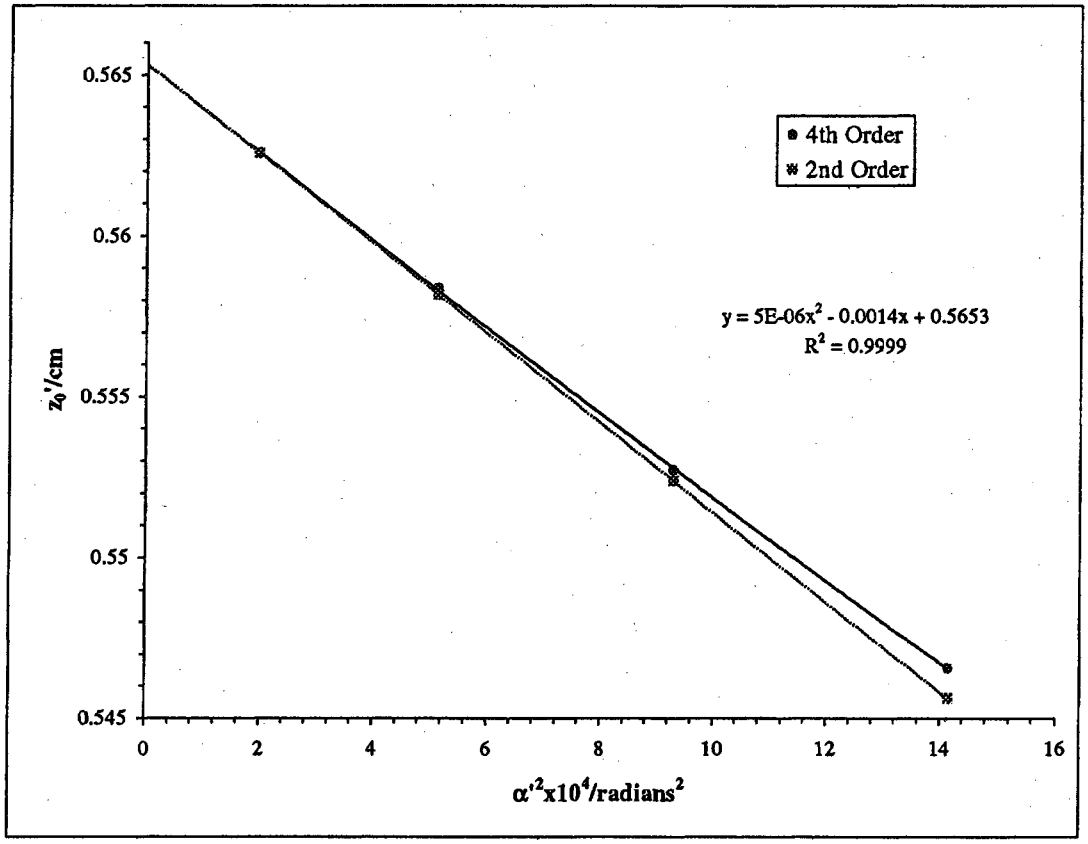

Mesh/inch	I/milliamps	Mesh	e'1/cm	d/cm	b/cm		Beam	Voltage	15 kV
2000	130	Rear	0.00127	26.1772	0.6985	DS			

Bar location/ units	Shadow Reading Y/cm	Spacing Δ/cm	E'/cm	M'	c/cm	$\alpha' \times 10^2$	$\alpha'^2 \times 10^4$	z'/cm
5.5	2.1852		1.152	164.972	0.160	4.375	19.144	0.539
4.5	2.3573	0.172	0.981	171.647	0.153	3.726	13.880	0.545
3.5	2.5491	0.192	0.794	178.720	0.147	3.018	9.107	0.551
2.5	2.7604	0.211	0.587	184.876	0.142	2.230	4.974	0.556
1.5	2.9886	0.228	0.364	190.947	0.138	1.382	1.911	0.561
0.5	3.2302	0.242	0.124	195.010	0.135	0.471	0.221	0.564
-0.5	3.4778	0.248						
-1.5	3.7162	0.238						
-2.5	3.9344	0.218						
-3.5	4.1379	0.204			Slope	z_0'/cm	C_s'/cm	
-4.5	4.3193	0.181		0.000010	-0.0015	0.564	14.85	
-5.5	4.4899	0.171						

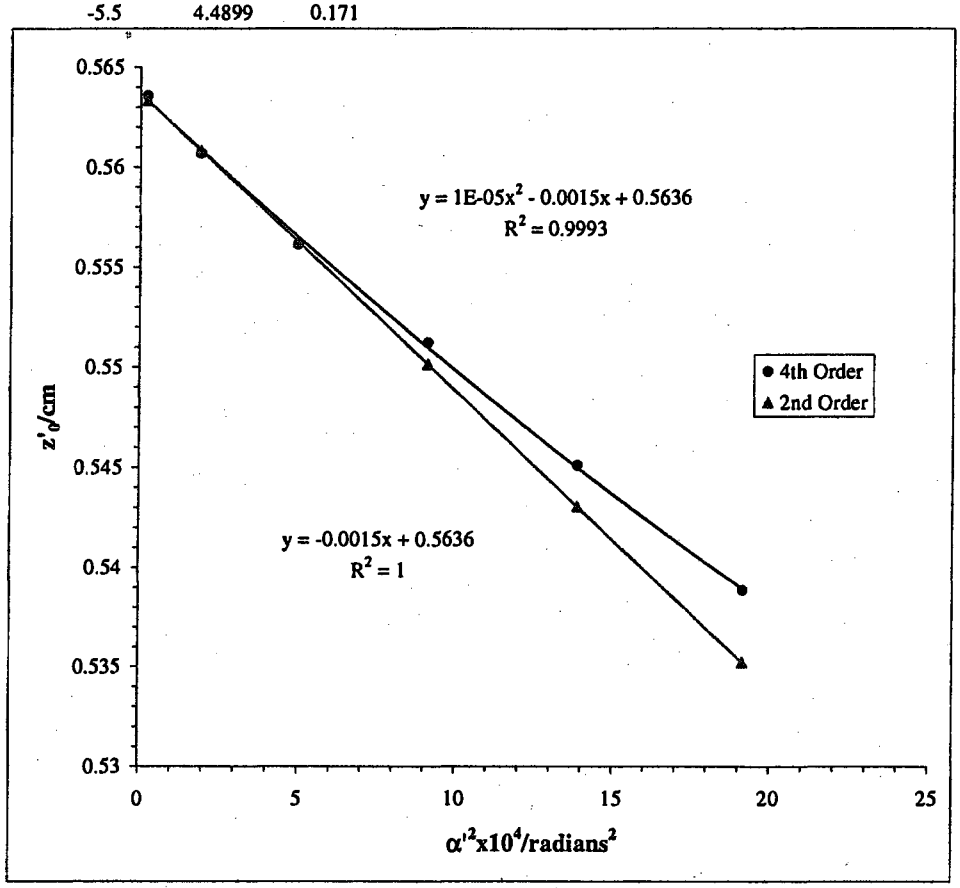

							Beam	Voltage	15 kV
Mesh/inch	I/milamp	Mesh	z/cm	e_1/cm	a/cm	z_{sp}/cm	z_0'/cm	C_z'/cm	$z_{sp}-z_o'$
600	130	Front	25.08	0.00423	15.56	26.8757	0.543	14.147	26.333

Bar location/ units	Shadow Reading X/cm	Spacing Δ/cm	E/cm	$\alpha \times 10^4$	$\alpha' \times 10^2$	$\alpha'^2 \times 10^4$	m	z'/cm	f/cm
4	1.3936		1.306	10.883	4.954	24.541	0.02197	0.508	0.540
3	1.7498	0.356	0.962	8.162	3.650	13.320	0.02236	0.524	0.549
2	2.0873	0.337	0.633	5.441	2.402	5.768	0.02266	0.535	0.556
1	2.4112	0.324	0.314	2.721	1.191	1.419	0.02284	0.541	0.561
0	2.7266	0.315							
-1	3.0387	0.312					g/cm	$(\rho/f_0)^2 = \delta =$	
-2	3.3525	0.314						$(m_0+1)^2 \alpha'^2$	
-3	3.6733	0.321					0.496	25.678	
-4	4.0061	0.333					0.512	13.937	
							0.522	6.035	
		Slope	m_o	μ_s			0.528	1.485	
	1.9E-07	0.0000	0.02290	-18.57					

f vs $(\delta)^2$ $S_f = slope_f / f_0$				g vs $(\delta)^2$ $S_g = slope_g / f_0$			
	$slope_f$	fo/cm	S_f		$slope_g$	go/cm	S_g
4.26E-06	-0.00097	0.562	-17.22	-2.22E-07	-0.00131	0.530	-23.26

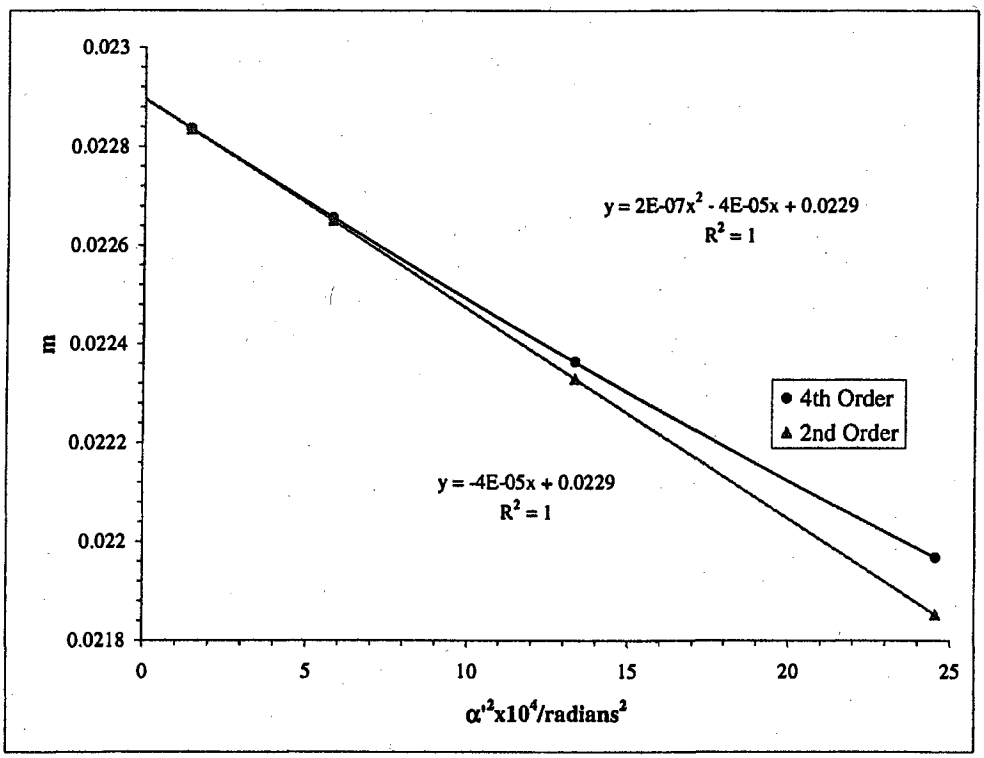

							Beam	Voltage	15 kV
Mesh/inch	I/milamp	Mesh	z/cm	e_1/cm	a/cm	z_{ap}/cm	z_0'/cm	C_s'/cm	z_{ap}-z_0'
600	130	Front	25.08	0.004233	15.56	26.88	0.543	14.15	26.33

Bar location/ units	Shadow Reading X/cm	Spacing Δ/cm	E/cm	$\alpha \times 10^4$	$\alpha' \times 10^2$	$\alpha'^2 \times 10^4$	m	z'/cm	f/cm
3.5	1.459		1.064	9.522	4.039	16.313	0.02358	0.520	0.579
2.5	1.775	0.316	0.750	6.802	2.848	8.109	0.02388	0.531	0.587
1.5	2.081	0.305	0.446	4.081	1.694	2.869	0.02410	0.539	0.592
0.5	2.379	0.299	0.148	1.360	0.562	0.316	0.02420	0.542	0.594
-0.5	2.675	0.296							
-1.5	2.973	0.297							
-2.5	3.276	0.303							
-3.5	3.588	0.312							

	Slope	m_o	μ_s
1.96E-07	0.0000	0.024215	-17.49

g/cm	$(\rho/f_0)^2 = \delta =$ $(m_0 + 1)^2 \alpha'^2$
0.506	17.112
0.517	8.507
0.524	3.009
0.528	0.331

f vs $(\delta)^2$ $S_f = slope_f / f_0$			
	$slope_f$	fo/cm	S_f
4.341E-06	-0.00096	0.595	-16.15

g vs $(\delta)^2$ $S_g = slope_g / f_0$			
	$slope_g$	go/cm	S_g
-2.4159E-07	-0.001301	0.528	-21.89

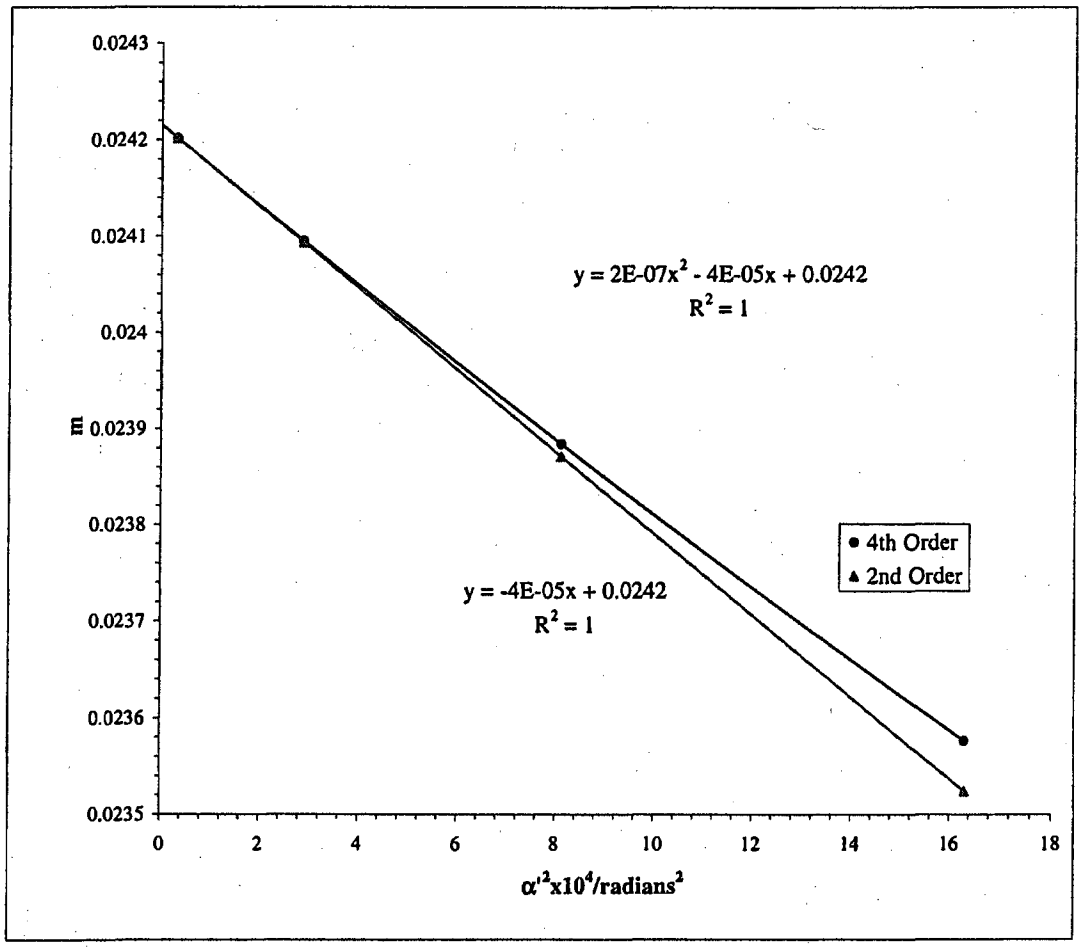

Beam Voltage	I/milamp	z/cm	z_0'/cm	Cs'/cm
15 kV	130	25.1	0.543	14.1

Average of m_o = 0.0236

Average of μ_s = -18.0

Paraxial properties :

f_o = 0.578 cm

g_o = 0.529 cm

S_f = -16.7

S_g = -22.6

Mesh/inch	I/milliamps	Mesh	e'_1/cm	d/cm	b/cm		Beam	Voltage	15 kV
2000	150	Rear	0.00127	26.39	0.483	DS			

Bar location/ units	Shadow Reading X/cm	Spacing Δ/cm	E'/cm	M'	c/cm	α' x 10^2	α'^2 x 10^4	z'/cm
8.5	0.545		2.443	226.3	0.117	9.22	84.94	0.365
7.5	0.742	0.197	2.251	236.3	0.112	8.49	72.11	0.370
6.5	0.952	0.210	2.044	247.6	0.107	7.71	59.47	0.376
5.5	1.181	0.229	1.820	260.6	0.102	6.87	47.20	0.381
4.5	1.435	0.254	1.572	275.1	0.096	5.93	35.22	0.386
3.5	1.716	0.281	1.296	291.6	0.091	4.89	23.95	0.392
2.5	2.037	0.321	0.983	309.6	0.086	3.71	13.78	0.397
1.5	2.409	0.372	0.620	325.3	0.081	2.34	5.48	0.401
0.5	2.820	0.411	0.216	339.5	0.078	0.81	0.66	0.405
-0.5	3.251	0.431						
-1.5	3.648	0.397						
-2.5	4.004	0.355						
-3.5	4.308	0.305						
-4.5	4.579	0.271						
-5.5	4.822	0.242			Slope	z_o'/cm	C_s'/cm	
-6.5	5.039	0.218		1.185E-06	-0.00056	0.405	5.603	
-7.5	5.243	0.204						
-8.5	5.431	0.188						

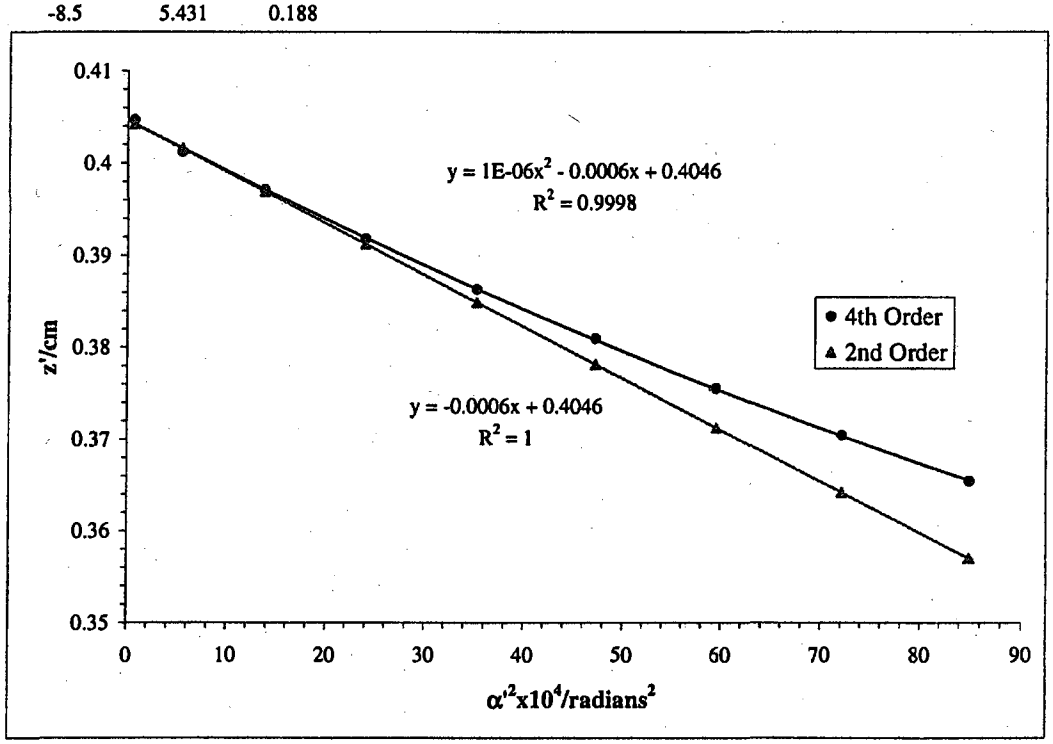

Mesh/inch	I/milliamps	Mesh	e'1/cm	d/cm	b/cm		Beam	Voltage	15 kV
2000	150	Rear	0.00127	26.39314	0.4826	DS			

Bar location/ units	Shadow Reading Y/cm	Spacing Δ/cm	E'/cm	M'	c/cm	α' x 10^2	α'^2 x 10^4	z'/cm
7.5	0.8646		2.248	236.0	0.112	8.48	71.93	0.370
6.5	1.0730	0.208	2.041	247.3	0.107	7.70	59.33	0.375
5.5	1.2997	0.227	1.814	259.6	0.102	6.84	46.85	0.381
4.5	1.5493	0.250	1.564	273.7	0.097	5.91	34.87	0.386
3.5	1.8252	0.276	1.287	289.6	0.091	4.86	23.62	0.391
2.5	2.1386	0.313	0.973	306.5	0.086	3.67	13.50	0.396
1.5	2.4955	0.357	0.614	322.3	0.082	2.32	5.38	0.400
0.5	2.8995	0.404	0.209	329.4	0.080	0.79	0.62	0.402
-0.5	3.3178	0.418						
-1.5	3.7235	0.406			Slope	z_0'/cm	C_s'/cm	
-2.5	4.0848	0.361		8.821E-07	-0.00052	0.403	5.165	
-3.5	4.3995	0.315						
-4.5	4.6778	0.278						
-5.5	4.9268	0.249						
-6.5	5.1554	0.229						
-7.5	5.3605	0.205						

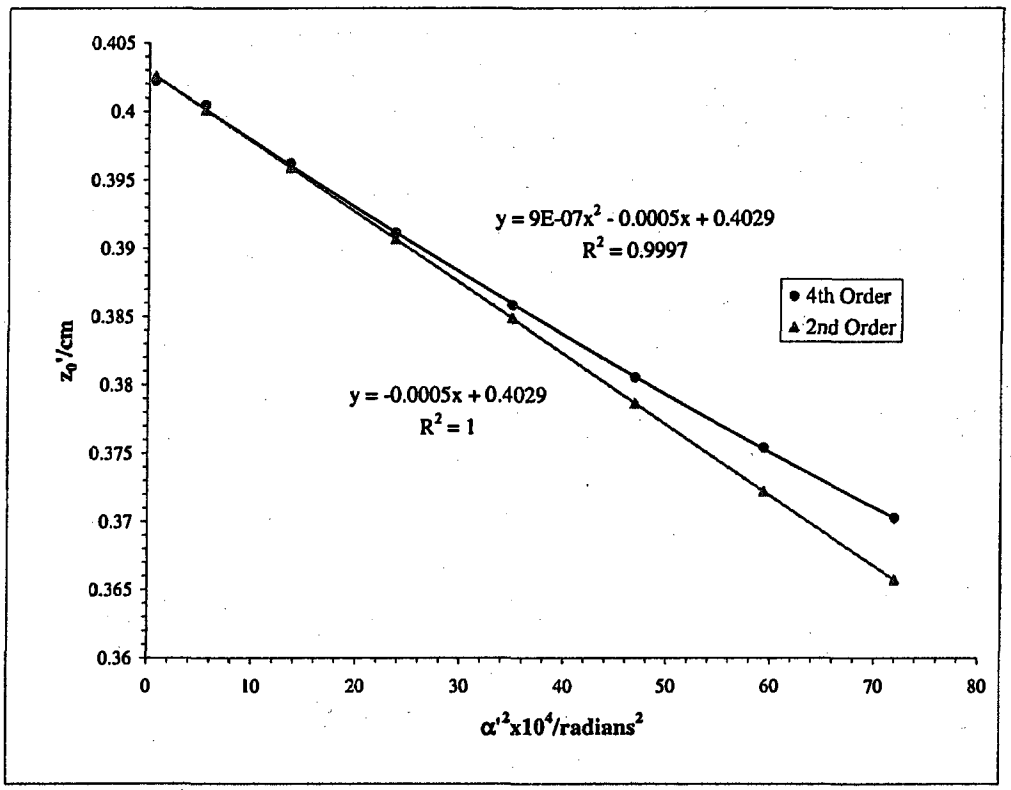

							Beam	Voltage	15 kV
Mesh/inch	I/milamp	Mesh	z/cm	e_1/cm	a/cm	z_{ap}/cm	z_0'/cm	C_s'/cm	$z_{ap}-z_0'$
600	150	Front	25.08	0.004233	15.56	26.88	0.404	5.384	26.47

Bar location/ units	Shadow Reading X/cm	Spacing Δ/cm	E/cm	$\alpha \times 10^4$	$\alpha' \times 10^2$	$\alpha'^2 \times 10^4$	m	z'/cm	f/cm
5	0.6213		2.169	13.600	8.183	66.968	0.01662	0.367693	0.41080
4	1.0991	0.478	1.685	10.880	6.361	40.458	0.01710	0.381965	0.42258
3	1.5430	0.444	1.238	8.160	4.673	21.837	0.01746	0.391991	0.43123
2	1.9662	0.423	0.813	5.440	3.070	9.424	0.01772	0.398674	0.43750
1	2.3743	0.408	0.403	2.720	1.524	2.321	0.01785	0.402498	0.44069
0	2.7785	0.404							
-1	3.1810	0.402					g/cm	$(\rho/f_0)^2 = (m_0+1)^2\alpha'^2$	
-2	3.5918	0.411							
-3	4.0182	0.426					0.36087	69.387	
-4	4.4695	0.451					0.37474	41.920	
-5	4.9599	0.490					0.38446	22.626	
							0.39092	9.765	
			Slope	m_0	μ_s		0.39463	2.405	
		2.1E-08	0.0000	0.017905	-11.50				

	f vs $(\rho/f_0)^2$ $S_f = slope_f / f_0$				g vs $(\rho/f_0)^2$ $S_g = slope_g / f_0$		
	$slope_f$	fo/cm	S_f		$slope_g$	go/cm	S_g
4.7E-07	-0.00048	0.442	-10.90	-2.5E-08	-0.00050	0.396	-11.36

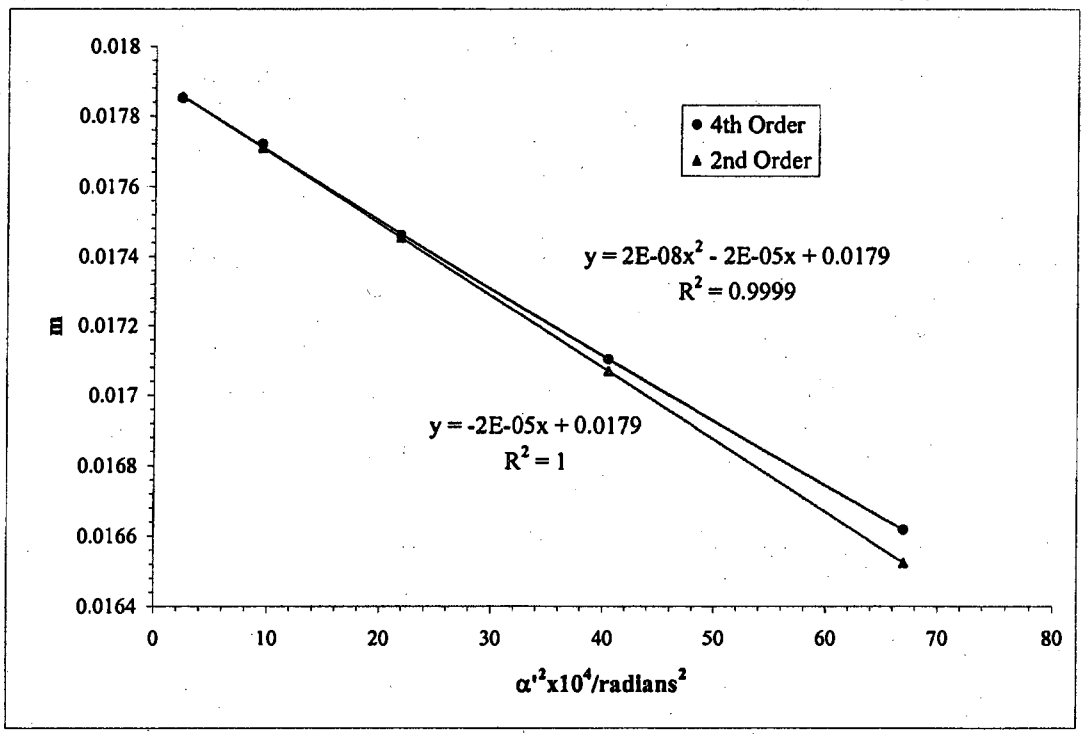

							Beam	Voltage	15 kV
Mesh/inch	I/milamp	Mesh	z/cm	e_t/cm	a/cm	z_{sp}/cm	z_o'/cm	C_s'/cm	$z_{sp}-z_o'$
600	150	Front	25.08	0.00423333	15.5639	26.87574	0.4037	5.384	26.472

Bar location/ units	Shadow Reading Y/cm	Spacing Δ/cm	E/cm	$\alpha \times 10^4$	$\alpha' \times 10^2$	$\alpha'^2 \times 10^4$	m	z'/cm	f/cm
4.5	0.6293		2.032	12.240	7.667	58.781	0.01596	0.372	0.395
3.5	1.1209	0.492	1.544	9.520	5.830	33.991	0.01633	0.385	0.403
2.5	1.5844	0.464	1.084	6.800	4.093	16.753	0.01661	0.395	0.410
1.5	2.0276	0.443	0.643	4.080	2.427	5.891	0.01681	0.401	0.415
0.5	2.4583	0.431	0.213	1.360	0.804	0.647	0.01691	0.403	0.417
-0.5	2.8842	0.426							
-1.5	3.3129	0.429							
-2.5	3.7521	0.439							
-3.5	4.2097	0.458							
-4.5	4.6933	0.484							

g/cm	$(\rho/f_o)^2 = (m_o + 1)^2 \alpha'^2$
0.366	60.79
0.379	35.15
0.388	17.32
0.394	6.09
0.396	0.67

	Slope	m_o	μ_s
4.8E-08	-1.91E-05	0.016920	-11.27

f vs $(\rho/f_o)^2$, $S_f = slope_f / f_o$

	$slope_f$	fo/cm	S_f
1.1E-06	-0.00045	0.41765	-10.69

g vs $(\rho/f_o)^2$, $S_g = slope_g / f_o$

	$slope_g$	go/cm	S_g
-4.2E-08	-0.00051	0.396681	-12.10

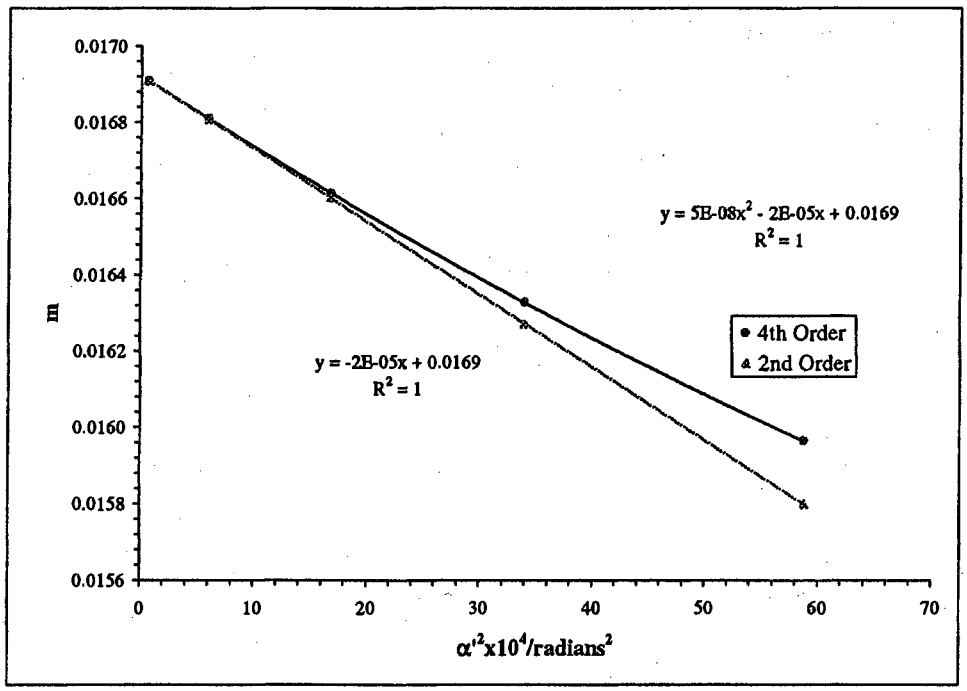

Beam Voltage	I/milamp	z/cm	z_0'/cm	C_s'/cm
15 kV	150	25.1	0.404	5.38

Average of m_o = 0.0174

Average of μ_s = -11.4

Paraxial properties :

f_o = 0.430 cm

g_o = 0.396 cm

S_f = -10.8

S_g = -11.7

Mesh/inch	I/milamp	Mesh	e'_1/cm	d/cm	b/cm		Beam	Voltage	15 kV
2000	180	Rear	0.00127	26.4439	0.4318	DS			

Bar location/ units	Shadow Reading X/cm	Spacing Δ/cm	E'/cm	M'	c/cm	α' x 10^2	α'^2 x 10^4	z'/cm
5.5	1.7276		1.3841	198.2	0.1341	5.2079	27.1218	0.2977
4.5	1.9664	0.2388	1.1478	200.8	0.1323	4.3189	18.6529	0.2995
3.5	2.2102	0.2438	0.9044	203.5	0.1306	3.4032	11.5816	0.3012
2.5	2.4633	0.2531	0.6533	205.8	0.1292	2.4584	6.0436	0.3026
1.5	2.7233	0.2600	0.3956	207.7	0.1279	1.4889	2.2168	0.3039
0.5	2.9871	0.2638	0.1321	208.1	0.1277	0.4973	0.2473	0.3041
-0.5	3.2514	0.2643						
-1.5	3.5146	0.2632						
-2.5	3.7698	0.2552			Slope	z_o'/cm	C_s'/cm	
-3.5	4.0189	0.2492		0.0000	-0.0003	0.3043	2.8553	
-4.5	4.2620	0.2430						
-5.5	4.4959	0.2339						

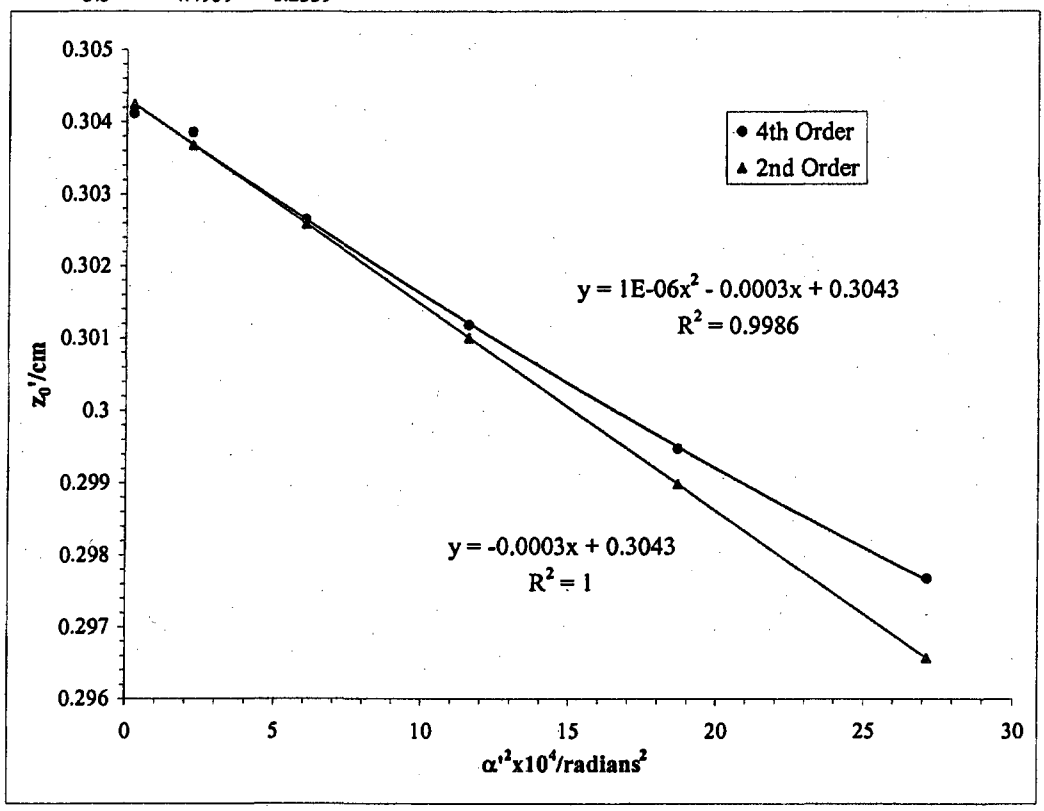

Mesh/inch	I/milamp	Mesh	e'_1/cm	d/cm	b/cm		Beam	Voltage	15 kV
2000	180	Rear	0.00127	26.4439	0.4318	DS			

Bar location/ units	Shadow Reading Y/cm	Spacing Δ/cm	E'/cm	M'	c/cm	α' x 10^2	α'^2 x 10^4	z'/cm
10	0.947		2.339	184.1	0.144	8.795	77.358	0.287
9	1.147	0.199	2.138	187.1	0.142	8.044	64.700	0.290
8	1.353	0.207	1.933	190.2	0.140	7.271	52.864	0.292
7	1.569	0.216	1.717	193.1	0.138	6.457	41.699	0.294
6	1.793	0.224	1.493	195.9	0.136	5.617	31.551	0.296
5	2.026	0.233	1.262	198.8	0.134	4.749	22.556	0.298
4	2.267	0.241	1.023	201.4	0.132	3.849	14.815	0.300
3	2.516	0.249	0.775	203.3	0.131	2.915	8.496	0.301
2	2.770	0.254	0.521	205.2	0.130	1.961	3.846	0.302
1	3.030	0.260	0.261	205.7	0.129	0.983	0.967	0.303
0	3.294	0.263						
-1	3.553	0.259		Slope	z_o'/cm	C_s'/cm		
-2	3.813	0.260	2.8E-07	-0.0002	0.3030	2.228		
-3	4.065	0.253						
-4	4.313	0.247						
-5	4.550	0.237						
-6	4.779	0.229						
-7	5.002	0.223						
-8	5.219	0.217						
-9	5.423	0.205						
-10	5.624	0.201						

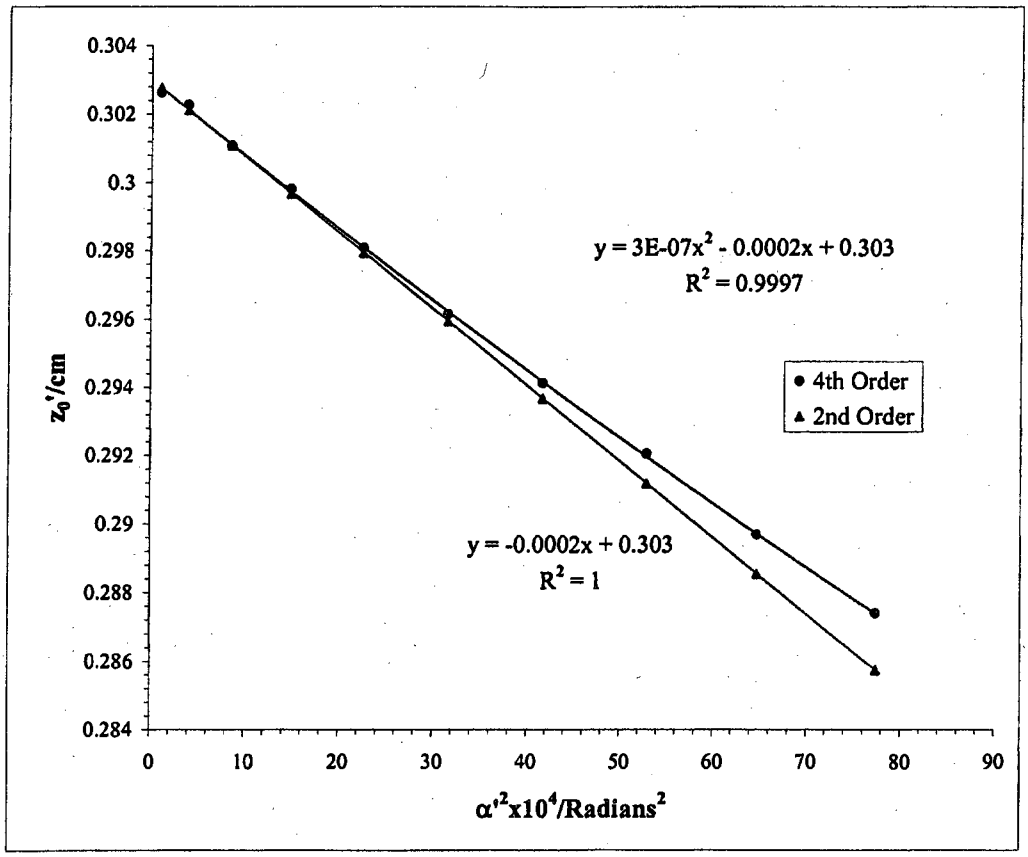

							Beam	Voltage	15 kV
Mesh/Inch	I/milamp	Mesh	z/cm	e_1/cm	a/cm	z_{sp}/cm	z_0'/cm	C_s'/cm	$z_{sp}-z_o'$
600	180	Front	25.08	0.0042333	15.56	26.88	0.304	2.542	26.57

Bar location/ units	Shadow Reading X/cm	Spacing Δ/cm	E/cm	$\alpha \times 10^4$	$\alpha' \times 10^2$	$\alpha'^2 \times 10^4$	m	z'/cm	f/cm
5	0.353		2.846	13.600	10.699	114.467	0.01271	0.275	0.315
4	1.001	0.648	2.213	10.880	8.321	69.240	0.01308	0.286	0.324
3	1.596	0.595	1.628	8.160	6.123	37.493	0.01333	0.294	0.330
2	2.160	0.565	1.069	5.440	4.022	16.177	0.01353	0.300	0.335
1	2.704	0.543	0.531	2.720	2.000	3.999	0.01360	0.303	0.337
0	3.232	0.528							
-1	3.767	0.534					g/cm	$(\rho/f_0)^2 = \delta =$ $(m_0+1)^2 \alpha'^2$	
-2	4.298	0.532							
-3	4.851	0.553					0.271	117.611	
-4	5.426	0.575					0.282	71.143	
-5	6.045	0.619					0.290	38.523	
							0.295	16.621	
							0.298	4.109	

	Slope	m_0	μ_s
1.43E-09	-8.31E-06	0.0136435	-6.09

f vs $(\delta)^2$

$S_f = slope_f / f_0$

	$slope_f$	f_o/cm	S_f
3.18E-08	-0.0002	0.338	-5.83

g vs $(\delta)^2$

$S_g = slope_g / f_0$

	$slope_g$	g_o/cm	S_g
-2E-09	-0.00024	0.299	-7.16

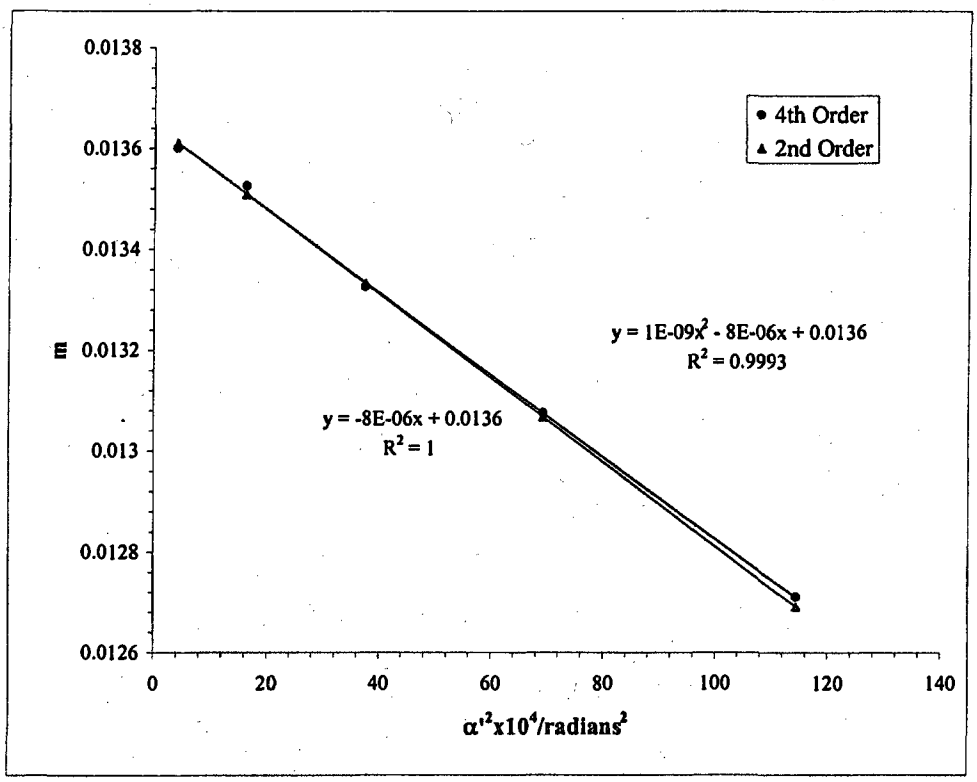

							Beam	Voltage	15 kV
Mesh/Inch	I/milamp	Mesh	z/cm	e_1/cm	a/cm	z_{zp}/cm	z_0'/cm	C_z'/cm	$z_{zp}-z_o'$
600	180	Front	25.08	0.00423	15.56	26.88	0.304	2.542	26.57

Bar location/ units	Shadow Reading Y/cm	Spacing Δ/cm	E/cm	α x 10^4	α' x 10^2	α'^{2} x 10^4	m	z'/cm	f/cm
4	0.434		2.416	10.880	9.086	82.555	0.01197	0.283	0.297
3	1.069	0.634	1.771	8.160	6.661	44.369	0.01225	0.292	0.304
2	1.674	0.605	1.161	5.440	4.367	19.072	0.01246	0.299	0.309
1	2.259	0.585	0.574	2.720	2.161	4.672	0.01258	0.302	0.312
0	2.833	0.574							
-1	3.407	0.575							
-2	3.995	0.588							
-3	4.610	0.615							
-4	5.267	0.657							

	Slope	m_o	μ_s
1.5E-08	-9.2E-06	0.012626	-7.26

g/cm	$(\rho/f_0)^2 = \delta = (m_0 + 1)^2 \alpha'^2$
0.279	84.65
0.289	45.50
0.295	19.56
0.299	4.79

f vs $(\delta)^2$

$S_f = slope_f / f_0$

	$slope_f$	fo/cm	S_f
3.616E-07	-0.00022	0.313	-6.99

g vs $(\delta)^2$

$S_g = slope_g / f_0$

	$slope_g$	go/cm	S_g
-1.0E-08	-0.00024	0.300	-7.75

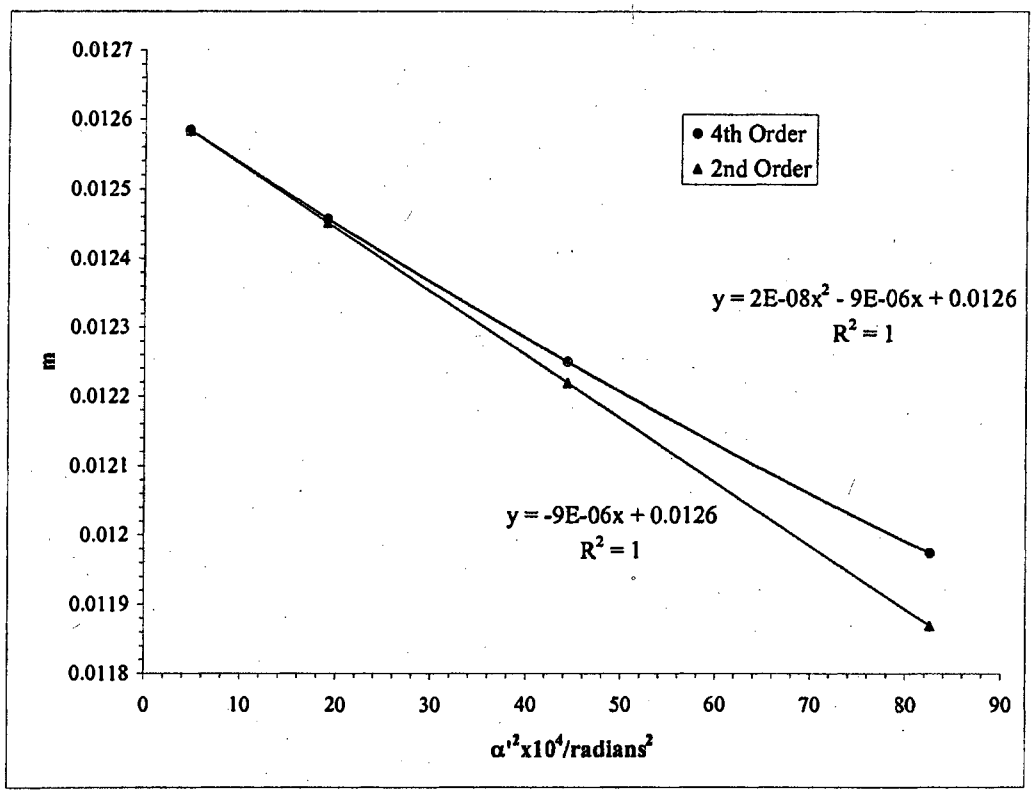

Beam Voltage	I/milamp	z/cm	z_0'/cm	C_s'/cm
15 kV	180	25.08	0.3036	2.54

Average of m_o = 0.0131

Average of μ_s = -6.68

Paraxial properties :

f_o = 0.325 cm

g_o = 0.299 cm

S_f = -6.41

S_g = -7.45

Mesh/inch	I/milliamp	Mesh	e'_1/cm	d/cm	b/cm		Beam	Voltage	15 kV
2000	200	Rear	0.00127	26.44	0.432	DS			

Bar location/ units	Shadow Reading X/cm	Spacing Δ/cm	E'/cm	M'	c/cm	$\alpha' \times 10^2$	$\alpha'^2 \times 10^4$	z'/cm
6.5	1.716		1.262	152.9	0.174	4.7422	22.4883	0.2577
5.5	1.904	0.188	1.074	153.7	0.173	4.0340	16.2735	0.2586
4.5	2.094	0.191	0.883	154.4	0.172	3.3159	10.9949	0.2594
3.5	2.287	0.193	0.689	155.0	0.172	2.5889	6.7023	0.2601
2.5	2.482	0.195	0.494	155.5	0.171	1.8546	3.4397	0.2606
1.5	2.679	0.197	0.297	155.8	0.171	1.1150	1.2433	0.2610
0.5	2.876	0.198	0.099	155.9	0.171	0.3720	0.1384	0.2611
-0.5	3.074	0.198						
-1.5	3.272	0.198		Slope	z_0'/cm	C_s'/cm		
-2.5	3.469	0.197	0.0000	-0.0002	0.2611	1.568		
-3.5	3.665	0.196						
-4.5	3.859	0.194						
-5.5	4.051	0.192						
-6.5	4.240	0.189						

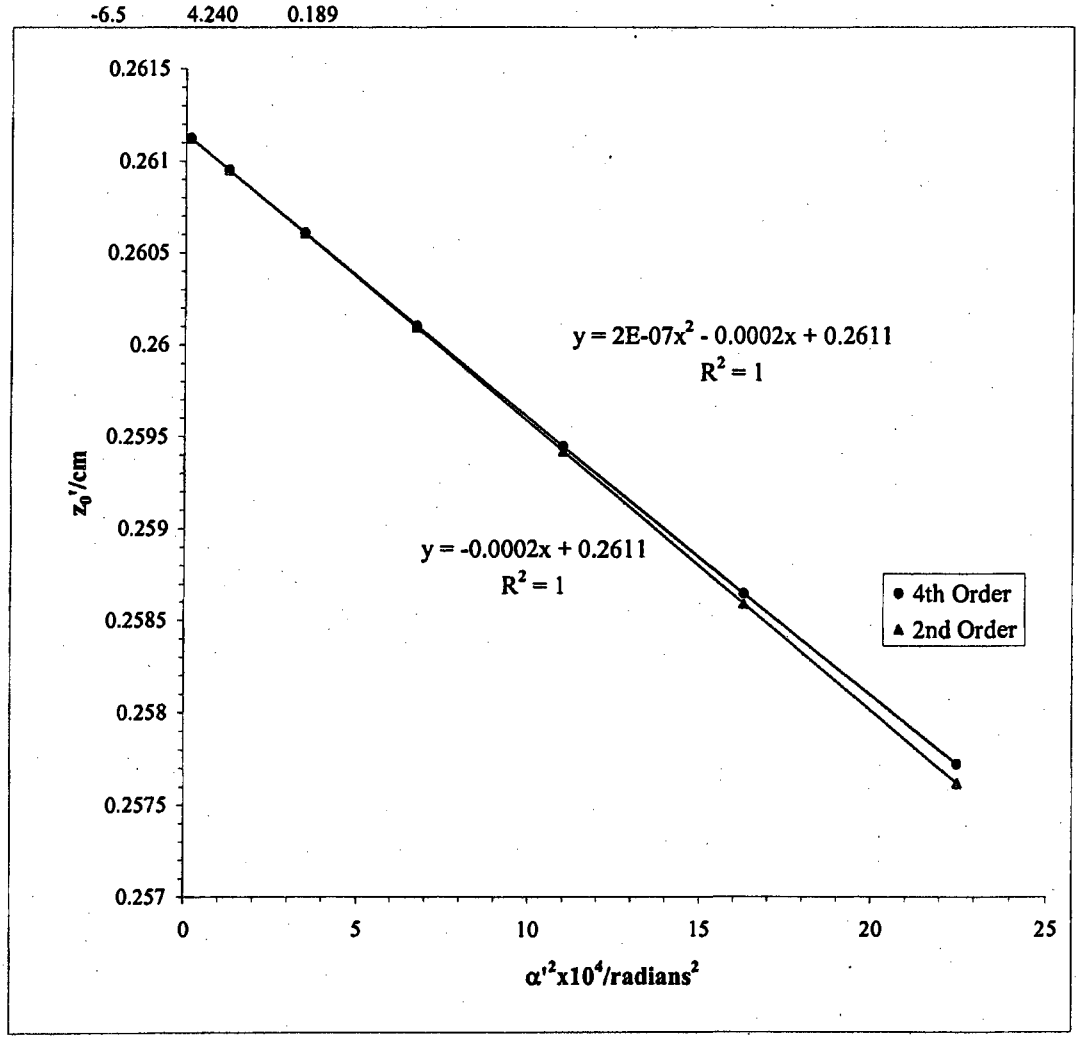

Mesh/inch	I/milliamp	Mesh	e'_1/cm	d/cm	b/cm		Beam	Voltage	15 kV
2000	200	Rear	0.00127	26.4439	0.4318	DS			

Bar location/ units	Shadow Reading Y/cm	Spacing Δ/cm	E'/cm	M'	c/cm	α' x 10^2	α'^2 x 10^4	z'/cm
12.5	0.144		2.331	146.8	0.1813	8.756	76.663	0.2505
11.5	0.313	0.169	2.162	148.0	0.1799	8.119	65.921	0.2519
10.5	0.485	0.172	1.989	149.2	0.1785	7.471	55.814	0.2533
9.5	0.661	0.176	1.813	150.3	0.1772	6.810	46.376	0.2546
8.5	0.841	0.180	1.633	151.3	0.1759	6.136	37.653	0.2559
7.5	1.024	0.183	1.451	152.3	0.1748	5.450	29.699	0.2570
6.5	1.211	0.187	1.265	153.2	0.1738	4.751	22.572	0.2580
5.5	1.401	0.190	1.076	154.0	0.1729	4.041	16.330	0.2589
4.5	1.593	0.192	0.884	154.7	0.1721	3.321	11.029	0.2597
3.5	1.787	0.195	0.690	155.2	0.1715	2.592	6.720	0.2603
2.5	1.984	0.196	0.494	155.6	0.1710	1.857	3.447	0.2608
1.5	2.181	0.197	0.297	155.9	0.1707	1.116	1.246	0.2611
0.5	2.379	0.198	0.099	156.1	0.1705	0.372	0.139	0.2613
-0.5	2.5773	0.198						
-1.5	2.7751	0.198						
-2.5	2.9719	0.197				Slope	z_0'/cm	C_s'/cm
-3.5	3.1672	0.195			6.97E-08	-0.0001	0.2613	1.4678
-4.5	3.3606	0.193						
-5.5	3.5517	0.191						
-6.5	3.740	0.188						
-7.5	3.925	0.185						
-8.5	4.108	0.182						
-9.5	4.287	0.179						
-10.5	4.463	0.176						
-11.5	4.636	0.173						
-12.5	4.806	0.170						

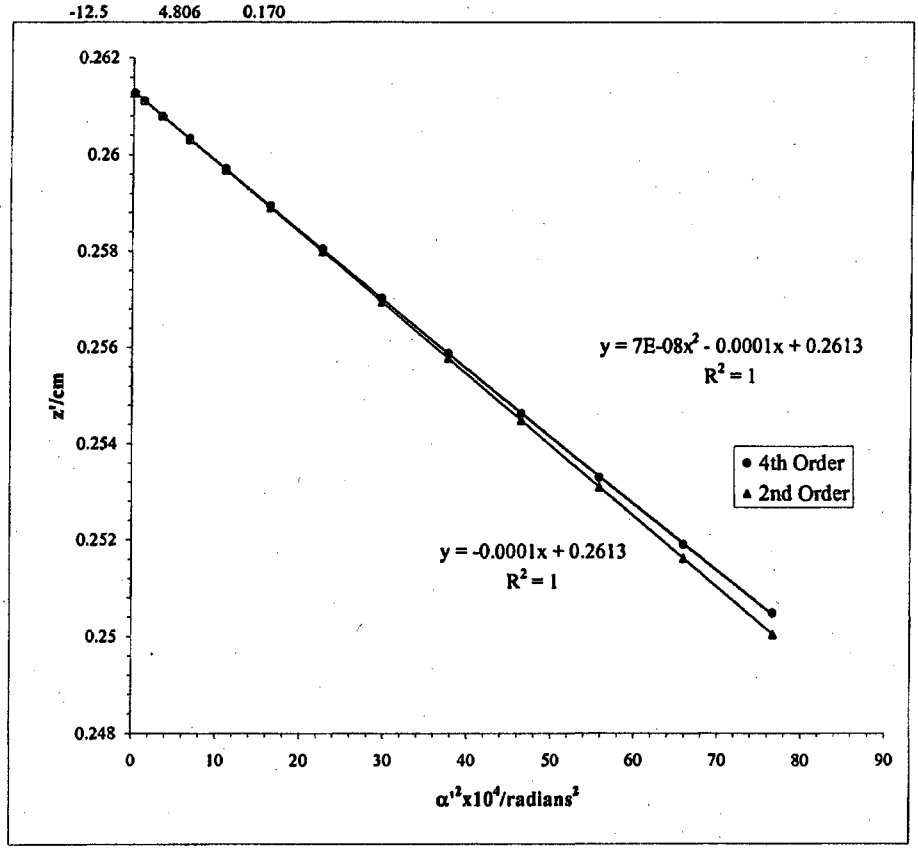

							Beam	Voltage	15 kV
Mesh/inch	I/milliamp	Mesh	z/cm	e_1/cm	a/cm	z_{sp}/cm	z_0'/cm	C_s'/cm	$z_{sp}-z_0'$/cm
2000	200	Front	25.08	0.00127	15.56	26.88	0.261	1.518	26.61

Bar location/ units	Shadow Reading X/cm	Spacing Δ/cm	E/cm	$\alpha \times 10^4$	$\alpha' \times 10^3$	$\alpha'^2 \times 10^4$	m	z'/cm	f/cm
6.5	2.088		1.343	5.304	5.044	25.445	0.01051	0.2574	0.2610
5.5	2.299	0.210	1.132	4.488	4.252	18.081	0.01055	0.2585	0.2620
4.5	2.507	0.208	0.923	3.672	3.468	12.028	0.01059	0.2594	0.2628
3.5	2.714	0.207	0.716	2.856	2.691	7.239	0.01061	0.2601	0.2634
2.5	2.919	0.205	0.511	2.040	1.918	3.679	0.01063	0.2607	0.2639
1.5	3.123	0.204	0.306	1.224	1.149	1.321	0.01065	0.2610	0.2643
0.5	3.327	0.204	0.102	0.408	0.383	0.147	0.01066	0.2612	0.2644
-0.5	3.531	0.204							
-1.5	3.735	0.204					g/cm	$(\rho/f_0)^2 = \delta =$	
-2.5	3.940	0.205						$(m_0+1)^2 \alpha'^2$	
-3.5	4.146	0.206					0.2546	25.990	
-4.5	4.353	0.207					0.2557	18.469	
-5.5	4.562	0.209					0.2566	12.285	
-6.5	4.774	0.211					0.2573	7.394	
							0.2579	3.758	
			Slope	m_o	μ_s		0.2582	1.350	
		8.8E-09	-5.78E-06	0.010656	-5.43		0.2584	0.150	

f vs $(\delta)^2$

$S_f = slope_f / f_0$

	$slope_f$	fo/cm	S_f
2.084E-07	-0.00014	0.264	-5.25

g vs $(\delta)^2$

$S_g = slope_g / f_0$

	$slope_g$	go/cm	S_g
-5.1E-09	-0.00015	0.258	-5.51

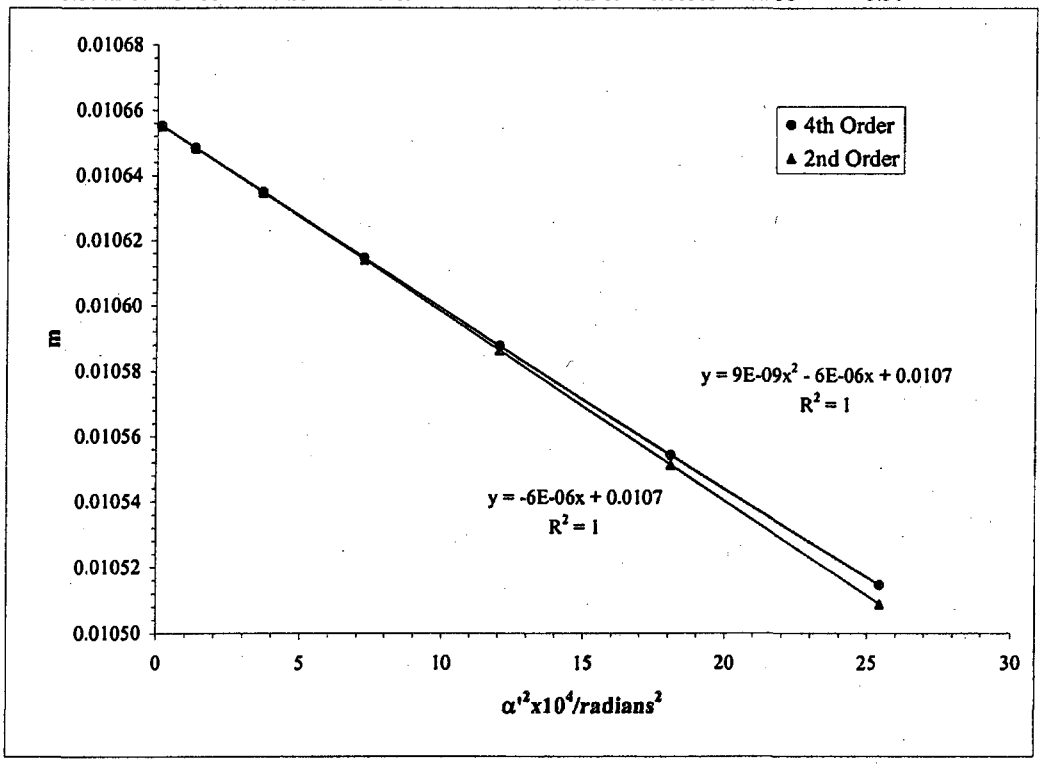

							Beam	Voltage	15 kV
Mesh/inch	I/milliamp	Mesh	z/cm	e_t/cm	a/cm	z_{sp}/cm	z_0'/cm	C_s'/cm	$z_{sp}-z_0'$/cm
2000	200	Front	25.08	0.00127	15.56	26.88	0.261	1.518	26.614

Bar location/ units	Shadow Reading Y/cm	Spacing Δ/cm	E/cm	$\alpha \times 10^4$	$\alpha' \times 10^2$	$\alpha'^2 \times 10^4$	m	z'/cm	f/cm
6	2.023		1.206	4.896	4.531	20.526	0.01081	0.258	0.268
5	2.227	0.205	1.002	4.080	3.764	14.165	0.01084	0.259	0.269
4	2.430	0.203	0.799	3.264	3.003	9.019	0.01087	0.260	0.270
3	2.631	0.201	0.598	2.448	2.248	5.053	0.01089	0.260	0.270
2	2.831	0.200	0.398	1.632	1.496	2.239	0.01091	0.261	0.271
1	3.031	0.199	0.199	0.816	0.748	0.559	0.01092	0.261	0.271
0	3.230	0.199							
-1	3.429	0.199					g/cm	$(\rho/f_0)^2 =$	
-2	3.628	0.199						$(m_0+1)^2\alpha'^2$	
-3	3.828	0.200					0.255	20.977	
-4	4.029	0.201					0.256	14.476	
-5	4.231	0.202					0.257	9.217	
-6	4.435	0.204					0.258	5.164	
							0.258	2.289	
			Slope	m_o	μ_s		0.258	0.571	
		8.2E-09	0.0000	0.010918	-5.15				

f vs $(\delta)^2$

$S_f = slope_f / f_0$

	$slope_f$	fo/cm	S_f
2.038E-07	-0.000138	0.271	-5.09

g vs $(\delta)^2$

$S_g = slope_g / f_0$

	$slope_g$	go/cm	S_g
-4.9E-09	-0.000146	0.258	-5.37

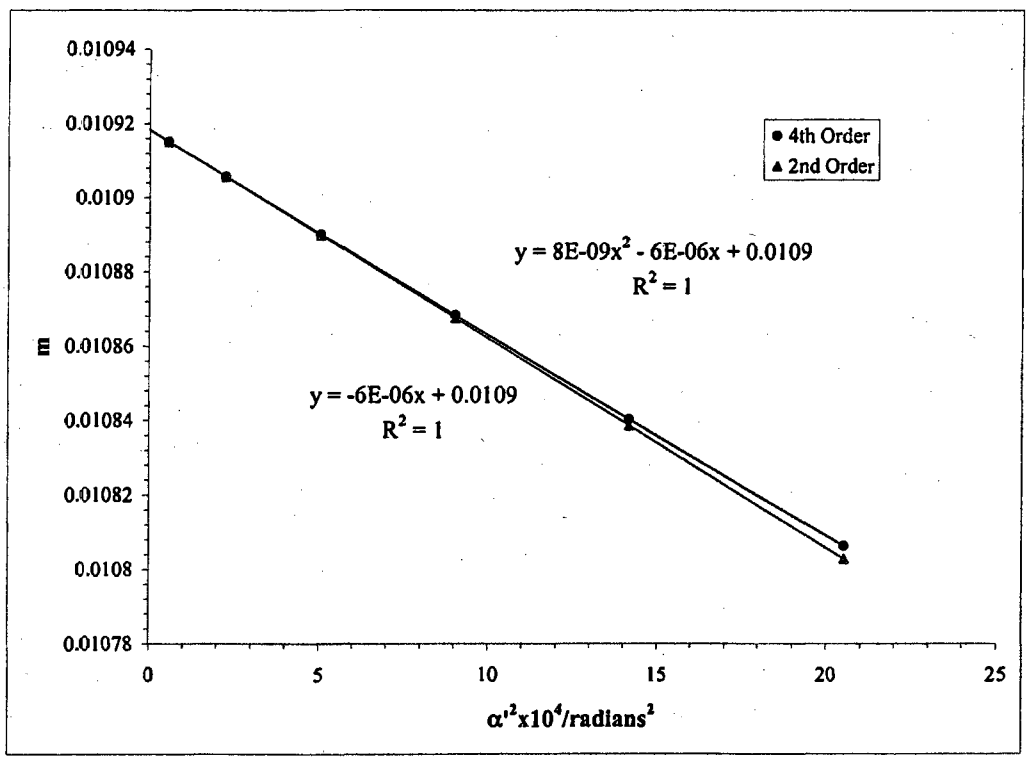

Beam Voltage	I/milliamp	z/cm	z_0'/cm	C_s'/cm
15 kV	200	25.1	0.261	1.52

Average of m_o = 0.0108

Average of μ_s = -5.15

Paraxial properties :

f_o = 0.268 cm

g_o = 0.258 cm

S_f = -5.17

S_g = -5.44

Mesh/inch	I/milliamp	Mesh	e'_1/cm	d/cm	b/cm		Beam	Voltage	15 kV
600	250	Rear	0.004233	26.44	0.432	DS			

Bar location/ units	Shadow Reading X/cm	Spacing Δ/cm	E'/cm	M'	c/cm	$\alpha' \times 10^2$	$\alpha'^2 \times 10^4$	z'/cm
5	0.902		2.208	104.3	0.2559	8.2705	68.4013	0.176
4	1.335	0.433	1.774	104.8	0.2548	6.6455	44.1626	0.177
3	1.773	0.438	1.335	105.2	0.2539	5.0019	25.0195	0.178
2	2.216	0.443	0.893	105.4	0.2532	3.3434	11.1785	0.179
1	2.661	0.445	0.447	105.6	0.2528	1.6744	2.8037	0.179
0	3.108	0.447						
-1	3.555	0.447						
-2	4.001	0.446						
-3	4.444	0.443			Slope	z_0'/cm	C_s'/cm	
-4	4.884	0.439		2.63E-08	-4.92E-05	0.179	0.492	
-5	5.318	0.435						

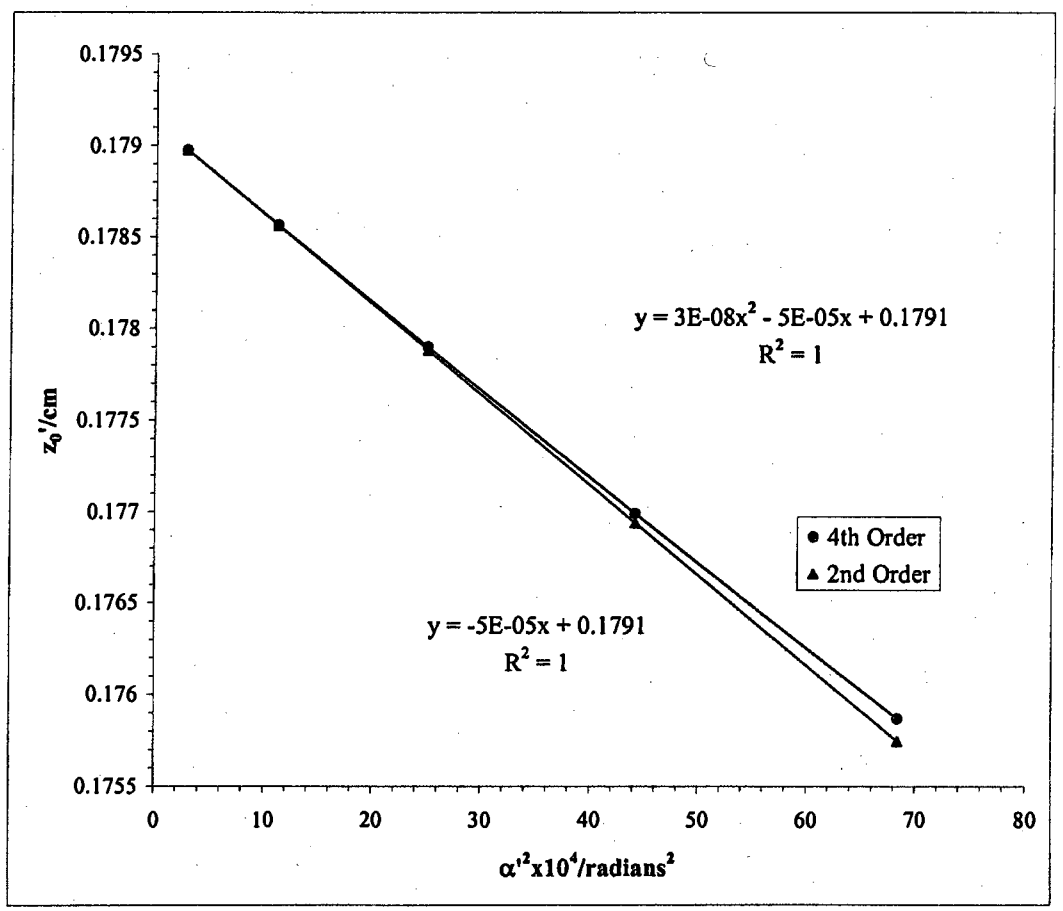

Mesh/inch	I/milliamp	Mesh	e'_1/cm	d/cm	b/cm		Beam	Voltage	15 kV
600	250	Rear	0.004233	26.44	0.432	DS			

Bar location/ units	Shadow Reading Y/cm	Spacing Δ/cm	E'/cm	M'	c/cm	$\alpha' \times 10^2$	$\alpha'^2 \times 10^4$	z'/cm
4	1.074		1.762	104.1	0.257	6.6002	43.5632	0.1752
3	1.508	0.435	1.327	104.5	0.256	4.9691	24.6924	0.1762
2	1.948	0.440	0.887	104.8	0.255	3.3225	11.0391	0.1770
1	2.391	0.443	0.444	105.0	0.254	1.6643	2.7700	0.1774
0	2.836	0.444						
-1	3.280	0.444						
-2	3.722	0.442						
-3	4.162	0.440						
-4	4.598	0.436						

	Slope	z_0'/cm	C_s'/cm
9.35E-08	-5.83E-05	0.178	0.583

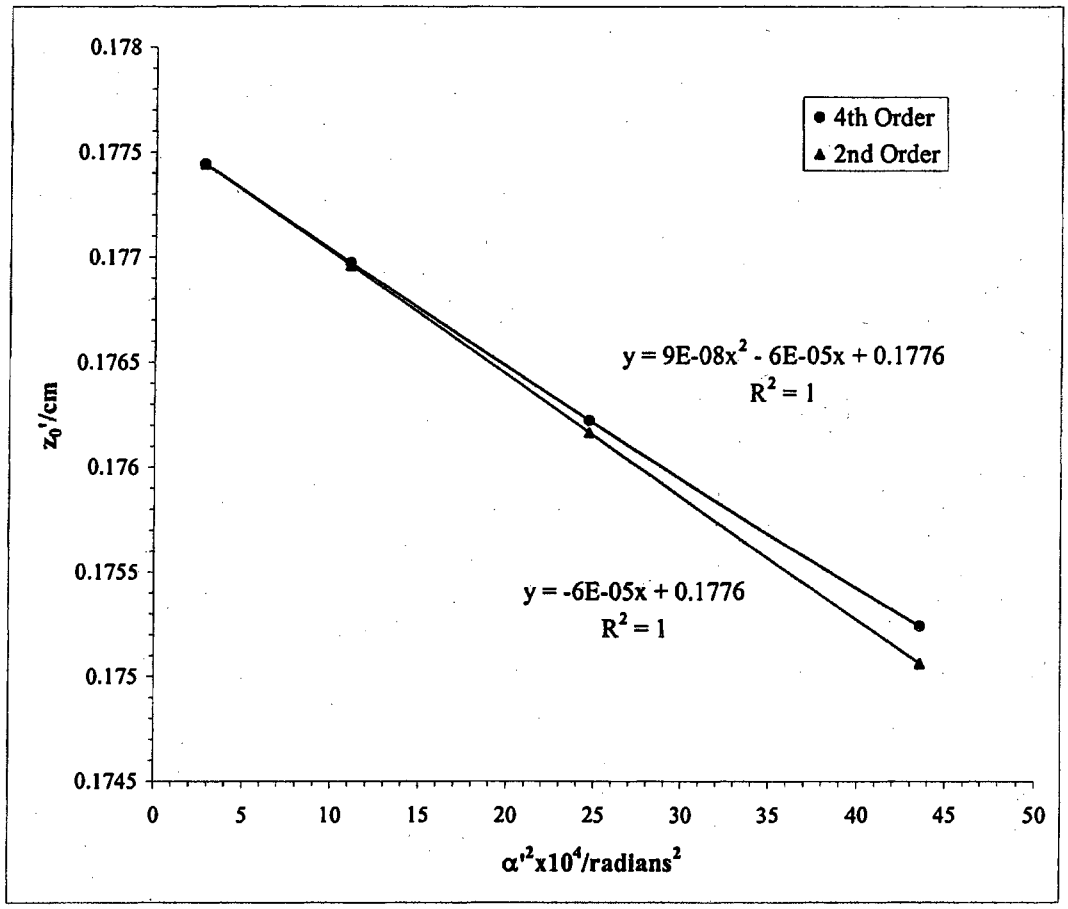

							Beam	Voltage	15 kV
Mesh/inch	I/milliamp	Mesh	z/cm	e_1/cm	a/cm	z_{sp}/cm	z_0'/cm	C_s'/cm	z_{sp}-z_o'
2000	250	Front	25.08	0.00127	15.56	26.88	0.177	0.583	26.70

Bar location/ units	Shadow Reading X/cm	Spacing Δ/cm	E/cm	α x 10^4	α' x 10^2	α'^{2} x 10^4	m	z'/cm	f/cm
6.5	0.487		1.940	5.305	7.264	52.768	0.00730	0.1743	0.1819
5.5	0.793	0.306	1.634	4.489	6.121	37.461	0.00733	0.1752	0.1826
4.5	1.094	0.301	1.333	3.673	4.991	24.911	0.00736	0.1759	0.1832
3.5	1.392	0.299	1.034	2.857	3.872	14.989	0.00738	0.1765	0.1837
2.5	1.689	0.297	0.737	2.040	2.760	7.616	0.00739	0.1769	0.1841
1.5	1.984	0.295	0.441	1.224	1.653	2.733	0.00741	0.1772	0.1844
0.5	2.279	0.294	0.147	0.408	0.551	0.303	0.00741	0.1774	0.1846
-0.5	2.573	0.294							
-1.5	2.867	0.294							
-2.5	3.163	0.296							
-3.5	3.460	0.297							
-4.5	3.759	0.299							
-5.5	4.061	0.302							
-6.5	4.366	0.305							

g/cm	$(\rho/f_0)^2 = \delta = (m_0 + 1)^2 \alpha'^2$
0.1730	53.553
0.1739	38.018
0.1746	25.282
0.1752	15.212
0.1756	7.729
0.1759	2.773
0.1760	0.308

	Slope	m_o	μ_s
3.1E-09	0.0000	0.007412	-2.9832

f vs $(\delta)^2$ S_f = $slope_f$ / f_0				g vs $(\delta)^2$ S_g = $slope_g$ / f_0			
	$slope_f$	fo/cm	S_f		$slope_g$	go/cm	S_g
7.60467E-08	-5.38288E-05	0.185	-2.92	-1.2E-09	-5.7E-05	0.176	-3.07

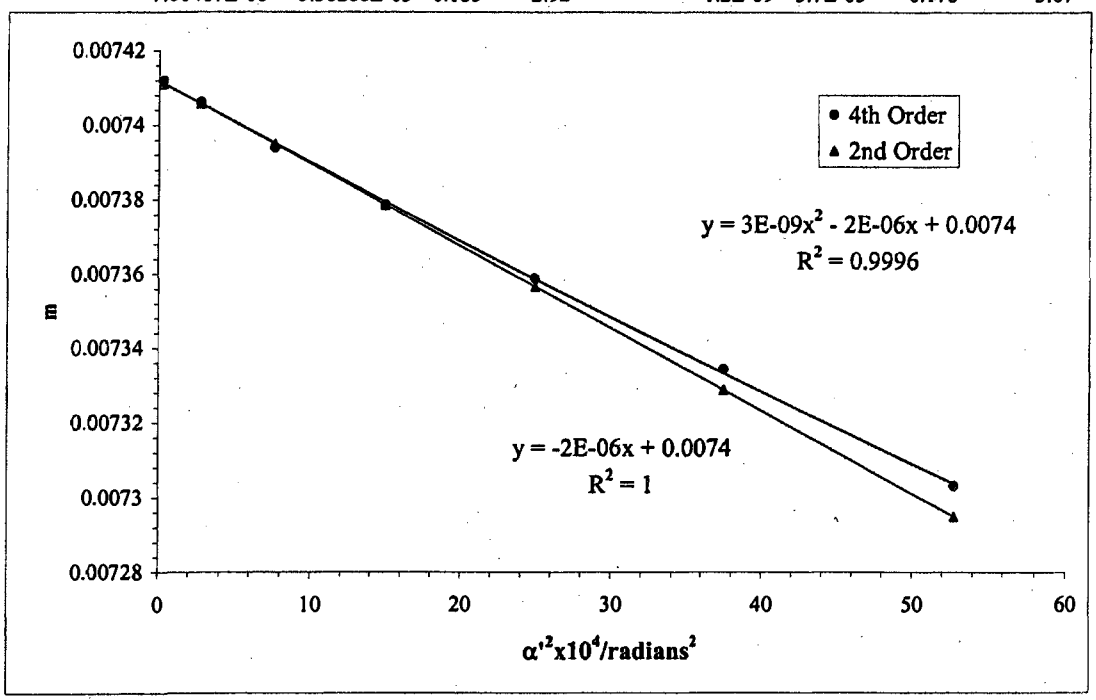

							Beam	Voltage	15 kV
Mesh/inch	I/milliamp	Mesh	z/cm	e_1/cm	a/cm	z_{sp}/cm	z_0'/cm	C_s'/cm	$z_{sp}-z_0'$
2000	250	Front	25.08	0.00127	15.56	26.88	0.177	0.583	26.70

Bar location/ units	Shadow Reading Y/cm	Spacing Δ/cm	E/cm	$\alpha \times 10^4$	$\alpha' \times 10^2$	$\alpha'^2 \times 10^4$	m	z'/cm	f/cm
7.5	0.091		2.193	6.121	8.212	67.444	0.00745	0.1735	0.1856
6.5	0.392	0.301	1.892	5.305	7.088	50.235	0.00749	0.1745	0.1864
5.5	0.690	0.297	1.595	4.489	5.976	35.707	0.00751	0.1753	0.1871
4.5	0.984	0.295	1.301	3.673	4.874	23.756	0.00754	0.1760	0.1877
3.5	1.276	0.292	1.009	2.857	3.781	14.294	0.00756	0.1766	0.1881
2.5	1.566	0.290	0.720	2.040	2.696	7.267	0.00757	0.1770	0.1885
1.5	1.854	0.288	0.431	1.224	1.615	2.609	0.00758	0.1772	0.1887
0.5	2.142	0.288	0.144	0.408	0.538	0.289	0.00759	0.1774	0.1889
-0.5	2.429	0.287							
-1.5	2.717	0.288							
-2.5	3.005	0.289							
-3.5	3.295	0.290							
-4.5	3.587	0.292							
-5.5	3.881	0.294							
-6.5	4.177	0.297							
-7.5	4.477	0.300							

	Slope	m_0	μ_s
3.4E-09	0.0000	0.007586	-2.87469

g/cm	$(\rho/f_0)^2 = \delta = (m_0+1)^2 \alpha'^2$
0.1721	68.471
0.1731	51.000
0.1739	36.251
0.1746	24.117
0.1751	14.512
0.1755	7.378
0.1758	2.649
0.1759	0.294

f vs $(\delta)^2$

$S_f = slope_f / f_0$

	$slope_f$	fo/cm	S_f
8.119E-08	-5.3E-05	0.189	-2.81

g vs $(\delta)^2$

$S_g = slope_g / f_0$

	$slope_g$	go/cm	S_g
-1.3E-09	-6E-05	0.176	-3.00

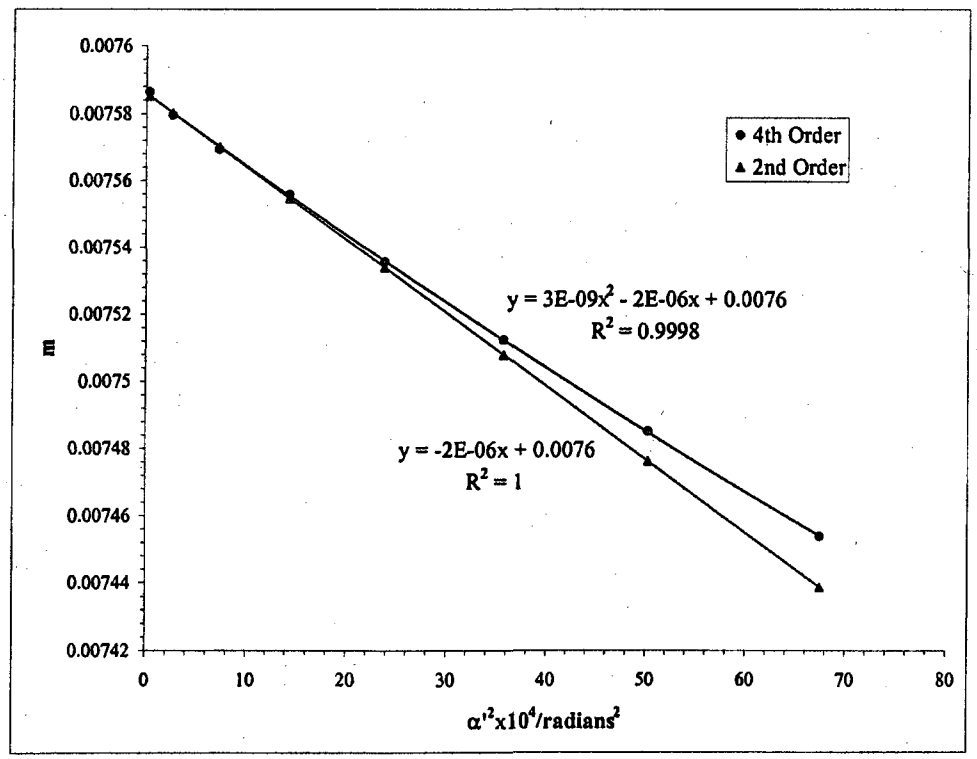

Beam Voltage	I/milliamp	z/cm	z_0'/cm	Cs'/cm
15 kV	250	25.1	0.177	0.583

Average of m_o = 0.00750

Average of μ_s = -2.87

Paraxial properties :

f_o = 0.187 cm

g_o = 0.176 cm

S_f = -2.86

S_g = -3.03

Mesh/inch	I/milliamps	Mesh	e'_1/cm	d/cm	b/cm		Beam	Voltage	15 kV
600	350	Rear	0.004233	26.44	0.432	DS			

Bar location/ units	Shadow Reading X/cm	Spacing Δ/cm	E'/cm	M'	c/cm	$\alpha' \times 10^2$	$\alpha'^2 \times 10^4$	z'/cm
5.5	1.769		1.8638	80.1	0.3345	6.9602	48.4445	0.0973
4.5	2.107	0.3374	1.5263	80.1	0.3342	5.6997	32.4867	0.0976
3.5	2.445	0.3382	1.1879	80.2	0.3340	4.4362	19.6800	0.0978
2.5	2.784	0.3389	0.8490	80.2	0.3338	3.1704	10.0514	0.0980
1.5	3.123	0.3393	0.5096	80.2	0.3337	1.9029	3.6210	0.0981
0.5	3.463	0.3396	0.1699	80.3	0.3336	0.6344	0.4025	0.0982
-0.5	3.802	0.3398						
-1.5	4.142	0.3397						
-2.5	4.482	0.3395						
-3.5	4.821	0.3391						
-4.5	5.159	0.3385						
-5.5	5.497	0.3377						

		Slope	z_0'/cm	C_s'/cm
	-3.00E-09	-1.81E-05	0.098	0.181

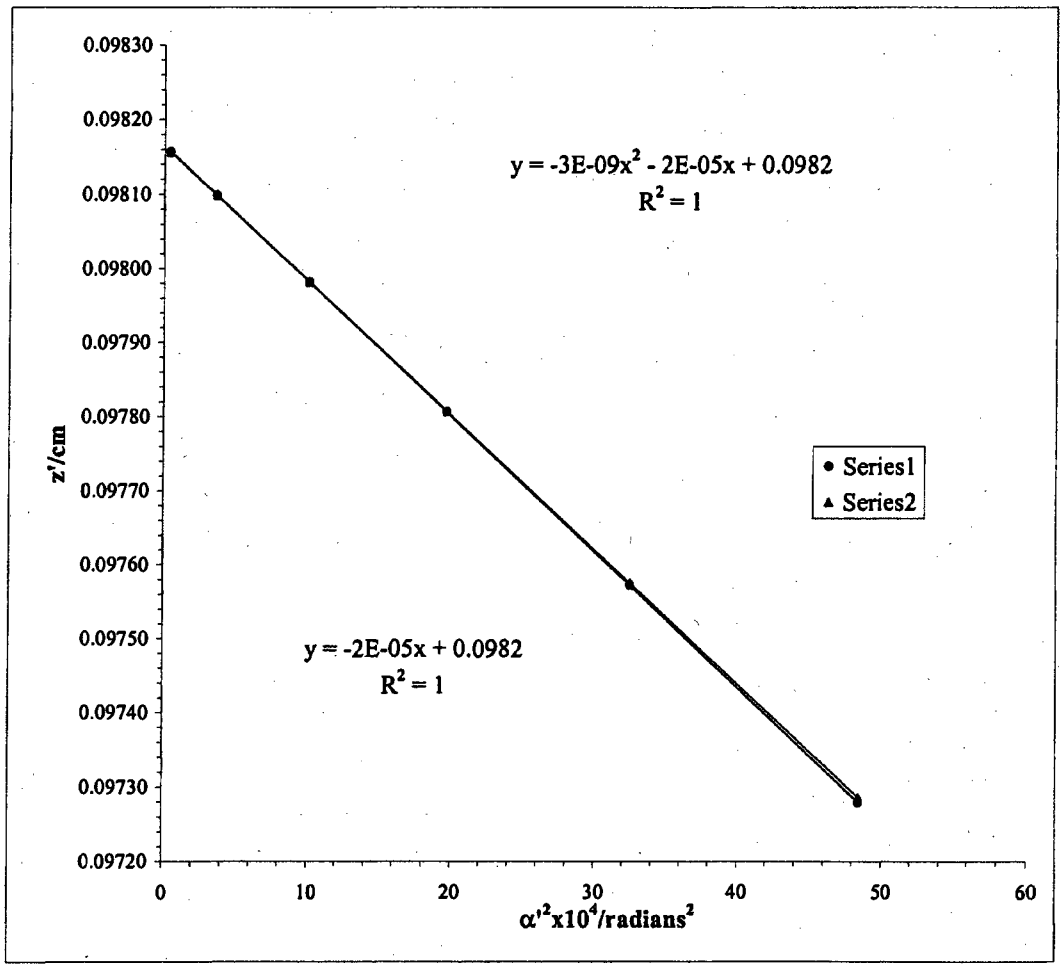

Mesh/inch	I/milliamps	Mesh	e'_1/cm	d/cm	b/cm		Beam	Voltage	15 kV
600	350	Rear	0.004233	26.44	0.432	DS			

Bar location/ units	Shadow Reading Y/cm	Spacing Δ/cm	E'/cm	M'	c/cm	α' x 10^2	α'^2 x 10^4	z'/cm
5.5	0.764		1.853	79.6	0.3365	6.9193	47.8763	0.0953
4.5	1.099	0.334	1.519	79.7	0.3360	5.6705	32.1541	0.0958
3.5	1.435	0.336	1.183	79.8	0.3355	4.4161	19.5019	0.0963
2.5	1.772	0.337	0.846	79.9	0.3352	3.1574	9.9694	0.0966
1.5	2.110	0.338	0.508	79.9	0.3350	1.8957	3.5937	0.0968
0.5	2.448	0.338	0.169	80.0	0.3349	0.6321	0.3996	0.0969
-0.5	2.787	0.339						
-1.5	3.125	0.338						
-2.5	3.463	0.338						
-3.5	3.800	0.337						
-4.5	4.136	0.336				Slope	z_o'/cm	C_s'/cm
-5.5	4.470	0.334			-1.07E-08	-3.40E-05	0.097	0.340

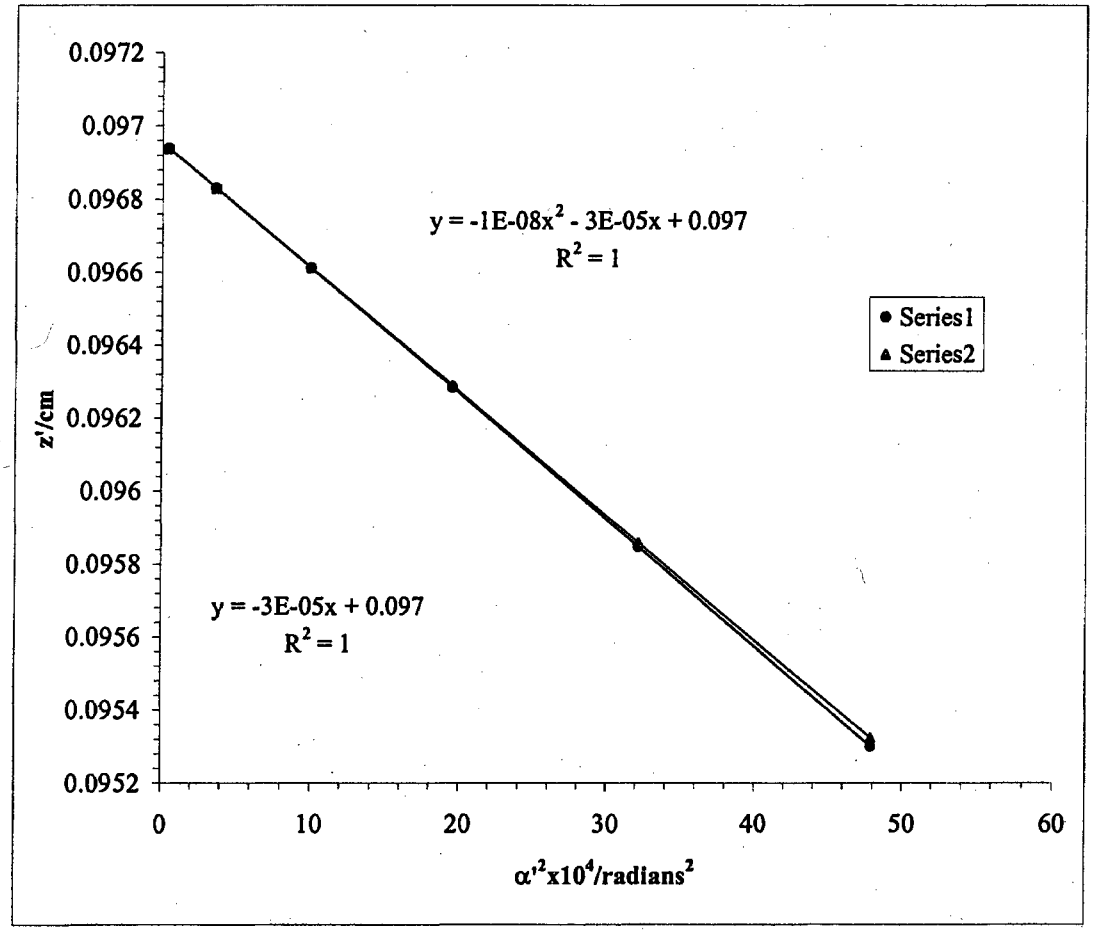

							Beam	Voltage	15 kV
Mesh/inch	I/milliamps	Mesh	z/cm	e_1/cm	a/cm	z_{sp}/cm	z_0'/cm	C_s'/cm	$z_{sp}-z_o'$
2000	350	Front	25.08	0.00127	15.56	26.88	0.098	0.261	26.78

Bar location/ units	Shadow Reading X/cm	Spacing Δ/cm	E/cm	α x 10^4	α' x 10^2	α'^{2} x 10^4	m	z'/cm	f/cm
4	1.657		1.919	3.265	7.164	51.330	0.00456	0.0962	0.1138
3	2.141	0.484	1.435	2.449	5.359	28.719	0.00457	0.0968	0.1141
2	2.622	0.481	0.955	1.632	3.565	12.710	0.00458	0.0972	0.1144
1	3.100	0.478	0.477	0.816	1.780	3.170	0.00458	0.0975	0.1145
0	3.577	0.477							
-1	4.054	0.477							
-2	4.531	0.478							
-3	5.011	0.480							
-4	5.495	0.483							

	g/cm	$(\rho/f_0)^2 = \delta =$ $(m_0 + 1)^2 \alpha'^2$
	0.0957	51.802
	0.0963	28.983
	0.0967	12.827
	0.0970	3.199

	Slope	m_o	μ_s
7.3E-10	0.0000	0.00459	-1.33

f vs $(\delta)^2$

$S_f = slope_f / f_0$

	$slope_f$	fo/cm	S_f
1.7858E-08	-1.492E-05	0.115	-1.30

g vs $(\delta)^2$

$S_g = slope_g / f_0$

	$slope_g$	go/cm	S_g
-1.71E-10	-2.57E-05	0.097	-2.24

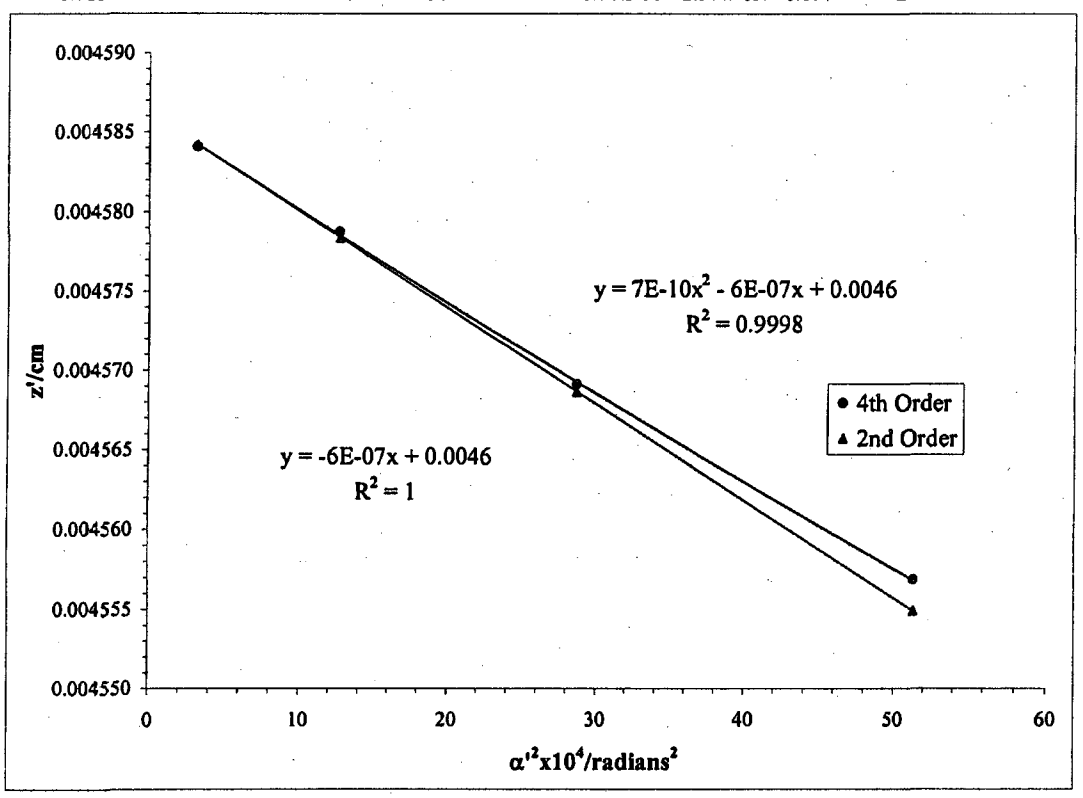

							Beam	Voltage	15 kV
Mesh/inch	I/milliamps	Mesh	z/cm	e_1/cm	a/cm	z_{sp}/cm	z_0'/cm	C_s'/cm	$z_{sp}-z_o'$
2000	210	Front	25.08	0.00127	15.56	26.88	0.098	0.261	26.78

Bar location/ units	Shadow Reading Y/cm	Spacing Δ/cm	E/cm	α x 10^4	α' x 10^3	α'² x 10^4	m	z'/cm	f/cm
6	0.4818		2.826	4.897	10.553	111.366	0.00464	0.094656	0.11593
5	0.9629	0.481	2.346	4.081	8.762	76.770	0.00466	0.095558	0.11635
4	1.4390	0.476	1.871	3.265	6.988	48.837	0.00467	0.096286	0.11670
3	1.9110	0.472	1.400	2.449	5.229	27.342	0.00468	0.096846	0.11697
2	2.3800	0.469	0.932	1.632	3.480	12.111	0.00469	0.097243	0.11717
1	2.8468	0.467	0.465	0.816	1.738	3.022	0.00470	0.097480	0.11729
0	3.3124	0.466							
-1	3.7777	0.465					g/cm	$(\rho/f_0)^2 = \delta =$ $(m_0+1)^2\alpha'^2$	
-2	4.2438	0.466							
-3	4.7115	0.468					0.09412	112.414	
-4	5.1819	0.470					0.09502	77.493	
-5	5.6557	0.474					0.09574	49.297	
-6	6.1342	0.478					0.09630	27.599	
							0.09669	12.225	
		Slope	m_o	μ_s			0.09693	3.050	
	1.7E-10	0.0000	0.004697	-1.12					

f vs $(\delta)^2$

$S_f = slope_f / f_0$

	$slope_f$	f_o/cm	S_f
4.038E-09	-1.288E-05	0.117	-1.10

g vs $(\delta)^2$

$S_g = slope_g / f_0$

	$slope_g$	g_o/cm	S_g
-4.39843E-11	-2.57E-05	0.097	-2.19

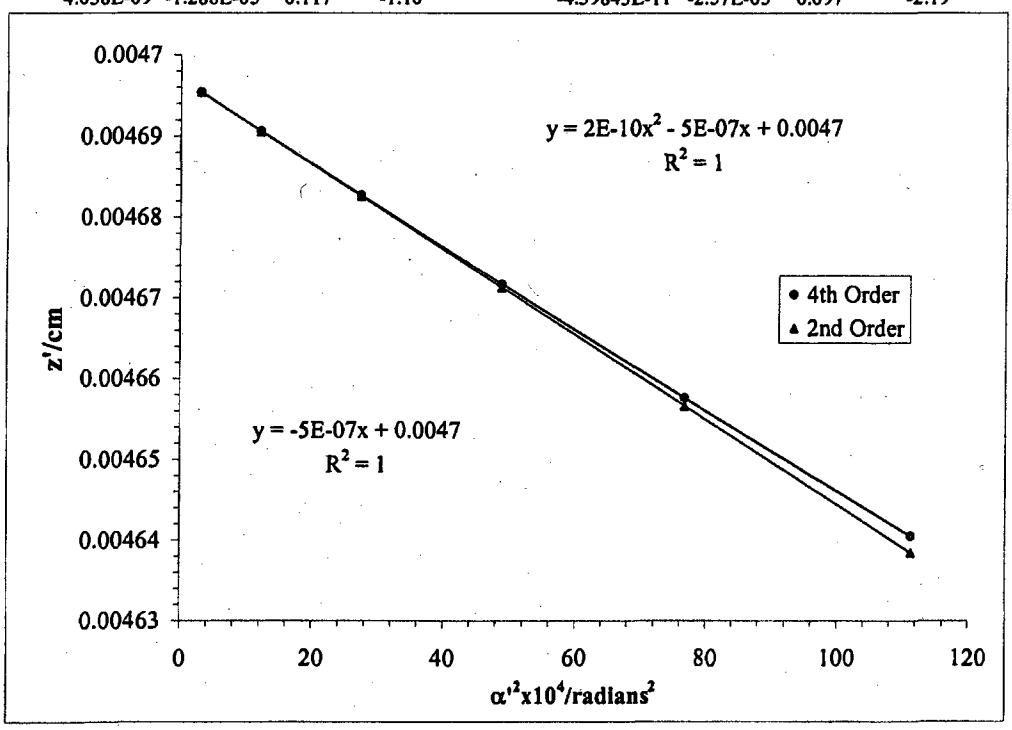

Beam Voltage	I/milliamps	z/cm	z_0'/cm	C_s'/cm
15 kV	350	25.1	0.0976	0.261

Average of m_o = 0.00464

Average of μ_s = -1.22

Paraxial properties :

f_o = 0.116 cm

g_o = 0.0970 cm

S_f = -1.20

S_g = -2.22

Magnetic Lens L_1 Data.
Acceleration Voltage 20 kV
Gap size 0.050 inches

Mesh/inch	I/milliamps	Mesh	e'1/cm	d/cm	b/cm		Beam	Voltage	20 kV
2000	130	Rear	0.00127	25.9	0.4318	US			

Bar location/ units	Shadow Reading X/cm	Spacing Δ/cm	E'/cm	M'	c/cm	$\alpha' \times 10^2$	$\alpha'^2 \times 10^4$	z'/cm
8	1.869		0.9339	-91.9221	-0.2787	3.6451	13.287	0.711
7	2.011	0.1425	0.7928	-89.1839	-0.2872	3.0955	9.582	0.719
6	2.141	0.1301	0.6635	-87.0761	-0.2941	2.5913	6.715	0.726
5	2.263	0.1219	0.5417	-85.3069	-0.3001	2.1160	4.478	0.732
4	2.379	0.1157	0.4255	-83.7664	-0.3055	1.6626	2.764	0.737
3	2.490	0.1105	0.3142	-82.4581	-0.3103	1.2277	1.507	0.742
2	2.596	0.1064	0.2069	-81.4427	-0.3142	0.8085	0.654	0.746
1	2.700	0.1036	0.1026	-80.7950	-0.3166	0.4011	0.161	0.748
0	2.802	0.1024						
-1	2.905	0.1028						
-2	3.010	0.1049						
-3	3.118	0.1082			Slope	zo'/cm	Cs'/cm	
-4	3.230	0.1122		8.82E-05	-0.0040	0.748	39.924	
-5	3.347	0.1167						
-6	3.468	0.1218						
-7	3.597	0.1285						
-8	3.737	0.1397						

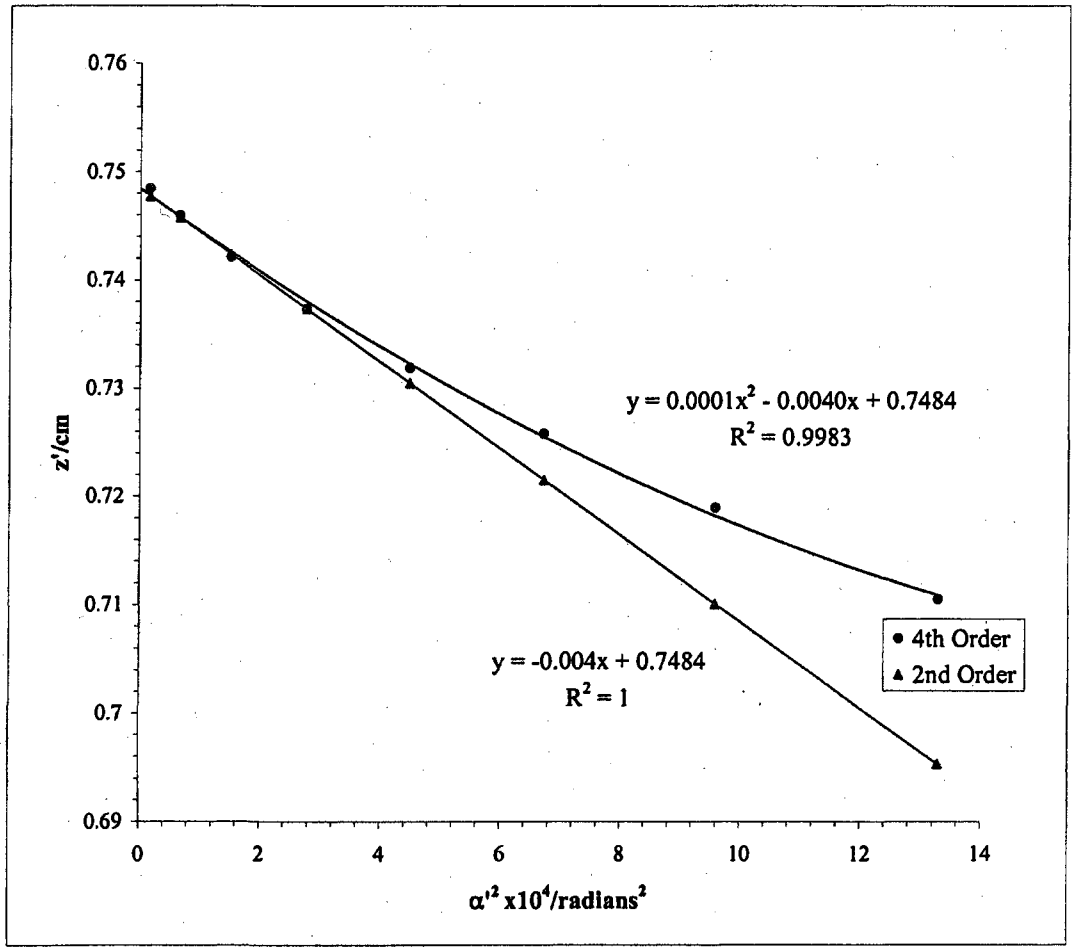

Mesh/inch	I/milliamps	Mesh	e'1/cm	d/cm	b/cm		Beam	Voltage	20 kV
2000	130	Rear	0.00127	25.90	0.432	US			

Bar location/ units	Shadow Reading Y/cm	Spacing Δ/cm	E'/cm	M'	c/cm	α' x 10^2	α'^{2} x 10^4	z'/cm
8.5	1.661	#REF!	0.991	-91.83	-0.279	3.8690	14.9692	0.711
7.5	1.813	0.152	0.843	-88.47	-0.289	3.2903	10.8263	0.721
6.5	1.948	0.135	0.709	-85.86	-0.298	2.7685	7.6645	0.730
5.5	2.071	0.123	0.587	-84.05	-0.305	2.2938	5.2614	0.736
4.5	2.188	0.117	0.472	-82.52	-0.310	1.8429	3.3962	0.742
3.5	2.299	0.111	0.360	-81.07	-0.316	1.4086	1.9841	0.747
2.5	2.404	0.105	0.255	-80.46	-0.318	0.9986	0.9971	0.750
1.5	2.507	0.103	0.151	-79.47	-0.322	0.5918	0.3503	0.754
0.5	2.609	0.102	0.052	-81.17	-0.315	0.2014	0.0406	0.747
-0.5	2.712	0.103						
-1.5	2.810	0.098						
-2.5	2.915	0.105						
-3.5	3.020	0.105						
-4.5	3.131	0.112						
-5.5	3.245	0.114			Slope	zo'/cm	Cs'/cm	
-6.5	3.365	0.120		4.4E-05	-0.0035	0.754	35.31	
-7.5	3.498	0.133						
-8.5	3.644	0.145						

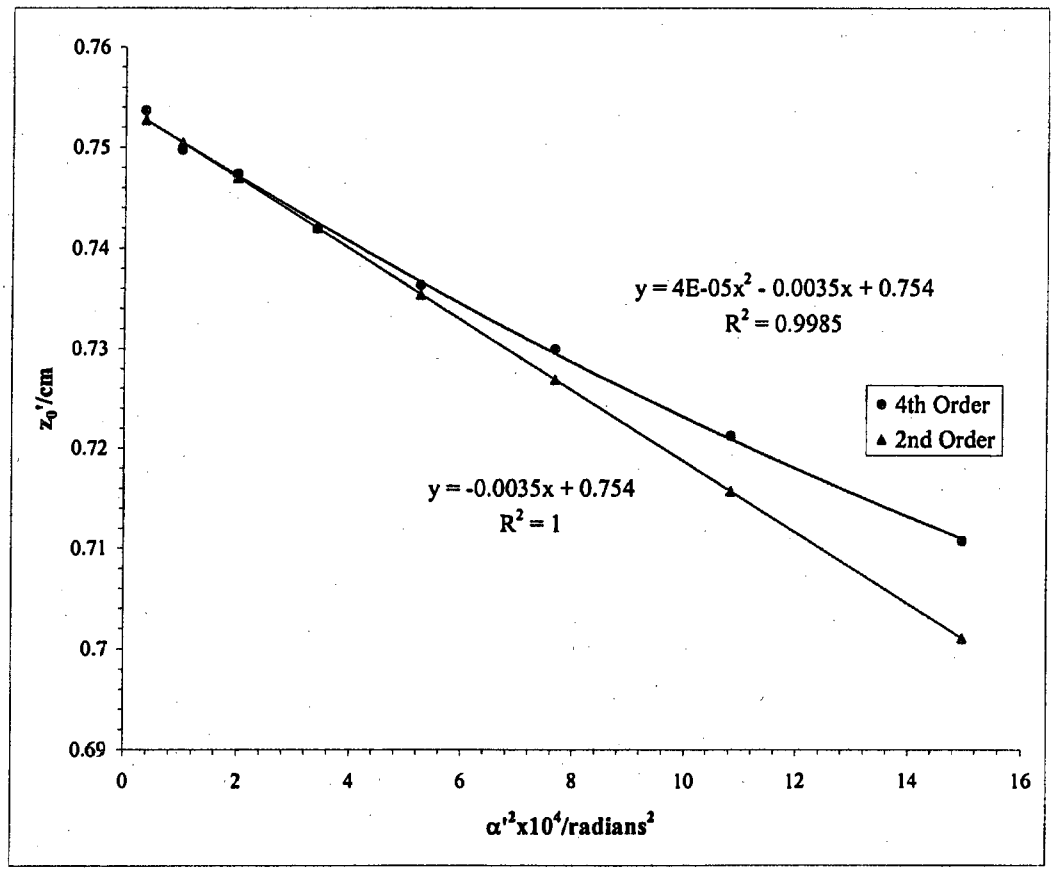

Mesh/inch	I/milliamps	Mesh	e'1/cm	d/cm	b/cm		Beam	Voltage	20 kV
2000	130	Rear	0.00127	25.49	0.843	DS			

Bar location/ units	Shadow Reading X/cm	Spacing Δ/cm	E'/cm	M'	c/cm	α' x 10^2	α'^{2} x 10^4	z'/cm
4.5	1.735		0.979	171.25	0.150	3.82	14.57	0.6936
3.5	1.885	0.150	0.820	184.38	0.139	3.20	10.23	0.7043
2.5	2.058	0.174	0.637	200.64	0.128	2.49	6.18	0.7156
1.5	2.271	0.212	0.415	217.62	0.118	1.62	2.62	0.7256
0.5	2.526	0.256	0.145	228.93	0.112	0.57	0.32	0.7315
-0.5	2.817	0.291						
-1.5	3.100	0.283						
-2.5	3.332	0.233						
-3.5	3.524	0.191						
-4.5	3.692	0.169						

	Slope	z_o'/cm	C_s'/cm
1E-05	-0.0028	0.733	28.37

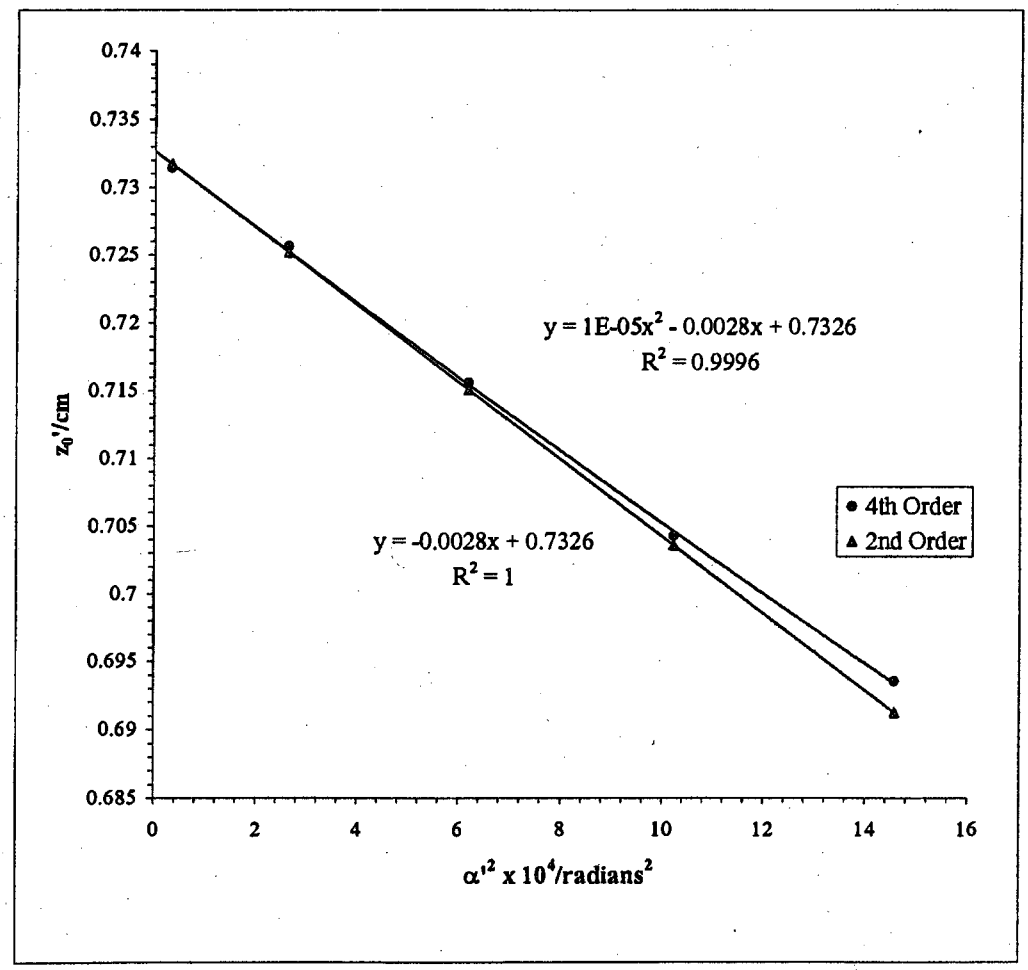

Mesh/inch	I/milliamps	Mesh	e'1/cm	d/cm	b/cm		Beam	Voltage	20 kV
2000	130	Rear	0.00127	25.49	0.843	DS			

Bar location/ units	Shadow Reading Y/cm	Spacing Δ/cm	E'/cm	M'	c/cm	$\alpha' \times 10^2$	$\alpha'^2 \times 10^4$	z'/cm
4.5	1.5389		0.994	173.92	0.147	3.877	15.032	0.696
3.5	1.7010	0.162	0.833	187.39	0.137	3.250	10.565	0.707
2.5	1.8902	0.189	0.645	203.30	0.126	2.520	6.350	0.717
1.5	2.1203	0.230	0.420	220.70	0.116	1.642	2.696	0.727
0.5	2.3973	0.277	0.148	233.46	0.110	0.579	0.335	0.734
-0.5	2.6938	0.296						
-1.5	2.9611	0.267						
-2.5	3.1811	0.220						
-3.5	3.3669	0.186						
-4.5	3.5268	0.160						

	Slope	z_0'/cm	Cs'/cm
1.72E-05	-0.0028	0.735	28.40

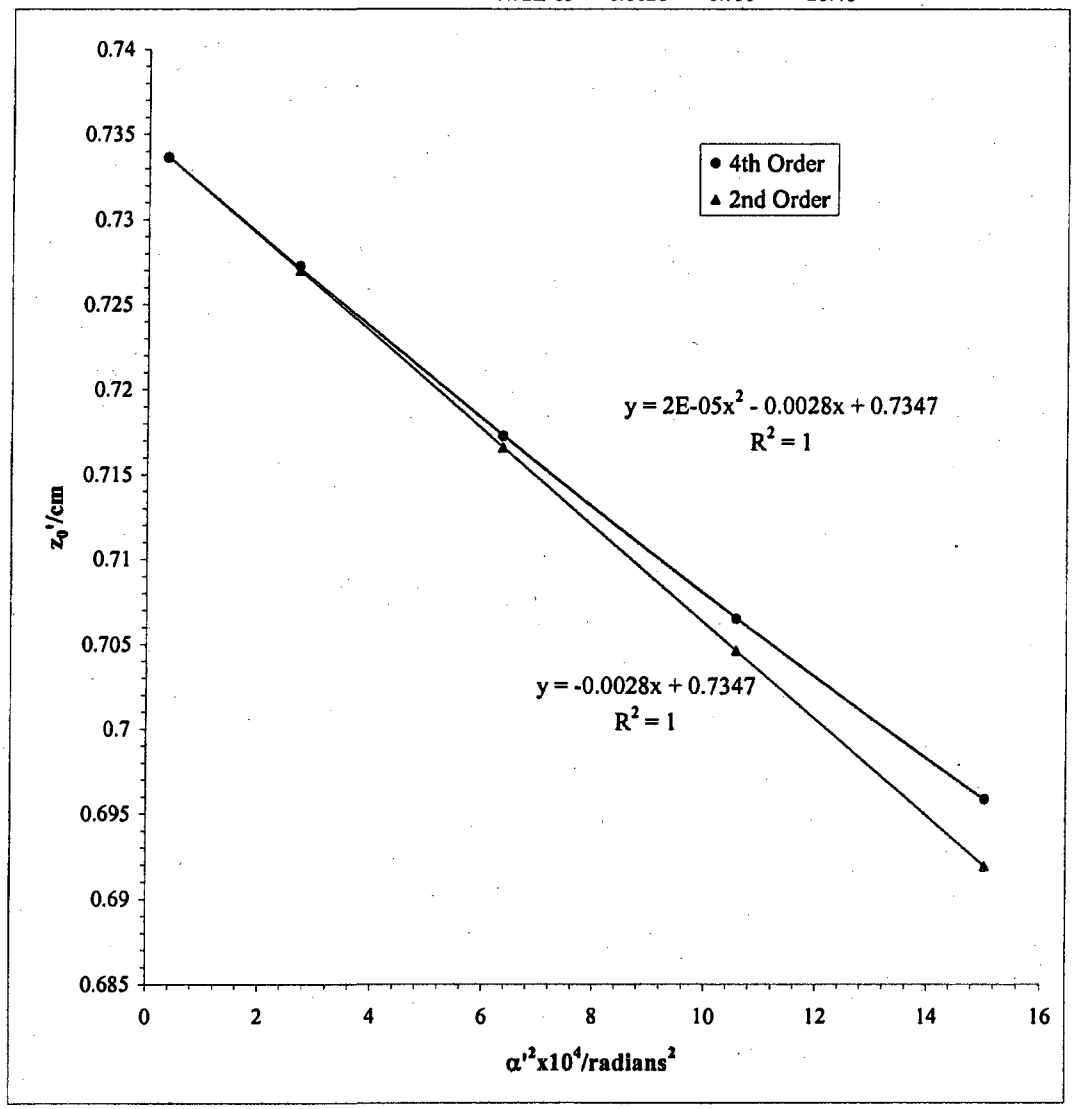

							Beam	Voltage	20 kV
Mesh/inch	I/milamp	Mesh	z/cm	e_1/cm	a/cm	z_{sp}/cm	z_0'/cm	C_s'/cm	$z_{sp}-z_0'$/cm
600	130	Front	30.35	0.00423	20.96	26.33	0.74	33.00	25.59

Bar location/ units	Shadow Reading X/cm	Spacing Δ/cm	E/cm	α x 10^4	α' x 10^2	α'^{2} x 10^4	m	z'/cm	f/cm
4.5	1.718		0.912	9.088	3.559	12.668	0.02553	0.701	0.757
3.5	1.933	0.215	0.697	7.069	2.720	7.401	0.02598	0.718	0.770
2.5	2.138	0.205	0.491	5.049	1.917	3.676	0.02633	0.730	0.780
1.5	2.337	0.199	0.292	3.029	1.140	1.300	0.02657	0.738	0.787
0.5	2.532	0.195	0.097	1.010	0.378	0.143	0.02669	0.742	0.791
-0.5	2.725	0.194							
-1.5	2.920	0.195					g/cm	$(\rho/f_0)^2 = (m_0+1)^2\alpha'^2$	
-2.5	3.120	0.200							
-3.5	3.326	0.207					0.681	13.4	
-4.5	3.543	0.216					0.698	7.80	
							0.710	3.88	
			Slope	m_o	μ_s		0.717	1.37	
		9.737E-07	-1.05E-04	0.02671	-39.26		0.721	0.151	

f vs $(\rho/f_o)^2$

$S_f = slope_f / f_0$

	$slope_f$	fo/cm	S_f
2.639E-05	-0.00288	0.791	-36.38

g vs $(\rho/f_o)^2$

$S_g = slope_g / f_0$

	$slope_g$	go/cm	S_g
-1.61E-06	-0.00298	0.721	-37.61

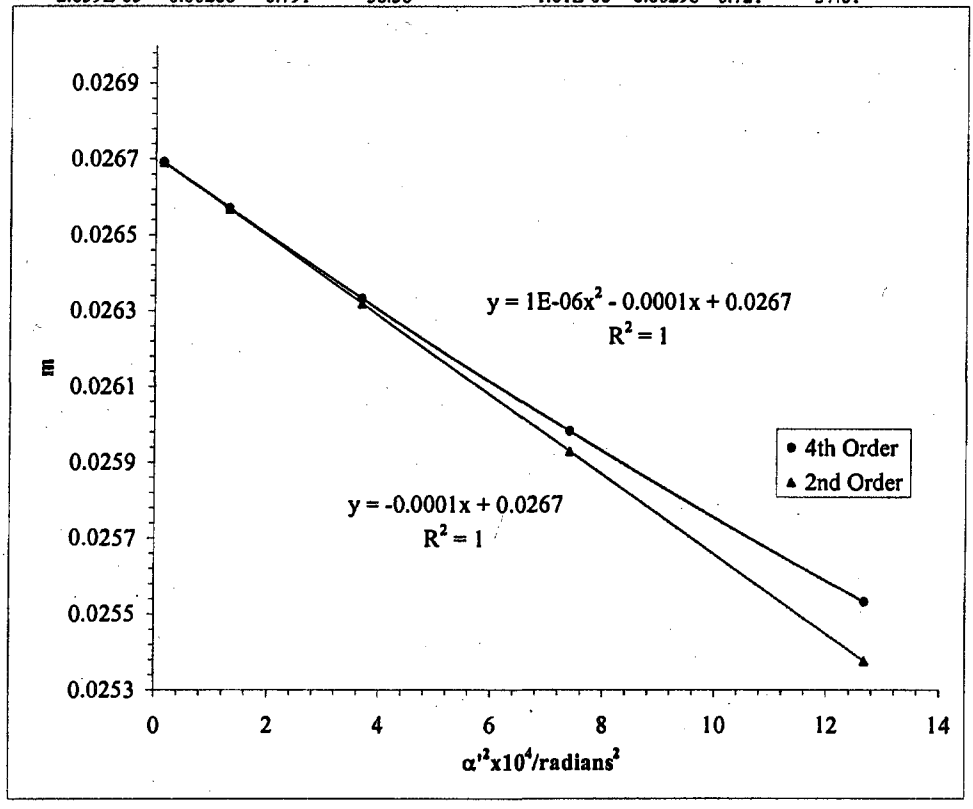

							Beam	Voltage	20 kV
Mesh/inch	I/milamp	Mesh	z/cm	e_1/cm	a/cm	z_{sp}/cm	z_0'/cm	C_z'/cm	$z_{sp}-z_o'$
600	130	Front	30.35	0.0042333	20.96	26.33	0.742	33.003	25.59

Bar location/ units	Shadow Reading Y/cm	Spacing Δ/cm	E/cm	α x 10^4	α' x 10^2	α'^{2} x 10^4	m	z'/cm	f/cm
4.5	1.400		0.909	9.088	3.552	12.615	0.02559	0.701	0.772
3.5	1.616	0.215	0.695	7.069	2.717	7.381	0.02602	0.718	0.786
2.5	1.822	0.206	0.490	5.049	1.916	3.671	0.02635	0.730	0.796
1.5	2.022	0.200	0.292	3.029	1.140	1.299	0.02658	0.738	0.803
0.5	2.217	0.195	0.097	1.010	0.378	0.143	0.02669	0.742	0.806
-0.5	2.411	0.194							
-1.5	2.605	0.194					g/cm	$(\rho/f_0)^2 = (m_0+1)^2\alpha'^2$	
-2.5	2.803	0.198							
-3.5	3.006	0.204					0.681	13.298	
-4.5	3.218	0.212					0.698	7.780	
							0.709	3.870	
			Slope	m_0	μ_s		0.717	1.369	
		8.84E-07	-1E-04	0.0267067	-37.39		0.720	0.151	

f vs $(\rho/f_o)^2$

S_f = slope$_f$ / f_0

slope$_f$	fo/cm	S_f
2.48E-05	-0.002902	0.807	-35.98

g vs $(\rho/f_o)^2$

S_g = slope$_g$ / f_0

slope$_g$	go/cm	S_g
-1.5E-06	-0.00298	0.721	-36.91

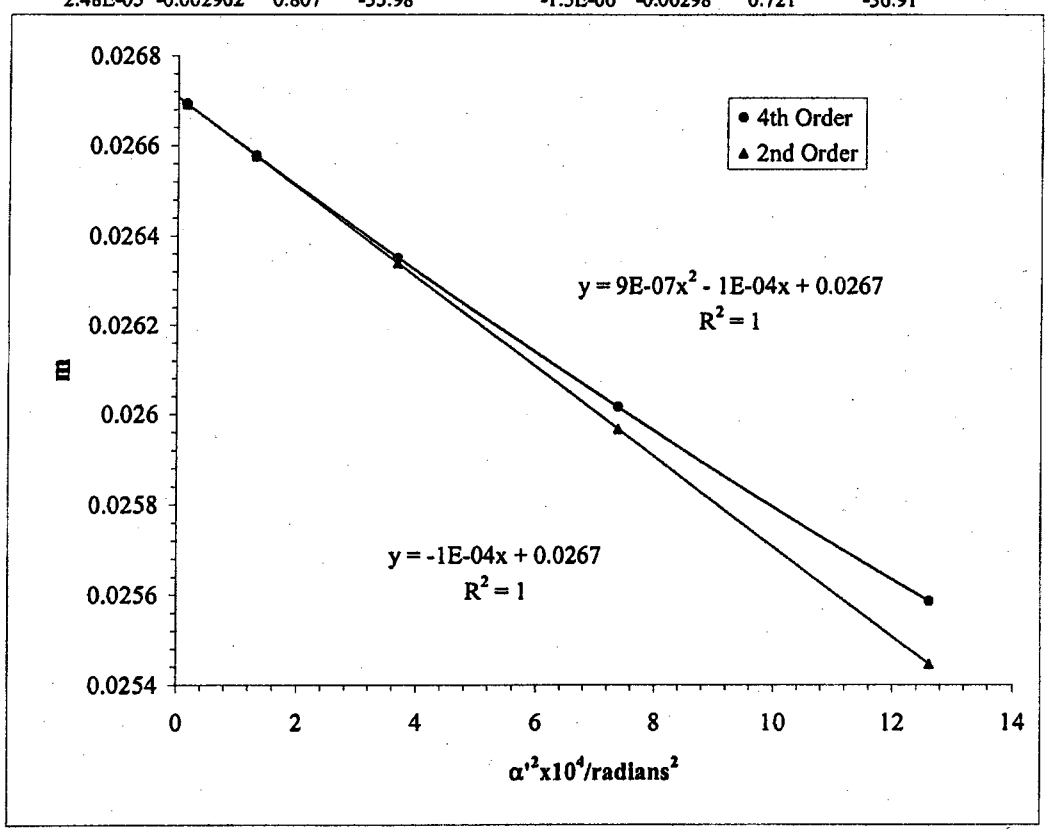

Beam Voltage	I/milamp	z/cm	z_0'/cm	C_s'/cm
20 kV	130	30.3	0.742	33.0

Average of m_o = 0.0267

Average of μ_s = -38.3

Paraxial properties :

f_o = 0.799 cm

g_o = 0.721 cm

S_f = -36.2

S_g = -37.3

Mesh/inch	I/milamp	Mesh	e'_1/cm	d/cm	b/cm		Beam	Voltage	20 kV
2000	150	Rear	0.00127	25.9	0.432	US			

Bar location/ units	Shadow Reading X/cm	Spacing Δ/cm	E'/cm	M'	c/cm	α' x 10^2	α'^{2} x 10^4	z'/cm
5	1.5726		0.899	-141.5	-0.182	3.494805	12.2137	0.613
4	1.7805	0.2079	0.693	-136.3	-0.189	2.693872	7.2569	0.620
3	1.9697	0.1892	0.506	-132.8	-0.194	1.968575	3.8753	0.625
2	2.1443	0.1747	0.332	-130.8	-0.197	1.292082	1.6695	0.628
1	2.3120	0.1677	0.164	-129.0	-0.199	0.637408	0.4063	0.631
0	2.4763	0.1642						
-1	2.6397	0.1634						
-2	2.8085	0.1689						
-3	2.9818	0.1732			Slope	zo'/cm	Cs'/cm	
-4	3.1657	0.1840		1.5E-05	-0.00165	0.631	16.50	
-5	3.3702	0.2045						

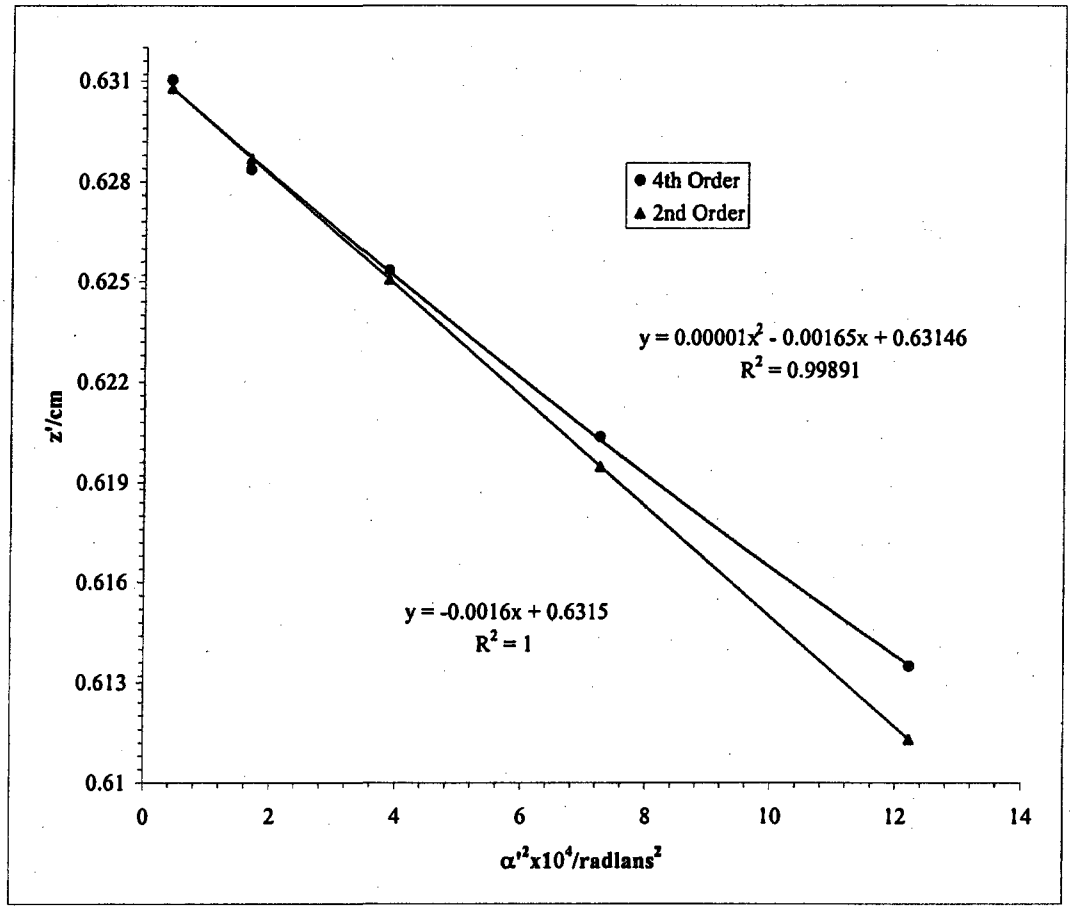

Mesh/inch	I/milamp	Mesh	e'_1/cm	d/cm	b/cm		Beam	Voltage	20 kV
2000	150	Rear	0.00127	25.9	0.432	US			

Bar location/ units	Shadow Reading Y/cm	Spacing Δ/cm	E'/cm	M'	c/cm	α' x 10^2	α'^2 x 10^4	z'/cm
5	0.956		0.891	-140.4	-0.183	3.47	12.01	0.615
4	1.154	0.198	0.689	-135.7	-0.190	2.68	7.18	0.621
3	1.336	0.182	0.504	-132.3	-0.194	1.96	3.84	0.626
2	1.507	0.171	0.331	-130.4	-0.197	1.29	1.66	0.629
1	1.674	0.167	0.164	-128.8	-0.199	0.64	0.41	0.631
0	1.838	0.164						
-1	2.002	0.163						
-2	2.170	0.168						
-3	2.344	0.174			Slope	z_o'/cm	Cs'/cm	
-4	2.532	0.188		1.20E-05	-0.001532	0.632	15.32	
-5	2.738	0.206						

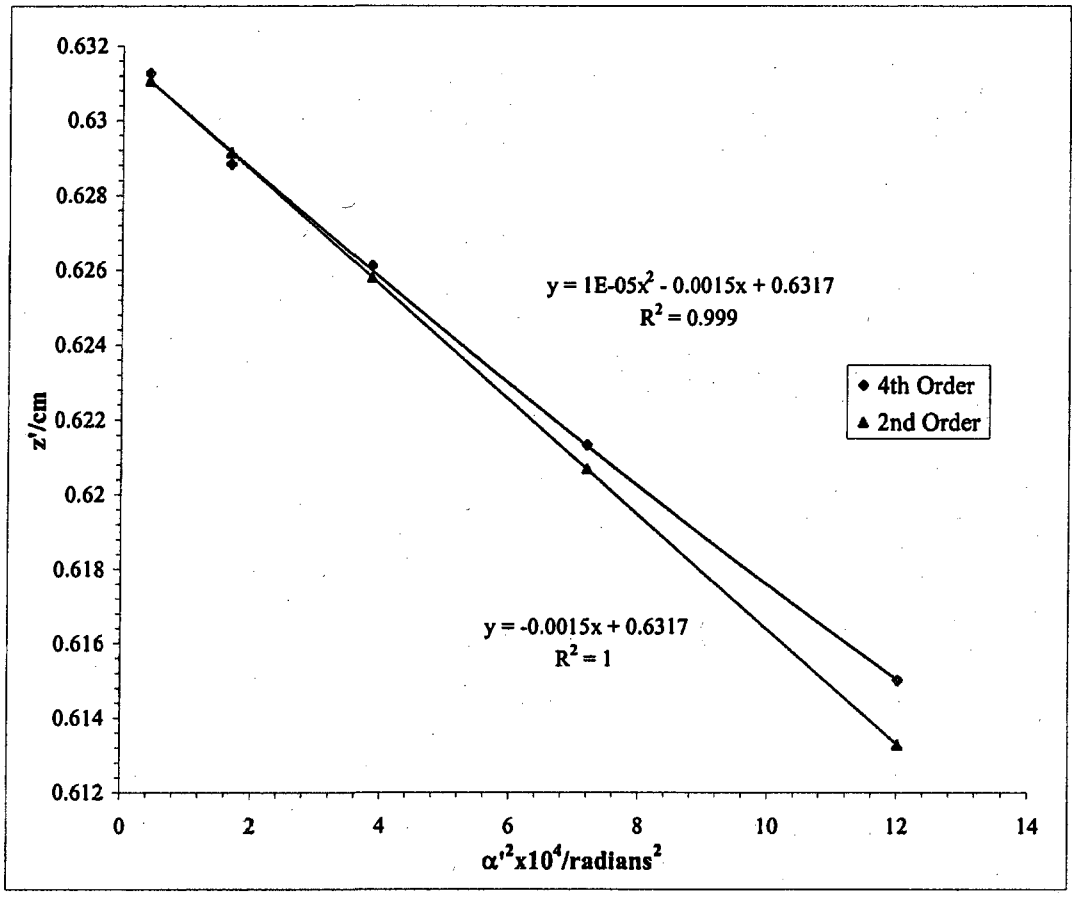

Mesh/inch	I/milamp	Mesh	e'_1/cm	d/cm	b/cm		Beam	Voltage	20 kV
2000	150	Rear	0.00127	25.64	0.690	DS			

Bar location/ units	Shadow Reading X/cm	Spacing Δ/cm	E'/cm	M'	c/cm	α' x 10^2	α'^2 x 10^4	z'/cm
6	1.3339		1.0346	135.77	0.1903	4.0051	16.0410	0.5000
5	1.4831	0.1491	0.8872	139.72	0.1848	3.4353	11.8015	0.5055
4	1.6415	0.1584	0.7300	143.70	0.1797	2.8272	7.9928	0.5106
3	1.8118	0.1703	0.5623	147.58	0.1749	2.1780	4.7437	0.5154
2	1.9924	0.1806	0.3833	150.92	0.1710	1.4850	2.2054	0.5193
1	2.1845	0.1921	0.1934	152.30	0.1695	0.7494	0.5616	0.5208
0	2.3775	0.1930						
-1	2.5713	0.1938						
-2	2.7590	0.1877						
-3	2.9363	0.1773						
-4	3.1015	0.1651			Slope	zo'/cm	Cs'/cm	
-5	3.2575	0.1560		1.25E-05	-0.00162	0.5228	16.17	
-6	3.4031	0.1456						

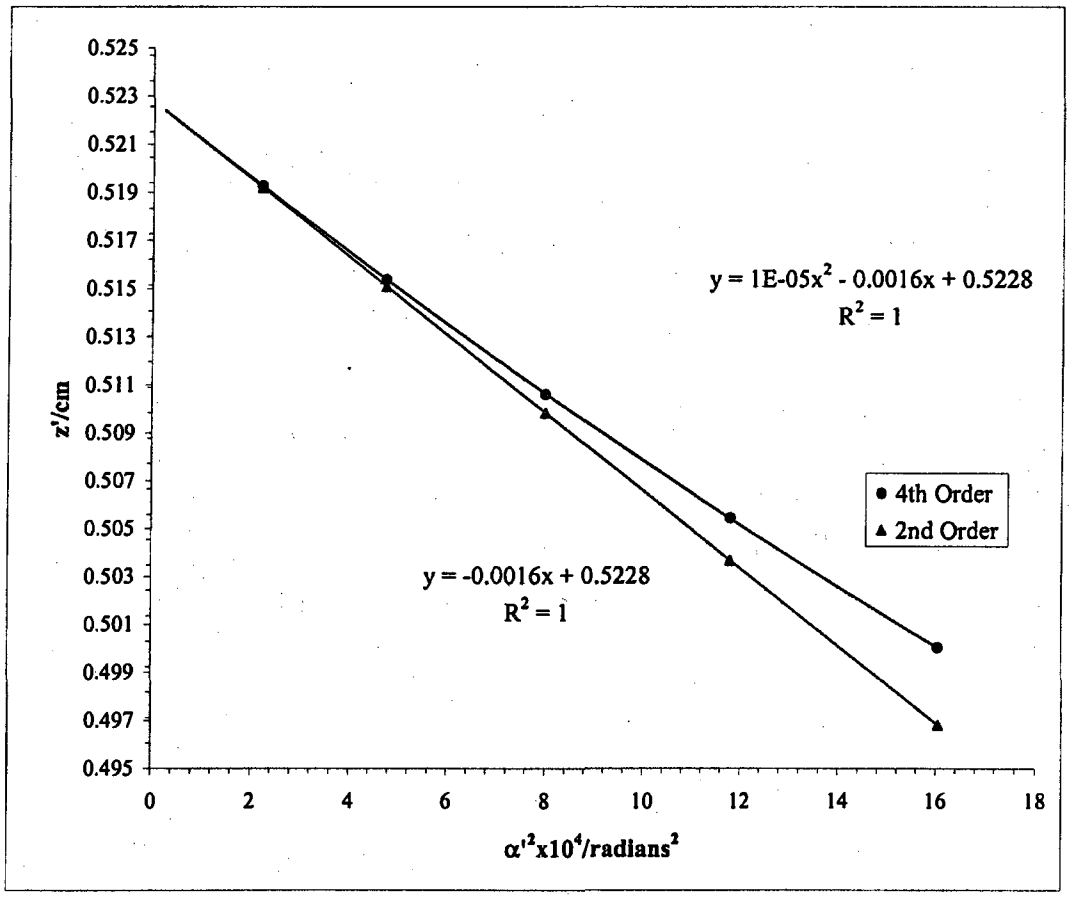

Mesh/inch	I/milamp	Mesh	e'_1/cm	d/cm	b/cm		Beam	Voltage	20 kV
2000	150	Rear	0.00127	25.64	0.690	DS			

Bar location/ units	Shadow Reading Y/cm	Spacing Δ/cm	E'/cm	M'	c/cm	α' x 10^2	α'^2 x 10^4	z'/cm
5.5	1.48		0.932	133.41	0.194	3.61	13.01	0.497
4.5	1.63	0.1462	0.784	137.12	0.188	3.03	9.20	0.502
3.5	1.78	0.1564	0.625	140.53	0.184	2.42	5.85	0.507
2.5	1.95	0.1658	0.456	143.58	0.180	1.77	3.12	0.510
1.5	2.13	0.1765	0.278	145.96	0.177	1.08	1.16	0.513
0.5	2.31	0.1843	0.093	146.94	0.176	0.36	0.13	0.515
-0.5	2.50	0.1866						
-1.5	2.68	0.1853						
-2.5	2.86	0.1792						
-3.5	3.03	0.1717						
-4.5	3.20	0.1616			Slope	zo'/cm	Cs'/cm	
-5.5	3.35	0.1504		6.12E-06	-0.0015	0.515	14.96	

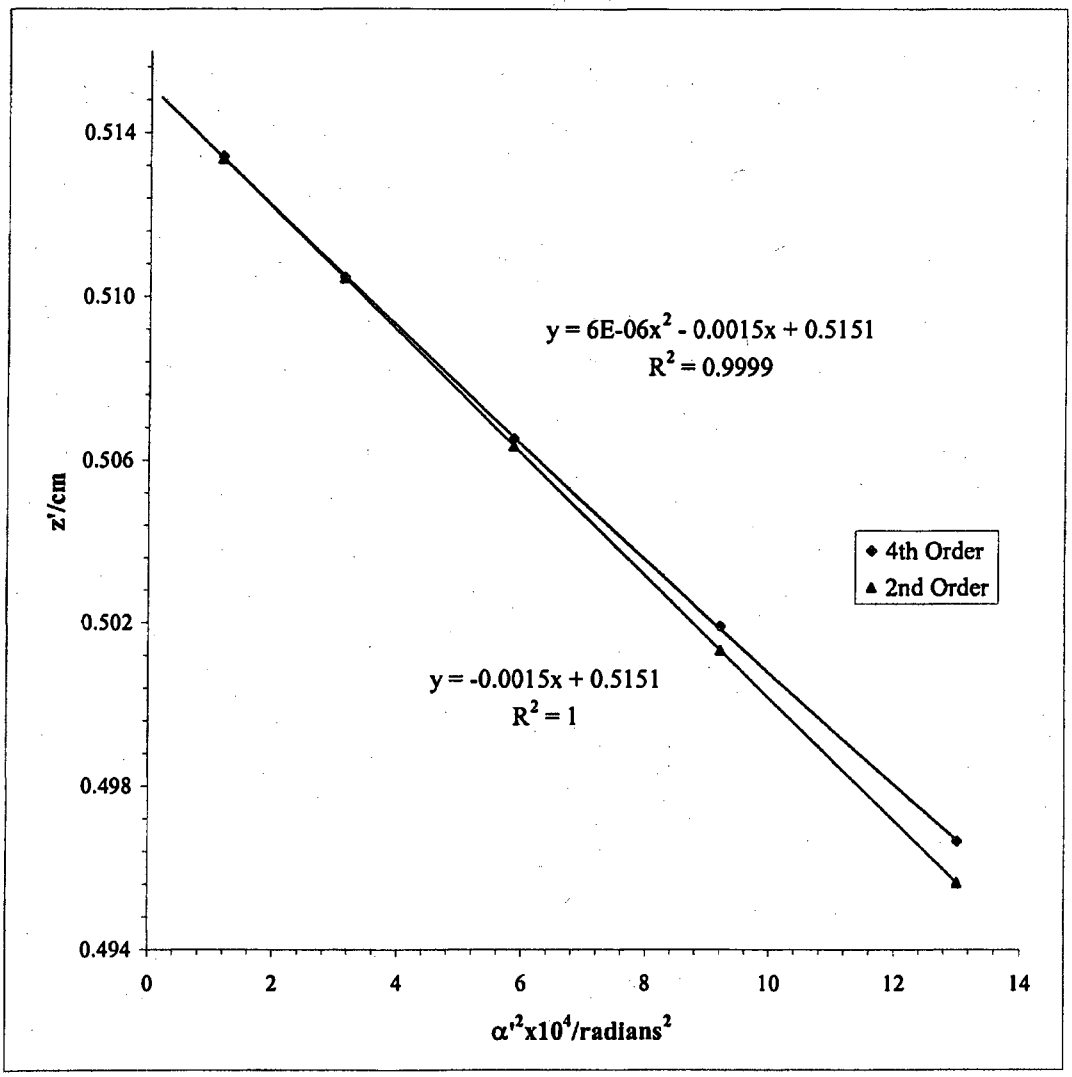

							Beam	Voltage	20 kV
Mesh/inch	I/milamp	Mesh	z/cm	e_t/cm	a/cm	z_{sp}/cm	z_0'/cm	C_s'/cm	$z_{sp}-z_o'$ /cm
600	150	Front	30.35	4.23E-03	20.96	26.33	0.58	15.74	25.76

Bar location/ units	Shadow Reading X/cm	Spacing Δ/cm	E/cm	α x 10^4	α^s x 10^2	α'^2 x 10^4	m	z'/cm	f/cm
3.5	1.211		0.972	7.069	3.769	14.209	0.01875	0.553	0.559
2.5	1.497	0.286	0.682	5.049	2.649	7.015	0.01906	0.564	0.568
1.5	1.773	0.275	0.405	3.029	1.571	2.470	0.01928	0.571	0.574
0.5	2.042	0.270	0.134	1.010	0.521	0.271	0.01939	0.575	0.577
-0.5	2.310	0.268							
-1.5	2.582	0.272							
-2.5	2.862	0.280							
-3.5	3.155	0.293							

	Slope	m_o	μ_s
3.21E-07	-5.00E-05	0.019399	-25.80

g/cm	$(\rho/f_0)^2 = (m_0+1)^2 \alpha'^2$
0.542	14.765
0.553	7.289
0.560	2.566
0.564	0.282

f vs $(\rho/f_o)^2$

S_f = slope$_f$ / f_0

	slope$_f$	fo/cm	S_f
9.029E-06	-0.00141	0.578	-24.42

g vs $(\rho/f_o)^2$

S_g = slope$_g$ / f_0

	slope$_g$	go/cm	S_g
-4.01609E-07	-0.00146	0.564	-25.25

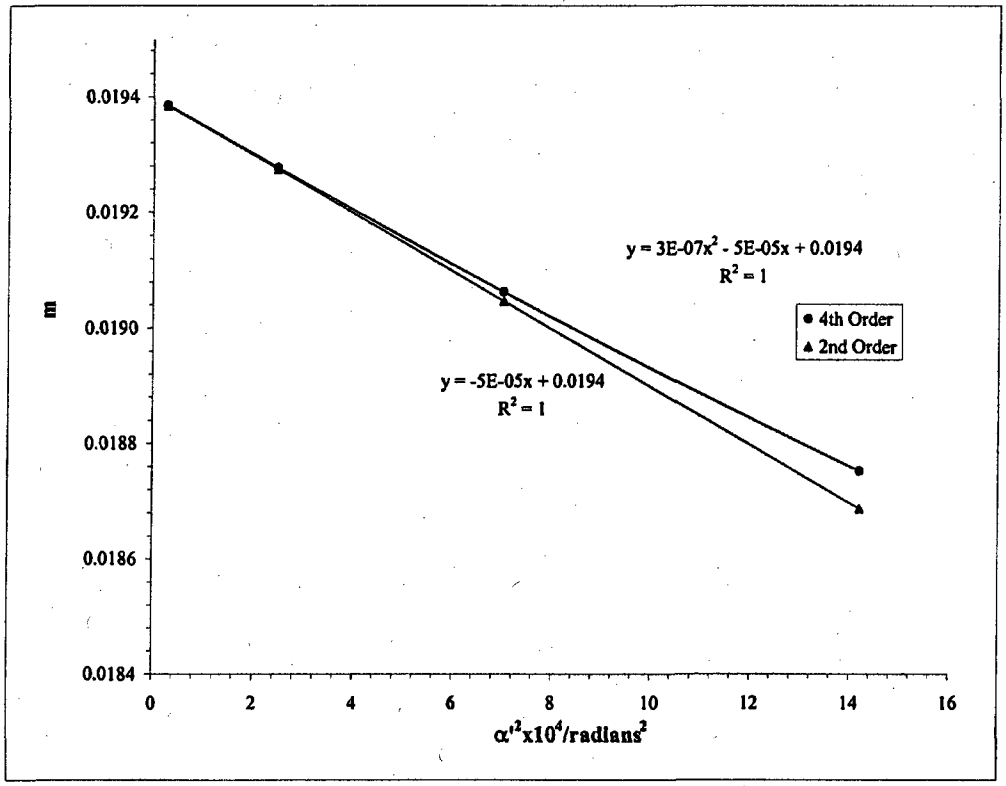

							Beam	Voltage	20 kV
Mesh/inch	I/milamp	Mesh	z/cm	e_1/cm	a/cm	z_{sp}/cm	z_0'/cm	C_s'/cm	$z_{sp}-z_o'$
600	150	Front	30.35	0.00423	20.96	26.33	0.575	15.74	25.76

Bar location/ units	Shadow Reading Y/cm	Spacing Δ/cm	E/cm	α x 10^4	α' x 10^2	α'² x 10^4	m	z'/cm	f/cm
4	2.124		1.133	8.078	4.392	19.293	0.0184	0.545	0.548
3	2.427	0.3032	0.833	6.059	3.231	10.436	0.0188	0.559	0.559
2	2.715	0.2878	0.547	4.039	2.123	4.508	0.0190	0.568	0.567
1	2.992	0.2773	0.271	2.020	1.052	1.108	0.0192	0.574	0.572
0	3.263	0.2716							
-1	3.534	0.2707					g/cm	$(\rho/f_0)^2 = (m_0+1)^2\alpha'^2$	
-2	3.809	0.2746							
-3	4.092	0.2833					0.535	20.043	
-4	4.389	0.2969					0.548	10.842	
							0.557	4.683	
		Slope	m_o	μ_s			0.563	1.151	
	3.09E-07	-5.01E-05	0.01924	-26.04					

f vs $(\rho/f_o)^2$

$S_f = slope_f / f_0$

	$slope_f$	fo/cm	S_f
8.46865E-06	-0.001408	0.573	-24.575

g vs $(\rho/f_o)^2$

$S_g = slope_g / f_0$

	$slope_g$	go/cm	S_g
-3.71E-07	-0.00146	0.564	-25.48

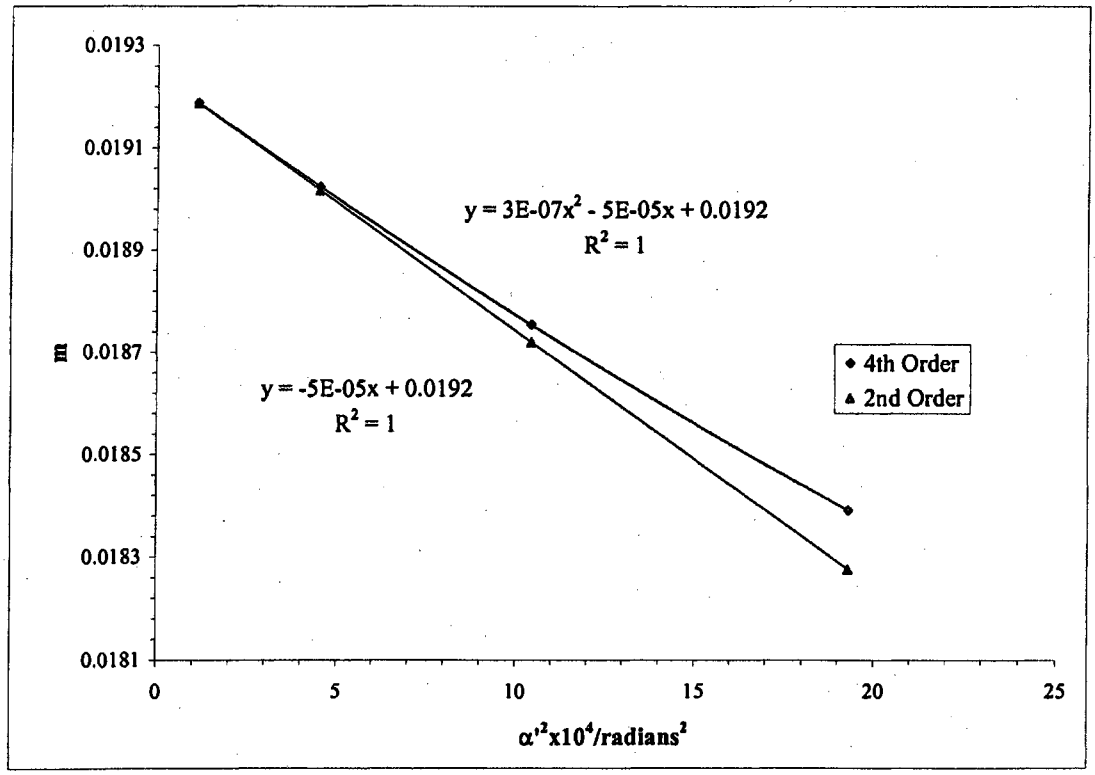

Beam Voltage	I/milamp	z/cm	z_0'/cm	C_s'/cm
20 kV	150	30.3	0.575	15.7

Average of m_o = 0.0193

Average of μ_s = -25.9

Paraxial properties :

f_o = 0.575 cm

g_o = 0.564 cm

S_f = -24.5

S_g = -25.4

Mesh/inch	I/milamp	Mesh	e'_1/cm	d/cm	b/cm		Beam	Voltage	20 kV
2000	180	Rear	0.00127	25.85	0.480	DS			

Bar location/ units	Shadow Reading X/cm	Spacing Δ/cm	E'/cm	M'	c/cm	$\alpha' \times 10^2$	$\alpha'^2 \times 10^4$	z'/cm
4	1.158		1.491	293.5	0.088	5.7479	33.0380	0.392
3	1.443	0.285	1.200	315.0	0.082	4.6272	21.4105	0.398
2	1.779	0.336	0.856	336.9	0.077	3.3004	10.8930	0.403
1	2.174	0.395	0.453	356.3	0.073	1.7457	3.0475	0.407
0	2.624	0.450						
-1	3.079	0.455						
-2	3.491	0.411						
-3	3.843	0.353		Slope	z_0'/cm	C_s'/cm		
-4	4.140	0.297	2.96E-07	-0.0005	0.409	5.307		

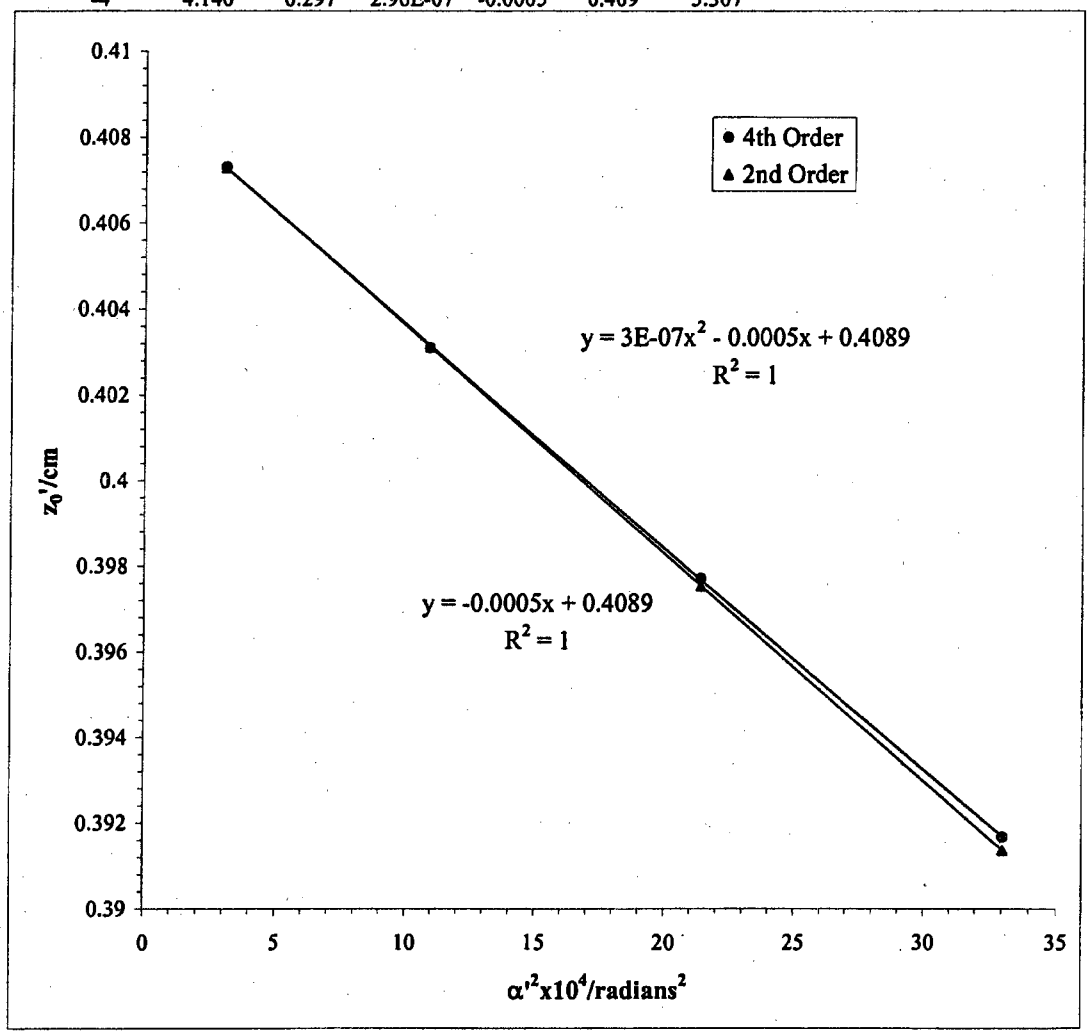

Mesh/inch	I/milamp	Mesh	e'_1/cm	d/cm	b/cm		Beam	Voltage	20 kV
2000	180	Rear	0.00127	25.85	0.480	DS			

Bar location/ units	Shadow Reading Y/cm	Spacing Δ/cm	E'/cm	M'	c/cm	$\alpha' \times 10^2$	$\alpha'^2 \times 10^4$	z'/cm
4	1.192		1.517	298.6	0.087	5.8483	34.2027	0.393
3	1.478	0.285	1.215	318.9	0.081	4.6852	21.9510	0.399
2	1.807	0.329	0.865	340.7	0.076	3.3376	11.1393	0.404
1	2.196	0.389	0.457	359.5	0.072	1.7612	3.1017	0.408
0	2.642	0.446						
-1	3.109	0.467						
-2	3.538	0.429						
-3	3.908	0.370						
-4	4.226	0.318						

	Slope	z_0'/cm	C_s'/cm
1.10E-06	-0.0005	0.410	5.157

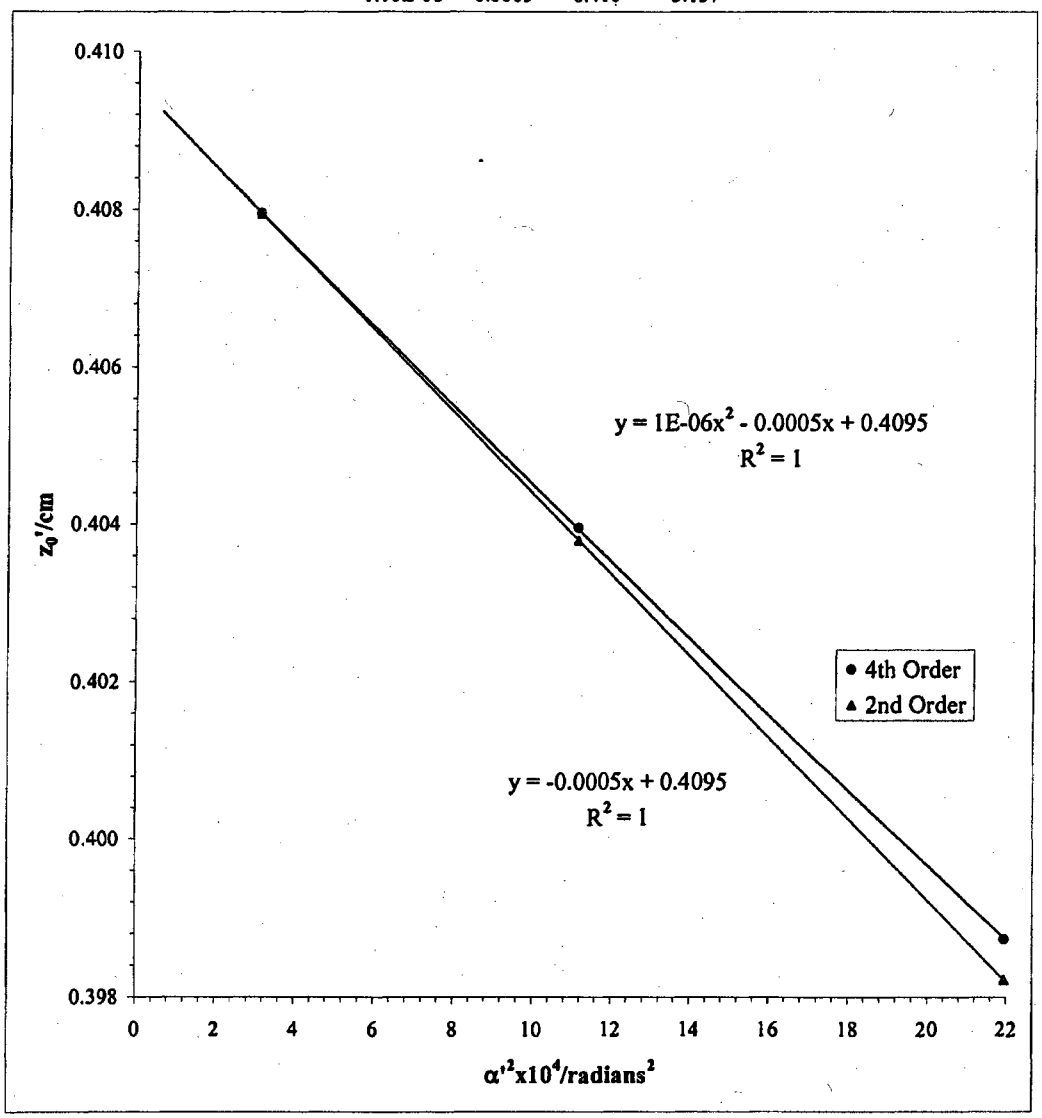

							Beam	Voltage	20 kV
Mesh/inch	I/milamp	Mesh	z/cm	e_1/cm	a/cm	z_{sp}/cm	z_0'/cm	C_s'/cm	$z_{sp}-z_o'$
600	180	Front	30.35	0.00423	20.96	26.33	0.409	5.232	25.92

Bar location/ units	Shadow Reading X/cm	Spacing Δ/cm	E/cm	$\alpha \times 10^4$	$\alpha' \times 10^2$	$\alpha'^2 \times 10^4$	m	z'/cm	f/cm
4	1.180		1.565	8.078	6.033	36.392	0.01339	0.3902	0.401
3	1.593	0.413	1.154	6.059	4.449	19.793	0.01362	0.3989	0.408
2	1.989	0.396	0.760	4.039	2.930	8.585	0.01379	0.4047	0.413
1	2.373	0.384	0.377	2.020	1.454	2.115	0.01389	0.4081	0.416
0	2.750	0.377							
-1	3.127	0.377					g/cm	$(\rho/f_0)^2 = (m_0+1)^2\alpha'^2$	
-2	3.508	0.382							
-3	3.901	0.393					0.385	37.412	
-4	4.310	0.409					0.393	20.348	
							0.399	8.826	
							0.402	2.174	

	Slope	m_0	μ_s
4.63E-08	-1.63E-05	0.01392	-11.69

f vs $(\rho/f_o)^2$

$S_f = slope_f / f_0$

	$slope_f$	fo/cm	S_f
1.31E-06	-0.000467	0.417	-11.20

g vs $(\rho/f_o)^2$

$S_g = slope_g / f_0$

	$slope_g$	go/cm	S_g
-4.2E-08	-0.0005	0.403	-11.89

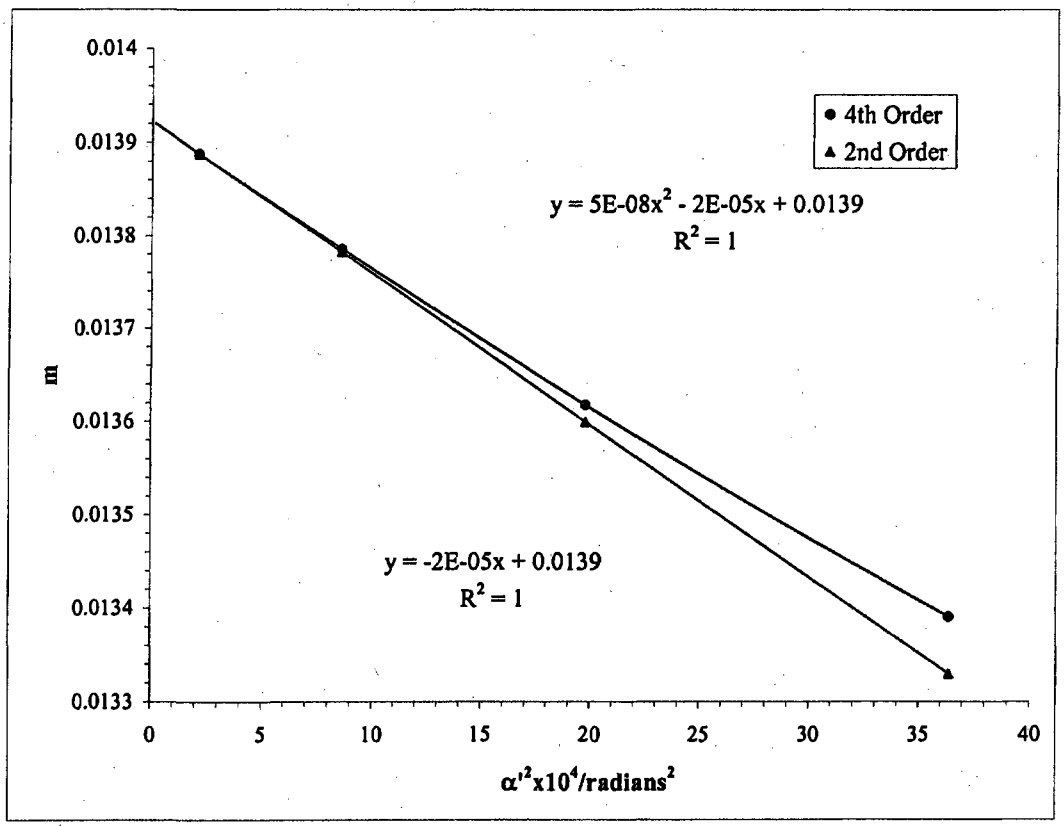

							Beam	Voltage	20 kV
Mesh/inch	I/milamp	Mesh	z/cm	ε_1/cm	a/cm	z_{sp}/cm	z_0'/cm	C_1'/cm	$z_{sp}-z_o'$
600	180	Front	30.35	0.004233	20.96	26.33	0.409	5.232	25.92

Bar location/ units	Shadow Reading Y/cm	Spacing Δ/cm	E/cm	$\alpha \times 10^4$	$\alpha' \times 10^2$	$\alpha'^2 \times 10^4$	m	z'/cm	f/cm
4	1.748		1.575	8.078	6.072	36.868	0.01330	0.3899	0.399
3	2.165	0.417	1.161	6.059	4.475	20.029	0.01354	0.3987	0.406
2	2.563	0.398	0.764	4.039	2.946	8.679	0.01371	0.4047	0.411
1	2.949	0.386	0.379	2.020	1.462	2.137	0.01382	0.4081	0.414
0	3.328	0.379							
-1	3.707	0.379					g/cm	$(\rho/f_0)^2 =$	
-2	4.091	0.384						$(m_0+1)^2\alpha'^2$	
-3	4.486	0.395					0.385	37.896	
-4	4.899	0.413					0.393	20.587	
							0.399	8.921	
		Slope	m_0	μ_s			0.402	2.196	
	4.80E-08	-1.66E-05	0.014	-11.97959					

f vs $(\rho/f_o)^2$

$S_f = slope_f / f_0$

	$slope_f$	fo/cm	S_f
1.3551E-06	-0.00048	0.415	-11.49

g vs $(\rho/f_o)^2$

$S_g = slope_g / f_0$

	$slope_g$	go/cm	S_g
-4.3E-08	-0.0005	0.403	-11.95

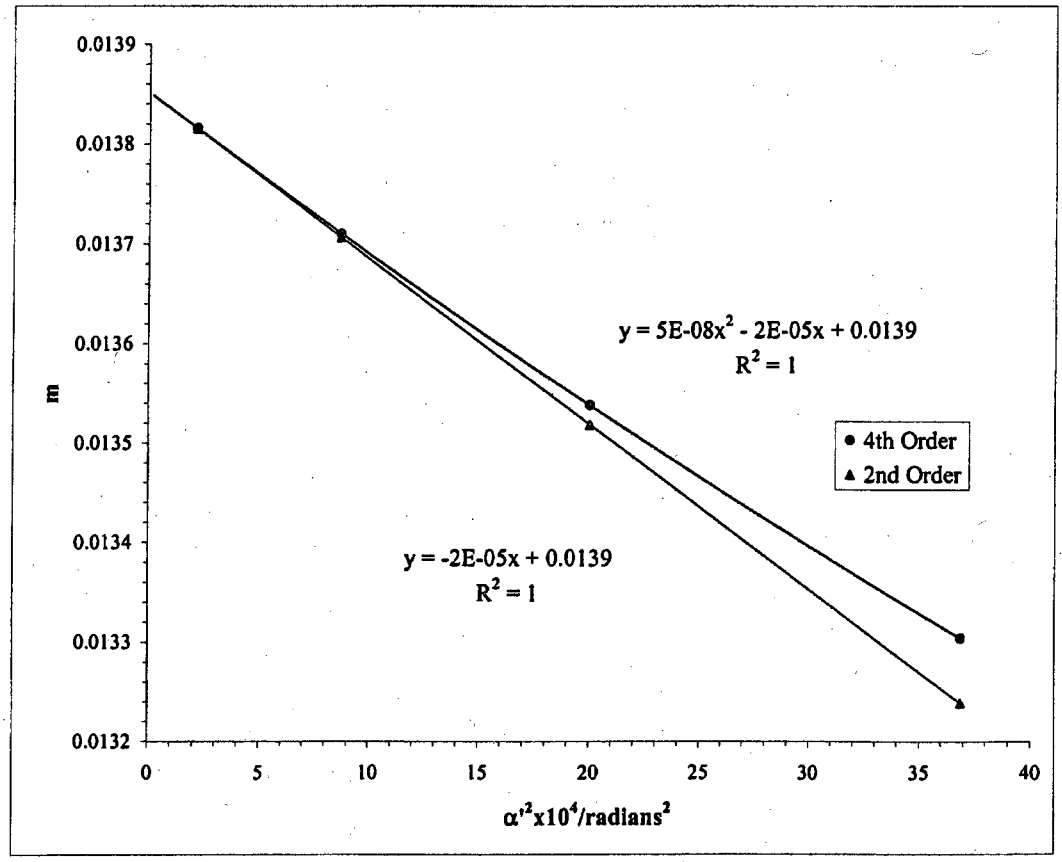

Beam Voltage	I/milamp	z/cm	z_0'/cm	C_s'/cm
20 kV	180	30.3	0.409	5.23

Average of m_o = 0.0139

Average of μ_s = -11.8

Paraxial properties :

f_o = 0.416 cm

g_o = 0.403 cm

S_f = -11.3

S_g = -11.9

Mesh/inch	I/milamp	Mesh	e'_1/cm	d/cm	b/cm		Beam	Voltage	20 kV
2000	200	Rear	0.00127	25.9	0.432	DS			

Bar location/ units	Shadow Reading X/cm	Spacing Δ/cm	E'/cm	M'	c/cm	$\alpha' \times 10^2$	$\alpha'^2 \times 10^4$	z'/cm
3.5	1.492		1.076	242.0	0.107	4.1355	17.1024	0.324
2.5	1.783	0.291	0.784	246.8	0.105	3.0129	9.0777	0.326
1.5	2.088	0.305	0.477	250.4	0.104	1.8344	3.3650	0.328
0.5	2.403	0.316	0.160	252.7	0.103	0.6171	0.3808	0.329
-0.5	2.724	0.321						
-1.5	3.042	0.318						
-2.5	3.350	0.308						
-3.5	3.643	0.293						

	Slope	z_0'/cm	C_s'/cm
1.64E-06	-0.000301	0.329	3.011

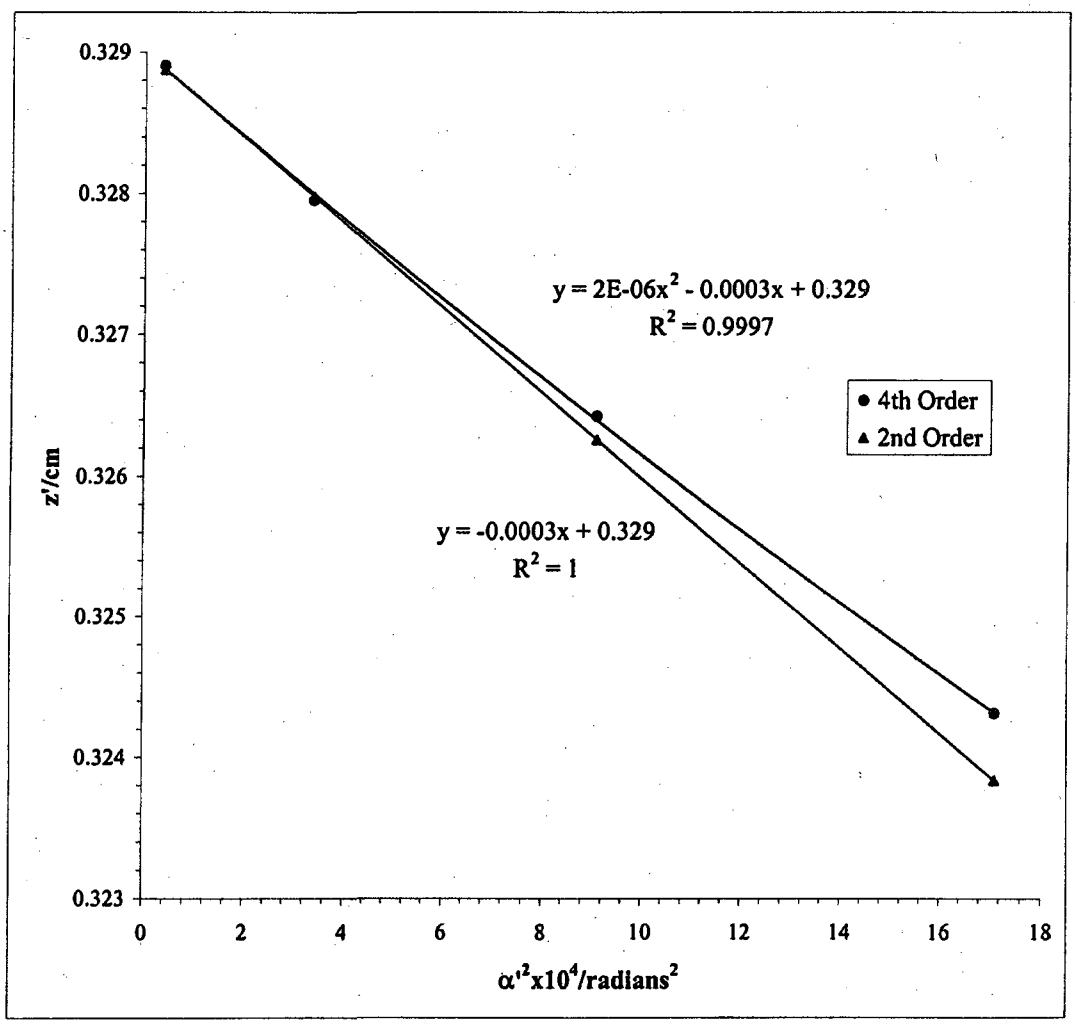

Mesh/inch	I/milamp	Mesh	e'_1/cm	d/cm	b/cm		Beam	Voltage	20 kV
2000	200	Rear	0.00127	25.9	0.4318	DS			

Bar location/ units	Shadow Reading Y/cm	Spacing Δ/cm	E'/cm	M'	c/cm	α' x 10^2	α'^2 x 10^4	z'/cm
4	1.955898		1.2156	239.3	0.1087	4.6737	21.8439	0.3231
3	2.236047	0.2801	0.9327	244.8	0.1062	3.5863	12.8619	0.3256
2	2.534343	0.2983	0.6330	249.2	0.1043	2.4344	5.9261	0.3275
1	2.84734	0.3130	0.3210	252.8	0.1029	1.2346	1.5243	0.3289
0	3.165452	0.3181						
-1	3.489416	0.3240						
-2	3.800417	0.3110						
-3	4.101394	0.3010						
-4	4.387058	0.2857						

	Slope	z_0'/cm	C_s'/cm
1.60E-06	-0.00032	0.3294	3.2169

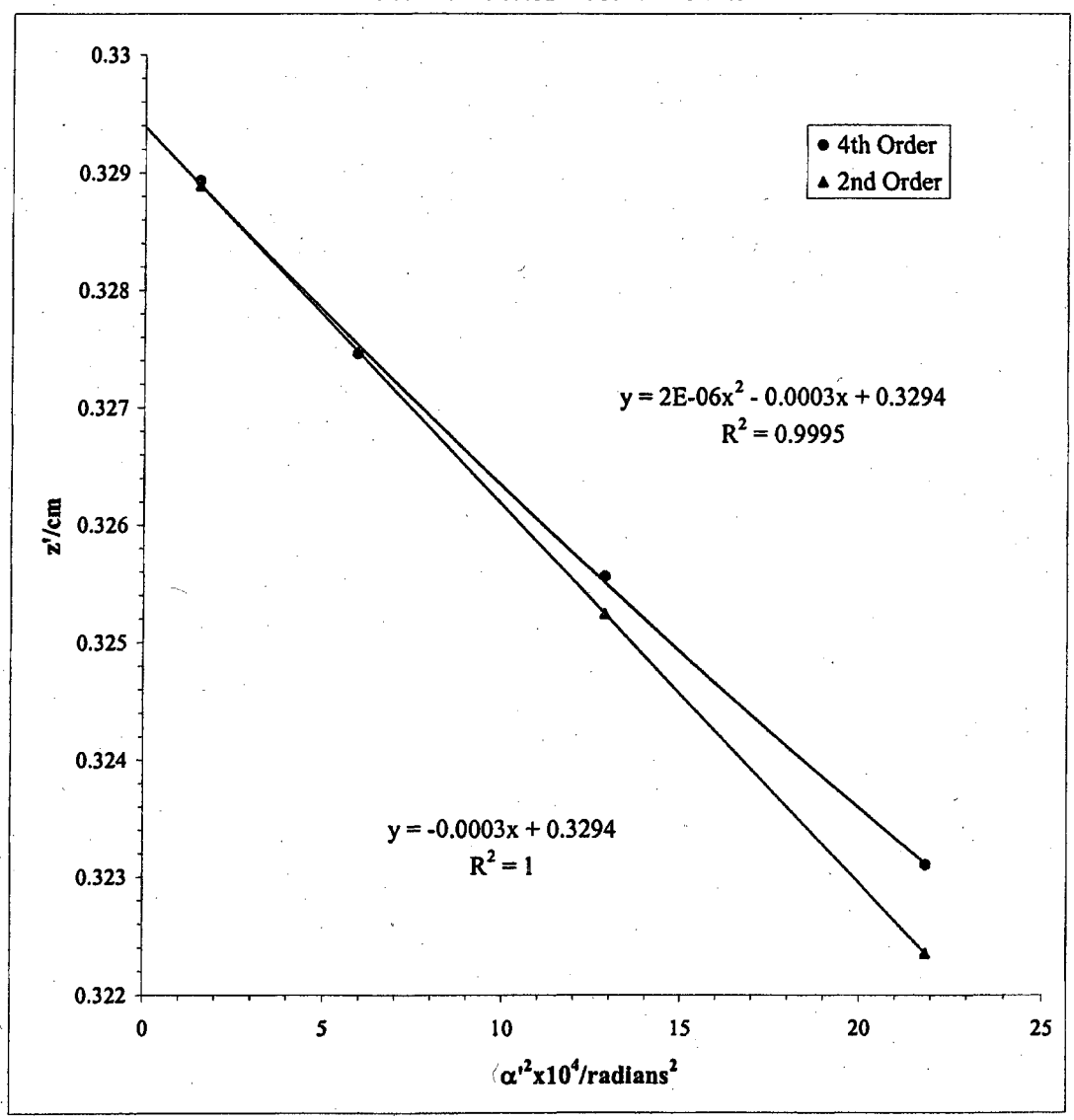

							Beam	Voltage	20 kV
Mesh/inch	I/milamp	Mesh	z/cm	e_1/cm	a/cm	z_{sp}/cm	z_0'/cm	C_s'/cm	$z_{sp}-z_o'$
2000	200	Front	30.35	0.00127	20.96	26.33	0.329	3.114	26.00

Bar location/ units	Shadow Reading X/cm	Spacing Δ/cm	E/cm	$\alpha \times 10^4$	$\alpha' \times 10^2$	$\alpha'^2 \times 10^4$	m	z'/cm	f/cm
7	2.597		0.967	4.241	3.718	13.822	0.01141	0.325	0.343
6	2.738	0.141	0.826	3.635	3.177	10.092	0.01144	0.326	0.344
5	2.877	0.139	0.687	3.029	2.640	6.971	0.01147	0.327	0.344
4	3.016	0.138	0.548	2.424	2.108	4.442	0.01150	0.328	0.345
3	3.153	0.138	0.410	1.818	1.578	2.490	0.01152	0.328	0.346
2	3.291	0.137	0.273	1.212	1.051	1.104	0.01153	0.329	0.346
1	3.427	0.137	0.137	0.606	0.525	0.276	0.01154	0.329	0.346
0	3.564	0.137							
-1	3.700	0.137					g/cm	$(\rho/f_0)^2 = (m_0+1)^2\alpha'^2$	
-2	3.837	0.137							
-3	3.974	0.137					0.321	14.143	
-4	4.112	0.138					0.322	10.326	
-5	4.251	0.139					0.323	7.133	
-6	4.390	0.140					0.324	4.546	
-7	4.531	0.141					0.324	2.548	
							0.325	1.130	
			Slope	m_o	μ_s		0.325	0.282	
			2.53E-08	-1.02E-05	0.011543	-8.7944			

f vs $(\rho/f_o)^2$

$S_f = slope_f / f_0$

	$slope_f$	fo/cm	S_f
7.23E-07	-0.000294	0.347	-8.50

g vs $(\rho/f_o)^2$

$S_g = slope_g / f_0$

	$slope_g$	go/cm	S_g
-1.9E-08	-0.000297	0.325	-8.58

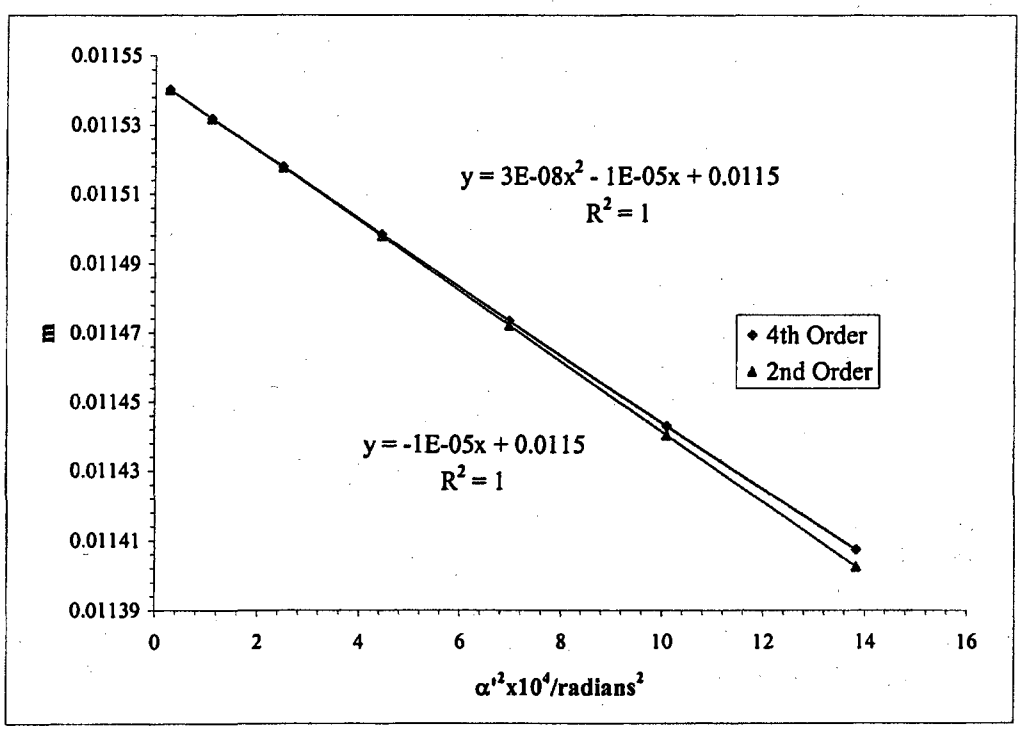

							Beam	Voltage	20 kV
Mesh/inch	I/milamp	Mesh	z/cm	e_1/cm	a/cm	z_{sp}/cm	z_0'/cm	C_s'/cm	$z_{sp}-z_0'$
2000	200	Front	30.347	0.00127	20.96	26.33	0.329	3.114	26.00

Bar location/ units	Shadow Reading Y/cm	Spacing Δ/cm	E/cm	$\alpha \times 10^4$	$\alpha' \times 10^2$	$\alpha'^2 \times 10^4$	m	z'/cm	f/cm
6.5	2.265		0.920	3.938	3.538	12.516	0.01113	0.325	0.334
5.5	2.409	0.144	0.776	3.332	2.984	8.906	0.01117	0.326	0.335
4.5	2.551	0.142	0.633	2.726	2.435	5.931	0.01119	0.327	0.336
3.5	2.692	0.141	0.492	2.121	1.890	3.573	0.01122	0.328	0.337
2.5	2.833	0.141	0.351	1.515	1.348	1.817	0.01124	0.329	0.337
1.5	2.974	0.140	0.210	0.909	0.808	0.653	0.01125	0.329	0.338
0.5	3.114	0.140	0.070	0.303	0.269	0.072	0.01125	0.329	0.338
-0.5	3.254	0.140							
-1.5	3.394	0.140					g/cm	$(\rho/f_0)^2 = (m_0+1)^2\alpha'^2$	
-2.5	3.534	0.141							
-3.5	3.676	0.141					0.322	12.80	
-4.5	3.818	0.142					0.323	9.11	
-5.5	3.961	0.143					0.324	6.07	
-6.5	4.105	0.144					0.324	3.65	
							0.325	1.86	
			Slope	m_0	μ_s		0.325	0.67	
		2.55E-08	-1E-05	0.01125	-8.93473		0.325	0.07	

f vs $(\rho/f_o)^2$

$S_f = slope_f / f_0$

	$slope_f$	fo/cm	S_f
7.3029E-07	-0.0002918	0.338	-8.64

g vs $(\rho/f_o)^2$

$S_g = slope_g / f_0$

	$slope_g$	go/cm	S_g
-1.9E-08	-0.000298	0.325	-8.82

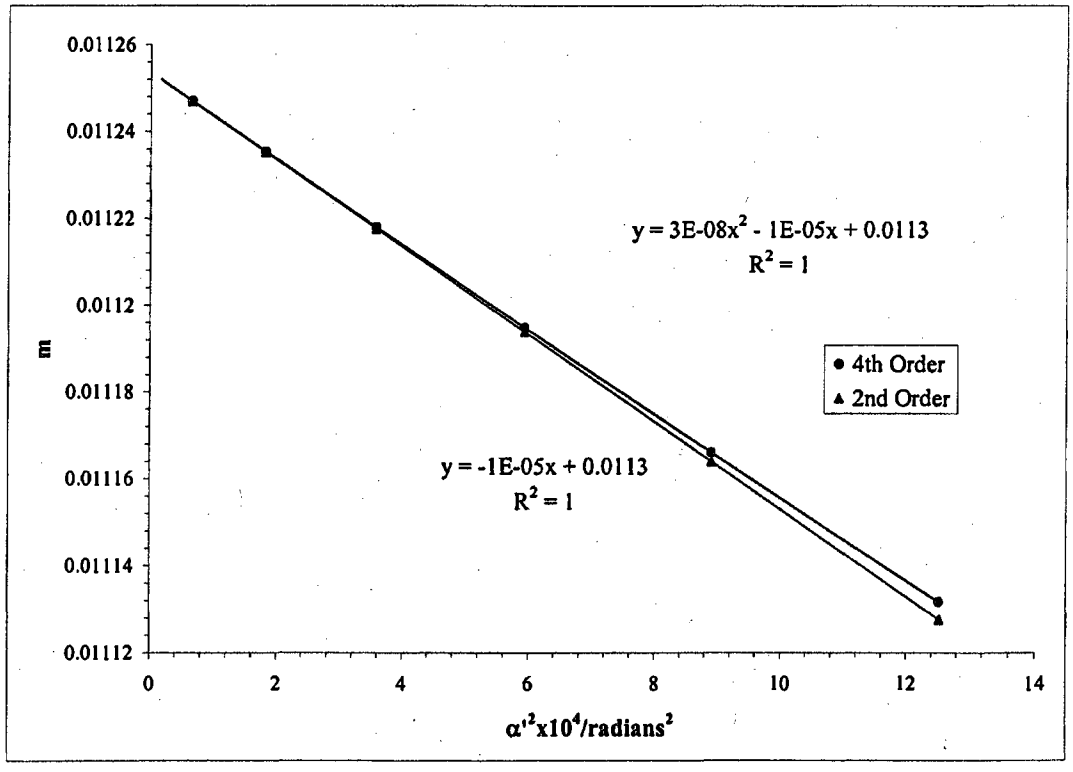

Beam Voltage	I/milamp	z/cm	z_0'/cm	C_s'/cm
20 kV	200	30.3	0.329	3.11

Average of m_o = 0.0114

Average of μ_s = -8.86

Paraxial properties :

f_o = 0.342 cm

g_o = 0.325 cm

S_f = -8.57

S_g = -8.70

Mesh/inch	I/milamp	Mesh	e'_1/cm	d/cm	b/cm		Beam	Voltage	20 kV
600	250	Rear	0.00423	25.9	0.4318	DS			

Bar location/ units	Shadow Reading X/cm	Spacing Δ/cm	E'/cm	M'	c/cm	α' x 10^2	α'^{2} x 10^4	z'/cm
4	0.6851		2.0625	121.8	0.2144	7.8980	62.3791	0.2174
3	1.1880	0.5029	1.5645	123.2	0.2120	5.9916	35.8994	0.2198
2	1.7040	0.5160	1.0525	124.3	0.2100	4.0310	16.2487	0.2218
1	2.2286	0.5246	0.5295	125.1	0.2087	2.0282	4.1134	0.2231
0	2.7584	0.5298						
-1	3.2877	0.5292						
-2	3.8090	0.5214			Slope	z_0'/cm	C_s'/cm	
-3	4.3171	0.5081		1.81E-07	-0.0001	0.224	1.09	
-4	4.8101	0.4930						

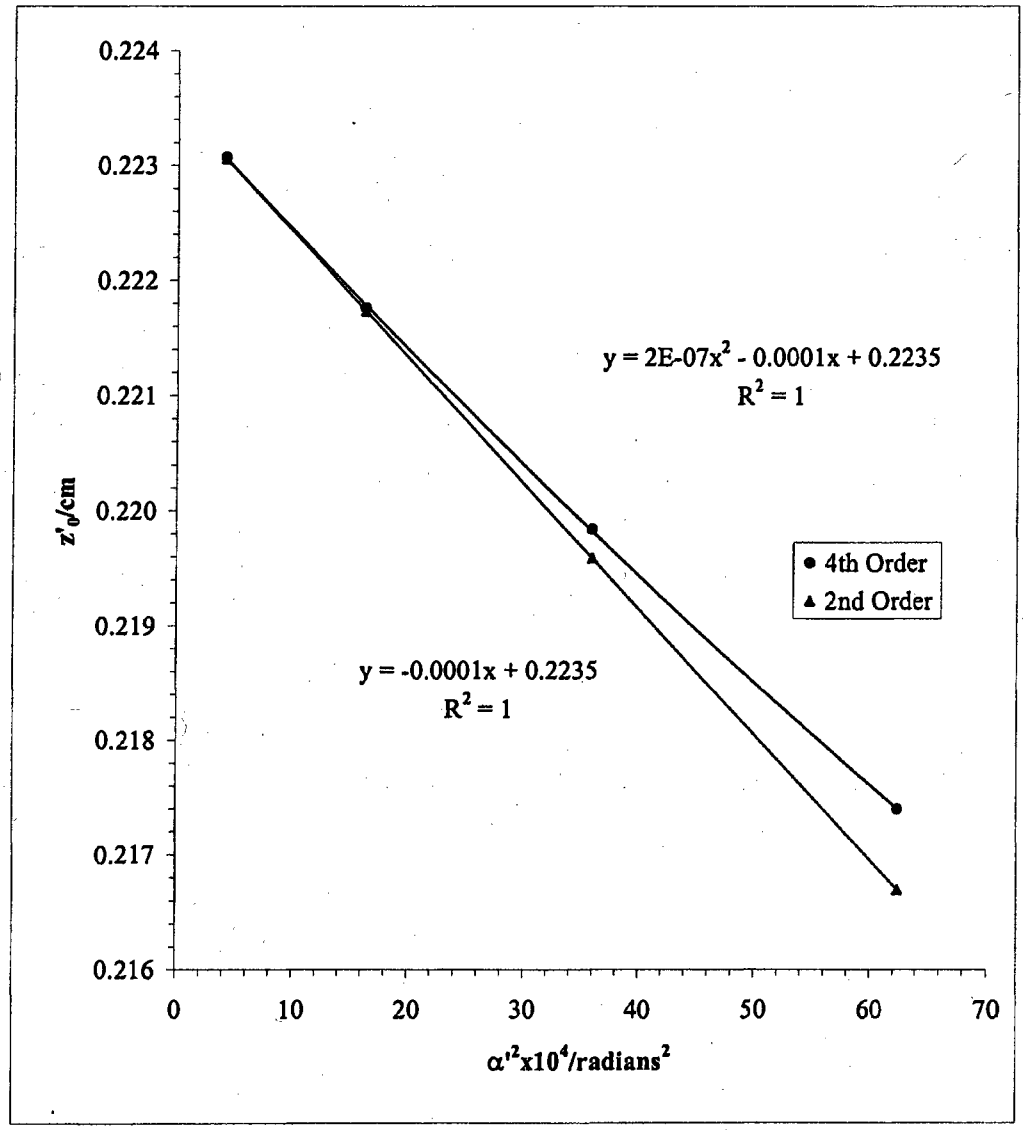

							Beam	Voltage	20 kV
Mesh/inch	I/milamp	Mesh	z/cm	e_1/cm	a/cm	z_{sp}/cm	z_0'/cm	C_z'/cm	$z_{sp}-z_o'$
2000	250	Front	30.35	0.00127	20.96	26.33	0.224	1.091	26.11

Bar location/ units	Shadow Reading X/cm	Spacing Δ/cm	E/cm	α x 10^4	α' x 10^2	α'^{2} x 10^4	m	z'/cm	f/cm
4.5	2.369		0.955	2.726	3.658	13.377	0.00745	0.2220	0.2246
3.5	2.586	0.2169	0.741	2.121	2.839	8.061	0.00747	0.2226	0.2250
2.5	2.801	0.2150	0.529	1.515	2.025	4.100	0.00748	0.2231	0.2253
1.5	3.015	0.2134	0.317	0.909	1.214	1.473	0.00749	0.2233	0.2256
0.5	3.227	0.2121	0.106	0.303	0.404	0.164	0.00749	0.2235	0.2257
-0.5	3.438	0.2112							
-1.5	3.648	0.2105					g/cm	$(\rho/f_0)^2 = (m_0+1)^2\alpha'^2$	
-2.5	3.859	0.2102							
-3.5	4.069	0.2102					0.2204	13.579	
-4.5	4.279	0.2105					0.2209	8.182	
							0.2214	4.162	
			Slope	m_0	μ_z		0.2217	1.495	
		3.14E-09	-2.83E-06	0.007492	-3.78		0.2218	0.166	

f vs $(\rho/f_o)^2$

$S_f = slope_f / f_0$

	$slope_f$	fo/cm	S_f
9.166E-08	-8.32E-05	0.226	-3.68

g vs $(\rho/f_o)^2$

$S_g = slope_g / f_0$

	$slope_g$	go/cm	S_g
-1.6E-09	-0.000106	0.222	-4.71

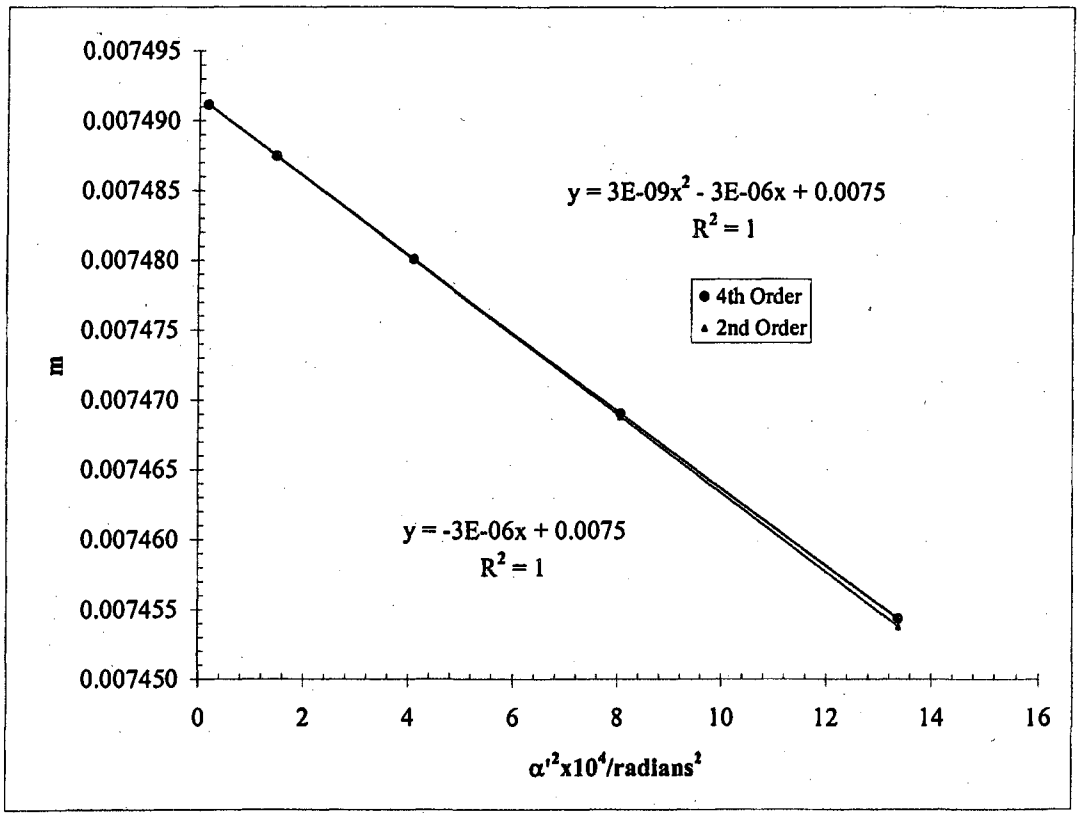

							Beam	Voltage	20 kV
Mesh/inch	l/milamp	Mesh	z/cm	e_1/cm	a/cm	z_{sp}/cm	z_0'/cm	C_s'/cm	$z_{sp}-z_0'$
2000	250	Front	30.35	0.00127	20.96	26.33	0.224	1.09	26.11

Bar location/ units	Shadow Reading Y/cm	Spacing Δ/cm	E/cm	$\alpha \times 10^4$	$\alpha' \times 10^2$	$\alpha'^2 \times 10^4$	m	z'/cm	$(\rho/f_0)^2 = (m_0+1)^2 \alpha'^2$
5	1.750		1.071	3.029	4.103	16.839	0.00738	0.2217	17.090
4	1.967	0.216	0.855	2.424	3.275	10.729	0.00740	0.2223	10.889
3	2.181	0.215	0.640	1.818	2.452	6.014	0.00741	0.2229	6.104
2	2.395	0.214	0.426	1.212	1.633	2.666	0.00742	0.2232	2.706
1	2.609	0.213	0.213	0.606	0.816	0.666	0.00743	0.2234	0.675
0	2.821	0.213							
-1	3.035	0.213					f/cm	g/cm	
-2	3.248	0.213							
-3	3.462	0.214					0.2224	0.2200	
-4	3.677	0.215					0.2229	0.2207	
-5	3.893	0.216					0.2233	0.2212	
							0.2236	0.2216	
		Slope	m_o	μ_s			0.2237	0.2218	
	3.04E-09	-2.78E-06	0.00743	-3.74					

f vs $(\rho/f_o)^2$

S_f = slope$_f$ / f_0

	slope$_f$	fo/cm	S_f
8.86387E-08	-8.176E-05	0.224	-3.65

g vs $(\rho/f_o)^2$

S_g = slope$_g$ / f_0

	slope$_g$	go/cm	S_g
-1.5E-09	-0.000106	0.222	-4.75

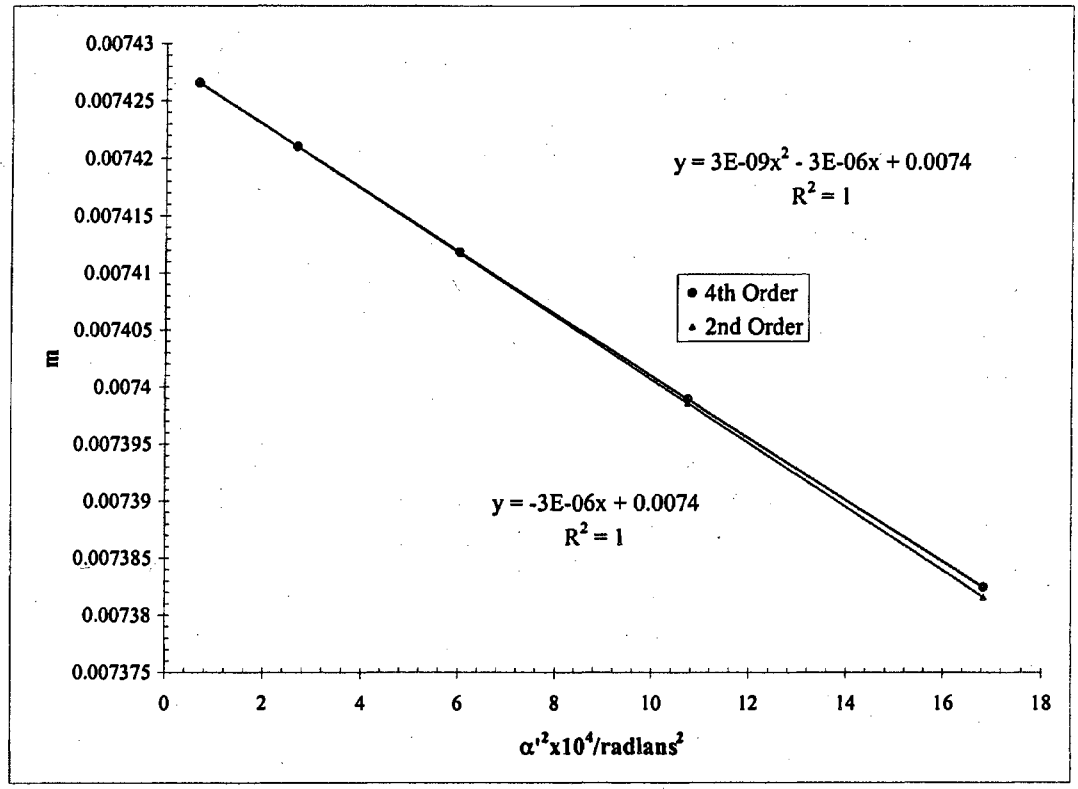

Beam Voltage	I/milamp	z/cm	z_0'/cm	C_s'/cm
20 kV	250	30.3	0.224	1.09

Average of m_o = 0.00746

Average of μ_s = -3.76

Paraxial properties :

f_o = 0.225 cm

g_o = 0.222 cm

S_f = -3.67

S_g = -4.73

Mesh/inch	I/milamp	Mesh	e'_1/cm	d/cm	b/cm		Beam	Voltage	20 kV
600	350	Rear	0.004233	25.9	0.4318	DS			

Bar location/ units	Shadow Reading X/cm	Spacing Δ/cm	E'/cm	M'	c/cm	$\alpha' \times 10^2$	$\alpha'^2 \times 10^4$	z'/cm
3.5	2.4582		1.2558	84.8	0.3092	4.7915	22.9587	0.1226
2.5	2.8160	0.3579	0.8979	84.8	0.3089	3.4258	11.7363	0.1229
1.5	3.1748	0.3587	0.5391	84.9	0.3087	2.0568	4.2305	0.1231
0.5	3.5341	0.3593	0.1797	84.9	0.3086	0.6858	0.4704	0.1232
-0.5	3.8936	0.3595						
-1.5	4.2529	0.3593						
-2.5	4.6118	0.3589						
-3.5	4.9698	0.3580						

	Slope	z_0'/cm	C_s'/cm
-6.8E-09	-3E-05	0.1232	0.264

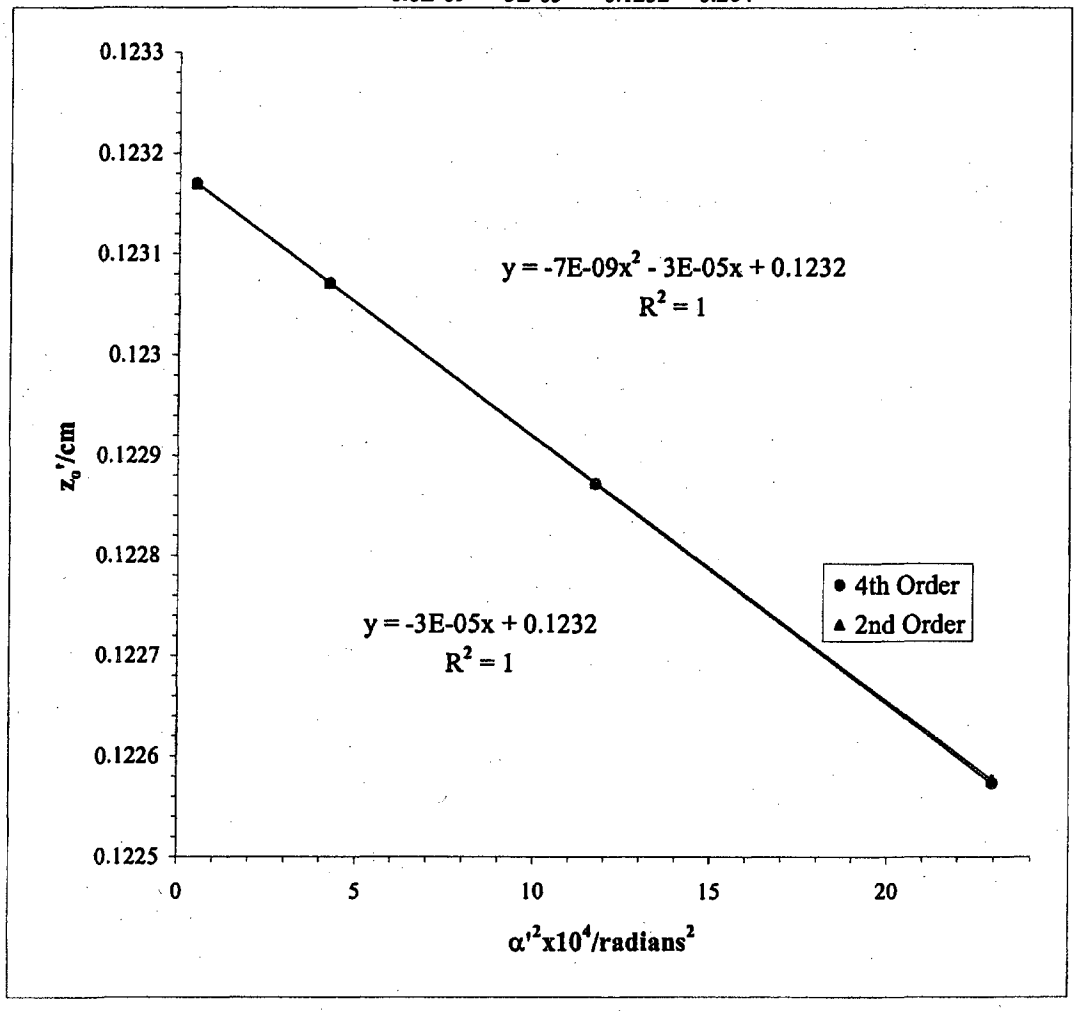

							Beam	Voltage	20 kV
Mesh/inch	I/milamp	Mesh	z/cm	e_1/cm	a/cm	z_{sp}/cm	z_0'/cm	C_s'/cm	$z_{sp}-z_0'$
2000	350	Front	30.3467	0.00127	20.96	26.33	0.1232	0.264	26.209

Bar #	Reading X/cm	Spacing Δ/cm	E/cm	$\alpha \times 10^4$	$\alpha' \times 10^2$	$\alpha'^2 \times 10^4$	m	z'/cm	$(\rho/f_0)^2 = (m_0+1)^2 \alpha'^2$
2.5	1.745		0.922	1.515	3.517	12.37	0.00431	0.123	12.475
1.5	2.114	0.369	0.552	0.909	2.108	4.44	0.00431	0.123	4.481
0.5	2.483	0.368	0.184	0.303	0.702	0.49	0.00431	0.123	0.497
-0.5	2.851	0.368							
-1.5	3.219	0.369					f/cm	g/cm	
-2.5	3.589	0.370					0.1302	0.1223	

	Slope	m_0	μ_s
2.64E-10	-6.2E-07	0.00431	-1.43

	0.1303	0.1225	
	0.1304	0.1226	

f vs $(\rho/f_o)^2$

$S_f = slope_f / f_0$

	$slope_f$	fo/cm	S_f
7.8E-09	-1.8E-05	0.130	-1.41

g vs $(\rho/f_o)^2$

$S_g = slope_g / f_0$

	$slope_g$	go/cm	S_g
-7.9E-11	-3E-05	0.123	-1.99

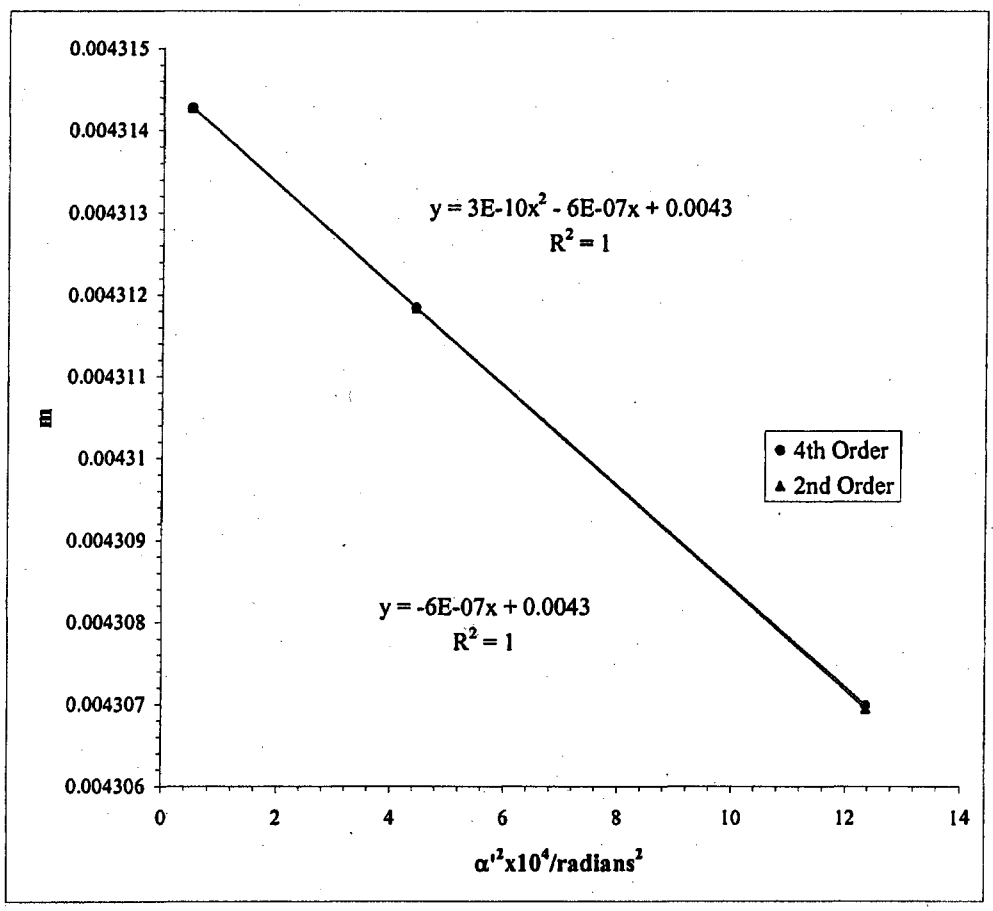

							Beam	Voltage	20 kV
Mesh/inch	I/milamp	Mesh	z/cm	e_1/cm	a/cm	z_{sp}/cm	z_0'/cm	C_s'/cm	$z_{sp}-z_o'$
2000	350	Front	30.35	0.00127	20.96	26.33	0.1232	0.264	26.21

	Bar location/ units	Shadow Reading Y/cm	Spacing Δ/cm	E/cm	$\alpha \times 10^4$	$\alpha' \times 10^2$	$\alpha'^2 \times 10^4$	m	z'/cm	$(\rho/f_0)^2 = (m_0+1)^2 \alpha'^2$
1	3	1.3810		1.077	1.818	4.109	16.89	0.004423	0.123	17.037
2	2	1.7411	0.360	0.717	1.212	2.736	7.49	0.004429	0.123	7.552
3	1	2.1000	0.359	0.358	0.606	1.367	1.87	0.004433	0.123	1.885
	0	2.4583	0.358							
	-1	2.8165	0.358					f/cm	g/cm	
	-2	3.1752	0.359							
	-3	3.5350	0.360					0.1337	0.1221	
								0.1339	0.1224	
				Slope	m_o	μ_s		0.1340	0.1225	
			2.7E-10	-6.4E-07	0.00443	-1.43				

f vs $(\rho/f_o)^2$

$S_f = slope_f / f_0$

0.3000	$slope_f$	fo/cm	S_f
8.02252E-09	-1.9E-05	0.134	-1.41

g vs $(\rho/f_o)^2$

$S_g = slope_g / f_0$

$slope_g$	go/cm	S_g
-8E-11	-2.6E-05	0.123	-1.94

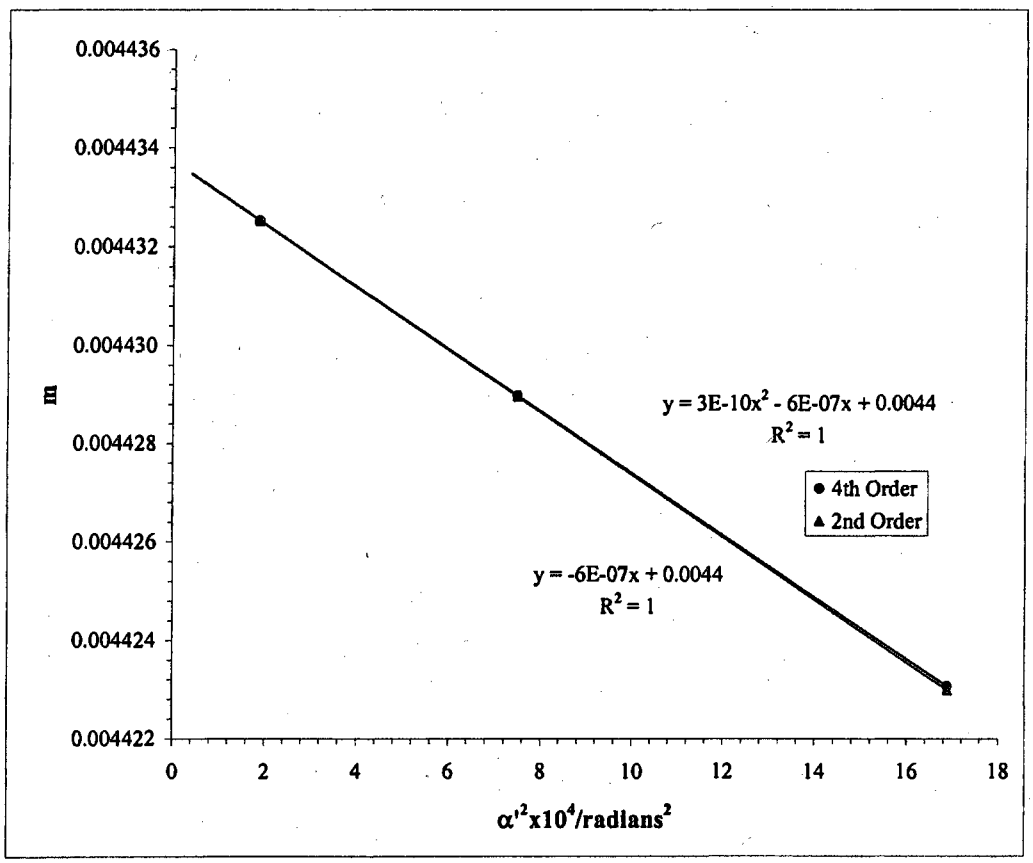

Beam Voltage	I/milamp	z/cm	z_0'/cm	C_s'/cm
20 kV	350	30.3	0.123	0.264

Average of m_o = 0.00437

Average of μ_s = -1.43

Paraxial properties :

f_o = 0.132 cm

g_o = 0.123 cm

S_f = -1.41

S_g = -1.97

Mesh/inch	I/milamp	Mesh	e'_1/cm	d/cm	b/cm		Beam	Voltage	20 kV
600	400	Rear	0.004233	25.9	0.432	DS			

Bar location/ units	Shadow Reading X/cm	Spacing Δ/cm	E'/cm	M'	c/cm	$\alpha' \times 10^2$	$\alpha'^2 \times 10^4$	z'/cm
4	1.4180		1.3198	77.9	0.3366	5.0303	25.3035	0.0952
3	1.7474	0.3294	0.9903	78.0	0.3365	3.7744	14.2458	0.0953
2	2.0772	0.3298	0.6604	78.0	0.3364	2.5170	6.3355	0.0954
1	2.4072	0.3301	0.3303	78.0	0.3363	1.2588	1.5845	0.0955
0	2.7375	0.3302						
-1	3.0677	0.3303						
-2	3.3979	0.3302						
-3	3.7279	0.3300			Slope	z_0'/cm	C_s'/cm	
-4	4.0575	0.3296		-1.6E-09	-1.35E-05	0.096	0.1346	

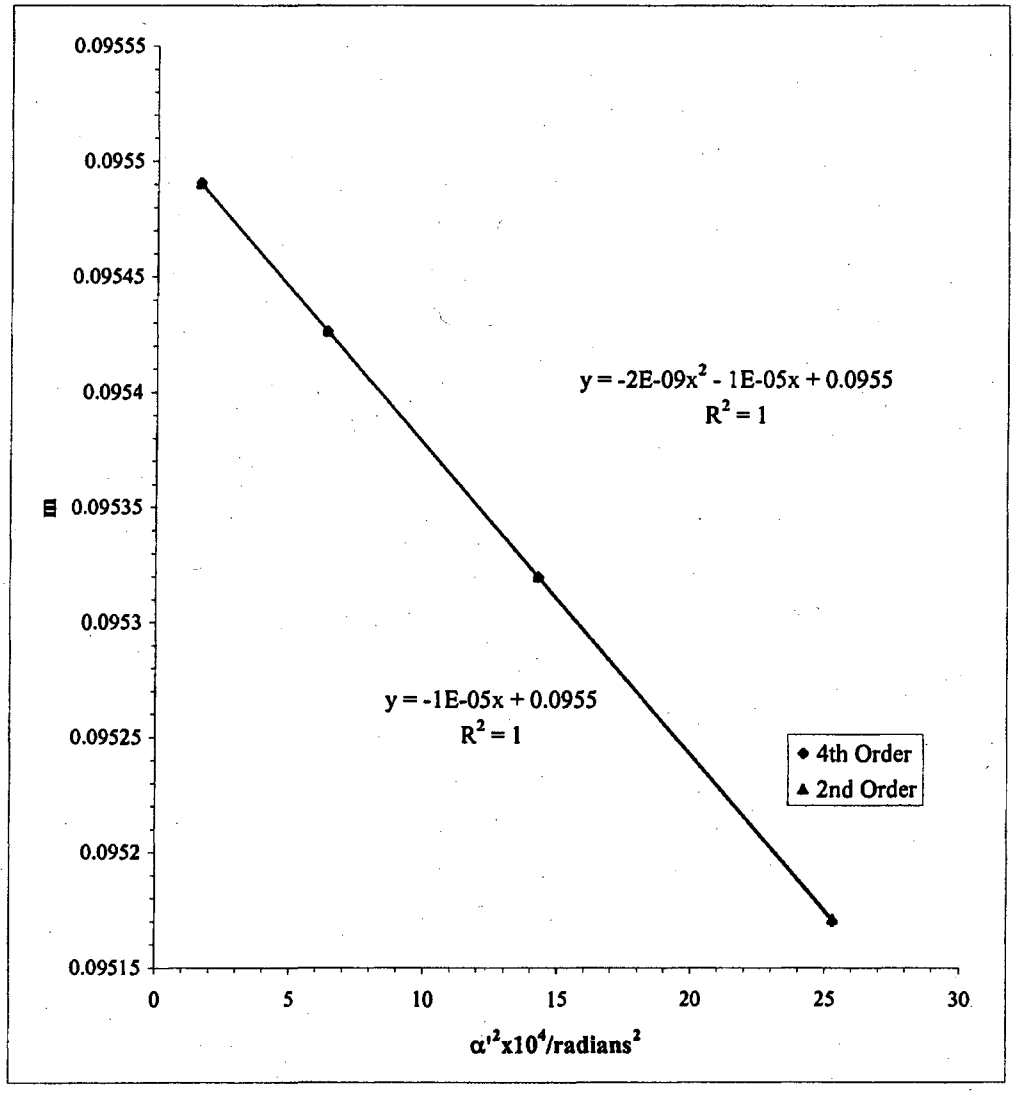

Mesh/inch	I/mllamp	Mesh	e'_1/cm	d/cm	b/cm		Beam	Voltage	20 kV
600	400	Rear	0.00423	25.9	0.432	DS			

Bar location/ units	Shadow Reading Y/cm	Spacing Δ/cm	E'/cm	M'	c/cm	$\alpha' \times 10^2$	$\alpha'^2 \times 10^4$	z'/cm
4	3.746		1.309	77.3	0.339	4.9905	24.9053	0.092
3	4.073	0.3270	0.982	77.4	0.339	3.7443	14.0196	0.093
2	4.400	0.3273	0.655	77.4	0.339	2.4968	6.2342	0.093
1	4.728	0.3275	0.328	77.4	0.339	1.2486	1.5591	0.093
0	5.055	0.3276						
-1	5.383	0.3276						
-2	5.711	0.3275						
-3	6.038	0.3273						
-4	6.365	0.3270						

Slope	z_o'/cm	C_s'/cm
-1.18E-09	-1.15E-05	0.0928	0.115

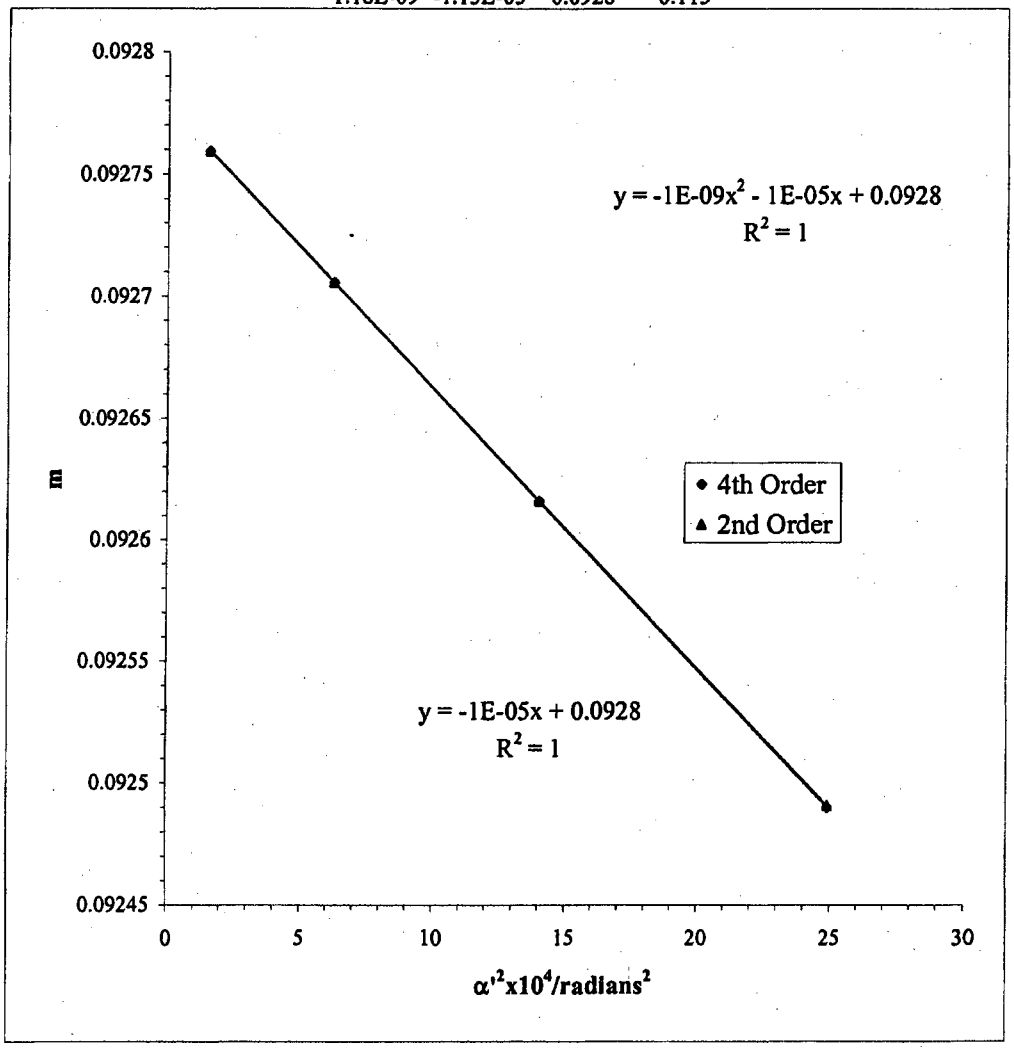

							Beam	Voltage	20 kV
Mesh/inch	I/milamp	Mesh	z/cm	e_1/cm	a/cm	z_{sp}/cm	z_0'/cm	C_s'/cm	$z_{sp}-z_0'$/cm
2000	400	Front	30.35	0.00127	20.96	26.33	0.094	0.213	26.24

Bar location/ units	Shadow Reading X/cm	Spacing Δ/cm	E/cm	$\alpha \times 10^4$	$\alpha' \times 10^2$	$\alpha'^2 \times 10^4$	m	z'/cm	f/cm
2.5	1.485		1.046	1.515	3.987	15.894	0.00380	0.09401	0.1149
1.5	1.904	0.419	0.627	0.909	2.389	5.709	0.00380	0.09423	0.1151
0.5	2.322	0.418	0.209	0.303	0.796	0.634	0.00381	0.09434	0.1151
-0.5	2.740	0.418							
-1.5	3.158	0.418						g/cm	$(\rho/f_0)^2 = (m_0+1)^2\alpha'^2$
-2.5	3.577	0.420						0.0936	16.015
								0.0938	5.753
								0.0939	0.639

	Slope	m_0	μ_s
1.3E-10	-4.08E-07	0.0038	-1.0723

f vs $(\rho/f)^2$

$S_f = slope_f / f_0$

	$slope_f$	fo/cm	S_f
3.9E-09	-1.22E-05	0.115	-1.057

g vs $(\rho/f)^2$

$S_g = slope_g / f_0$

	$slope_g$	go/cm	S_g
-5.14E-11	-2.1E-05	0.094	-1.83

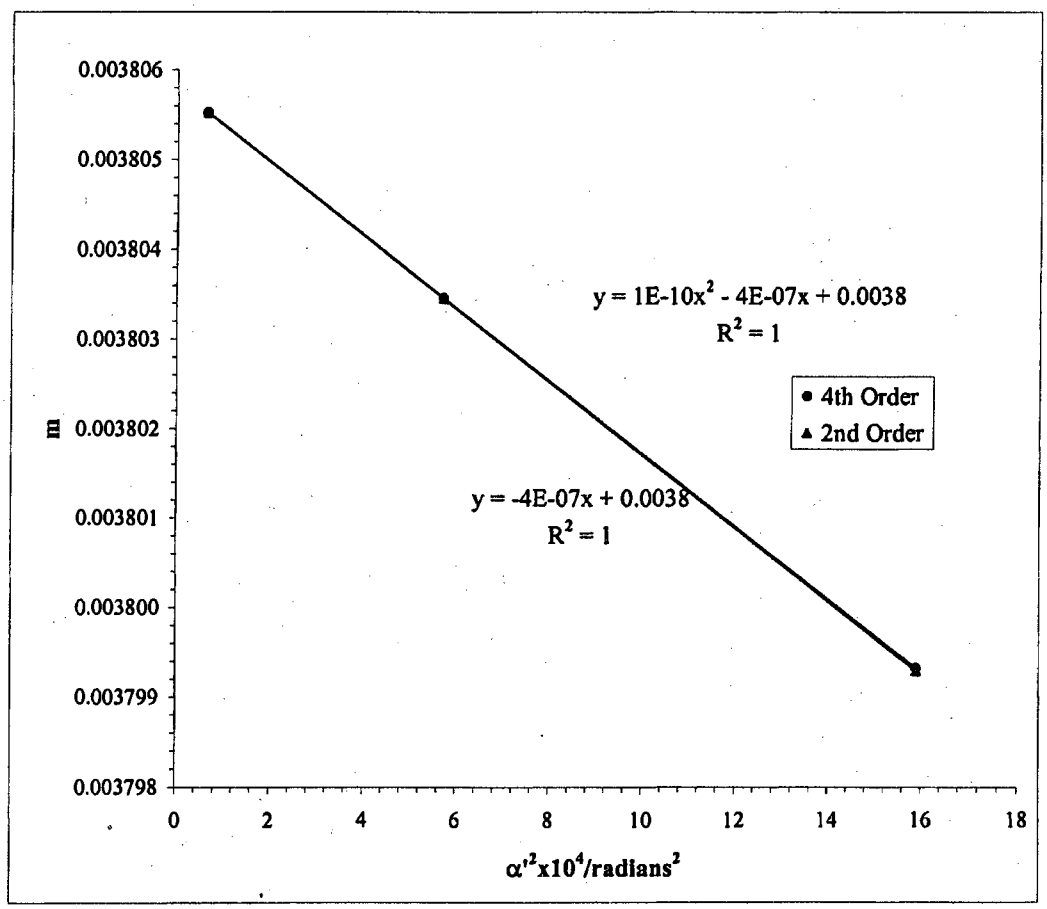

							Beam	Voltage	20 kV
Mesh/inch	I/milamp	Mesh	z/cm	e_1/cm	a/cm	z_{sp}/cm	z_0'/cm	C_s'/cm	$z_{sp}-z_o'$
2000	400	Front	30.3467	0.00127	20.96	26.33	0.094	0.213	26.24

Bar location/ units	Shadow Reading Y/cm	Spacing Δ/cm	E/cm	$\alpha \times 10^4$	$\alpha' \times 10^2$	$\alpha'^2 \times 10^4$	m	z'/cm	$(\rho/f_0)^2 = (m_0+1)^2\alpha'^2$
9	0.223		3.896	5.453	14.847	220.433	0.00367	0.08966	222.093
8	0.673	0.450	3.447	4.847	13.135	172.518	0.00369	0.09068	173.817
7	1.117	0.444	3.003	4.241	11.444	130.974	0.00371	0.09156	131.960
6	1.556	0.439	2.565	3.635	9.773	95.521	0.00372	0.09232	96.240
5	1.991	0.435	2.130	3.029	8.119	65.921	0.00373	0.09295	66.418
4	2.422	0.431	1.700	2.424	6.479	41.974	0.00374	0.09346	42.290
3	2.850	0.428	1.272	1.818	4.849	23.516	0.00375	0.09385	23.693
2	3.275	0.426	0.847	1.212	3.228	10.422	0.00375	0.09413	10.500
1	3.700	0.424	0.423	0.606	1.613	2.601	0.00376	0.09430	2.621
0	4.123	0.423							
-1	4.546	0.423						f/cm	g/cm
-2	4.970	0.424							
-3	5.395	0.425						0.1111	0.0893
-4	5.822	0.427						0.1117	0.0903
-5	6.252	0.430						0.1121	0.0911
-6	6.685	0.434						0.1125	0.0919
-7	7.123	0.438						0.1129	0.0925
-8	7.566	0.443						0.1132	0.0930
-9	8.015	0.449		Slope	m_o	μ_s		0.1134	0.0934
			1.2E-10	-4.12E-07	0.0038	-1.0974		0.1136	0.0937
								0.1137	0.0939

f vs $(\rho/f_o)^2$

$S_f = slope_f / f_0$

	$slope_f$	fo/cm	S_f
3.566E-09	-1E-05	0.114	-1.08

g vs $(\rho/f_o)^2$

$S_g = slope_g / f_0$

	$slope_g$	go/cm	S_g
-3.09E-11	-2.1E-05	0.094	-1.85

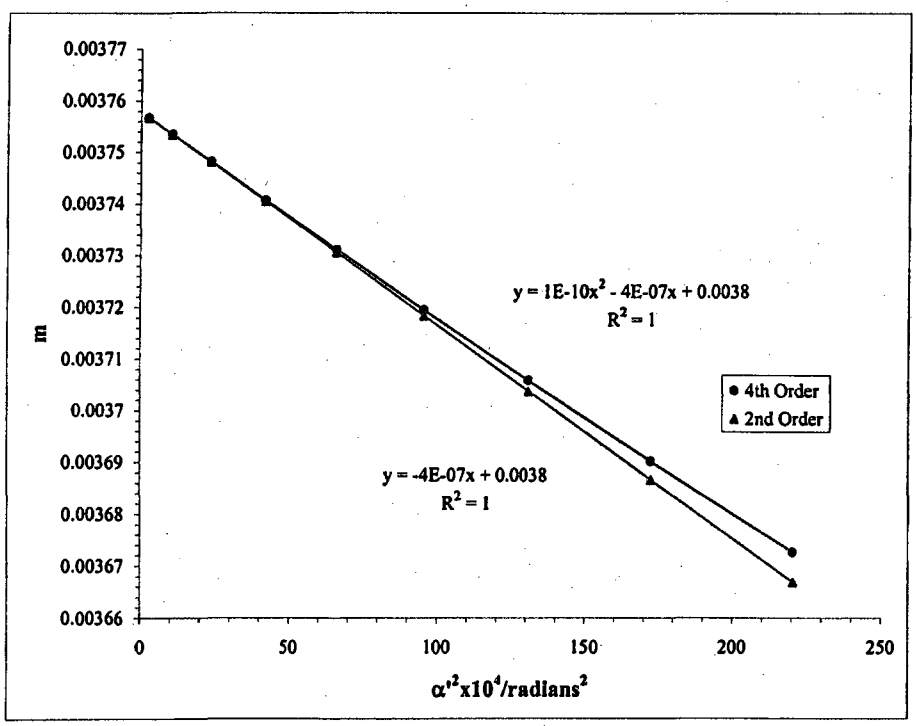

Beam Voltage	I/milamp	z/cm	z_0'/cm	C_s'/cm
20 kV	400	30.3	0.0944	0.213

Average of m_0 = 0.00381

Average of μ_s = -1.07

Paraxial properties :

f_0 = 0.115 cm

g_0 = 0.0939 cm

S_f = -1.06

S_g = -1.83

Magnetic Lens L_2 Data.
Acceleration Voltage 20 kV
Gap size 0.100 inches

Mesh/Inch	I/milliamps	Mesh	e'_1/cm	d/cm	b/cm		Beam	Voltage	20 kV
600	100	Rear	0.004233	26.49	0.442	US			
							0.1 inch gap		

Bar location/ units	Shadow Reading X/cm	Spacing Δ/cm	E'/cm	M'	c/cm	$\alpha' \times 10^2$	$\alpha'^2 \times 10^4$	z'/cm
10	0.468		0.7521	-17.8	-1.4117	2.9988	8.9927	1.854
9	0.554	0.086	0.6657	-17.5	-1.4341	2.6568	7.0584	1.876
8	0.636	0.083	0.5829	-17.2	-1.4547	2.3281	5.4199	1.897
7	0.716	0.080	0.5032	-17.0	-1.4734	2.0112	4.0449	1.915
6	0.793	0.077	0.4262	-16.8	-1.4900	1.7046	2.9058	1.932
5	0.867	0.075	0.3516	-16.6	-1.5044	1.4070	1.9796	1.946
4	0.940	0.073	0.2789	-16.5	-1.5163	1.1167	1.2471	1.958
3	1.011	0.071	0.2078	-16.4	-1.5258	0.8324	0.6928	1.968
2	1.081	0.070	0.1379	-16.3	-1.5326	0.5524	0.3052	1.975
1	1.150	0.069	0.0687	-16.2	-1.5367	0.2755	0.0759	1.979
0	1.219	0.069						
-1	1.287	0.069						
-2	1.357	0.069						
-3	1.427	0.070			Slope	z_o'/cm	C_s'/cm	
-4	1.498	0.071		0.00039	-0.01745	1.980	174.55	
-5	1.571	0.073						
-6	1.645	0.075						
-7	1.722	0.077						
-8	1.802	0.080						
-9	1.885	0.083						
-10	1.972	0.087						

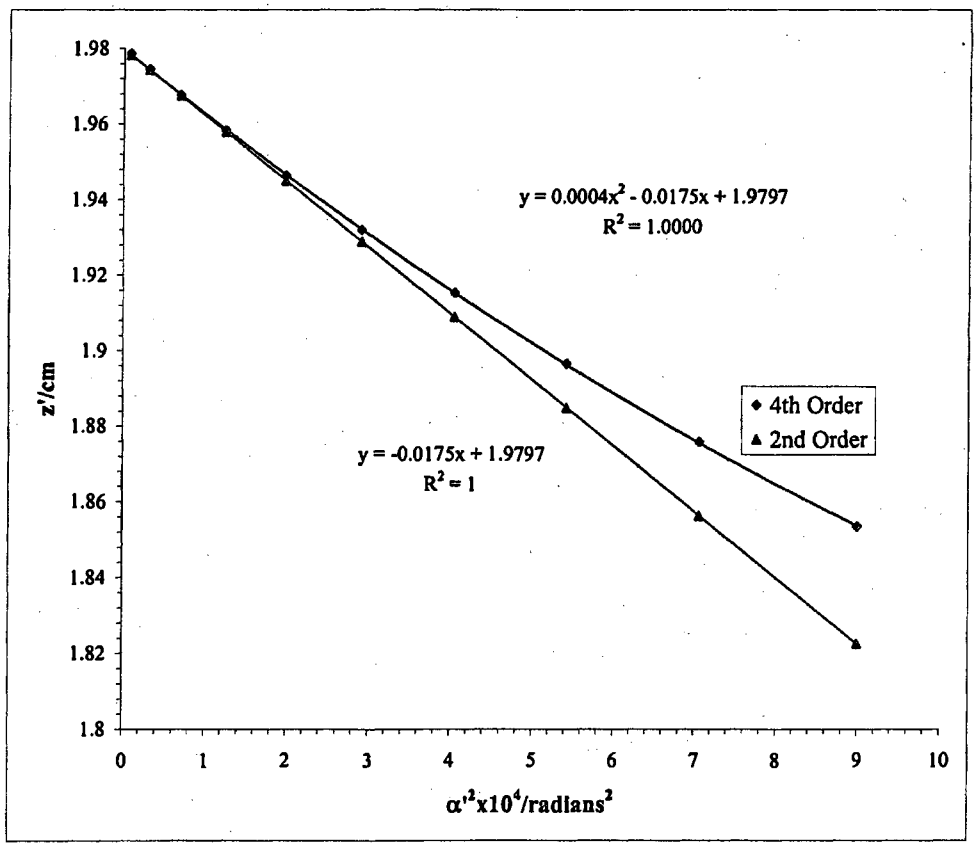

Mesh/inch	I/milliamps	Mesh	e'_1/cm	d/cm	b/cm		Beam	Voltage	20 kV
600	100	Rear	0.0042333	26.49	0.442	US			

Bar #	Reading Y/cm	Spacing Δ/cm	E'/cm	M'	c/cm	α' x 10^2	0.1 inch gap α'^2 x 10^4	z'/cm
10	0.413		0.7554	-17.8	-1.406	3.0113	9.0679	1.848
9	0.500	0.0866	0.6686	-17.5	-1.428	2.6674	7.1153	1.870
8	0.583	0.0830	0.5853	-17.3	-1.449	2.3371	5.4620	1.891
7	0.663	0.0799	0.5052	-17.0	-1.468	2.0187	4.0752	1.910
6	0.740	0.0771	0.4278	-16.8	-1.485	1.7108	2.9270	1.927
5	0.815	0.0748	0.3529	-16.7	-1.499	1.4120	1.9936	1.941
4	0.888	0.0728	0.2799	-16.5	-1.511	1.1206	1.2557	1.953
3	0.959	0.0713	0.2086	-16.4	-1.521	0.8352	0.6975	1.963
2	1.029	0.0701	0.1384	-16.3	-1.527	0.5543	0.3072	1.969
1	1.098	0.0693	0.0690	-16.3	-1.532	0.2764	0.0764	1.974
0	1.167	0.0690						
-1	1.236	0.0690						
-2	1.306	0.0694						
-3	1.376	0.0703						
-4	1.447	0.0715			Slope	z_o'/cm	C_s'/cm	
-5	1.521	0.0731		0.00039	-0.017454	1.975	174.5	
-6	1.596	0.0751						
-7	1.673	0.0775						
-8	1.754	0.0803						
-9	1.837	0.0836						
-10	1.924	0.0872						

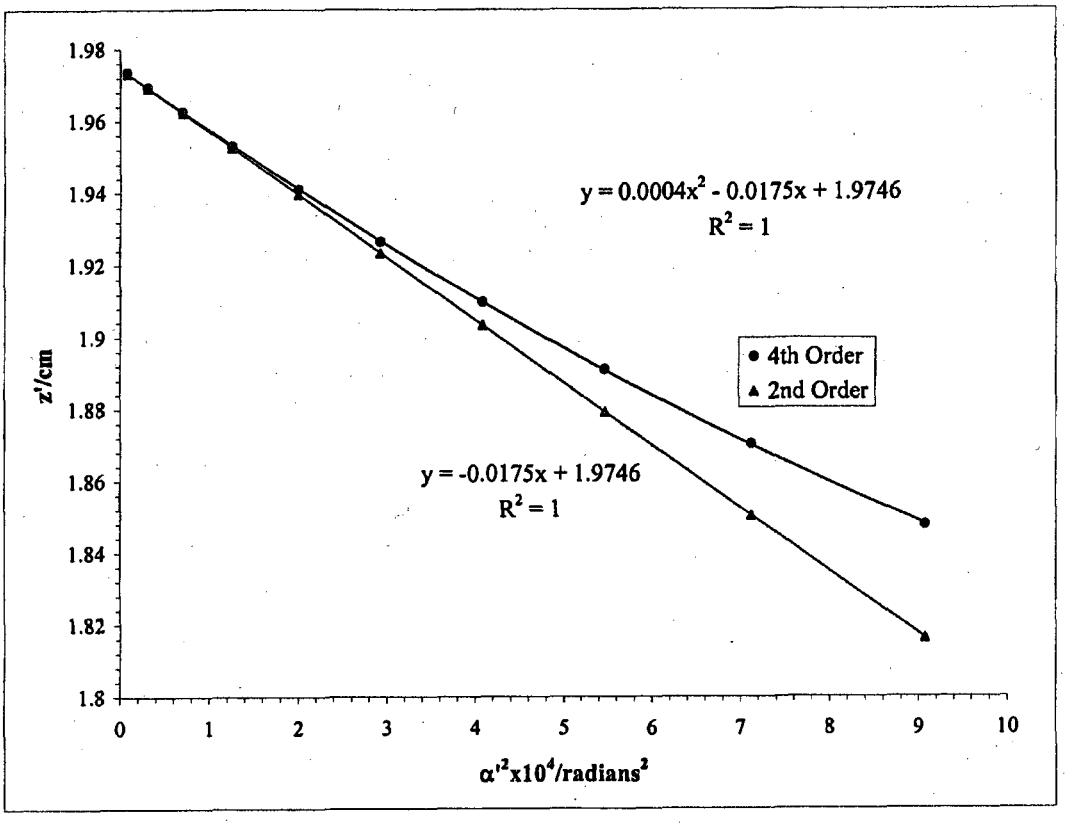

Mesh/inch	I/milliamps	Mesh	e'_1/cm	d/cm	b/cm		Beam	Voltage	20 kV
600	100	Rear	0.00423	24.71	2.22	DS			

0.1 inch gap

Bar location/ units	Shadow Reading X/cm	Spacing Δ/cm	E'/cm	M'	c/cm	α' x 10^2	α'^{2} x 10^4	z'/cm
5	0.3779		0.8653	40.88	0.6197	3.4157	11.6668	1.6003
4	0.4996	0.1216	0.7436	43.91	0.5759	2.9402	8.6445	1.6440
3	0.6399	0.1403	0.6038	47.54	0.5310	2.3918	5.7208	1.6890
2	0.8026	0.1627	0.4413	52.12	0.4835	1.7512	3.0667	1.7365
1	1.0064	0.2039	0.2372	56.02	0.4492	0.9425	0.8883	1.7708
0	1.2434	0.2370						
-1	1.4807	0.2373						
-2	1.6851	0.2043			Slope	z_0'/cm	C_s'/cm	
-3	1.8475	0.1624		0.0002	-0.01795	1.788	179.55	
-4	1.9867	0.1392						
-5	2.1086	0.1219						

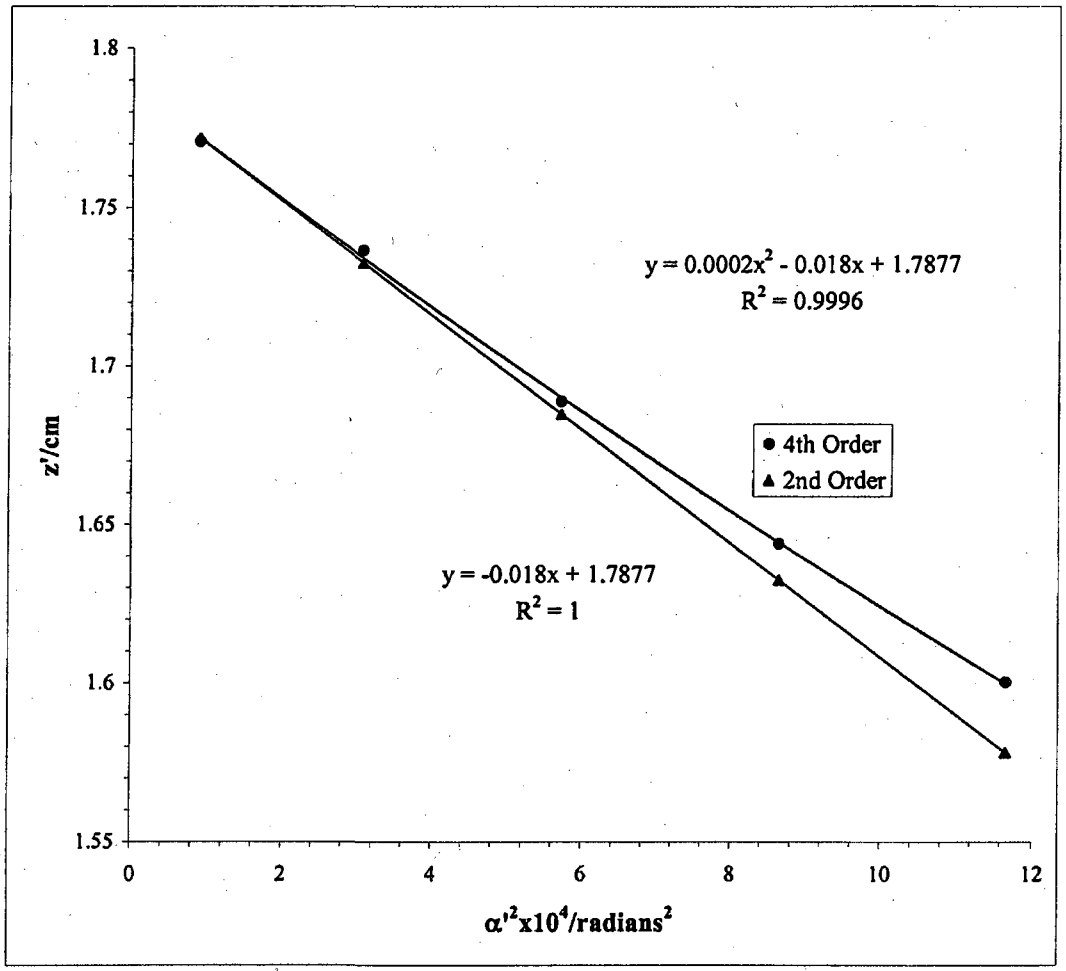

Mesh/inch	I/milliamps	Mesh	e'_1/cm	d/cm	b/cm		Beam	Voltage	20 kV
600	100	Rear	0.00423	24.71	2.220	DS			
							0.1 inch gap		

Bar location/ units	Shadow Reading Y/cm	Spacing Δ/cm	E'/cm	M'	e/cm	$\alpha' \times 10^2$	$\alpha'^2 \times 10^4$	z'/cm
4	0.4997		0.7434	43.90	0.5761	2.9394	8.6401	1.6439
3	0.6390	0.1393	0.6045	47.60	0.5303	2.3947	5.7345	1.6896
2	0.8037	0.1647	0.4399	51.96	0.4850	1.7458	3.0480	1.7350
1	1.0048	0.2011	0.2386	56.37	0.4463	0.9485	0.8996	1.7736
0	1.2433	0.2385						
-1	1.4821	0.2388						
-2	1.6836	0.2015			Slope	z_0'/cm	C_s'/cm	
-3	1.8481	0.1645		0.0002	-0.02	1.790	188.01	
-4	1.9865	0.1384						

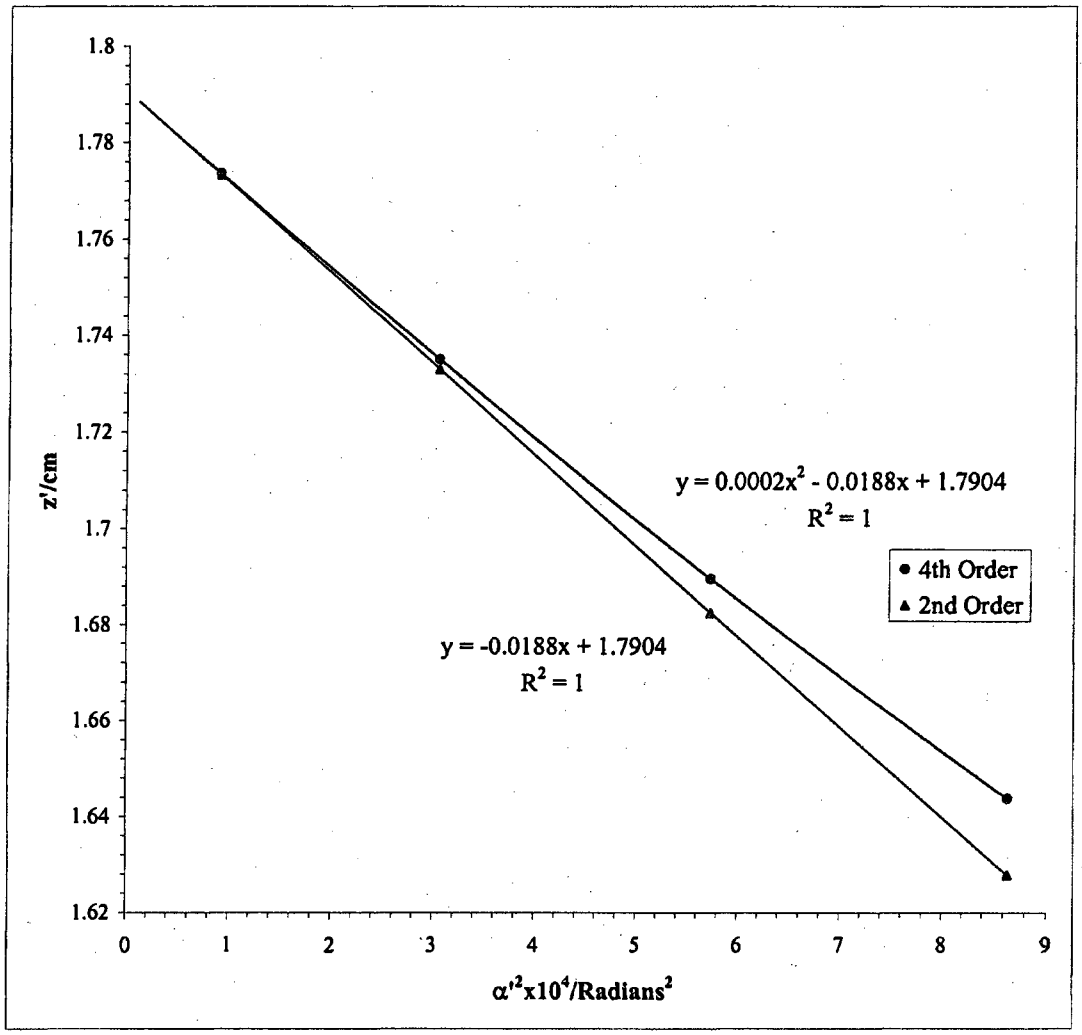

			0.1 inch gap				Beam	Voltage	20 kV
Mesh/inch	I/milliamp	Mesh	z/cm	e_1/cm	a/cm	z_{sp}/cm	z_0'/cm	C_s'/cm	$z_{sp}-z_0'$
600	100	Front	25.03	0.00423	15.63	26.93	1.789	179.16	25.15

Bar location/ units	Shadow Reading X/cm	Spacing Δ/cm	E/cm	$\alpha \times 10^4$	$\alpha' \times 10^2$	$\alpha'^2 \times 10^4$	m	z'/cm	f/cm
8.5	0.525		0.910	23.026	3.587	12.864	0.0642	1.5586	1.5128
7.5	0.659	0.1333	0.780	20.317	3.080	9.489	0.0660	1.6190	1.5505
6.5	0.781	0.1224	0.660	17.608	2.610	6.813	0.0675	1.6670	1.5829
5.5	0.895	0.1139	0.547	14.899	2.168	4.701	0.0687	1.7048	1.6101
4.5	1.002	0.1074	0.441	12.190	1.748	3.056	0.0697	1.7343	1.6320
3.5	1.105	0.1026	0.339	9.481	1.344	1.808	0.0705	1.7566	1.6491
2.5	1.204	0.0992	0.240	6.772	0.953	0.907	0.0711	1.7728	1.6616
1.5	1.301	0.0969	0.143	4.063	0.569	0.323	0.0715	1.7832	1.6697
0.5	1.397	0.0955	0.048	1.354	0.189	0.036	0.0717	1.7884	1.6738
-0.5	1.492	0.0951							
-1.5	1.587	0.0954							
-2.5	1.683	0.0965							
-3.5	1.782	0.0985							
-4.5	1.883	0.1015							
-5.5	1.989	0.1056							
-6.5	2.100	0.1111							
-7.5	2.218	0.1183							
-8.5	2.346	0.1275							

				g/cm	$(\rho/f_0)^2 = (m_0+1)^2\alpha'^2$
				1.461	14.775
				1.517	10.899
				1.560	7.825
				1.594	5.400
				1.620	3.510
				1.640	2.076
				1.655	1.042
	Slope	m_0	μ_s	1.664	0.371
	6.23604E-06	-0.000663	0.07169	-92.48	1.668	0.041

f vs $(\rho/f_0)^2$

$S_f = slope_f / f_0$

	$slope_f$	f_0/cm	S_f
0.0001051	-0.01250407	1.674	-74.68

g vs $(\rho/f_0)^2$

$S_g = slope_g / f_0$

	$slope_g$	g_0/cm	S_g
-2E-05	-0.01375	1.669	-82.11

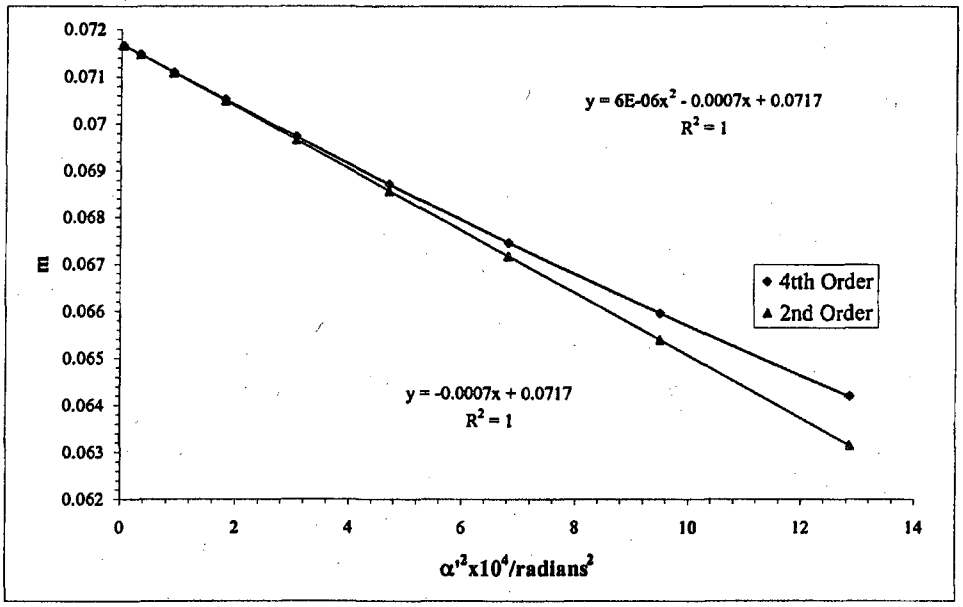

0.1 inch gap							Beam	Voltage	20 kV
Mesh/inch	I/milliamp	Mesh	z/cm	e_1/cm	a/cm	z_{sp}/cm	z_0'/cm	C_s'/cm	$z_{sp}-z_0'$
600	100	Front	25.03	0.00423	15.63	26.93	1.789	179.16	25.15

Bar location/ units	Shadow Reading Y/cm	Spacing Δ/cm	E/cm	$\alpha \times 10^4$	$\alpha' \times 10^2$	$\alpha'^2 \times 10^4$	m	z'/cm	f/cm
9.5	0.286		1.006	25.73	3.957	15.661	0.0650	1.5084	1.5358
8.5	0.411	0.126	0.880	23.03	3.468	12.024	0.0664	1.5736	1.5642
7.5	0.530	0.119	0.760	20.32	3.001	9.008	0.0677	1.6276	1.5912
6.5	0.642	0.113	0.646	17.61	2.556	6.535	0.0689	1.6719	1.6162
5.5	0.750	0.107	0.537	14.90	2.130	4.538	0.0699	1.7077	1.6388
4.5	0.853	0.103	0.434	12.19	1.720	2.960	0.0709	1.7360	1.6585
3.5	0.953	0.100	0.333	9.48	1.324	1.753	0.0716	1.7576	1.6748
2.5	1.049	0.097	0.236	6.77	0.938	0.880	0.0722	1.7733	1.6873
1.5	1.144	0.095	0.141	4.06	0.560	0.313	0.0726	1.7834	1.6958
0.5	1.238	0.094	0.047	1.35	0.186	0.035	0.0728	1.7884	1.7002
-0.5	1.332	0.094							
-1.5	1.426	0.094					g/cm	$(\rho/f_0)^2 = (m_0+1)^2\alpha'^2$	
-2.5	1.521	0.096							
-3.5	1.619	0.098					1.4086	18.024	
-4.5	1.720	0.101					1.4697	13.838	
-5.5	1.825	0.105					1.5199	10.367	
-6.5	1.934	0.109					1.5606	7.521	
-7.5	2.049	0.115					1.5931	5.223	
-8.5	2.170	0.121					1.6185	3.406	
-9.5	2.299	0.128					1.6377	2.017	
							1.6515	1.013	
			Slope	m_0	μ_s		1.6603	0.361	
			1.12E-05	-0.001	0.07277	-91.74	1.6647	0.040	

f vs $(\rho/f_0)^2$

$S_f = slope_f / f_0$

	$slope_f$	fo/cm	S_f
0.000194	-0.0125706	1.700	-73.95

g vs $(\rho/f_0)^2$

$S_g = slope_g / f_0$

	$slope_g$	go/cm	S_g
-3.1E-05	-0.01369	1.665	-80.56

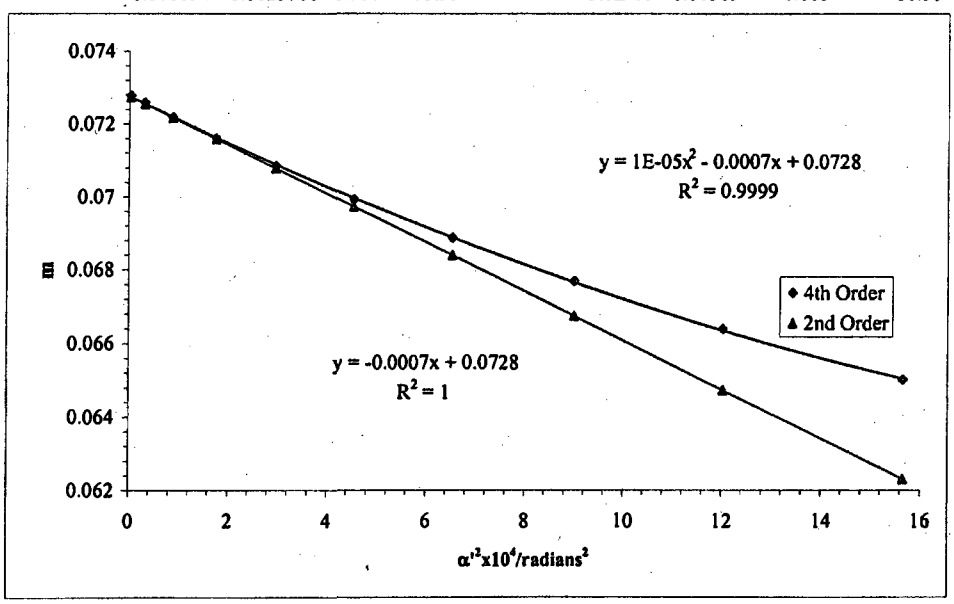

Beam Voltage	I/milliamp	z/cm	z_0'/cm	C_s'/cm	0.1 inch gap
20 kV	100	25.03	1.789	179.16	

Average of m_o = 0.07223

Average of μ_s = -92.11

Paraxial properties :

f_o = 1.687 cm

g_o = 1.667 cm

S_f = -74.31

S_g = -81.34

Mesh/inch	I/milliamps	Mesh	e'_1/cm	d/cm	b/cm		Beam	Voltage	20 kV
600	130	Rear	0.004233	26.49	0.442	US			
							0.1 inch gap		

Bar location/ units	Shadow Reading X/cm	Spacing Δ/cm	E'/cm	M'	c/cm	$\alpha' \times 10^2$	$\alpha'^2 \times 10^4$	z'/cm
5.5	1.128		0.905	-38.9	-0.665	3.5038	12.2766	1.106
4.5	1.311	0.183	0.719	-37.7	-0.684	2.7852	7.7571	1.126
3.5	1.482	0.171	0.546	-36.9	-0.699	2.1186	4.4886	1.141
2.5	1.643	0.161	0.384	-36.3	-0.710	1.4901	2.2203	1.152
1.5	1.799	0.156	0.228	-35.9	-0.719	0.8834	0.7804	1.161
0.5	1.951	0.151	0.075	-35.6	-0.723	0.2926	0.0856	1.165
-0.5	2.101	0.151						
-1.5	2.255	0.153						
-2.5	2.412	0.157						
-3.5	2.575	0.163						
-4.5	2.749	0.174						
-5.5	2.938	0.190						

	Slope	z_0'/cm	C_s'/cm
7.73E-05	-0.00573	1.165	57.32

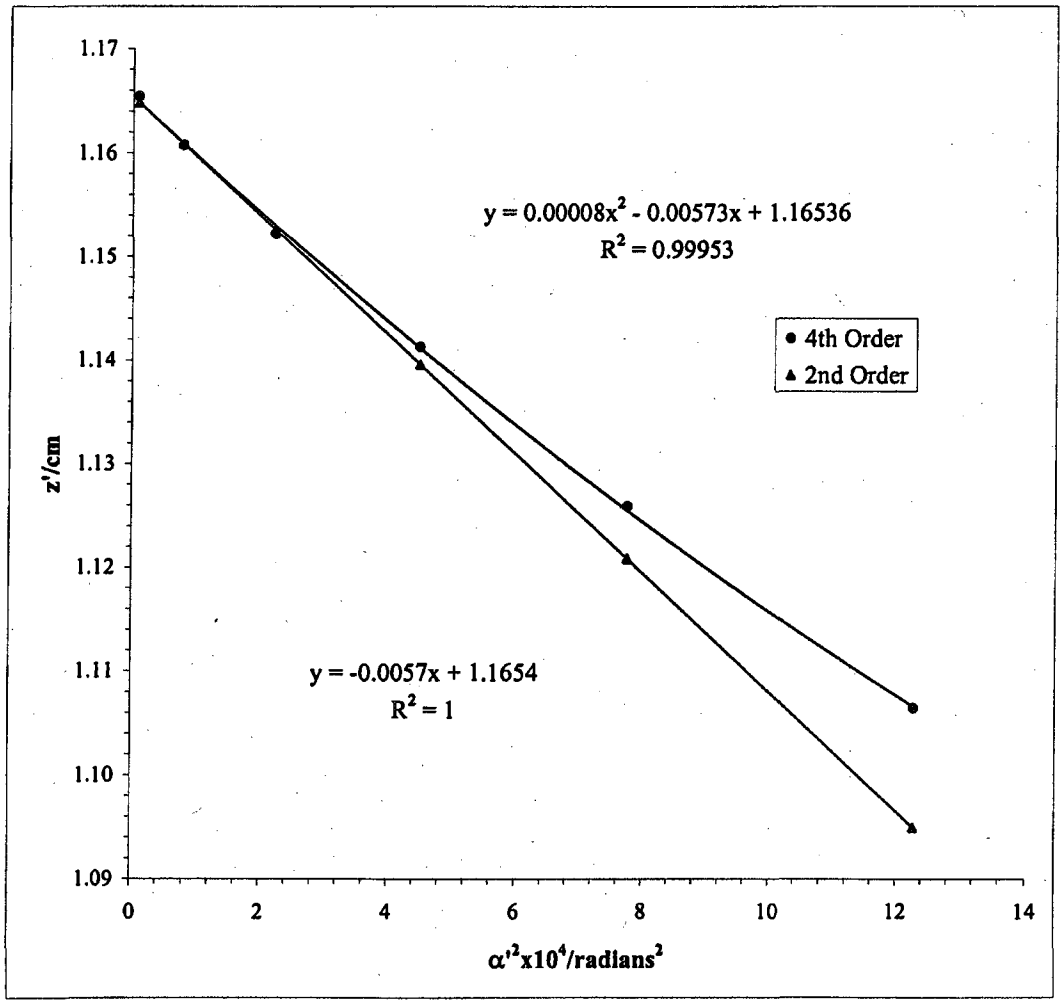

Mesh/inch	I/milliamps	Mesh	e'_1/cm	d/cm	b/cm		Beam	Voltage	20 kV
600	130	Rear	0.00423	26.49	0.442	US			
							0.1 inch gap		

Bar location/ units	Shadow Reading Y/cm	Spacing Δ/cm	E'/cm	M'	c/cm	$\alpha' \times 10^2$	$\alpha'^2 \times 10^4$	z'/cm
7.5	0.284		1.405	-44.3	-0.585	5.4245	29.4251	1.027
6.5	0.594	0.310	1.134	-41.2	-0.627	4.3862	19.2391	1.069
5.5	0.829	0.234	0.917	-39.4	-0.656	3.5508	12.6083	1.098
4.5	1.030	0.202	0.726	-38.1	-0.678	2.8117	7.9055	1.119
3.5	1.212	0.181	0.551	-37.2	-0.693	2.1372	4.5674	1.135
2.5	1.380	0.168	0.387	-36.6	-0.705	1.5007	2.2522	1.147
1.5	1.539	0.159	0.230	-36.2	-0.712	0.8923	0.7963	1.154
0.5	1.694	0.155	0.077	-36.3	-0.710	0.2982	0.0889	1.152
-0.5	1.848	0.154						
-1.5	1.999	0.151						
-2.5	2.154	0.155						
-3.5	2.314	0.161						
-4.5	2.482	0.168						
-5.5	2.663	0.181		Slope	z_o'/cm	C_s'/cm		
-6.5	2.863	0.200	1.8E-05	-0.005	1.158	49.70		
-7.5	3.095	0.232						

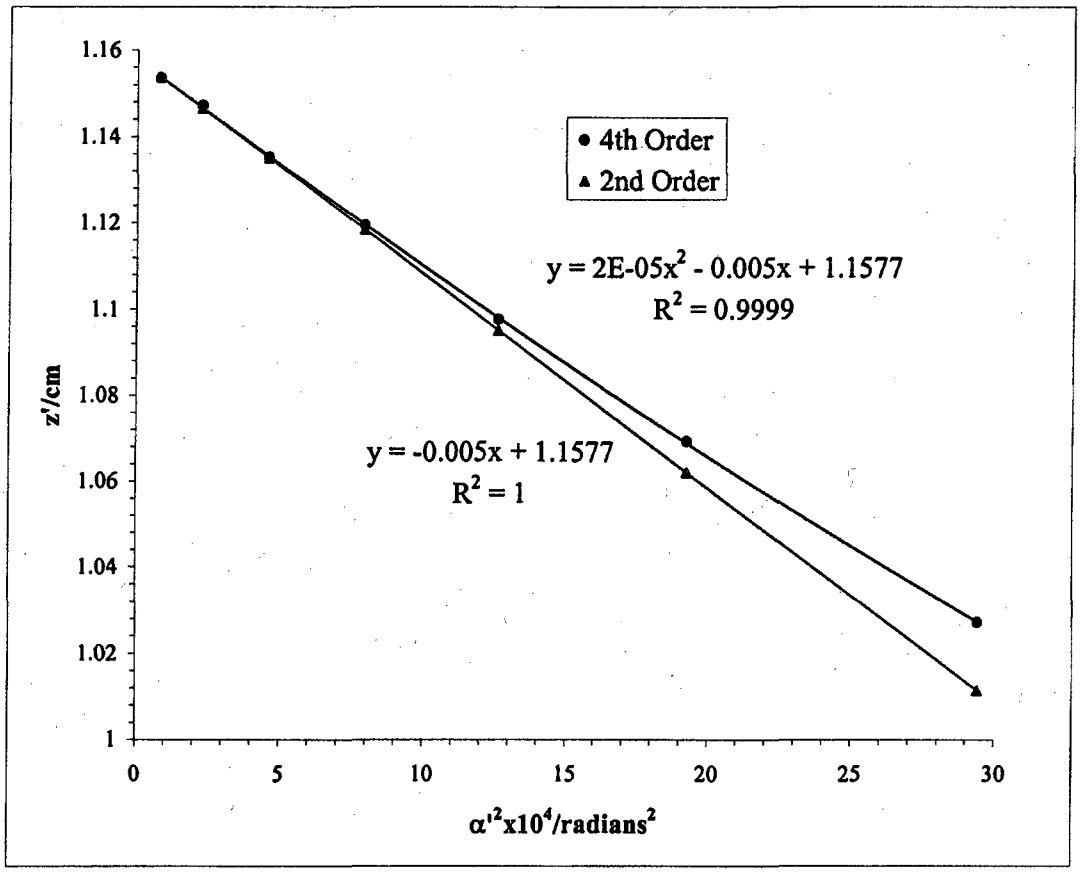

Mesh/inch	I/milliamps	Mesh	e'_1/cm	d/cm	b/cm		Beam	Voltage	20 kV
600	130	Rear	0.00423	25.35	1.585	DS			
							0.1 inch gap		

Bar location/ units	Shadow Reading X/cm	Spacing Δ/cm	E'/cm	M'	c/cm	$\alpha' \times 10^2$	$\alpha'^2 \times 10^4$	z'/cm
4.5	0.930		1.009	52.96	0.488	3.9050	15.2491	1.097
3.5	1.120	0.190	0.822	55.50	0.465	3.1855	10.1473	1.120
2.5	1.331	0.211	0.615	58.11	0.444	2.3845	5.6857	1.141
1.5	1.565	0.234	0.384	60.50	0.426	1.4906	2.2218	1.159
0.5	1.821	0.256	0.131	61.94	0.416	0.5089	0.2589	1.169
-0.5	2.083	0.262						
-1.5	2.333	0.250						
-2.5	2.561	0.227						
-3.5	2.765	0.204						
-4.5	2.948	0.184						

	Slope	z_o'/cm	C_s'/cm
3.5E-05	-0.005349	1.170	53.49

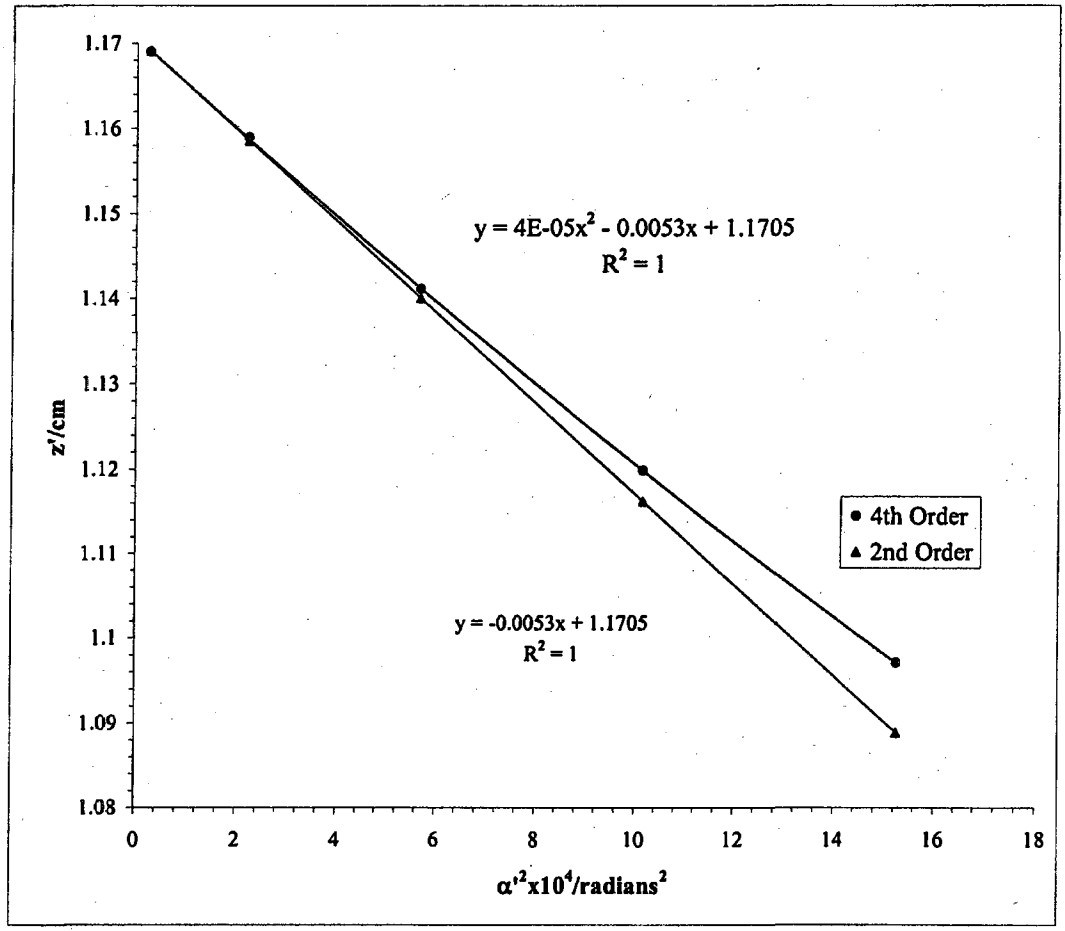

Mesh/inch	I/milliamps	Mesh	e'_1/cm	d/cm	b/cm		Beam	Voltage	20 kV
600	130	Rear	0.00423	25.35	1.585	DS			
							0.1 inch gap		

Bar location/ units	Shadow Reading Y/cm	Spacing Δ/cm	E'/cm	M'	c/cm	$\alpha' \times 10^2$	$\alpha'^2 \times 10^4$	z'/cm
5	0.712		1.084	51.23	0.505	4.1942	17.5912	1.080
4	0.888	0.177	0.907	53.58	0.482	3.5124	12.3367	1.103
3	1.082	0.194	0.712	56.04	0.461	2.7575	7.6038	1.124
2	1.299	0.216	0.495	58.44	0.441	1.9186	3.6812	1.144
1	1.539	0.240	0.255	60.27	0.428	0.9899	0.9798	1.157
0	1.794	0.256						
-1	2.049	0.255						
-2	2.288	0.239						
-3	2.506	0.217						
-4	2.703	0.197		Slope	z_o'/cm	C_t'/cm		
-5	2.880	0.178	3.2E-05	-0.005224	1.162	52.24		

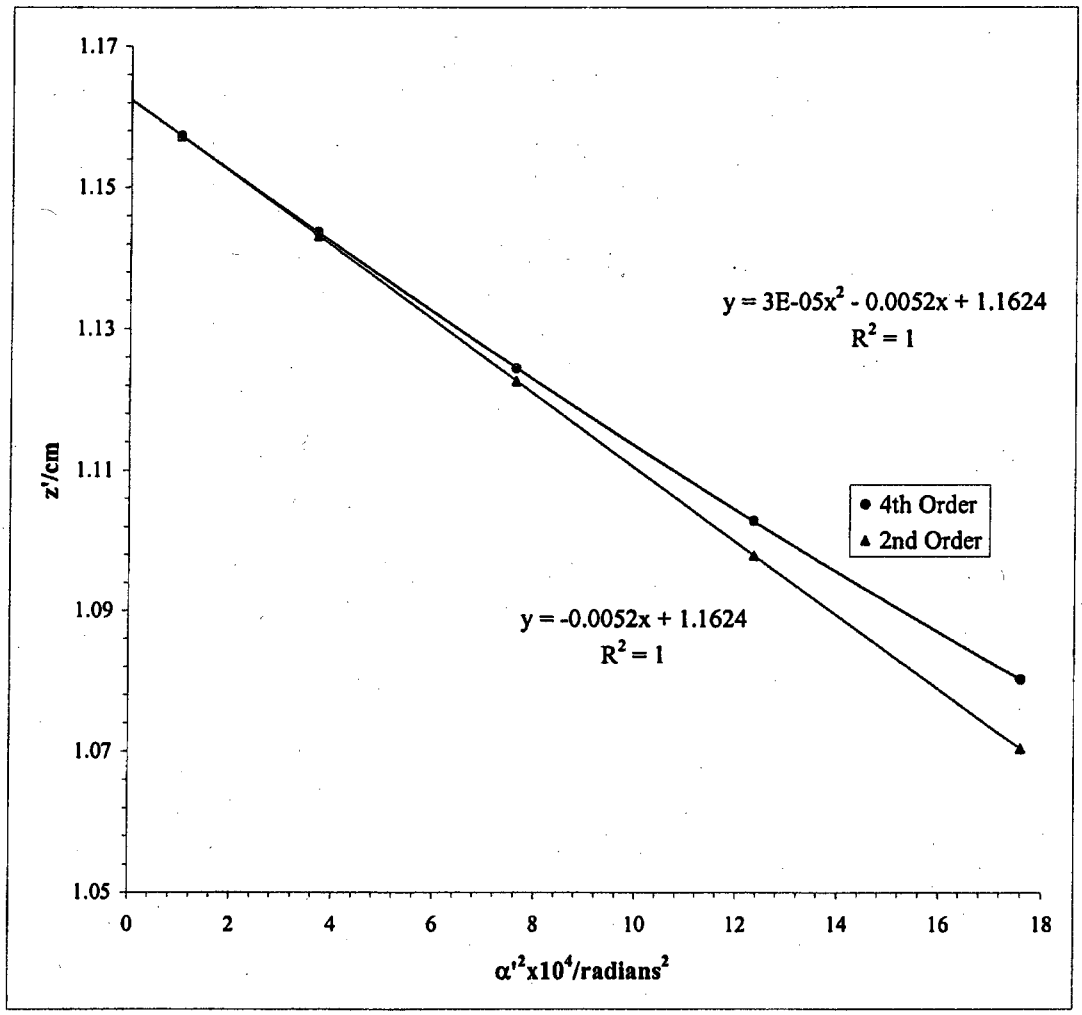

			0.1 inch gap				Beam	Voltage	20 kV
Mesh/inch	I/milliamp	Mesh	z/cm	e_1/cm	a/cm	z_{sp}/cm	z_0'/cm	C_s'/cm	$z_{sp}-z_0'$
600	130	Front	25.03	0.00423	15.63	26.93	1.164	53.19	25.77

Bar location/ units	Shadow Reading X/cm	Spacing Δ/cm	E/cm	$\alpha \times 10^4$	$\alpha' \times 10^2$	$\alpha'^2 \times 10^4$	m	z'/cm	f/cm
6	1.175		0.942	16.254	3.647	13.302	0.04457	1.093	1.069
5	1.345	0.170	0.773	13.545	2.996	8.974	0.04521	1.116	1.083
4	1.508	0.163	0.611	10.836	2.368	5.607	0.04576	1.134	1.096
3	1.665	0.158	0.454	8.127	1.759	3.094	0.04620	1.148	1.106
2	1.819	0.154	0.300	5.418	1.165	1.356	0.04652	1.157	1.113
1	1.970	0.151	0.149	2.709	0.580	0.336	0.04671	1.162	1.117
0	2.120	0.150							
-1	2.269	0.149					g/cm	$(\rho/f_0)^2 = (m_0+1)^2\alpha'^2$	
-2	2.420	0.151							
-3	2.573	0.153					1.046	14.575	
-4	2.729	0.157					1.067	9.833	
-5	2.891	0.162					1.084	6.143	
-6	3.060	0.168					1.096	3.391	
							1.105	1.486	
			Slope	m_0	μ_s		1.110	0.369	
		1.9E-06	-0.0002	0.04677	-40.759				

f vs $(\rho/f_o)^2$

S_f = slope$_f$ / f_0

	slope$_f$	fo/cm	S_f
3.65E-05	-0.00395	1.119	-35.33

g vs $(\rho/f_o)^2$

S_g = slope$_g$ / f_0

	slope$_g$	go/cm	S_g
-3.9E-06	-0.00448	1.112	-40.02

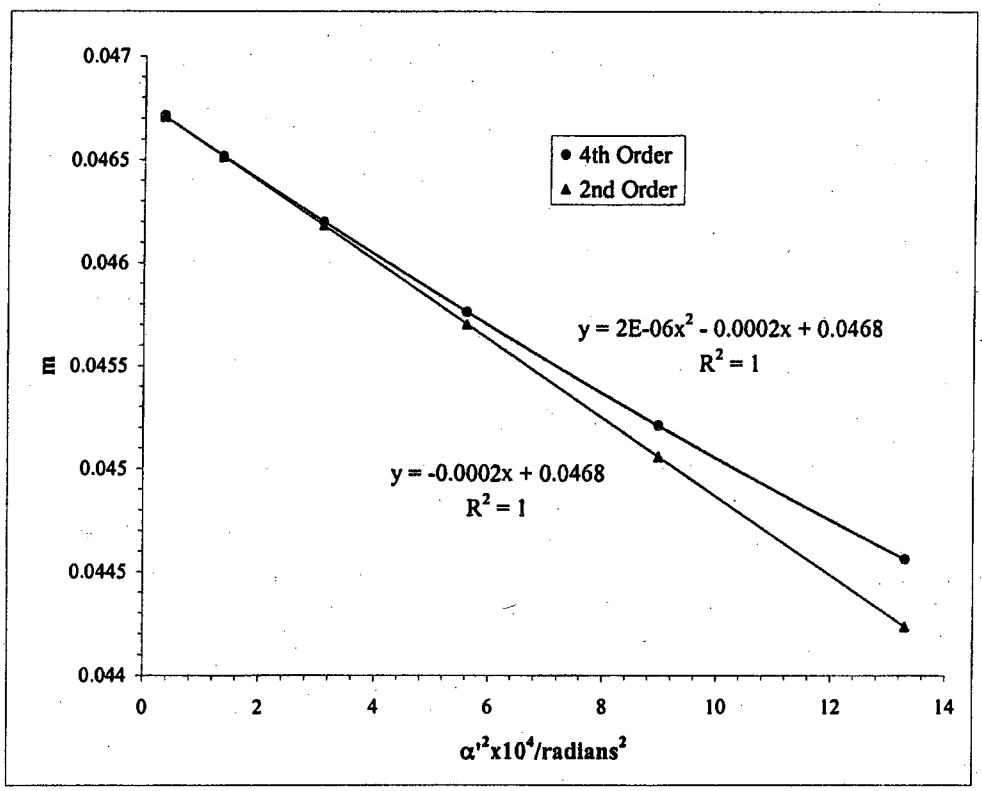

0.1 inch gap							Beam	Voltage	20 kV
Mesh/inch	I/milliamp	Mesh	z/cm	e_1/cm	a/cm	z_{sp}/cm	z_0'/cm	C_s'/cm	$z_{sp}-z_o'$
600	130	Front	25.03	0.00423	15.63	26.93	1.164	53.19	25.77

Bar location/ units	Shadow Reading Y/cm	Spacing Δ/cm	E/cm	α x 10^4	α' x 10^2	α'^{2} x 10^4	m	z'/cm	f/cm
6.5	0.802		1.036	17.608	4.005	16.043	0.04396	1.079	1.055
5.5	0.979	0.177	0.861	14.899	3.333	11.111	0.04470	1.105	1.071
4.5	1.148	0.169	0.694	12.190	2.689	7.230	0.04533	1.126	1.086
3.5	1.310	0.162	0.533	9.481	2.067	4.274	0.04586	1.141	1.098
2.5	1.467	0.157	0.377	6.772	1.464	2.143	0.04626	1.153	1.107
1.5	1.620	0.153	0.225	4.063	0.873	0.762	0.04654	1.160	1.113
0.5	1.771	0.151	0.075	1.354	0.290	0.084	0.04667	1.164	1.116
-0.5	1.920	0.150							
-1.5	2.070	0.150					g/cm	$(\rho/f_0)^2 = (m_0+1)^2\alpha'^2$	
-2.5	2.222	0.152							
-3.5	2.376	0.155					1.032	17.576	
-4.5	2.536	0.159					1.057	12.172	
-5.5	2.701	0.165					1.076	7.921	
-6.5	2.873	0.172					1.091	4.683	
							1.101	2.348	
			Slope	m_o	μ_s		1.108	0.835	
		2.0E-06	-0.0002	0.04669	-43.10		1.111	0.092	

f vs $(\rho/f_o)^2$

S_f = slope$_f$ / f_0

slope$_f$	fo/cm	S_f
3.86E-05	-0.004185	1.116	-37.49

g vs $(\rho/f_o)^2$

S_g = slope$_g$ / f_0

slope$_g$	go/cm	S_g
-4.06E-06	-0.004457	1.112	-39.92

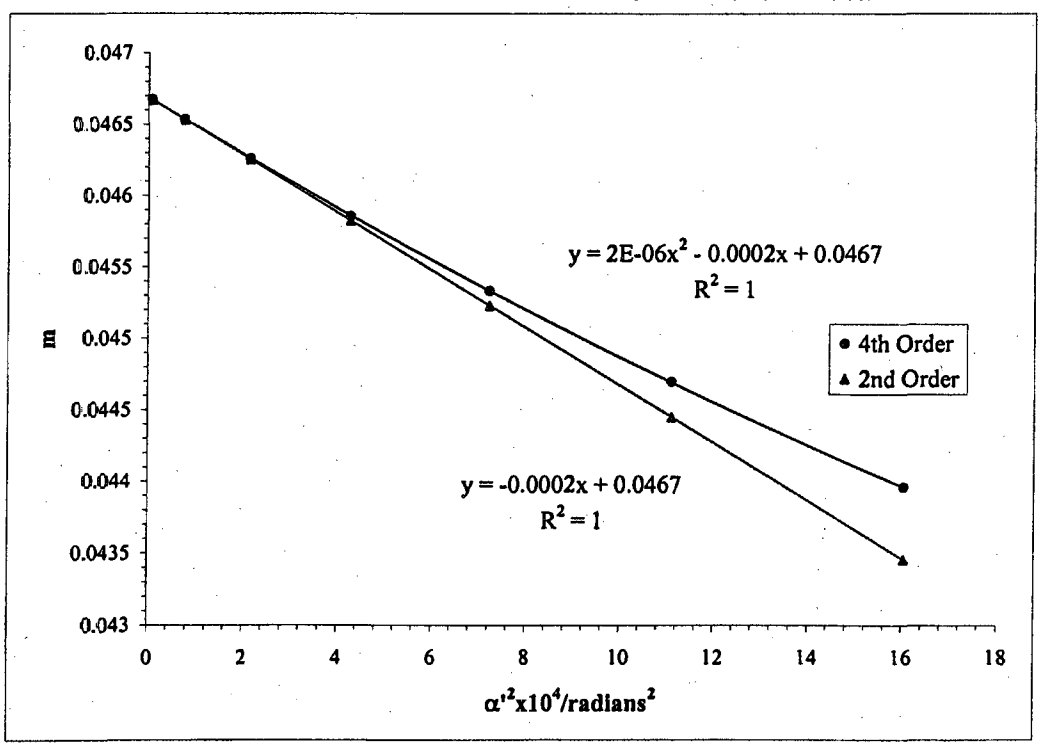

Beam Voltage	I/milamp	z/cm	z_0'/cm	C_s'/cm
20 kV	130	25.03	1.164	53.19

Average of m_o = 0.04673

Average of μ_s = -41.93

Paraxial properties :

f_o = 1.117 cm

g_o = 1.112 cm

S_f = -36.41

S_g = -39.97

Mesh/inch	I/milliamps	Mesh	e'_1/cm	d/cm	b/cm		Beam	Voltage	20 kV
600	150	Rear	0.00423	26.49	0.442	US			

0.1 inch gap

Bar location/ units	Shadow Reading X/cm	Spacing Δ/cm	E'/cm	M'	c/cm	$\alpha' \times 10^2$	$\alpha'^2 \times 10^4$	z'/cm
3.5	0.982		0.9273	-62.6	-0.417	3.5562	12.6463	0.859
2.5	1.268	0.286	0.6419	-60.7	-0.430	2.4629	6.0657	0.872
1.5	1.534	0.266	0.3769	-59.4	-0.439	1.4468	2.0933	0.881
0.5	1.787	0.253	0.1243	-58.7	-0.444	0.4771	0.2276	0.886
-0.5	2.035	0.249						
-1.5	2.288	0.252						
-2.5	2.552	0.264						
-3.5	2.837	0.285						

	Slope	z_0'/cm	C_s'/cm
3.2E-05	-0.002586	0.886	25.86

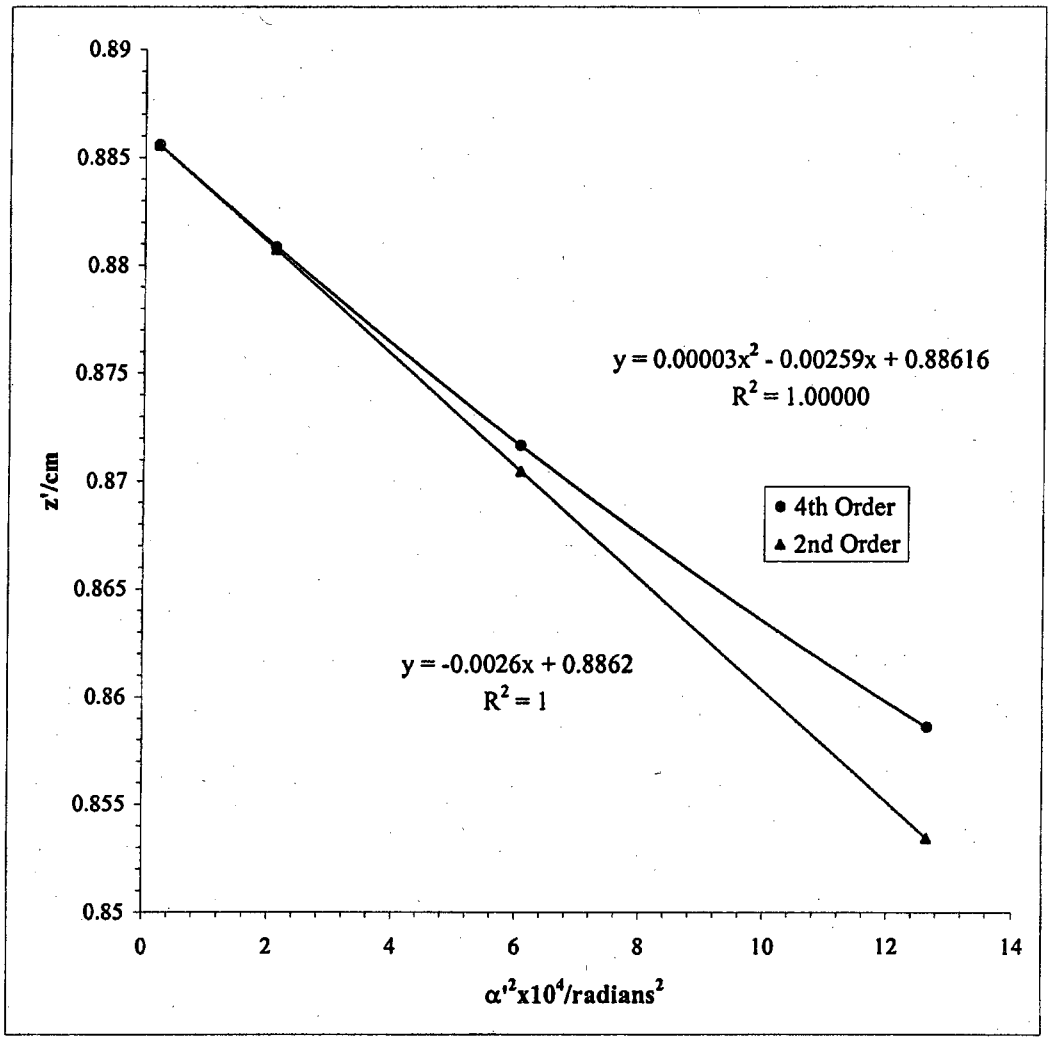

Mesh/inch	I/milliamps	Mesh	e'_1/cm	d/cm	b/cm		Beam	Voltage	20 kV
600	150	Rear	0.00423	25.73	1.20	DS			
							0.1 inch gap		

Bar location/ units	Shadow Reading X/cm	Spacing Δ/cm	E'/cm	M'	c/cm	α' x 10^2	α'^{2} x 10^4	z'/cm
3.5	1.141		1.036	69.92	0.3733	3.9687	15.7509	0.831
2.5	1.407	0.265	0.768	72.58	0.3595	2.9443	8.6686	0.845
1.5	1.697	0.290	0.475	74.79	0.3487	1.8211	3.3165	0.855
0.5	2.008	0.311	0.162	76.38	0.3413	0.6201	0.3846	0.863
-0.5	2.331	0.323						
-1.5	2.646	0.315						
-2.5	2.943	0.296						
-3.5	3.213	0.270						

	Slope	z_0'/cm	C_s'/cm
1.83017E-05	-0.00236	0.863	23.60

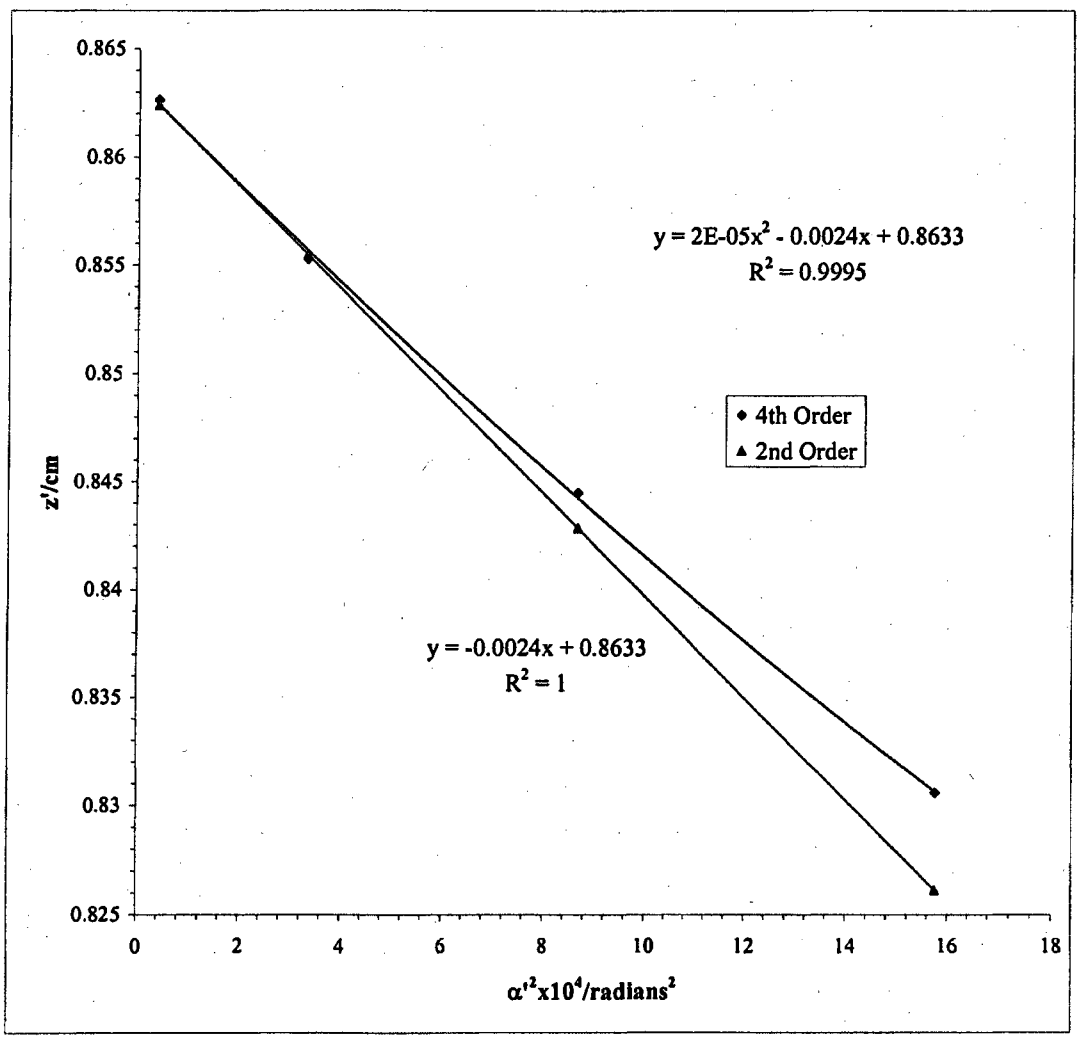

Mesh/Inch	I/milliamps	Mesh	e'_1/cm	d/cm	b/cm		Beam	Voltage	20 kV
600	150	Rear	0.00423	25.73	1.204	DS	0.1 inch gap		

Bar location/ units	Shadow Reading Y/cm	Spacing Δ/cm	E'/cm	M'	c/cm	$\alpha'^2 \times 10^2$	$\alpha'^2 \times 10^4$	z'/cm
8.5	0.268		2.061	57.27	0.4572	7.8699	61.9357	0.7467
7.5	0.444	0.176	1.882	59.29	0.4414	7.1927	51.7349	0.7625
6.5	0.633	0.189	1.692	61.47	0.4255	6.4672	41.8244	0.7785
5.5	0.835	0.202	1.486	63.83	0.4095	5.6858	32.3289	0.7945
4.5	1.055	0.220	1.263	66.31	0.3940	4.8356	23.3832	0.8100
3.5	1.295	0.240	1.021	68.88	0.3791	3.9089	15.2792	0.8249
2.5	1.557	0.262	0.756	71.43	0.3653	2.8969	8.3919	0.8386
1.5	1.844	0.287	0.466	73.41	0.3553	1.7870	3.1935	0.8486
0.5	2.149	0.306	0.158	74.64	0.3494	0.6058	0.3670	0.8545
-0.5	2.465	0.316						
-1.5	2.776	0.311						
-2.5	3.069	0.293			Slope	z_o'/cm	C_s'/cm	
-3.5	3.336	0.267		4.5E-06	-0.002025	0.855	20.25	
-4.5	3.581	0.246						
-5.5	3.808	0.226						
-6.5	4.016	0.209						
-7.5	4.209	0.192						
-8.5	4.390	0.181						

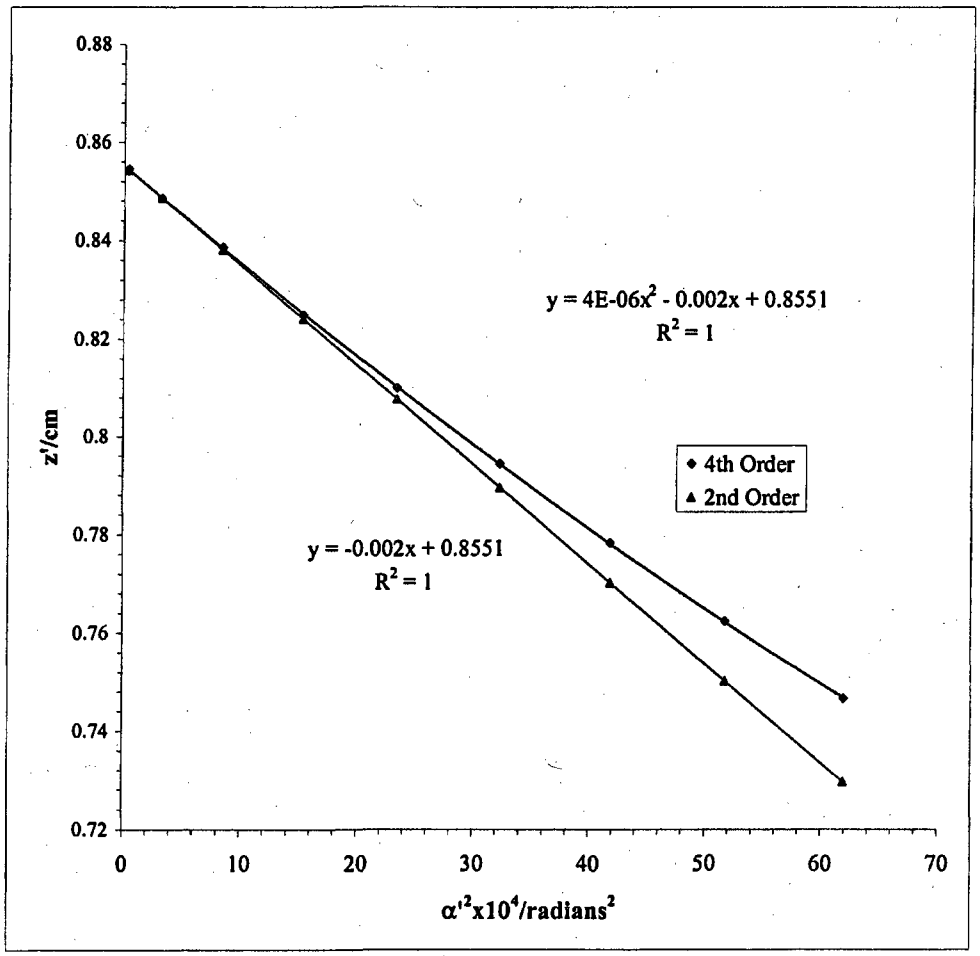

			0.1 inch gap				Beam	Voltage	20 kV
Mesh/inch	I/milliamp	Mesh	z/cm	e_t/cm	a/cm	z_{ap}/cm	z_o'/cm	C_s'/cm	$z_{ap}-z_o'$
600	150	Front	25.03	0.004233	15.63	26.93	0.868	23.24	26.07

Bar location/ units	Shadow Reading X/cm	Spacing Δ/cm	E/cm	$\alpha \times 10^4$	$\alpha' \times 10^2$	$\alpha'^2 \times 10^4$	m	z'/cm	f/cm
9	0.466		1.943	24.380	7.419	55.041	0.0329	0.740	0.799
8	0.721	0.2549	1.693	21.671	6.469	41.848	0.0335	0.771	0.813
7	0.963	0.2421	1.454	18.962	5.563	30.944	0.0341	0.796	0.827
6	1.194	0.2308	1.226	16.254	4.695	22.045	0.0346	0.817	0.839
5	1.415	0.2211	1.008	13.545	3.861	14.907	0.0351	0.834	0.850
4	1.628	0.2129	0.797	10.836	3.055	9.332	0.0355	0.847	0.859
3	1.834	0.2063	0.592	8.127	2.271	5.159	0.0358	0.856	0.866
2	2.035	0.2012	0.392	5.418	1.505	2.264	0.0360	0.863	0.871
1	2.233	0.1976	0.195	2.709	0.750	0.562	0.0361	0.867	0.874
0	2.429	0.1956							
-1	2.624	0.1951					g/cm	$(\rho/f_0)^2 = (m_0+1)^2\alpha'^2$	
-2	2.820	0.1962							
-3	3.019	0.1988					0.714	59.096	
-4	3.222	0.2030					0.744	44.930	
-5	3.430	0.2087					0.768	33.223	
-6	3.646	0.2159					0.788	23.668	
-7	3.871	0.2247					0.804	16.005	
-8	4.106	0.2350					0.816	10.020	
-9	4.353	0.2468					0.825	5.539	
			Slope	m_o	μ_s		0.832	2.431	
		3.2E-07	-0.0001	0.03617418	-21.40		0.835	0.603	

f vs $(\rho/f_o)^2$

S_f = slope$_f$/ f_0

	slope$_f$	fo/cm	S_f
6.548E-06	-0.0016713	0.875	-19.10

g vs $(\rho/f_o)^2$

S_g = slope$_g$/ f_0

	slope$_g$	go/cm	S_g
-5.27E-07	-0.002042	0.837	-23.34

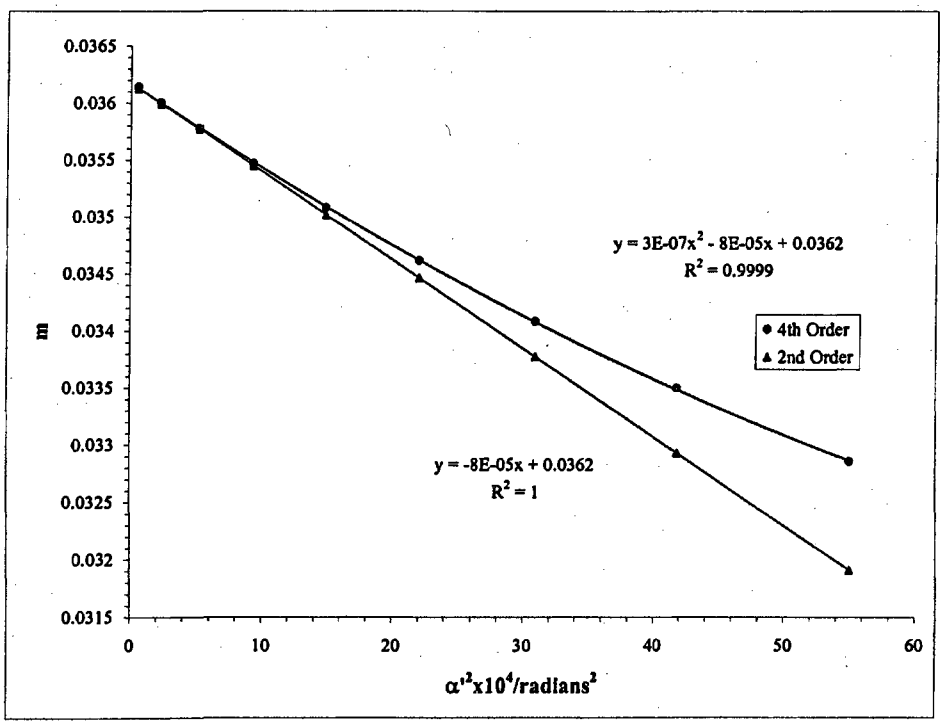

0.1 inch gap | Beam Voltage 20 kV

Mesh/inch	I/milliamp	Mesh	z/cm	e_1/cm	a/cm	z_{ap}/cm	z_0'/cm	C_s'/cm	$z_{ap}-z_0'$
600	150	Front	25.03	0.00423	15.63	26.93	0.8682	23.24	26.07

Bar location/ units	Shadow Reading Y/cm	Spacing Δ/cm	E/cm	$\alpha \times 10^4$	$\alpha' \times 10^2$	$\alpha'^2 \times 10^4$	m	z'/cm	f/cm
8.5	0.519		1.839	23.026	7.023	49.321	0.03279	0.754	0.797
7.5	0.770	0.251	1.589	20.317	6.075	36.901	0.03345	0.782	0.812
6.5	1.008	0.238	1.351	17.608	5.172	26.744	0.03405	0.806	0.826
5.5	1.236	0.227	1.125	14.899	4.308	18.559	0.03458	0.825	0.838
4.5	1.454	0.218	0.908	12.190	3.478	12.098	0.03505	0.840	0.849
3.5	1.664	0.210	0.698	9.481	2.676	7.163	0.03543	0.852	0.857
2.5	1.868	0.204	0.494	6.772	1.896	3.595	0.03572	0.860	0.864
1.5	2.068	0.200	0.295	4.063	1.131	1.280	0.03591	0.865	0.869
0.5	2.265	0.197	0.098	1.354	0.376	0.141	0.03601	0.868	0.871
-0.5	2.461	0.196							
-1.5	2.657	0.197					g/cm	$(\rho/f_0)^2 = (m_0+1)^2\alpha'^2$	
-2.5	2.857	0.199							
-3.5	3.060	0.203					0.727	52.938	
-4.5	3.269	0.209					0.755	39.606	
-5.5	3.485	0.216					0.778	28.706	
-6.5	3.711	0.226					0.796	19.920	
-7.5	3.947	0.236					0.810	12.986	
-8.5	4.196	0.249					0.821	7.688	
			Slope	m_0	μ_s		0.829	3.859	
		3.8E-07	-0.0001	0.03601615	-23.29		0.834	1.374	
							0.837	0.152	

f vs $(\rho/f_0)^2$

$S_f = slope_f / f_0$

	$slope_f$	f_0/cm	S_f
7.81258E-06	-0.001818	0.871	-20.87

g vs $(\rho/f_0)^2$

$S_g = slope_g / f_0$

	$slope_g$	g_0/cm	S_g
-6.3E-07	-0.00203	0.837	-23.34

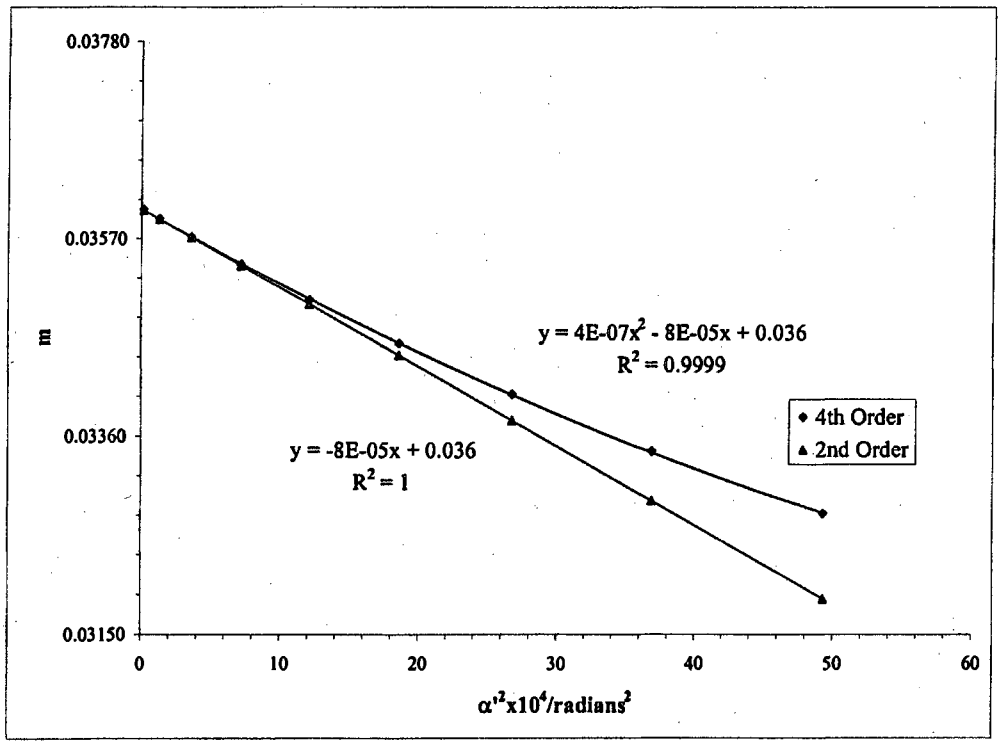

Beam Voltage	I/milamp	z/cm	z_0'/cm	C_s'/cm
20 kV	150	25.03	0.868	23.24

Average of m_o = 0.036095

Average of μ_s = -22.35

Paraxial properties :

f_o = 0.873 cm

g_o = 0.837 cm

S_f = -19.98

S_g = -23.34

Mesh/inch	I/milliamps	Mesh	e'_1/cm	d/cm	b/cm		Beam	Voltage	20 kV
600	180	Rear	0.00423	26.24	0.696	DS			
							0.1 inch gap		
Bar location/ units	Shadow Reading X/cm	Spacing Δ/cm	E'/cm	M'	c/cm	$\alpha' \times 10^2$	$\alpha'^2 \times 10^4$	z'/cm	
4	0.0486		2.4313	143.58	0.1840	9.2017	84.6711	0.5119	
3	0.4776	0.4290	1.9878	156.52	0.1687	7.5277	56.6657	0.5272	
2	0.9883	0.5107	1.4570	172.09	0.1534	5.5209	30.4799	0.5426	
1	1.6193	0.6310	0.7983	188.58	0.1399	3.0265	9.1596	0.5561	
0	2.4045	0.7853							
-1	3.2159	0.8114							
-2	3.9024	0.6865		0.00	-0.0007	0.5621	6.6202		
-3	4.4533	0.5509			Slope	z_0'/cm	C_s'/cm		
-4	4.9112	0.4580		8.2913E-07	-0.000662	0.562	6.620		

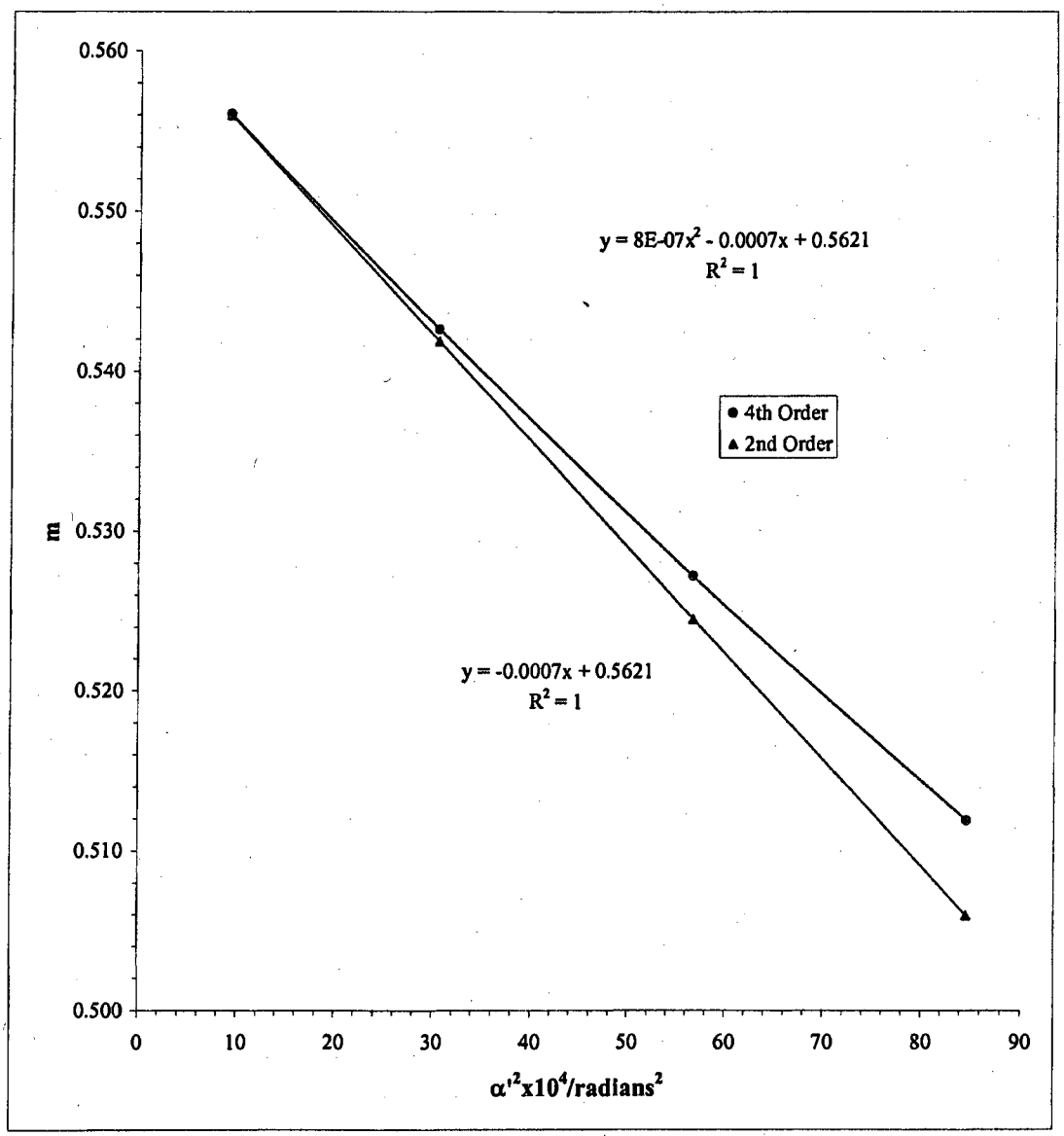

Mesh/inch	I/milliamps	Mesh	e'_1/cm	d/cm	b/cm		Beam	Voltage	20 kV
600	180	Rear	0.004233	26.24	0.696	DS			
							0.1 inch gap		

Bar location/ units	Shadow Reading Y/cm	Spacing Δ/cm	E'/cm	M'	c/cm	α' x 10^2	α'^2 x 10^4	z'/cm
3	0.851		1.990	156.69	0.169	7.5358	56.7881	0.527
2	1.361	0.510	1.459	172.28	0.153	5.5268	30.5459	0.543
1	1.989	0.628	0.799	188.83	0.140	3.0304	9.1835	0.556
0	2.775	0.786						
-1	3.588	0.813						
-2	4.278	0.690			Slope	z_o'/cm	C_s'/cm	
-3	4.831	0.553		9.96E-07	-0.00067	0.562	6.714	

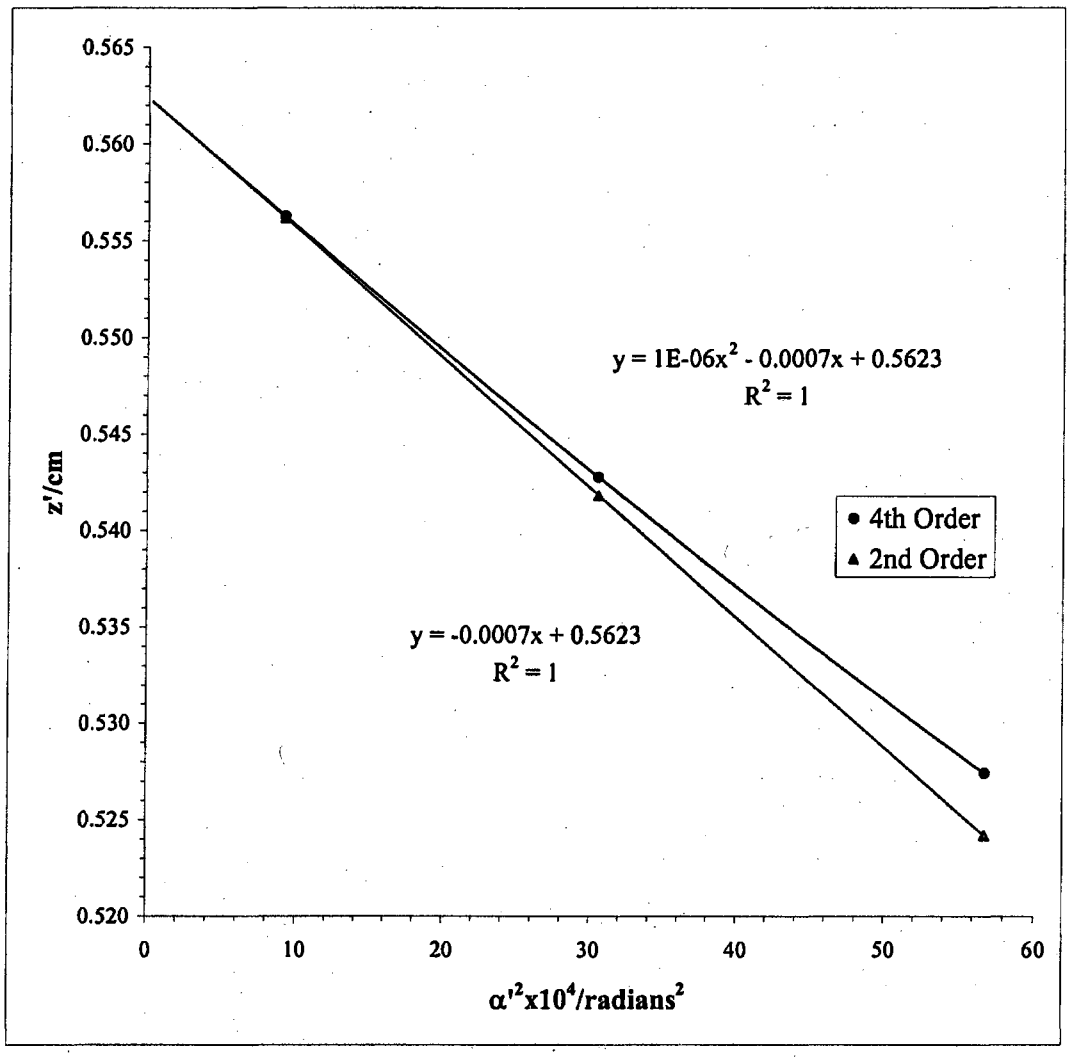

			0.1 inch gap				Beam	Voltage	20 kV
Mesh/inch	I/milliamp	Mesh	z/cm	e_1/cm	a/cm	z_{xp}/cm	z_0'/cm	C_1'/cm	$z_{xp}-z_0'$
600	180	Front	25.03	0.00423	15.63	26.93	0.562	6.667	26.37

Bar location/ units	Shadow Reading Y/cm	Spacing Δ/cm	E/cm	$\alpha \times 10^4$	$\alpha' \times 10^2$	$\alpha'^2 \times 10^4$	m	z'/cm	f/cm
7	1.030		2.084	18.962	7.889	62.244	0.02404	0.521	0.589
6	1.353	0.323	1.760	16.254	6.665	44.418	0.02439	0.533	0.598
5	1.663	0.311	1.448	13.545	5.485	30.083	0.02469	0.542	0.605
4	1.964	0.301	1.146	10.836	4.343	18.858	0.02495	0.550	0.611
3	2.257	0.293	0.852	8.127	3.230	10.436	0.02516	0.555	0.616
2	2.544	0.287	0.565	5.418	2.141	4.584	0.02531	0.559	0.620
1	2.827	0.283	0.281	2.709	1.067	1.138	0.02539	0.561	0.622
0	3.108	0.281							
-1	3.390	0.281					g/cm	$(\rho/f_0)^2 = (m_0+1)^2\alpha'^2$	
-2	3.673	0.284							
-3	3.961	0.288					0.507	65.45	
-4	4.256	0.294					0.518	46.71	
-5	4.559	0.303					0.527	31.63	
-6	4.872	0.313					0.534	19.83	
-7	5.197	0.326					0.540	10.97	
							0.543	4.82	
			Slope	m_0	μ_0		0.546	1.20	
		6.0E-08	-0.00003	0.025423	-10.24				

f vs $(\rho/f_0)^2$

$S_f = slope_f / f_0$

$slope_f$	f_0/cm	S_f
1.319E-06	-0.000591	0.622	-9.49

g vs $(\rho/f_0)^2$

$S_g = slope_g / f_0$

$slope_g$	g_0/cm	S_g
-7.613E-08	-0.0006	0.546	-9.70

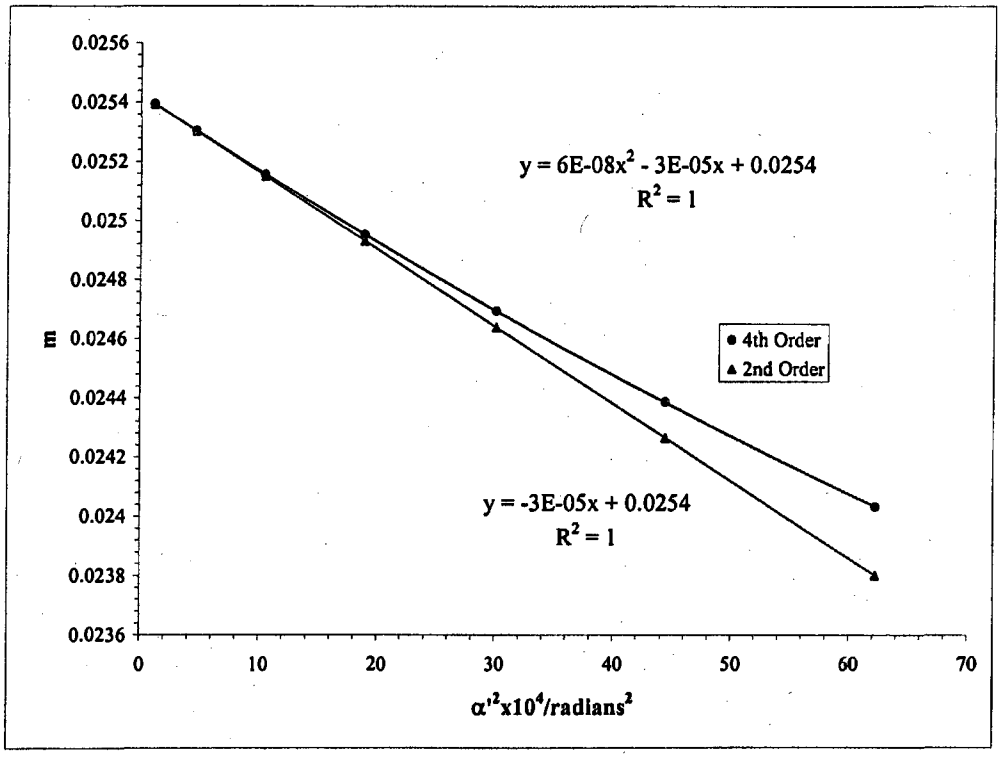

Beam Voltage	I/milamp	z/cm	z_0'/cm	C_s'/cm
20 kV	180	25.03	0.562	6.67

Average of m_o = 0.025676

Average of μ_s = -10.24

Paraxial properties :

f_o = 0.625 cm

g_o = 0.546 cm

S_f = -9.49

S_g = -9.70

Mesh/inch	I/milliamps	Mesh	e'_1/cm	d/cm	b/cm		Beam	Voltage	20 kV
600	200	Rear	0.00423	26.24	0.696	DS			
						0.1 inch gap			

Bar location/ units	Shadow Reading X/cm	Spacing Δ/cm	E'/cm	M'	c/cm	α' x 10^2	α'^2 x 10^4	z'/cm
4	0.986		1.894	111.84	0.237	7.153	51.168	0.459
3	1.410	0.424	1.472	115.89	0.228	5.561	30.922	0.468
2	1.871	0.461	1.013	119.59	0.221	3.827	14.644	0.475
1	2.368	0.497	0.518	122.31	0.216	1.957	3.831	0.480
0	2.886	0.518						
-1	3.403	0.518						
-2	3.896	0.493						
-3	4.353	0.458			Slope	z_o'/cm	C_s'/cm	
-4	4.774	0.421		7.25949E-07	-0.000471	0.481	4.714	

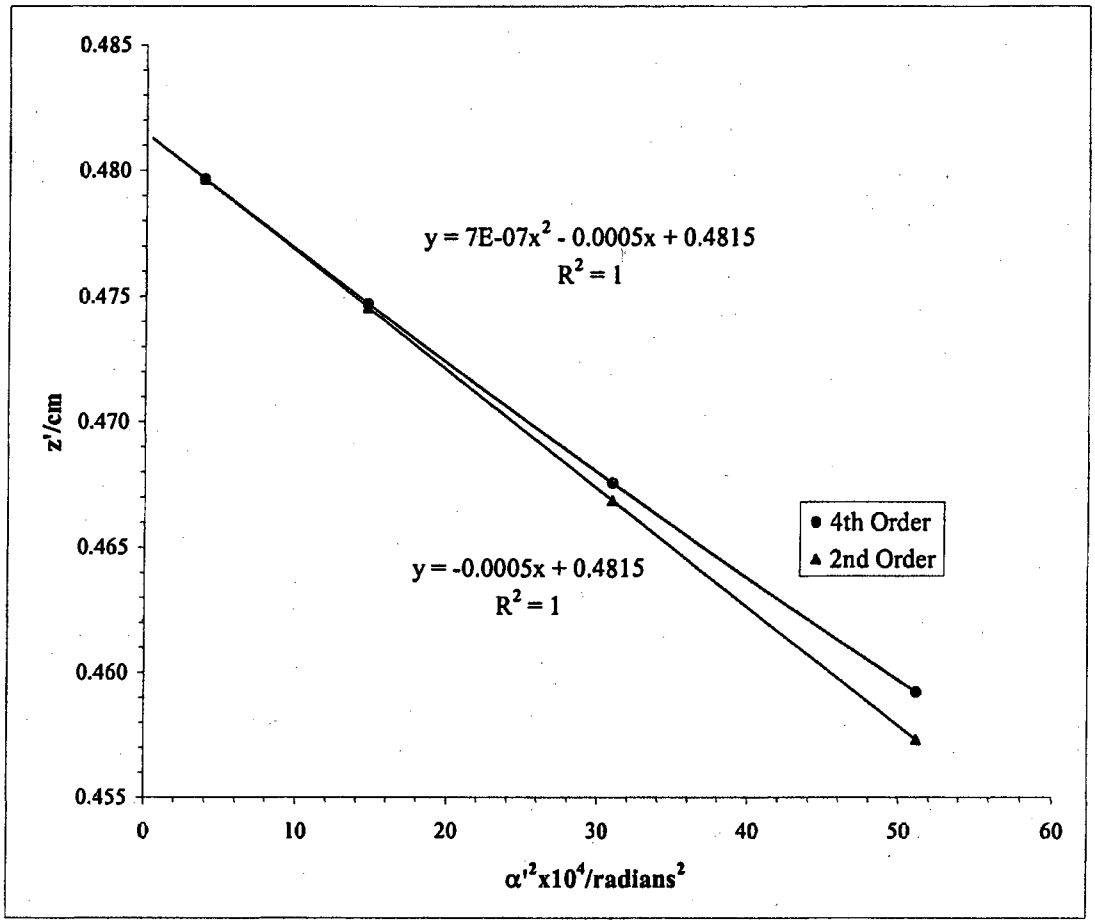

Mesh/inch	I/milliamps	Mesh	e'_1/cm	d/cm	b/cm		Beam	Voltage	20 kV
600	200	Rear	0.0042	26.2382	0.69596	DS			
							0.1 inch gap		

Bar location units	Shadow Reading Y/cm	Spacing Δ/cm	E'/cm	M'	c/cm	α' x 10^2	α'^{2} x 10^4	z'/cm
4	0.181		1.887	111.44	0.238	7.1273	50.7981	0.458
3	0.601	0.420	1.465	115.37	0.229	5.5358	30.6453	0.467
2	1.057	0.456	1.006	118.87	0.223	3.8036	14.4677	0.473
1	1.547	0.490	0.515	121.60	0.218	1.9459	3.7864	0.478
0	2.062	0.515						
-1	2.577	0.515						
-2	3.070	0.493			Slope	z_0'/cm	C_s'/cm	
-3	3.531	0.461		8.914E-07	-0.000473	0.480	4.732	
-4	3.955	0.424						

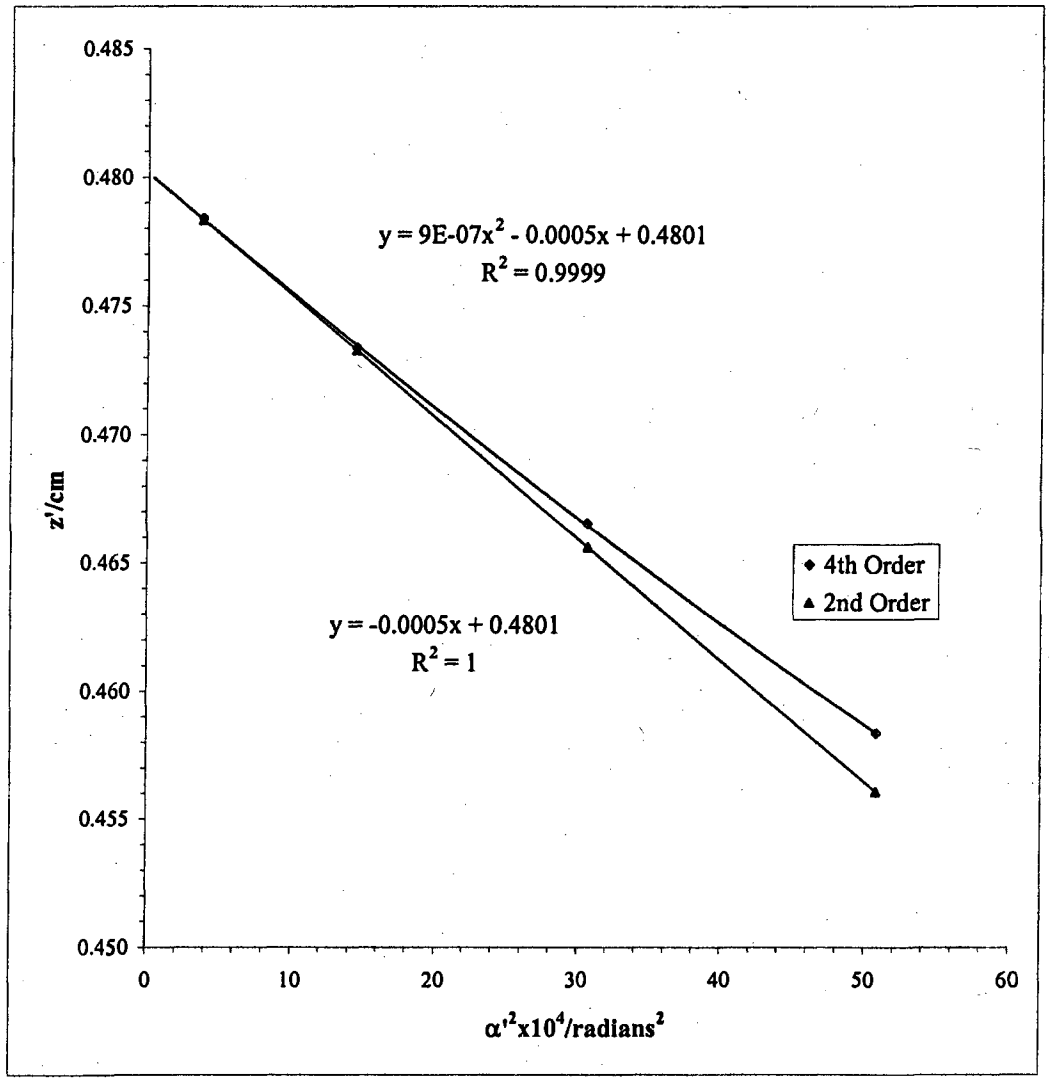

		0.1 inch gap					Beam	Voltage	20 kV
Mesh/inch	I/milliamp	Mesh	z/cm	e_1/cm	a/cm	z_{sp}/cm	z_o'/cm	C_s'/cm	$z_{sp}-z_o'$
600	200	Front	25.03	0.00423	15.63	26.93	0.481	4.723	26.45

Bar location/ units	Shadow Reading X/cm	Spacing Δ/cm	E/cm	α x 10^4	α' x 10^2	α'^{2} x 10^4	m	z'/cm	f/cm
4	1.180		1.342	10.836	5.070	25.704	0.02137	0.469	0.525
3	1.524	0.344	0.999	8.127	3.774	14.246	0.02153	0.474	0.529
2	1.862	0.337	0.662	5.418	2.503	6.265	0.02165	0.478	0.532
1	2.194	0.333	0.330	2.709	1.247	1.556	0.02172	0.480	0.533
0	2.525	0.330							
-1	2.854	0.330					g/cm	$(\rho/f_0)^2 = (m_0+1)^2\alpha'^2$	
-2	3.186	0.332							
-3	3.522	0.336					0.458	26.834	
-4	3.864	0.342					0.463	14.873	
							0.466	6.540	
		Slope	m_o	μ_s			0.468	1.625	
	2.9E-08	0.0000	0.02174	-6.89					

f vs $(\rho/f_o)^2$

$S_f = slope_f / f_0$

$slope_f$	fo/cm	S_f
6.413E-07	-3E-04	0.534	-6.44

g vs $(\rho/f_o)^2$

$S_g = slope_g / f_0$

$slope_g$	go/cm	S_g
-3.2E-08	-0.00039	0.469	-7.38

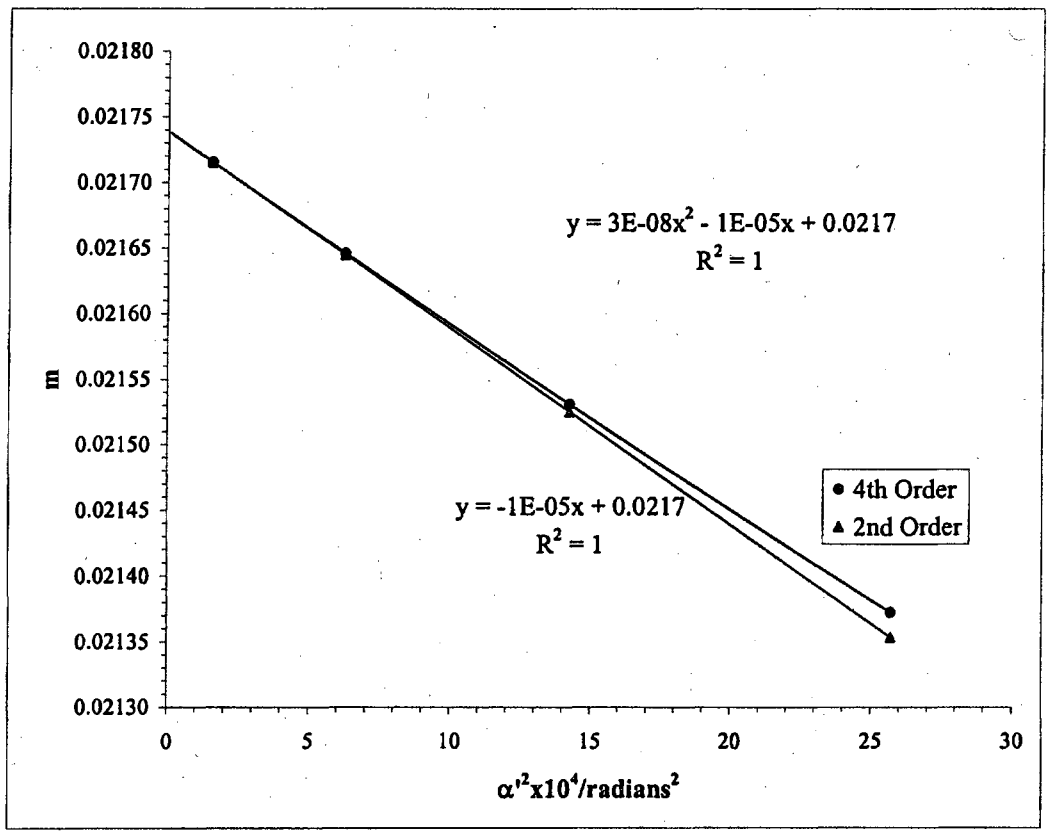

0.1 inch gap | Beam Voltage 20 kV

Mesh/inch	I/milliamp	Mesh	z/cm	e_t/cm	a/cm	z_{sp}/cm	z_0'/cm	C_t'/cm	$z_{sp}-z_o'$
600	200	Front	25.03	0.00423	15.63	26.93	0.481	4.723	26.45

Bar location/ units	Shadow Reading Y/cm	Spacing Δ/cm	E/cm	$\alpha \times 10^4$	$\alpha' \times 10^2$	$\alpha'^2 \times 10^4$	m	z'/cm	f/cm
4	1.033		1.366	10.836	5.161	26.636	0.02100	0.469	0.516
3	1.381	0.348	1.016	8.127	3.840	14.747	0.02116	0.474	0.520
2	1.723	0.341	0.673	5.418	2.545	6.480	0.02128	0.478	0.523
1	2.060	0.337	0.336	2.709	1.268	1.609	0.02136	0.480	0.524
0	2.395	0.335							
-1	2.731	0.336							
-2	3.070	0.339							
-3	3.413	0.344							
-4	3.765	0.351							

g/cm	$(\rho/f_0)^2 = (m_0+1)^2 \alpha'^2$
0.458	27.787
0.463	15.384
0.467	6.760
0.469	1.678

	Slope	m_o	μ_s
3.0E-08	0.0000	0.02138	-7.1695

f vs $(\rho/f_o)^2$

$S_f = slope_f / f_0$

	$slope_f$	fo/cm	S_f
6.78E-07	-0.000352	0.525	-6.71

g vs $(\rho/f_o)^2$

$S_g = slope_g / f_0$

	$slope_g$	go/cm	S_g
-3.34E-08	-0.0003943	0.469	-7.51

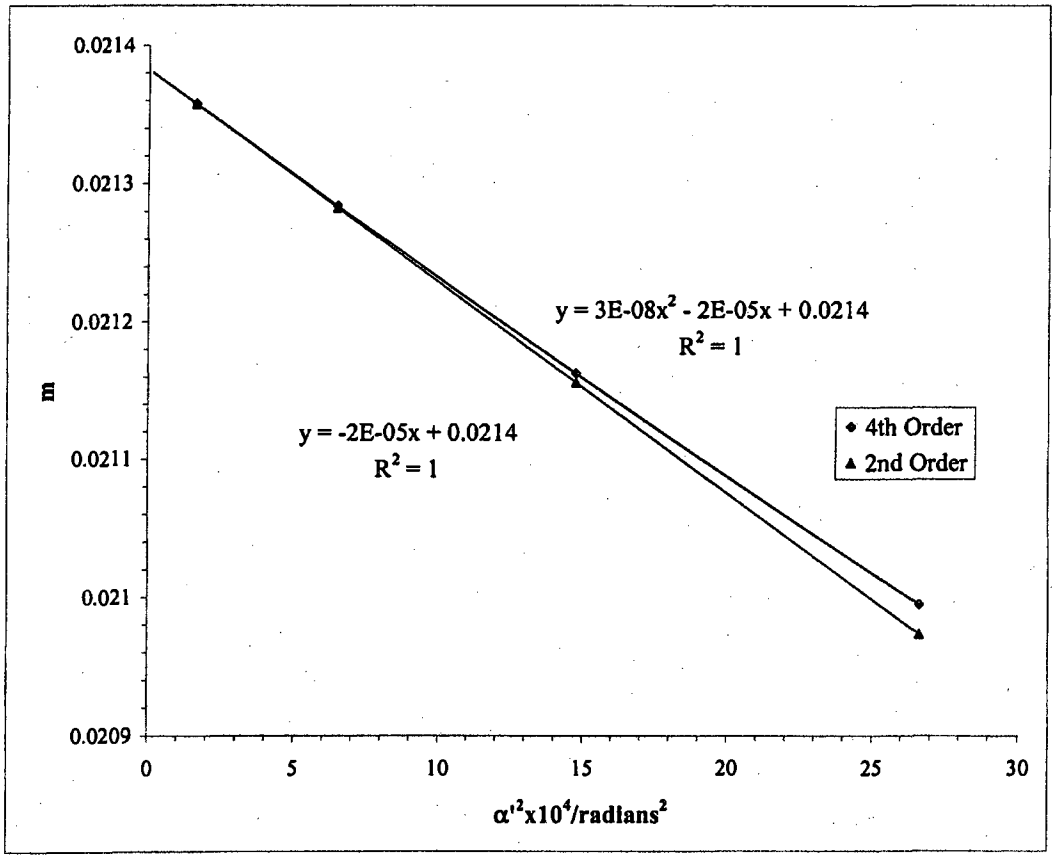

Beam Voltage	I/milliamp	z/cm	z_0'/cm	C_s'/cm
20 kV	200	25.0	0.481	4.72

Average of m_0 = 0.0216

Average of μ_s = -7.03

Paraxial properties :

f_o = 0.529 cm

g_o = 0.469 cm

S_f = -6.58

S_g = -7.45

Mesh/inch	I/milliamps	Mesh	e'_1/cm	d/cm	b/cm		Beam	Voltage	20 kV
600	250	Rear	0.004233	26.24	0.696	DS			
							0.1 inch gap		

Bar location/ units	Shadow Reading X/cm	Spacing Δ/cm	E'/cm	M'	c/cm	α' x 10^2	α'^{2} x 10^4	z'/cm
8.5	0.450		2.3621	65.64	0.4059	8.8653	78.5933	0.290
7.5	0.717	0.266	2.0954	66.00	0.4037	7.8649	61.8568	0.292
6.5	0.988	0.271	1.8250	66.32	0.4017	6.8505	46.9288	0.294
5.5	1.262	0.274	1.5510	66.61	0.3999	5.8225	33.9020	0.296
4.5	1.540	0.278	1.2738	66.87	0.3983	4.7823	22.8705	0.298
3.5	1.820	0.281	0.9939	67.08	0.3971	3.7314	13.9232	0.299
2.5	2.103	0.283	0.7116	67.24	0.3961	2.6717	7.1382	0.300
1.5	2.388	0.284	0.4277	67.35	0.3955	1.6057	2.5782	0.300
0.5	2.673	0.285	0.1427	67.40	0.3951	0.5357	0.2869	0.301
-0.5	2.958	0.285						
-1.5	3.243	0.285						
-2.5	3.526	0.284						
-3.5	3.808	0.282						
-4.5	4.087	0.279			Slope	z_o'/cm	C_s'/cm	
-5.5	4.364	0.277		8.47404E-08	-0.000144	0.301	1.440	
-6.5	4.637	0.273						
-7.5	4.908	0.270						
-8.5	5.175	0.267						

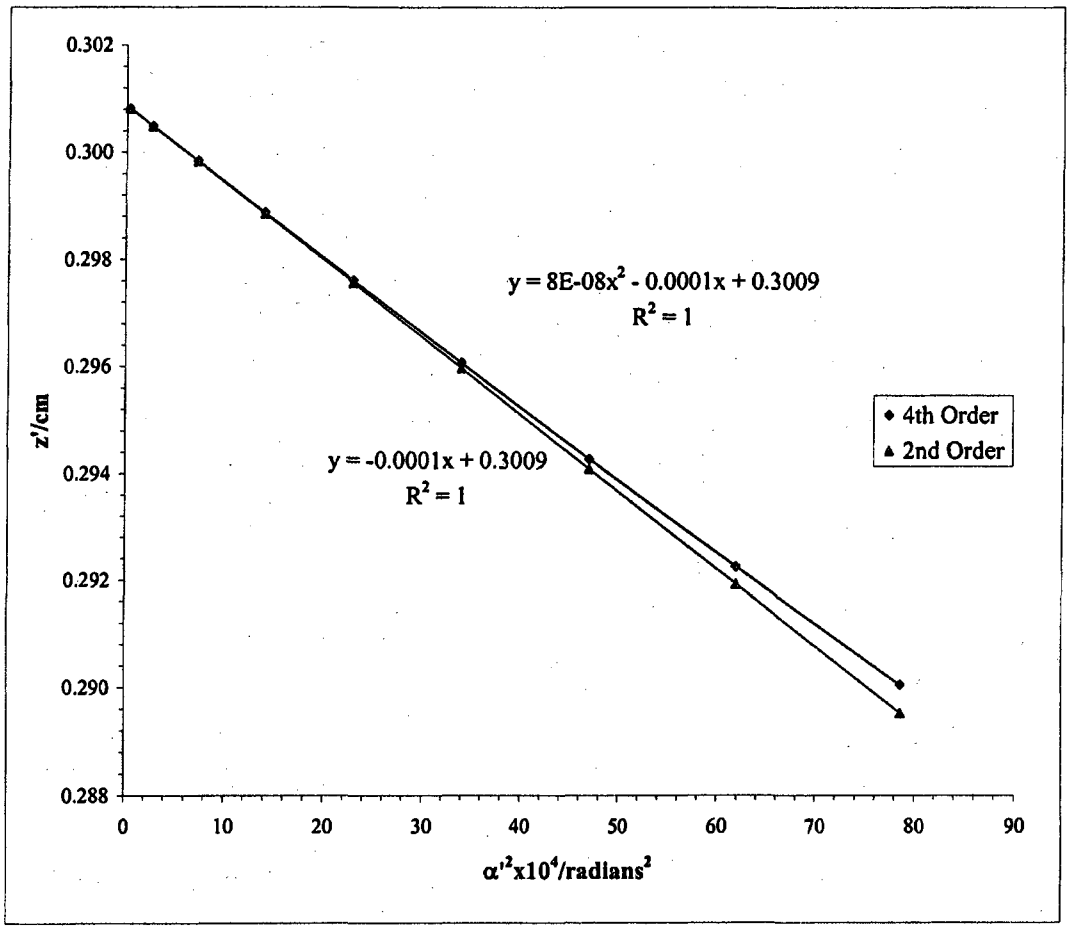

Mesh/inc	I/milliamps	Mesh	e'_1/cm	d/cm	b/cm		Beam	Voltage	20 kV
600	250	Rear	0.0042	26.24	0.696	DS	0.1 inch gap		

Bar location, units	Shadow Reading Y/cm	Spacing Δ/cm	E'/cm	M'	c/cm	$\alpha' \times 10^2$	$\alpha'^2 \times 10^4$	z'/cm
7	1.053		1.959	66.12	0.4029	7.3549	54.0951	0.293
6	1.325	0.272	1.687	66.42	0.4010	6.3334	40.1117	0.295
5	1.602	0.277	1.411	66.66	0.3996	5.2971	28.0592	0.296
4	1.881	0.279	1.132	66.87	0.3983	4.2512	18.0725	0.298
3	2.162	0.281	0.851	67.04	0.3973	3.1967	10.2191	0.299
2	2.446	0.283	0.569	67.19	0.3964	2.1359	4.5623	0.300
1	2.729	0.284	0.285	67.27	0.3960	1.0691	1.1431	0.300
0	3.015	0.285						
-1	3.299	0.284						
-2	3.583	0.284						
-3	3.865	0.282						
-4	4.146	0.281						
-5	4.424	0.278						
-6	4.699	0.275						
-7	4.972	0.273						

	Slope	z_0'/cm	C_s'/cm
	-0.000139	0.300	1.392
1.623E-07			

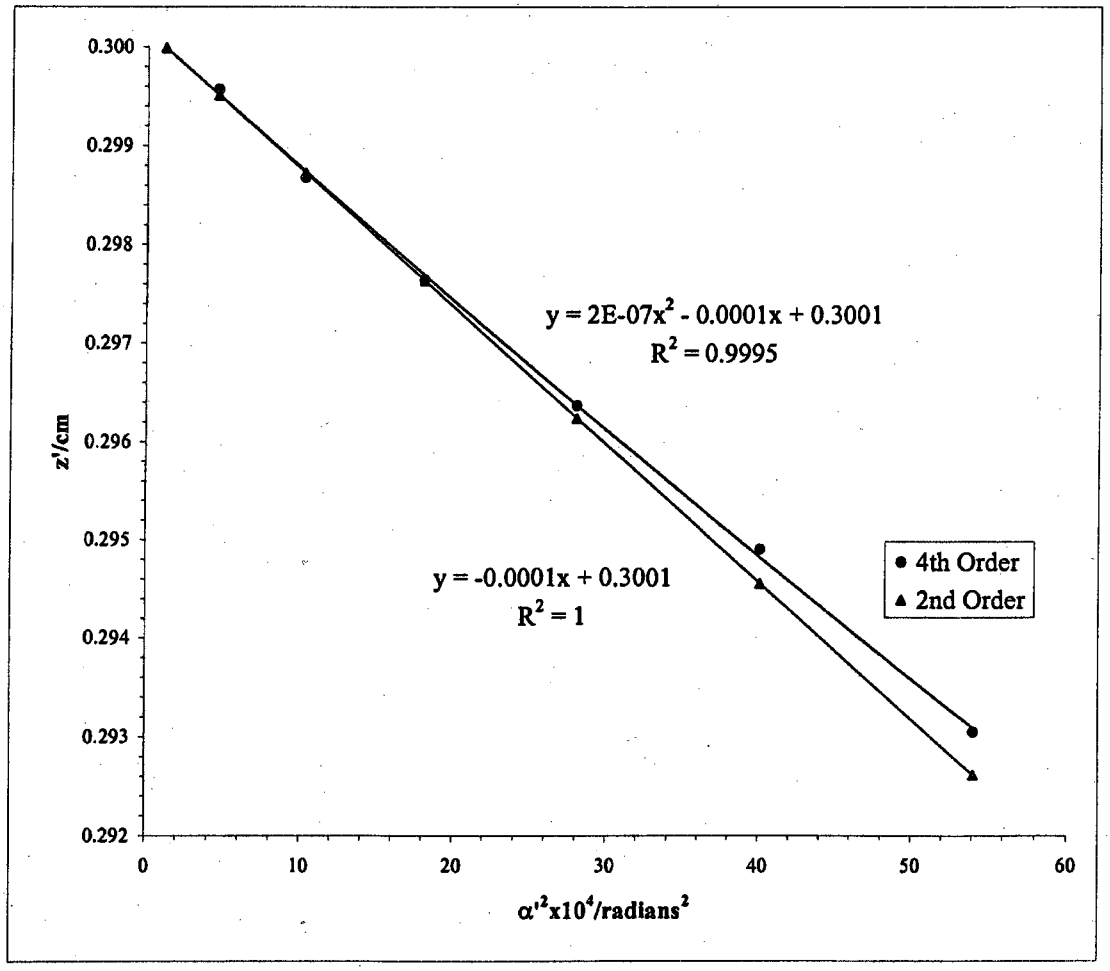

		0.1 inch gap				Beam	Voltage	20 kV
Mesh/inch	I/milliamp	Mesh	z/cm	e_f/cm	a/cm	z_{sp}/cm	z_0'/cm	C_s'/cm	$z_{sp}-z_0'$
2000	250	Front	25.03	0.00127	15.63	26.93	0.301	1.416	26.63

Bar location/ units	Shadow Reading X/cm	Spacing Δ/cm	E/cm	$\alpha \times 10^4$	$\alpha' \times 10^2$	$\alpha'^2 \times 10^4$	m	z'/cm	f/cm
6.5	2.374		0.966	5.282	3.625	13.141	0.01457	0.299	0.360
5.5	2.523	0.150	0.816	4.470	3.064	9.388	0.01459	0.299	0.361
4.5	2.673	0.149	0.667	3.657	2.504	6.272	0.01460	0.299	0.361
3.5	2.821	0.149	0.518	2.844	1.946	3.789	0.01461	0.300	0.361
2.5	2.970	0.148	0.370	2.032	1.389	1.931	0.01462	0.300	0.362
1.5	3.118	0.148	0.222	1.219	0.833	0.695	0.01463	0.300	0.362
0.5	3.266	0.148	0.074	0.406	0.278	0.077	0.01463	0.300	0.362
-0.5	3.414	0.148							
-1.5	3.562	0.148							
-2.5	3.710	0.148							
-3.5	3.858	0.148							
-4.5	4.007	0.149							
-5.5	4.156	0.149							
-6.5	4.305	0.149							

	Slope	m_0	μ_s
4.2E-09	-4.53E-06	0.014631	-3.10

g/cm	$(\rho/f_0)^2 = (m_0+1)^4 \alpha'^4$
0.293	13.529
0.294	9.664
0.294	6.457
0.294	3.900
0.295	1.988
0.295	0.715
0.295	0.079

f vs $(\rho/f_o)^2$

$S_f = slope_f / f_0$

	$slope_f$	fo/cm	S_f
9.7122E-08	-0.00011	0.362	-2.96

g vs $(\rho/f_o)^2$

$S_g = slope_g / f_0$

	$slope_g$	go/cm	S_g
-3.303E-09	-0.0001	0.295	-3.45

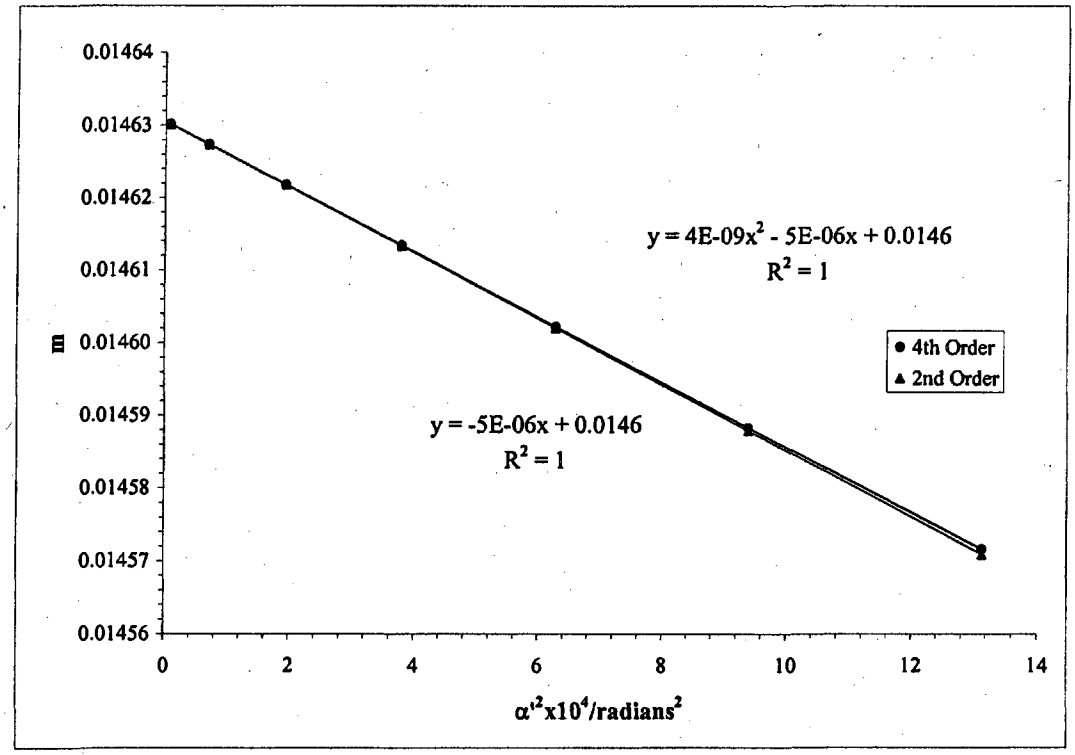

0.1 inch gap | Beam Voltage 20 kV

Mesh/incl	I/milliamp	Mesh	z/cm	e_1/cm	a/cm	z_{sp}/cm	z_0'/cm	C_s'/cm	$z_{sp}-z_o'$
2000	250	Front	25.03	0.00127	15.63	26.93	0.301	1.416	26.63

Bar location/ units	Shadow Reading Y/cm	Spacing Δ/cm	E/cm	$\alpha \times 10^4$	$\alpha' \times 10^2$	$\alpha'^2 \times 10^4$	m	z'/cm	f/cm
7	2.604		1.055	5.689	3.961	15.686	0.0144	0.298	0.355
6	2.755	0.152	0.903	4.876	3.390	11.495	0.0144	0.299	0.356
5	2.907	0.151	0.752	4.063	2.822	7.966	0.0144	0.299	0.356
4	3.058	0.151	0.601	3.251	2.256	5.089	0.0144	0.300	0.356
3	3.208	0.151	0.450	2.438	1.691	2.859	0.0144	0.300	0.357
2	3.358	0.150	0.300	1.625	1.127	1.269	0.0144	0.300	0.357
1	3.509	0.150	0.150	0.813	0.563	0.317	0.0144	0.300	0.357
0	3.659	0.150							
-1	3.809	0.150					g/cm	$(\rho/f_0)^2 = (m_0+1)^2\alpha'^2$	
-2	3.959	0.150							
-3	4.109	0.150					0.293	16.142	
-4	4.259	0.151					0.294	11.829	
-5	4.410	0.151					0.294	8.197	
-6	4.562	0.151					0.294	5.237	
-7	4.713	0.152					0.295	2.942	
							0.295	1.306	
			Slope	m_0	μ_s		0.295	0.326	
			4.1E-09	0.0000	0.014433	-3.08907			

f vs $(\rho/f_o)^2$

S_f = slope$_f$ / f_0

slope$_f$	fo/cm	S_f
9.4851E-08	-0.000105	0.357	-2.95

g vs $(\rho/f_o)^2$

S_g = slope$_g$ / f_0

slope$_g$	go/cm	S_g
-3.18E-09	-0.000125	0.295	-3.50

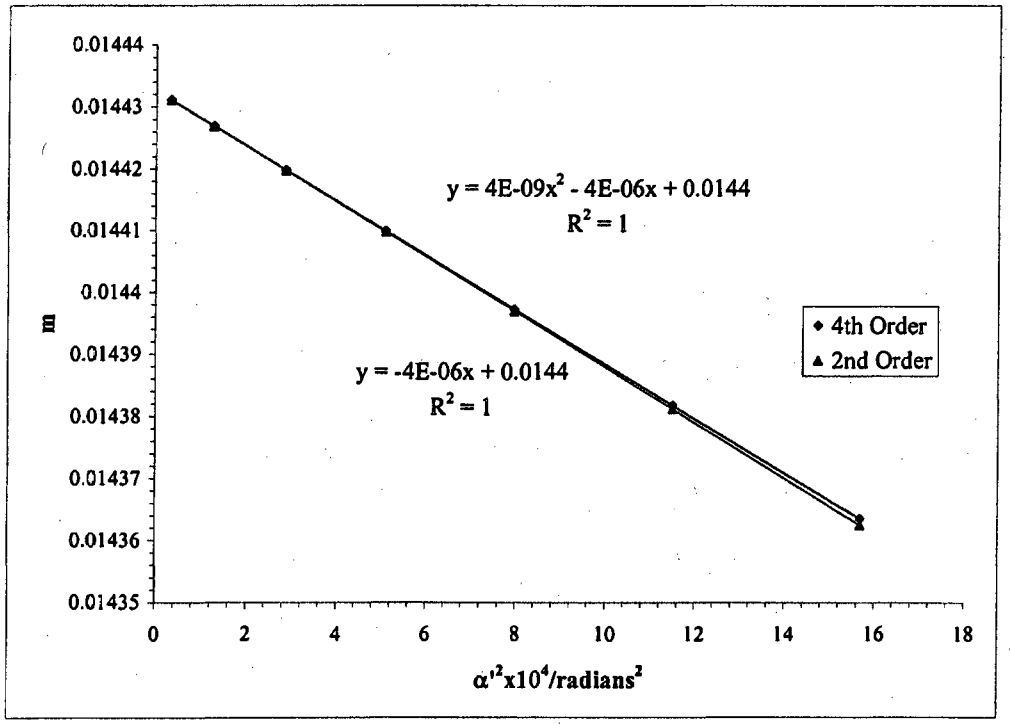

Beam Voltage	I/milliamp	z/cm	z_0'/cm	C_s'/cm	0.1 inch gap
20 kV	250	25.0	0.301	1.42	

Average of m_o = 0.0145

Average of μ_s = -3.09

Paraxial properties :

f_o = 0.359 cm

g_o = 0.295 cm

S_f = -2.96

S_g = -3.48

Mesh/inch	I/milliamps	Mesh	e'_1/cm	d/cm	b/cm		Beam	Voltage	20 kV
600	300	Rear	0.00423	26.49	0.442	DS			
							0.1 inch gap		

Bar location/ units	Shadow Reading X/cm	Spacing Δ/cm	E'/cm	M'	c/cm	α' x 10^2	α'^{2} x 10^4	z'/cm
3.5	1.070		1.8317	123.62	0.216	6.8582	47.0345	0.226
2.5	1.584	0.514	1.3169	124.43	0.215	4.9309	24.3135	0.227
1.5	2.106	0.522	0.7944	125.09	0.213	2.9745	8.8475	0.228
0.5	2.634	0.528	0.2657	125.52	0.213	0.9949	0.9898	0.229
-0.5	3.165	0.531						
-1.5	3.695	0.530			Slope	z_o'/cm	C_s'/cm	
-2.5	4.218	0.523		4.21E-07	-9.12435E-05	0.229	0.912	
-3.5	4.733	0.515						

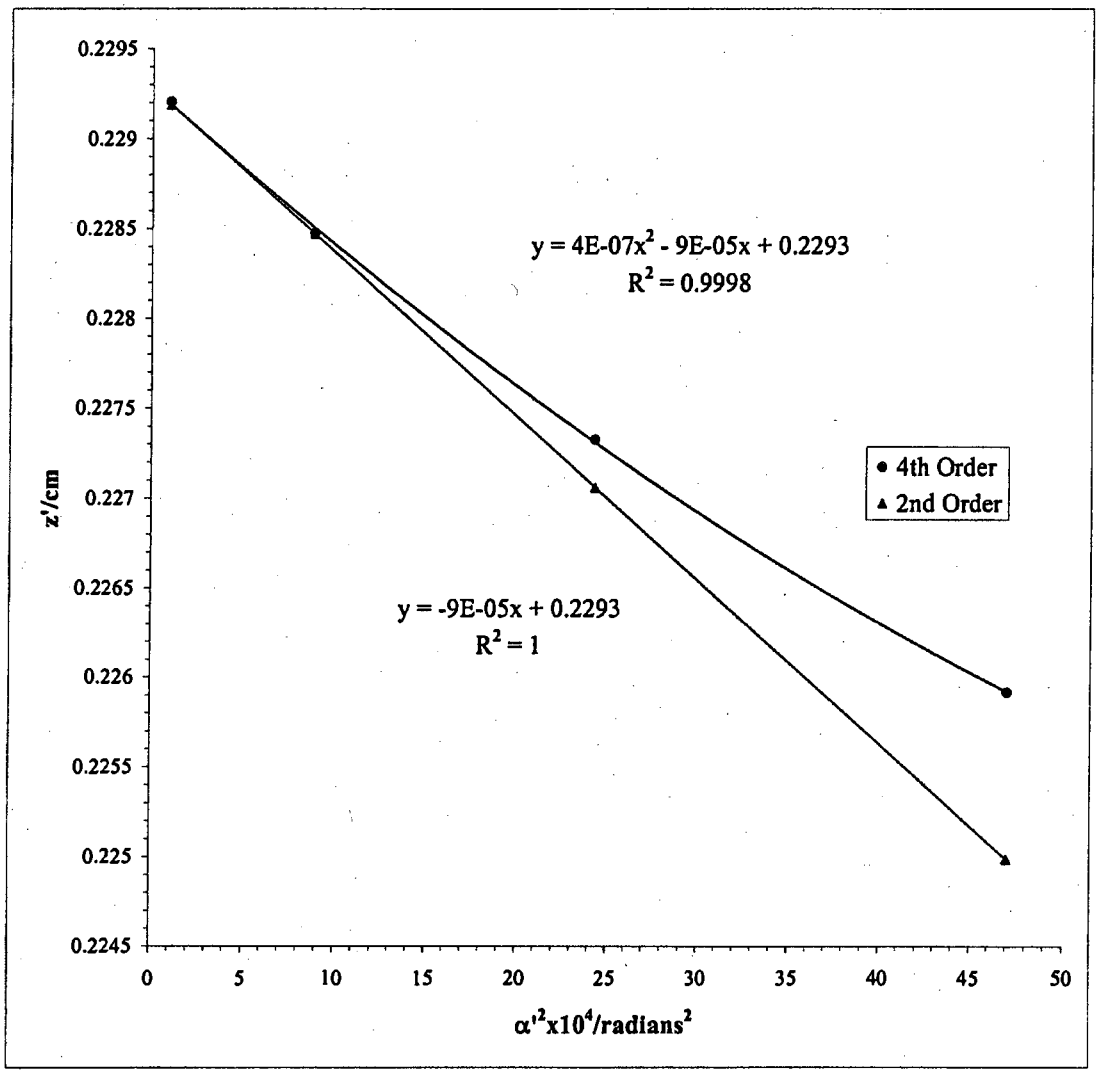

Mesh/inch	I/milliamps	Mesh	e'_1/cm	d/cm	b/cm		Beam	Voltage	20 kV
600	300	Rear	0.00423	26.49	0.442	DS	0.1 inch gap		

Bar location/ units	Shadow Reading Y/cm	Spacing Δ/cm	E'/cm	M'	c/cm	$\alpha' \times 10^2$	$\alpha'^2 \times 10^4$	z'/cm
4	0.6987		2.086	123.18	0.217	7.8096	60.9899	0.225
3	1.2110	0.512	1.576	124.13	0.215	5.9025	34.8396	0.227
2	1.7339	0.523	1.057	124.89	0.214	3.9594	15.6771	0.228
1	2.2626	0.529	0.530	125.28	0.213	1.9860	3.9443	0.229
0	2.7933	0.531						
-1	3.3234	0.530						
-2	3.8487	0.525						
-3	4.3638	0.515			Slope	z_0'/cm	C_s'/cm	
-4	4.8705			1.24E-07	-7.55E-05	0.229	0.755	

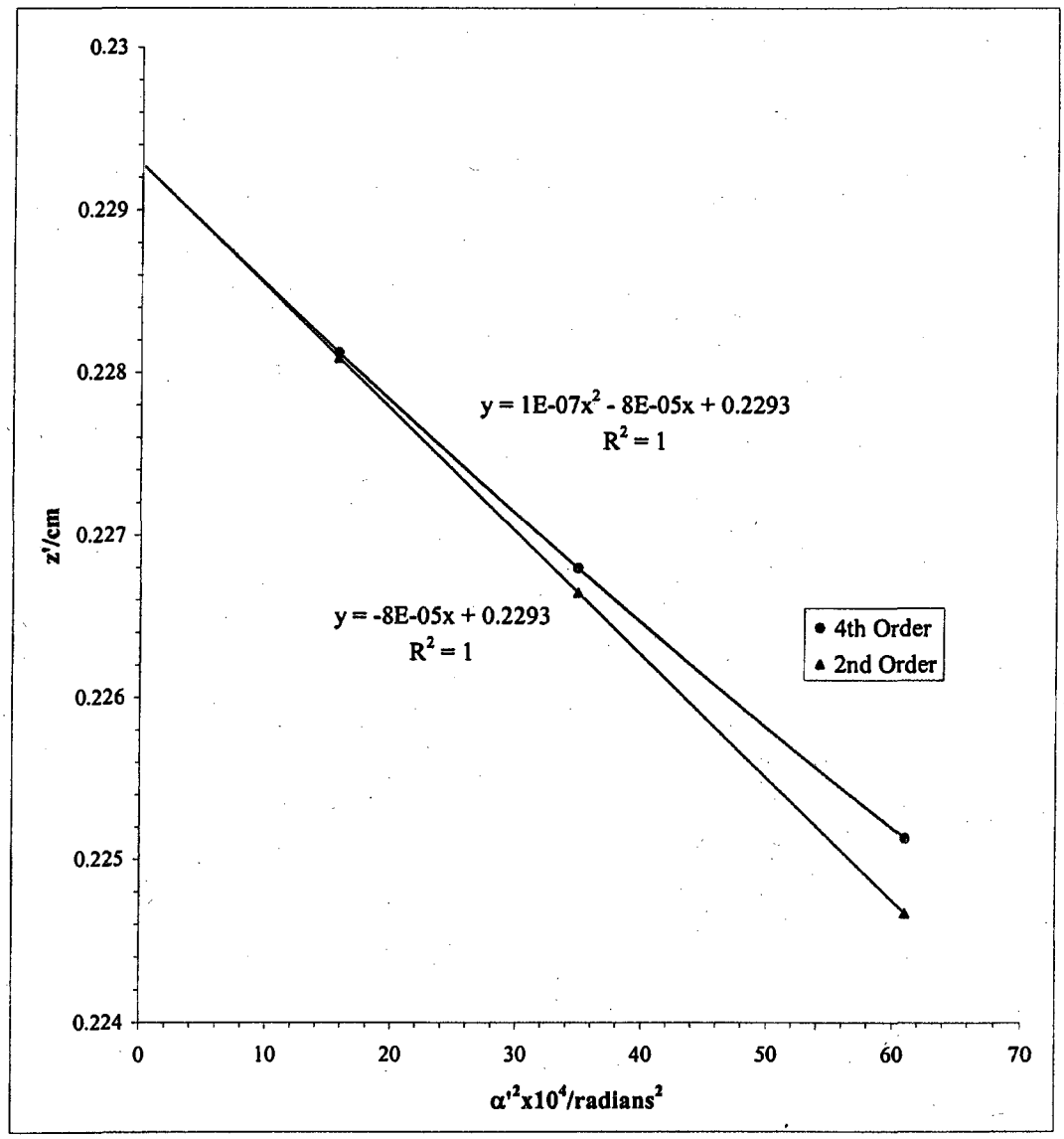

			0.1 inch gap				Beam	Voltage	20 kV
Mesh/inch	l/milliamp	Mesh	z/cm	e_1/cm	a/cm	z_{ap}/cm	z_0'/cm	C_s'/cm	$z_{ap}-z_0'$
2000	300	Front	25.03	0.00127	15.63	26.93	0.229	0.834	26.705

Bar location/ units	Shadow Reading X/cm	Spacing Δ/cm	E/cm	$\alpha \times 10^4$	$\alpha' \times 10^2$	$\alpha'^2 \times 10^4$	m	z'/cm	f/cm
10	1.242		2.011	8.127	7.528	56.677	0.01079	0.225	0.267745
9	1.446	0.20429	1.806	7.314	6.763	45.735	0.01082	0.226	0.268244
8	1.649	0.20322	1.603	6.501	6.001	36.013	0.01083	0.227	0.268693
7	1.852	0.20227	1.400	5.689	5.243	27.490	0.01085	0.227	0.269090
6	2.053	0.20144	1.199	4.876	4.488	20.144	0.01086	0.228	0.269435
5	2.254	0.20074	0.998	4.063	3.736	13.958	0.01088	0.228	0.269728
4	2.454	0.20015	0.797	3.251	2.986	8.917	0.01089	0.229	0.269968
3	2.654	0.19969	0.598	2.438	2.238	5.009	0.01089	0.229	0.270155
2	2.853	0.19936	0.398	1.625	1.491	2.224	0.01090	0.229	0.270289
1	3.052	0.19914	0.199	0.813	0.745	0.556	0.01090	0.229	0.270369
0	3.251	0.19905							
-1	3.450	0.19908					g/cm	$(\rho/f_0)^2 = (m_0+1)^2\alpha'^2$	
-2	3.650	0.19923							
-3	3.849	0.19950					0.222298	57.919	
-4	4.049	0.19990					0.223053	46.737	
-5	4.249	0.20042					0.223724	36.803	
-6	4.450	0.20106					0.224312	28.093	
-7	4.652	0.20182					0.224819	20.586	
-8	4.855	0.20271					0.225245	14.264	
-9	5.059	0.20371					0.225593	9.113	
-10	5.264	0.20484					0.225862	5.119	
							0.226054	2.273	
			Slope	m_0	μ_s		0.226169	0.568	
		1.0E-09	-1.97E-06	0.0109	-1.81				

f vs $(\rho/f_0)^2$

$S_f = slope_f / f_0$

$slope_f$	fo/cm	S_f
2.43E-08	-4.72E-05	0.270	-1.74

g vs $(\rho/f_0)^2$

$S_g = slope_g / f_0$

$slope_g$	go/cm	S_g
-6.1E-10	-6.746E-05	0.226	-2.49

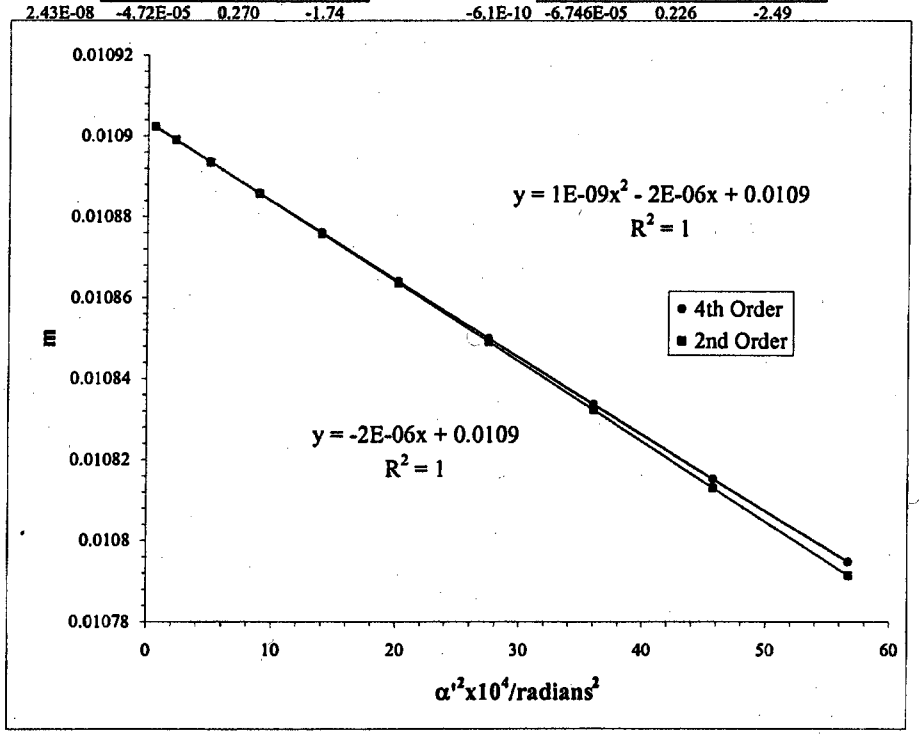

			0.1 inch gap				Beam	Voltage	20 kV
Mesh/inch	I/milliamp	Mesh	z/cm	e_1/cm	a/cm	z_{sp}/cm	z_0'/cm	C_1'/cm	$z_{sp}-z_o'$
2000	300	Front	25.03	0.00127	15.63	26.93	0.229	0.834	26.70

Bar location/ units	Shadow Reading Y/cm	Spacing Δ/cm	E/cm	$\alpha \times 10^4$	$\alpha' \times 10^2$	$\alpha'^2 \times 10^4$	m	z'/cm	f/cm
10.5	1.588		2.146	8.533	8.035	64.555	0.01062	0.2246	0.2634
9.5	1.796	0.208	1.938	7.720	7.255	52.630	0.01064	0.2255	0.2640
8.5	2.003	0.207	1.730	6.908	6.479	41.980	0.01066	0.2262	0.2644
7.5	2.209	0.206	1.524	6.095	5.708	32.577	0.01068	0.2269	0.2648
6.5	2.414	0.205	1.319	5.282	4.940	24.399	0.01069	0.2274	0.2652
5.5	2.619	0.204	1.115	4.470	4.174	17.426	0.01071	0.2279	0.2655
4.5	2.822	0.204	0.911	3.657	3.412	11.642	0.01072	0.2283	0.2658
3.5	3.025	0.203	0.708	2.844	2.652	7.031	0.01073	0.2287	0.2660
2.5	3.228	0.203	0.505	2.032	1.893	3.583	0.01073	0.2289	0.2662
1.5	3.430	0.202	0.303	1.219	1.135	1.289	0.01074	0.2291	0.2663
0.5	3.632	0.202	0.101	0.406	0.378	0.143	0.01074	0.2291	0.2663
-0.5	3.834	0.202							
-1.5	4.037	0.202					g/cm	$(\rho/f_0)^2 = (m_0+1)^2\alpha'^2$	
-2.5	4.239	0.202							
-3.5	4.442	0.203					0.2218	65.949	
-4.5	4.645	0.203					0.2227	53.767	
-5.5	4.848	0.204					0.2234	42.886	
-6.5	5.053	0.204					0.2240	33.280	
-7.5	5.258	0.205					0.2246	24.926	
-8.5	5.464	0.206					0.2251	17.803	
-9.5	5.671	0.207					0.2255	11.893	
-10.5	5.880	0.208					0.2258	7.183	
							0.2260	3.660	
			Slope	m_o	μ_1		0.2262	1.317	
		9.8E-10	-1.92E-06	0.01074	-1.79		0.2263	0.146	

f vs $(\rho/f_o)^2$ — $S_f = slope_f / f_0$

	$slope_f$	fo/cm	S_f
2.32E-08	-4.59E-05	0.266	-1.72

g vs $(\rho/f_o)^2$ — $S_g = slope_g / f_0$

	$slope_g$	go/cm	S_g
-6E-10	-6.75E-05	0.226	-2.54

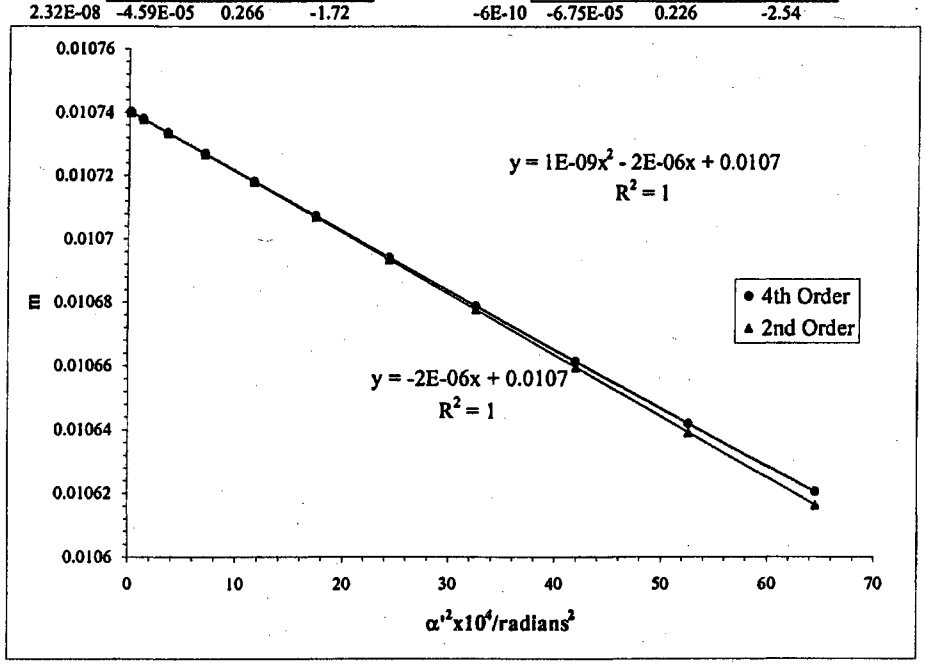

Beam Voltage	I/milliamp	z/cm	z_0'/cm	C_s'/cm
20 kV	300	25.0	0.229	0.834

Average of m_o = 0.0108

Average of μ_s = -1.80

Paraxial properties :

f_o = 0.268 cm

g_o = 0.226 cm

S_f = -1.73

S_g = -2.51

Mesh/inch	I/milliamps	Mesh	e'_1/cm	d/cm	b/cm		Beam	Voltage	20 kV
600	350	Rear	0.004233	26.4922	0.44196	DS	0.1 inch gap		

Bar location/ units	Shadow Reading X/cm	Spacing Δ/cm	E'/cm	M'	c/cm	α' x 10^2	α'^{2} x 10^4	z'/cm
2.5	2.369		1.021	96.50	0.2774	3.8151	14.5548	0.1646
1.5	2.777	0.408	0.613	96.59	0.2772	2.2911	5.2494	0.1648
0.5	3.186	0.409	0.205	96.63	0.2770	0.7641	0.5838	0.1649
-0.5	3.595	0.409						
-1.5	4.004	0.409						
-2.5	4.411	0.408						

		Slope	z_o'/cm	C_s'/cm
	-8.06E-09	-2.71649E-05	0.165	0.272

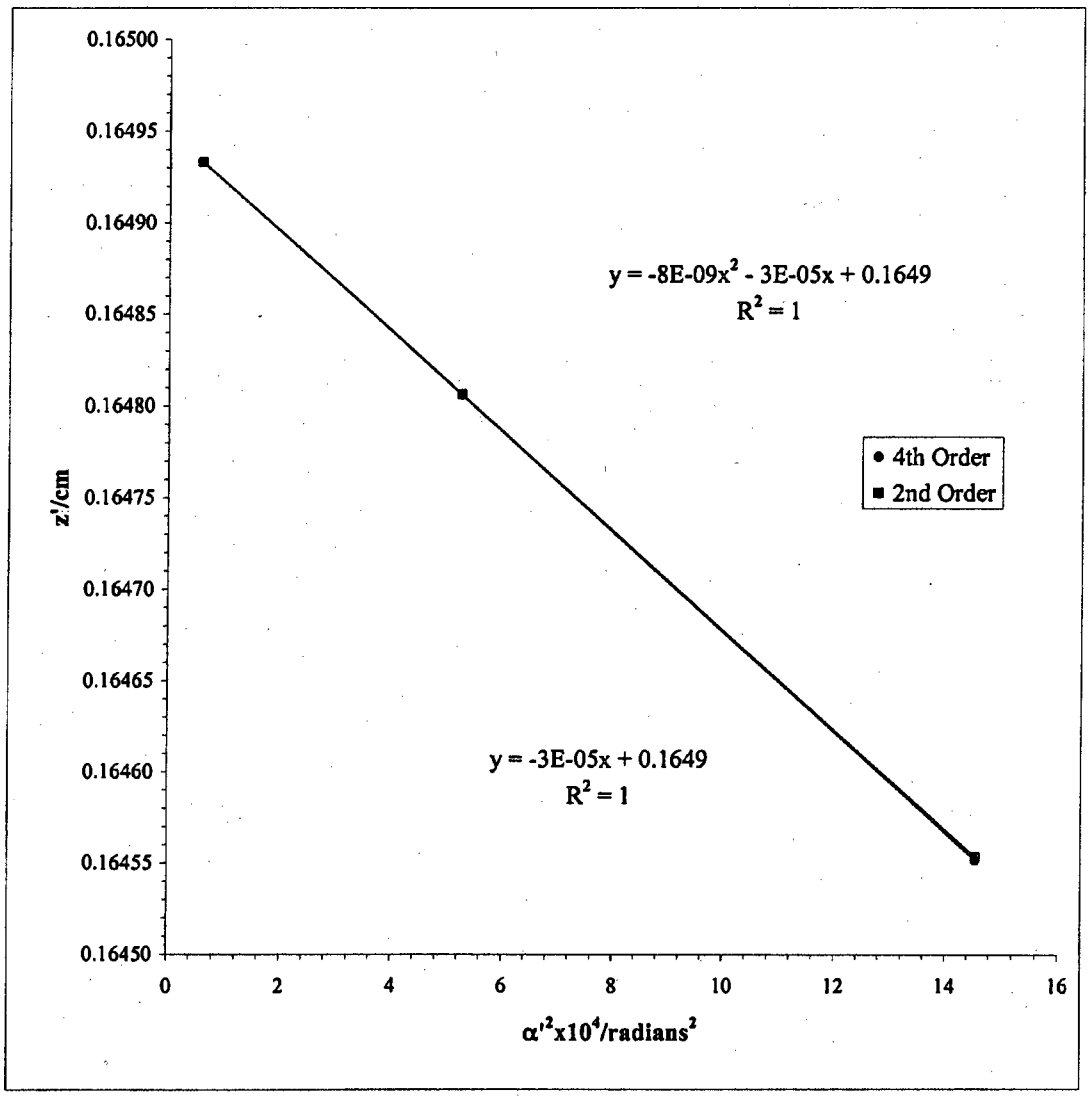

Mesh/inch	I/milliamps	Mesh	e'_1/cm	d/cm	b/cm		Beam	Voltage	20 kV
600	350	Rear	0.004233	26.49	0.442	DS	0.1 inch gap		

Bar location/ units	Shadow Reading Y/cm	Spacing Δ/cm	E'/cm	M'	c/cm	α' x 10^2	α'^2 x 10^4	z'/cm
2.5	2.053		1.025	96.88	0.2763	3.8304	14.6716	0.1657
1.5	2.462	0.4092	0.616	97.00	0.2760	2.3010	5.2944	0.1660
0.5	2.873	0.4104	0.205	97.05	0.2758	0.7674	0.5890	0.1662
-0.5	3.283	0.4109						
-1.5	3.694	0.4106						
-2.5	4.104	0.4096						

	Slope	z_o'/cm	C_s'/cm
-1.3E-08	-3.50209E-05	0.166	0.350

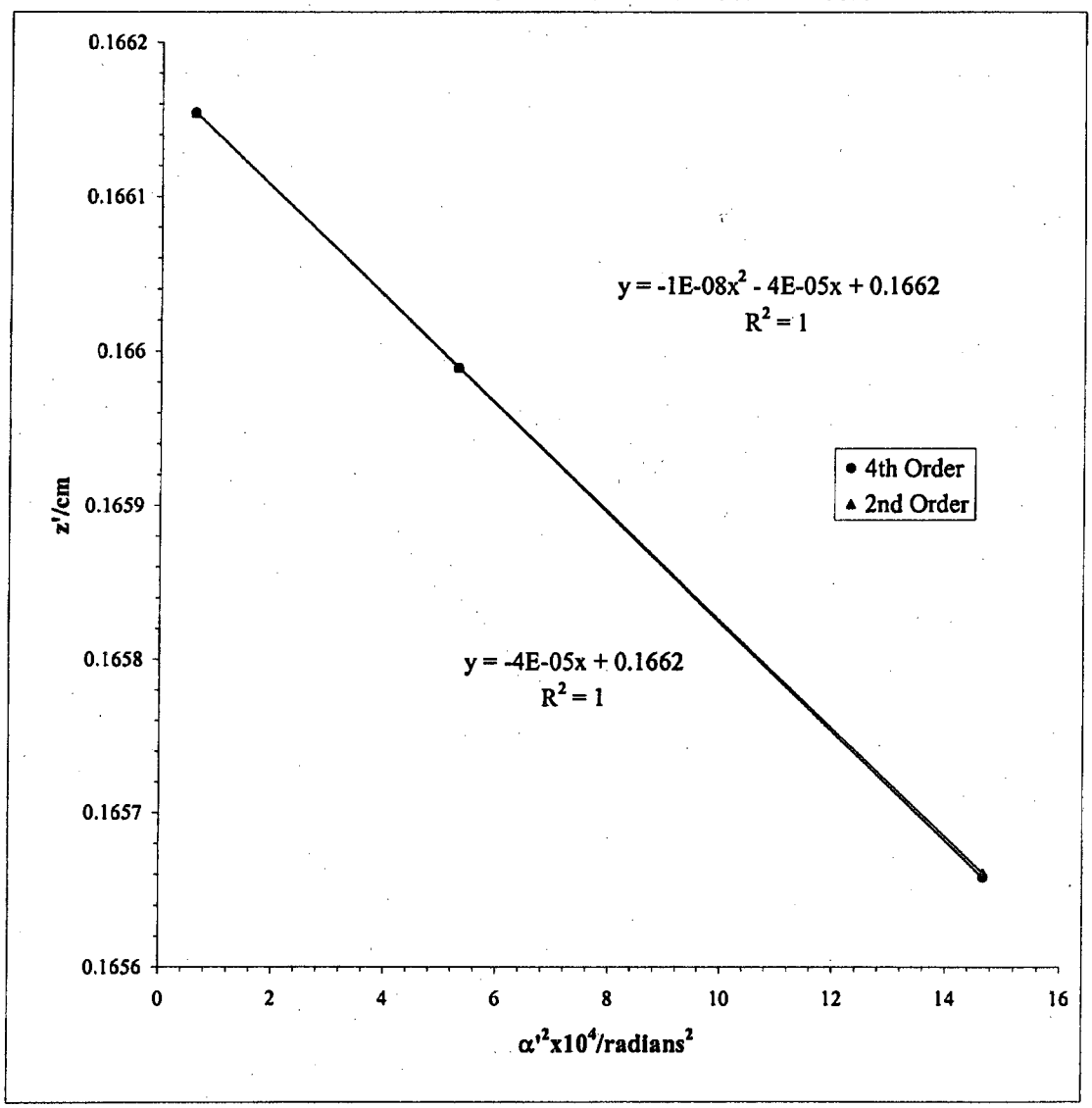

0.1 inch gap | Beam Voltage 20 kV

Mesh/inch	I/milliamp	Mesh	z/cm	e_1/cm	a/cm	z_{sp}/cm	z_0'/cm	C_s'/cm	$z_{sp}-z_0'$
2000	350	Front	25.03	0.00127	15.63	26.93	0.166	0.311	26.77

Bar location/ units	Shadow Reading X/cm	Spacing Δ/cm	E/cm	$\alpha \times 10^4$	$\alpha' \times 10^2$	$\alpha'^2 \times 10^4$	m	z'/cm	f/cm
4.5	1.3646		1.143	3.657	4.271	18.238	0.008563	0.164980	0.2129
3.5	1.6193	0.2547	0.888	2.844	3.319	11.015	0.008570	0.165249	0.2131
2.5	1.8735	0.2542	0.634	2.032	2.369	5.613	0.008575	0.165451	0.2132
1.5	2.1273	0.2538	0.380	1.219	1.421	2.019	0.008579	0.165585	0.2133
0.5	2.3809	0.2536	0.127	0.406	0.474	0.224	0.008581	0.165652	0.2133
-0.5	2.6344	0.2535							
-1.5	2.8881	0.2536							
-2.5	3.1419	0.2539							
-3.5	3.3962	0.2543							
-4.5	3.6510	0.2548							

Slope	m_0	μ_s
0.0000	0.008581	-1.12

g/cm	$(\rho/f_0)^2 = (m_0+1)^2 \alpha'^2$
0.1632	18.552
0.1634	11.205
0.1636	5.710
0.1638	2.054
0.1638	0.228

f vs $(\rho/f_0)^2$

S_f = slope$_f$ / f_0

	slope$_f$	fo/cm	S_f
7.6672E-09	-2.31099E-05	0.213	-1.08

g vs $(\rho/f_0)^2$

S_g = slope$_g$ / f_0

	slope$_g$	go/cm	S_g
-1.5E-10	-3.6E-05	0.164	-1.70

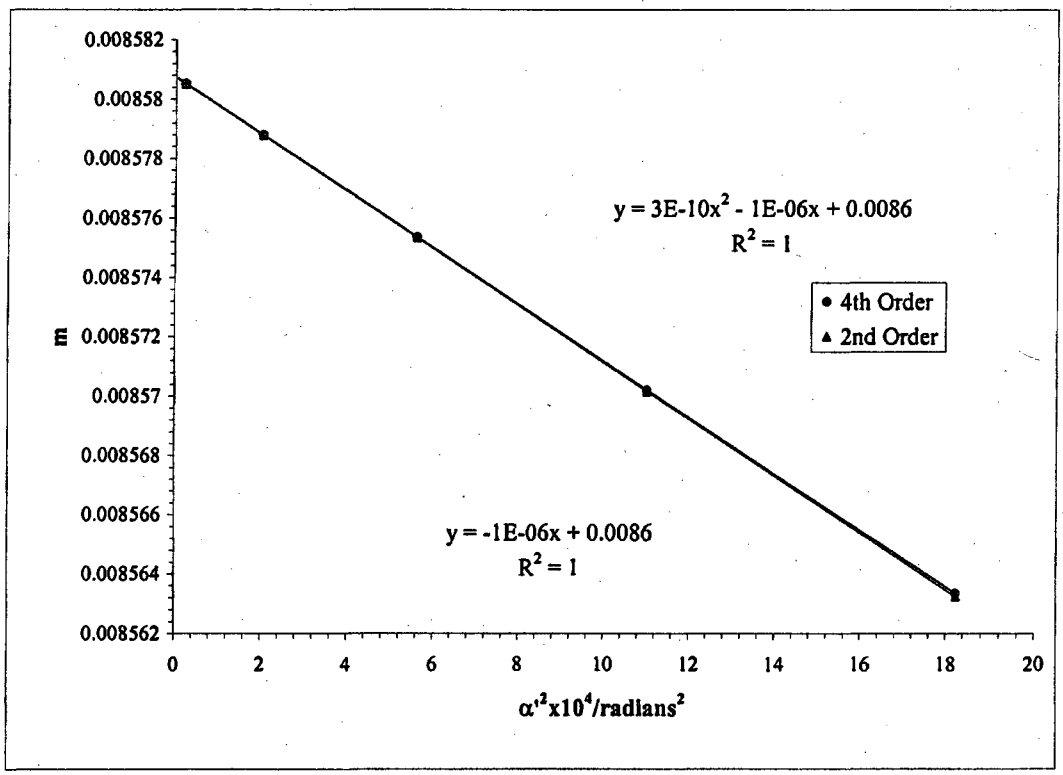

Beam Voltage	I/milliamp	z/cm	z_0'/cm	C_s'/cm	0.1 inch gap
20 kV	350	25.0	0.166	0.311	

Average of m_0 = 0.008581

Average of μ_s = -1.12

Paraxial properties :

f_0 = 0.213 cm

g_o = 0.164 cm

S_f = -1.08

S_g = -1.70

Magnetic Lens L_1 Data.
Acceleration Voltage 25 kV
Gap size 0.050 inches

Mesh/Inch	I/milliamps	Mesh	e'1/cm	d/cm	b/cm		Beam	Voltage	25 kV
2000	100	Rear	0.00127	25.28	1.593	DS			

Bar location/ units	Shadow Reading X/cm	Spacing Δ/cm	E'/cm	M'	c/cm	$\alpha' \times 10^2$	$\alpha'^2 \times 10^4$	z'/cm
7.5	1.127414		0.730	76.661	0.334	2.850	8.125	1.258
6.5	1.190602	0.063	0.669	81.072	0.316	2.614	6.835	1.277
5.5	1.25349	0.063	0.602	86.199	0.297	2.354	5.540	1.296
4.5	1.325593	0.072	0.527	92.266	0.277	2.063	4.256	1.316
3.5	1.411544	0.086	0.440	99.026	0.258	1.723	2.970	1.335
2.5	1.519225	0.108	0.342	107.763	0.237	1.341	1.797	1.356
1.5	1.64151	0.122	0.221	115.920	0.220	0.866	0.750	1.373
0.5	1.788932	0.147	0.078	123.170	0.207	0.307	0.094	1.386
-0.5	1.945358	0.156						
-1.5	2.083163	0.138						
-2.5	2.203517	0.120						
-3.5	2.291883	0.088						
-4.5	2.380196	0.088						
-5.5	2.45769	0.077						
-6.5	2.529107	0.071			Slope	z_o'/cm	C_s'/cm	
-7.5	2.587803	0.059		0.000276	-0.0180	1.387	179.89	

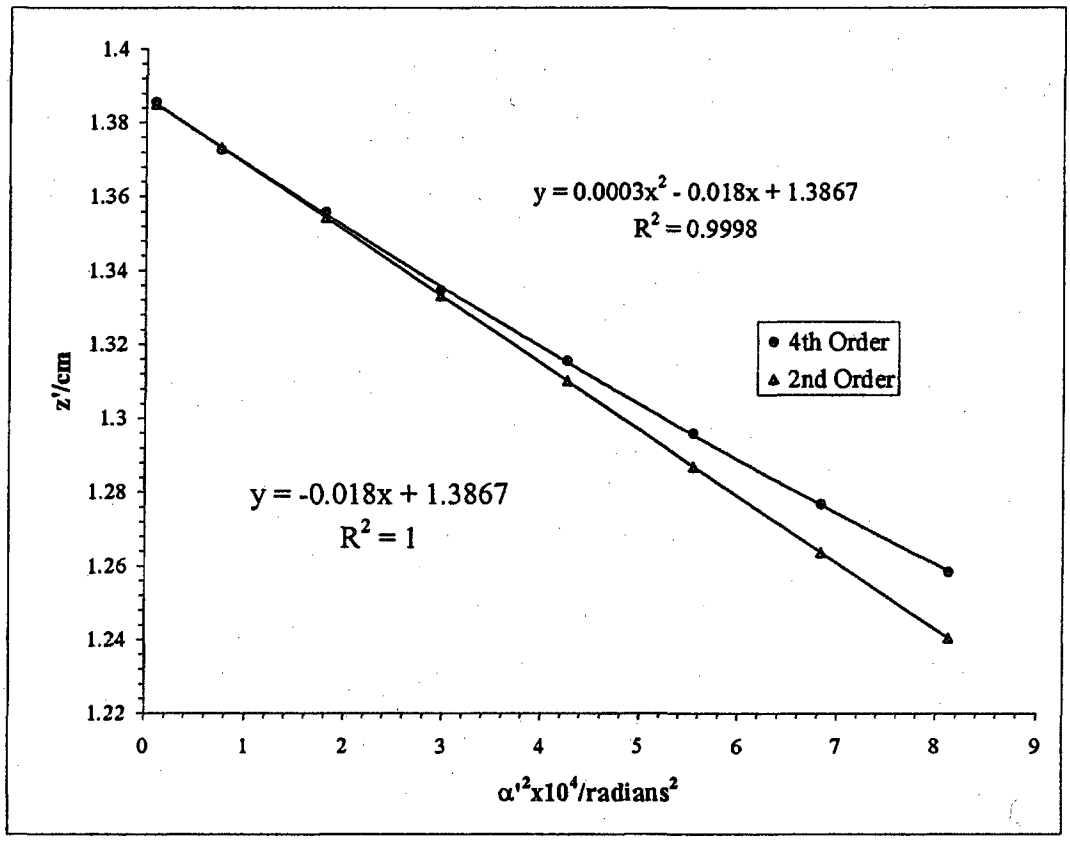

Mesh/Inch	I/milliamps	Mesh	e'1/cm	d/cm	b/cm		Beam	Voltage	25 kV
2000	100	Rear	0.00127	25.28	1.593	DS			

Bar location/ units	Shadow Reading Y/cm	Spacing Δ/cm	E'/cm	M'	c/cm	$\alpha' \times 10^2$	$\alpha'^2 \times 10^4$	z'/cm
5.5	1.2491		0.606	86.723	0.295	2.368	5.609	1.298
4.5	1.3224	0.073	0.531	92.844	0.275	2.076	4.310	1.317
3.5	1.4067	0.084	0.447	100.515	0.254	1.750	3.061	1.339
2.5	1.5129	0.106	0.346	108.986	0.234	1.356	1.839	1.358
1.5	1.6340	0.121	0.225	118.317	0.216	0.884	0.781	1.377
0.5	1.7827	0.149	0.080	125.594	0.203	0.313	0.098	1.390
-0.5	1.9422	0.160						
-1.5	2.0847	0.143						
-2.5	2.2049	0.120			Slope	z_o'/cm	C_s'/cm	
-3.5	2.3003	0.095		0.000277	-0.0183	1.391	182.75	
-4.5	2.3836	0.083						
-5.5	2.4606	0.077						

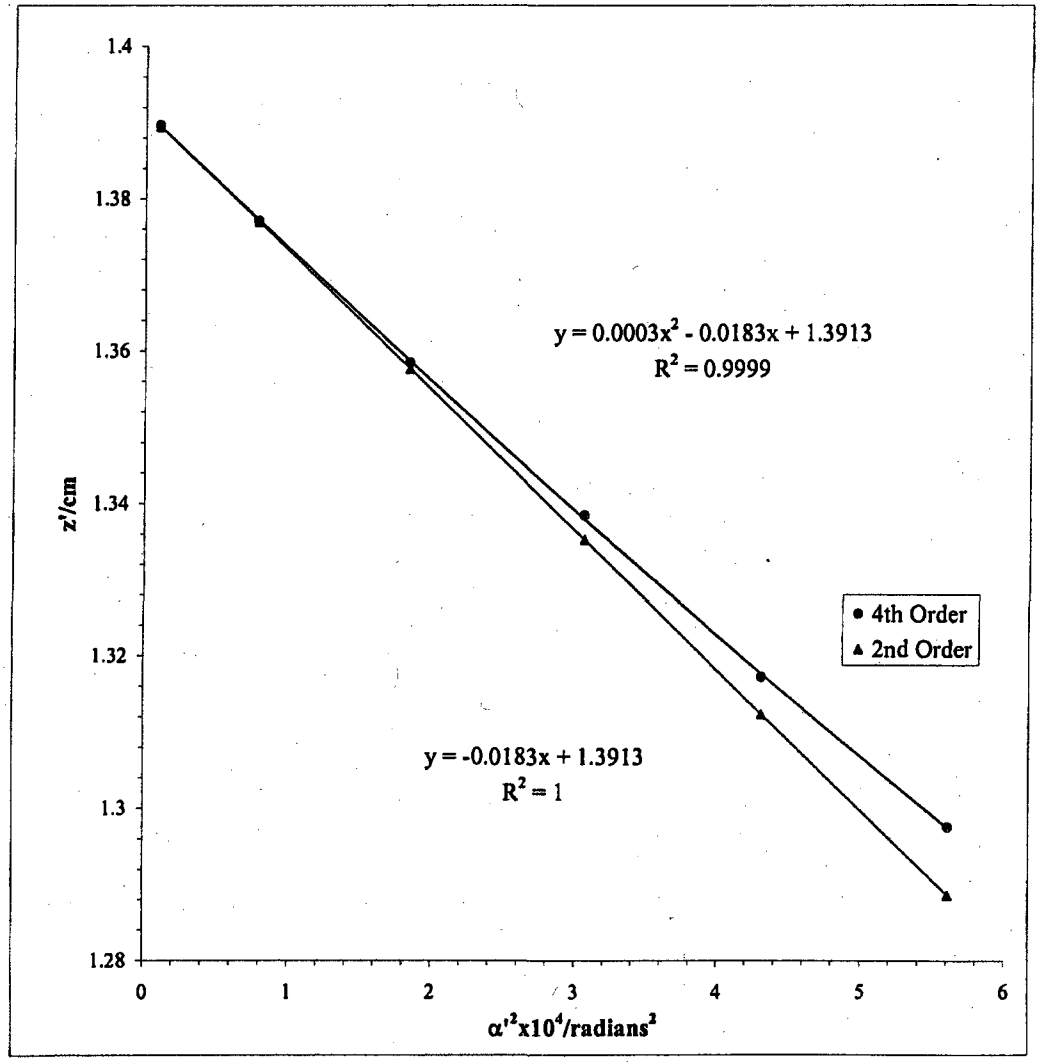

							Beam	Voltage	25 kV
Mesh/inch	I/milliamps	Mesh	z/cm	e_1/cm	a/cm	z_{sp}/cm	z_0'/cm	C_s'/cm	$z_{sp}-z_o'$
600	100	Front	25.08	0.00423	15.56	26.8757	1.389	181.32	25.49

Bar location/ units	Shadow Reading X/cm	Spacing Δ/cm	E/cm	$\alpha \times 10^4$	$\alpha' \times 10^2$	$\alpha'^2 \times 10^4$	m	z'/cm	f/cm
6.5	0.831		0.842	17.684	3.278	10.745	0.05395	1.194	1.292
5.5	0.983	0.152	0.691	14.964	2.699	7.283	0.05545	1.257	1.325
4.5	1.124	0.141	0.551	12.243	2.156	4.650	0.05678	1.305	1.354
3.5	1.257	0.132	0.420	9.522	1.645	2.705	0.05790	1.340	1.379
2.5	1.382	0.125	0.295	6.802	1.157	1.339	0.05878	1.365	1.399
1.5	1.503	0.120	0.175	4.081	0.687	0.472	0.05938	1.380	1.412
0.5	1.620	0.117	0.058	1.360	0.228	0.052	0.05968	1.388	1.419
-0.5	1.736	0.116							
-1.5	1.853	0.117					g/cm	$(\rho/f_0)^2 = (m_0+1)^2\alpha'^2$	
-2.5	1.973	0.120							
-3.5	2.097	0.124					1.124	12.066	
-4.5	2.227	0.130					1.183	8.179	
-5.5	2.366	0.139					1.228	5.222	
-6.5	2.515	0.149					1.260	3.038	
							1.282	1.504	
		Slope	m_o	μ_s			1.296	0.530	
	1.55E-05	-0.0007	0.0597	-117.42			1.303	0.058	

f vs $(\rho/f_o)^2$

$S_f = slope_f / f_0$

	$slope_f$	fo/cm	S_f
0.0002885	-0.01399	1.419	-98.57

g vs $(\rho/f_o)^2$

$S_g = slope_g / f_0$

	$slope_g$	go/cm	S_g
-3.8E-05	-0.01445	1.304	-101.77

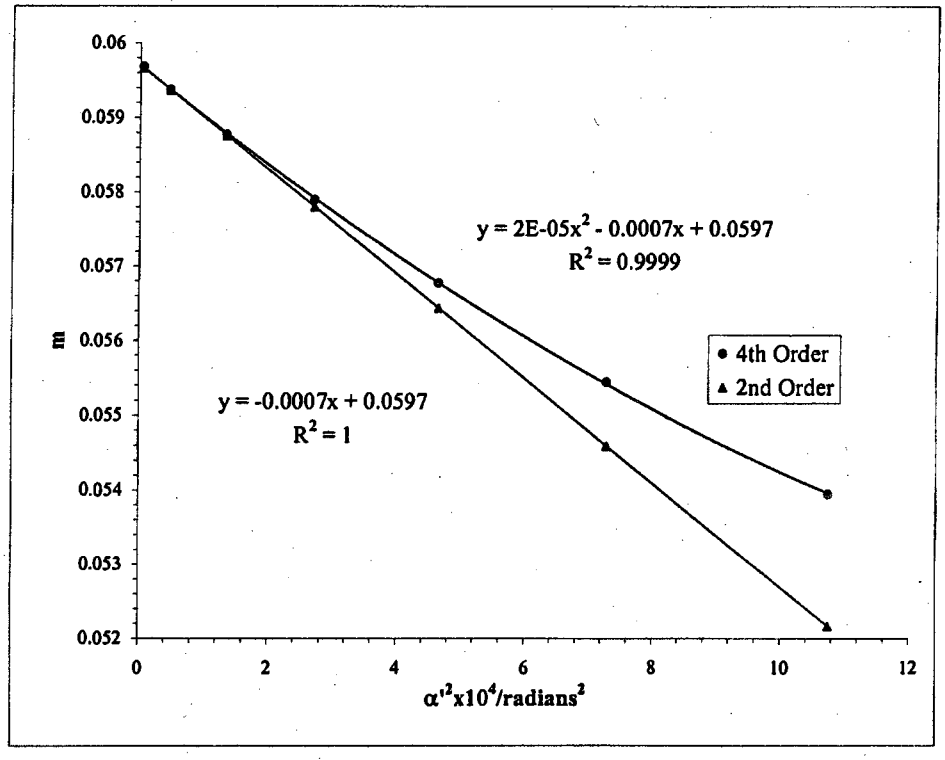

							Beam	Voltage	25 kV
Mesh/inch	I/milliamps	Mesh	z/cm	e_1/cm	a/cm	z_{ip}/cm	z_0'/cm	C_s'/cm	z_{ip}-z_0'
600	100	Front	25.08	0.00423	15.56	26.88	1.389	181.32	25.49

Bar location/ units	Shadow Reading Y/cm	Spacing Δ/cm	E/cm	$\alpha \times 10^4$	$\alpha' \times 10^2$	$\alpha'^2 \times 10^4$	m	z'/cm	f/cm
6	1.417		0.790	16.324	3.078	9.477	0.05303	1.217	1.269
5	1.565	0.147	0.640	13.603	2.498	6.241	0.05445	1.276	1.300
4	1.702	0.138	0.499	10.883	1.954	3.819	0.05569	1.320	1.327
3	1.832	0.130	0.367	8.162	1.439	2.072	0.05670	1.351	1.350
2	1.957	0.125	0.242	5.441	0.947	0.897	0.05746	1.373	1.367
1	2.078	0.121	0.120	2.721	0.470	0.221	0.05792	1.385	1.377
0	2.198	0.119							
-1	2.318	0.120							
-2	2.440	0.123							
-3	2.567	0.127							
-4	2.701	0.134							
-5	2.844	0.143							
-6	2.997	0.153							

g/cm	$(\rho/f_0)^2 = (m_0 + 1)^2 \alpha'^2$
1.150	10.609
1.205	6.987
1.246	4.275
1.275	2.319
1.294	1.004
1.305	0.247

	Slope	m_0	μ_s
1.55E-05	-0.0007	0.058053	-116.5

f vs $(\rho/f_o)^2$

$S_f = slope_f / f_0$

	$slope_f$	fo/cm	S_f
0.0002891	-0.013524	1.380	-98.00

g vs $(\rho/f_o)^2$

$S_g = slope_g / f_0$

	$slope_g$	go/cm	S_g
-3.72216E-05	-0.0146	1.309	-105.77

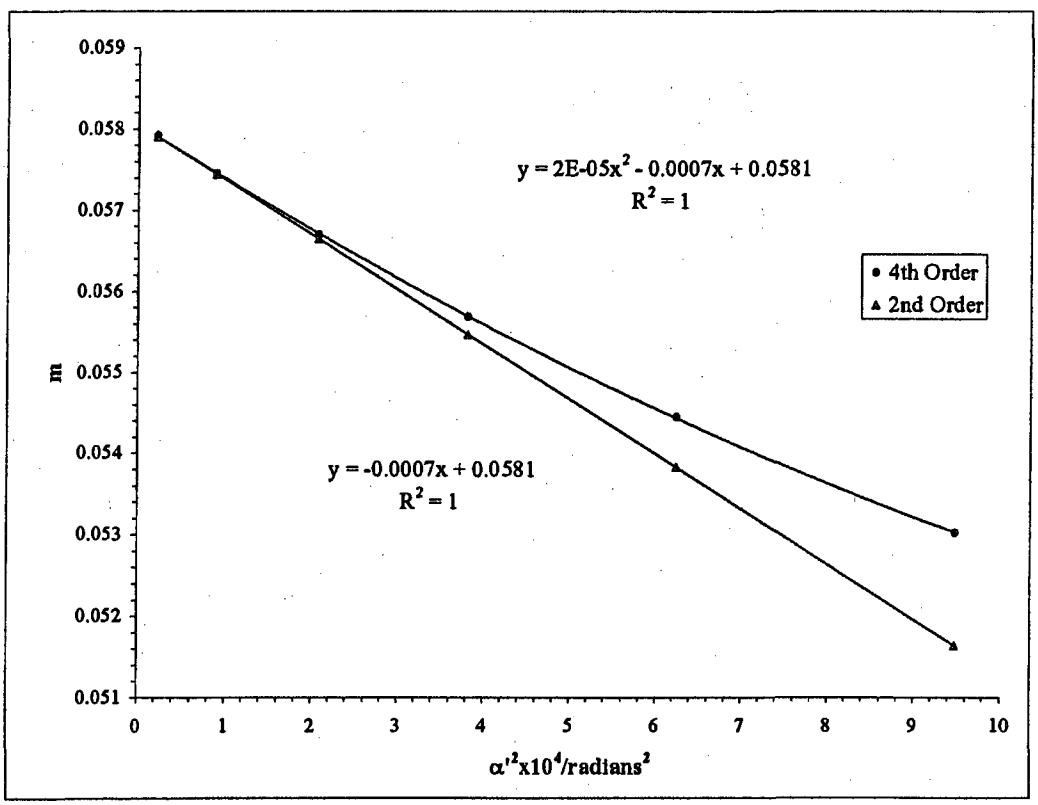

Beam Voltage	I/milliamps	z/cm	z_0'/cm	C_s'/cm
25 kV	100	25.08	1.39	181.3

Average of m_o = 0.0589

Average of μ_s = -117.0

Paraxial properties :

f_o = 1.40 cm

g_o = 1.31 cm

S_f = -98.3

S_g = -103.8

Mesh/inch	I/milliamps	Mesh	e'1/cm	d/cm	b/cm		Beam	Voltage	25 kV
2000	130	Rear	0.00127	26.44	0.432	US			

Bar location/ units	Shadow Reading X/cm	Spacing Δ/cm	E'/cm	M'	c/cm	α' x 10^2	α'^2 x 10^4	z'/cm
11.5	1.644		1.007	-68.98	-0.378	3.8650	14.9383	0.810
10.5	1.763	0.119	0.894	-67.04	-0.389	3.4309	11.7710	0.820
9.5	1.870	0.107	0.790	-65.52	-0.398	3.0348	9.2099	0.829
8.5	1.970	0.100	0.694	-64.26	-0.405	2.6642	7.0978	0.837
7.5	2.064	0.094	0.602	-63.18	-0.412	2.3117	5.3438	0.844
6.5	2.153	0.090	0.514	-62.21	-0.418	1.9732	3.8936	0.850
5.5	2.239	0.086	0.428	-61.34	-0.424	1.6466	2.7113	0.856
4.5	2.322	0.083	0.346	-60.56	-0.430	1.3305	1.7703	0.861
3.5	2.403	0.080	0.266	-59.91	-0.434	1.0238	1.0481	0.866
2.5	2.481	0.078	0.189	-59.39	-0.438	0.7250	0.5257	0.870
1.5	2.557	0.076	0.112	-59.02	-0.441	0.4324	0.1870	0.872
0.5	2.632	0.075	0.037	-58.84	-0.442	0.1437	0.0206	0.874
-0.5	2.707	0.075						
-1.5	2.782	0.075						
-2.5	2.858	0.076			Slope	z_0'/cm	C_s'/cm	
-3.5	2.935	0.077		0.0001	-0.0056	0.871	56.02	
-4.5	3.015	0.079						
-5.5	3.096	0.082						
-6.5	3.180	0.084						
-7.5	3.267	0.087						
-8.5	3.357	0.090						
-9.5	3.451	0.094						
-10.5	3.551	0.100						
-11.5	3.659	0.108						

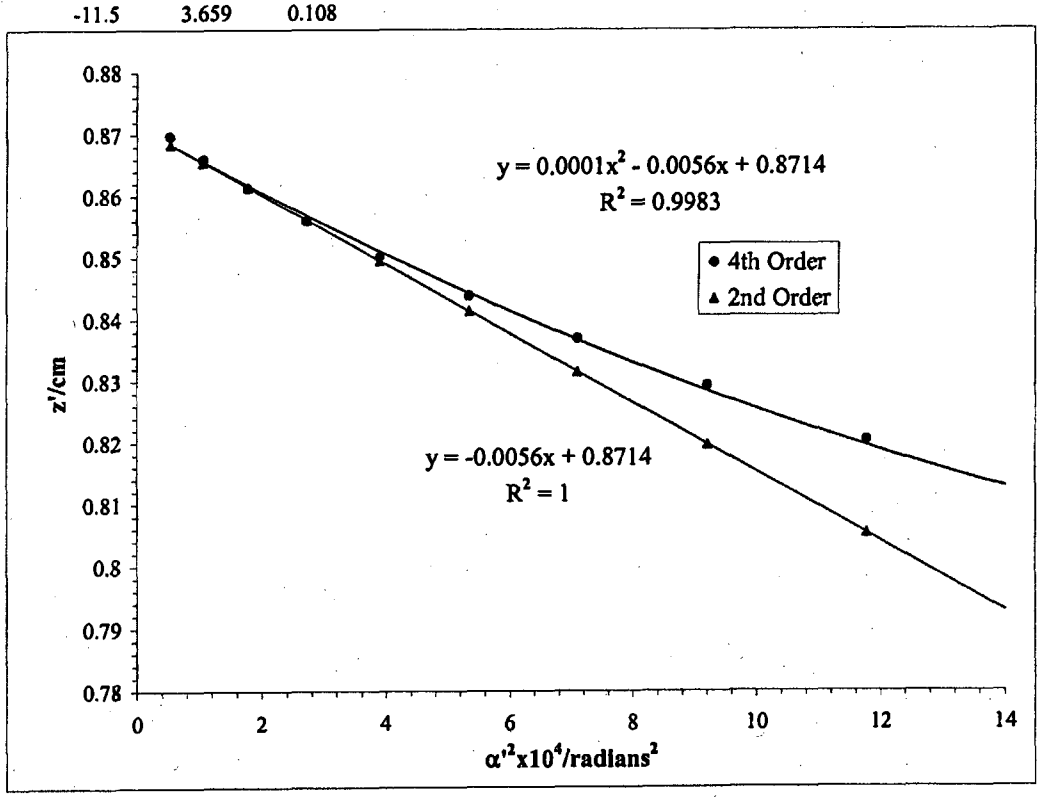

Mesh/inch	I/milliamps	Mesh	e'1/cm	d/cm	b/cm		Beam	Voltage	25 kV
2000	130	Rear	0.00127	26.44	0.432	US			

Bar location/ units	Shadow Reading Y/cm	Spacing Δ/cm	E'/cm	M'	c/cm	$\alpha' \times 10^2$	$\alpha'^2 \times 10^4$	z'/cm
10.5	1.972		0.903	-67.73	-0.385	3.4661	12.0136	0.817
9.5	2.073	0.102	0.798	-66.11	-0.394	3.0620	9.3760	0.826
8.5	2.169	0.095	0.699	-64.80	-0.402	2.6860	7.2148	0.834
7.5	2.260	0.091	0.607	-63.70	-0.409	2.3305	5.4311	0.841
6.5	2.347	0.087	0.518	-62.76	-0.415	1.9905	3.9619	0.847
5.5	2.431	0.085	0.433	-61.96	-0.420	1.6629	2.7654	0.852
4.5	2.514	0.082	0.350	-61.27	-0.425	1.3458	1.8111	0.856
3.5	2.594	0.080	0.270	-60.71	-0.429	1.0372	1.0759	0.860
2.5	2.672	0.078	0.191	-60.27	-0.432	0.7357	0.5412	0.863
1.5	2.749	0.077	0.114	-59.97	-0.434	0.4393	0.1929	0.865
0.5	2.825	0.076	0.038	-59.82	-0.435	0.1461	0.0213	0.867
-0.5	2.901	0.076						
-1.5	2.978	0.076						
-2.5	3.055	0.077			Slope	z_o'/cm	C_s'/cm	
-3.5	3.133	0.079		9.29E-05	-0.0052	0.866	52.01	
-4.5	3.214	0.081						
-5.5	3.297	0.083						
-6.5	3.383	0.086						
-7.5	3.473	0.090						
-8.5	3.568	0.095						
-9.5	3.669	0.101						
-10.5	3.778	0.109						

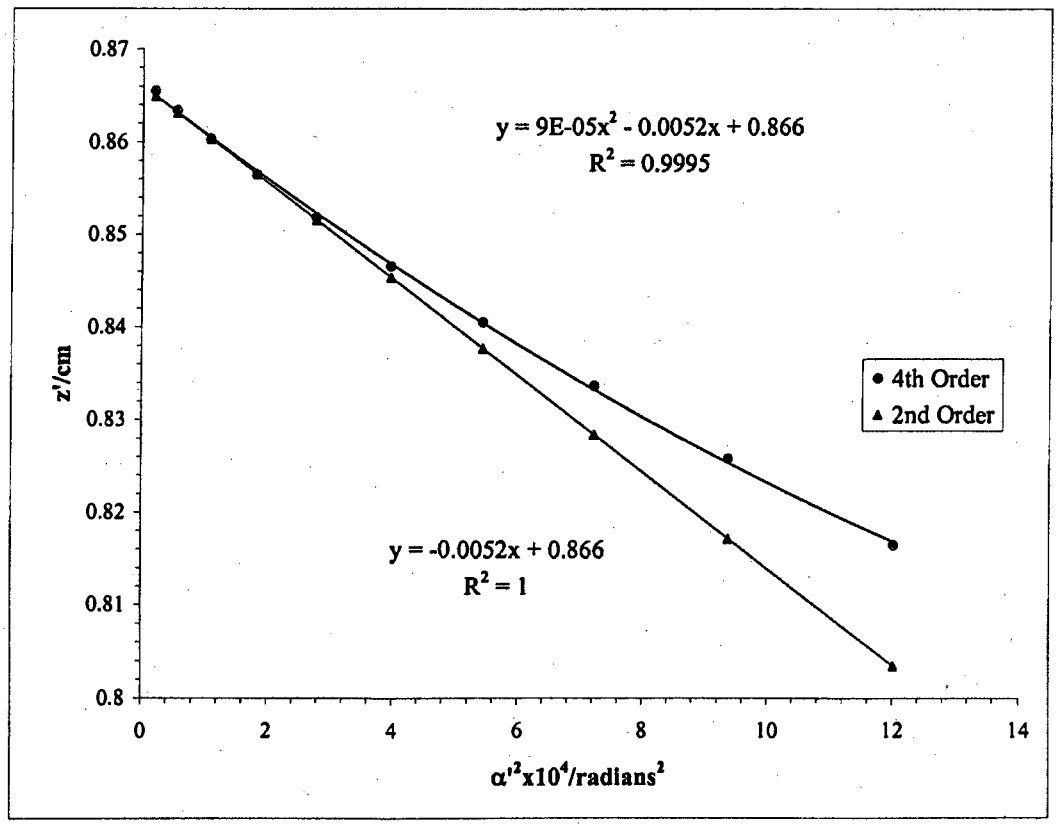

Mesh/inch	I/milliamps	Mesh	e'1/cm	d/cm	b/cm		Beam	Voltage	25 kV
2000	130	Rear	0.00127	25.91	0.965	DS			

Bar location/ units	Shadow Reading X/cm	Spacing Δ/cm	E'/cm	M'	c/cm	α' x 10^2	α'^{2} x 10^4	z'/cm
5	1.923		0.945	148.86	0.175	3.624	13.132	0.790
4	2.059	0.135	0.813	159.99	0.163	3.117	9.717	0.802
3	2.216	0.158	0.662	173.83	0.150	2.541	6.459	0.815
2	2.409	0.193	0.480	189.10	0.138	1.844	3.400	0.827
1	2.641	0.232	0.259	204.05	0.128	0.995	0.990	0.838
0	2.907	0.266						
-1	3.160	0.253						
-2	3.370	0.210			Slope	z_o'/cm	C_s'/cm	
-3	3.541	0.171		2.9E-05	-0.0043	0.842	43.36	
-4	3.684	0.143						
-5	3.814	0.130						

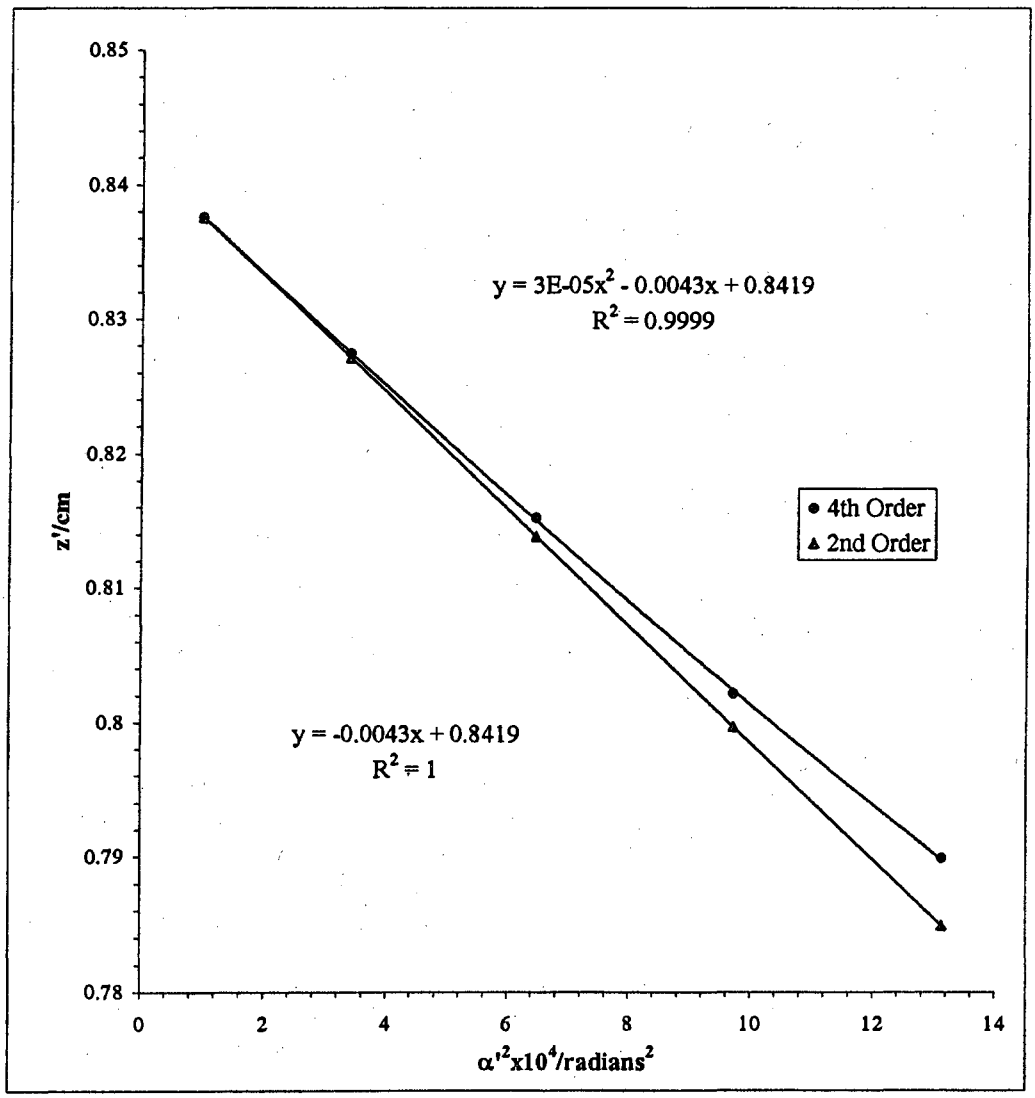

Mesh/inch	I/milliamps	Mesh	e'1/cm	d/cm	b/cm		Beam	Voltage	25 kV
2000	130	Rear	0.00127	25.91	0.965	DS			

Bar location/ units	Shadow Reading Y/cm	Spacing Δ/cm	E'/cm	M'	c/cm	α' x 10^2	α'^2 x 10^4	z'/cm
5.5	1.994	1.994	1.003	143.53	0.182	3.842	14.763	0.783
4.5	2.118	0.124	0.878	153.56	0.170	3.365	11.323	0.795
3.5	2.258	0.141	0.736	165.61	0.157	2.824	7.975	0.808
2.5	2.423	0.164	0.569	179.26	0.145	2.184	4.772	0.820
1.5	2.618	0.196	0.370	194.30	0.134	1.421	2.020	0.831
0.5	2.855	0.237	0.132	207.12	0.126	0.505	0.255	0.839
-0.5	3.118	0.263						
-1.5	3.359	0.240						
-2.5	3.561	0.203						
-3.5	3.731	0.170						
-4.5	3.873	0.142			Slope	z_0'/cm	C_s'/cm	
-5.5	3.999	0.126		3.9E-05	-0.0044	0.840	44.19	

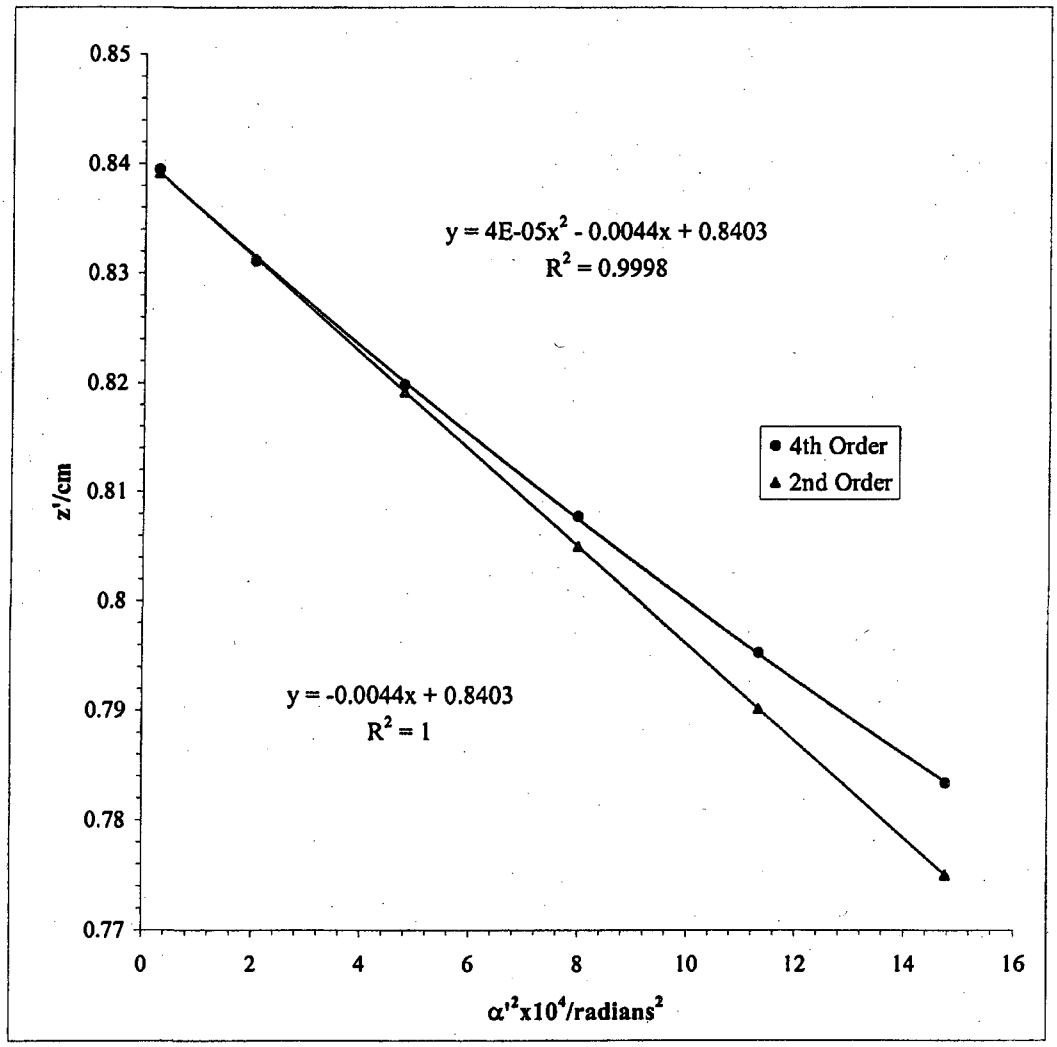

							Beam	Voltage	25 kV
Mesh/inch	I/milliamps	Mesh	z/cm	e_1/cm	a/cm	z_{sp}/cm	z_0'/cm	C_s'/cm	$z_{sp}-z_0'$
600	130	Front	25.08	0.00423	15.56	26.88	0.855	48.89	26.02

Bar location/ units	Shadow Reading X/cm	Spacing Δ/cm	E/cm	$\alpha \times 10^4$	$\alpha' \times 10^2$	$\alpha'^2 \times 10^4$	m	z'/cm	f/cm
5.5	1.610		1.180	14.964	4.516	20.396	0.03313	0.755	0.807
4.5	1.857	0.247	0.937	12.243	3.593	12.912	0.03407	0.792	0.828
3.5	2.086	0.229	0.712	9.522	2.731	7.459	0.03487	0.818	0.847
2.5	2.301	0.215	0.499	6.802	1.916	3.673	0.03549	0.837	0.861
1.5	2.506	0.205	0.296	4.081	1.136	1.291	0.03592	0.849	0.872
0.5	2.705	0.199	0.098	1.360	0.376	0.142	0.03614	0.854	0.877
-0.5	2.900	0.196							
-1.5	3.097	0.197					g/cm	$(\rho/f_0)^2 = (m_0+1)^2\alpha'^2$	
-2.5	3.299	0.202							
-3.5	3.509	0.210					0.728	21.898	
-4.5	3.731	0.222					0.764	13.863	
-5.5	3.969	0.238					0.789	8.008	
							0.806	3.943	
		Slope	m_0	μ_s			0.817	1.386	
	1.91E-06	-0.00019	0.036161	-51.77			0.823	0.152	

f vs $(\rho/f_o)^2$

$S_f = slope_f / f_0$

	$slope_f$	f_0/cm	S_f
3.9706E-05	-0.00408	0.877	-46.48

g vs $(\rho/f_o)^2$

$S_g = slope_g / f_0$

	$slope_g$	g_0/cm	S_g
-3.2E-06	-0.0042566	0.823	-48.53

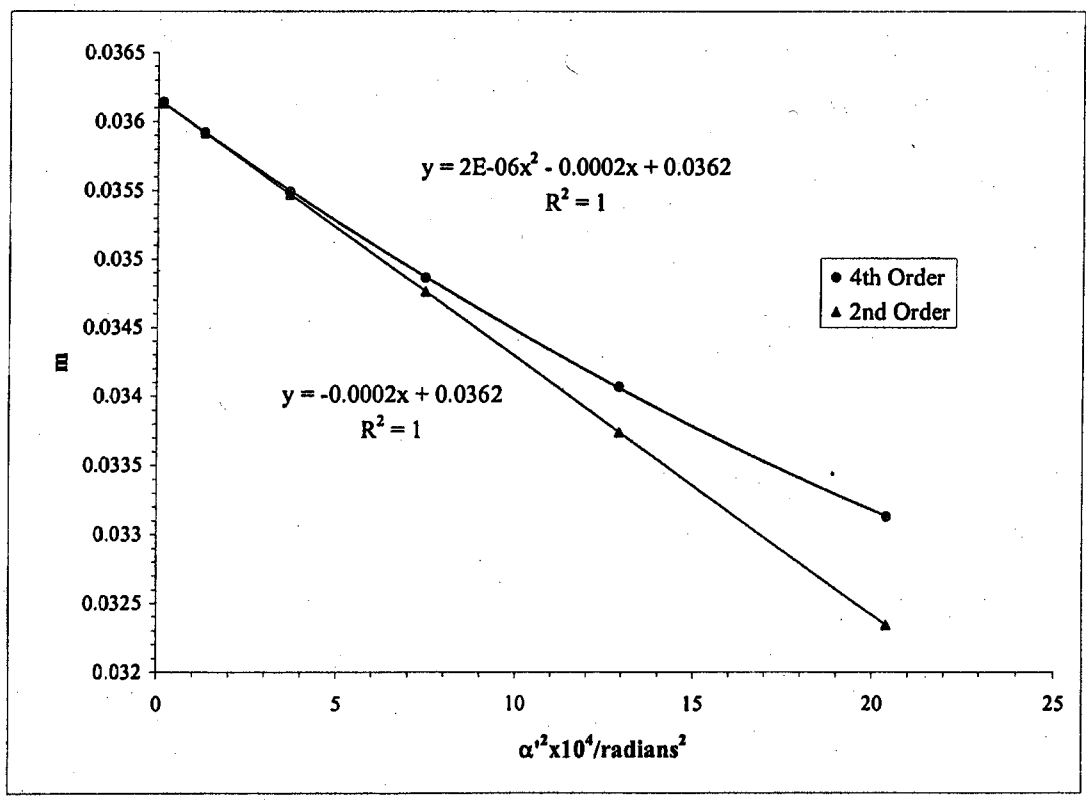

							Beam	Voltage	25 kV
Mesh/inch	I/milliamps	Mesh	z/cm	e_1/cm	a/cm	z_{sp}/cm	z_0'/cm	C_s'/cm	$z_{sp}-z_0'$
600	130	Front	25.08	0.00423	15.56	26.88	0.855	48.89	26.02

Bar location/ units	Shadow Reading Y/cm	Spacing Δ/cm	E/cm	$\alpha \times 10^4$	$\alpha' \times 10^2$	$\alpha'^2 \times 10^4$	m	z'/cm	f/cm
5	1.678		1.109	13.603	4.247	18.034	0.03203	0.767	0.780
4	1.926	0.247	0.860	10.883	3.298	10.878	0.03300	0.802	0.802
3	2.155	0.229	0.630	8.162	2.418	5.844	0.03376	0.826	0.820
2	2.370	0.215	0.412	5.441	1.584	2.510	0.03434	0.843	0.833
1	2.577	0.207	0.206	2.721	0.791	0.626	0.03440	0.852	0.834
0	2.784	0.207							
-1	2.989	0.205							
-2	3.195	0.206							
-3	3.414	0.219							
-4	3.645	0.231							
-5	3.896	0.250							

m	g/cm	$(\rho/f_0)^2 = (m_0+1)^2\alpha'^2$
	0.742	19.310
	0.775	11.648
	0.799	6.258
	0.814	2.688
	0.823	0.670

	Slope	m_o	μ_s
1.79E-06	-0.0002	0.03479	-53.24

f vs $(\rho/f_o)^2$

S_f = slope$_f$ / f_0

	slope$_f$	fo/cm	S_f
3.749E-05	-0.004	0.844	-47.98

g vs $(\rho/f_o)^2$

S_g = slope$_g$ / f_0

	slope$_g$	go/cm	S_g
-3E-06	-0.0043	0.826	-50.75

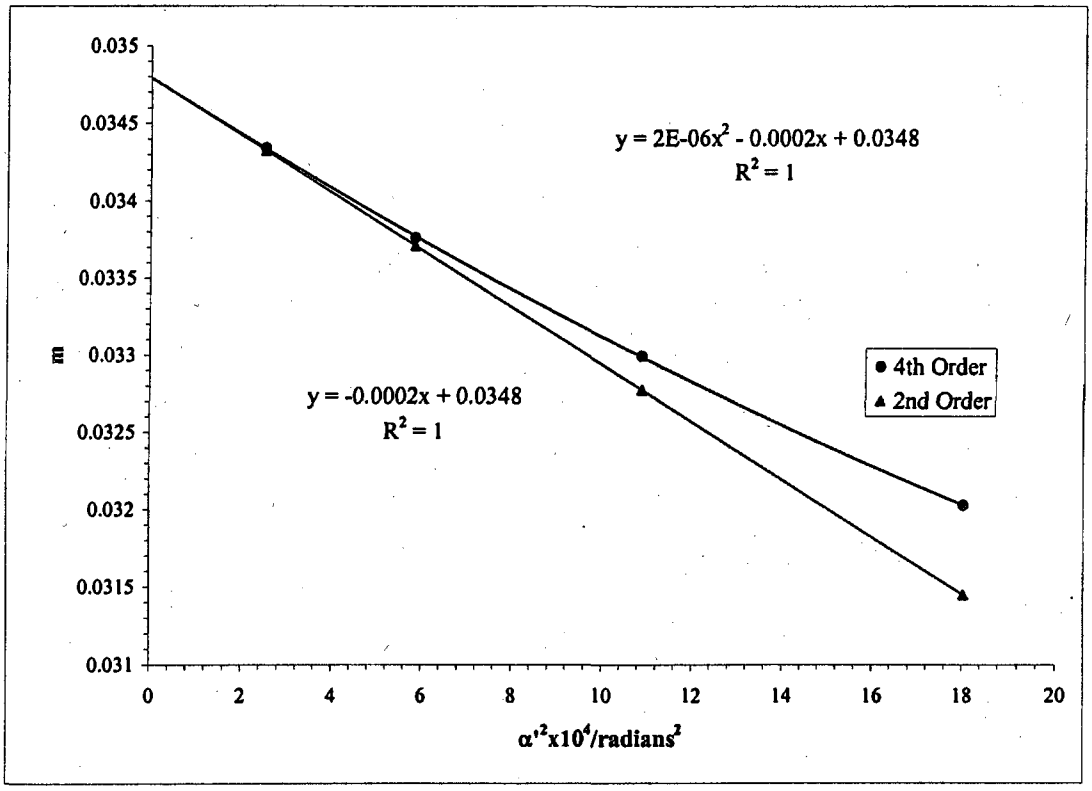

Beam Voltage	I/milliamps	z/cm	z_0'/cm	C_s'/cm
25 kV	130	25.08	0.855	48.9

Average of m_o = 0.0355

Average of μ_s = -52.5

Paraxial properties :

f_o = 0.861 cm

g_o = 0.824 cm

S_f = -47.2

S_g = -49.6

Mesh/inch	I/milliamps	Mesh	e'_1/cm	d/cm	b/cm		Beam	Voltage	25 kV
2000	150	Rear	0.00127	26.44	0.432	US			

Bar location/ units	Shadow Reading X/cm	Spacing Δ/cm	E'/cm	M'	c/cm	α' x 10^2	α'^2 x 10^4	z'/cm
6.5	1.245		0.891	-108.0	-0.243	3.402	11.5761	0.674
5.5	1.400	0.155	0.738	-105.6	-0.248	2.816	7.9316	0.680
4.5	1.546	0.146	0.592	-103.6	-0.253	2.262	5.1146	0.685
3.5	1.685	0.139	0.454	-102.1	-0.257	1.732	3.0013	0.688
2.5	1.819	0.134	0.320	-100.9	-0.260	1.223	1.4962	0.691
1.5	1.949	0.130	0.191	-100.1	-0.262	0.728	0.5303	0.693
0.5	2.077	0.128	0.063	-99.7	-0.263	0.242	0.0585	0.694
-0.5	2.203	0.127						
-1.5	2.330	0.127						
-2.5	2.460	0.129						
-3.5	2.593	0.133			Slope	z_0'/cm	C_s'/cm	
-4.5	2.731	0.138		3.45E-05	-0.0021	0.695	21.32	
-5.5	2.875	0.145						
-6.5	3.028							

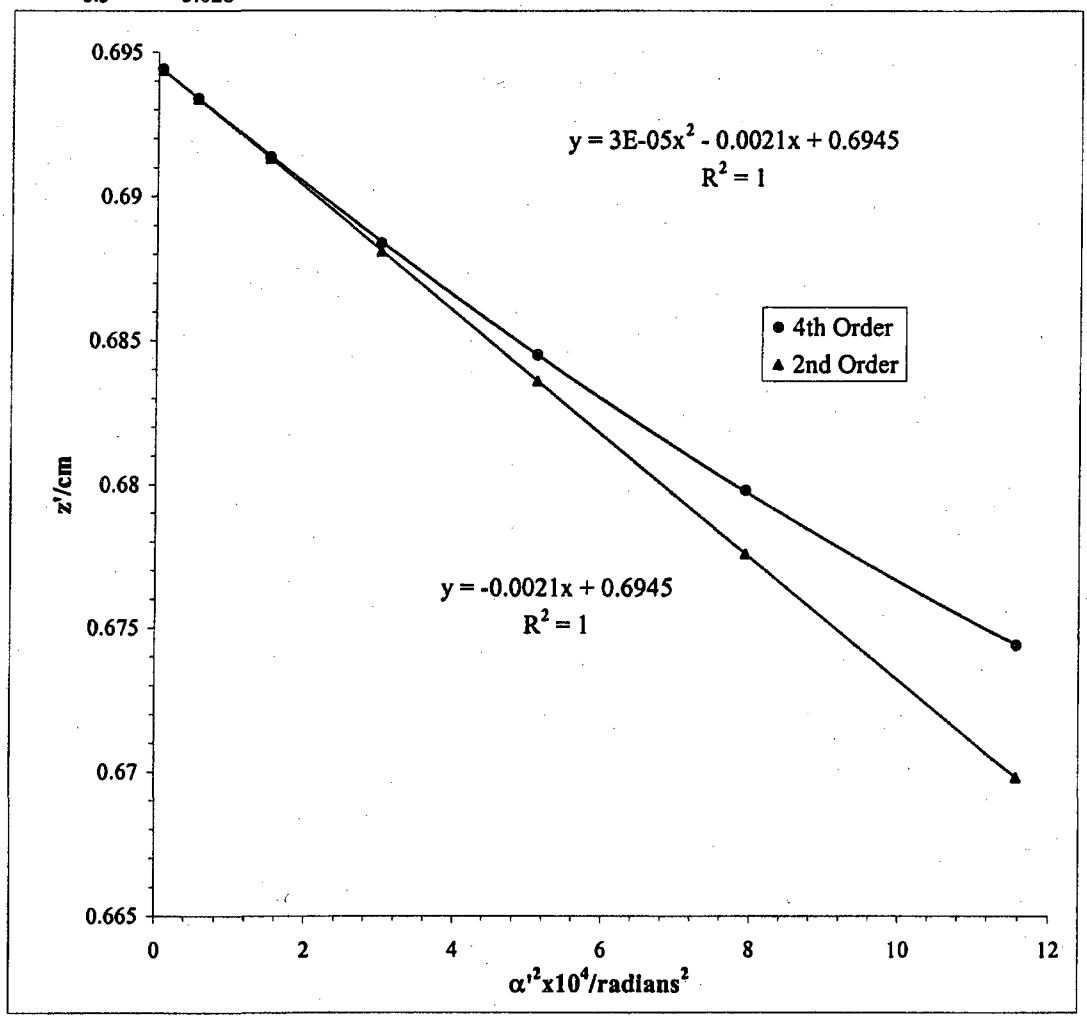

Mesh/inch	I/milliamps	Mesh	e'_1/cm	d/cm	b/cm		Beam	Voltage	25 kV
2000	150	Rear	0.00127	26.44	0.432	US			

Bar location/ units	Shadow Reading Y/cm	Spacing Δ/cm	E'/cm	M'	c/cm	$\alpha' \times 10^2$	$\alpha'^2 \times 10^4$	z'/cm
6	1.478		0.966	-126.7	-0.207	3.6804	13.5452	0.639
5	1.657	0.179	0.769	-121.1	-0.217	2.9309	8.5899	0.648
4	1.821	0.163	0.596	-117.3	-0.223	2.2733	5.1679	0.655
3	1.974	0.154	0.438	-115.0	-0.228	1.6706	2.7909	0.660
2	2.121	0.146	0.288	-113.4	-0.231	1.0988	1.2074	0.663
1	2.266	0.145	0.142	-111.9	-0.234	0.5422	0.2939	0.666
0	2.412	0.146						
-1	2.550	0.138						
-2	2.697	0.147						
-3	2.850	0.153			Slope	z_0'/cm	C_s'/cm	
-4	3.013	0.162		1.42E-05	-0.0022	0.666	22.01	
-5	3.195	0.182						
-6	3.410	0.215						

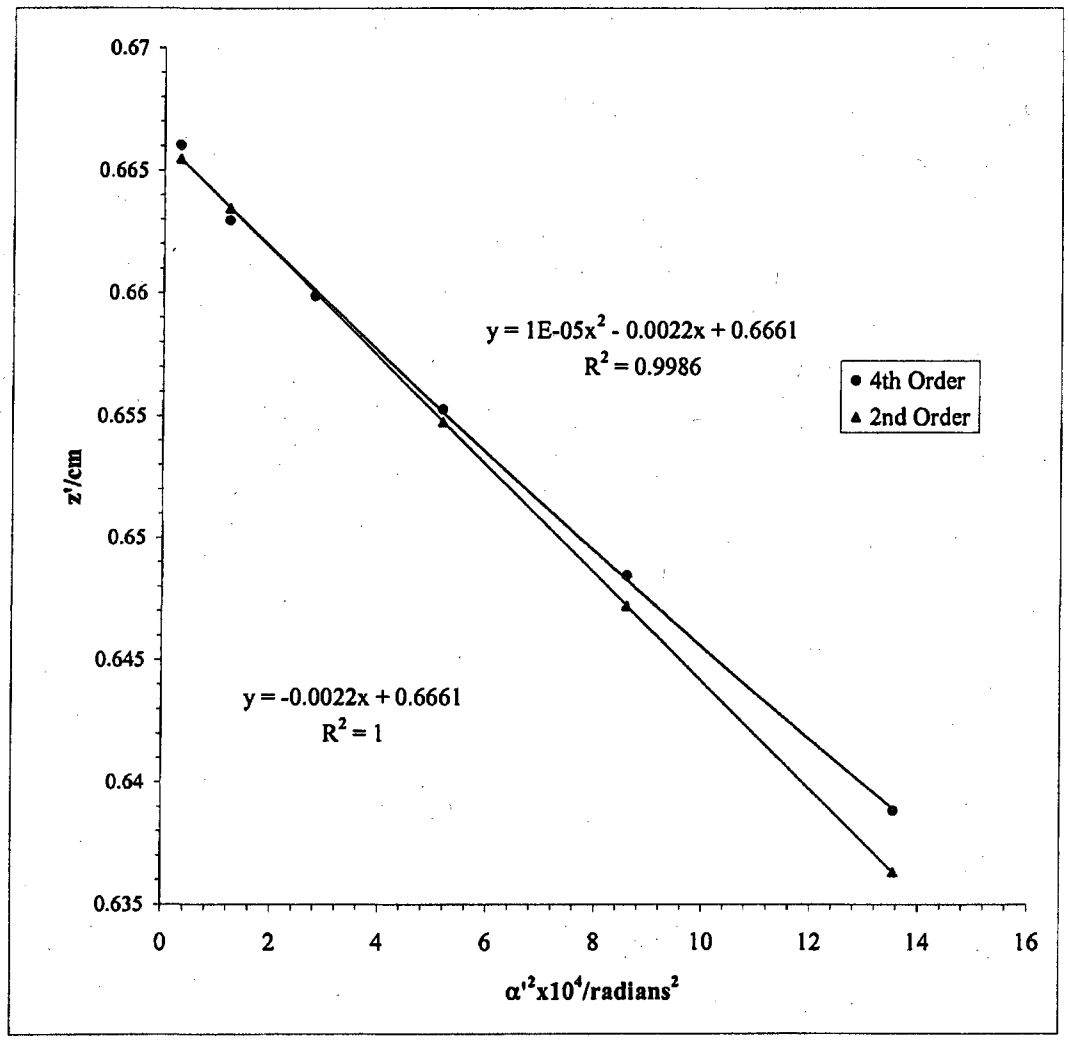

Mesh/inch	I/milliamps	Mesh	e'_1/cm	d/cm	b/cm		Beam	Voltage	25 kV
2000	150	Rear	0.00127	26.11	0.767	DS			

Bar location/ units	Shadow Reading X/cm	Spacing Δ/cm	E'/cm	M'	c/cm	α' x 10^2	α'^2 x 10^4	z'/cm
4.5	1.699		1.027	179.8	0.146	3.9133	15.3141	0.621
3.5	1.875	0.176	0.852	191.7	0.137	3.2464	10.5393	0.630
2.5	2.079	0.204	0.650	204.6	0.128	2.4763	6.1321	0.639
1.5	2.320	0.242	0.414	217.3	0.121	1.5784	2.4913	0.646
0.5	2.593	0.273	0.144	226.8	0.116	0.5491	0.3015	0.651
-0.5	2.881	0.288						
-1.5	3.148	0.267						
-2.5	3.378	0.230			Slope	z_0'/cm	C_s'/cm	
-3.5	3.579	0.200		0.0000	-0.0022	0.652	22.19	
-4.5	3.754	0.175						

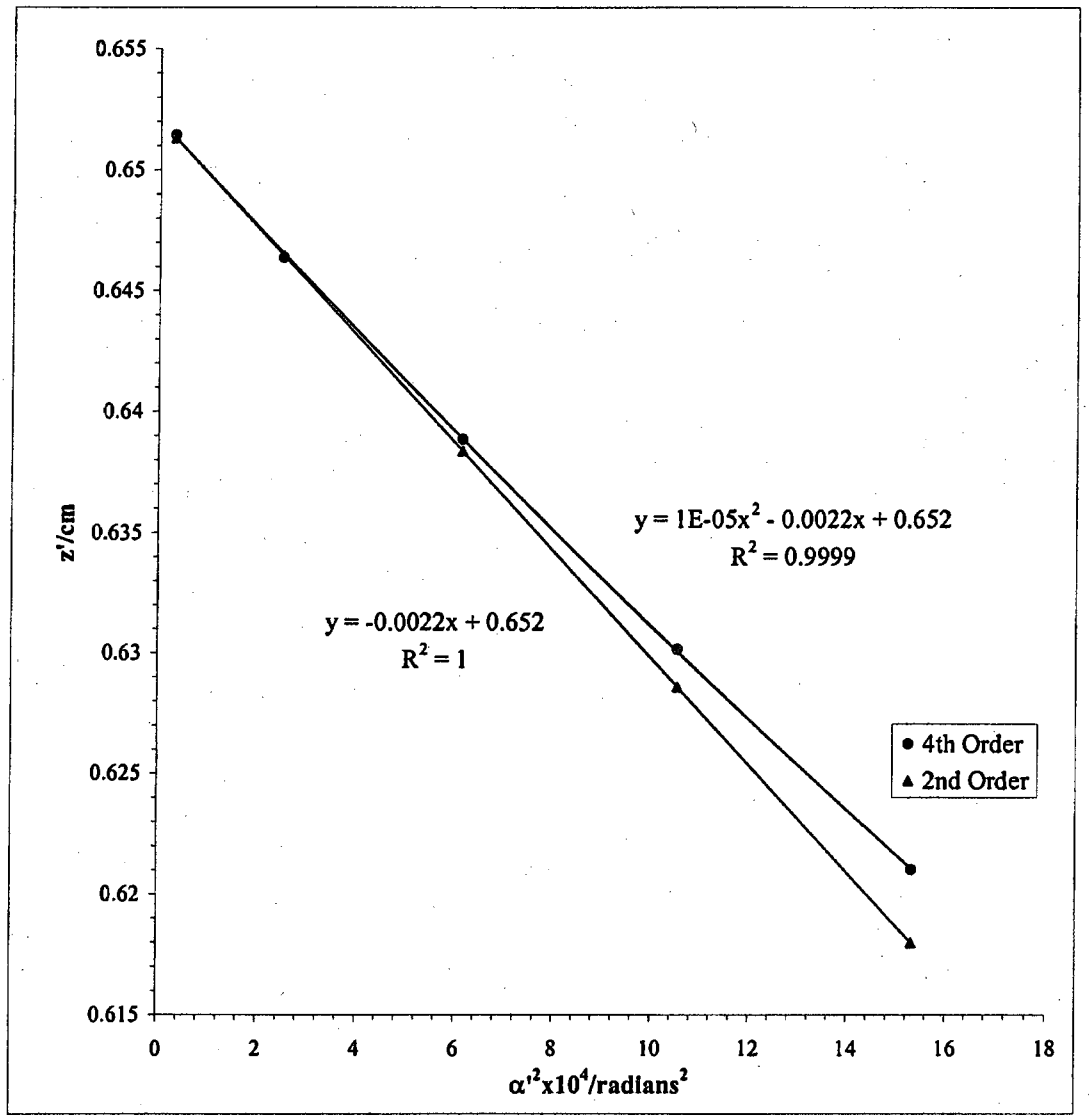

Mesh/inch	I/milliamps	Mesh	e'_1/cm	d/cm	b/cm	Number	Beam	Voltage	25 kV
2000	150	Rear	0.00127	26.11	0.767	DS			

Bar location/ units	Shadow Reading Y/cm	Spacing Δ/cm	E'/cm	M'	c/cm	$\alpha'^2 \times 10^2$	$\alpha'^2 \times 10^4$	z'/cm
4.5	2.187	2.187	1.0222	178.9	0.147	3.8931	15.1564	0.620
3.5	2.368	0.181	0.8440	189.9	0.138	3.2157	10.3406	0.629
2.5	2.573	0.205	0.6433	202.6	0.130	2.4517	6.0108	0.638
1.5	2.814	0.241	0.4088	214.6	0.122	1.5585	2.4289	0.645
0.5	3.086	0.273	0.1416	223.1	0.118	0.5401	0.2917	0.650
-0.5	3.370	0.283						
-1.5	3.631	0.262						
-2.5	3.860	0.228						
-3.5	4.056	0.196						
-4.5	4.232	0.176						

	Slope	z_0'/cm	C_s'/cm
1.55E-05	-0.0022	0.650	22.08

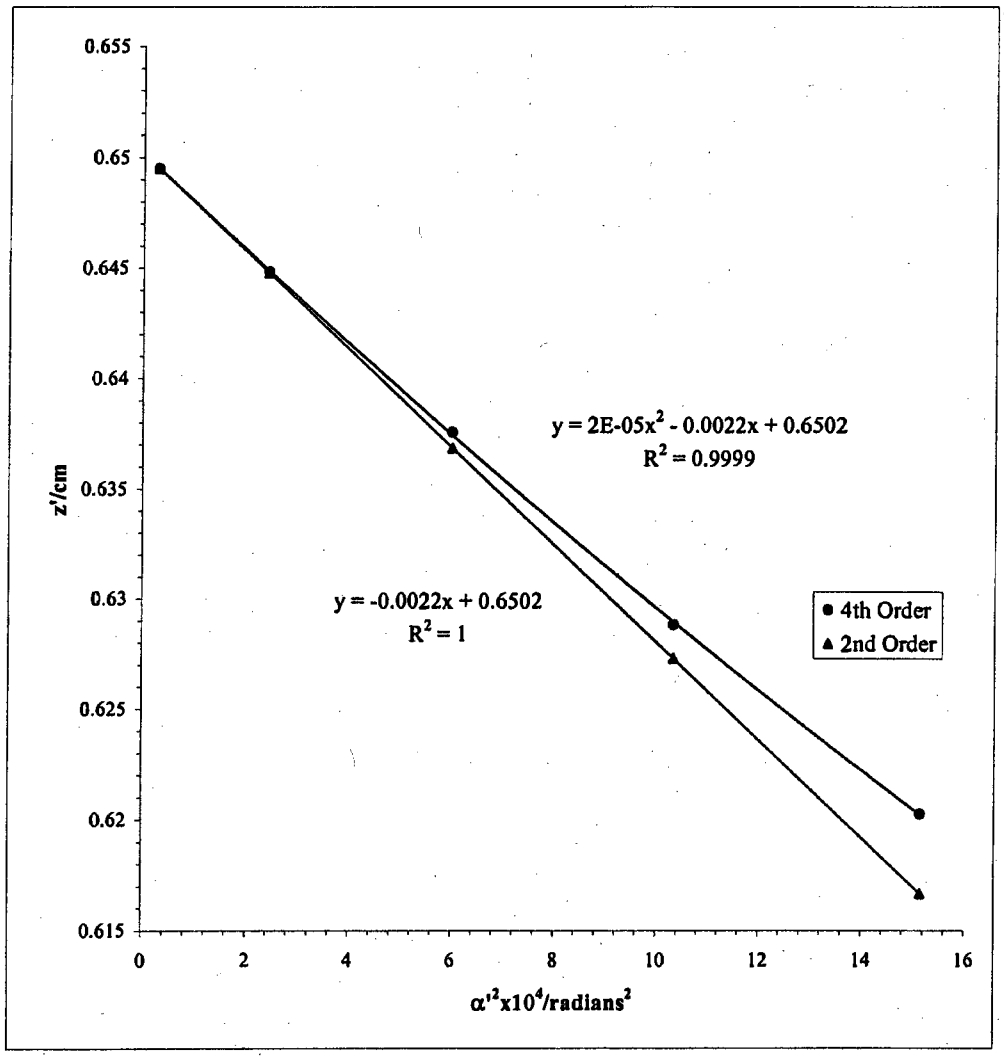

							Beam	Voltage	25 kV
Mesh/inch	I/milliamps	Mesh	z/cm	e_1/cm	a/cm	z_{sp}/cm	z_0'/cm	C_0'/cm	$z_{sp}-z_o'$
600	150	Front	25.08	0.00423	15.56	26.88	0.666	21.90	26.21

Bar location/ units	Shadow Reading X/cm	Spacing Δ/cm	E/cm	$\alpha \times 10^4$	$\alpha' \times 10^2$	$\alpha'^2 \times 10^4$	m	z'/cm	f/cm
7	1.331		2.155	19.045	8.177	66.861	0.02329	0.519	0.572
6	1.715	0.384	1.771	16.324	6.732	45.323	0.02425	0.566	0.595
5	2.060	0.345	1.426	13.603	5.426	29.439	0.02507	0.601	0.614
4	2.373	0.313	1.110	10.883	4.229	17.885	0.02573	0.627	0.630
3	2.667	0.294	0.812	8.162	3.095	9.580	0.02637	0.645	0.645
2	2.941	0.273	0.534	5.441	2.037	4.150	0.02671	0.657	0.653
1	3.210	0.269	0.264	2.721	1.008	1.017	0.02698	0.663	0.659
0	3.473	0.264							
-1	3.738	0.265					g/cm	$(\rho/f_0)^2 = (m_0+1)^2\alpha'^2$	
-2	4.009	0.270							
-3	4.2910	0.282					0.506	70.525	
-4	4.5933	0.302					0.552	47.807	
-5	4.9113	0.318					0.586	31.052	
-6	5.2573	0.346					0.610	18.865	
-7	5.6413	0.384					0.628	10.105	
							0.639	4.378	
			Slope	m_0	μ_s		0.646	1.072	
		2.9E-07	-0.0001	0.02704	-27.97				

f vs $(\rho/f_o)^2$

$S_f = slope_f / f_0$

	$slope_f$	fo/cm	S_f
6.398E-06	-0.0017	0.661	-25.72

g vs $(\rho/f_o)^2$

$S_g = slope_g / f_0$

	$slope_g$	go/cm	S_g
-3.9E-07	-0.00198	0.648	-30.05

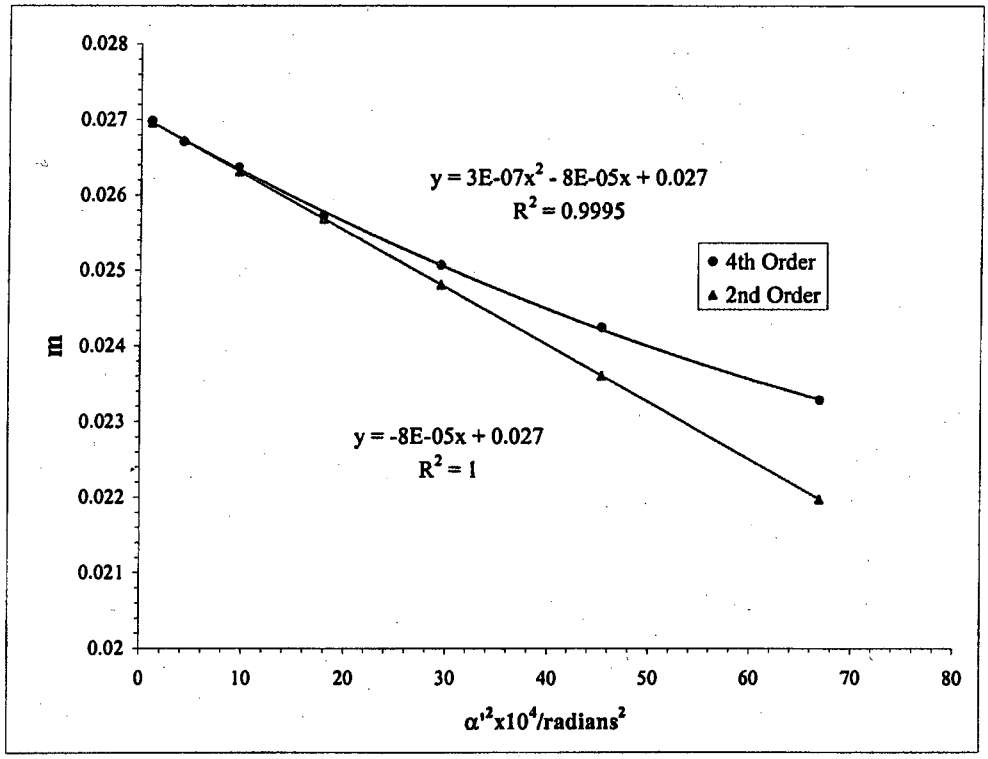

							Beam	Voltage	25 kV
Mesh/inch	I/milliamps	Mesh	z/cm	e_1/cm	a/cm	z_{sp}/cm	z_0'/cm	C_s'/cm	$z_{sp}-z_o'$
600	150	Δ/cm	25.08	0.00423	15.56	26.88	0.666	21.90	26.21

Bar location/ units	Shadow Reading Y/cm	Spacing D/cm	E/cm	$\alpha \times 10^4$	$\alpha' \times 10^2$	$\alpha'^2 \times 10^4$	m	z'/cm	f/cm
7.5	0.341		2.441	20.405	9.245	85.478	0.02207	0.478	0.543
6.5	0.777	0.436	2.009	17.684	7.629	58.206	0.02318	0.538	0.569
5.5	1.159	0.382	1.628	14.964	6.191	38.331	0.02417	0.582	0.592
4.5	1.504	0.345	1.286	12.243	4.899	23.996	0.02499	0.613	0.612
3.5	1.819	0.314	0.973	9.522	3.709	13.759	0.02567	0.636	0.628
2.5	2.110	0.291	0.682	6.802	2.602	6.770	0.02614	0.651	0.639
1.5	2.391	0.281	0.402	4.081	1.532	2.349	0.02663	0.661	0.651
0.5	2.660	0.269	0.133	1.360	0.508	0.258	0.02676	0.665	0.654
-0.5	2.927	0.266							
-1.5	3.195	0.268						g/cm	$(\rho/f_0)^2 = (m_0+1)^2 \alpha'^2$
-2.5	3.475								
-3.5	3.7654							0.466	90.111
-4.5	4.0774							0.525	61.361
-5.5	4.4153							0.567	40.409
-6.5	4.7958			Slope	m_o	μ_a		0.598	25.296
-7.5	5.2221		2.8E-07	-0.0001	0.026743	-29.35		0.619	14.505
								0.634	7.137
								0.643	2.476
								0.648	0.272

f vs $(\rho/f_o)^2$

$S_f = slope_f / f_0$

	$slope_f$	fo/cm	S_f
6.124E-06	-0.0017679	0.653	-27.06

g vs $(\rho/f_o)^2$

$S_g = slope_g / f_0$

	$slope_g$	go/cm	S_g
-3.7E-07	-0.001984	0.648	-30.37

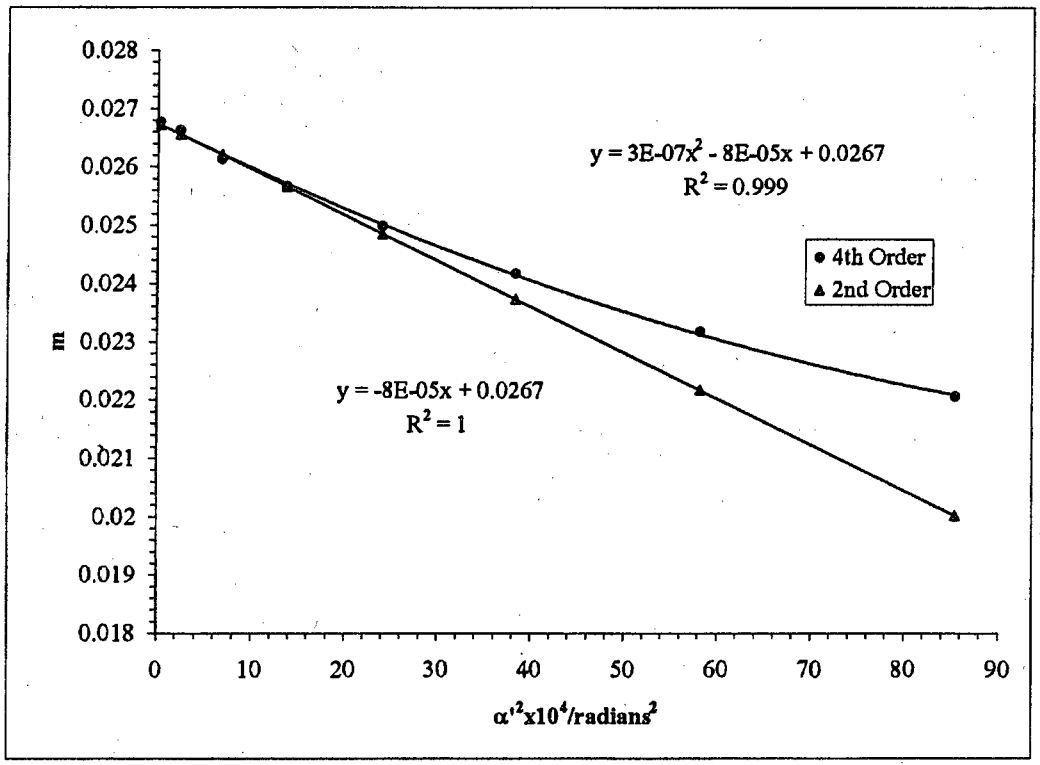

Beam Voltage	I/milliamps	z/cm	z_0'/cm	C_s'/cm
25 kV	150	25.1	0.666	21.9

Average of m_0 = 0.0269

Average of μ_s = -28.7

Paraxial properties :

f_o = 0.657 cm

g_o = 0.648 cm

S_f = -26.4

S_g = -30.2

Mesh/inch	I/milliamps	Mesh	e'_1/cm	d/cm	b/cm		Beam	Voltage	25 kV
2000	180	Rear	0.00127	26.33	0.541	DS			

Bar location/ units	Shadow Reading X/cm	Spacing Δ/cm	E'/cm	M'	c/cm	α' x 10^2	α'^2 x 10^4	z'/cm
3.5	1.712		1.272	286.2	0.092	4.8132	23.1673	0.449
2.5	2.013	0.301	0.981	308.9	0.086	3.7116	13.7757	0.455
1.5	2.368	0.355	0.635	333.1	0.079	2.4025	5.7718	0.462
0.5	2.788	0.420	0.222	349.4	0.076	0.8401	0.7057	0.465
-0.5	3.232	0.444						
-1.5	3.637	0.405			Slope	z_o'/cm	C_s'/cm	
-2.5	3.974	0.337		0.0000	-0.0008	0.466	7.738	
-3.5	4.256	0.282						

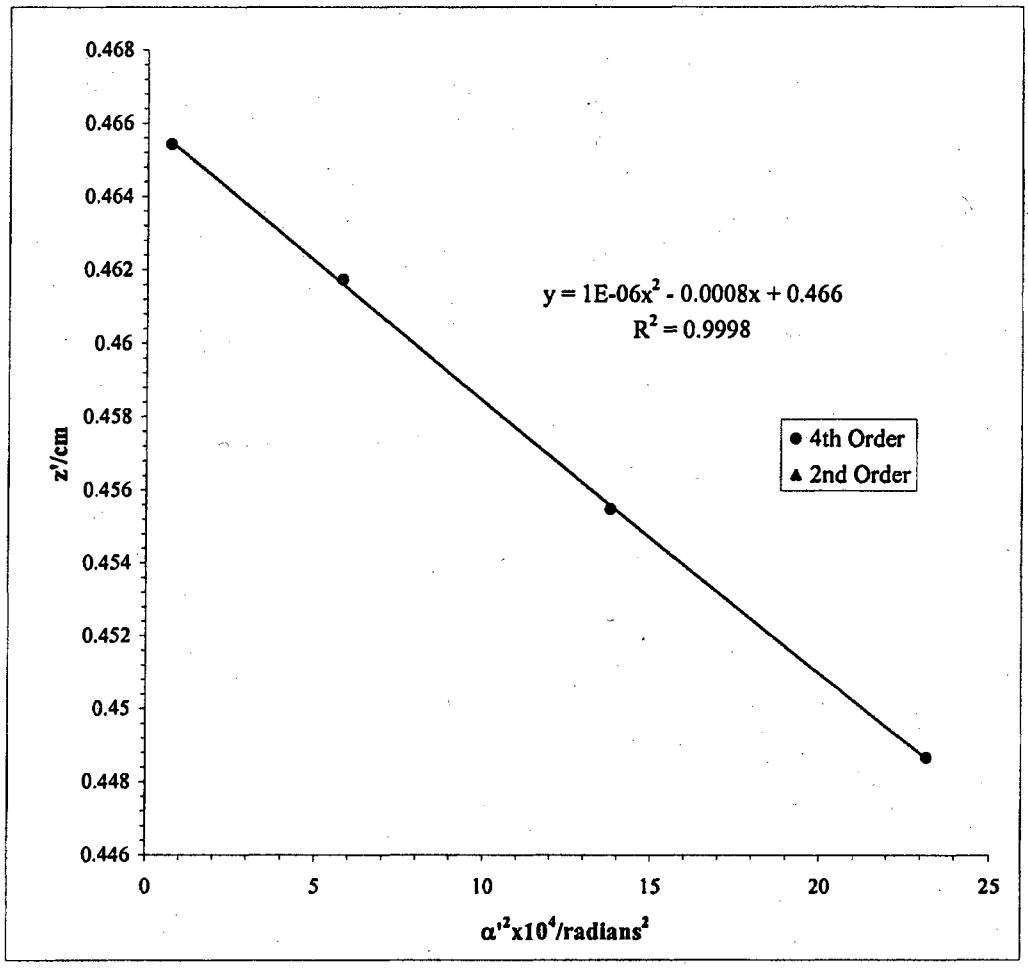

Mesh/inch	I/milliamps	Mesh	e'_1/cm	d/cm	b/cm		Beam	Voltage	25 kV
2000	180	Rear	0.00127	26.33	0.541	DS			

Bar location/ units	Shadow Reading Y/cm	Spacing Δ/cm	E'/cm	M'	c/cm	α' x 10^2	α'^2 x 10^4	z'/cm
3.5	1.87		1.2812	288.2	0.0917	4.8484	23.5067	0.4493
2.5	2.16	0.2933	0.9907	312.0	0.0847	3.7500	14.0624	0.4564
1.5	2.51	0.3458	0.6435	337.8	0.0782	2.4364	5.9361	0.4628
0.5	2.92	0.4159	0.2267	357.1	0.0740	0.8585	0.7371	0.4671
-0.5	3.37	0.4535						
-1.5	3.79	0.4177			Slope	z_o'/cm	C_s'/cm	
-2.5	4.14	0.3485		2.5E-06	-0.0008	0.468	8.393	
-3.5	4.43	0.2877						

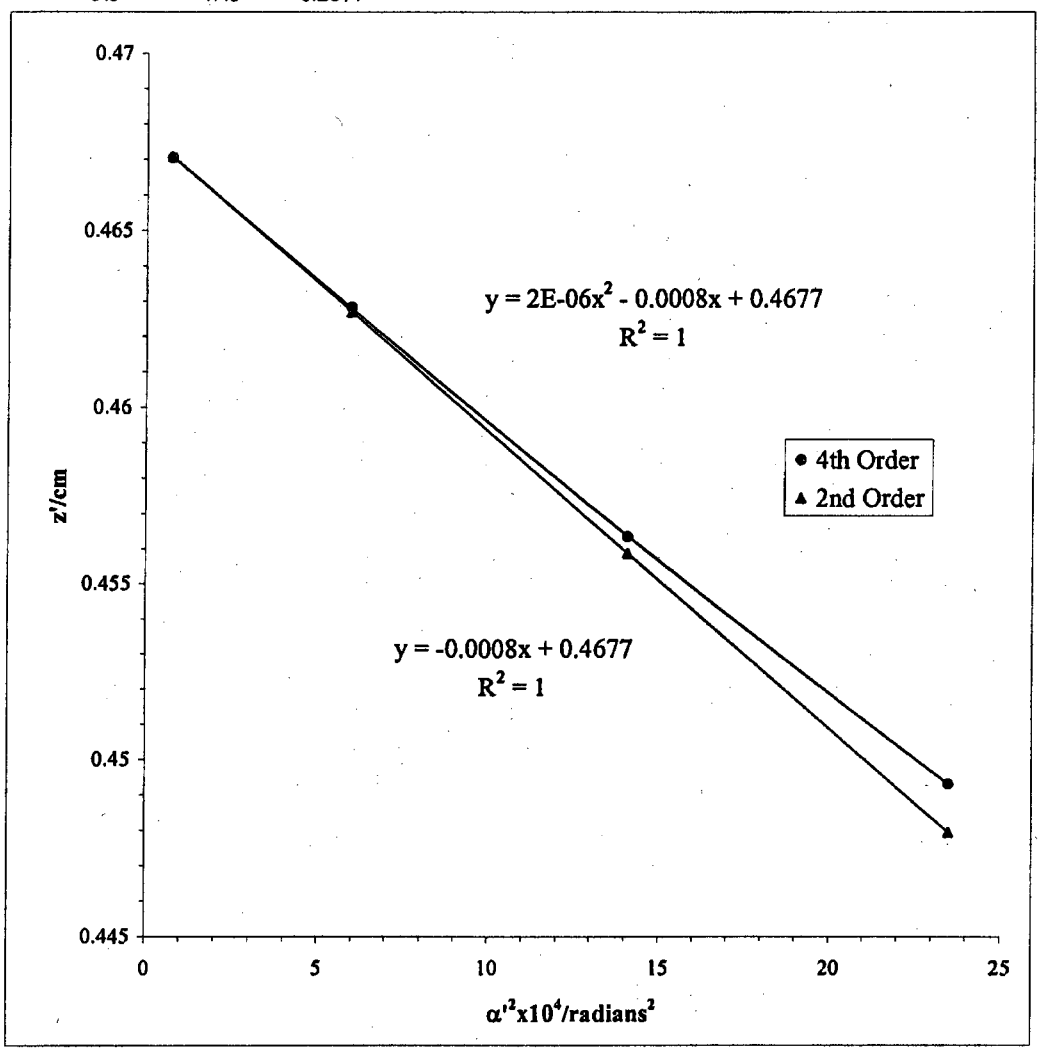

							Beam	Voltage	25 kV
Mesh/inch	I/milliamps	Mesh	z/cm	e_1/cm	a/cm	z_{sp}/cm	z_0'/cm	C_s'/cm	$z_{sp}-z_0'$
600	180	Front	25.08	0.00423	15.56	26.88	0.467	8.065	26.41

Bar location/ units	Shadow Reading X/cm	Spacing Δ/cm	E/cm	α x 10^4	α' x 10^2	α'² x 10^4	m	z'/cm	f/cm
3.5	1.860		1.257	9.522	4.757	22.630	0.02002	0.448611	0.49324
2.5	2.231	0.371	0.884	6.802	3.348	11.209	0.02032	0.457823	0.50043
1.5	2.589	0.358	0.525	4.081	1.989	3.955	0.02052	0.463673	0.50536
0.5	2.939	0.350	0.174	1.360	0.660	0.435	0.02062	0.466512	0.50786
-0.5	3.288	0.348							
-1.5	3.639	0.352					g/cm	$(\rho/f_0)^2 = (m_0+1)^2\alpha'^2$	
-2.5	4.000	0.360							
-3.5	4.374	0.375					0.43874	23.574	
							0.44766	11.676	
			Slope	m_0	μ_s		0.45330	4.120	
		0.0000	0.0000	0.020638	-14.52		0.45604	0.453	

f vs $(\rho/f_o)^2$

$S_f = slope_f / f_0$

	$slope_f$	fo/cm	S_f
2.5256E-06	-0.00069	0.508	-13.64

g vs $(\rho/f_o)^2$

$S_g = slope_g / f_0$

	$slope_g$	go/cm	S_g
-1.2E-07	-0.000745	0.456	-14.67

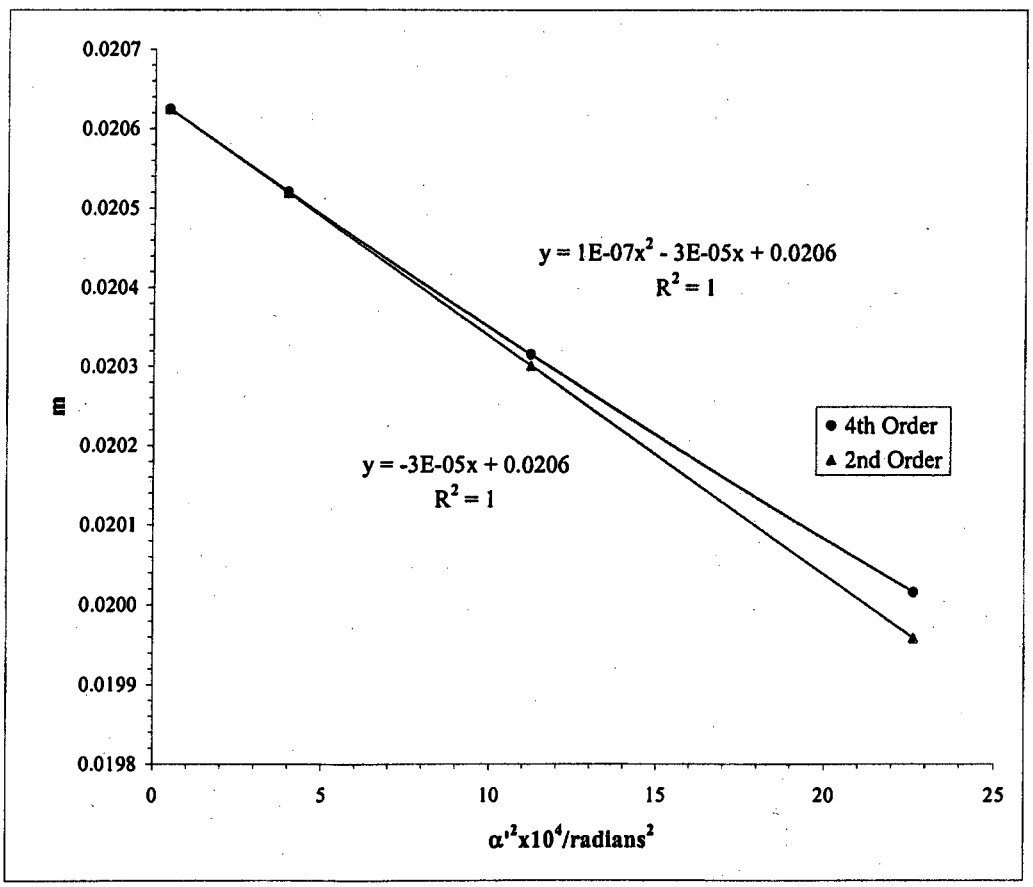

							Beam	Voltage	25 kV
Mesh/Inch	I/milliamps	Mesh	z/cm	e_1/cm	a/cm	z_{sp}/cm	z_0'/cm	C_s'/cm	$z_{sp}-z_o'$
600	180	Front	25.08	0.00423	15.56	26.88	0.467	8.065	26.41

Bar location/ units	Shadow Reading Y/cm	Spacing Δ/cm	E/cm	α x 10^4	α' x 10^2	α'^{2} x 10^4	m	z'/cm	f/cm
5.5	0.723		2.179	14.964	8.232	67.772	0.01818	0.412	0.449
4.5	1.172	0.450	1.733	12.243	6.555	42.969	0.01868	0.432	0.461
3.5	1.592	0.419	1.318	9.522	4.986	24.857	0.01910	0.447	0.471
2.5	1.987	0.395	0.925	6.802	3.501	12.255	0.01943	0.457	0.479
1.5	2.365	0.378	0.548	4.081	2.076	4.310	0.01966	0.463	0.484
0.5	2.733	0.368	0.182	1.360	0.688	0.473	0.01977	0.466	0.487
-0.5	3.096	0.363							
-1.5	3.462	0.366					g/cm	$(\rho/f_0)^2 = (m_0+1)^2\alpha'^2$	
-2.5	3.837	0.375							
-3.5	4.227	0.390					0.404	70.258	
-4.5	4.639	0.412					0.424	44.589	
-5.5	5.080	0.441					0.438	25.816	
							0.448	12.735	
			Slope	m_0	μ_s		0.454	4.481	
		8.4E-08	-2.9E-05	0.019779	-14.844		0.457	0.492	

f vs $(\rho/f_o)^2$

S_f = slope$_f$ / f_0

	slope$_f$	fo/cm	S_f
1.964E-06	-7E-04	0.487	-14.10

g vs $(\rho/f_o)^2$

S_g = slope$_g$ / f_0

	slope$_g$	go/cm	S_g
-1.18E-07	-0.0007	0.457	-15.37

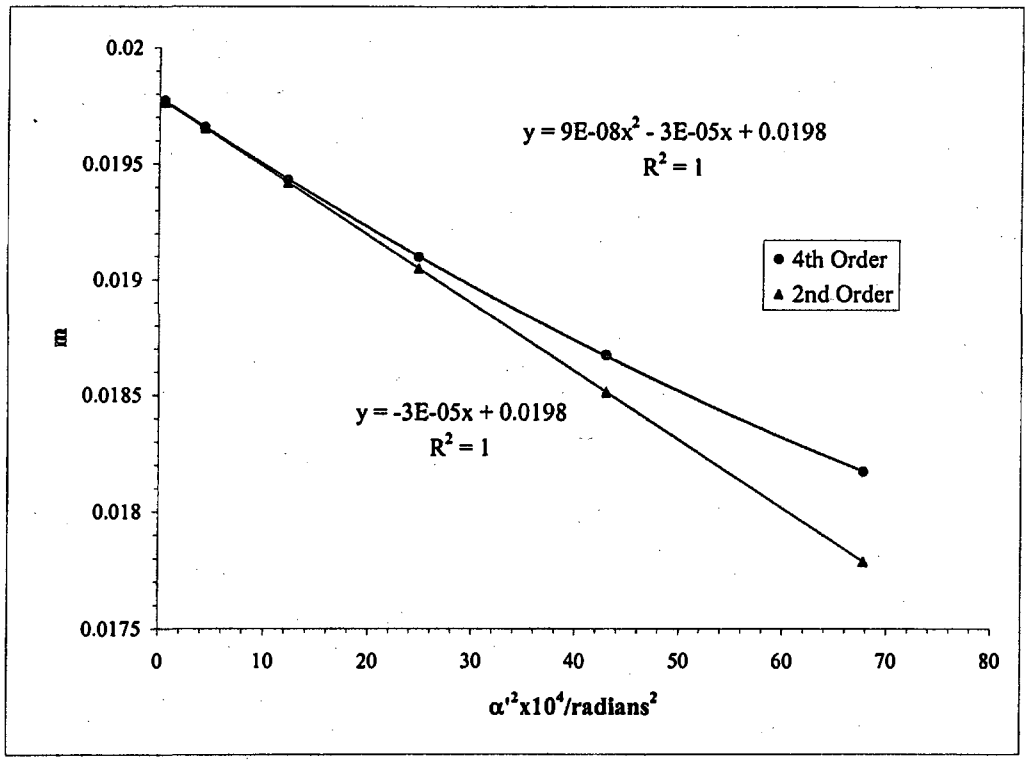

Beam Voltage	I/milliamps	z/cm	z_0'/cm	C_s'/cm
25 kV	180	25.08	0.467	8.07

Average of m_o = 0.0202

Average of μ_s = -14.68

Paraxial properties :

f_o = 0.498 cm

g_o = 0.457 cm

S_f = -13.87

S_g = -15.02

Mesh/inch	I/milliamps	Mesh	e'_1/cm	d/cm	b/cm		Beam	Voltage	25 kV
2000	200	Rear	0.00127	26.33	0.541	DS			

Bar location/ units	Shadow Reading X/cm	Spacing Δ/cm	E'/cm	M'	c/cm	α' x 10^2	α'^2 x 10^4	z'/cm
13	1.052		2.408	145.8	0.182	9.0797	82.4417	0.359
12	1.193	0.141	2.264	148.6	0.178	8.5396	72.9248	0.363
11	1.336	0.143	2.118	151.6	0.175	7.9895	63.8321	0.366
10	1.486	0.150	1.964	154.6	0.171	7.4097	54.9041	0.370
9	1.645	0.159	1.803	157.7	0.168	6.8022	46.2698	0.373
8	1.809	0.163	1.637	161.2	0.164	6.1790	38.1797	0.377
7	1.978	0.170	1.462	164.5	0.161	5.5190	30.4593	0.380
6	2.160	0.181	1.280	167.9	0.158	4.8305	23.3338	0.383
5	2.346	0.186	1.087	171.2	0.155	4.1044	16.8457	0.386
4	2.545	0.199	0.885	174.2	0.152	3.3406	11.1598	0.389
3	2.754	0.209	0.674	177.0	0.150	2.5459	6.4817	0.391
2	2.969		0.456	179.4	0.148	1.7210	2.9619	0.393
1	3.195		0.229	180.1	0.147	0.8635	0.7457	0.394
0	3.421							
-1	3.652				Slope	z_0'/cm	C_s'/cm	
-2	3.881			1.04E-06	-0.0005	0.395	5.162	
-3	4.102							
-4	4.315							
-5	4.520							
-6	4.719							
-7	4.903							
-8	5.083							
-9	5.251							
-10	5.414							
-11	5.572							
-12	5.721							
-13	5.867							

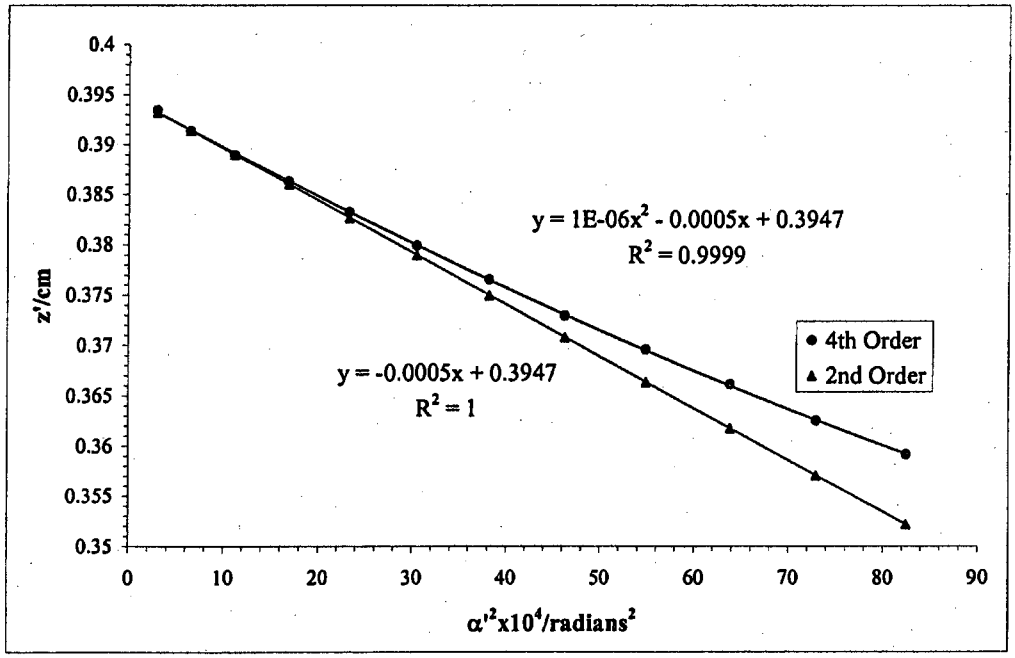

Mesh/Inch	I/milliamps	Mesh	e'_1/cm	d/cm	b/cm		Beam	Voltage	25 kV
2000	200	Rear	0.00127	26.33	0.541	DS			

Bar location/ units	Shadow Reading Y/cm	Spacing Δ/cm	E'/cm	M'	c/cm	$\alpha' \times 10^2$	$\alpha'^2 \times 10^4$	z'/cm
13	0.371		2.402	145.5	0.182	9.0602	82.0873	0.359
12	0.513	0.142	2.260	148.3	0.179	8.5252	72.6799	0.362
11	0.660	0.147	2.114	151.4	0.175	7.9760	63.6167	0.366
10	0.813	0.153	1.963	154.6	0.171	7.4073	54.8680	0.370
9	0.971	0.157	1.805	157.9	0.168	6.8100	46.3762	0.373
8	1.137	0.167	1.638	161.3	0.164	6.1829	38.2278	0.377
7	1.312	0.174	1.465	164.8	0.161	5.5299	30.5803	0.380
6	1.494	0.182	1.283	168.4	0.157	4.8428	23.4529	0.384
5	1.687	0.194	1.090	171.6	0.154	4.1144	16.9282	0.387
4	1.890	0.203	0.889	174.9	0.151	3.3551	11.2570	0.390
3	2.099	0.209	0.678	177.9	0.149	2.5598	6.5527	0.392
2	2.3212		0.458	180.1	0.147	1.7277	2.9849	0.394
1	2.5480		0.232	182.5	0.145	0.8751	0.7657	0.396
0	2.7803							
-1	3.0115				Slope	z_o'/cm	C_s'/cm	
-2	3.2363			0.0000	-0.0005	0.396	5.43	
-3	3.4548							
-4	3.6673							
-5	3.8671							
-6	4.0596							
-7	4.2419							
-8	4.4142							
-9	4.5803							
-10	4.7400							
-11	4.8887							
-12	5.0335							
-13	5.1756							

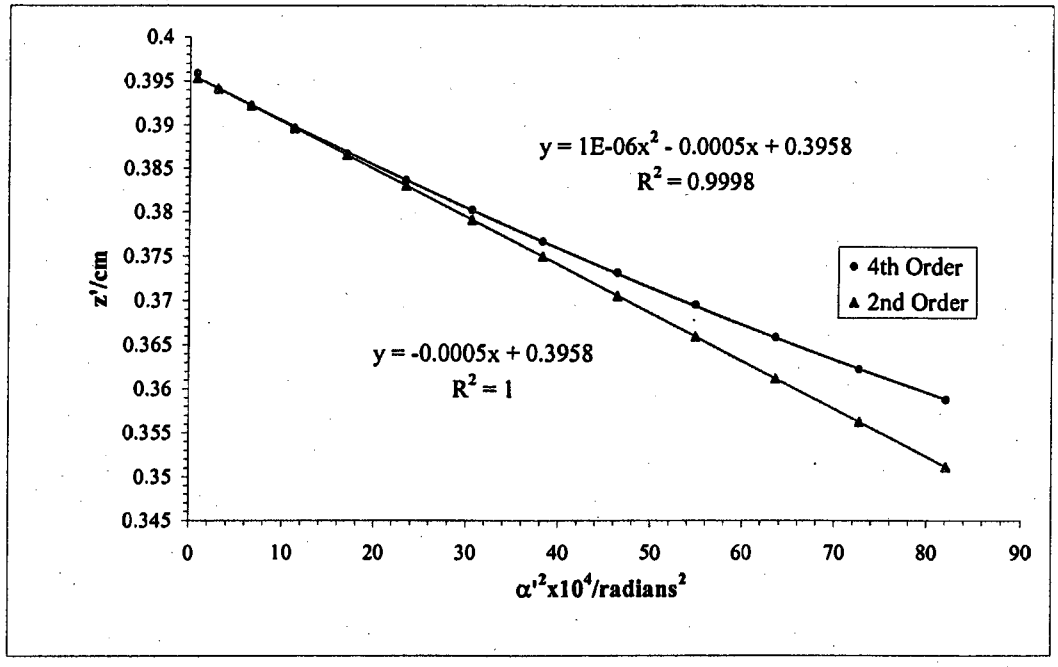

							Beam	Voltage	25 kV
Mesh/inch	I/milliamps	Mesh	z/cm	e_1/cm	a/cm	z_{sp}/cm	z_0'/cm	C_s'/cm	z_{sp}-z_0'
2000	200	Front	25.08	0.00127	15.56	26.88	0.395	5.297	26.48

Bar location/ units	Shadow Reading X/cm	Spacing Δ/cm	E/cm	$\alpha \times 10^4$	$\alpha' \times 10^2$	$\alpha'^2 \times 10^4$	m	z'/cm	f/cm
9	1.790		1.184	7.346	4.469	19.974	0.01644	0.385	0.406
8	1.927	0.137	1.048	6.530	3.956	15.649	0.01651	0.387	0.408
7	2.061	0.135	0.913	5.713	3.448	11.891	0.01657	0.389	0.409
6	2.195	0.133	0.780	4.897	2.946	8.679	0.01662	0.391	0.411
5	2.327	0.132	0.648	4.081	2.448	5.994	0.01667	0.392	0.412
4	2.458	0.131	0.518	3.265	1.954	3.819	0.01671	0.393	0.413
3	2.588	0.130	0.387	2.449	1.463	2.140	0.01674	0.394	0.413
2	2.718	0.130	0.258	1.632	0.974	0.949	0.01676	0.395	0.414
1	2.847	0.129	0.129	0.816	0.487	0.237	0.01677	0.395	0.414
0	2.976	0.129							
-1	3.105	0.129					g/cm	$(\rho/f_0)^2 = (m_0+1)^2\alpha'^2$	
-2	3.234	0.129							
-3	3.363	0.129					0.378	20.636	
-4	3.493	0.130					0.380	16.170	
-5	3.624	0.131					0.382	12.289	
-6	3.755	0.132					0.384	8.970	
-7	3.888	0.133					0.385	6.195	
-8	4.022	0.134					0.386	3.947	
-9	4.158	0.136					0.387	2.213	
							0.388	0.981	
			Slope	m_0	μ_s		0.388	0.245	
		5.2E-08	0.0000	0.01677	-10.74				

f vs $(\rho/f_o)^2$

$S_f = slope_f / f_0$

	$slope_f$	fo/cm	S_f
1.1945E-06	-0.00042	0.414	-10.18

g vs $(\rho/f_o)^2$

$S_g = slope_g / f_0$

	$slope_g$	go/cm	S_g
-6.2E-08	-0.0005	0.388	-12.03

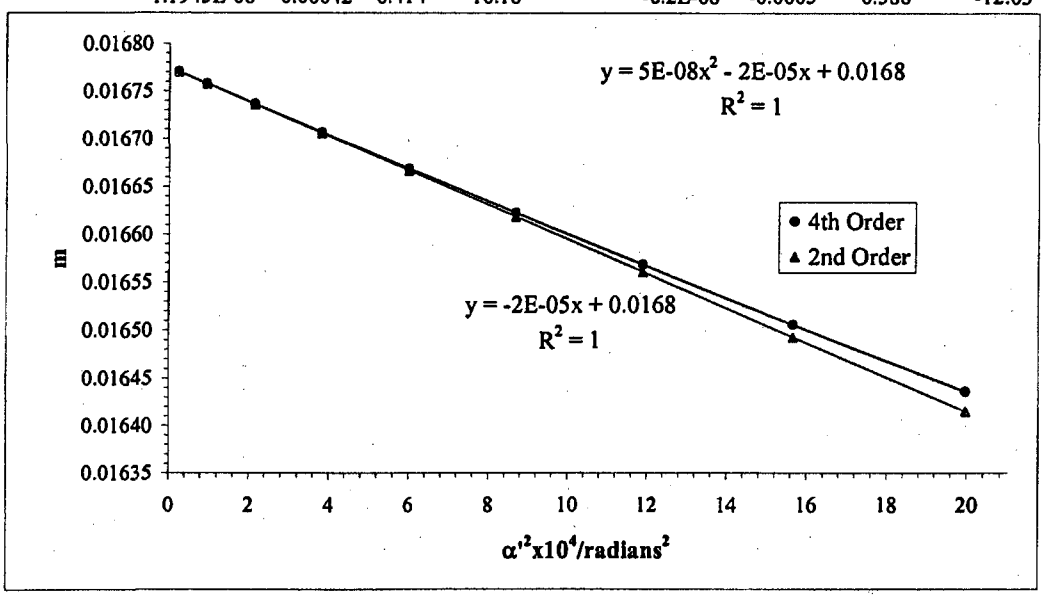

							Beam	Voltage	25 kV
Mesh/inch	I/milliamps	Mesh	z/cm	e_1/cm	a/cm	z_{sp}/cm	z_0'/cm	C_s'/cm	$z_{sp}-z_0'$
2000	200	Front	25.08	0.00127	15.56	26.8757	0.3953	5.297	26.480

Bar location/ units	Shadow Reading Y/cm	Spacing D/cm	E/cm	$\alpha \times 10^4$	$\alpha' \times 10^2$	$\alpha'^2 \times 10^4$	m	z'/cm	f/cm
13	2.002		1.727	10.611	6.516	42.461	0.01628	0.373	0.402
12	2.147	0.146	1.583	9.794	5.972	35.663	0.01640	0.376	0.405
11	2.290	0.143	1.441	8.978	5.438	29.570	0.01651	0.380	0.408
10	2.430	0.140	1.302	8.162	4.913	24.140	0.01661	0.382	0.410
9	2.568	0.138	1.165	7.346	4.397	19.336	0.01671	0.385	0.413
8	2.703	0.135	1.030	6.530	3.889	15.125	0.01679	0.387	0.415
7	2.837	0.134	0.897	5.713	3.388	11.477	0.01686	0.389	0.417
6	2.968	0.132	0.766	4.897	2.893	8.367	0.01693	0.391	0.418
5	3.099	0.130	0.636	4.081	2.403	5.772	0.01699	0.392	0.419
4	3.228	0.129	0.508	3.265	1.917	3.674	0.01703	0.393	0.421
3	3.356	0.128	0.380	2.449	1.435	2.058	0.01707	0.394	0.421
2	3.483	0.127	0.253	1.632	0.955	0.912	0.01709	0.395	0.422
1	3.610	0.127	0.126	0.816	0.477	0.228	0.01711	0.395	0.422
0	3.736	0.126							
-1	3.863	0.126					g/cm	$(\rho/f_0)^2 = (m_0+1)^2\alpha'^2$	
-2	3.989	0.126							
-3	4.116	0.127					0.366	43.927	
-4	4.243	0.127					0.370	36.894	
-5	4.371	0.128					0.373	30.590	
-6	4.501	0.129					0.376	24.973	
-7	4.631	0.131					0.378	20.003	
-8	4.763	0.132					0.380	15.647	
-9	4.897	0.134					0.382	11.873	
-10	5.033	0.136					0.384	8.656	
-11	5.171	0.138					0.385	5.972	
-12	5.3121	0.141					0.386	3.801	
-13	5.4555	0.143					0.387	2.129	
		Slope	m_s	μ_s			0.388	0.943	
	6.9E-08	0.0000	0.017114	-13.1226			0.388	0.235	

f vs $(\rho/f_o)^2$

$S_f = slope_f / f_0$

	$slope_f$	fo/cm	S_f
1.58E-06	-0.00053	0.423	-12.49

g vs $(\rho/f_o)^2$

$S_g = slope_g / f_0$

	$slope_g$	go/cm	S_g
-6.16E-08	-0.00049	0.388	-11.69

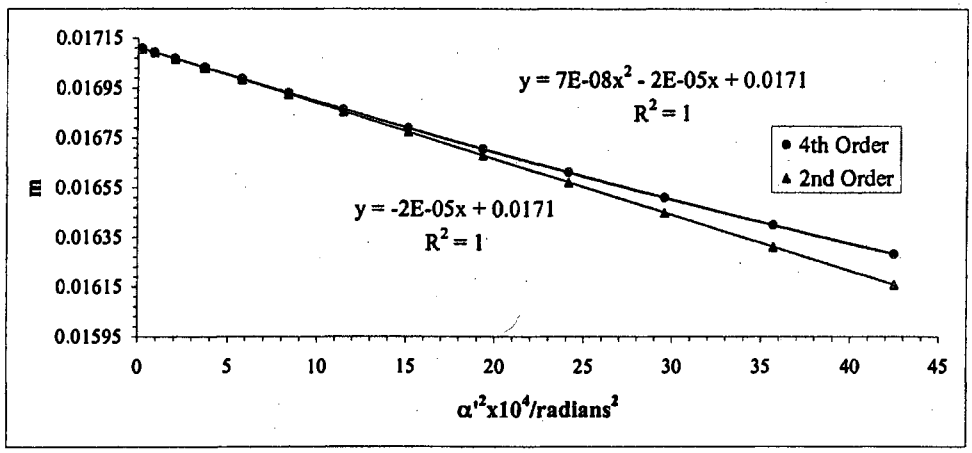

Beam Voltage	I/milliamps	z/cm	z_0'/cm	C_s'/cm
25 kV	200	25.08	0.395	5.30

Average of m_o = 0.0169

Average of μ_s = -11.9

Paraxial properties :

f_o =	0.418	cm
g_o =	0.388	cm
S_f =	-11.3	
S_g =	-11.9	

Mesh/inch	I/milliamps	Mesh	e'_1/cm	d/cm	b/cm		Beam	Voltage	25 kV
600	250	Rear	0.00423	26.44	0.432	DS			

Bar location/ units	Shadow Reading X/cm	Spacing Δ/cm	E'/cm	M'	c/cm	α' x 10^2	α'^2 x 10^4	z'/cm
4	3.5571		2.6204	154.7	0.1720	9.8451	96.9270	0.2598
3	4.1549	0.5978	2.0228	159.3	0.1671	7.6015	57.7823	0.2647
2	4.8014	0.6465	1.3825	163.3	0.1629	5.1959	26.9978	0.2689
1	5.4872	0.6858	0.7027	166.0	0.1603	2.6414	6.9770	0.2715
0	6.1923	0.7051						
-1	6.8926	0.7003						
-2	7.5663	0.6737						
-3	8.2005	0.6342						
-4	8.7978							

	Slope	z_0'/cm	C_s'/cm
8E-08	-0.0001	0.273	1.390

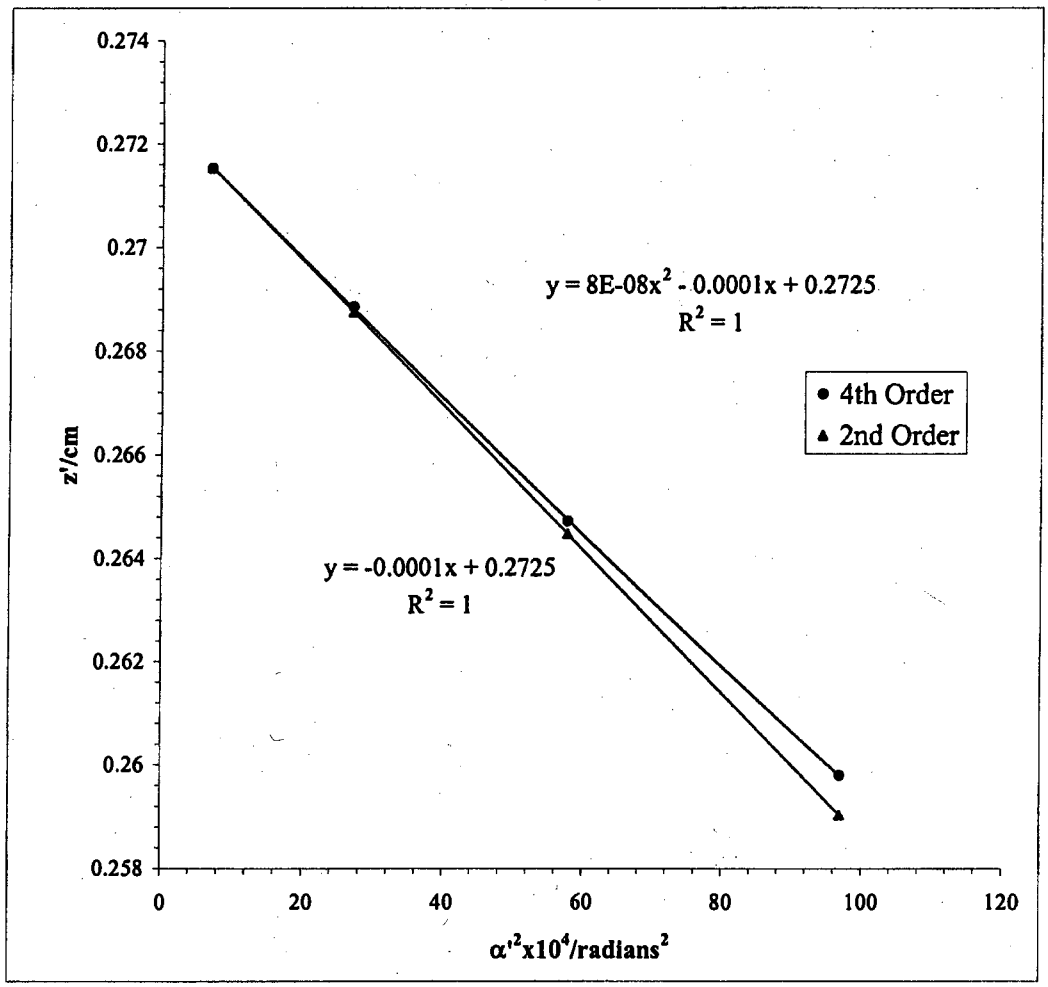

Mesh/inch	I/milliamps	Mesh	e'_1/cm	d/cm	b/cm		Beam	Voltage	25 kV
600	250	Rear	0.00423	26.44	0.432	DS			

Bar location/ units	Shadow Reading Y/cm	Spacing Δ/cm	E'/cm	M'	c/cm	α' x 10^2	α'^2 x 10^4	z'/cm
4	0.133		2.574	152.0	0.1751	9.6697	93.5029	0.257
3	0.710	0.577	1.990	156.7	0.1699	7.4760	55.8908	0.262
2	1.329	0.619	1.362	160.9	0.1654	5.1184	26.1979	0.266
1	1.991	0.662	0.693	163.7	0.1625	2.6051	6.7864	0.269
0	2.681	0.690						
-1	3.377	0.696						
-2	4.053	0.676			Slope	z_0'/cm	C_s'/cm	
-3	4.690	0.637		1.11E-07	-1.57E-04	0.270	1.5690	
-4	5.281							

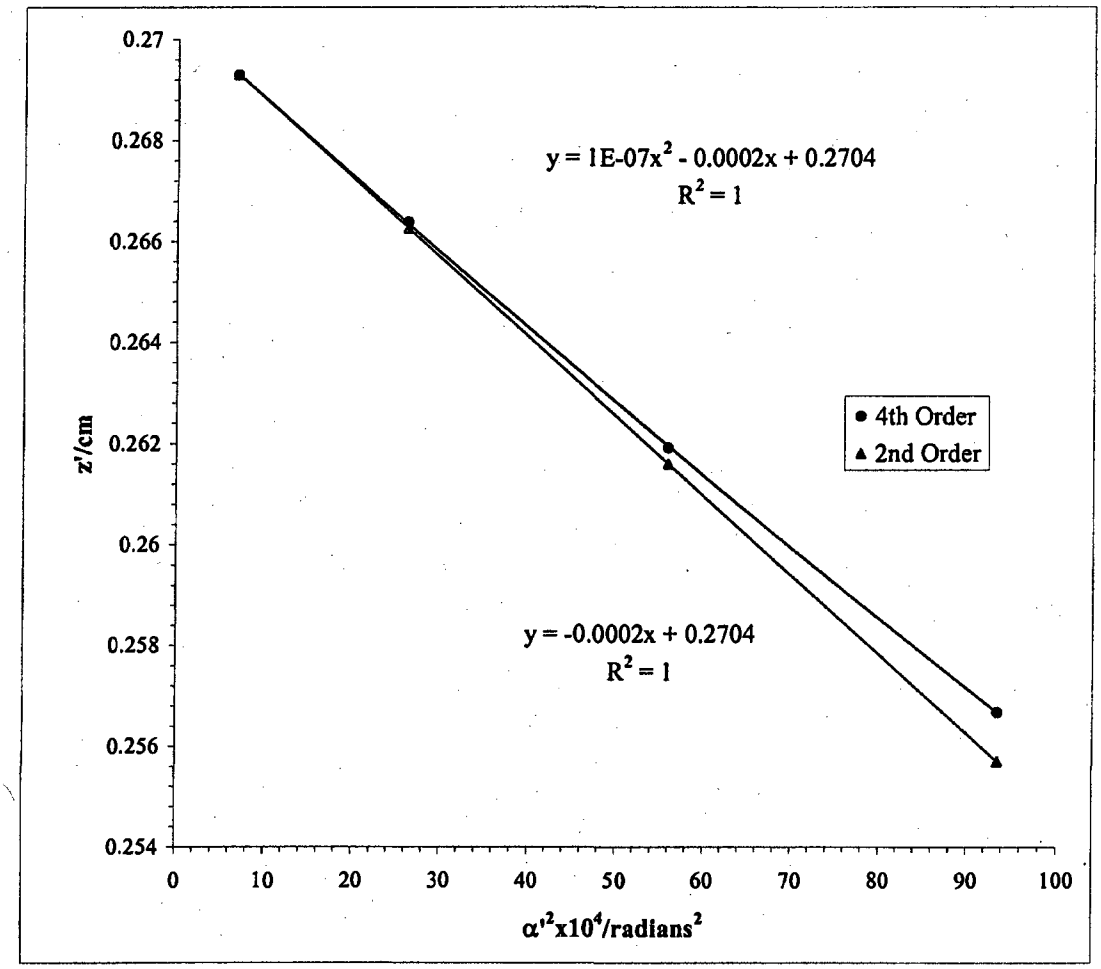

							Beam	Voltage	25 kV
Mesh/inch	I/milliamps	Mesh	z/cm	e_1/cm	a/cm	z_{sp}/cm	z_0'/cm	C_s'/cm	$z_{sp}-z_0'$
2000	250	Front	25.08	0.00127	15.56	26.88	0.271	1.479	26.60

Bar location/ units	Shadow Reading X/cm	Spacing Δ/cm	E/cm	$\alpha \times 10^4$	$\alpha' \times 10^2$	$\alpha'^2 \times 10^4$	m	z'/cm	f/cm
6	1.925		1.153	4.897	4.333	18.778	0.01130	0.269	0.280
5	2.120	0.195	0.958	4.081	3.601	12.967	0.01133	0.270	0.281
4	2.314	0.194	0.765	3.265	2.874	8.261	0.01136	0.270	0.282
3	2.507	0.193	0.572	2.449	2.152	4.630	0.01138	0.271	0.282
2	2.698	0.192	0.381	1.632	1.433	2.053	0.01139	0.271	0.283
1	2.889	0.191	0.190	0.816	0.716	0.512	0.01140	0.271	0.283
0	3.080	0.190							
-1	3.270	0.190					g/cm	$(\rho/f_0)^2 = (m_0+1)^2\alpha'^2$	
-2	3.461	0.191							
-3	3.652	0.191					0.265	19.209	
-4	3.844	0.192					0.266	13.265	
-5	4.037	0.193					0.267	8.450	
-6	4.231	0.194					0.268	4.736	
							0.268	2.100	
							0.268	0.524	

	Slope	m_0	μ_s
8.3E-09	0.0000	0.011406	-5.03

f vs $(\rho/f_o)^2$

S_f = slope$_f$ / f_0

	slope$_f$	fo/cm	S_f
1.96E-07	-0.00014	0.283	-4.86

g vs $(\rho/f_o)^2$

S_g = slope$_g$ / f_0

	slope$_g$	go/cm	S_g
-5.2E-09	-0.00014	0.268	-5.00

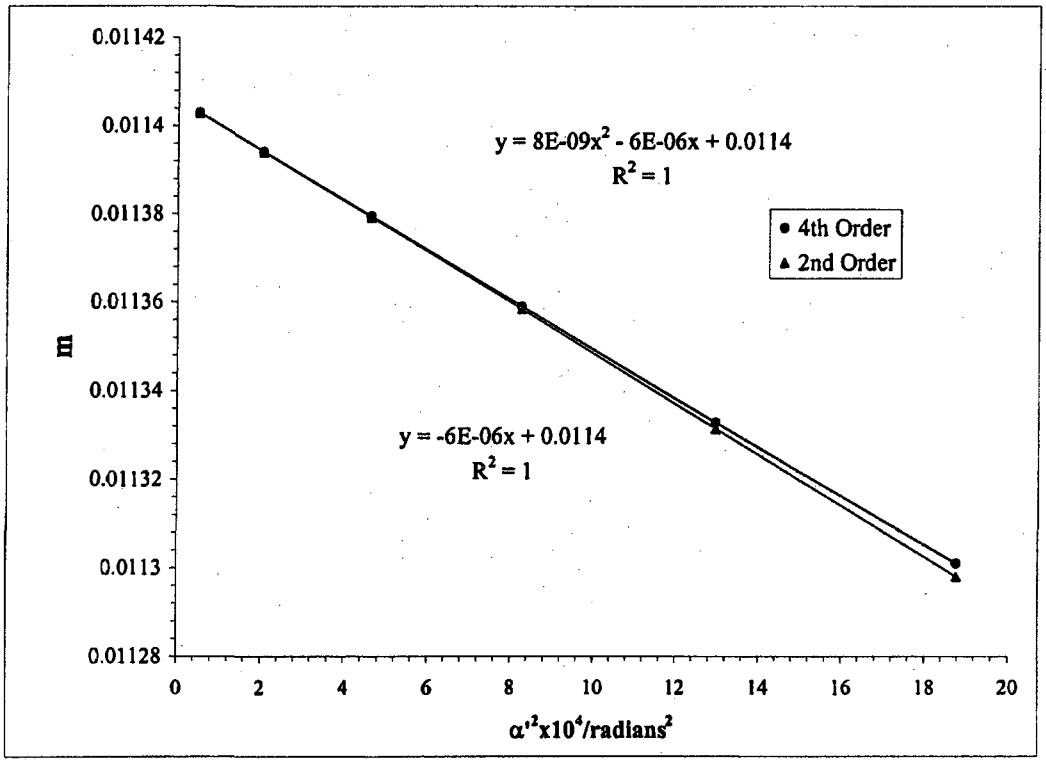

							Beam	Voltage	25 kV
Mesh/inch	I/milliamps	Mesh	z/cm	e_1/cm	a/cm	z_{sp}/cm	z_0'/cm	C_s'/cm	$z_{sp}-z_o'$
2000	250	Front	25.08	0.00127	15.56	26.88	0.271	1.479	26.60

Bar location/ units	Shadow Reading Y/cm	Spacing Δ/cm	E/cm	$\alpha \times 10^4$	$\alpha' \times 10^2$	$\alpha'^2 \times 10^4$	m	z'/cm	f/cm
5.5	1.475		1.066	4.489	4.008	16.061	0.01120	0.269	0.278
4.5	1.671	0.196	0.870	3.673	3.270	10.695	0.01123	0.270	0.279
3.5	1.865	0.195	0.675	2.857	2.538	6.442	0.01125	0.270	0.279
2.5	2.059	0.194	0.482	2.040	1.810	3.276	0.01127	0.271	0.280
1.5	2.252	0.193	0.289	1.224	1.085	1.177	0.01128	0.271	0.280
0.5	2.444	0.192	0.096	0.408	0.361	0.131	0.01129	0.271	0.280
-0.5	2.637	0.192							
-1.5	2.829	0.193					g/cm	$(\rho/f_0)^2 = (m_0+1)^2\alpha'^2$	
-2.5	3.022	0.193							
-3.5	3.216	0.194					0.266	16.426	
-4.5	3.411	0.195					0.267	10.938	
-5.5	3.608	0.196					0.267	6.589	
							0.268	3.351	
		Slope	m_o	μ_s			0.268	1.204	
	8.5E-09	0.0000	0.01129	-5.10			0.268	0.134	

f vs $(\rho/f_o)^2$

$S_f = slope_f / f_0$

	$slope_f$	fo/cm	S_f
2.005E-07	-0.000138	0.280	-4.93

g vs $(\rho/f_o)^2$

$S_g = slope_g / f_0$

	$slope_g$	go/cm	S_g
-5.3E-09	-0.000142	0.268	-5.05

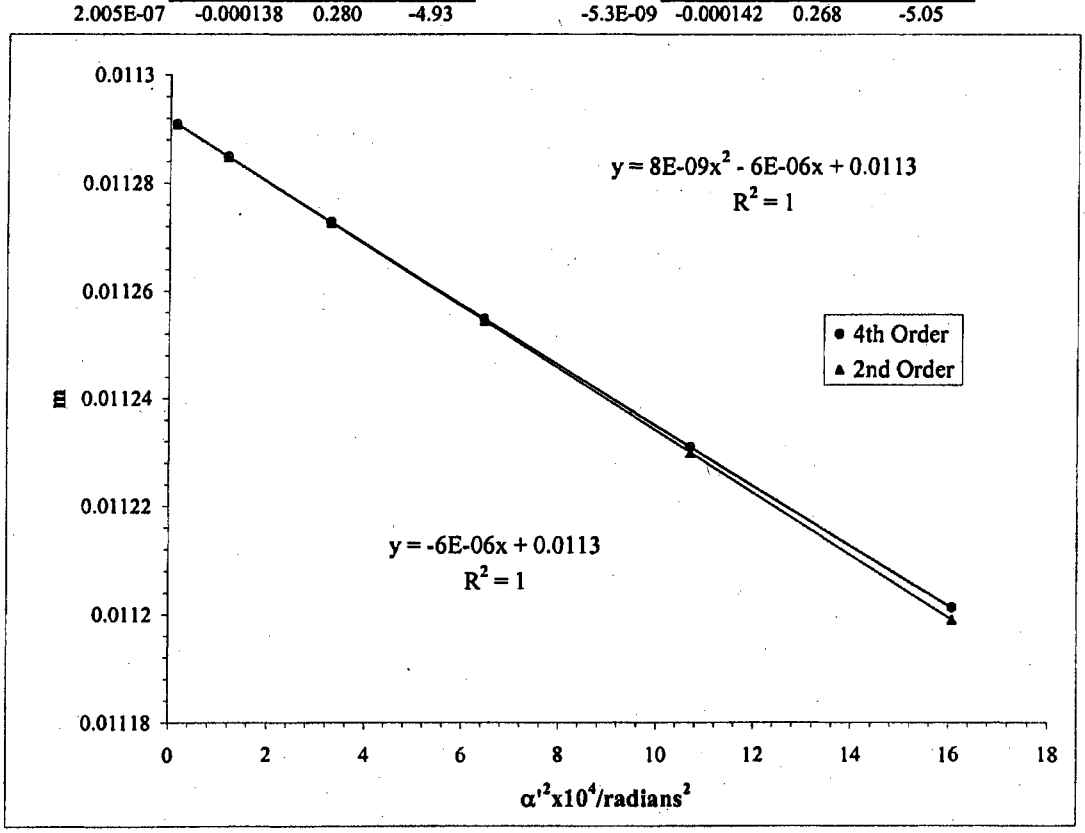

Beam Voltage	I/milliamps	z/cm	z_0'/cm	C_s'/cm
25 kV	250	25.1	0.271	1.48

Average of m_o = 0.0113

Average of μ_s = -5.06

Paraxial properties :

f_o = 0.282 cm

g_o = 0.268 cm

S_f = -4.89

S_g = -5.03

Mesh/inch	I/milliamps	Mesh	e'_1/cm	d/cm	b/cm		Beam	Voltage	25 kV
600	350	Rear	0.00423	26.44	0.432	DS			

Bar location/ units	Shadow Reading X/cm	Spacing Δ/cm	E'/cm	M'	c/cm	α' x 10^2	α'^{2} x 10^4	z'/cm
5	0.233		1.999	94.4	0.283	7.4798	55.9473	0.149
4	0.628	0.395	1.604	94.7	0.282	6.0016	36.0196	0.150
3	1.026	0.398	1.206	94.9	0.282	4.5111	20.3497	0.150
2	1.427	0.401	0.805	95.1	0.281	3.0118	9.0708	0.151
1	1.829	0.402	0.403	95.2	0.281	1.5080	2.2740	0.151
0	2.232	0.403						
-1	2.635	0.403						
-2	3.037	0.402						
-3	3.437	0.401						
-4	3.836	0.398			Slope	z_0'/cm	C_6'/cm	
-5	4.231	0.396		2.6E-08	-4.3E-05	0.151	0.425	

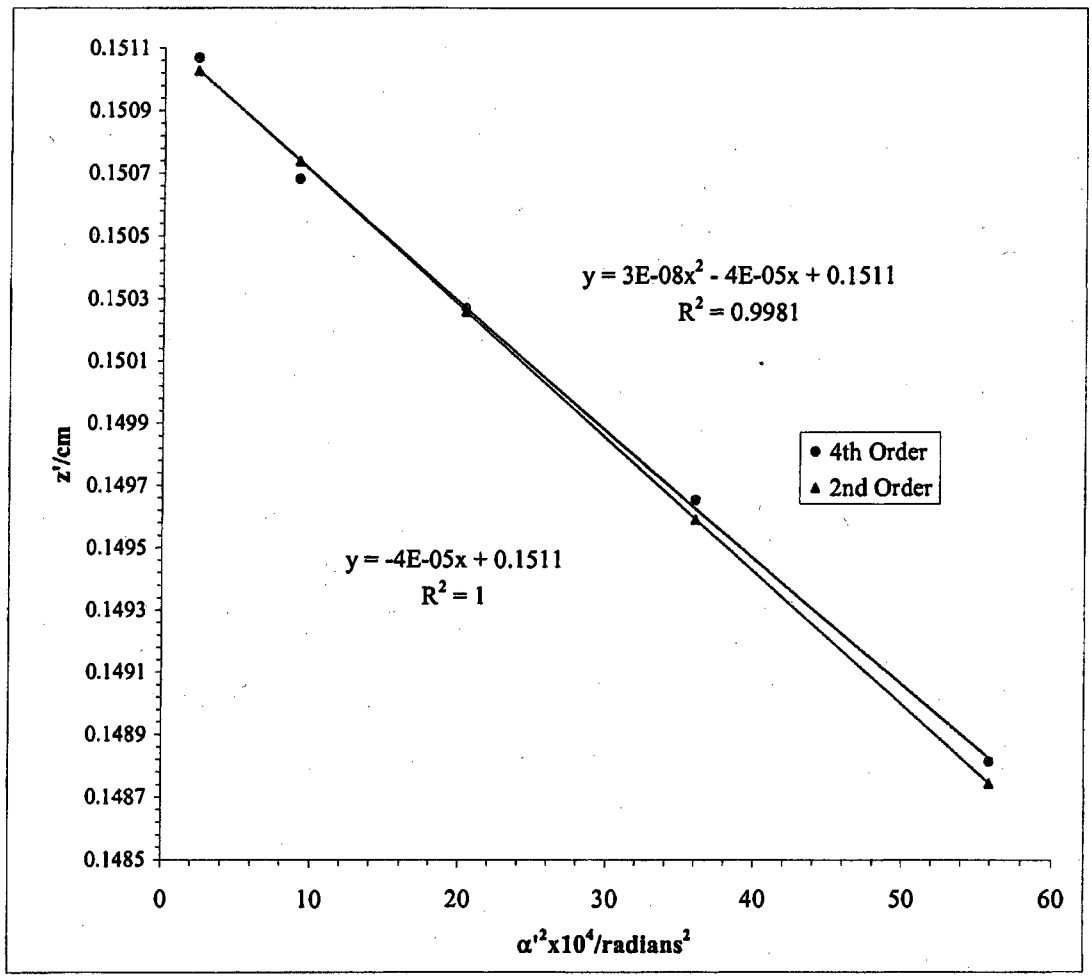

Mesh/inch	I/milliamps	Mesh	e'_1/cm	d/cm	b/cm		Beam	Voltage	25 kV
600	350	Rear	0.00423	26.44	0.432	DS			

Bar location/ units	Shadow Reading Y/cm	Spacing Δ/cm	E'/cm	M'	c/cm	$\alpha' \times 10^2$	$\alpha'^2 \times 10^4$	z'/cm
5.5	0.460		2.193	94.2	0.2838	8.2040	67.3049	0.1480
4.5	0.856	0.395	1.798	94.4	0.2832	6.7263	45.2431	0.1486
3.5	1.253	0.397	1.401	94.5	0.2827	5.2403	27.4609	0.1491
2.5	1.652	0.399	1.002	94.6	0.2824	3.7478	14.0461	0.1494
1.5	2.052	0.400	0.601	94.7	0.2822	2.2506	5.0651	0.1496
0.5	2.453	0.401	0.201	94.8	0.2820	0.7505	0.5633	0.1498
-0.5	2.854	0.401						
-1.5	3.255	0.401						
-2.5	3.655	0.400			Slope	z_o'/cm	C_s'/cm	
-3.5	4.054	0.399		4.1E-08	-3E-05	0.150	0.280	
-4.5	4.451	0.397						
-5.5	4.846	0.395						

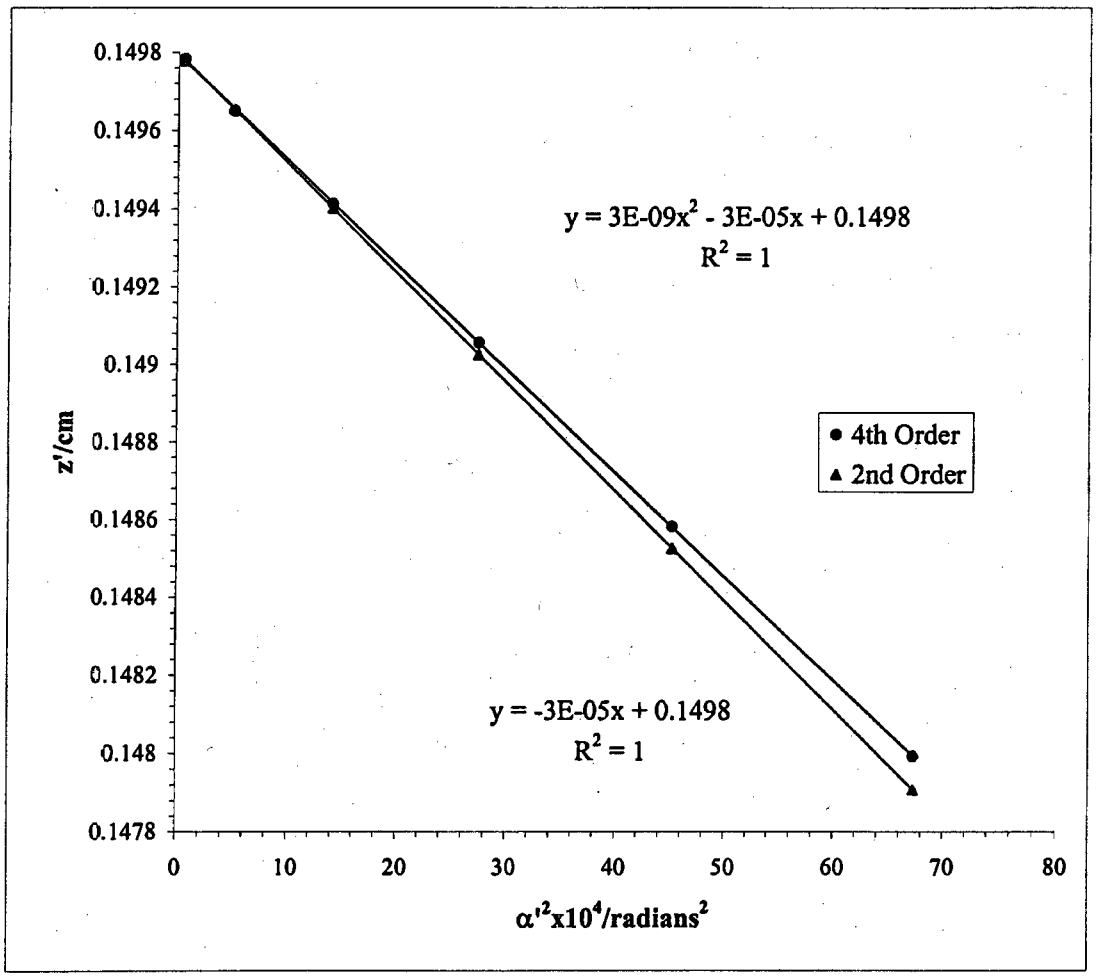

							Beam	Voltage	25 kV
Mesh/inch	I/milliamps	Mesh	z/cm	e_i/cm	a/cm	z_{sp}/cm	z_0'/cm	C_s'/cm	$z_{sp}-z_o'$
2000	350	Front	25.08	0.00127	15.56	26.88	0.1505	0.353	26.73

Bar location/ units	Shadow Reading X/cm	Spacing Δ/cm	E/cm	$\alpha \times 10^4$	$\alpha' \times 10^2$	$\alpha'^2 \times 10^4$	m	z'/cm	f/cm
4	1.738		1.334	3.265	4.991	24.914	0.006541	0.1496	0.1631
3	2.073	0.335	0.999	2.449	3.736	13.960	0.006553	0.1500	0.1634
2	2.407	0.333	0.665	1.632	2.487	6.188	0.006562	0.1502	0.1636
1	2.739	0.332	0.332	0.816	1.243	1.544	0.006568	0.1504	0.1637
0	3.071	0.332							
-1	3.403	0.332							
-2	3.736	0.333							
-3	4.070	0.334							
-4	4.407	0.336							

	Slope	m_o	μ_z
6.2E-10	-1E-06	0.006570	-1.79

g/cm	$(\rho/f_0)^2 = (m_0 + 1)^2 \alpha'^2$
0.1485	25.243
0.1489	14.144
0.1492	6.269
0.1493	1.565

f vs $(\rho/f_o)^2$

$S_f = slope_f / f_0$

	$slope_f$	fo/cm	S_f
1.496E-08	-2.9E-05	0.164	-1.75

g vs $(\rho/f_o)^2$

$S_g = slope_g / f_0$

$slope_g$	go/cm	S_g
-2E-10	-3.4E-05	0.149	-2.10

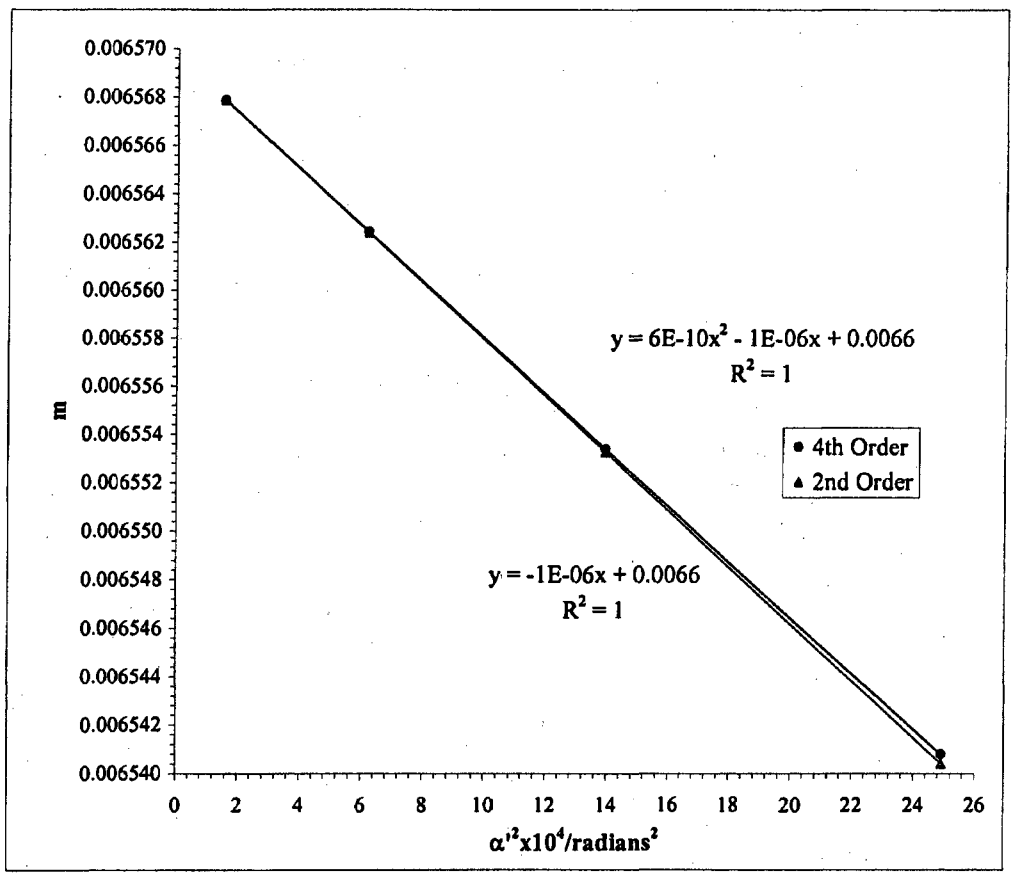

							Beam	Voltage	25 kV
Mesh/inch	I/milliamps	Mesh	z/cm	e_1/cm	a/cm	z_{sp}/cm	z_0'/cm	C_s'/cm	$z_{sp}-z_o'$
2000	130	Front	25.08	0.00127	15.56	26.88	0.150	0.353	26.73

Bar location/ units	Shadow Reading Y/cm	Spacing Δ/cm	E/cm	$\alpha \times 10^4$	$\alpha' \times 10^2$	$\alpha'^2 \times 10^4$	m	z'/cm	f/cm
3.5	2.0148		1.167	2.857	4.367	19.072	0.00654	0.1498	0.1631
2.5	2.3499	0.335	0.832	2.040	3.114	9.698	0.00655	0.1501	0.1634
1.5	2.6835	0.334	0.499	1.224	1.866	3.483	0.00656	0.1503	0.1635
0.5	3.0162	0.333	0.166	0.408	0.622	0.387	0.00656	0.1504	0.1636
-0.5	3.3485	0.332							
-1.5	3.6811	0.333						g/cm	$(\rho/f_0)^2 =$
-2.5	4.0145	0.333							$(m_0+1)^2 \alpha'^2$
-3.5	4.3491	0.335						0.1487	19.322
								0.1490	9.825
		Slope	m_o	μ_s				0.1493	3.529
	6.4E-10	0.0000	0.0066	-1.82				0.1494	0.392

f vs $(\rho/f_o)^2$

$S_f = slope_f / f_0$

	$slope_f$	fo/cm	S_f
1.556E-08	-2.9199E-05	0.164	-1.78

g vs $(\rho/f_o)^2$

$S_g = slope_g / f_0$

	$slope_g$	go/cm	S_g
-3E-10	-3.44E-05	0.149	-2.10

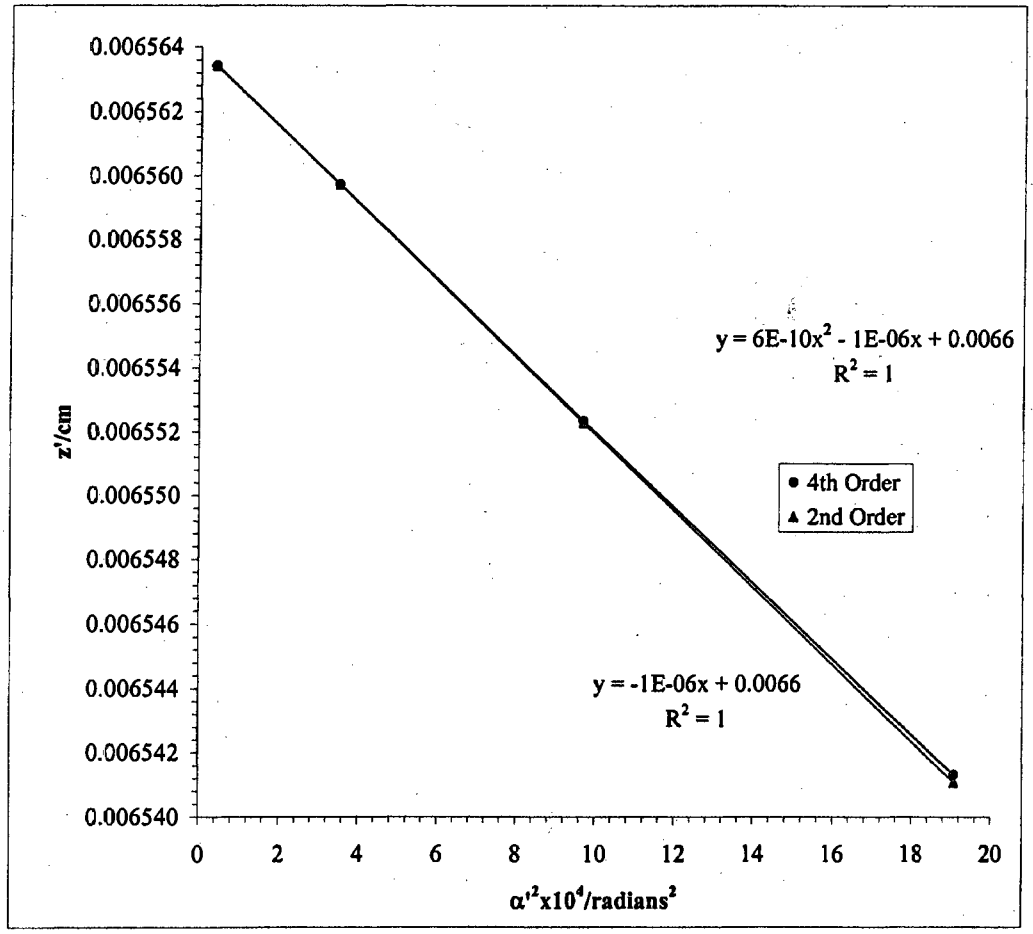

Beam Voltage	I/milliamps	z/cm	z_0'/cm	C_s'/cm
25 kV	350	25.1	0.150	0.353

Average of m_o = 0.00657

Average of μ_s = -1.80

Paraxial properties :

f_o = 0.164 cm

g_o = 0.149 cm

S_f = -1.77

S_g = -2.10

Mesh/inch	I/milliamps	Mesh	e'_1/cm	d/cm	b/cm		Beam	Voltage	25 kV
600	400	Rear	0.00423	26.44	0.432	DS			

Bar location/ units	Shadow Reading X/cm	Spacing Δ/cm	E'/cm	M'	c/cm	α' x 10^2	α'^2 x 10^4	z'/cm
4.5	1.5328		1.6377	86.0	0.3112	6.1210	37.4672	0.1206
3.5	1.8943	0.3615	1.2756	86.1	0.3108	4.7678	22.7316	0.1210
2.5	2.2573	0.3630	0.9121	86.2	0.3104	3.4093	11.6232	0.1214
1.5	2.6214	0.3641	0.5477	86.2	0.3102	2.0471	4.1904	0.1216
0.5	2.9863	0.3649	0.1826	86.3	0.3101	0.6826	0.4659	0.1217
-0.5	3.3515	0.3652						
-1.5	3.7167	0.3652						
-2.5	4.0815	0.3648						
-3.5	4.4455	0.3640			Slope	z_o'/cm	C_s'/cm	
-4.5	4.8082	0.3627		-9.1E-09	-3.0E-05	0.122	0.303	

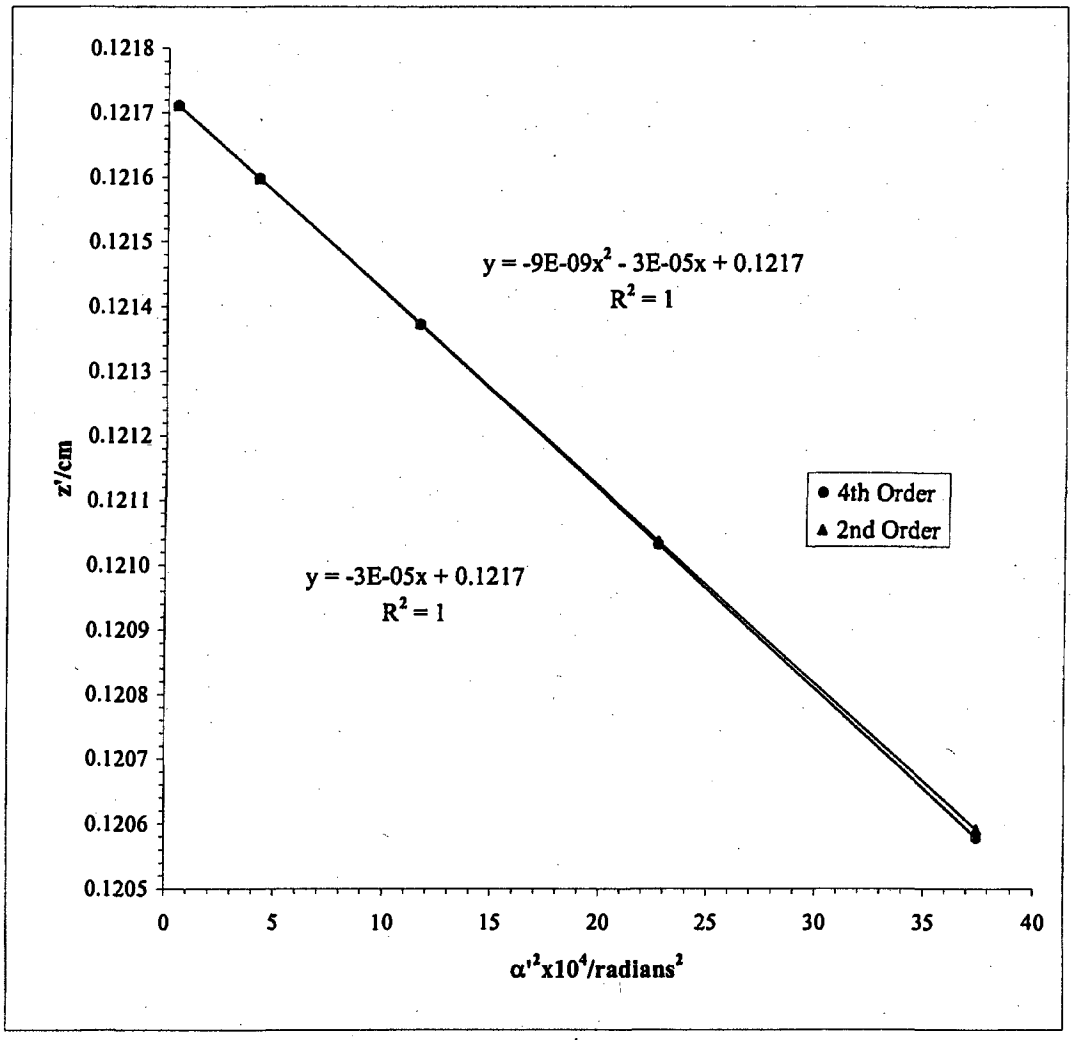

Mesh/Inch	I/milliamps	Mesh	e'_1/cm	d/cm	b/cm		Beam	Voltage	25 kV
600	400	Rear	0.00423	26.44	0.432	DS			

Bar location/ units	Shadow Reading Y/cm	Spacing Δ/cm	E'/cm	M'	c/cm	α' x 10^2	α'^2 x 10^4	z'/cm
3.5	2.6062		1.2707	85.8	0.3120	4.7491	22.5542	0.1198
2.5	2.9686	0.3623	0.9083	85.8	0.3117	3.3949	11.5251	0.1201
1.5	3.3316	0.3630	0.5453	85.9	0.3116	2.0380	4.1533	0.1202
0.5	3.6950	0.3635	0.1818	85.9	0.3115	0.6795	0.4617	0.1203
-0.5	4.0586	0.3636						
-1.5	4.4221	0.3635			Slope	z_0'/cm	C_s'/cm	
-2.5	4.7852	0.3631		-4.6E-09	-2.2E-05	0.1203	0.2173	
-3.5	5.1476	0.3624						

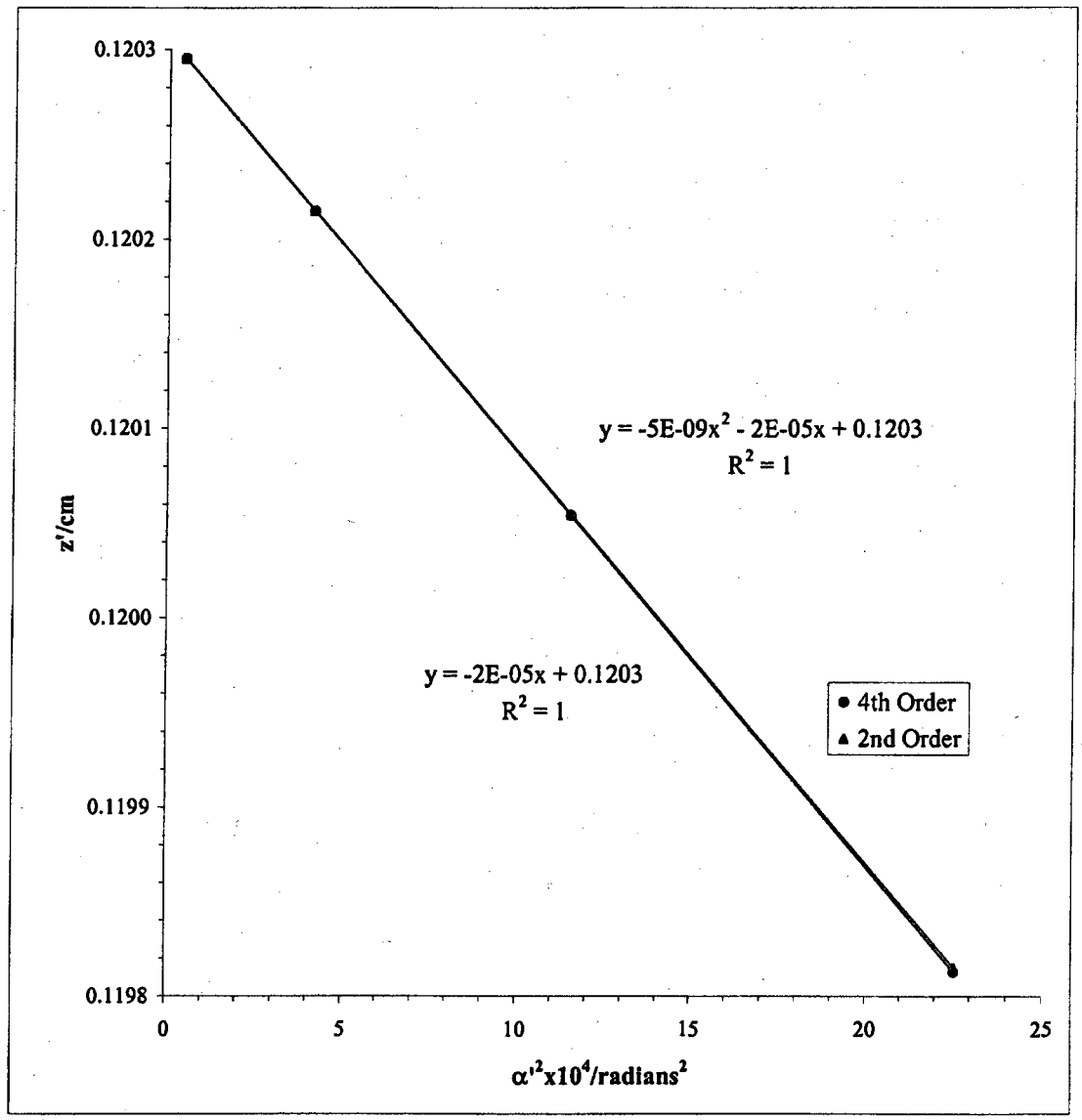

							Beam	Voltage	25 kV
Mesh/inch	I/milliamps	Mesh	z/cm	e_1/cm	a/cm	z_{sp}/cm	z_o'/cm	C_s'/cm	$z_{sp}-z_o'$
2000	400	Front	25.08	0.00127	15.56	26.88	0.121	0.260	26.75

Bar location/ units	Shadow Reading X/cm	Spacing Δ/cm	E/cm	$\alpha \times 10^4$	$\alpha' \times 10^2$	$\alpha'^2 \times 10^4$	m	z'/cm	f/cm
5	2.175		2.014	4.081	7.528	56.672	0.00542	0.1195	0.13531
4	2.582	0.408	1.606	3.265	6.002	36.029	0.00544	0.1201	0.13576
3	2.987	0.404	1.201	2.449	4.490	20.161	0.00545	0.1205	0.13611
2	3.388	0.402	0.799	1.632	2.988	8.927	0.00546	0.1208	0.13637
1	3.788	0.400	0.399	0.816	1.492	2.227	0.00547	0.1210	0.13652
0	4.187	0.399							
-1	4.586	0.399					g/cm	$(\rho/f_0)^2 = (m_0+1)^2\alpha'^2$	
-2	4.987	0.400							
-3	5.389	0.402					0.11881	57.294	
-4	5.794	0.405					0.11934	36.425	
-5	6.203	0.409					0.11975	20.383	
							0.12004	9.025	
		Slope	m_o	m_s			0.12021	2.251	
	4.4E-10	0.0000	0.0055	-1.6762					

f vs $(\rho/f_o)^2$

$S_f = slope_f / f_0$

	$slope_f$	fo/cm	S_f
1.0681E-08	-2E-05	0.137	-1.65

g vs $(\rho/f_o)^2$

$S_g = slope_g / f_0$

	$slope_g$	go/cm	S_g
-1.36E-10	-3E-05	0.120	-1.86

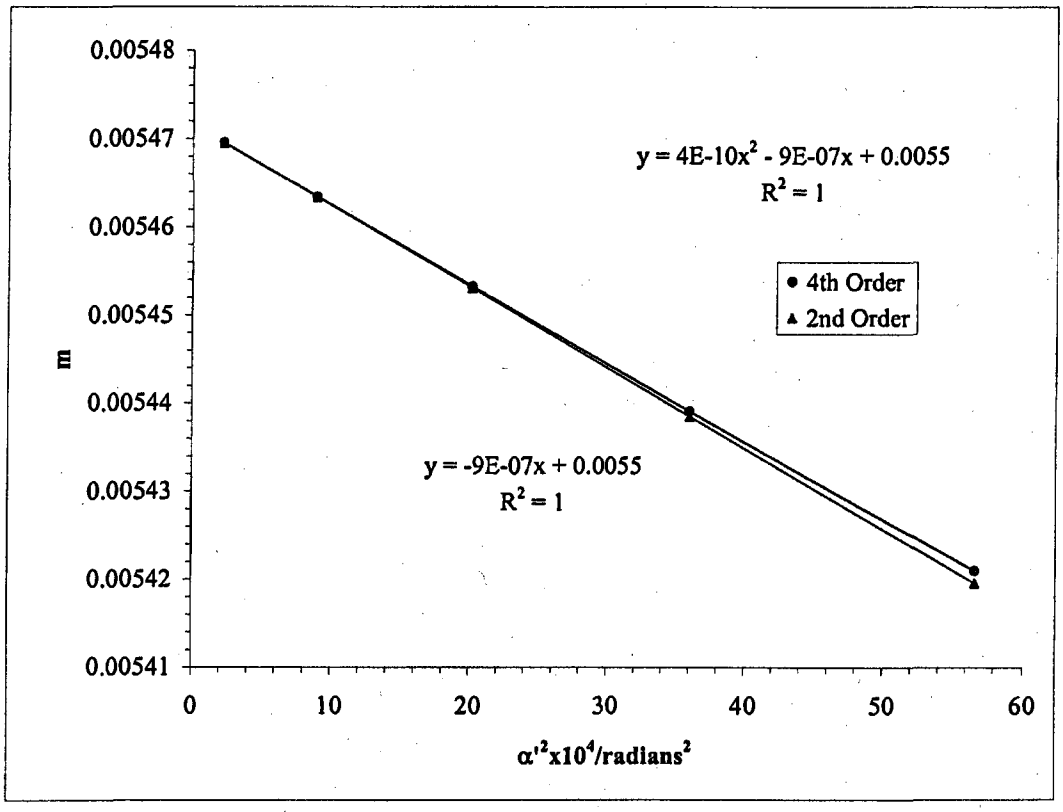

							Beam	Voltage	25 kV
Mesh/inch	I/milliamps	Mesh	z/cm	e_1/cm	a/cm	z_{sp}/cm	z_0'/cm	C_s'/cm	$z_{sp}-z_0'$
2000	400	Front	25.08	0.00127	15.56	26.88	0.121	0.260	26.75

Bar location/ units	Shadow Reading Y/cm	Spacing Δ/cm	E/cm	$\alpha \times 10^4$	$\alpha' \times 10^2$	$\alpha'^2 \times 10^4$	m	z'/cm	f/cm
4	0.6382		1.634	3.265	6.109	37.315	0.00534	0.1200	0.13340
3	1.0497	0.412	1.222	2.449	4.569	20.877	0.00536	0.1205	0.13376
2	1.4586	0.409	0.813	1.632	3.040	9.243	0.00537	0.1208	0.13402
1	1.8656	0.407	0.406	0.816	1.518	2.305	0.00538	0.1210	0.13417
0	2.2718	0.406							
-1	2.6780	0.406					g/cm	$(\rho/f_0)^2 = (m_0+1)^2 \alpha'^2$	
-2	3.0854	0.407							
-3	3.4947	0.409					0.11933	37.717	
-4	3.9070	0.412					0.11976	21.102	
							0.12006	9.342	
		Slope	m_o	μ_s			0.12023	2.330	
	4.4E-10	0.0000	0.0054	-1.68362					

f vs $(\rho/f_o)^2$

$S_f = slope_f / f_0$

	$slope_f$	fo/cm	S_f
1.0792E-08	-2E-05	0.134	-1.66

g vs $(\rho/f_o)^2$

$S_g = slope_g / f_0$

	$slope_g$	go/cm	S_g
-1.3E-10	-2.5E-05	0.120	-1.90

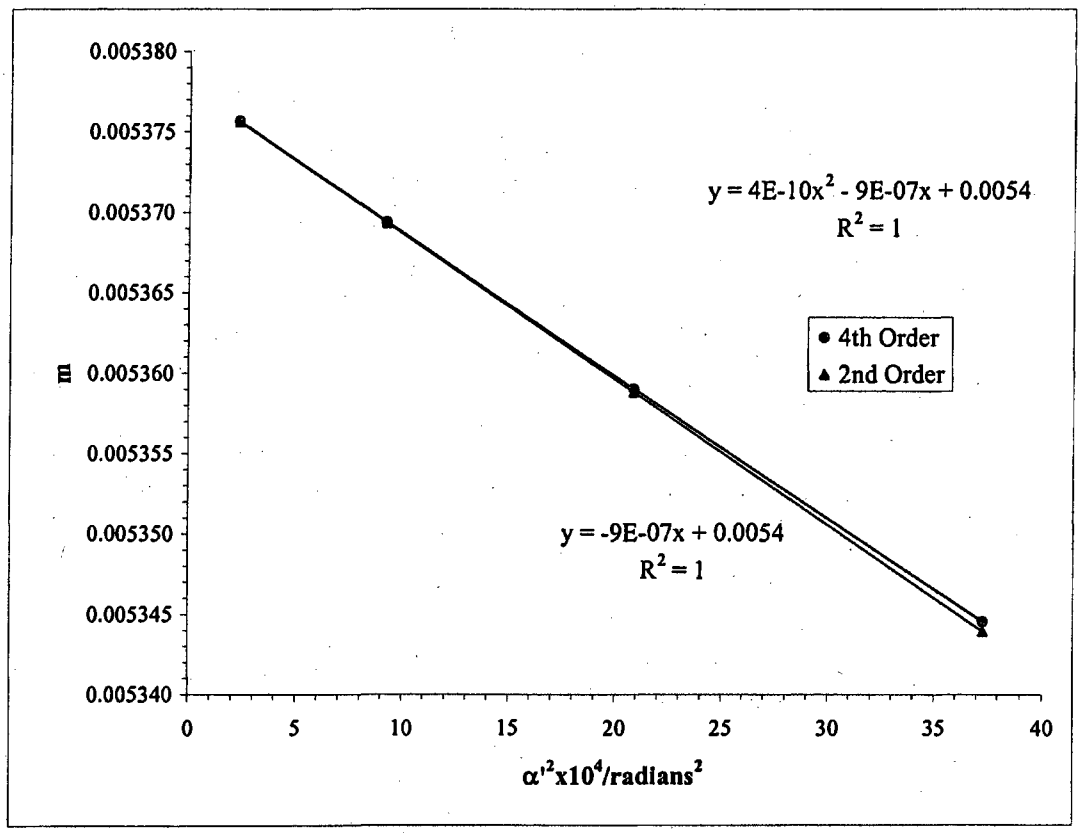

Beam Voltage	I/milliamps	z/cm	z_0'/cm	C_s'/cm
25 kV	400	25.1	0.121	0.260

Average of m_o = 0.00547

Average of μ_s = -1.68

Paraxial properties :

f_o = 0.135 cm

g_o = 0.120 cm

S_f = -1.65

S_g = -1.88

Elektros Electrostatic Objective Lens L_3 Data.

Mesh/inch	V Ratio	Mesh	e'_1/cm	d/cm	b/cm		Beam	Voltage	20 kV
2000	0.60	Rear	0.00127	31.95	2.170	US			
								L3 Elektros obj.	

Bar location/ units	Shadow Reading X/cm	Spacing Δ/cm	E'/cm	M'	c/cm	α' x 10^2	α'^{2} x 10^4	z'/cm
6.5	0.771		0.452	-54.70	-0.574	1.439	2.071	2.744
5.5	0.883	0.113	0.336	-48.09	-0.651	1.073	1.152	2.821
4.5	0.961	0.078	0.257	-45.03	-0.694	0.823	0.678	2.865
3.5	1.027	0.066	0.191	-43.05	-0.725	0.613	0.376	2.896
2.5	1.085	0.058	0.133	-41.95	-0.744	0.427	0.182	2.914
1.5	1.139	0.054	0.079	-41.27	-0.756	0.252	0.064	2.926
0.5	1.191	0.052	0.027	-42.03	-0.742	0.086	0.007	2.913
-0.5	1.244	0.053						
-1.5	1.296	0.052						
-2.5	1.351	0.055						
-3.5	1.410	0.058			Slope	z_0'/cm	C_s'/cm	
-4.5	1.476	0.066		0.006445	-0.104711	2.933	1047.11	
-5.5	1.555	0.079						
-6.5	1.674	0.119						

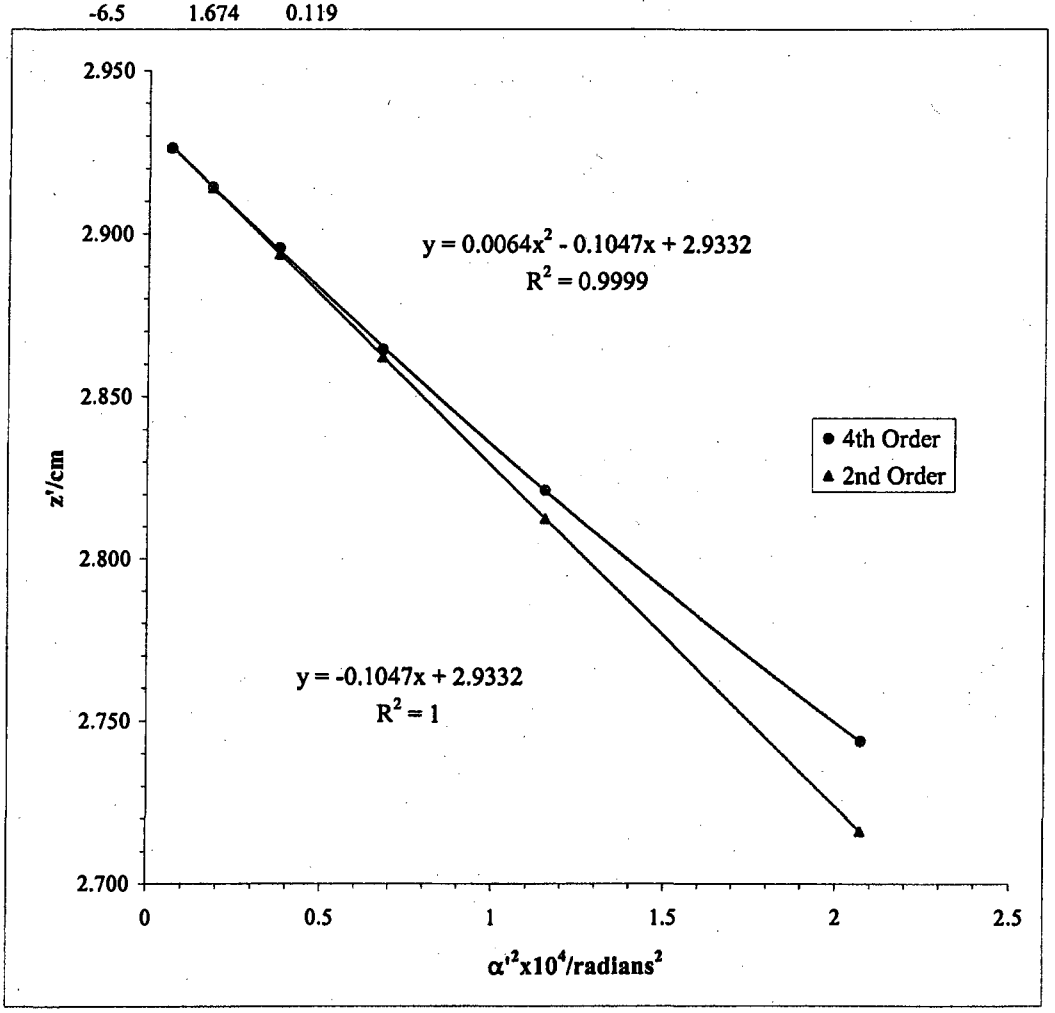

Mesh/inch	V Ratio	Mesh	e'_1/cm	d/cm	b/cm		Beam	Voltage	20 kV
2000	0.60	Rear	0.00127	31.95	2.17	US			
								L3 Elektros obj.	

Bar location/ units	Shadow Reading Y/cm	Spacing Δ/cm	E'/cm	M'	c/cm	α' x 10^2	α'^2 x 10^4	z'/cm
6	0.942		0.388	-50.91	-0.615	1.238	1.533	2.786
5	1.032	0.090	0.295	-46.51	-0.672	0.944	0.892	2.843
4	1.102	0.070	0.224	-44.04	-0.709	0.716	0.513	2.880
3	1.163	0.061	0.163	-42.67	-0.732	0.521	0.271	2.902
2	1.219	0.056	0.106	-41.60	-0.750	0.339	0.115	2.920
1	1.273	0.054	0.052	-40.92	-0.762	0.167	0.028	2.933
0	1.324	0.051						
-1	1.377	0.053						
-2	1.430	0.054						
-3	1.488	0.058						
-4	1.549	0.061						
-5	1.623	0.073						
-6	1.718	0.095						

	Slope	z_0'/cm	C_s'/cm
0.010226	-1.120E-01	2.934	1120.09

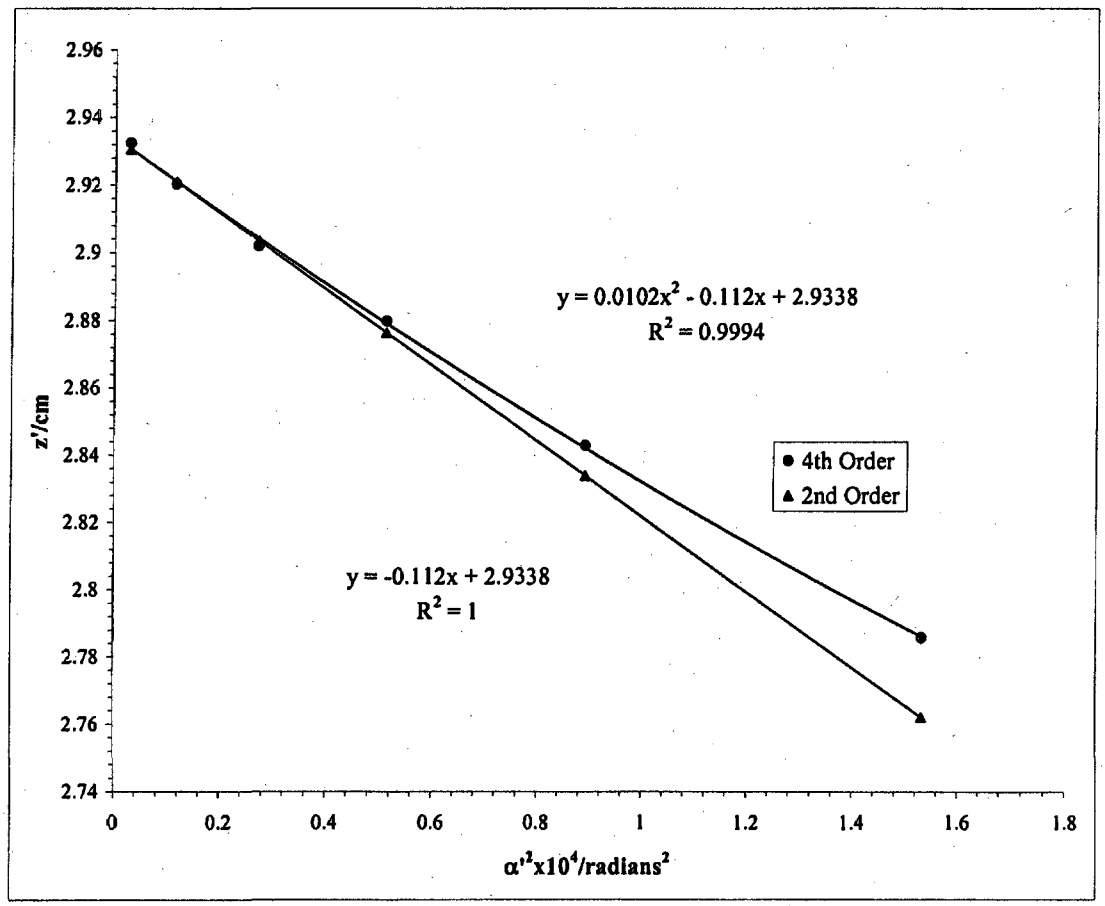

Mesh/inch	V Ratio	Mesh	e'_1/cm	d/cm	b/cm		Beam	Voltage	20 kV
2000	0.60	Rear	0.00127	30.73	3.39	DS			
								L3 Elektros obj.	

Bar location/ units	Shadow Reading X/cm	Spacing Δ/cm	E'/cm	M'	c/cm	α' x 10^2	α'^2 x 10^4	z'/cm
7.5	0.672		0.448	47.08	0.667	1.4284	2.0403	2.723
6.5	0.713	0.042	0.407	49.27	0.637	1.2967	1.6814	2.753
5.5	0.760	0.047	0.362	51.77	0.605	1.1541	1.3319	2.784
4.5	0.810	0.050	0.312	54.55	0.574	0.9958	0.9917	2.816
3.5	0.867	0.057	0.255	57.47	0.544	0.8168	0.6672	2.845
2.5	0.930	0.063	0.193	60.81	0.514	0.6180	0.3819	2.876
1.5	1.003	0.073	0.122	63.82	0.489	0.3895	0.1517	2.900
0.5	1.083	0.080	0.042	65.94	0.473	0.1342	0.0180	2.916
-0.5	1.167	0.084						
-1.5	1.246	0.080						
-2.5	1.316	0.070						
-3.5	1.378	0.062						
-4.5	1.434	0.055						
-5.5	1.484	0.050			Slope	z_o'/cm	C_s'/cm	
-6.5	1.527	0.043		0.00772	-0.110915	2.917	1109.15	
-7.5	1.568	0.042						

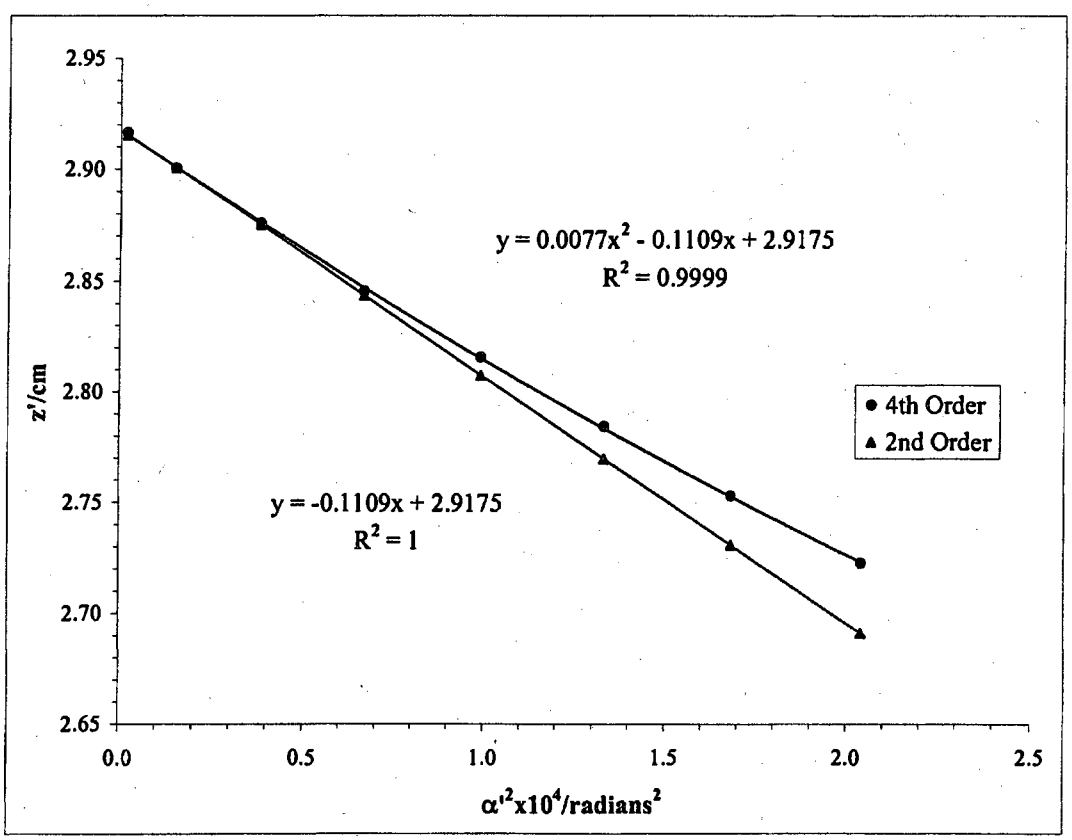

Mesh/inch	V Ratio	Mesh	e'_1/cm	d/cm	b/cm		Beam	Voltage	20 kV
2000	0.60	Rear	0.00127	30.73	3.39	DS			
								L3 Elektros obj.	

Bar location/ units	Shadow Reading Y/cm	Spacing Δ/cm	E'/cm	M'	c/cm	α' x 10^2	α'^{2} x 10^4	z'/cm
13.5	0.442		0.662	38.64	0.816	2.0999	4.4094	2.573
12.5	0.473	0.031	0.631	39.76	0.793	2.0023	4.0092	2.597
11.5	0.506	0.032	0.599	41.03	0.768	1.9023	3.6186	2.622
10.5	0.539	0.034	0.565	42.38	0.743	1.7956	3.2240	2.647
9.5	0.573	0.034	0.531	44.00	0.715	1.6884	2.8505	2.675
8.5	0.610	0.037	0.494	45.74	0.687	1.5718	2.4706	2.703
7.5	0.650	0.040	0.453	47.60	0.660	1.4443	2.0859	2.730
6.5	0.691	0.041	0.412	49.86	0.629	1.3125	1.7226	2.761
5.5	0.737	0.046	0.365	52.27	0.599	1.1654	1.3582	2.790
4.5	0.787	0.050	0.314	54.97	0.569	1.0037	1.0073	2.820
3.5	0.842	0.055	0.258	58.08	0.538	0.8256	0.6817	2.851
2.5	0.905	0.063	0.194	61.13	0.511	0.6213	0.3860	2.879
1.5	0.976	0.071	0.122	64.24	0.486	0.3920	0.1537	2.904
0.5	1.054	0.078	0.043	67.10	0.465	0.1366	0.0187	2.925
-0.5	1.139	0.085						
-1.5	1.220	0.081						
-2.5	1.293	0.073			Slope	z_o'/cm	C_s'/cm	
-3.5	1.358	0.065		0.00543	-0.1024	2.920	1023.59	
-4.5	1.415	0.057						
-5.5	1.467	0.052						
-6.5	1.514	0.047						
-7.5	1.557	0.042						
-8.5	1.598	0.041						
-9.5	1.635	0.037						
-10.5	1.670	0.035						
-11.5	1.704	0.034						
-12.5	1.736	0.032						
-13.5	1.767	0.032						

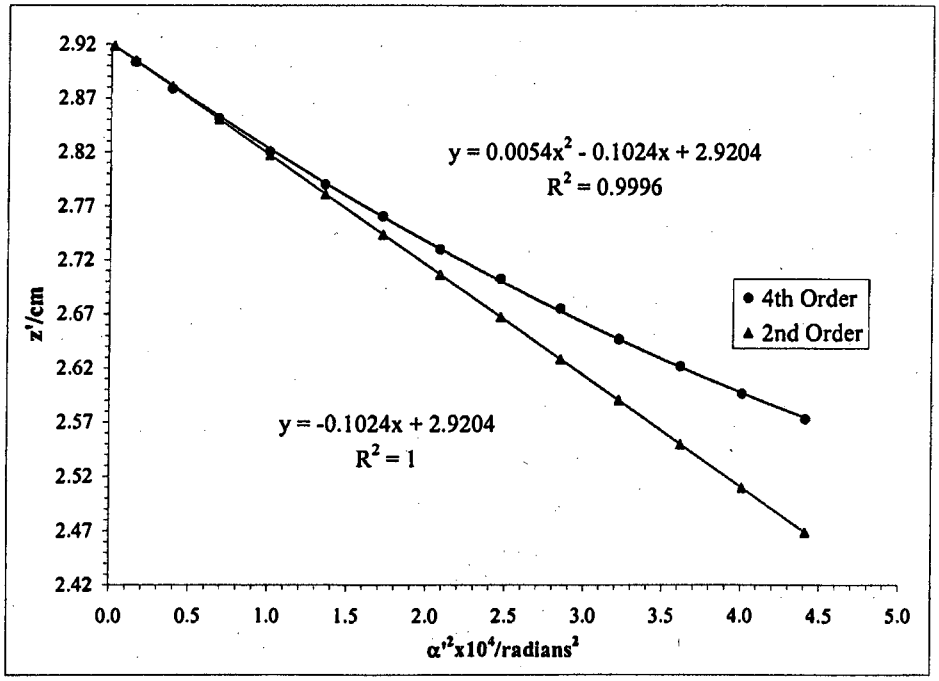

L3 Elektros obj. Beam Voltage 20 kV

Mesh/inch	V Ratio	Mesh	z/cm	e_1/cm	a/cm	z_{ap}/cm	z_0'/cm	C_s'/cm	$z_{ap}-z_o'$
600	0.60	Front	25.00	0.00423	22.40	34.12	2.926	1090.41	31.19

Bar location/ units	Shadow Reading X/cm	Spacing Δ/cm	E/cm	$\alpha \times 10^4$	$\alpha' \times 10^2$	$\alpha'^2 \times 10^4$	m	z'/cm	f/cm
15	0.073		0.942	28.348	2.926	8.563	0.09687	1.992	2.250
14	0.162	0.090	0.854	26.458	2.666	7.110	0.09923	2.151	2.290
13	0.246	0.084	0.771	24.568	2.420	5.856	0.10152	2.287	2.330
12	0.324	0.078	0.694	22.679	2.186	4.779	0.10374	2.405	2.369
11	0.398	0.073	0.621	20.789	1.964	3.857	0.10585	2.505	2.408
10	0.467	0.069	0.553	18.899	1.753	3.071	0.10784	2.591	2.445
9	0.532	0.065	0.488	17.009	1.551	2.404	0.10969	2.664	2.480
8	0.594	0.062	0.426	15.119	1.357	1.842	0.11139	2.725	2.512
7	0.654	0.059	0.367	13.229	1.172	1.373	0.11292	2.776	2.542
6	0.711	0.057	0.311	11.339	0.992	0.985	0.11427	2.819	2.568
5	0.766	0.055	0.256	9.449	0.819	0.670	0.11543	2.853	2.591
4	0.819	0.053	0.203	7.560	0.649	0.422	0.11639	2.880	2.610
3	0.871	0.052	0.151	5.670	0.484	0.234	0.11715	2.900	2.625
2	0.922	0.051	0.100	3.780	0.321	0.103	0.11769	2.915	2.636
1	0.972	0.050	0.050	1.890	0.160	0.026	0.11801	2.923	2.642
0	1.022	0.050							
-1	1.072	0.050							
-2	1.123	0.050							
-3	1.173	0.051							
-4	1.225	0.052							
-5	1.278	0.053							
-6	1.332	0.054							
-7	1.388	0.056							
-8	1.447	0.058							
-9	1.508	0.061							
-10	1.572	0.064							
-11	1.640	0.068							
-12	1.712	0.072							
-13	1.788	0.076							
-14	1.869	0.081							
-15	1.957	0.087							

	Slope	m_o	μ_s
1.5E-04	-0.0037	0.11792	-315.31

g/cm	$(\rho/f_0)^2 = (m_0+1)^2 \alpha'^2$
1.774	10.702
1.923	8.885
2.051	7.319
2.159	5.973
2.250	4.821
2.327	3.838
2.392	3.005
2.445	2.302
2.489	1.715
2.525	1.231
2.554	0.838
2.576	0.527
2.593	0.293
2.604	0.129
2.611	0.032

f vs $(\rho/f_o)^2$

$S_f = slope_f / f_0$

	$slope_f$	fo/cm	S_f
0.00209	-0.05832	2.640	-220.95

g vs $(\rho/f_o)^2$

$S_g = slope_g / f_0$

	$slope_g$	go/cm	S_g
-0.000533	-0.07298	2.615	-276.46

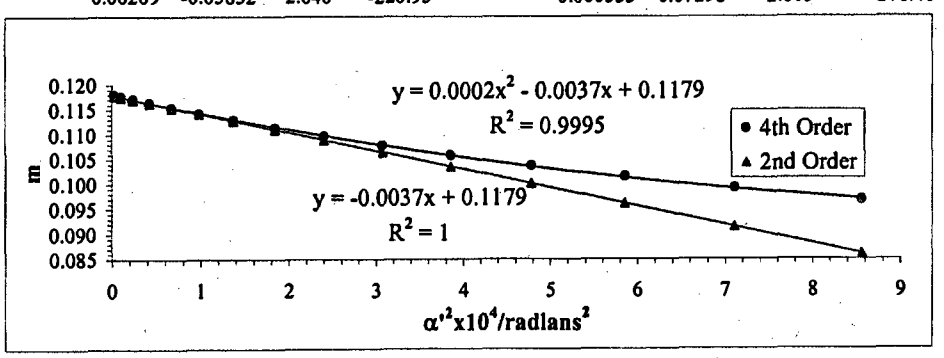

L3 Elektros obj.							Beam	Voltage	20 kV
Mesh/inch	V Ratio	Mesh	z/cm	e_1/cm	a/cm	z_{ap}/cm	z_0'/cm	C_1'/cm	$z_{ap}-z_o'$
600	0.60	Front	25.00	0.00423	22.40	34.12	2.926	1090.41	31.19

Bar location/ units	Shadow Reading Y/cm	Spacing Δ/cm	E/cm	α x 10^4	α' x 10^2	α'^{2} x 10^4	m	z'/cm	f/cm
12	0.482		0.670	22.679	2.115	4.473	0.10723	2.438	2.448
11	0.549	0.067	0.603	20.789	1.908	3.640	0.10896	2.529	2.478
10	0.613	0.064	0.539	18.899	1.709	2.919	0.11061	2.608	2.507
9	0.674	0.061	0.477	17.009	1.516	2.299	0.11217	2.675	2.536
8	0.733	0.059	0.418	15.119	1.331	1.771	0.11362	2.733	2.563
7	0.790	0.057	0.361	13.229	1.151	1.324	0.11495	2.782	2.588
6	0.844	0.055	0.306	11.339	0.976	0.953	0.11614	2.822	2.611
5	0.898	0.053	0.252	9.449	0.806	0.650	0.11717	2.855	2.631
4	0.950	0.052	0.200	7.560	0.640	0.410	0.11803	2.881	2.648
3	1.000	0.051	0.149	5.670	0.478	0.228	0.11871	2.901	2.661
2	1.050	0.050	0.099	3.780	0.317	0.101	0.11921	2.915	2.671
1	1.100	0.050	0.049	1.890	0.158	0.025	0.11951	2.923	2.677
0	1.149	0.049							
-1	1.199	0.049					g/cm	$(\rho/f_0)^2 = (m_0+1)^2\alpha'^2$	
-2	1.248	0.050							
-3	1.299	0.050					2.176	5.606	
-4	1.350	0.051					2.259	4.563	
-5	1.402	0.052					2.330	3.659	
-6	1.456	0.054					2.391	2.882	
-7	1.511	0.055					2.442	2.219	
-8	1.568	0.057					2.484	1.660	
-9	1.628	0.060					2.519	1.195	
-10	1.690	0.062					2.547	0.815	
-11	1.755	0.065					2.569	0.514	
-12	1.823	0.068					2.585	0.286	
							2.597	0.126	
			Slope	m_o	μ_s		2.603	0.031	
		2.2E-04	-0.0037	0.12	-311.80				

f vs $(\rho/f_o)^2$

$S_f = slope_f / f_0$

	$slope_f$	fo/cm	S_f
0.003098	-0.05809	2.677	-216.98

g vs $(\rho/f_o)^2$

$S_g = slope_g / f_0$

	$slope_g$	go/cm	S_g
-0.000802	-0.0723053	2.606	-270.08

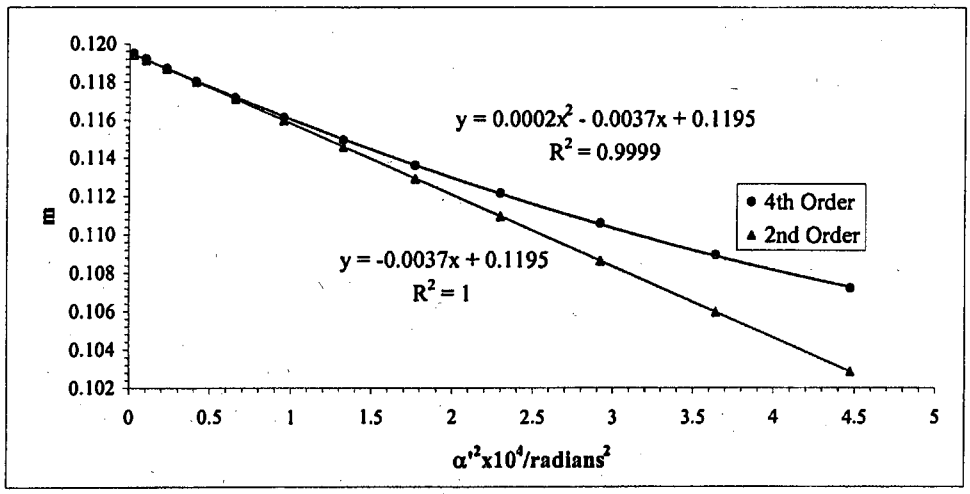

Beam Voltage	Volt Ratio	z/cm	z_0'/cm	C_s'/cm
20 kV	0.60	25.0	2.93	1090.41

L3 Elektros obj.

Average of m_0 = 0.119

Average of μ_s = -314

Paraxial properties :

f_0 = 2.66 cm

g_0 = 2.61 cm

S_f = -219

S_g = -273

Mesh/inch	V Ratio	Mesh	e'_1/cm	d/cm	b/cm		Beam	Voltage	20 kV
2000	0.70	Rear	0.00127	32.86	1.256	US			
								L3 Elektros obj.	

Bar location/ units	Shadow Reading X/cm	Spacing Δ/cm	E'/cm	M'	c/cm	α' x 10^2	α'^2 x 10^4	z'/cm
7	1.237		0.746	-83.91	-0.387	2.2968	5.275	1.643
6	1.413	0.176	0.581	-76.25	-0.425	1.7911	3.208	1.681
5	1.539	0.126	0.458	-72.17	-0.449	1.4139	1.999	1.705
4	1.646	0.107	0.352	-69.37	-0.467	1.0878	1.183	1.723
3	1.743	0.097	0.257	-67.38	-0.481	0.7928	0.629	1.737
2	1.832	0.089	0.168	-66.02	-0.490	0.5180	0.268	1.746
1	1.917	0.084	0.084	-65.79	-0.492	0.2581	0.067	1.748
0	2.000	0.083						
-1	2.084	0.084						
-2	2.168	0.084						
-3	2.256	0.089						
-4	2.351	0.095						
-5	2.456	0.104						
-6	2.575	0.119			Slope	z_0'/cm	C_s'/cm	
-7	2.729	0.154		0.00068124	-0.024047	1.75	240.47	

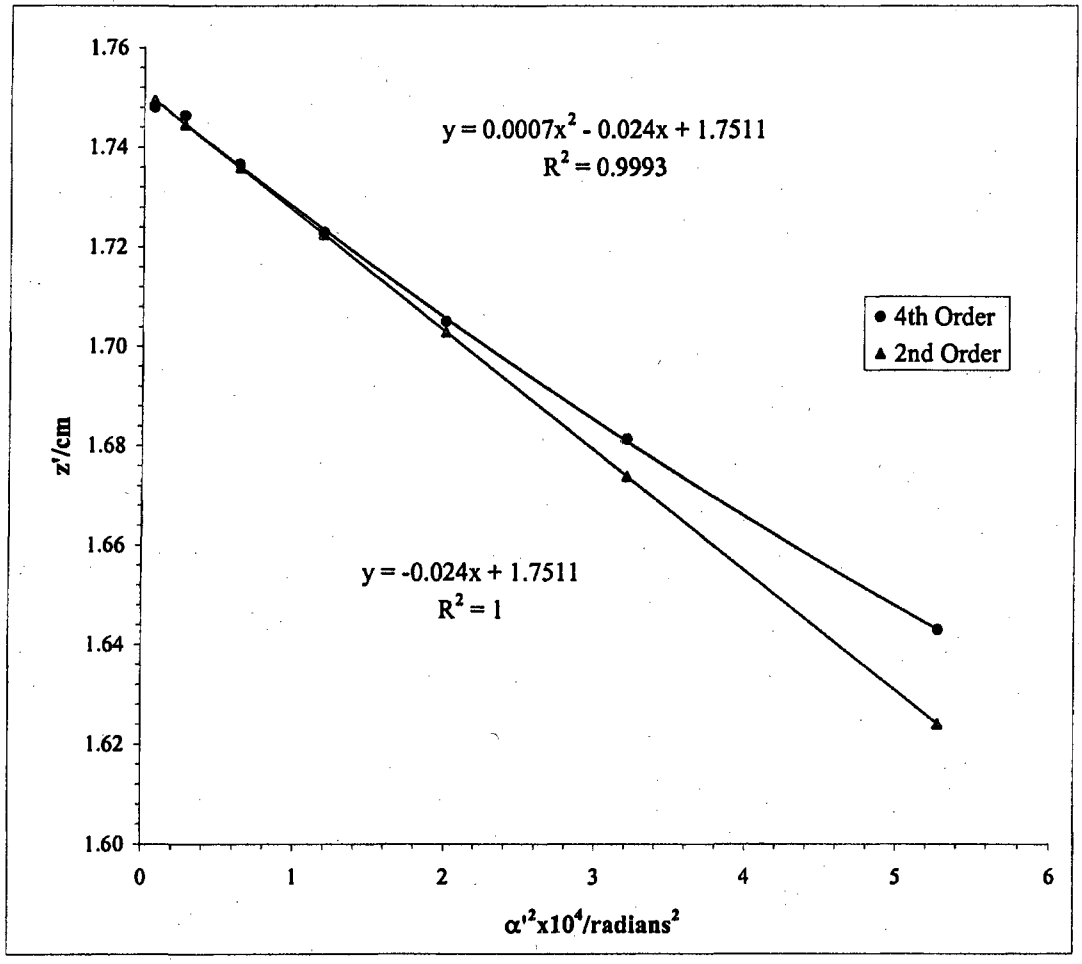

Mesh/inch	V Ratio	Mesh	e'_1/cm	d/cm	b/cm		Beam	Voltage	20 kV
2000	0.70	Rear	0.00127	32.86	1.26	US			
								L3 Elektros obj.	

Bar location/ units	Shadow Reading Y/cm	Spacing Δ/cm	E'/cm	M'	c/cm	α' x 10^2	α'^2 x 10^4	z'/cm
7	0.854		0.743	-83.56	-0.389	2.2874	5.232	1.645
6	1.016	0.162	0.579	-76.03	-0.427	1.7861	3.190	1.683
5	1.140	0.124	0.456	-71.81	-0.451	1.4068	1.979	1.707
4	1.244	0.105	0.352	-69.21	-0.468	1.0853	1.178	1.724
3	1.339	0.094	0.257	-67.47	-0.480	0.7938	0.630	1.736
2	1.426	0.088	0.169	-66.37	-0.488	0.5207	0.271	1.744
1	1.512	0.086	0.083	-65.11	-0.497	0.2555	0.065	1.753
0	1.596	0.083						
-1	1.678	0.082						
-2	1.764	0.086						
-3	1.853	0.089						
-4	1.948	0.095						
-5	2.052	0.104						
-6	2.175	0.123			Slope	z_o'/cm	C_z'/cm	
-7	2.340	0.165		0.000725	-2.429E-02	1.752	242.87	

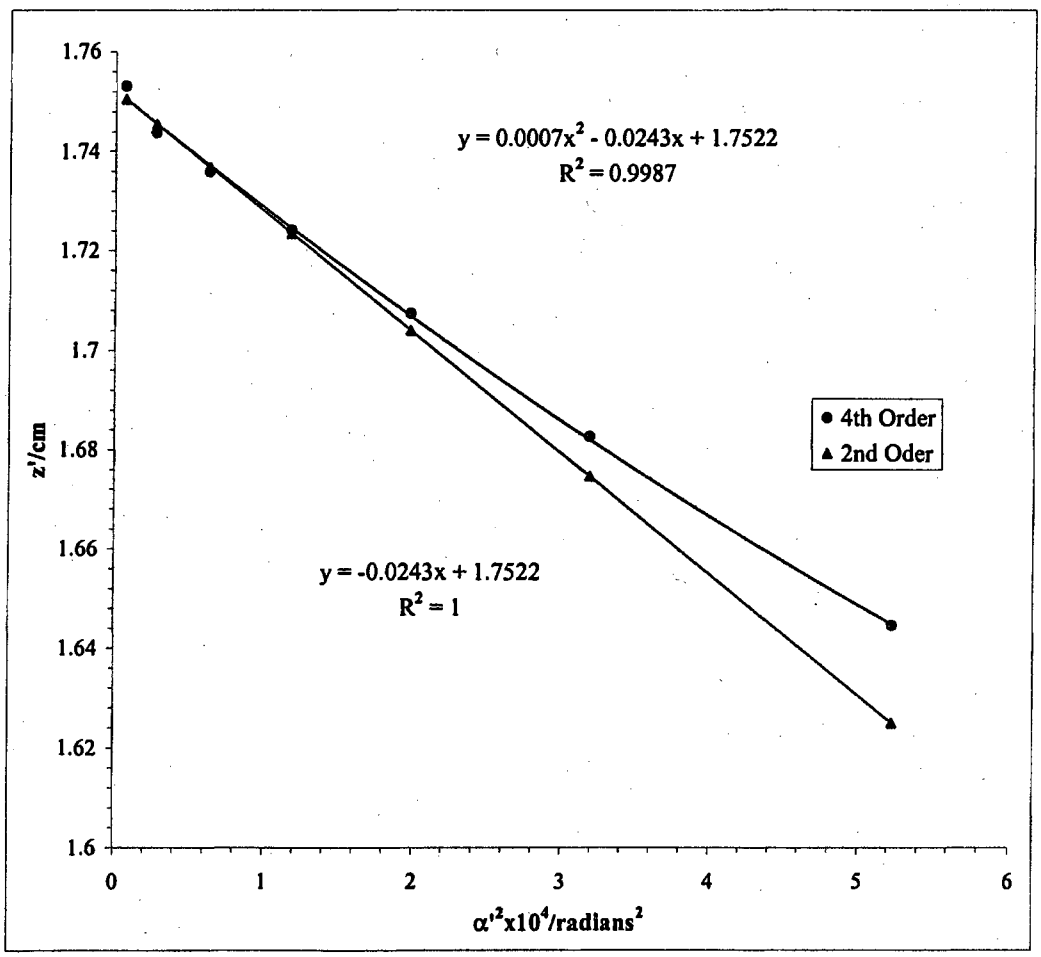

Mesh/Inch	V Ratio	Mesh	e'_1/cm	d/cm	b/cm		Beam	Voltage	20 kV
2000	0.70	Rear	0.00127	32.13	1.99	DS			
								L3 Elektros obj.	

Bar location/ units	Shadow Reading X/cm	Spacing Δ/cm	E'/cm	M'	c/cm	α' x 10^2	α'^2 x 10^4	z'/cm
14.5	1.005		1.208	65.62	0.497	3.7038	13.7180	1.495
13.5	1.055	0.050	1.159	67.59	0.482	3.5536	12.6279	1.510
12.5	1.110	0.054	1.105	69.63	0.468	3.3915	11.5020	1.525
11.5	1.164	0.054	1.051	71.94	0.453	3.2250	10.4005	1.540
10.5	1.222	0.058	0.994	74.52	0.437	3.0517	9.3128	1.556
9.5	1.282	0.060	0.934	77.38	0.421	2.8684	8.2277	1.572
8.5	1.347	0.065	0.871	80.65	0.403	2.6764	7.1632	1.589
7.5	1.415	0.068	0.803	84.29	0.386	2.4693	6.0975	1.607
6.5	1.490	0.075	0.730	88.41	0.368	2.2460	5.0447	1.625
5.5	1.570	0.080	0.651	93.23	0.348	2.0052	4.0210	1.644
4.5	1.660	0.091	0.563	98.55	0.329	1.7353	3.0112	1.663
3.5	1.761	0.100	0.465	104.68	0.310	1.4345	2.0579	1.683
2.5	1.877	0.116	0.353	111.28	0.291	1.0898	1.1878	1.701
1.5	2.010	0.133	0.225	117.97	0.275	0.6936	0.4811	1.718
0.5	2.160	0.150	0.077	122.03	0.265	0.2392	0.0572	1.727
-0.5	2.315	0.155						
-1.5	2.459	0.144						
-2.5	2.584	0.124			Slope	z_o'/cm	C_s'/cm	
-3.5	2.691	0.108		0.00039	-0.022135	1.728	221.35	
-4.5	2.787	0.095						
-5.5	2.872	0.085						
-6.5	2.950	0.077						
-7.5	3.021	0.071						
-8.5	3.088	0.068						
-9.5	3.149	0.061						
-10.5	3.210	0.060						
-11.5	3.265	0.056						
-12.5	3.321	0.055						
-13.5	3.373	0.052						
-14.5	3.422	0.049						

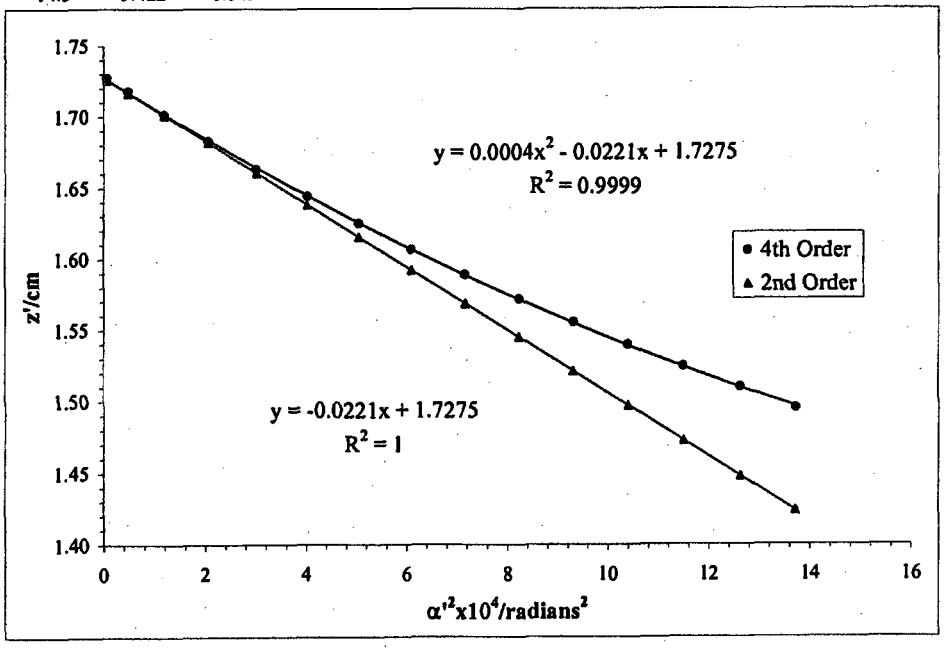

Mesh/inc	V Ratio	Mesh	e'_1/cm	d/cm	b/cm		Beam	Voltage	20 kV
2000	0.70	Rear	0.00127	32.13	1.99	DS			
								L3 Elektros obj.	

Bar location units	Shadow Reading Y/cm	Spacing Δ/cm	E'/cm	M'	c/cm	α' x 10^2	α'^2 x 10^4	z'/cm
14.5	1.274		1.218	66.16	0.493	3.7348	13.9488	1.500
13.5	1.326	0.052	1.167	68.08	0.479	3.5795	12.8131	1.514
12.5	1.379	0.054	1.114	70.18	0.464	3.4185	11.6861	1.528
11.5	1.434	0.054	1.060	72.55	0.449	3.2528	10.5808	1.544
10.5	1.492	0.059	1.002	75.12	0.433	3.0766	9.4656	1.559
9.5	1.552	0.060	0.942	78.06	0.417	2.8939	8.3748	1.576
8.5	1.618	0.066	0.878	81.29	0.400	2.6979	7.2787	1.593
7.5	1.687	0.068	0.810	85.01	0.382	2.4907	6.2034	1.610
6.5	1.762	0.076	0.736	89.10	0.365	2.2638	5.1249	1.628
5.5	1.844	0.082	0.656	93.93	0.346	2.0205	4.0822	1.647
4.5	1.935	0.091	0.568	99.47	0.326	1.7517	3.0685	1.666
3.5	2.036	0.101	0.470	105.74	0.307	1.4491	2.0999	1.686
2.5	2.154	0.117	0.357	112.30	0.289	1.0999	1.2098	1.704
1.5	2.288	0.135	0.226	118.81	0.273	0.6985	0.4880	1.720
0.5	2.441	0.152	0.078	122.74	0.264	0.2406	0.0579	1.729
-0.5	2.596	0.156						
-1.5	2.741	0.144						
-2.5	2.867	0.126			Slope	z_o'/cm	C_s'/cm	
-3.5	2.976	0.110		0.000364	-0.021498	1.730	214.98	
-4.5	3.072	0.096						
-5.5	3.157	0.085						
-6.5	3.233	0.077						
-7.5	3.306	0.073						
-8.5	3.373	0.067						
-9.5	3.436	0.063						
-10.5	3.496	0.060						
-11.5	3.553	0.057						
-12.5	3.607	0.055						
-13.5	3.660	0.052						
-14.5	3.710	0.051						

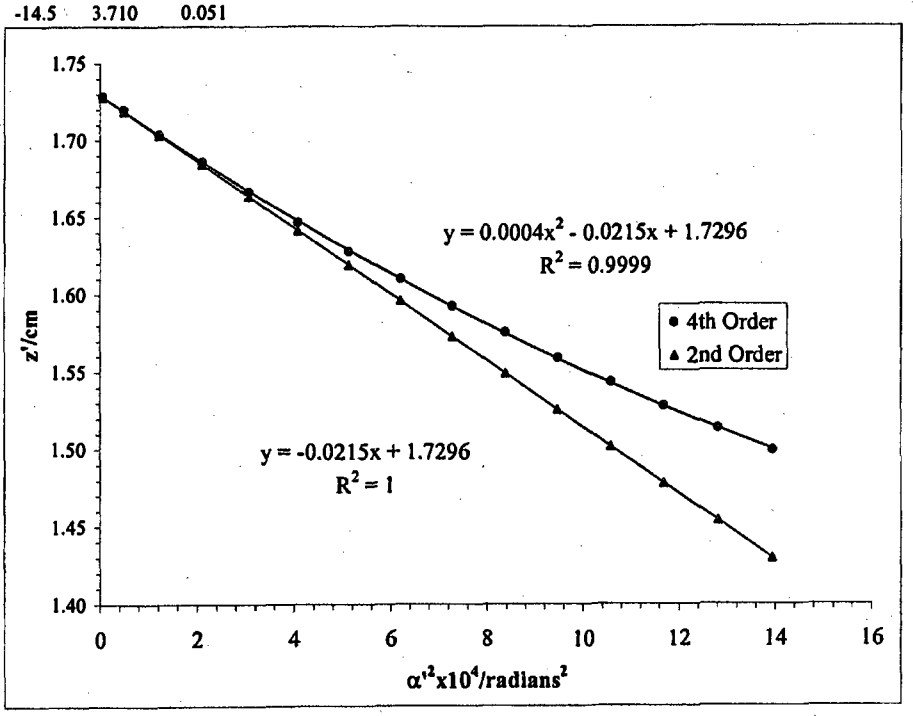

L3 Elektros obj. Beam Voltage 20 kV

Mesh/inch	V Ratio	Mesh	z/cm	e_1/cm	a/cm	z_{xp}/cm	z_o'/cm	C_t'/cm	$z_{xp}-z_o'$
600	0.70	Front	25.00	0.00423	22.40	34.12	1.744	263.79	32.38

Bar location/ units	Shadow Reading X/cm	Spacing Δ/cm	E/cm	$\alpha \times 10^4$	$\alpha' \times 10^2$	$\alpha'^2 \times 10^4$	m	z'/cm	f/cm
12	1.010		1.201	22.679	3.670	13.466	0.06180	1.388	1.465
11	1.136	0.126	1.076	20.789	3.293	10.843	0.06313	1.458	1.492
10	1.254	0.118	0.957	18.899	2.936	8.619	0.06437	1.516	1.518
9	1.366	0.112	0.845	17.009	2.596	6.740	0.06552	1.566	1.542
8	1.473	0.107	0.739	15.119	2.272	5.160	0.06656	1.607	1.564
7	1.575	0.102	0.637	13.229	1.960	3.843	0.06748	1.642	1.584
6	1.673	0.098	0.539	11.339	1.660	2.756	0.06830	1.671	1.601
5	1.767	0.095	0.444	9.449	1.370	1.876	0.06899	1.694	1.616
4	1.859	0.092	0.352	7.560	1.087	1.181	0.06956	1.712	1.628
3	1.949	0.090	0.262	5.670	0.810	0.656	0.07001	1.726	1.637
2	2.038	0.088	0.174	3.780	0.537	0.289	0.07033	1.736	1.644
1	2.125	0.087	0.087	1.890	0.268	0.072	0.07052	1.742	1.648
0	2.212	0.087							
-1	2.298	0.087							
-2	2.386	0.087							
-3	2.474	0.088							
-4	2.564	0.090							
-5	2.656	0.092							
-6	2.750	0.095							
-7	2.848	0.098							
-8	2.950	0.102							
-9	3.057	0.107							
-10	3.169	0.112							
-11	3.287	0.118							
-12	3.413	0.126							

g/cm	$(\rho/f)^2 = (m+1)^2 \alpha'^2$
1.298	15.433
1.363	12.427
1.418	9.878
1.465	7.724
1.503	5.914
1.535	4.404
1.562	3.159
1.583	2.150
1.599	1.353
1.612	0.752
1.620	0.331
1.625	0.082

	Slope	m_o	μ_s
1.5E-05	-0.0009	0.07	-120.59

f vs $(\rho/f_o)^2$

$S_f = slope_f / f_0$

	$slope_f$	fo/cm	S_f
0.00026	-0.015916	1.649	-96.51

g vs $(\rho/f_o)^2$

$S_g = slope_g / f_0$

	$slope_g$	go/cm	S_g
-4.19295E-05	-0.020706	1.627	-125.56

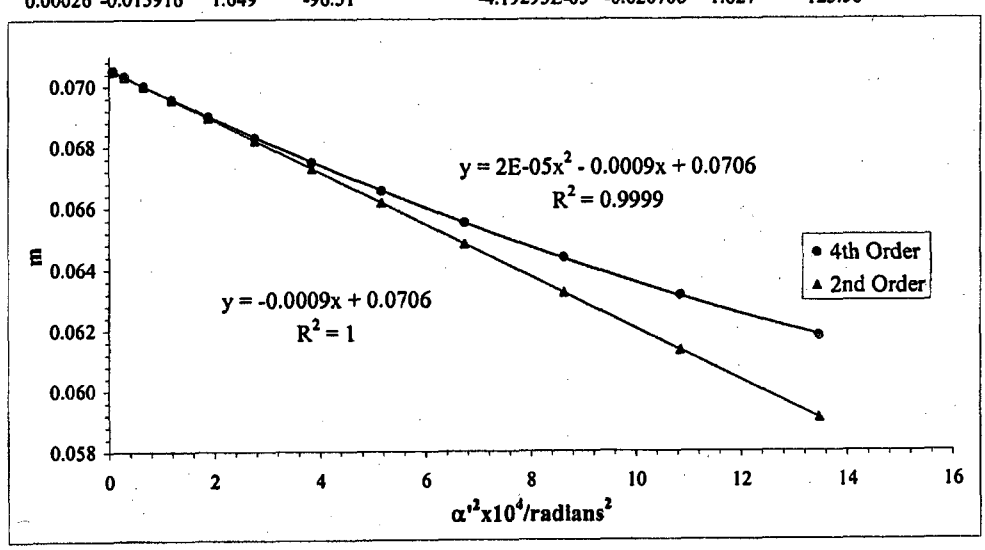

L3 Elektros obj. Beam Voltage 20 kV

Mesh/inch	V Ratio	Mesh	z/cm	e_1/cm	a/cm	z_{sp}/cm	z_0'/cm	C_s'/cm	$z_{sp}-z_0'$
600	0.70	Front	25.00	0.00423	22.40	34.12	1.744	263.79	32.38

Bar location/ units	Shadow Reading Y/cm	Spacing Δ/cm	E/cm	$\alpha \times 10^4$	$\alpha' \times 10^2$	$\alpha'^2 \times 10^4$	m	z'/cm	f/cm
12	1.371		1.200	22.679	3.665	13.432	0.0619	1.389	1.467
11	1.497	0.126	1.075	20.789	3.290	10.821	0.0632	1.458	1.494
10	1.616	0.119	0.957	18.899	2.935	8.617	0.0644	1.516	1.518
9	1.728	0.112	0.845	17.009	2.597	6.742	0.0655	1.566	1.542
8	1.835	0.107	0.739	15.119	2.273	5.168	0.0665	1.607	1.563
7	1.937	0.102	0.637	13.229	1.963	3.851	0.0674	1.642	1.582
6	2.036	0.099	0.539	11.339	1.662	2.761	0.0682	1.671	1.599
5	2.132	0.096	0.444	9.449	1.369	1.875	0.0690	1.694	1.616
4	2.224	0.093	0.352	7.560	1.087	1.182	0.0695	1.712	1.627
3	2.314	0.089	0.263	5.670	0.811	0.657	0.0699	1.726	1.636
2	2.401	0.087	0.175	3.780	0.542	0.293	0.0698	1.736	1.631
1	2.490	0.089	0.087	1.890	0.268	0.072	0.0704	1.742	1.646
0	2.577	0.087							
-1	2.664	0.086							
-2	2.752	0.088							
-3	2.839	0.087							
-4	2.929	0.090							
-5	3.020	0.091							
-6	3.115	0.095							
-7	3.212	0.097							
-8	3.314	0.102							
-9	3.419	0.105							
-10	3.530	0.111							
-11	3.646	0.116							
-12	3.771	0.125							

g/cm	$(\rho/f_0)^2 = (m_0+1)^2\alpha'^2$
1.298	15.389
1.364	12.398
1.419	9.872
1.465	7.724
1.503	5.921
1.535	4.413
1.562	3.164
1.583	2.148
1.599	1.355
1.612	0.753
1.622	0.336
1.626	0.082

	Slope	m_0	μ_s
1.3E-05	-0.0008	0.0704	-114.51

f vs $(\rho/f_0)^2$

$S_f = slope_f / f_0$

	$slope_f$	fo/cm	S_f
0.000224	-0.01499	1.645	-91.17

g vs $(\rho/f_0)^2$

$S_g = slope_g / f_0$

$slope_g$	go/cm	S_g
-3.65205E-05	-0.020845	1.628	-126.75

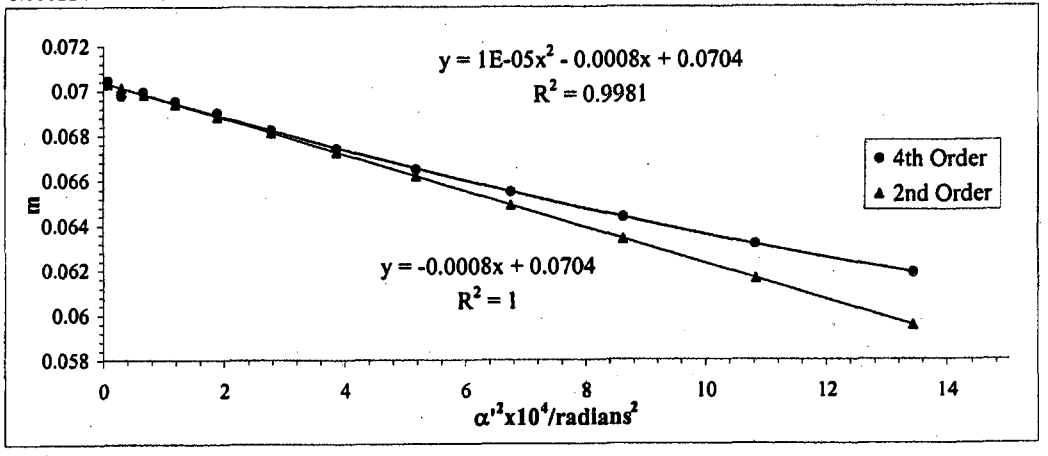

Beam Voltage	Volt Ratio	z/cm	z_0'/cm	C_s'/cm	L3 Elektros obj.
20 kV	0.70	25.00	1.744	263.79	

Average of m_o = 0.0705

Average of μ_s = -117.55

Paraxial properties :

f_o = 1.647 cm

g_o = 1.628 cm

S_f = -93.84

S_g = -126.15

Mesh/inch	V Ratio	Mesh	e'_1/cm	d/cm	b/cm		Beam	Voltage	20 kV
2000	0.80	Rear	0.00127	33.32	0.799	US			
								L3 Elektros obj.	

Bar location/ units	Shadow Reading X/cm	Spacing Δ/cm	E'/cm	M'	c/cm	$\alpha' \times 10^2$	$\alpha'^2 \times 10^4$	z'/cm
5.5	1.770		0.897	-128.41	-0.257	2.7128	7.359	1.056
4.5	1.968	0.198	0.690	-120.76	-0.274	2.0883	4.361	1.072
3.5	2.138	0.170	0.515	-115.89	-0.285	1.5594	2.432	1.084
2.5	2.291	0.153	0.359	-113.11	-0.292	1.0873	1.182	1.091
1.5	2.436	0.145	0.212	-111.35	-0.297	0.6423	0.413	1.095
0.5	2.577	0.142	0.071	-111.24	-0.297	0.2139	0.046	1.096
-0.5	2.719	0.141						
-1.5	2.860	0.141						
-2.5	3.009	0.149						
-3.5	3.168	0.159						
-4.5	3.349	0.180						
-5.5	3.564	0.215						

	Slope	z_0'/cm	C_s'/cm
4.3087E-05	-0.005974	1.098	59.74

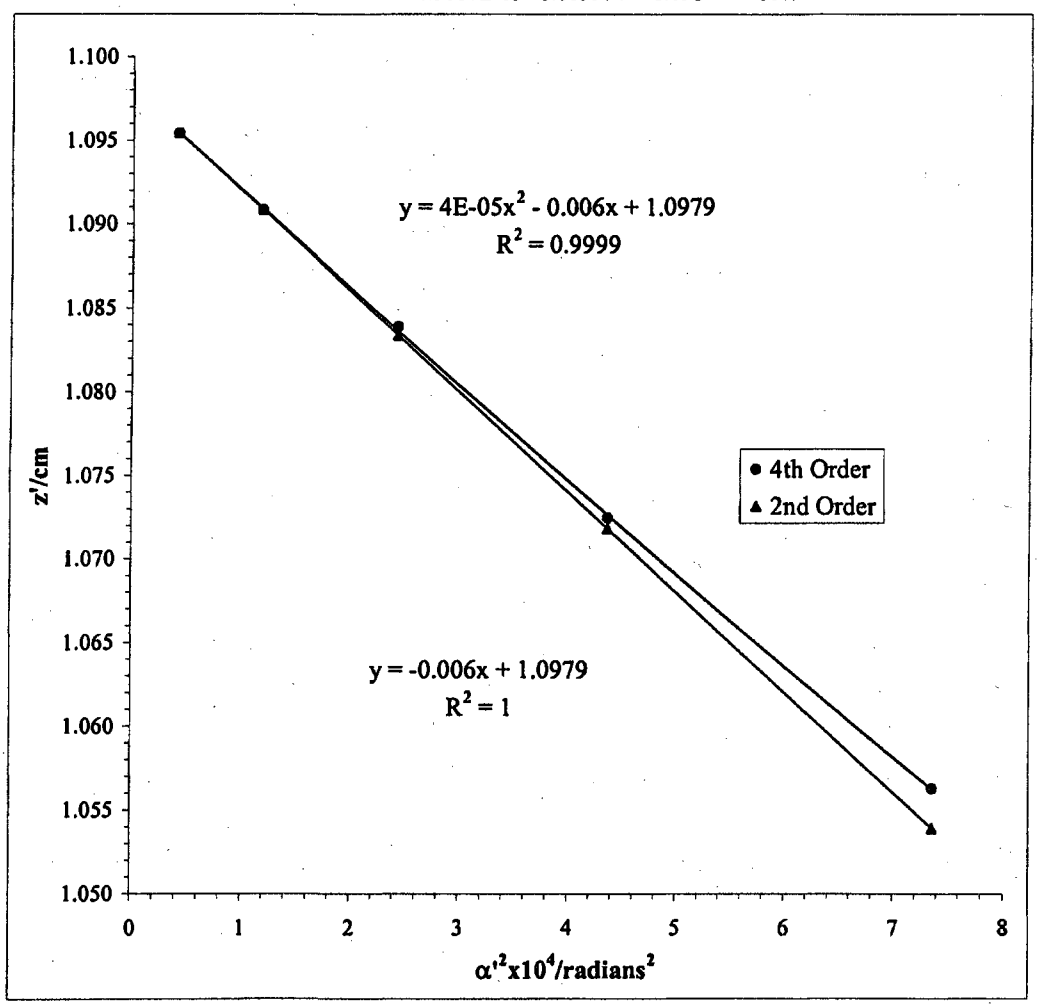

Mesh/inch	V Ratio	Mesh	e'_1/cm	d/cm	b/cm	Number	Beam	Voltage	20 kV
2000	0.80	Rear	0.00127	33.32	0.799	US			
								L3 Elektros obj.	

Bar location/ units	Shadow Reading Y/cm	Spacing Δ/cm	E'/cm	M'	c/cm	α' x 10^2	α'^{2} x 10^4	z'/cm
6.5	1.611		1.203	-145.75	-0.227	3.6356	13.218	1.026
5.5	1.939	0.327	0.902	-129.20	-0.256	2.7293	7.449	1.055
4.5	2.156	0.217	0.693	-121.31	-0.272	2.0977	4.401	1.071
3.5	2.336	0.180	0.517	-116.42	-0.284	1.5663	2.453	1.083
2.5	2.495	0.160	0.360	-113.26	-0.292	1.0887	1.185	1.090
1.5	2.643	0.148	0.213	-111.69	-0.296	0.6443	0.415	1.095
0.5	2.786	0.143	0.070	-109.80	-0.301	0.2112	0.045	1.100
-0.5	2.925	0.139						
-1.5	3.069	0.143						
-2.5	3.215	0.146						
-3.5	3.371	0.156						
-4.5	3.542	0.171						
-5.5	3.744	0.202						
-6.5	4.018	0.274						

	Slope	z_o'/cm	C_s'/cm
5.44E-05	-6.121E-03	1.097	61.21

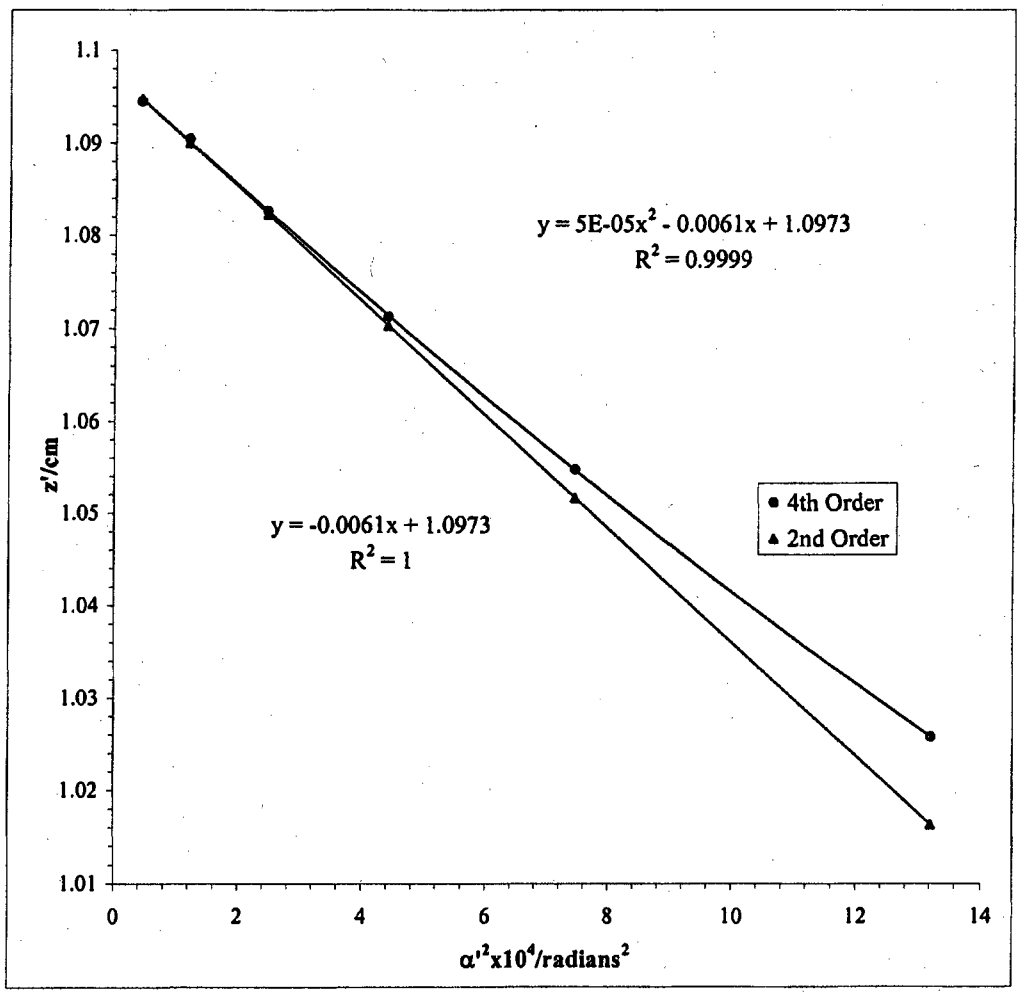

Mesh/inch	V Ratio	Mesh	e'_1/cm	d/cm	b/cm		Beam	Voltage	20 kV
2000	0.80	Rear	0.00127	32.86	1.26	DS			
								L3 Elektros obj.	

Bar location/ units	Shadow Reading X/cm	Spacing Δ/cm	E'/cm	M'	c/cm	α' x 10^2	α'^2 x 10^4	z'/cm
7.5	1.265		1.277	134.04	0.247	3.8561	14.8691	1.009
6.5	1.379	0.115	1.161	140.59	0.235	3.5064	12.2949	1.021
5.5	1.505	0.125	1.035	148.21	0.223	3.1288	9.7892	1.033
4.5	1.642	0.137	0.897	156.96	0.211	2.7122	7.3562	1.045
3.5	1.796	0.155	0.741	166.79	0.198	2.2424	5.0283	1.058
2.5	1.973	0.177	0.563	177.29	0.186	1.7031	2.9007	1.070
1.5	2.177	0.204	0.357	187.25	0.176	1.0796	1.1656	1.080
0.5	2.410	0.233	0.122	192.06	0.172	0.3692	0.1363	1.084
-0.5	2.654	0.244						
-1.5	2.890	0.237						
-2.5	3.099	0.209			Slope	z_o'/cm	C_s'/cm	
-3.5	3.279	0.180		3.9E-05	-0.005744	1.086	57.44	
-4.5	3.436	0.157						
-5.5	3.575	0.140						
-6.5	3.701	0.125						
-7.5	3.818	0.118						

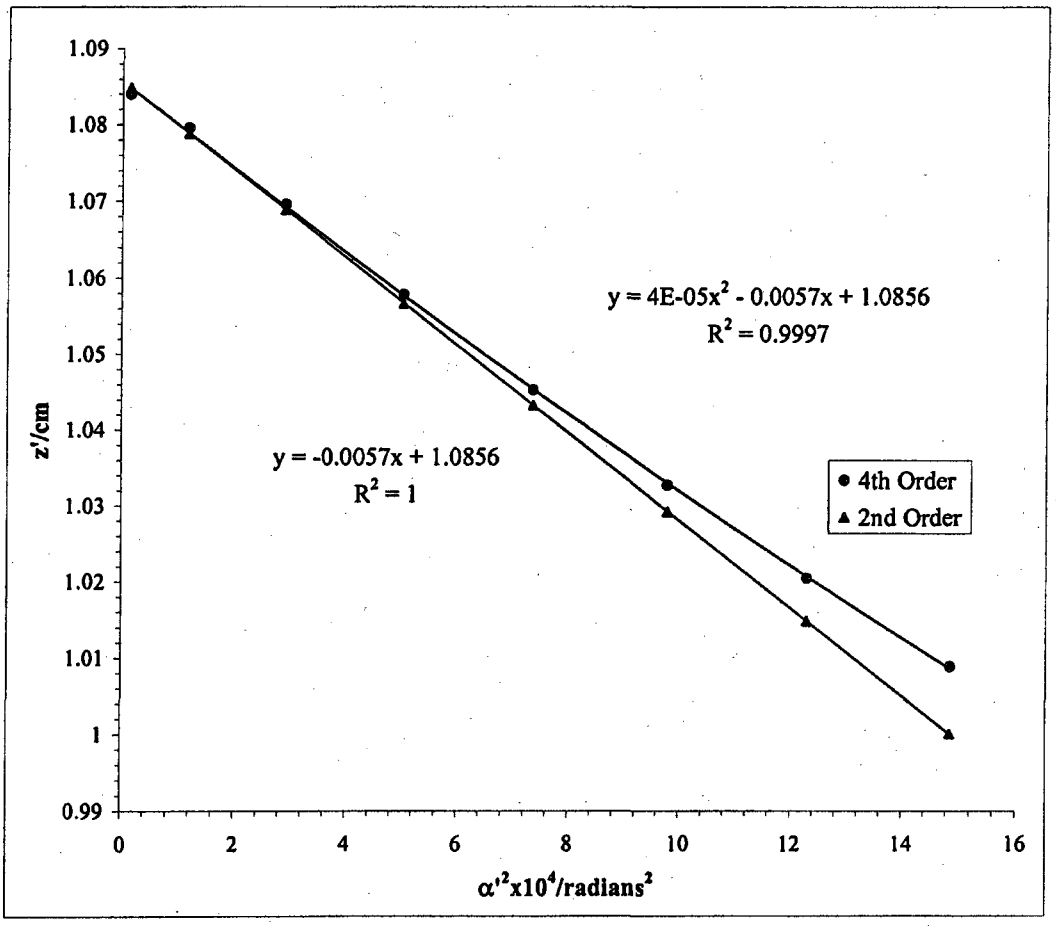

Mesh/inch	V Ratio	Mesh	e'_1/cm	d/cm	b/cm		Beam	Voltage	20 kV
2000	0.80	Rear	0.00127	32.86	1.26	DS			
								L3 Elektros obj.	

Bar location/ units	Shadow Reading Y/cm	Spacing Δ/cm	E'/cm	M'	c/cm	α' x 10^2	α'^2 x 10^4	z'/cm
7	1.280		1.210	136.11	0.243	3.6550	13.3588	1.013
6	1.398	0.118	1.090	143.07	0.231	3.2941	10.8511	1.025
5	1.526	0.128	0.960	151.16	0.219	2.9013	8.4178	1.037
4	1.670	0.144	0.814	160.32	0.206	2.4628	6.0653	1.050
3	1.830	0.160	0.650	170.53	0.194	1.9654	3.8629	1.062
2	2.015	0.186	0.460	180.96	0.183	1.3909	1.9347	1.073
1	2.229	0.214	0.241	189.97	0.174	0.7303	0.5333	1.082
0	2.469	0.240						
-1	2.712	0.243						
-2	2.935	0.223						
-3	3.129	0.194						
-4	3.299	0.170			Slope	z_o'/cm	C_s'/cm	
-5	3.446	0.147		6.04E-05	-0.006241	1.085	62.41	
-6	3.578	0.132						
-7	3.700	0.122						

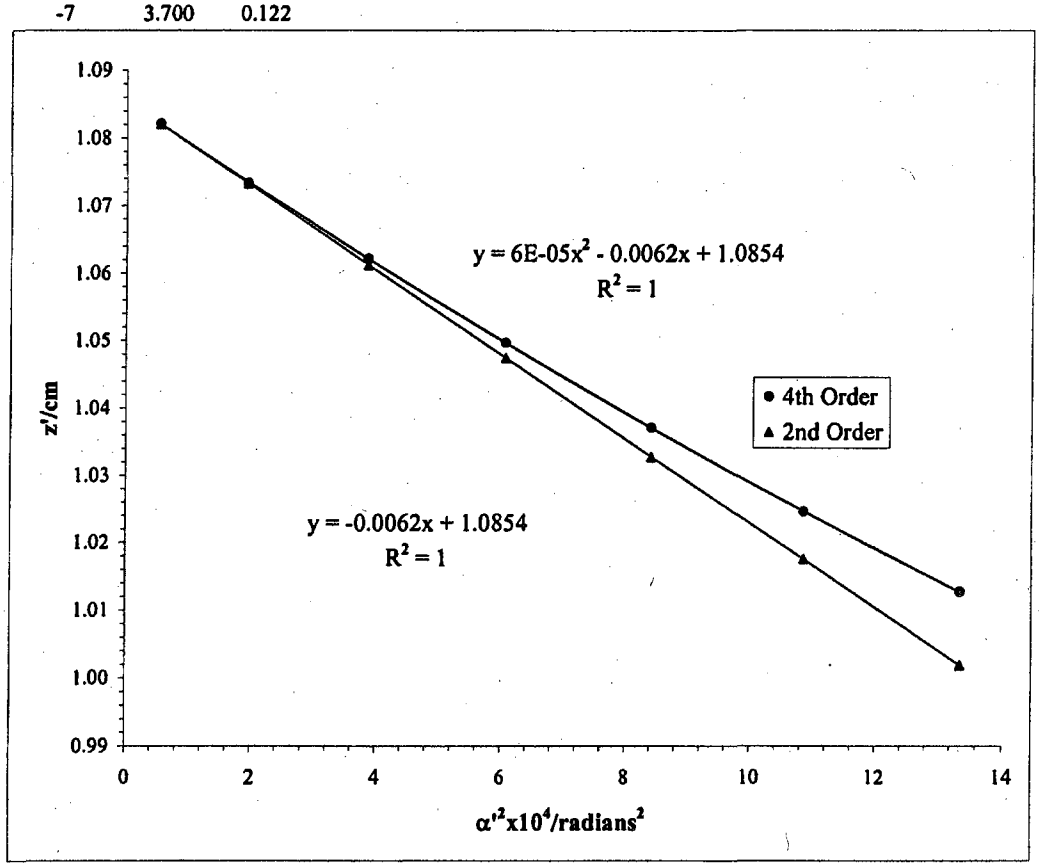

L3 Elektros obj. **Beam Voltage 20 kV**

Mesh/inch	V Ratio	Mesh	z/cm	e_1/cm	a/cm	z_{sp}/cm	z_0'/cm	C_s'/cm	$z_{sp}-z_o'$
600	0.80	Front	25.00	0.00423	22.40	34.12	1.094	68.02	33.03

Bar location/ units	Shadow Reading X/cm	Spacing Δ/cm	E/cm	$\alpha \times 10^4$	$\alpha' \times 10^2$	$\alpha'^2 \times 10^4$	m	z'/cm	f/cm
8	1.221		1.204	15.119	3.635	13.213	0.04159	1.004	1.000
7	1.389	0.168	1.036	13.229	3.130	9.796	0.04227	1.027	1.015
6	1.550	0.161	0.875	11.339	2.645	6.995	0.04287	1.046	1.029
5	1.705	0.155	0.720	9.449	2.177	4.740	0.04340	1.062	1.041
4	1.855	0.150	0.570	7.560	1.724	2.973	0.04385	1.074	1.051
3	2.000	0.146	0.424	5.670	1.283	1.646	0.04420	1.083	1.059
2	2.143	0.143	0.281	3.780	0.850	0.723	0.04445	1.089	1.065
1	2.284	0.141	0.140	1.890	0.424	0.180	0.04461	1.093	1.069
0	2.424	0.140							
-1	2.564	0.140							
-2	2.705	0.141							
-3	2.848	0.143							
-4	2.994	0.146							
-5	3.144	0.150							
-6	3.299	0.155							
-7	3.460	0.161							
-8	3.629	0.168							

g/cm	$(\rho/f_0)^2 = (m_0+1)^2\alpha'^2$
0.962	14.419
0.984	10.690
1.002	7.633
1.017	5.173
1.028	3.244
1.036	1.796
1.042	0.789
1.045	0.196

	Slope	m_0	μ_z
3.6E-06	-0.0003	0.04465	-62.51

f vs $(\rho/f_o)^2$

$S_f = slope_f / f_0$

$slope_f$	fo/cm	S_f
7.26E-05	-0.00587	1.069	-54.93

g vs $(\rho/f_o)^2$

$S_g = slope_g / f_0$

$slope_g$	go/cm	S_g
-7.28313E-06	-0.005701	1.046	-53.31

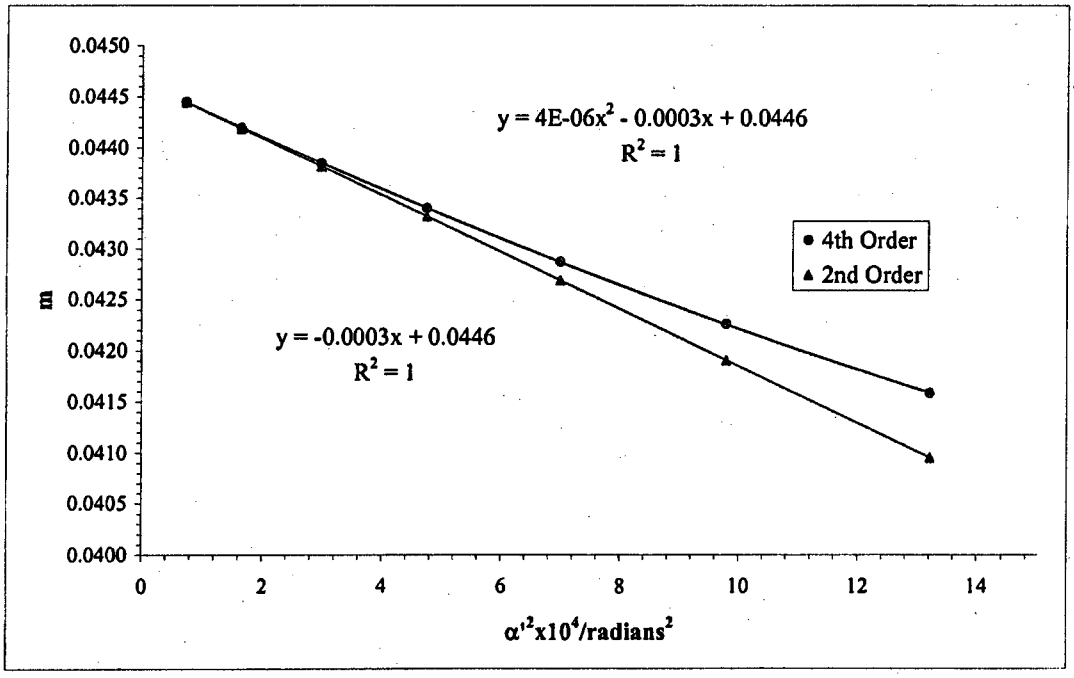

L3 Elektros obj. **Beam** **Voltage** **20 kV**

Mesh/inch	V Ratio	Mesh	z/cm	e_i/cm	a/cm	z_{sp}/cm	z_0'/cm	C_s'/cm	$z_{sp}-z_0'$
600	0.80	Front	25.00	0.00423	22.40	34.12	1.094	68.02	33.03

Bar location/ units	Shadow Reading Y/cm	Spacing Δ/cm	E/cm	$\alpha \times 10^4$	$\alpha' \times 10^2$	$\alpha'^2 \times 10^4$	m	z'/cm	f/cm
10	0.760024		1.557	18.899	4.692	22.014	0.0403	0.944	0.971
9	0.942806	0.1828	1.375	17.009	4.149	17.217	0.0410	0.977	0.986
8	1.117305	0.1745	1.202	15.119	3.630	13.174	0.0417	1.004	1.001
7	1.284417	0.1671	1.036	13.229	3.130	9.798	0.0423	1.027	1.015
6	1.445044	0.1606	0.876	11.339	2.649	7.017	0.0428	1.046	1.027
5	1.600088	0.1550	0.722	9.449	2.183	4.767	0.0433	1.062	1.038
4	1.750458	0.1504	0.572	7.560	1.731	2.996	0.0437	1.074	1.047
3	1.897063	0.1466	0.426	5.670	1.289	1.661	0.0440	1.083	1.054
2	2.040815	0.1438	0.282	3.780	0.855	0.731	0.0442	1.089	1.059
1	2.182625	0.1418	0.141	1.890	0.426	0.182	0.0444	1.093	1.063
0	2.323404	0.1408							
-1	2.464064	0.1407							
-2	2.605514	0.1414							
-3	2.748658	0.1431							
-4	2.894401	0.1457							
-5	3.04364	0.1492							
-6	3.197268	0.1536							
-7	3.356174	0.1589							
-8	3.521237	0.1651							
-9	3.69333	0.1721							
-10	3.873318	0.1800							

Slope	m_o	μ_s
2.5E-06	-0.0002	0.04439	-54.36

g/cm	$(\rho/f)^2 = (m+1)^2 \alpha'^2$
0.905	24.012
0.936	18.780
0.963	14.369
0.984	10.687
1.002	7.654
1.017	5.200
1.028	3.268
1.036	1.812
1.042	0.797
1.046	0.198

f vs $(\rho/f_o)^2$

S_f = slope$_f$ / f_0

slope$_f$	fo/cm	S_f
4.99E-05	-0.005045	1.063	-47.45

g vs $(\rho/f_o)^2$

S_g = slope$_g$ / f_0

slope$_g$	go/cm	S_g
-4.9E-06	-0.00578	1.047	-54.39

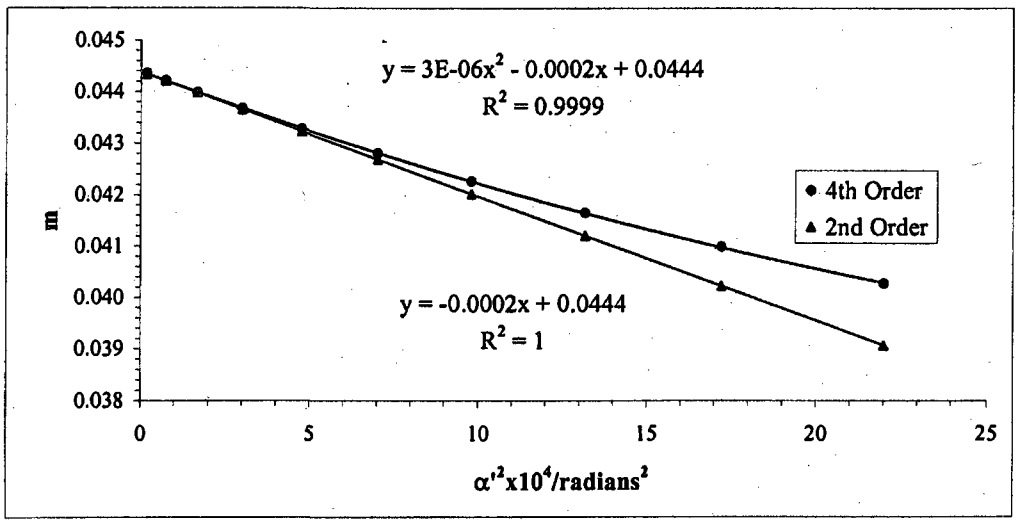

Beam Voltage	Volt Ratio	z/cm	z_0'/cm	C_s'/cm	L3 Elektros obj.
20 kV	0.80	25.0	1.09	68.0	

Average of m_o = 0.0445

Average of μ_s = -58.4

Paraxial properties :

f_o = 1.07 cm

g_o = 1.05 cm

S_f = -51.2

S_g = -53.8

Mesh/inch	V Ratio	Mesh	e'_1/cm	d/cm	b/cm		Beam	Voltage	20 kV
2000	0.90	Rear	0.00127	33.60	0.519	US			
								L3 Elektros obj.	

Bar location/ units	Shadow Reading X/cm	Spacing Δ/cm	E'/cm	M'	c/cm	α' x 10^2	α'^2 x 10^4	z'/cm
5.5	0.952		1.125	-161.10	-0.207	3.3699	11.356	0.727
4.5	1.199	0.247	0.883	-154.47	-0.216	2.6444	6.993	0.736
3.5	1.418	0.218	0.667	-150.08	-0.222	1.9986	3.994	0.742
2.5	1.619	0.201	0.467	-147.08	-0.227	1.3993	1.958	0.746
1.5	1.811	0.192	0.277	-145.14	-0.230	0.8286	0.687	0.749
0.5	1.996	0.186	0.092	-144.82	-0.230	0.2756	0.076	0.750
-0.5	2.180	0.184						
-1.5	2.364	0.183						
-2.5	2.553	0.189						
-3.5	2.752	0.199						
-4.5	2.965	0.213			Slope	z_0'/cm	C_s'/cm	
-5.5	3.203	0.238		1.7E-05	-0.0023	0.7509	23.18	

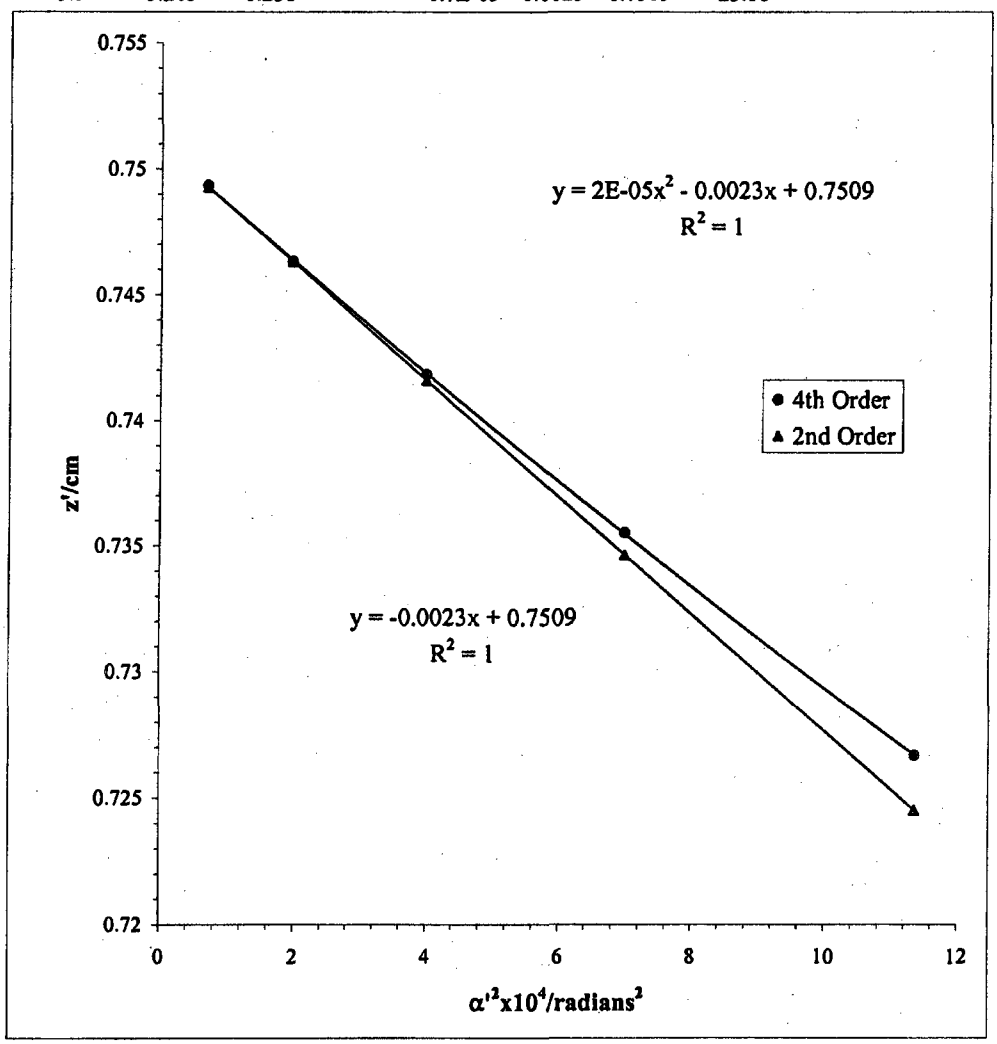

Mesh/inch	V Ratio	Mesh	e'_1/cm	d/cm	b/cm		Beam	Voltage	20 kV
2000	0.90	Rear	0.00127	33.60	0.52	US			
								L3 Elektros obj.	

Bar location/ units	Shadow Reading Y/cm	Spacing Δ/cm	E'/cm	M'	c/cm	α' x 10^2	α'^{2} x 10^4	z'/cm
5.5	1.570		1.119	-160.22	-0.208	3.3516	11.233	0.728
4.5	1.807	0.238	0.879	-153.83	-0.217	2.6334	6.935	0.736
3.5	2.020	0.213	0.664	-149.40	-0.223	1.9897	3.959	0.743
2.5	2.219	0.199	0.465	-146.60	-0.228	1.3947	1.945	0.747
1.5	2.407	0.188	0.277	-145.16	-0.230	0.8287	0.687	0.749
0.5	2.592	0.185	0.092	-145.16	-0.230	0.2762	0.076	0.749
-0.5	2.776	0.184						
-1.5	2.960	0.184						
-2.5	3.150	0.190						
-3.5	3.348	0.199			Slope	z_o'/cm	C_s'/cm	
-4.5	3.565	0.217		1E-05	-2.2E-03	0.751	22.29	
-5.5	3.808	0.242						

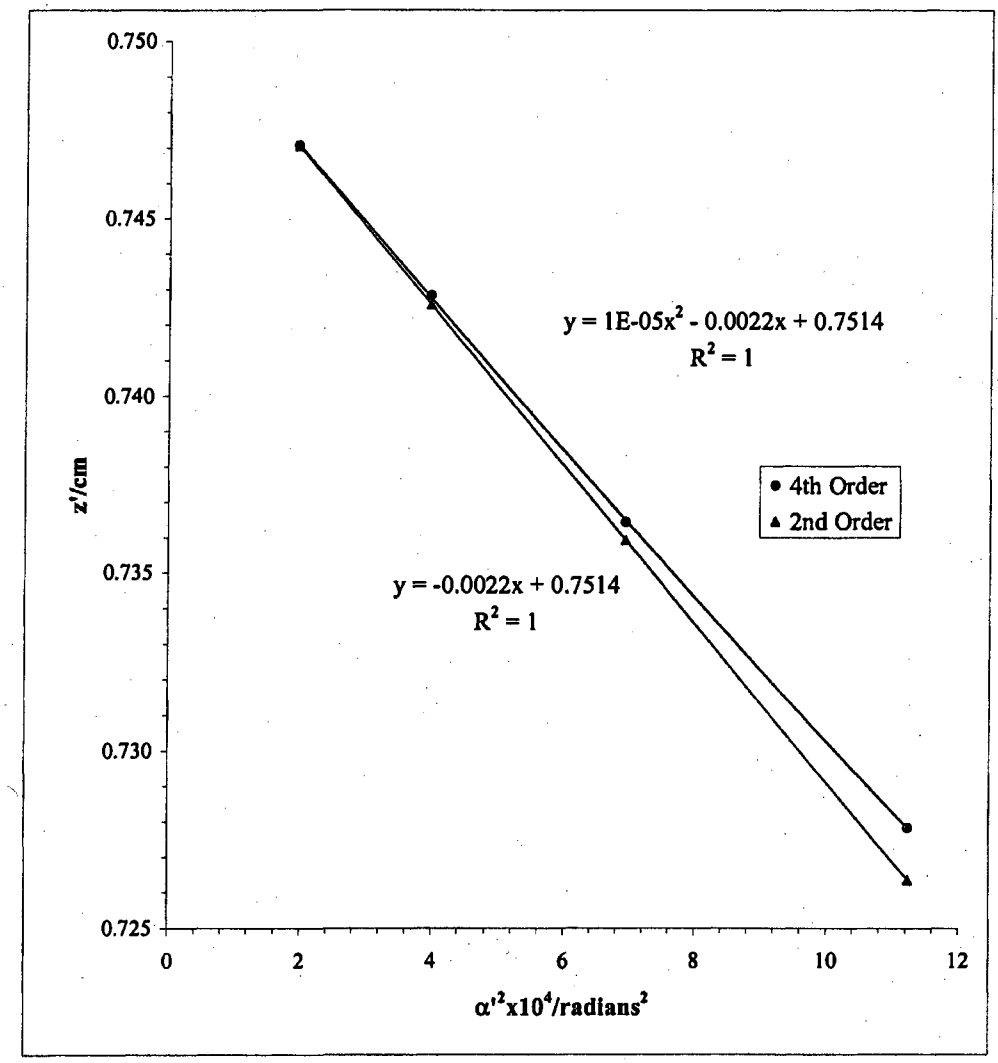

Mesh/inch	V Ratio	Mesh	e'_1/cm	d/cm	b/cm		Beam	Voltage	20 kV
2000	0.90	Rear	0.00127	33.19	0.93	DS			
								L3 Elektros obj.	

Bar location/ units	Shadow Reading X/cm	Spacing Δ/cm	E'/cm	M'	c/cm	α' x 10^2	α'^{2} x 10^4	z'/cm
6	1.289		1.214	159.36	0.210	3.6352	13.2149	0.716
5	1.457	0.168	1.046	164.66	0.203	3.1307	9.8016	0.723
4	1.638	0.181	0.863	169.93	0.196	2.5853	6.6838	0.729
3	1.834	0.196	0.667	174.95	0.191	1.9966	3.9863	0.735
2	2.045	0.211	0.455	179.02	0.186	1.3622	1.8556	0.739
1	2.269	0.224	0.231	181.72	0.184	0.6914	0.4781	0.742
0	2.499	0.230						
-1	2.731	0.231			Slope	z_o'/cm	C_t'/cm	
-2	2.955	0.224		3.7E-06	-0.002094	0.743	20.94	
-3	3.168	0.213						
-4	3.365	0.197						
-5	3.548	0.184						
-6	3.717	0.169						

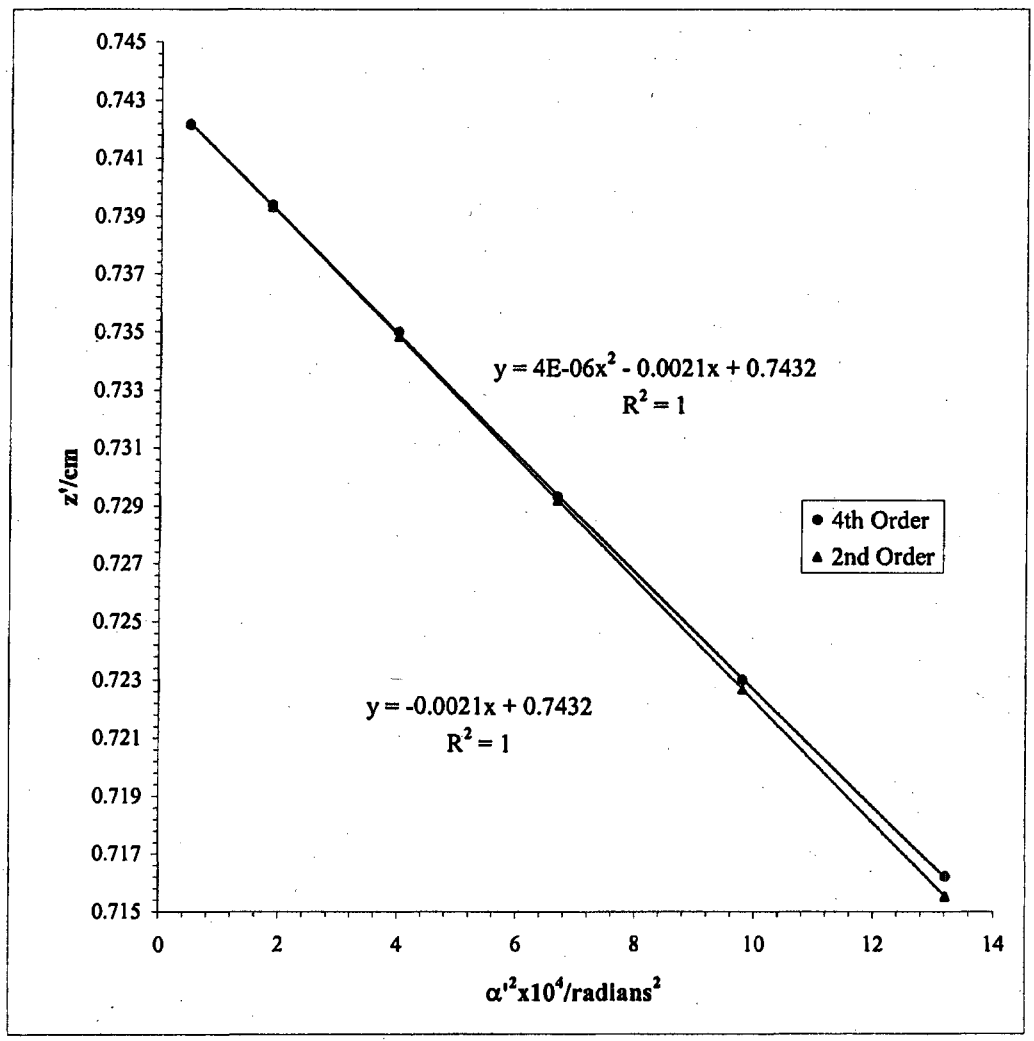

Mesh/inch	V Ratio	Mesh	e'_1/cm	d/cm	b/cm		Beam	Voltage	20 kV
2000	0.90	Rear	0.00127	33.19	0.93	DS			
								L3 Elektros obj.	

Bar location/ units	Shadow Reading Y/cm	Spacing Δ/cm	E'/cm	M'	c/cm	α' x 10^2	α'^2 x 10^4	z'/cm
7	1.194		1.359	152.91	0.219	4.0683	16.5513	0.707
6	1.352	0.158	1.203	157.85	0.212	3.6006	12.9641	0.714
5	1.520	0.168	1.036	163.16	0.205	3.1020	9.6227	0.721
4	1.702	0.182	0.855	168.37	0.198	2.5614	6.5607	0.727
3	1.896	0.195	0.661	173.44	0.192	1.9792	3.9174	0.733
2	2.108	0.212	0.450	177.35	0.188	1.3494	1.8209	0.738
1	2.330	0.221	0.230	180.84	0.185	0.6881	0.4734	0.741
0	2.560	0.230						
-1	2.789	0.229						
-2	3.009	0.220						
-3	3.218	0.209						
-4	3.412	0.194			Slope	z_0'/cm	C_s'/cm	
-5	3.592	0.180		1.27E-05	-0.002313	0.7421	23.13	
-6	3.758	0.166						
-7	3.913	0.155						

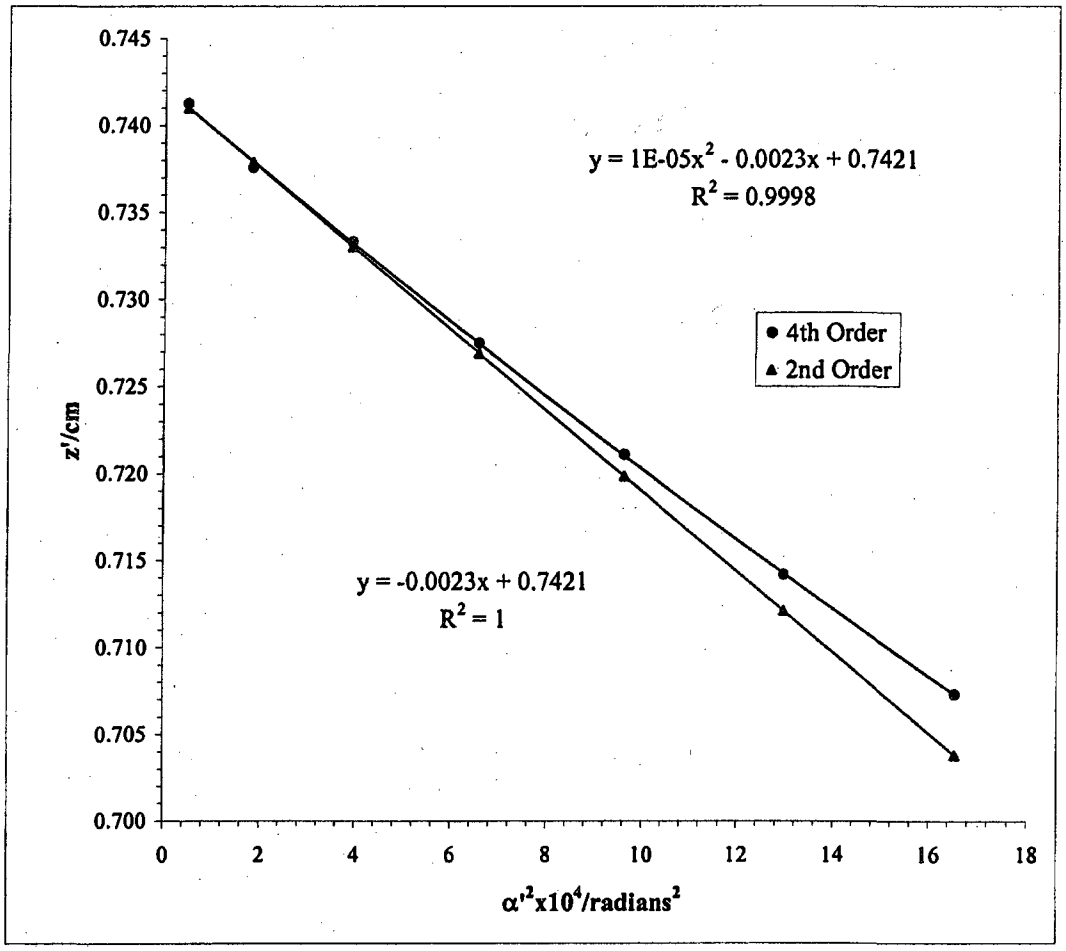

L3 Elektros obj. Beam Voltage 20 kV

Mesh/inch	V Ratio	Mesh	z/cm	e_f/cm	a/cm	z_{sp}/cm	z_0'/cm	C_z'/cm	$z_{sp}-z_0'$
600	0.90	Front	25.00	0.00423	22.40	34.12	0.748	22.15	33.37

Bar location/ units	Shadow Reading X/cm	Spacing Δ/cm	E/cm	α x 10^4	α' x 10^2	α'^{2} x 10^4	m	z'/cm	f/cm
6	1.278		1.285	11.339	3.847	14.798	0.02948	0.715	0.716
5	1.506	0.228	1.057	9.449	3.165	10.020	0.02985	0.725	0.725
4	1.727	0.221	0.837	7.560	2.506	6.280	0.03017	0.734	0.733
3	1.942	0.215	0.622	5.670	1.864	3.475	0.03042	0.740	0.739
2	2.152	0.210	0.412	3.780	1.235	1.526	0.03060	0.744	0.743
1	2.359	0.207	0.205	1.890	0.615	0.379	0.03071	0.747	0.745
0	2.565	0.205							
-1	2.770	0.205					g/cm	$(\rho/f_0)^2 = (m_0+1)^2\alpha'^2$	
-2	2.977	0.207							
-3	3.186	0.210					0.694	15.722	
-4	3.401	0.214					0.704	10.646	
-5	3.621	0.220					0.712	6.672	
-6	3.848	0.228					0.717	3.692	
							0.722	1.621	
			Slope	m_o	μ_s		0.724	0.402	
		7.3E-07	-0.0001	0.03074	-31.29				

f vs $(\rho/f_o)^2$

S_f = slope$_f$ / f_0

slope$_f$	fo/cm	S_f
1.548E-05	-0.002138	0.746	-28.65

g vs $(\rho/f_o)^2$

S_g = slope$_g$ / f_0

slope$_g$	go/cm	S_g
-1.1E-06	-0.00195	0.725	-26.16

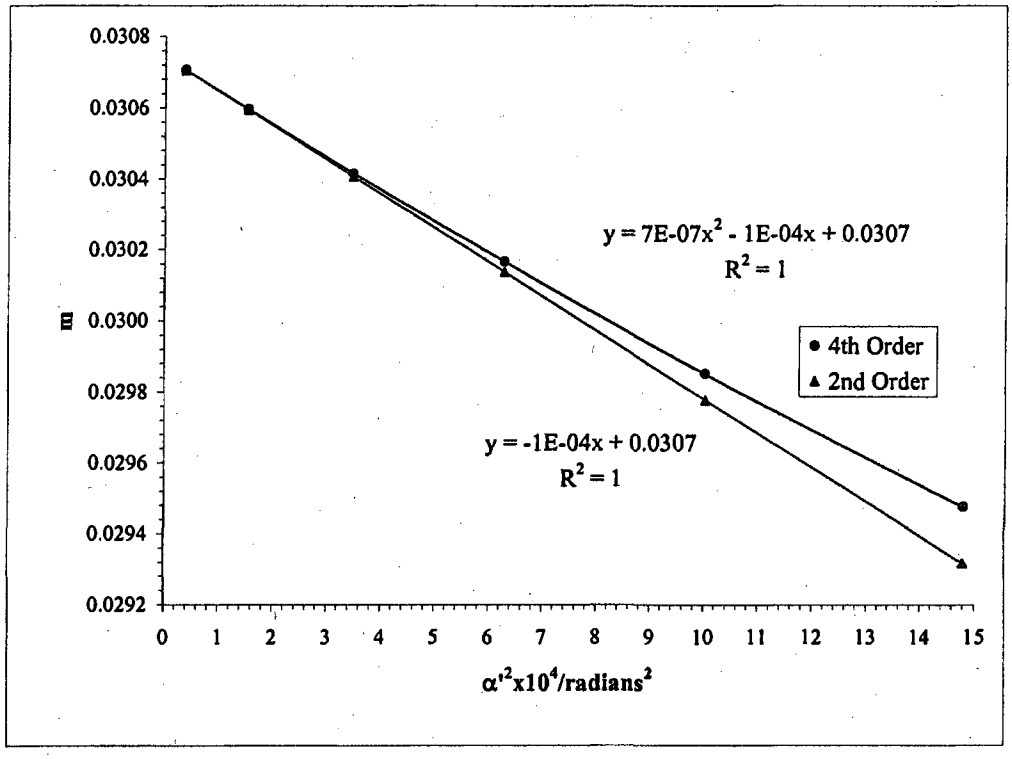

L3 Elektros obj. **Beam** **Voltage** **20 kV**

Mesh/inch	V Ratio	Mesh	z/cm	e_1/cm	a/cm	z_{sp}/cm	z_0'/cm	C_s'/cm	$z_{sp}-z_0'$
600	0.90	Front	25.00	0.00423	22.40	34.12	0.748	22.15	33.37

Bar location/ units	Shadow Reading Y/cm	Spacing Δ/cm	E/cm	$\alpha \times 10^4$	$\alpha' \times 10^2$	$\alpha'^2 \times 10^4$	m	z'/cm	f/cm
8	0.839		1.763	15.119	5.275	27.821	0.028664	0.686	0.698
7	1.088	0.248	1.518	13.229	4.544	20.647	0.029114	0.702	0.708
6	1.325	0.237	1.284	11.339	3.843	14.766	0.029509	0.715	0.717
5	1.553	0.228	1.057	9.449	3.166	10.023	0.029847	0.725	0.725
4	1.773	0.220	0.838	7.560	2.509	6.297	0.030125	0.734	0.732
3	1.988	0.215	0.624	5.670	1.869	3.491	0.030343	0.740	0.737
2	2.198	0.210	0.414	3.780	1.239	1.536	0.030499	0.744	0.740
1	2.406	0.208	0.206	1.890	0.618	0.382	0.030593	0.747	0.743
0	2.612	0.206							
-1	2.818	0.206							
-2	3.025	0.207							
-3	3.235	0.210							
-4	3.449	0.214							
-5	3.667	0.219							
-6	3.892	0.225							
-7	4.125	0.233							
-8	4.366	0.242							

g/cm	$(\rho/f_0)^2 = (m_0+1)^2 \alpha'^2$
0.666	29.551
0.681	21.931
0.694	15.684
0.704	10.647
0.712	6.689
0.718	3.708
0.722	1.631
0.724	0.405

	Slope	m_o	μ_s
3.9E-07	-0.0001	0.03062	-26.53

f vs $(\rho/f_o)^2$

S_f = slope$_f$ / f_0

	slope$_f$	fo/cm	S_f
8.31544E-06	-0.001797	0.743	-24.17

g vs $(\rho/f_o)^2$

S_g = slope$_g$ / f_0

	slope$_g$	go/cm	S_g
-6E-07	-0.00197	0.725	-26.56

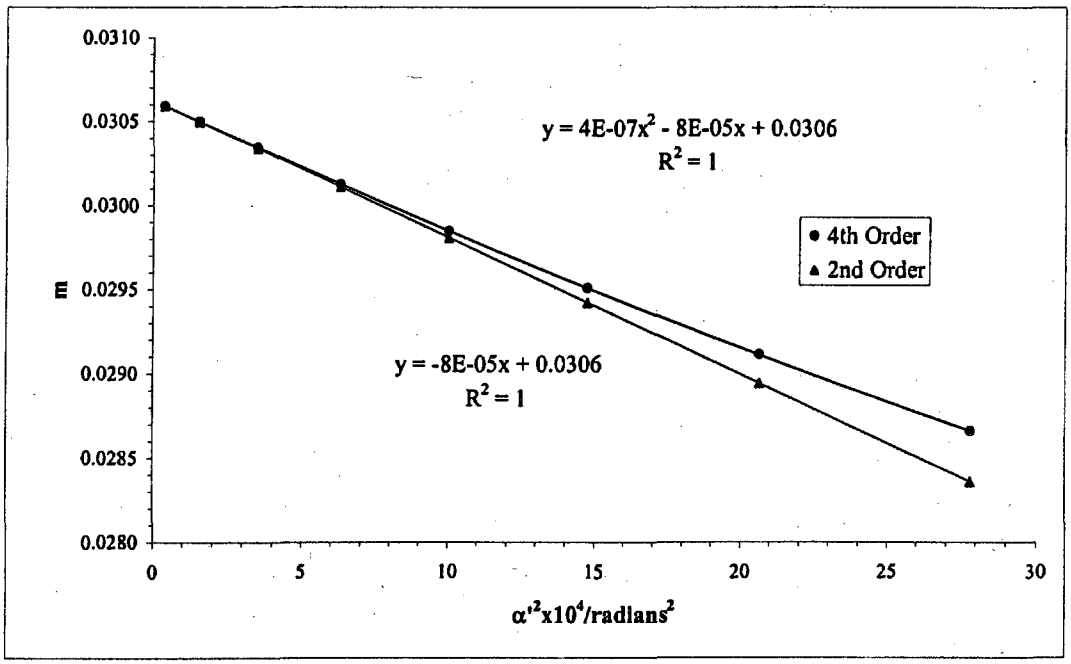

Beam Voltage	Volt Ratio	z/cm	z_0'/cm	C_s'/cm	L3 Elektros obj.
20 kV	0.90	25.0	0.748	22.2	

Average of m_o = 0.0307

Average of μ_s = -28.9

Paraxial properties :

f_o = 0.745 cm

g_o = 0.725 cm

S_f = -26.41

S_g = -26.36

Mesh/inch	V Ratio	Mesh	e'_1/cm	d/cm	b/cm		Beam	Voltage	20 kV
2000	0.95	Rear	0.00127	33.73	0.392	US			
								L3 Elektros obj.	

Bar location/ units	Shadow Reading X/cm	Spacing Δ/cm	E'/cm	M'	c/cm	α' x 10^2	α'^2 x 10^4	z'/cm
6	0.981		1.608	-211.03	-0.159	4.7905	22.949	0.551
5	1.321	0.340	1.270	-200.06	-0.168	3.7855	14.330	0.560
4	1.612	0.291	0.979	-192.79	-0.174	2.9189	8.520	0.566
3	1.876	0.264	0.716	-187.99	-0.178	2.1349	4.558	0.571
2	2.122	0.246	0.469	-184.61	-0.182	1.3978	1.954	0.574
1	2.360	0.237	0.232	-182.89	-0.183	0.6924	0.479	0.576
0	2.592	0.232						
-1	2.824	0.232						
-2	3.060	0.236			Slope	z_0'/cm	C_s'/cm	
-3	3.308	0.248		5.85E-06	-0.00122	0.576	12.20	
-4	3.571	0.262						
-5	3.861	0.291						
-6	4.197	0.336						

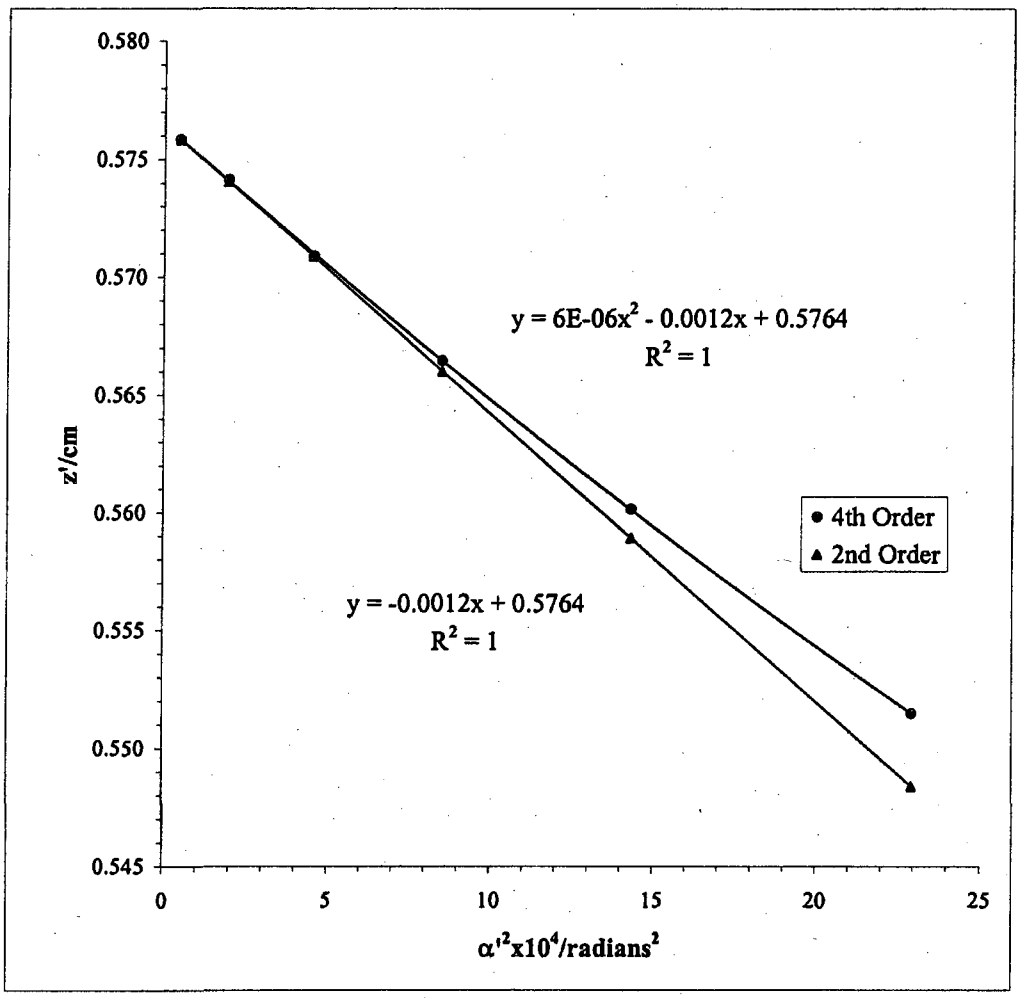

Mesh/inch	V Ratio	Mesh	e'_1/cm	d/cm	b/cm		Beam	Voltage	20 kV
2000	0.95	Rear	0.00127	33.73	0.392	US			

L3 Elektros obj.

Bar location/ units	Shadow Reading Y/cm	Spacing Δ/cm	E'/cm	M'	c/cm	$\alpha' \times 10^2$	$\alpha'^2 \times 10^4$	z'/cm
7	0.253		2.039	-229.30	-0.146	6.0704	36.850	0.539
6	0.670	0.417	1.621	-212.75	-0.158	4.8292	23.321	0.550
5	1.018	0.348	1.273	-200.51	-0.167	3.7939	14.393	0.560
4	1.316	0.298	0.977	-192.27	-0.175	2.9110	8.474	0.567
3	1.580	0.265	0.713	-187.23	-0.179	2.1263	4.521	0.572
2	1.825	0.245	0.468	-184.13	-0.182	1.3942	1.944	0.575
1	2.061	0.236	0.233	-183.27	-0.183	0.6939	0.481	0.575
0	2.293	0.233						
-1	2.526	0.233						
-2	2.761	0.234			Slope	z_o'/cm	C_s'/cm	
-3	3.007	0.246		7.97E-06	-1.342E-03	0.577	13.42	
-4	3.269	0.262						
-5	3.564	0.295						
-6	3.912	0.348						
-7	4.330	0.418						

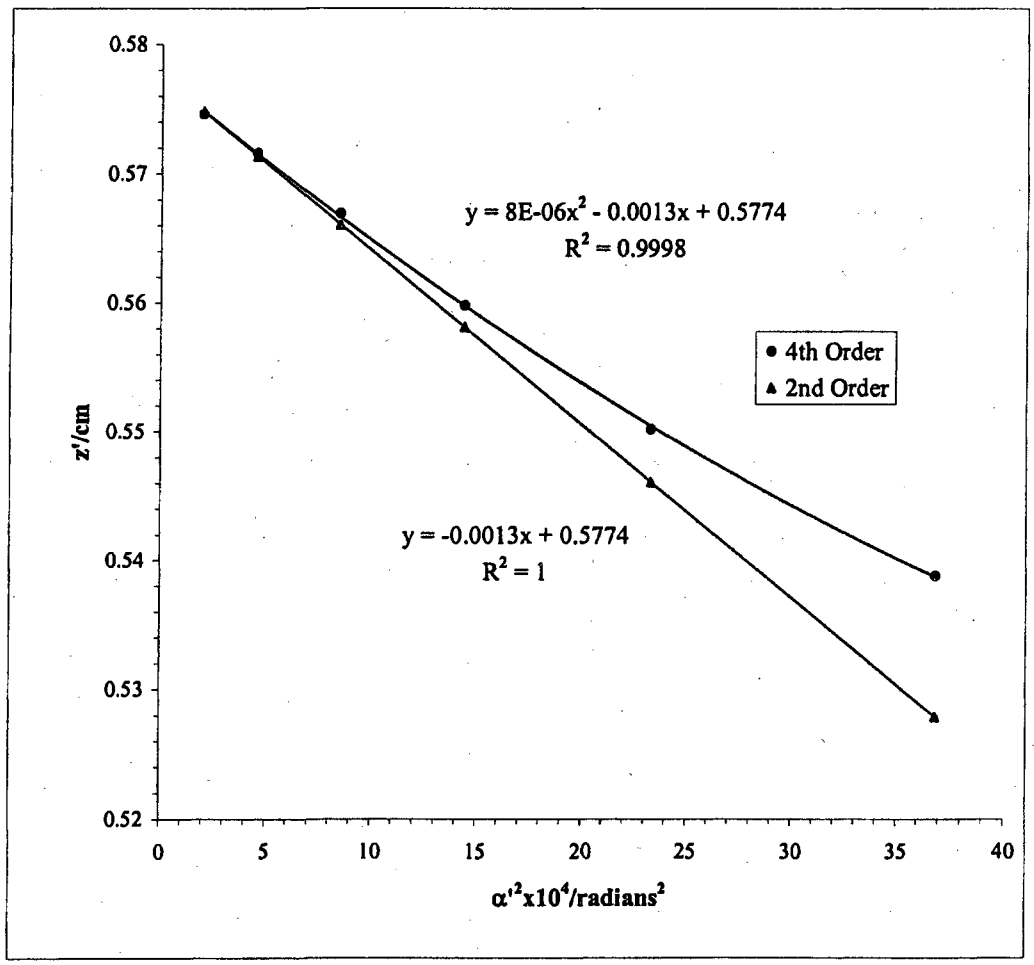

Mesh/inch	V Ratio	Mesh	e'_1/cm	d/cm	b/cm		Beam	Voltage	20 kV
2000	0.95	Rear	0.00127	33.37	0.75	DS			
								L3 Elektros obj.	

Bar location/ units	Shadow Reading X/cm	Spacing Δ/cm	E'/cm	M'	c/cm	α' x 10^2	α'^2 x 10^4	z'/cm
11	0.094		2.215	158.58	0.212	6.5967	43.5164	0.536
10	0.241	0.147	2.066	162.64	0.206	6.1515	37.8415	0.542
9	0.398	0.156	1.907	166.83	0.201	5.6798	32.2600	0.547
8	0.563	0.165	1.741	171.33	0.196	5.1856	26.8904	0.552
7	0.734	0.171	1.566	176.10	0.191	4.6646	21.7583	0.557
6	0.918	0.184	1.379	180.98	0.185	4.1095	16.8880	0.563
5	1.113	0.196	1.180	185.82	0.181	3.5167	12.3674	0.567
4	1.321	0.208	0.968	190.48	0.176	2.8844	8.3198	0.572
3	1.542	0.221	0.742	194.86	0.172	2.2132	4.8984	0.576
2	1.779	0.236	0.503	197.99	0.169	1.4994	2.2481	0.579
1	2.025	0.246	0.254	200.05	0.168	0.7575	0.5738	0.580
0	2.278	0.253						
-1	2.533	0.255						
-2	2.784	0.251						
-3	3.027	0.243						
-4	3.257	0.229			Slope	z_0'/cm	C_s'/cm	
-5	3.473	0.216		2.7E-06	-0.00115	0.5812	11.50	
-6	3.676	0.203						
-7	3.865	0.189						
-8	4.044	0.179						
-9	4.211	0.167						
-10	4.373	0.161						
-11	4.525	0.152						

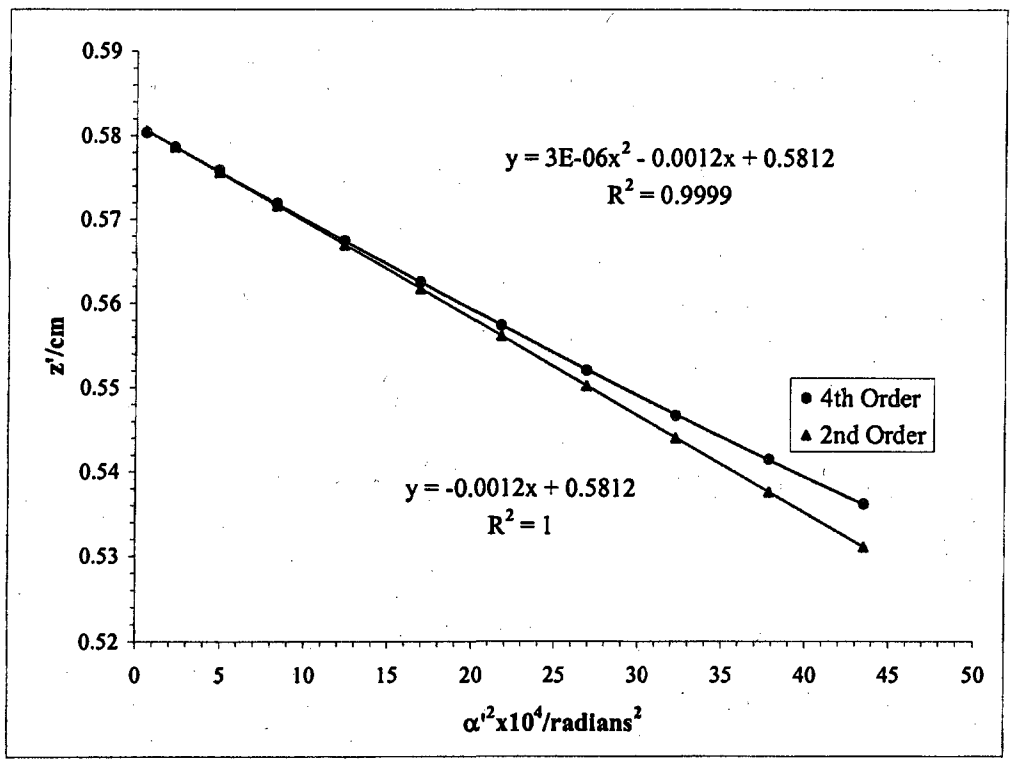

Mesh/Inch	V Ratio	Mesh	e'_1/cm	d/cm	b/cm		Beam	Voltage	20 kV
2000	0.95	Rear	0.00127	33.37	0.75	DS			
								L3 Elektros obj.	

Bar location/ units	Shadow Reading Y/cm	Spacing Δ/cm	E'/cm	M'	c/cm	α' x 10^2	α'^2 x 10^4	z'/cm
5.5	1.249		1.269	181.73	0.185	3.7829	14.3101	0.563
4.5	1.449	0.200	1.063	186.04	0.180	3.1689	10.0419	0.568
3.5	1.662	0.212	0.848	190.73	0.176	2.5271	6.3861	0.572
2.5	1.888	0.227	0.617	194.41	0.173	1.8401	3.3860	0.575
1.5	2.126	0.238	0.376	197.44	0.170	1.1214	1.2575	0.578
0.5	2.373	0.247	0.127	199.91	0.168	0.3785	0.1433	0.580
-0.5	2.627	0.254						
-1.5	2.878	0.251						
-2.5	3.123	0.245			Slope	z_0'/cm	C_s'/cm	
-3.5	3.357	0.234		9.17E-06	-0.001279	0.580	12.79	
-4.5	3.576	0.219						
-5.5	3.788	0.212						

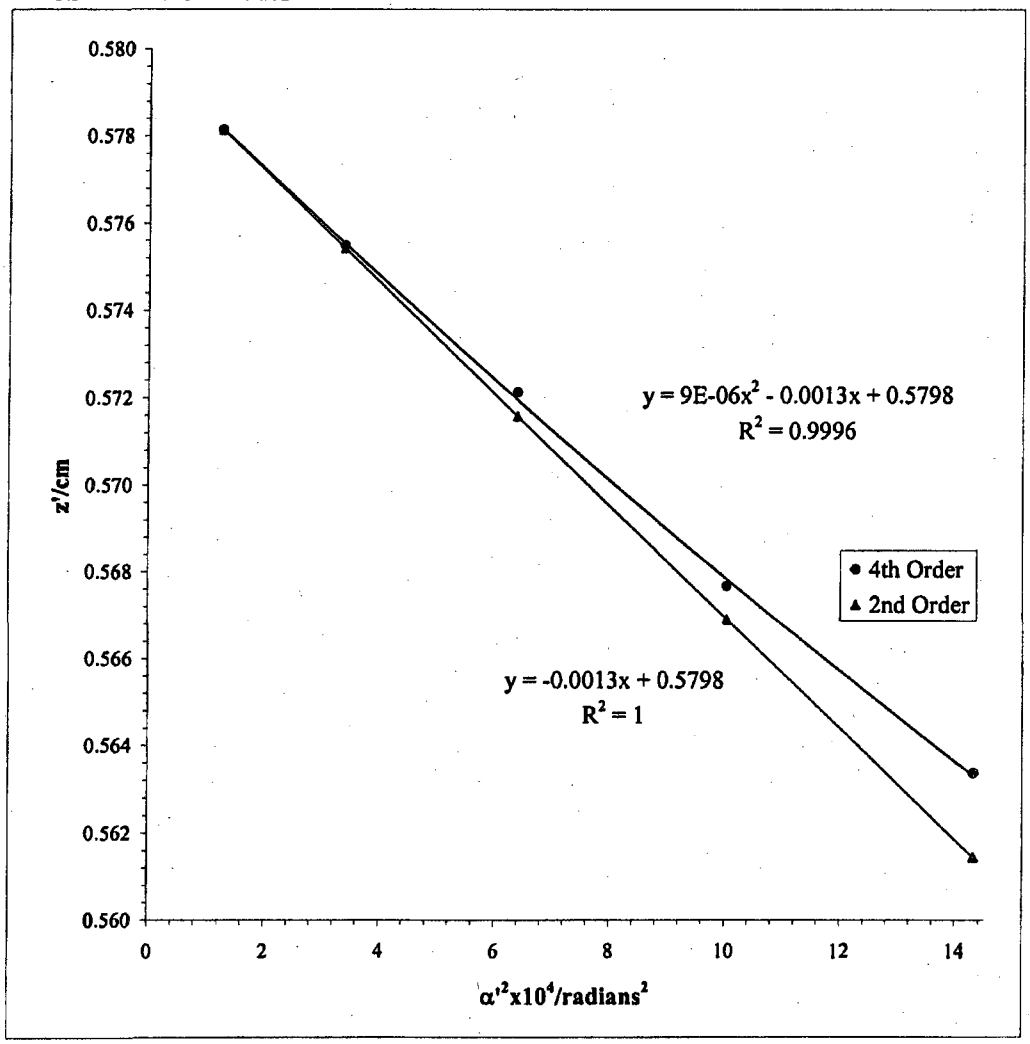

L3 Elektros obj.							Beam	Voltage	20 kV
Mesh/inch	V Ratio	Mesh	z/cm	e_t/cm	a/cm	z_{sp}/cm	z_o'/cm	C_s'/cm	$z_{sp}-z_o'$
600	0.95	Front	25.00	0.00423	22.40	34.12	0.579	11.77	33.54

Bar location/ units	Shadow Reading X/cm	Spacing Δ/cm	E/cm	$\alpha \times 10^4$	$\alpha' \times 10^2$	$\alpha'^2 \times 10^4$	m	z'/cm	f/cm
5	1.543		1.348	9.449	4.018	16.143	0.0235	0.560	0.575
4	1.825	0.282	1.066	7.560	3.178	10.102	0.0238	0.567	0.581
3	2.099	0.274	0.793	5.670	2.363	5.582	0.0240	0.572	0.587
2	2.367	0.268	0.525	3.780	1.565	2.450	0.0241	0.576	0.590
1	2.631	0.264	0.261	1.890	0.780	0.608	0.0242	0.578	0.592
0	2.892	0.262							
-1	3.154	0.261					g/cm	$(\rho/f_o)^2 = (m_o+1)^2\alpha'^2$	
-2	3.417	0.263							
-3	3.685	0.267					0.546	16.936	
-4	3.958	0.273					0.553	10.598	
-5	4.240	0.282					0.558	5.857	
		Slope	m_o	μ_s			0.561	2.570	
	2.7E-07	-0.0001	0.02427	-21.07			0.563	0.638	

f vs $(\rho/f_o)^2$

$S_f = slope_f / f_0$

$slope_f$	fo/cm	S_f
6.027E-06	-0.00117	0.593	-19.65

g vs $(\rho/f_o)^2$

$S_g = slope_g / f_0$

$slope_g$	go/cm	S_g
-3.4E-07	-0.00107	0.564	-17.96

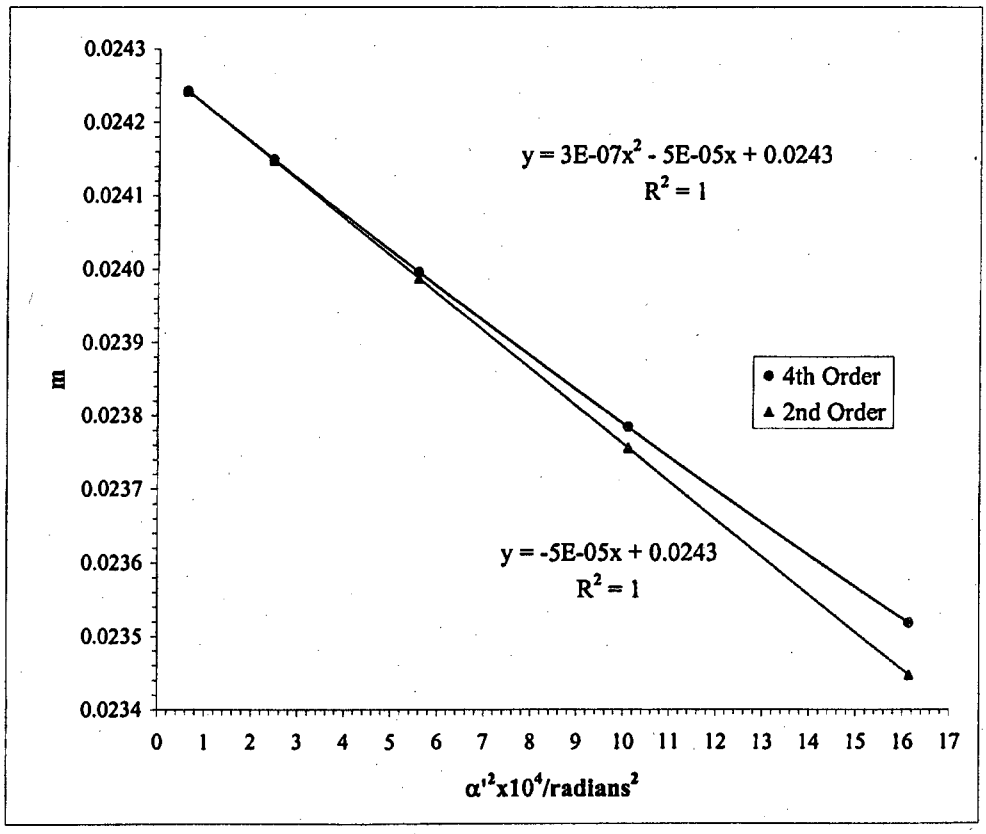

L3 Elektros obj. Beam Voltage 20 kV

Mesh/inch	V Ratio	Mesh	z/cm	e_1/cm	a/cm	z_{sp}/cm	z_0'/cm	C_s'/cm	$z_{sp}-z_0'$
600	0.95	Front	25.00	0.00423	22.40	34.12	0.579	11.77	33.54

Bar location/ units	Shadow Reading Y/cm	Spacing Δ/cm	E/cm	$\alpha \times 10^4$	$\alpha' \times 10^2$	$\alpha'^2 \times 10^4$	m	z'/cm	f/cm
4	1.436		1.067	7.560	3.179	10.106	0.02378	0.567	0.581
3	1.710	0.275	0.793	5.670	2.365	5.593	0.02397	0.572	0.586
2	1.977	0.267	0.526	3.780	1.569	2.461	0.02409	0.576	0.589
1	2.242	0.265	0.262	1.890	0.781	0.609	0.02421	0.578	0.592
0	2.504	0.262							
-1	2.766	0.262							
-2	3.029	0.263							
-3	3.297	0.268							
-4	3.569	0.272							

g/cm	$(\rho/f_0)^2 = (m_0+1)^2 \alpha'^2$
0.553	10.592
0.558	5.864
0.561	2.581
0.563	0.639

	Slope	m_o	μ_s
8.1E-07	-0.0001	0.02424	-21.94

f vs $(\rho/f_o)^2$

$S_f = slope_f / f_0$

	$slope_f$	fo/cm	S_f
1.80266E-05	-0.00121	0.592	-20.48

g vs $(\rho/f_o)^2$

$S_g = slope_g / f_0$

	$slope_g$	go/cm	S_g
-1.00073E-06	-0.00106	0.564	-17.95

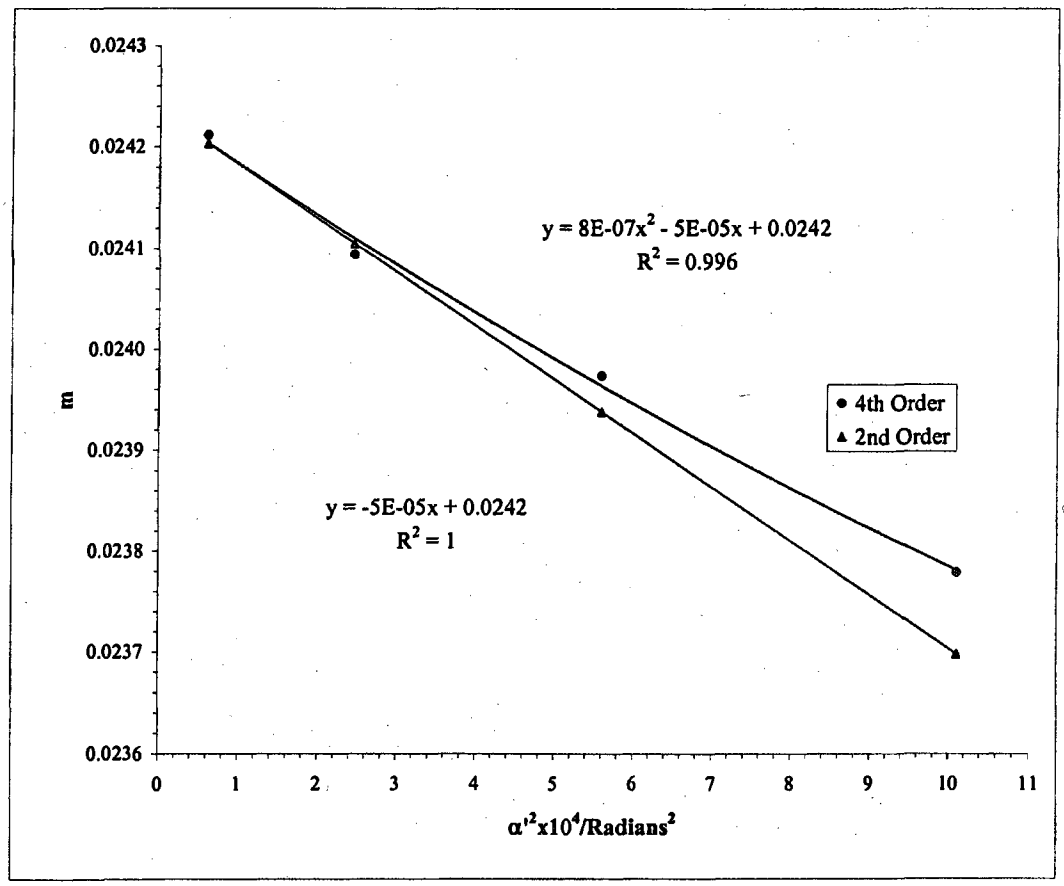

Beam Voltage	Volt Ratio	z/cm	z_0'/cm	C_s'/cm	L3 Elektros obj.
20 kV	0.95	25.0	0.579	11.8	

Average of m_o = 0.0243

Average of μ_s = -21.5

Paraxial properties :

f_o = 0.593 cm

g_o = 0.564 cm

S_f = -20.1

S_g = -18.0

Mesh/inch	V Ratio	Mesh	e'_1/cm	d/cm	b/cm		Beam	Voltage	20 kV
2000	1.00	Rear	0.00127	33.52	0.60	DS			
								L3 Elektros obj.	

Bar location/ units	Shadow Reading X/cm	Spacing Δ/cm	E'/cm	M'	c/cm	α' x 10^2	α'^2 x 10^4	z'/cm
7.5	0.707		1.970	206.82	0.163	5.8479	34.1977	0.433
6.5	0.927	0.220	1.752	212.19	0.159	5.2004	27.0446	0.437
5.5	1.165	0.238	1.518	217.39	0.155	4.5086	20.3274	0.441
4.5	1.412	0.247	1.273	222.76	0.151	3.7804	14.2914	0.444
3.5	1.676	0.264	1.012	227.69	0.148	3.0057	9.0341	0.448
2.5	1.953	0.277	0.737	232.05	0.145	2.1883	4.7885	0.451
1.5	2.244	0.291	0.447	234.71	0.143	1.3281	1.7637	0.452
0.5	2.543	0.298	0.150	235.61	0.143	0.4444	0.1975	0.453
-0.5	2.842	0.299						
-1.5	3.138	0.297			Slope	z_o'/cm	C_s'/cm	
-2.5	3.426	0.288		4E-07	-0.000612	0.453	6.12	
-3.5	3.700	0.274						
-4.5	3.958	0.258						
-5.5	4.202	0.244						
-6.5	4.430	0.228						
-7.5	4.647	0.217						

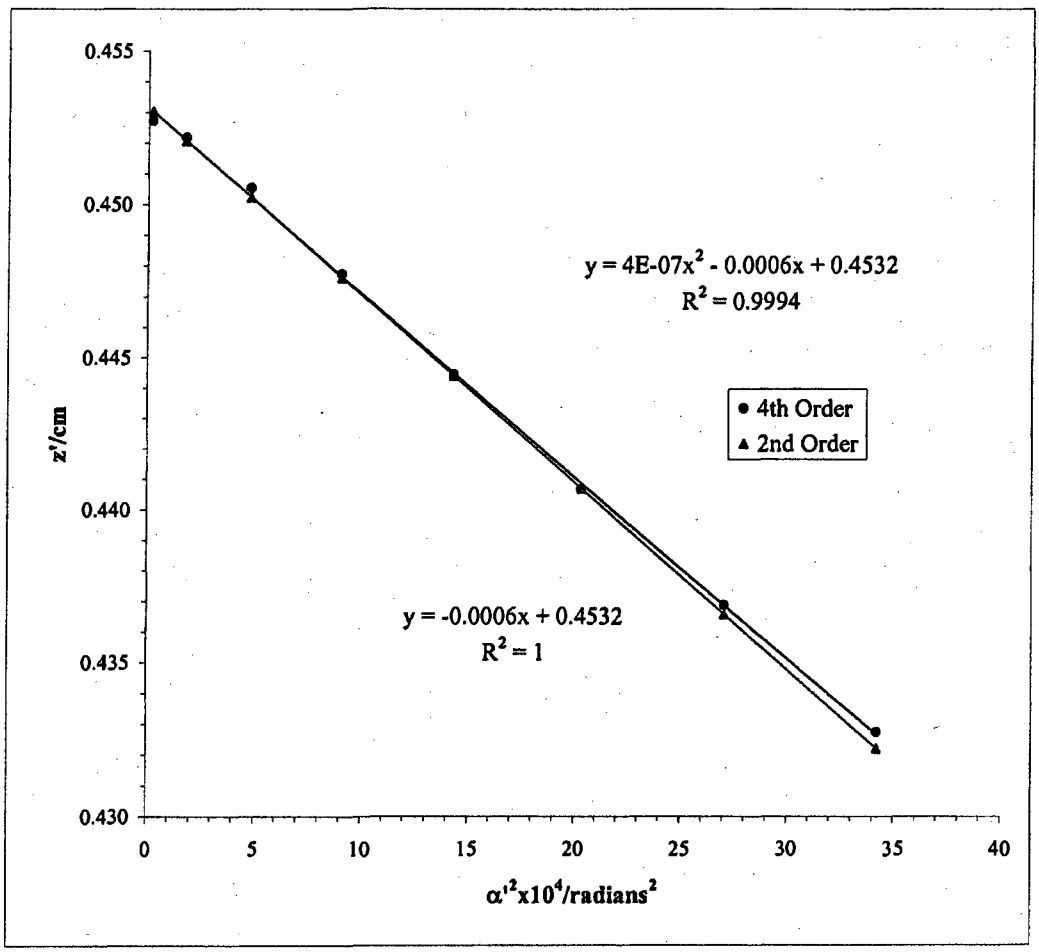

Mesh/inch	V Ratio	Mesh	e'_1/cm	d/cm	b/cm		Beam	Voltage	20 kV
2000	1.00	Rear	0.00127	33.52	0.60	DS			
								L3 Elektros obj.	

Bar location/ units	Shadow Reading Y/cm	Spacing Δ/cm	E'/cm	M'	c/cm	α' x 10^2	α'^2 x 10^4	z'/cm
6.5	0.925		1.691	204.80	0.164	5.0183	25.1829	0.4311
5.5	1.150	0.225	1.466	209.89	0.160	4.3523	18.9427	0.4351
4.5	1.386	0.236	1.230	215.27	0.156	3.6527	13.3424	0.4392
3.5	1.637	0.251	0.979	220.28	0.153	2.9074	8.4530	0.4427
2.5	1.901	0.265	0.713	224.46	0.150	2.1163	4.4787	0.4456
1.5	2.178	0.277	0.433	227.48	0.148	1.2869	1.6562	0.4476
0.5	2.465	0.287	0.146	229.79	0.147	0.4334	0.1878	0.4491
-0.5	2.757	0.292						
-1.5	3.045	0.288						
-2.5	3.327	0.282			Slope	z_0'/cm	C_s'/cm	
-3.5	3.595	0.268		2.73E-06	-0.000784	0.449	7.84	
-4.5	3.846	0.251						
-5.5	4.082	0.236						
-6.5	4.307	0.225						

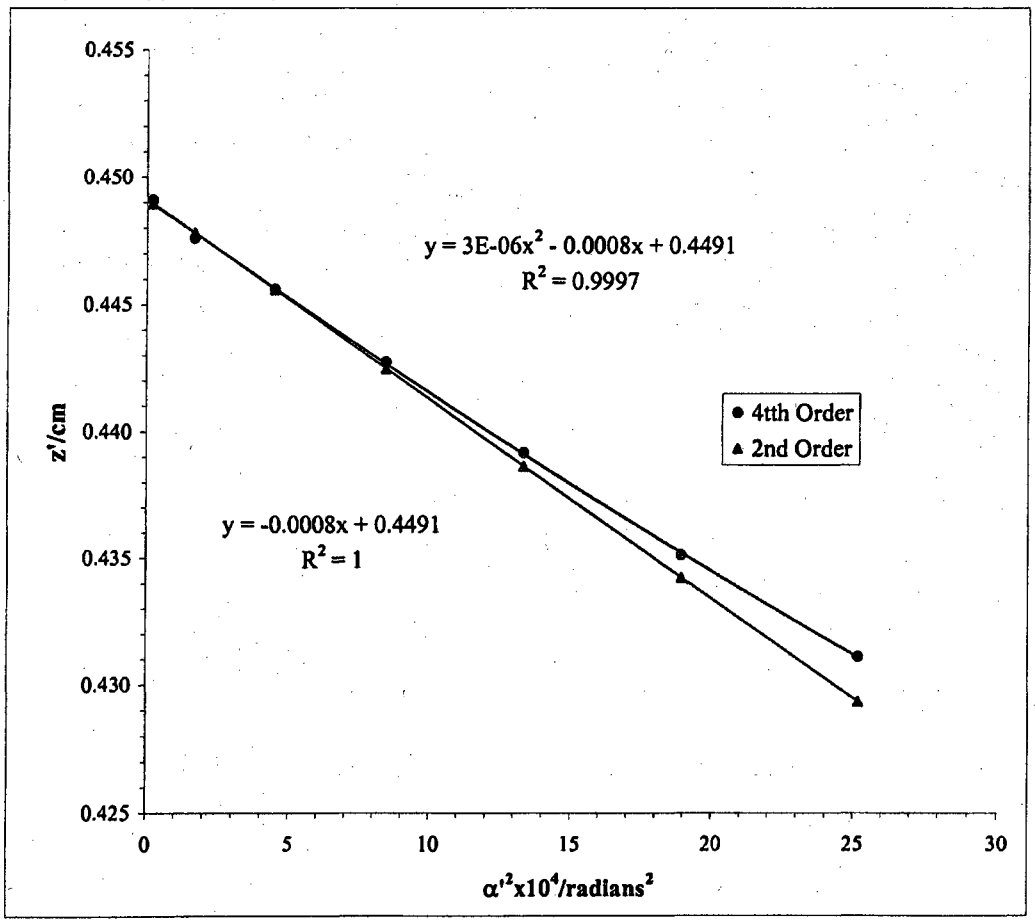

L3 Elektros obj. Beam Voltage 20 kV

Mesh/inch	V Ratio	Mesh	z/cm	e_i/cm	a/cm	z_{ap}/cm	z_o'/cm	C_s'/cm	$z_{ap}-z_o'$
600	1.00	Front	25.00	0.00423	22.40	34.12	0.451	6.44	33.67

Bar location/ units	Shadow Reading X/cm	Spacing Δ/cm	E/cm	α x 10^4	α' x 10^2	α'² x 10^4	m	z'/cm	f/cm
4	1.189		1.356	7.560	4.026	16.210	0.01878	0.440	0.461
3	1.538	0.349	1.009	5.670	2.995	8.970	0.01893	0.445	0.465
2	1.879	0.340	0.668	3.780	1.985	3.941	0.01904	0.448	0.468
1	2.216	0.338	0.332	1.890	0.987	0.975	0.01914	0.450	0.470
0	2.549	0.333							
-1	2.881	0.332							
-2	3.215	0.335							
-3	3.555	0.340							
-4	3.901	0.345							

	Slope	m_o	μ_s
4.2E-07	0.0000	0.01917	-16.06

g/cm	$(\rho/f_o)^2 = (m_o+1)^2\alpha'^2$
0.432	16.838
0.436	9.312
0.439	4.093
0.441	1.012

f vs $(\rho/f_o)^2$

S_f = slope$_f$ / f_0

	slope$_f$	fo/cm	S_f
9.59559E-06	-0.000717	0.471	-15.23

g vs $(\rho/f_o)^2$

S_g = slope$_g$ / f_0

	slope$_g$	go/cm	S_g
-3.39552E-07	-0.00059	0.442	-12.59

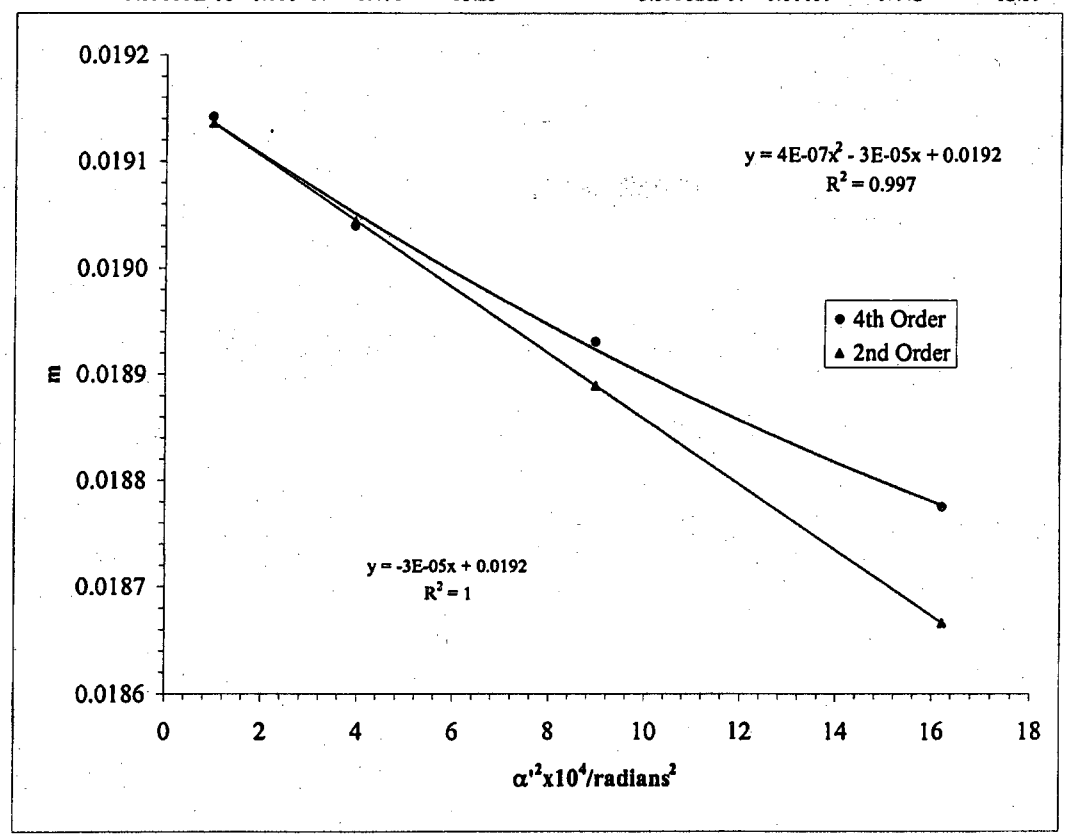

L3 Elektros obj. Beam Voltage 20 kV

Mesh/inch	V Ratio	Mesh	z/cm	e_1/cm	a/cm	z_{sp}/cm	z_0'/cm	C_s'/cm	$z_{sp}-z_o'$
600	1.00	Front	25.00	0.00423	22.40	34.12	0.451	6.44	33.67

Bar location/ units	Shadow Reading Y/cm	Spacing Δ/cm	E/cm	$\alpha \times 10^4$	$\alpha' \times 10^2$	$\alpha'^2 \times 10^4$	m	z'/cm	f/cm
6	0.937		2.086	11.339	6.191	38.328	0.0183	0.426	0.450
5	1.311	0.374	1.712	9.449	5.082	25.832	0.0186	0.434	0.457
4	1.671	0.360	1.352	7.560	4.016	16.126	0.0188	0.440	0.462
3	2.019	0.348	1.004	5.670	2.983	8.895	0.0190	0.445	0.467
2	2.359	0.340	0.665	3.780	1.974	3.898	0.0191	0.448	0.470
1	2.693	0.334	0.331	1.890	0.983	0.966	0.0192	0.450	0.472
0	3.024	0.331							
-1	3.355	0.331							
-2	3.689	0.334							
-3	4.028	0.339							
-4	4.376	0.348							
-5	4.735	0.359							
-6	5.108	0.373							

g/cm	$(\rho/f)^2 = (m+1)^2 \alpha'^2$
0.418	39.818
0.426	26.836
0.432	16.753
0.436	9.241
0.439	4.050
0.441	1.004

	Slope	m_o	μ_g
9.4E-08	0.0000	0.0193	-14.55

f vs $(\rho/f_o)^2$

$S_f = slope_f / f_0$

	$slope_f$	f_o/cm	S_f
2.12E-06	-0.00065	0.473	-13.77

g vs $(\rho/f_o)^2$

$S_g = slope_g / f_0$

	$slope_g$	g_o/cm	S_g
-9.31E-08	-0.000594	0.442	-12.57

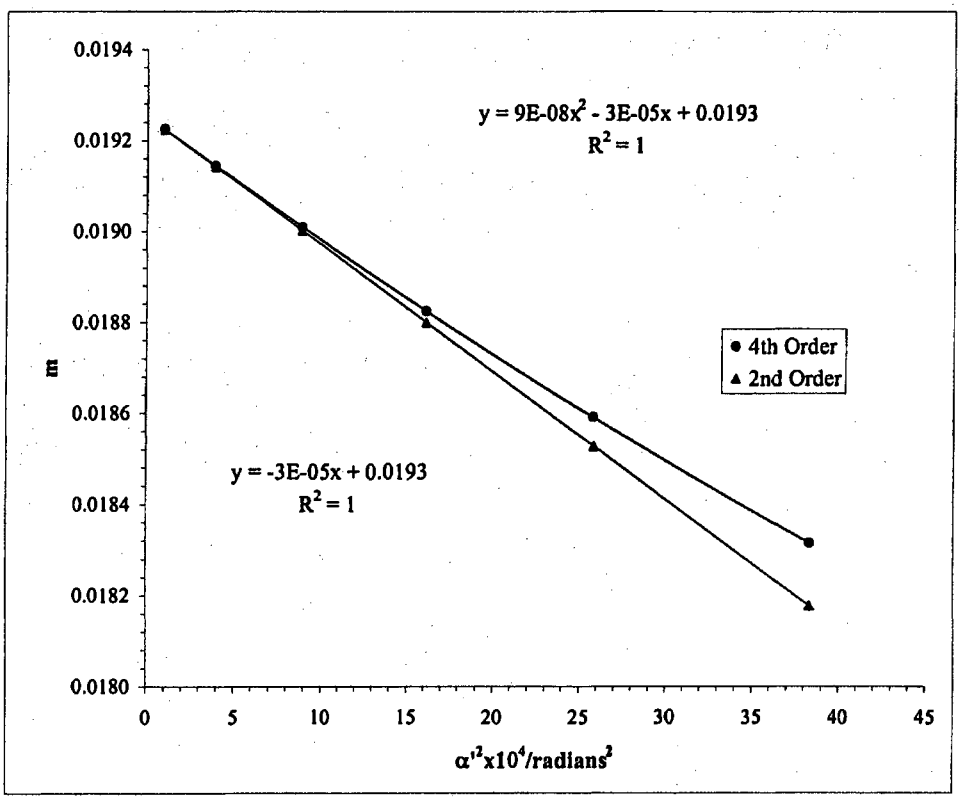

Beam Voltage	Volt Ratio	z/cm	z_0'/cm	C_s'/cm	L3 Elektros obj.
20 kV	1.00	25.0	0.451	6.44	

Average of m_o = 0.0192

Average of μ_s = -15.3

Paraxial properties :

f_o = 0.472 cm

g_o = 0.442 cm

S_f = -14.5

S_g = -12.6

PEM II Electrostatic Objective Lens L_4 Data.

Mesh/inch	V Ratio	Mesh	e'_1/cm	d/cm	b/cm		Beam	Voltage	20 kV
2000	0.70	Rear	0.00127	32.37	1.748	US			
								L4 Objective Lens	

Bar location/ units	Shadow Reading X/cm	Spacing Δ/cm	E'/cm	M'	c/cm	α' x 10^2	α'^2 x 10^4	z'/cm
7	1.021		0.571	-64.2	-0.496	1.7913	3.2086	2.244
6	1.146	0.124	0.449	-58.9	-0.540	1.4110	1.9910	2.288
5	1.241	0.095	0.355	-55.9	-0.569	1.1156	1.2445	2.317
4	1.322	0.081	0.274	-53.9	-0.590	0.8610	0.7413	2.338
3	1.396	0.073	0.201	-52.7	-0.603	0.6315	0.3988	2.351
2	1.466	0.070	0.132	-51.9	-0.612	0.4147	0.1720	2.360
1	1.533	0.067	0.065	-51.1	-0.621	0.2045	0.0418	2.369
0	1.597	0.064						
-1	1.663	0.066			Slope	z_o'/cm	C_s'/cm	
-2	1.729	0.067		0.004193	-0.0474	2.369	474.01	
-3	1.797	0.067						
-4	1.869	0.073						
-5	1.951	0.081						
-6	2.044	0.093						
-7	2.163	0.119						

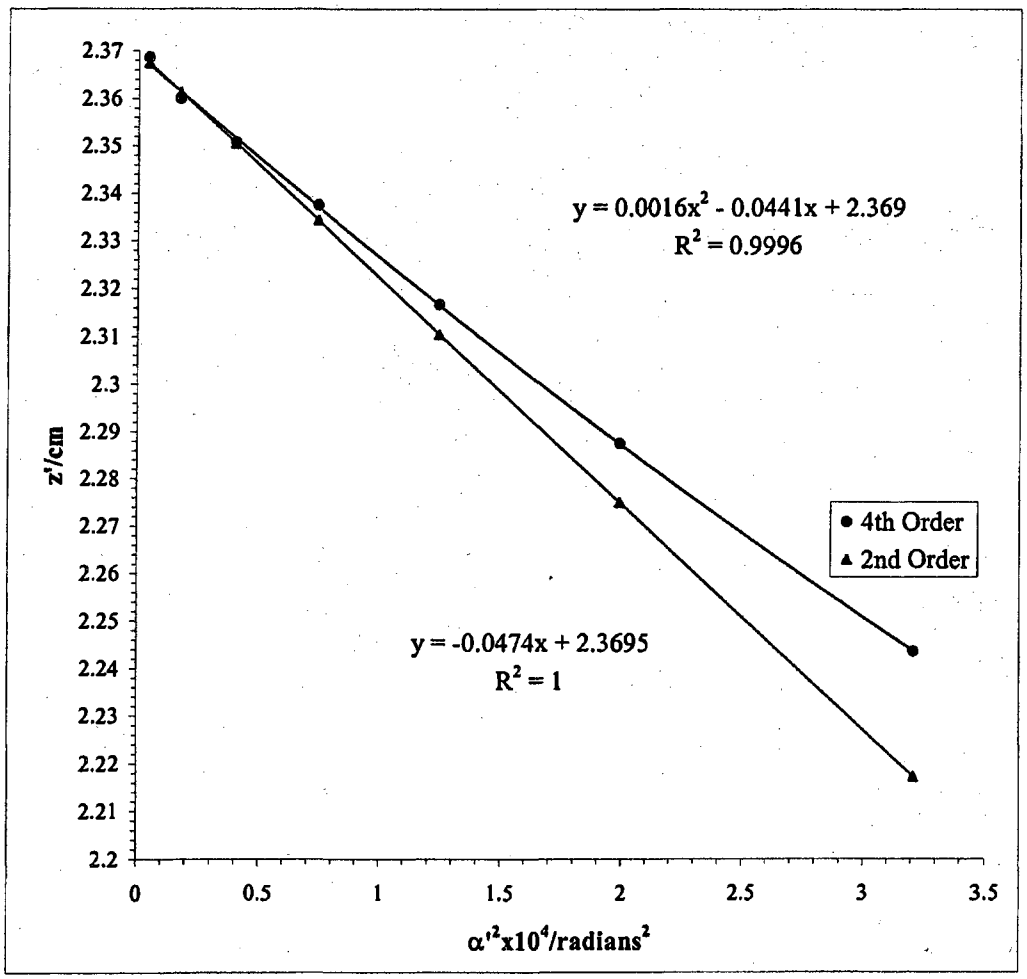

Mesh/inch	V Ratio	Mesh	e'_1/cm	d/cm	b/cm		Beam	Voltage	20 kV
2000	0.70	Rear	0.00127	32.37	1.748	US			
								L4 Objective Lens	

Bar location/ units	Shadow Reading Y/cm	Spacing Δ/cm	E'/cm	M'	c/cm	α' x 10^2	α'^2 x 10^4	z'/cm
6	1.033		0.434	-56.9	-0.559	1.3630	1.8578	2.307
5	1.127	0.095	0.343	-54.1	-0.588	1.0803	1.1672	2.335
4	1.207	0.080	0.265	-52.2	-0.609	0.8344	0.6962	2.356
3	1.279	0.072	0.194	-50.9	-0.623	0.6111	0.3735	2.371
2	1.345	0.066	0.128	-50.3	-0.632	0.4022	0.1618	2.379
1	1.410	0.064	0.063	-49.8	-0.638	0.1992	0.0397	2.385
0	1.475	0.065						
-1	1.536	0.061						
-2	1.601	0.065						
-3	1.667	0.067						
-4	1.737	0.070			Slope	z_o'/cm	C_s'/cm	
-5	1.814	0.077		0.000748	-0.04469	2.387	446.89	
-6	1.900	0.086						

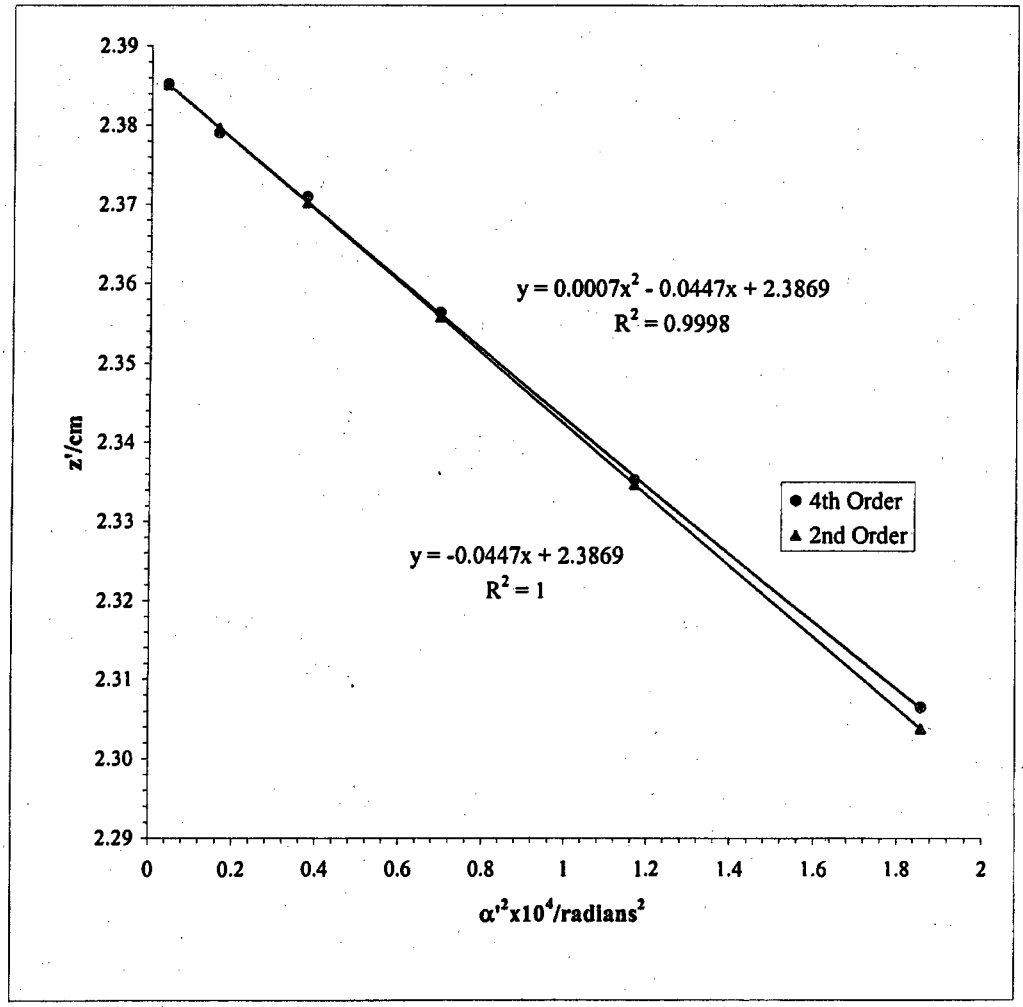

Mesh/inch	V Ratio	Mesh	e'_1/cm	d/cm	b/cm		Beam	Voltage	20 kV
2000	0.70	Rear	0.00127	31.23	2.891	DS			
								L4 Objective Lens	

Bar location/ units	Shadow Reading X/cm	Spacing Δ/cm	E'/cm	M'	c/cm	$\alpha' \times 10^2$	$\alpha'^2 \times 10^4$	z'/cm
7	0.985		0.471	52.98	0.601	1.4798	2.1897	2.290
6	1.037	0.052	0.419	54.93	0.579	1.3159	1.7317	2.311
5	1.097	0.060	0.360	56.68	0.561	1.1322	1.2820	2.330
4	1.159	0.062	0.297	58.45	0.544	0.9346	0.8734	2.347
3	1.227	0.068	0.229	60.17	0.528	0.7219	0.5212	2.363
2	1.298	0.071	0.157	61.69	0.515	0.4937	0.2437	2.376
1	1.373	0.076	0.080	62.98	0.504	0.2520	0.0635	2.387
0	1.454	0.081						
-1	1.533	0.079						
-2	1.611	0.078						
-3	1.685	0.074						
-4	1.753	0.067						
-5	1.817	0.064			Slope	z_0'/cm	C_s'/cm	
-6	1.874	0.057		0.001628	-0.048172	2.388	481.72	
-7	1.9270	0.053						

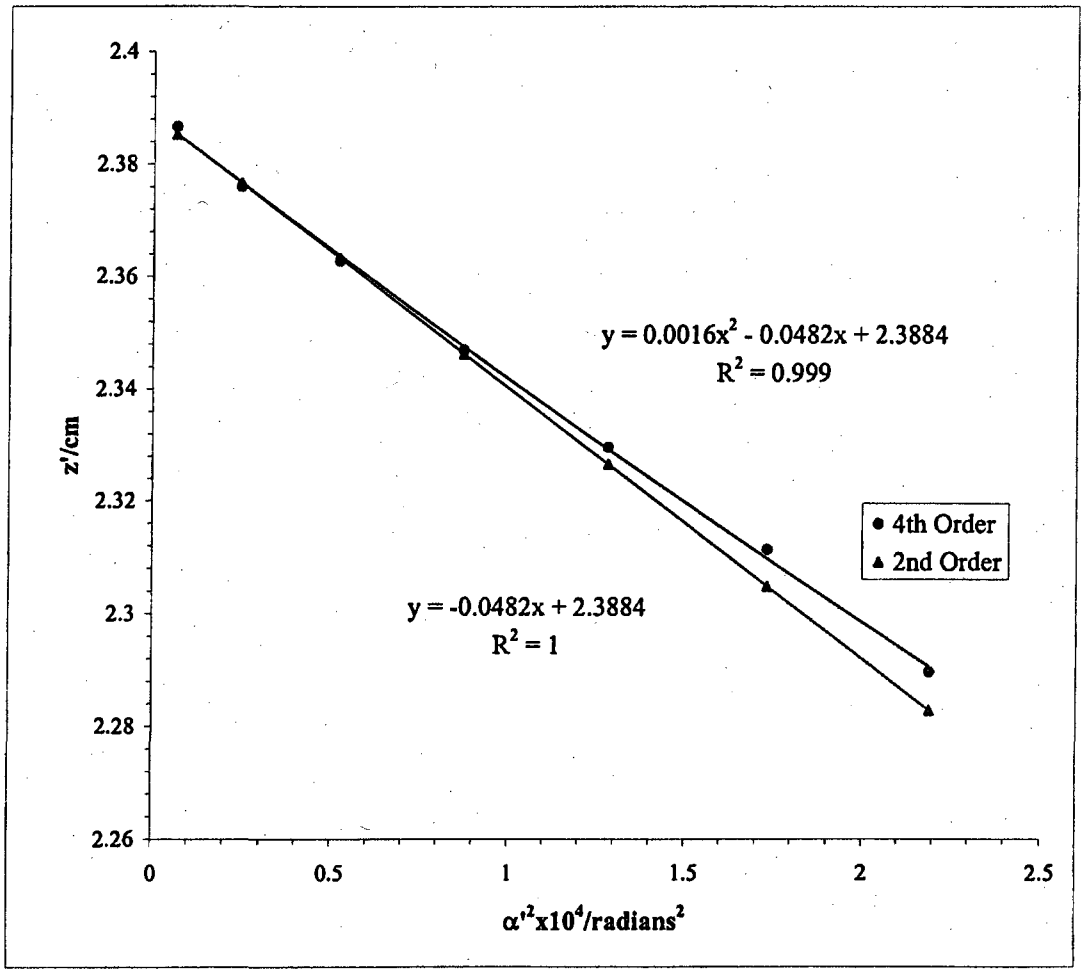

Mesh/inch	V Ratio	Mesh	e'_1/cm	d/cm	b/cm		Beam	Voltage	20 kV
2000	0.70	Rear	0.00127	31.23	2.891	DS			
								L4 Objective Lens	

Bar location/ units	Shadow Reading Y/cm	Spacing Δ/cm	E'/cm	M'	c/cm	$\alpha' \times 10^2$	$\alpha'^2 \times 10^4$	z'/cm
7.5	1.087		0.489	51.33	0.620	1.5351	2.3566	2.270
6.5	1.138	0.051	0.438	53.10	0.599	1.3773	1.8969	2.291
5.5	1.193	0.056	0.383	54.88	0.580	1.2052	1.4525	2.311
4.5	1.254	0.061	0.323	56.46	0.563	1.0149	1.0301	2.327
3.5	1.317	0.063	0.259	58.31	0.545	0.8157	0.6654	2.346
2.5	1.386	0.069	0.189	59.53	0.534	0.5951	0.3541	2.357
1.5	1.458	0.072	0.116	60.89	0.521	0.3653	0.1335	2.369
0.5	1.534	0.076	0.039	62.14	0.5107	0.1243	0.0155	2.3798
-0.5	1.613	0.079						
-1.5	1.690	0.077						
-2.5	1.764	0.074						
-3.5	1.836	0.072			Slope	z_0'/cm	C_s'/cm	
-4.5	1.900	0.064		0.001925	-0.04957	2.377	495.67	
-5.5	1.960	0.060						
-6.5	2.014	0.054						
-7.5	2.0645	0.050						

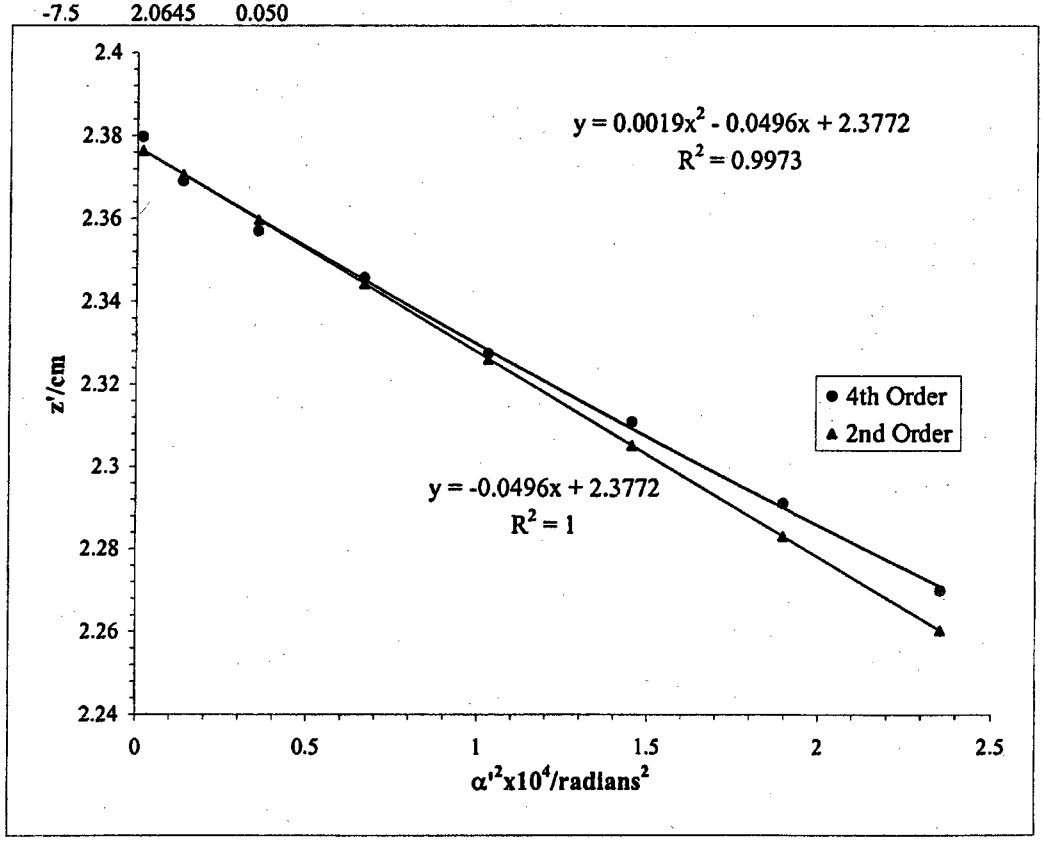

L4 Objective Lens — **Beam Voltage 20 kV**

Mesh/inch	V Ratio	Mesh	z/cm	e_1/cm	a/cm	z_{ap}/cm	z_0'/cm	C_s'/cm	$z_{ap}-z_o'$
600	0.70	Front	29.20	0.00423	27.40	34.12	2.381	474.57	31.74

Bar location/ units	Shadow Reading X/cm	Spacing Δ/cm	E/cm	$\alpha \times 10^4$	$\alpha' \times 10^2$	$\alpha'^2 \times 10^4$	m	z'/cm	f/cm
15.5	0.346		1.077	23.951	3.337	11.134	0.07178	1.852	1.973
14.5	0.434	0.088	0.990	22.406	3.074	9.450	0.07288	1.932	1.998
13.5	0.518	0.084	0.906	20.860	2.820	7.955	0.07396	2.003	2.023
12.5	0.599	0.081	0.826	19.315	2.575	6.632	0.07500	2.066	2.047
11.5	0.676	0.078	0.748	17.770	2.338	5.466	0.07601	2.121	2.070
10.5	0.751	0.075	0.674	16.225	2.108	4.445	0.07696	2.170	2.093
9.5	0.823	0.072	0.602	14.680	1.886	3.555	0.07785	2.212	2.114
8.5	0.893	0.070	0.532	13.134	1.669	2.787	0.07868	2.248	2.134
7.5	0.961	0.068	0.465	11.589	1.459	2.128	0.07944	2.279	2.152
6.5	1.027	0.066	0.399	10.044	1.254	1.572	0.08011	2.306	2.169
5.5	1.091	0.064	0.335	8.499	1.053	1.109	0.08071	2.328	2.183
4.5	1.154	0.063	0.272	6.953	0.856	0.733	0.08121	2.346	2.196
3.5	1.215	0.062	0.210	5.408	0.663	0.439	0.08162	2.360	2.206
2.5	1.276	0.061	0.150	3.863	0.472	0.222	0.08193	2.370	2.213
1.5	1.336	0.060	0.090	2.318	0.282	0.080	0.08214	2.377	2.218
0.5	1.396	0.060	0.030	0.773	0.094	0.009	0.08224	2.380	2.221
-0.5	1.456	0.060							
-1.5	1.515	0.060					g/cm	$(\rho/f_0)^2 = (m_0+1)^2 \alpha'^2$	
-2.5	1.575	0.060							
-3.5	1.636	0.061					1.710	13.039	
-4.5	1.698	0.062					1.786	11.068	
-5.5	1.760	0.063					1.853	9.316	
-6.5	1.824	0.064					1.912	7.766	
-7.5	1.890	0.066					1.964	6.401	
-8.5	1.957	0.067					2.009	5.205	
-9.5	2.027	0.069					2.047	4.164	
-10.5	2.098	0.072					2.080	3.264	
-11.5	2.173	0.074					2.109	2.493	
-12.5	2.250	0.077		Slope	m_o	μ_s	2.132	1.841	
-13.5	2.330	0.080	3.69E-05	-0.001338	0.08219	-162.77	2.152	1.299	
-14.5	2.414	0.084					2.167	0.859	
-15.5	2.501	0.087					2.180	0.514	
							2.189	0.260	
							2.195	0.093	
							2.197	0.010	

f vs $(\rho/f_o)^2$	$S_f = slope_f / f_0$			g vs $(\rho/f_o)^2$	$S_g = slope_g / f_0$		
	$slope_f$	fo/cm	S_f		$slope_g$	go/cm	S_g
0.000712	-0.028	2.219	-126.05	-0.00013	-0.0357817	2.198	-161.22

Graph on page 434

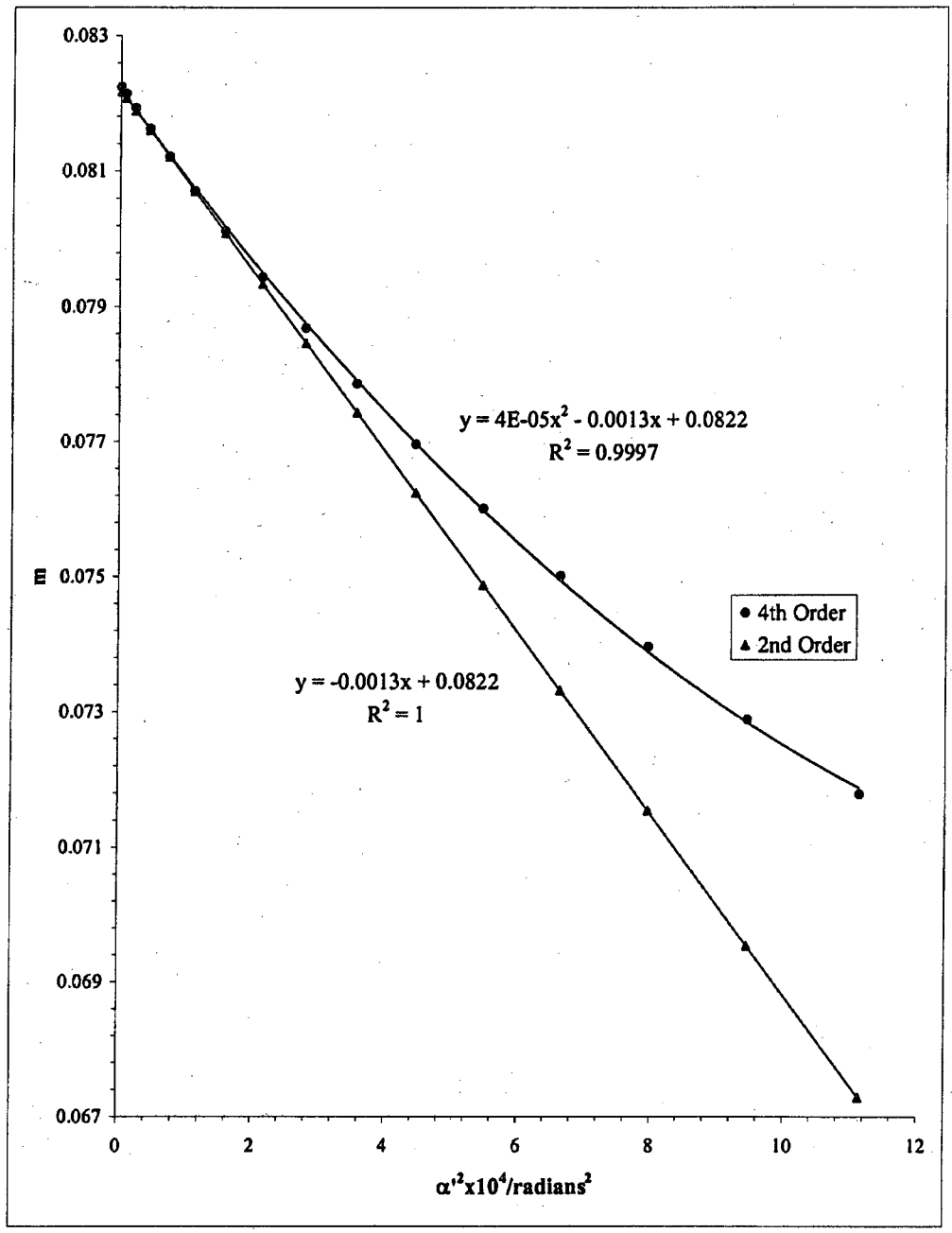

Graph from Page 433

L4 Objective Lens | **Beam Voltage** | **20 kV**

Mesh/inch	V Ratio	Mesh	z/cm	e_1/cm	a/cm	z_{sp}/cm	z_0'/cm	C_s'/cm	$z_{sp}-z_o'$
600	0.70	Front	29.20	0.00423	27.40	34.12	2.381	474.57	31.74

Bar location/ units	Shadow Reading Y/cm	Spacing Δ/cm	E/cm	$\alpha \times 10^4$	$\alpha' \times 10^2$	$\alpha'^2 \times 10^4$	m	z'/cm	f/cm
16.5	0.087		1.178	25.496	3.637	13.225	0.07011	1.753	1.934
15.5	0.179	0.092	1.086	23.951	3.363	11.307	0.07123	1.844	1.959
14.5	0.267	0.088	0.998	22.406	3.098	9.597	0.07233	1.925	1.983
13.5	0.352	0.084	0.913	20.860	2.842	8.077	0.07340	1.997	2.008
12.5	0.433	0.081	0.832	19.315	2.595	6.733	0.07444	2.061	2.032
11.5	0.511	0.078	0.754	17.770	2.356	5.549	0.07544	2.117	2.055
10.5	0.586	0.075	0.679	16.225	2.124	4.511	0.07639	2.166	2.077
9.5	0.658	0.072	0.606	14.680	1.900	3.608	0.07728	2.209	2.099
8.5	0.728	0.070	0.536	13.134	1.682	2.828	0.07811	2.246	2.118
7.5	0.796	0.068	0.468	11.589	1.470	2.160	0.07886	2.278	2.137
6.5	0.863	0.066	0.402	10.044	1.263	1.595	0.07954	2.305	2.153
5.5	0.927	0.064	0.337	8.499	1.061	1.125	0.08013	2.327	2.168
4.5	0.990	0.063	0.274	6.953	0.862	0.744	0.08063	2.345	2.180
3.5	1.052	0.062	0.212	5.408	0.667	0.445	0.08104	2.359	2.190
2.5	1.113	0.061	0.151	3.863	0.475	0.225	0.08135	2.370	2.197
1.5	1.174	0.061	0.090	2.318	0.284	0.081	0.08156	2.377	2.203
0.5	1.234	0.060	0.030	0.773	0.095	0.009	0.08166	2.380	2.205
-0.5	1.294	0.060							
-1.5	1.354	0.060							
-2.5	1.415	0.061							
-3.5	1.476	0.061							
-4.5	1.538	0.062							
-5.5	1.601	0.063							
-6.5	1.666	0.065							
-7.5	1.732	0.066							
-8.5	1.800	0.068							
-9.5	1.871	0.070							
-10.5	1.943	0.073							
-11.5	2.019	0.075							
-12.5	2.097	0.078							
-13.5	2.178	0.081							
-14.5	2.263	0.085							
-15.5	2.351	0.088							
-16.5	2.443	0.092							

	Slope	m_o	μ_s
3.24E-05	-0.001287	0.081581	-157.742

g/cm	$(\rho/f_o)^2 = (m_o+1)^2 \alpha'^2$
1.617	15.471
1.704	13.227
1.782	11.226
1.850	9.449
1.910	7.876
1.962	6.491
2.008	5.277
2.047	4.221
2.081	3.308
2.110	2.526
2.134	1.865
2.153	1.316
2.169	0.870
2.182	0.521
2.191	0.264
2.197	0.094
2.200	0.010

f vs $(\rho/f_o)^2$

$S_f = slope_f / f_0$

	$slope_f$	fo/cm	S_f
0.0006258	-0.02685	2.203	-121.88

g vs $(\rho/f_o)^2$

$S_g = slope_g / f_0$

	$slope_g$	go/cm	S_g
-0.00011	-0.03606	2.201	-163.69

Graph on page 436

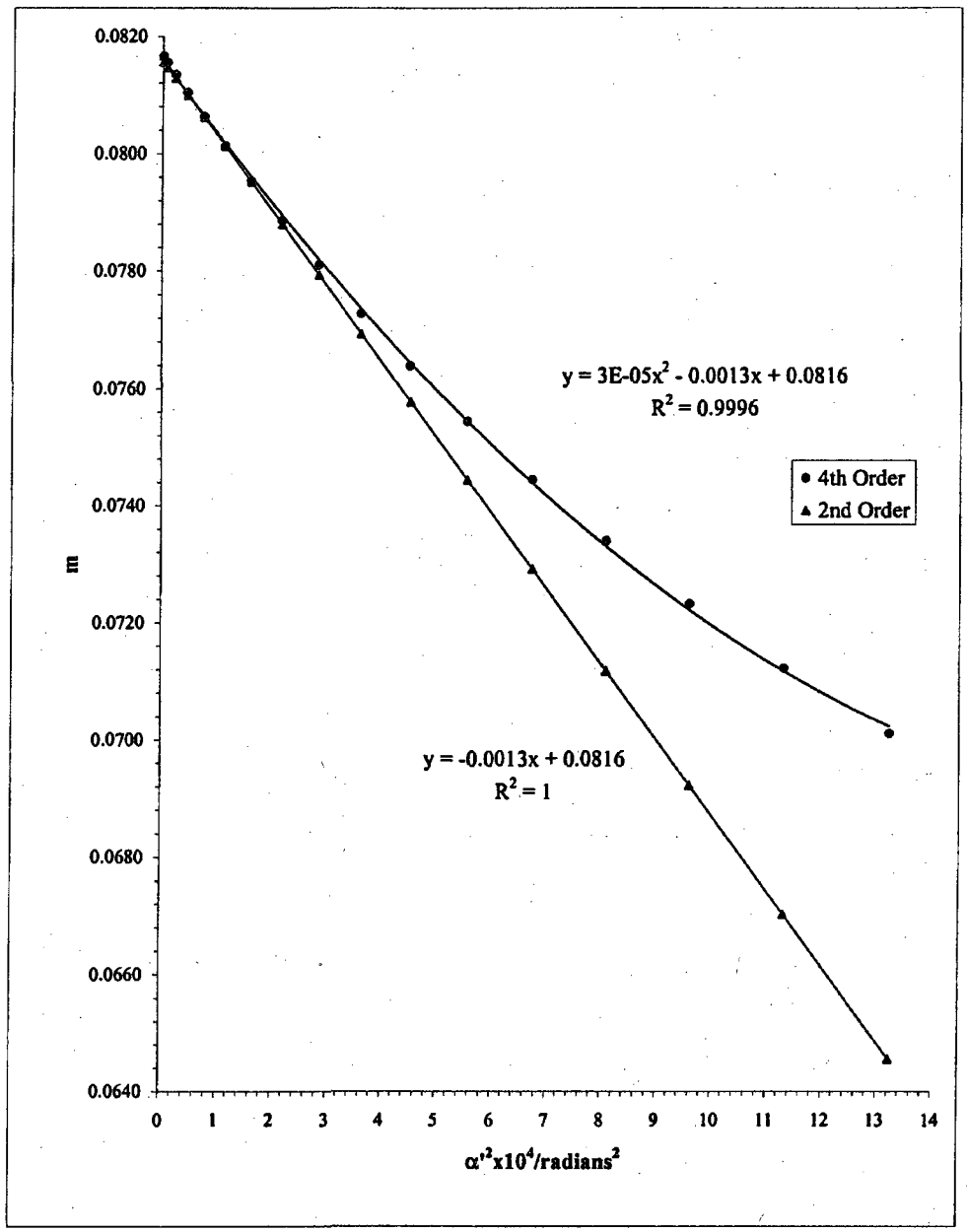

Graph from Page 435

Beam Voltage	Volt Ratio	z/cm	z_0'/cm	C_s'/cm	L4 Objective Lens
20 kV	0.70	29.2	2.38	475	

Average of m_o = 0.0819

Average of μ_s = -160

Paraxial properties :

f_o = 2.21 cm

g_o = 2.20 cm

S_f = -124

S_g = -162

Mesh/inch	V Ratio	Mesh	e'_1/cm	d/cm	b/cm		Beam	Voltage	20 kV
2000	0.80	Rear	0.00127	33.01	1.11	US			
								L4 Objective Lens	

Bar location/ units	Shadow Reading X/cm	Spacing Δ/cm	E'/cm	M'	c/cm	α' x 10^2	α'^2 x 10^4	z'/cm
8	1.084		0.775	-76.3	-0.427	2.3788	5.6586	1.540
7	1.217	0.133	0.641	-72.1	-0.451	1.9696	3.8793	1.564
6	1.330	0.113	0.528	-69.2	-0.470	1.6216	2.6296	1.582
5	1.430	0.100	0.427	-67.3	-0.483	1.3141	1.7270	1.596
4	1.523	0.093	0.334	-65.8	-0.494	1.0278	1.0564	1.607
3	1.610	0.087	0.247	-64.8	-0.502	0.7595	0.5768	1.614
2	1.695	0.085	0.162	-64.0	-0.508	0.5000	0.2500	1.621
1	1.776	0.081	0.081	-63.8	-0.510	0.2492	0.0621	1.622
0	1.856	0.080						
-1	1.938	0.082						
-2	2.020	0.082			Slope	z_0'/cm	C_s'/cm	
-3	2.103	0.084		0.00036	-0.01699	1.624	169.90	
-4	2.191	0.088						
-5	2.285	0.094						
-6	2.385	0.101						
-7	2.499	0.114						
-8	2.634	0.135						

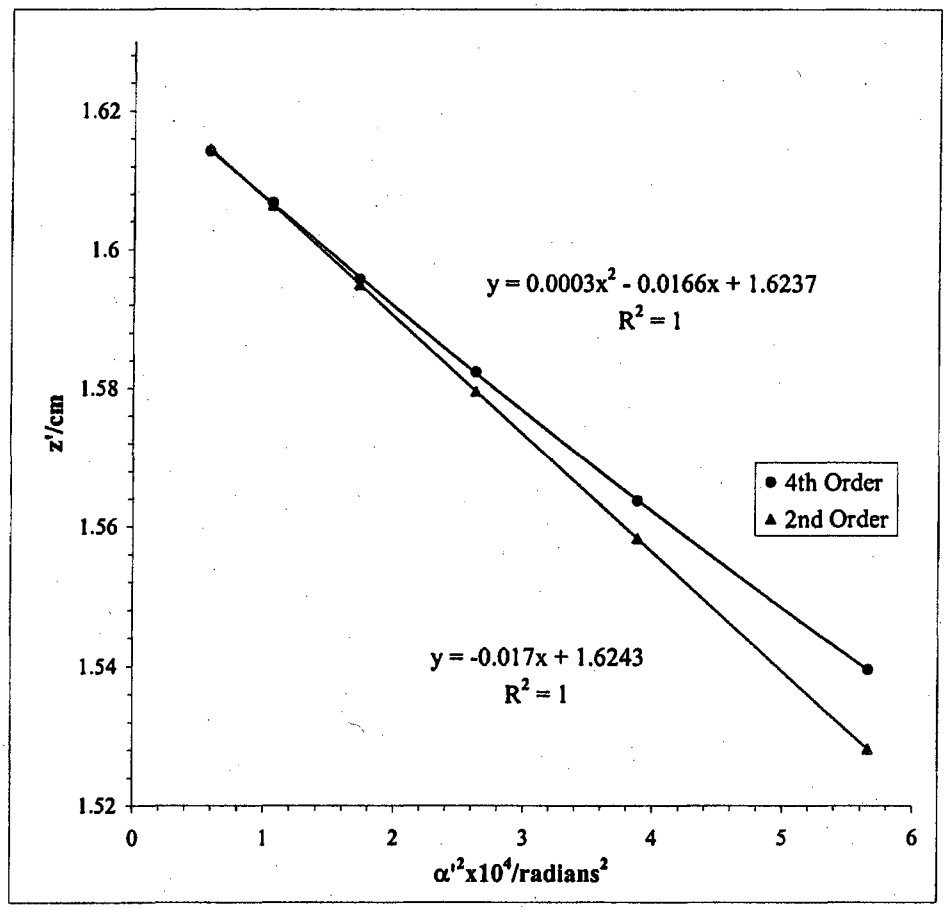

Mesh/inch	V Ratio	Mesh	e'_1/cm	d/cm	b/cm		Beam	Voltage	20 kV
2000	0.80	Rear	0.00127	33.01	1.113	US			
								L4 Objective Lens	

Bar location/ units	Shadow Reading Y/cm	Spacing Δ/cm	E'/cm	M'	c/cm	α' x 10^2	α'^2 x 10^4	z'/cm
9.5	0.096		1.158	-96.0	-0.340	3.5454	12.5699	1.453
8.5	0.386	0.290	0.888	-82.3	-0.396	2.7240	7.4202	1.509
7.5	0.557	0.170	0.726	-76.3	-0.427	2.2298	4.9722	1.540
6.5	0.688	0.131	0.599	-72.6	-0.448	1.8407	3.3882	1.561
5.5	0.802	0.114	0.489	-69.9	-0.465	1.5014	2.2543	1.578
4.5	0.903	0.101	0.389	-68.2	-0.477	1.1974	1.4337	1.590
3.5	0.995	0.093	0.298	-66.9	-0.486	0.9151	0.8374	1.598
2.5	1.084	0.089	0.210	-66.0	-0.493	0.6445	0.4154	1.605
1.5	1.170	0.086	0.124	-65.2	-0.498	0.3824	0.1462	1.611
0.5	1.253	0.083	0.041	-64.4	-0.505	0.1258	0.0158	1.617
-0.5	1.335	0.082						
-1.5	1.419	0.084						
-2.5	1.503	0.085						
-3.5	1.590	0.087			Slope	z_o'/cm	C_s'/cm	
-4.5	1.682	0.091		0.000251	-0.01582	1.612	158.15	
-5.5	1.779	0.097						
-6.5	1.886	0.107						
-7.5	2.010	0.123						
-8.5	2.163	0.153						
-9.5	2.413	0.250						

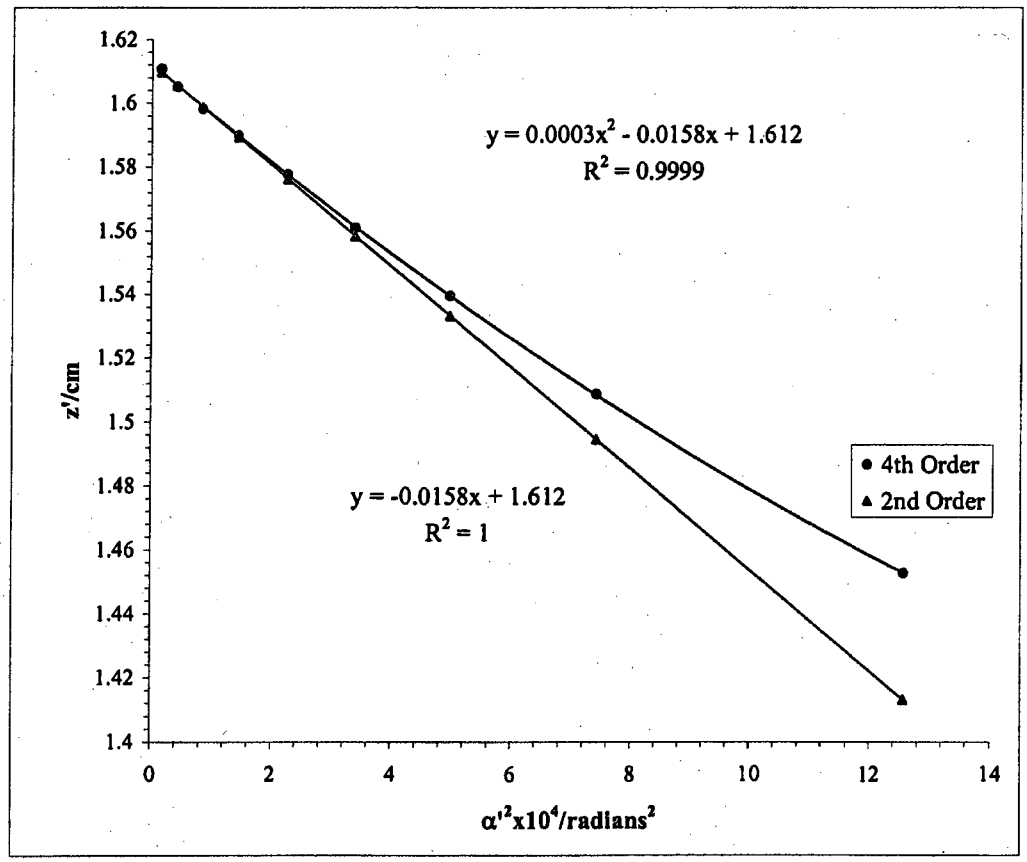

Mesh/inch	V Ratio	Mesh	e'_1/cm	d/cm	b/cm		Beam	Voltage	20 kV
2000	0.80	Rear	0.00127	31.99	2.129	DS			
								L4 Objective Lens	

Bar location/ units	Shadow Reading X/cm	Spacing Δ/cm	E'/cm	M'	c/cm	α' x 10^2	α'^{2} x 10^4	z'/cm
9	1.655		0.667	58.34	0.558	2.0488	4.1977	1.571
8	1.716	0.061	0.605	59.52	0.547	1.8586	3.4542	1.582
7	1.781	0.064	0.538	60.55	0.537	1.6550	2.7390	1.591
6	1.846	0.066	0.471	61.83	0.526	1.4489	2.0993	1.603
5	1.917	0.070	0.400	62.93	0.517	1.2293	1.5112	1.612
4	1.990	0.073	0.325	63.96	0.508	0.9997	0.9995	1.620
3	2.065	0.075	0.248	65.00	0.500	0.7622	0.5810	1.629
2	2.143	0.079	0.167	65.91	0.493	0.5154	0.2656	1.636
1	2.226	0.083	0.084	65.92	0.493	0.2577	0.0664	1.636
0	2.311	0.085						
-1	2.394	0.083						
-2	2.478	0.084						
-3	2.560	0.082						
-4	2.639	0.079						
-5	2.716	0.077			Slope	z_0'/cm	C_s'/cm	
-6	2.789	0.073		0.00082	-0.01994	1.640	199.43	
-7	2.857	0.069						
-8	2.926	0.068						
-9	2.989	0.063						

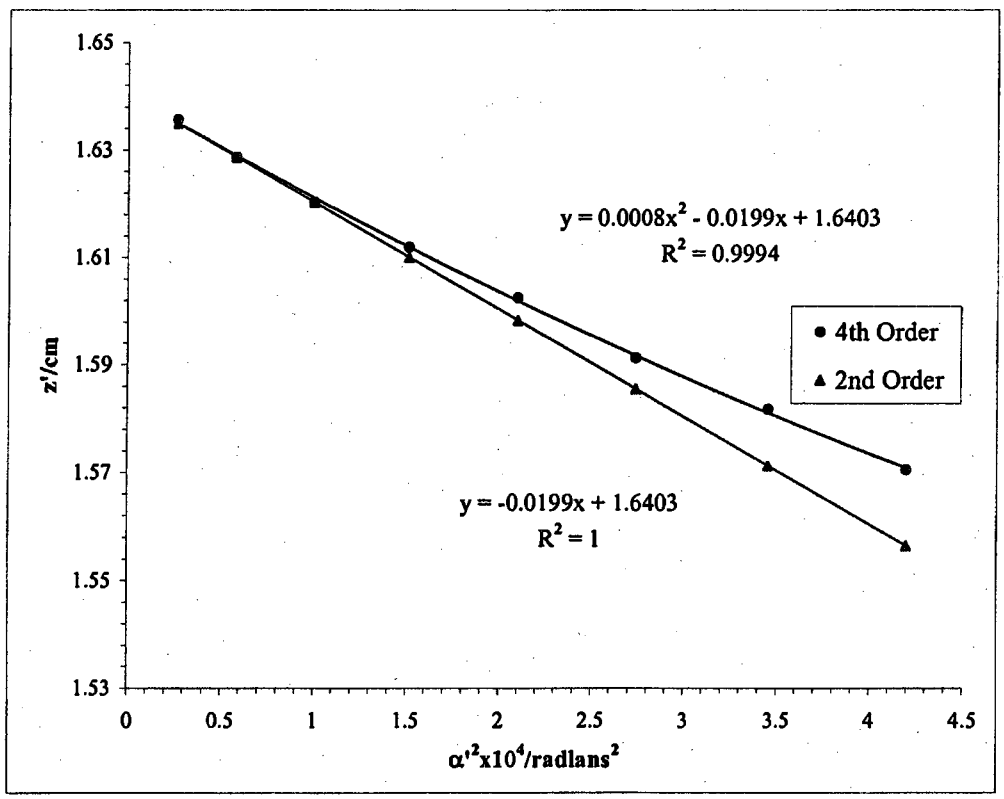

Mesh/inch	V Ratio	Mesh	e'_1/cm	d/cm	b/cm		Beam	Voltage	20 kV
2000	0.80	Rear	0.00127	31.99	2.129	DS			
								L4 Objective Lens	

Bar location/ units	Shadow Reading Y/cm	Spacing Δ/cm	E'/cm	M'	c/cm	α' x 10^2	α'^2 x 10^4	z'/cm
7.5	2.232		0.578	60.71	0.536	1.7779	3.1610	1.593
6.5	2.299	0.067	0.513	62.11	0.524	1.5768	2.4864	1.605
5.5	2.370	0.071	0.441	63.16	0.515	1.3572	1.8421	1.614
4.5	2.446	0.075	0.367	64.24	0.506	1.1298	1.2765	1.623
3.5	2.522	0.077	0.291	65.39	0.497	0.8947	0.8004	1.632
2.5	2.603	0.081	0.210	66.12	0.491	0.6463	0.4177	1.637
1.5	2.687	0.084	0.128	66.97	0.485	0.3928	0.1543	1.644
0.5	2.774	0.087	0.041	64.96	0.500	0.1270	0.0161	1.628
-0.5	2.857	0.083						
-1.5	2.942	0.086						
-2.5	3.023	0.081						
-3.5	3.103	0.080						
-4.5	3.180	0.076						
-5.5	3.252	0.073			Slope	z_0'/cm	C_s'/cm	
-6.5	3.325	0.072		0.000475	-0.018	1.646	180.02	
-7.5	3.389	0.064						

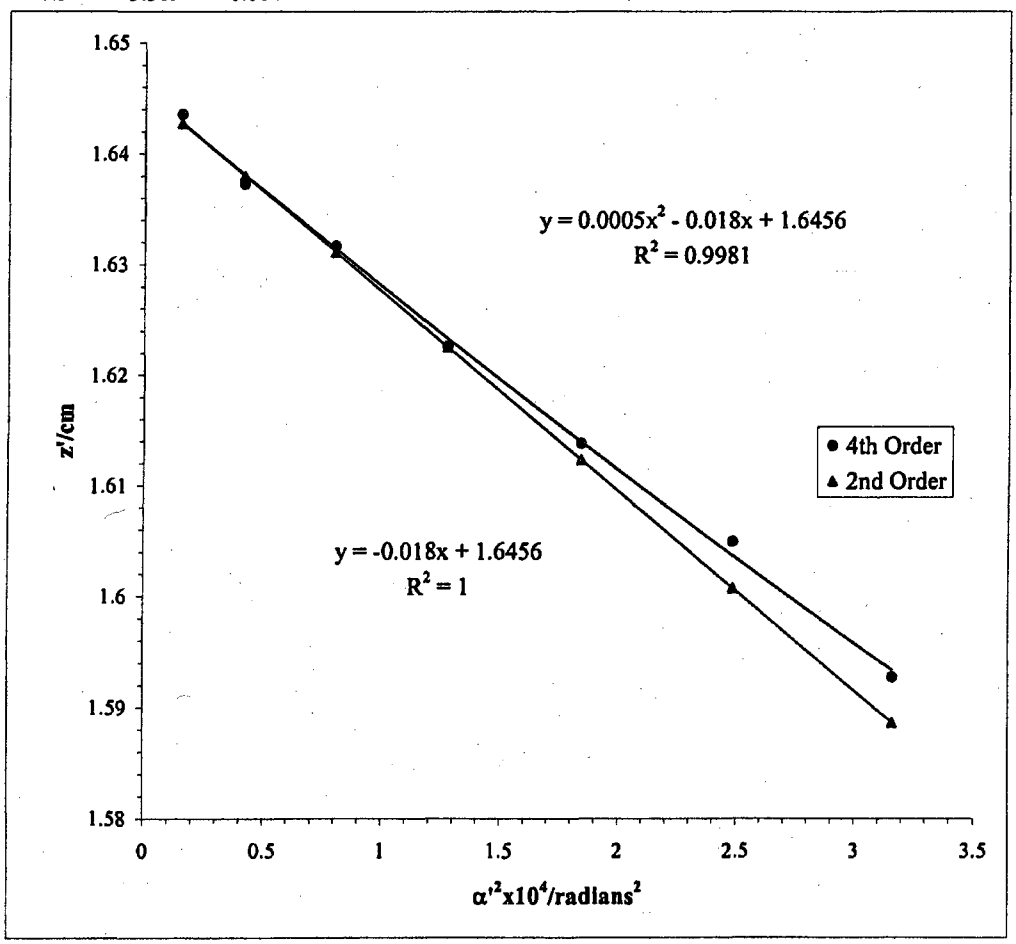

L4 Objective Lens — **Beam Voltage** **20 kV**

Mesh/inch	V Ratio	Mesh	z/cm	e_1/cm	a/cm	z_{sp}/cm	z_0'/cm	C_s'/cm	$z_{sp}-z_0'$
600	0.80	Front	29.20	0.00423	27.40	34.12	1.631	176.87	32.49

Bar location/ units	Shadow Reading X/cm	Spacing Δ/cm	E/cm	$\alpha \times 10^4$	$\alpha' \times 10^2$	$\alpha'^2 \times 10^4$	m	z'/cm	f/cm
12.5	1.176		1.278	19.315	3.900	15.213	0.04952	1.361	1.382
11.5	1.298	0.122	1.153	17.770	3.524	12.419	0.05043	1.411	1.405
10.5	1.418	0.120	1.034	16.225	3.166	10.025	0.05124	1.453	1.426
9.5	1.530	0.111	0.923	14.680	2.827	7.994	0.05192	1.489	1.443
8.5	1.639	0.109	0.814	13.134	2.497	6.233	0.05261	1.520	1.460
7.5	1.741	0.103	0.709	11.589	2.177	4.741	0.05323	1.547	1.476
6.5	1.842	0.101	0.608	10.044	1.868	3.489	0.05377	1.569	1.490
5.5	1.939	0.097	0.510	8.499	1.568	2.457	0.05422	1.587	1.502
4.5	2.034	0.095	0.414	6.953	1.273	1.620	0.05463	1.602	1.512
3.5	2.129	0.094	0.319	5.408	0.982	0.965	0.05505	1.613	1.524
2.5	2.222	0.093	0.227	3.863	0.698	0.487	0.05533	1.622	1.531
1.5	2.313	0.091	0.136	2.318	0.419	0.175	0.05533	1.627	1.530
0.5	2.404	0.091	0.045	0.773	0.139	0.019	0.05558	1.630	1.537
-0.5	2.494	0.090							
-1.5	2.585	0.091					g/cm	$(\rho/f_0)^2 = (m_0+1)^2\alpha'^2$	
-2.5	2.676	0.091							
-3.5	2.767	0.091					1.293	16.949	
-4.5	2.862	0.095					1.340	13.835	
-5.5	2.959	0.097					1.380	11.169	
-6.5	3.058	0.099					1.414	8.906	
-7.5	3.160	0.102					1.443	6.944	
-8.5	3.266	0.106					1.468	5.282	
-9.5	3.375	0.108		Slope	m_o	m_s	1.489	3.888	
-10.5	3.487	0.112	8.1E-06	-0.00051	0.055495	-92.26	1.506	2.737	
-11.5	3.603	0.116					1.519	1.805	
-12.5	3.732	0.128					1.530	1.075	
							1.537	0.543	

f vs $(\rho/f_o)^2$ — g vs (ρ/f_o)

$S_f = slope_f / f_0$ — $S_g = slope_g / f_0$

$slope_f$	fo/cm	S_f	$slope_g$	go/cm	S_g
0.0001765	-0.01192	1.535	-77.65	-2.2E-05	-0.01453	1.545	-94.66

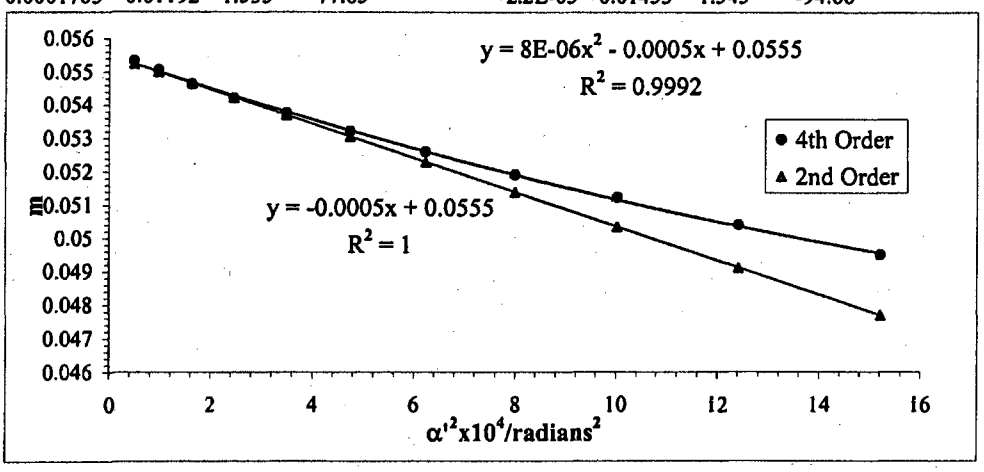

L4 Objective Lens — **Beam Voltage 20 kV**

Mesh/inch	V Ratio	Mesh	z/cm	e_1/cm	a/cm	z_{sp}/cm	z_0'/cm	C_s'/cm	$z_{sp}-z_o'$
600	0.80	Front	29.20	0.004233	27.40	34.12	1.631	176.87	32.49

Bar location/ units	Shadow Reading X/cm	Spacing Δ/cm	E/cm	$\alpha \times 10^4$	$\alpha' \times 10^2$	$\alpha'^2 \times 10^4$	m	z'/cm	f/cm
12.5	1.377		1.257	19.315	3.838	14.729	0.050329	1.370	1.404
11.5	1.499	0.122	1.135	17.770	3.470	12.039	0.051214	1.418	1.427
10.5	1.615	0.116	1.018	16.225	3.117	9.718	0.052046	1.459	1.448
9.5	1.726	0.111	0.907	14.680	2.779	7.724	0.052818	1.494	1.468
8.5	1.833	0.107	0.800	13.134	2.454	6.021	0.053526	1.524	1.486
7.5	1.935	0.103	0.697	11.589	2.140	4.578	0.054167	1.550	1.502
6.5	2.035	0.099	0.597	10.044	1.835	3.367	0.054735	1.571	1.517
5.5	2.131	0.096	0.501	8.499	1.539	2.368	0.055229	1.589	1.530
4.5	2.225	0.094	0.406	6.953	1.250	1.562	0.055644	1.603	1.541
3.5	2.317	0.092	0.314	5.408	0.966	0.933	0.055980	1.614	1.549
2.5	2.408	0.091	0.223	3.863	0.687	0.472	0.056233	1.622	1.556
1.5	2.497	0.090	0.134	2.318	0.411	0.169	0.056402	1.628	1.560
0.5	2.586	0.089	0.044	0.773	0.137	0.019	0.056487	1.630	1.563
-0.5	2.675	0.089							
-1.5	2.764	0.089							
-2.5	2.854	0.090							
-3.5	2.945	0.091							
-4.5	3.038	0.093							
-5.5	3.132	0.095							
-6.5	3.229	0.097							
-7.5	3.329	0.100							
-8.5	3.433	0.103							
-9.5	3.540	0.107							
-10.5	3.652	0.112							
-11.5	3.769	0.117							
-12.5	3.891	0.123							

g/cm	$(\rho/f_0)^2 = (m_0+1)^2 \alpha'^2$
1.299	16.439
1.345	13.437
1.383	10.847
1.416	8.622
1.445	6.720
1.468	5.109
1.488	3.758
1.504	2.643
1.517	1.743
1.527	1.042
1.535	0.527
1.540	0.188
1.542	0.021
1.542	-92.15

Slope	m_o	m_s
8.47E-06	-0.00054	0.05648	-95.76

f vs $(\rho/f_o)^2$

$S_f = slope_f / f_0$

	$slope_f$	fo/cm	S_f
0.000184	-0.0126	1.562	-80.67

g vs $(\rho/f_o)^2$

$S_g = slope_g / f_0$

	$slope_g$	go/cm	S_g
-2.4E-05	-0.0144	1.542	-92.15

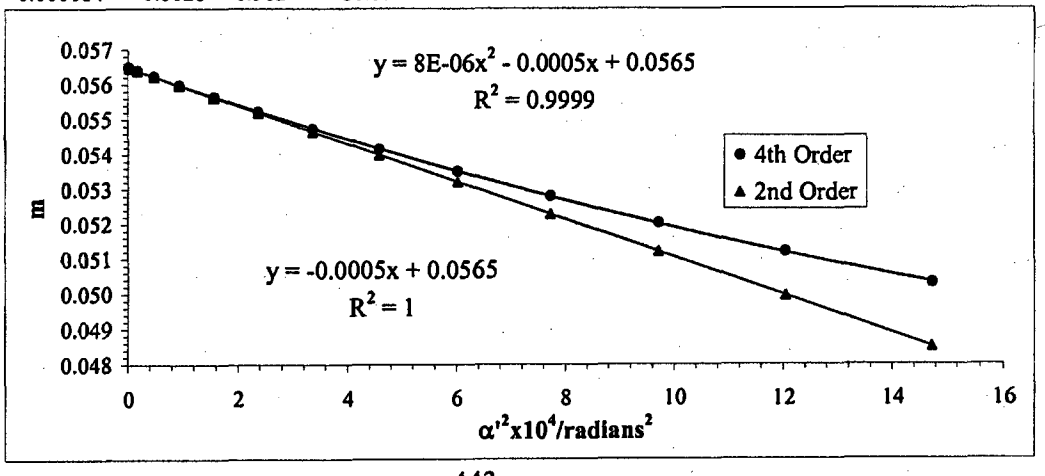

L4 Objective Lens

Beam Voltage	Volt Ratio	z/cm	z_0'/cm	Cs'/cm
20 kV	0.80	29.2	1.63	177

Average of m_o = 0.0551

Average of μ_s = -75.4

Paraxial properties :

f_o = 1.55 cm

g_o = 1.54 cm

S_f = -79.2

S_g = -93.4

Mesh/inch	V Ratio	Mesh	e'_1/cm	d/cm	b/cm		Beam	Voltage	20 kV
2000	0.85	Rear	0.00127	33.26	0.859	US			
								L4 Objective Lens	

Bar location/ units	Shadow Reading X/cm	Spacing Δ/cm	E'/cm	M'	c/cm	α' x 10^2	α'^{2} x 10^4	z'/cm
10.5	1.777		1.132	-84.9	-0.387	3.4423	11.8495	1.246
9.5	1.943	0.166	0.966	-80.0	-0.410	2.9397	8.6415	1.269
8.5	2.080	0.137	0.828	-76.7	-0.428	2.5234	6.3677	1.286
7.5	2.200	0.120	0.708	-74.3	-0.442	2.1568	4.6518	1.300
6.5	2.310	0.111	0.598	-72.4	-0.453	1.8221	3.3202	1.312
5.5	2.412	0.102	0.496	-71.0	-0.462	1.5116	2.2848	1.321
4.5	2.509	0.097	0.399	-69.8	-0.470	1.2172	1.4816	1.328
3.5	2.600	0.091	0.307	-69.2	-0.474	0.9377	0.8792	1.333
2.5	2.690	0.090	0.218	-68.7	-0.477	0.6657	0.4432	1.335
1.5	2.778	0.088	0.130	-68.2	-0.481	0.3964	0.1571	1.339
0.5	2.865	0.087	0.043	-68.0	-0.482	0.1318	0.0174	1.340
-0.5	2.951	0.086						
-1.5	3.038	0.087			Slope	zo'/cm	Cs'/cm	
-2.5	3.127	0.088		8.59E-05	-9.00E-03	1.340	90.01	
-3.5	3.215	0.088						
-4.5	3.307	0.092						
-5.5	3.404	0.097						
-6.5	3.506	0.102						
-7.5	3.615	0.109						
-8.5	3.737	0.121						
-9.5	3.874	0.137						
-10.5	4.040	0.166						

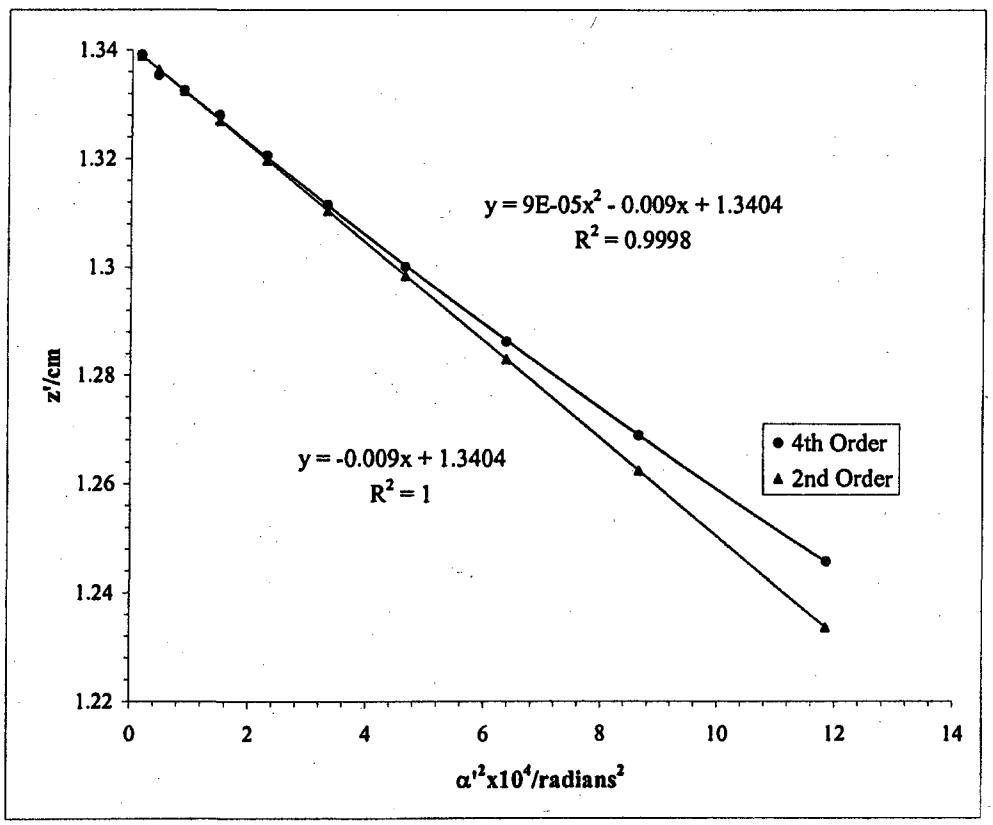

Mesh/inch	V Ratio	Mesh	e'_1/cm	d/cm	b/cm		Beam	Voltage	20 kV
2000	0.85	Rear	0.00127	33.26	0.859	US			
								L4 Objective Lens	

Bar location/ units	Shadow Reading Y/cm	Spacing Δ/cm	E'/cm	M'	c/cm	α' x 10^2	α'^2 x 10^4	z'/cm
11	2.028		1.198	-85.7	-0.384	3.6426	13.2689	1.242
10	2.205	0.177	1.019	-80.3	-0.409	3.1031	9.6293	1.268
9	2.347	0.142	0.875	-76.6	-0.429	2.6654	7.1044	1.287
8	2.470	0.123	0.751	-73.9	-0.444	2.2890	5.2397	1.302
7	2.581	0.111	0.640	-71.9	-0.456	1.9496	3.8010	1.315
6	2.682	0.102	0.537	-70.5	-0.465	1.6370	2.6799	1.324
5	2.779	0.097	0.440	-69.3	-0.473	1.3418	1.8003	1.332
4	2.872	0.093	0.347	-68.3	-0.480	1.0580	1.1193	1.339
3	2.961	0.088	0.258	-67.7	-0.484	0.7864	0.6185	1.343
2	3.048	0.088	0.170	-67.0	-0.489	0.5196	0.2700	1.347
1	3.134	0.086	0.084	-66.4	-0.494	0.2572	0.0661	1.352
0	3.218	0.084						
-1	3.303	0.084						
-2	3.389	0.086						
-3	3.476	0.087						
-4	3.566	0.090			Slope	z_o'/cm	Cs'/cm	
-5	3.659	0.093		1.33E-04	-9.89E-03	1.350	98.90	
-6	3.756	0.097						
-7	3.860	0.104						
-8	3.972	0.112						
-9	4.097	0.125						
-10	4.244	0.147						
-11	4.423	0.180						

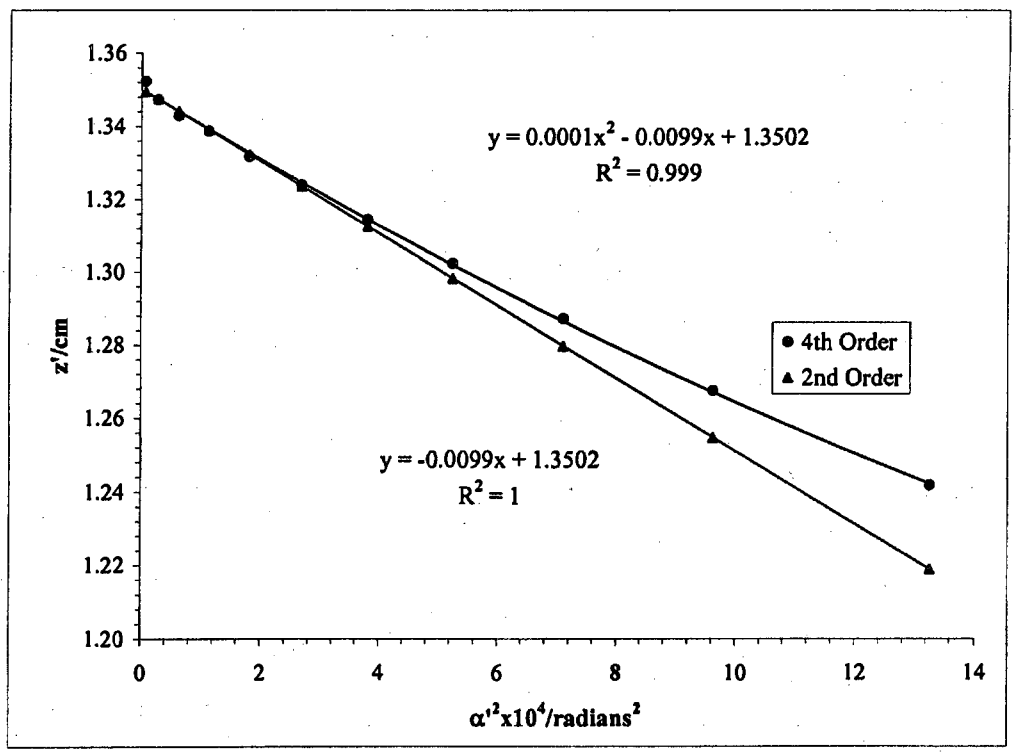

Mesh/inch	V Ratio	Mesh	e'_1/cm	d/cm	b/cm		Beam	Voltage	20 kV
2000	0.85	Rear	0.00127	32.50	1.621	DS			
								L4 Objective Lens	

Bar location/ units	Shadow Reading X/cm	Spacing Δ/cm	E'/cm	M'	c/cm	$\alpha' \times 10^2$	$\alpha'^2 \times 10^4$	z'/cm
12	1.372		1.239	81.33	0.405	3.7669	14.1899	1.216
11	1.444	0.073	1.167	83.57	0.394	3.5495	12.5990	1.227
10	1.520	0.076	1.092	85.97	0.382	3.3205	11.0254	1.238
9	1.600	0.080	1.013	88.59	0.371	3.0806	9.4902	1.249
8	1.685	0.085	0.928	91.34	0.360	2.8245	7.9776	1.261
7	1.775	0.090	0.838	94.31	0.348	2.5525	6.5154	1.272
6	1.870	0.095	0.743	97.55	0.337	2.2638	5.1247	1.284
5	1.973	0.103	0.641	101.00	0.325	1.9540	3.8182	1.296
4	2.085	0.112	0.531	104.46	0.314	1.6172	2.6153	1.306
3	2.205	0.120	0.411	107.78	0.304	1.2518	1.5671	1.316
2	2.335	0.130	0.281	110.53	0.297	0.8561	0.7328	1.324
1	2.473	0.138	0.143	112.24	0.292	0.4347	0.1890	1.328
0	2.615	0.142						
-1	2.758	0.143						
-2	2.897	0.138						
-3	3.026	0.129			Slope	z_0'/cm	C_s'/cm	
-4	3.146	0.120		1.09E-04	-9.61E-03	1.331	96.06	
-5	3.256	0.109						
-6	3.357	0.101						
-7	3.452	0.095						
-8	3.541	0.089						
-9	3.625	0.084						
-10	3.703	0.079						
-11	3.779	0.076						
-12	3.850	0.071						

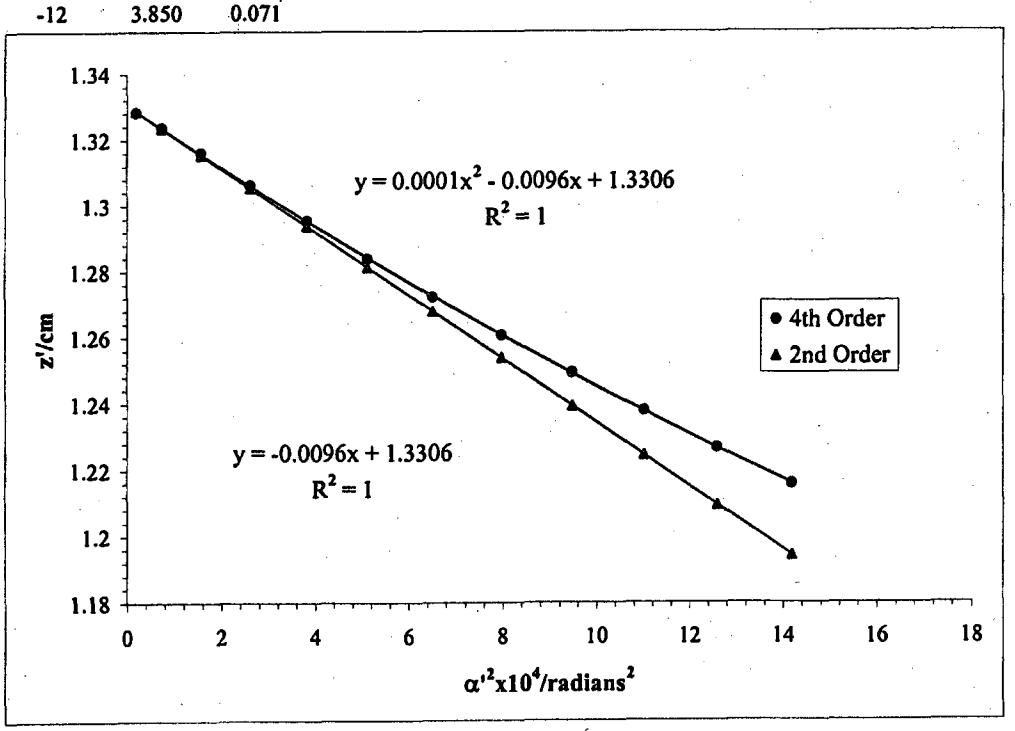

Mesh/inch	V Ratio	Mesh	e'_1/cm	d/cm	b/cm		Beam	Voltage	20 kV
2000	0.85	Rear	0.00127	32.50	1.621	DS			
								L4 Objective Lens	

Bar location/ units	Shadow Reading Y/cm	Spacing Δ/cm	E'/cm	M'	c/cm	$\alpha' \times 10^2$	$\alpha'^2 \times 10^4$	z'/cm
10.5	1.7537		1.1228	84.20	0.3906	3.4138	11.6543	1.2299
9.5	1.8319	0.0782	1.0446	86.58	0.3797	3.1771	10.0940	1.2408
8.5	1.9152	0.0833	0.9623	89.15	0.3687	2.9280	8.5733	1.2518
7.5	2.0022	0.0870	0.8761	91.97	0.3572	2.6664	7.1098	1.2633
6.5	2.0938	0.0916	0.7844	95.02	0.3457	2.3882	5.7037	1.2749
5.5	2.1941	0.1004	0.6852	98.10	0.3347	2.0870	4.3556	1.2858
4.5	2.3008	0.1066	0.5794	101.39	0.3237	1.7654	3.1166	1.2968
3.5	2.4161	0.1154	0.4646	104.52	0.3139	1.4159	2.0049	1.3066
2.5	2.5413	0.1252	0.3410	107.42	0.3054	1.0397	1.0809	1.3151
1.5	2.6735	0.1321	0.2091	109.78	0.2987	0.6377	0.4066	1.3218
0.5	2.8121	0.1386	0.0710	111.78	0.2933	0.2165	0.0469	1.3272
-0.5	2.9541	0.1420						
-1.5	3.0917	0.1377						
-2.5	3.2234	0.1317			Slope	z_0'/cm	C_s'/cm	
-3.5	3.3453	0.1219		1.40E-04	-9.90E-03	1.326	98.95	
-4.5	3.4596	0.1143						
-5.5	3.5646	0.1050						
-6.5	3.6625	0.0980						
-7.5	3.7543	0.0918						
-8.5	3.8399	0.0856						
-9.5	3.9210	0.0812						
-10.5	3.9993	0.0782						

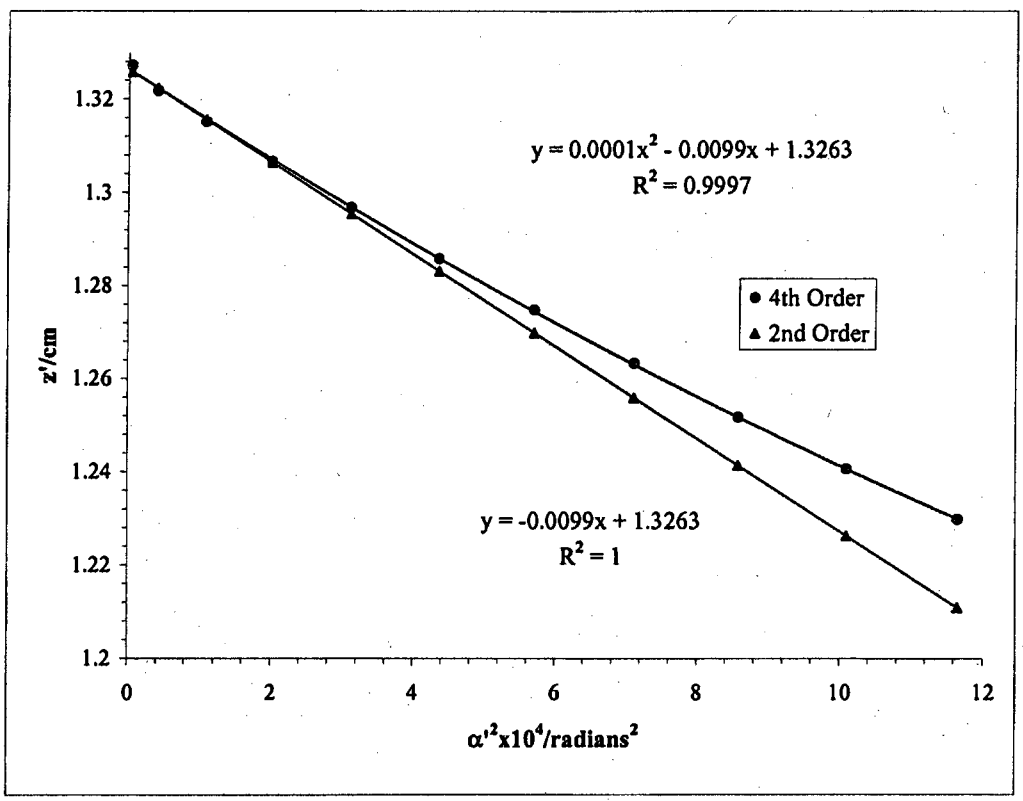

L4 Objective Lens — **Beam Voltage** **20 kV**

Mesh/inch	V Ratio	Mesh	z/cm	e_1/cm	a/cm	z_{sp}/cm	z_0'/cm	C_s'/cm	$z_{sp}-z_o'$
600	0.85	Front	29.20	0.0042333	27.40	34.12	1.34	108.32	32.78

Bar location/ units	Shadow Reading X/cm	Spacing Δ/cm	E/cm	α x 10^4	α' x 10^2	α'^{2} x 10^4	m	z'/cm	f/cm
10.5	1.357		1.239	16.225	3.761	14.145	0.043140	1.183668	1.21102
9.5	1.492	0.135	1.103	14.680	3.354	11.246	0.043773	1.215065	1.22749
8.5	1.621	0.129	0.974	13.134	2.962	8.771	0.044349	1.241879	1.24252
7.5	1.746	0.125	0.849	11.589	2.583	6.672	0.044866	1.264612	1.25604
6.5	1.867	0.121	0.728	10.044	2.216	4.911	0.045322	1.283686	1.26800
5.5	1.984	0.117	0.610	8.499	1.859	3.456	0.045715	1.299448	1.27832
4.5	2.098	0.114	0.495	6.953	1.510	2.281	0.046045	1.312180	1.28699
3.5	2.210	0.112	0.383	5.408	1.168	1.364	0.046309	1.322109	1.29395
2.5	2.321	0.110	0.272	3.863	0.831	0.690	0.046508	1.329409	1.29920
1.5	2.430	0.109	0.163	2.318	0.497	0.247	0.046641	1.334207	1.30270
0.5	2.539	0.109	0.054	0.773	0.165	0.027	0.046708	1.336585	1.30446
-0.5	2.647	0.108							
-1.5	2.756	0.109						g/cm	$(\rho/f_0)^2 =$
-2.5	2.866	0.110		Slope	m_o	μ_s		$(m_0+1)^2\,\alpha'^2$	
-3.5	2.976	0.111	3.28E-06	-0.000299	0.04671	-63.94	1.13143	15.497	
-4.5	3.089	0.113					1.16133	12.322	
-5.5	3.204	0.115		f vs $(\rho/f_o)^2$			1.18677	9.610	
-6.5	3.322	0.118	$S_f = slope_f / f_0$				1.20826	7.310	
-7.5	3.443	0.121		$slope_f$	fo/cm	S_f	1.22622	5.381	
-8.5	3.568	0.125	7.5E-05	-0.007187	1.305	-55.09	1.24101	3.786	
-9.5	3.699	0.130					1.25292	2.499	
-10.5	3.834	0.136		g vs $(\rho/f_o)^2$			1.26219	1.494	
			$S_g = slope_g / f_0$				1.26899	0.756	
				$slope_g$	go/cm	S_g	1.27345	0.271	
			-8E-06	-0.009199	1.276	-70.52	1.27566	0.030	

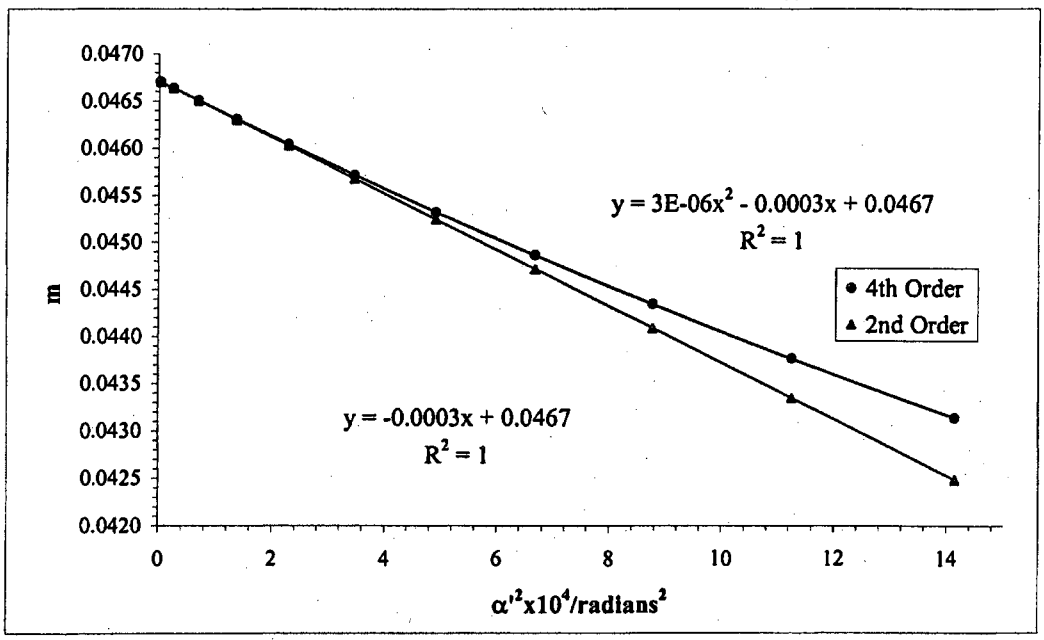

L4 Objective Lens							Beam	Voltage	20 kV
Mesh/inch	V Ratio	Mesh	z/cm	e_1/cm	a/cm	z_{sp}/cm	z_0'/cm	C_s'/cm	$z_{sp}-z_o'$
600	0.85	Front	29.20	0.004233	27.40	34.12	1.34	108.32	32.78

Bar location/ units	Shadow Reading Y/cm	Spacing Δ/cm	E/cm	α x 10^4	α' x 10^2	α'^{2} x 10^4	m	z'/cm	f/cm
11	1.240		1.317	16.997	3.997	15.976	0.0425	1.164	1.195
10	1.381	0.142	1.178	15.452	3.579	12.811	0.0432	1.198	1.211
9	1.516	0.135	1.045	13.907	3.178	10.102	0.0438	1.227	1.226
8	1.645	0.129	0.918	12.362	2.792	7.795	0.0443	1.252	1.240
7	1.770	0.124	0.794	10.816	2.418	5.846	0.0447	1.274	1.252
6	1.890	0.120	0.674	9.271	2.054	4.220	0.0451	1.291	1.262
5	2.007	0.117	0.558	7.726	1.699	2.888	0.0455	1.306	1.271
4	2.121	0.114	0.443	6.181	1.351	1.826	0.0457	1.317	1.278
3	2.233	0.112	0.331	4.636	1.009	1.018	0.0459	1.326	1.284
2	2.344	0.111	0.220	3.090	0.670	0.449	0.0461	1.332	1.288
1	2.454	0.110	0.110	1.545	0.335	0.112	0.0462	1.336	1.290
0	2.564	0.110							
-1	2.673	0.110					g/cm	$(\rho/f_0)^2 =$	
-2	2.784	0.110		Slope	m_o	μ_g		$(m_0+1)^2\alpha'^2$	
-3	2.895	0.111	2.2E-06	-0.00027	0.04622	-57.57	1.113	17.486	
-4	3.007	0.113					1.146	14.023	
-5	3.122	0.114		f vs $(\rho/f_o)^2$			1.174	11.057	
-6	3.238	0.117	$S_f = slope_f / f_0$				1.198	8.532	
-7	3.358	0.119		$slope_f$	fo/cm	S_f	1.218	6.399	
-8	3.481	0.123	5E-05	-0.00636	1.291	-49.29	1.234	4.619	
-9	3.607	0.127					1.248	3.161	
-10	3.738	0.131		g vs $(\rho/f_o)^2$			1.259	1.999	
-11	3.874	0.136	$S_g = slope_g / f_0$				1.267	1.114	
				$slope_g$	go/cm	S_g	1.273	0.492	
			-6E-06	-0.00929	1.277	-71.99	1.276	0.123	

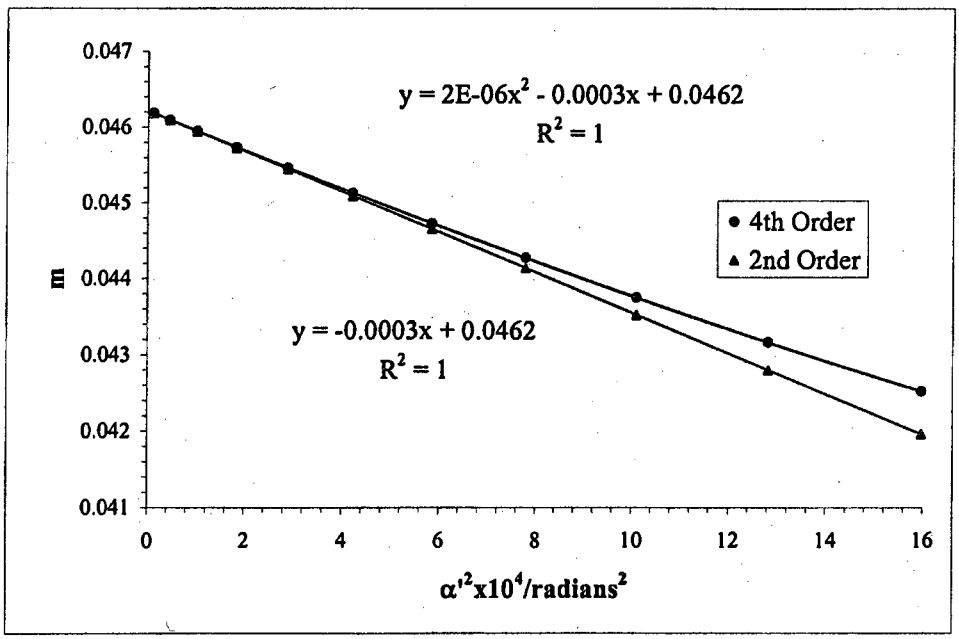

Beam Voltage	Volt Ratio	z/cm	z_0'/cm	C_s'/cm	L4 Objective Lens
20 kV	0.70	29.2	1.34	108	

Average of m_o = 0.0465

Average of μ_s = -60.8

Paraxial properties :

f_o = 1.30 cm

g_o = 1.28 cm

S_f = -52.2

S_g = -71.3

Mesh/inch	V Ratio	Mesh	e'_1/cm	d/cm	b/cm		Beam	Voltage	20 kV
2000	0.90	Rear	0.00127	33.39	0.732	US			
								L4 Objective Lens	

Bar location/ units	Shadow Reading X/cm	Spacing Δ/cm	E'/cm	M'	c/cm	α' x 10^2	α'^2 x 10^4	z'/cm
11	0.650		1.374	-98.3	-0.336	4.1560	17.2722	1.068
10	0.850	0.200	1.174	-92.4	-0.357	3.5541	12.6314	1.089
9	1.016	0.166	1.009	-88.2	-0.374	3.0554	9.3354	1.106
8	1.159	0.143	0.866	-85.3	-0.387	2.6252	6.8916	1.119
7	1.286	0.128	0.739	-83.1	-0.397	2.2391	5.0136	1.129
6	1.405	0.119	0.620	-81.3	-0.406	1.8789	3.5301	1.137
5	1.518	0.113	0.508	-80.0	-0.412	1.5398	2.3710	1.144
4	1.625	0.106	0.401	-79.0	-0.417	1.2176	1.4825	1.149
3	1.728	0.103	0.298	-78.2	-0.422	0.9036	0.8165	1.153
2	1.828	0.101	0.197	-77.6	-0.425	0.5977	0.3573	1.156
1	1.927	0.099	0.098	-77.1	-0.427	0.2972	0.0884	1.159
0	2.027	0.099						
-1	2.123	0.097						
-2	2.223	0.099			Slope	z_0'/cm	C_s'/cm	
-3	2.323	0.101		5.2E-05	-0.0061	1.158	61.38	
-4	2.428	0.104						
-5	2.534	0.106						
-6	2.644	0.111						
-7	2.764	0.119						
-8	2.891	0.128						
-9	3.033	0.142						
-10	3.198	0.165						
-11	3.39726	0.199						

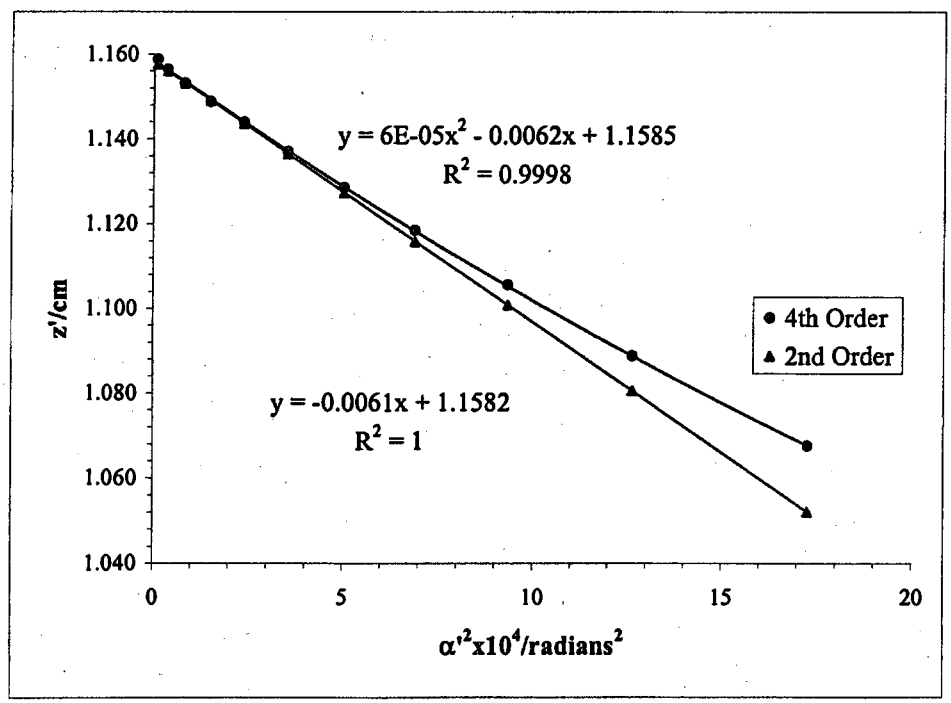

Mesh/inch	V Ratio	Mesh	e'_1/cm	d/cm	b/cm		Beam	Voltage	20 kV
2000	0.90	Rear	0.00127	33.39	0.732	US			
									L4 Objective Lens

Bar location/ units	Shadow Reading Y/cm	Spacing Δ/cm	E'/cm	M'	c/cm	α' x 10^2	α'^2 x 10^4	z'/cm
10.5	1.266		1.302	-97.6	-0.338	3.9396	15.5206	1.070
9.5	1.449	0.183	1.113	-92.3	-0.358	3.3704	11.3596	1.089
8.5	1.602	0.153	0.957	-88.6	-0.373	2.8973	8.3946	1.104
7.5	1.738	0.136	0.818	-85.8	-0.385	2.4771	6.1360	1.116
6.5	1.863	0.125	0.692	-83.8	-0.394	2.0968	4.3965	1.125
5.5	1.980	0.117	0.574	-82.2	-0.401	1.7402	3.0283	1.133
4.5	2.090	0.111	0.463	-81.0	-0.407	1.4041	1.9716	1.139
3.5	2.197	0.106	0.356	-80.0	-0.412	1.0790	1.1642	1.143
2.5	2.299	0.103	0.252	-79.4	-0.415	0.7650	0.5853	1.147
1.5	2.401	0.102	0.151	-79.2	-0.416	0.4576	0.2094	1.148
0.5	2.502	0.101	0.050	-79.2	-0.416	0.1526	0.0233	1.148
-0.5	2.602	0.101						
-1.5	2.703	0.100		Slope	z_0'/cm	C_s'/cm		
-2.5	2.804	0.101	3.71E-05	-0.006	1.150	57.13		
-3.5	2.908	0.105						
-4.5	3.017	0.108						
-5.5	3.128	0.111						
-6.5	3.247	0.119						
-7.5	3.373	0.127						
-8.5	3.515	0.142						
-9.5	3.676	0.161						
-10.5	3.870	0.195						

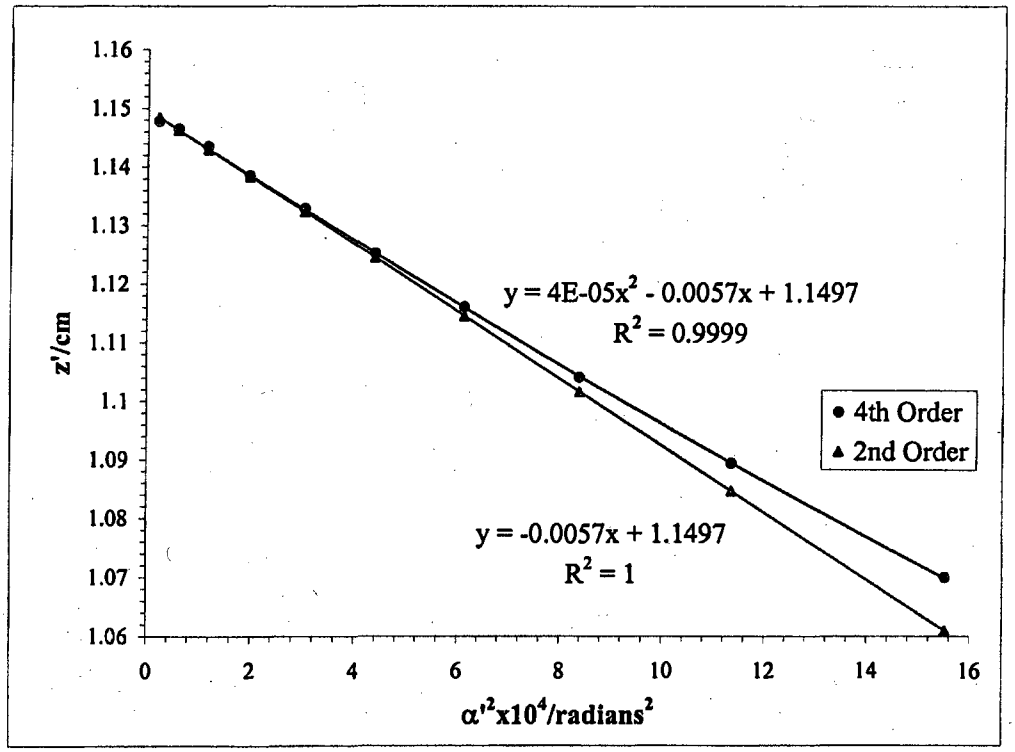

Mesh/inch	V Ratio	Mesh	e'_1/cm	d/cm	b/cm		Beam	Voltage	20 kV
2000	0.90	Rear	0.00127	32.63	1.494	DS			
								L4 Objective Lens	

Bar location/ units	Shadow Reading X/cm	Spacing Δ/cm	E'/cm	M'	c/cm	α' x 10^2	α'^2 x 10^4	z'/cm
12.5	1.568		1.203	75.75	0.436	3.6373	13.2300	1.057
11.5	1.646	0.078	1.126	77.10	0.429	3.4069	11.6072	1.065
10.5	1.725	0.078	1.047	78.49	0.421	3.1673	10.0317	1.072
9.5	1.808	0.084	0.965	79.95	0.413	2.9195	8.5234	1.080
8.5	1.893	0.085	0.880	81.49	0.405	2.6633	7.0932	1.088
7.5	1.982	0.089	0.791	83.01	0.398	2.3943	5.7327	1.096
6.5	2.075	0.093	0.698	84.58	0.390	2.1149	4.4726	1.103
5.5	2.172	0.097	0.601	86.00	0.384	1.8199	3.3119	1.110
4.5	2.274	0.102	0.500	87.43	0.377	1.5140	2.2923	1.116
3.5	2.380	0.106	0.394	88.64	0.372	1.1940	1.4257	1.121
2.5	2.489	0.109	0.285	89.64	0.368	0.8627	0.7442	1.125
1.5	2.603	0.113	0.172	90.21	0.366	0.5209	0.2713	1.128
0.5	2.717	0.114	0.057	90.33	0.365	0.1739	0.0302	1.128
-0.5	2.831	0.115						
-1.5	2.946	0.115						
-2.5	3.058	0.112						
-3.5	3.168	0.109			Slope	z_o'/cm	C_s'/cm	
-4.5	3.273	0.106		6.E-05	-0.00632	1.130	63.17	
-5.5	3.373	0.100						
-6.5	3.472	0.098						
-7.5	3.563	0.092						
-8.5	3.652	0.089						
-9.5	3.737	0.085						
-10.5	3.818	0.081						
-11.5	3.899	0.081						
-12.5	3.973	0.074						

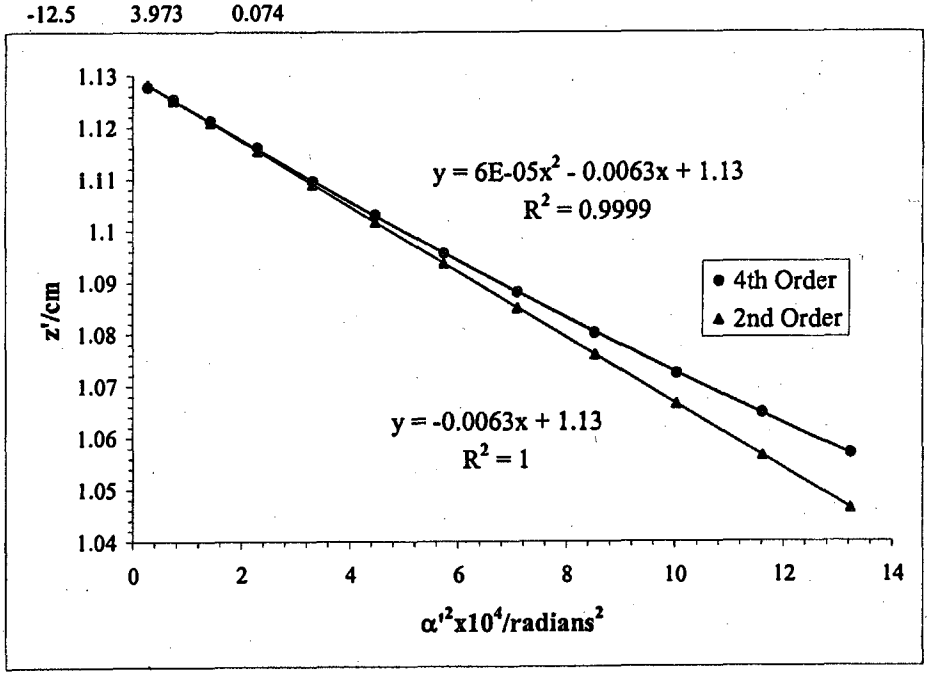

Mesh/inch	V Ratio	Mesh	e'_1/cm	d/cm	b/cm		Beam	Voltage	20 kV
2000	0.90	Rear	0.00127	32.63	1.494	DS			
									L4 Objective Lens

Bar location/ units	Shadow Reading Y/cm	Spacing Δ/cm	E'/cm	M'	c/cm	α' x 10^2	α'^2 x 10^4	z'/cm
12.5	1.529		1.212	76.33	0.433	3.6654	13.4354	1.060
11.5	1.603	0.074	1.137	77.82	0.425	3.4389	11.8262	1.069
10.5	1.684	0.081	1.057	79.23	0.417	3.1976	10.2246	1.076
9.5	1.765	0.082	0.974	80.75	0.409	2.9493	8.6982	1.084
8.5	1.850	0.085	0.890	82.41	0.401	2.6937	7.2559	1.093
7.5	1.938	0.088	0.799	83.93	0.393	2.4211	5.8616	1.100
6.5	2.032	0.094	0.705	85.44	0.386	2.1365	4.5645	1.107
5.5	2.128	0.097	0.607	86.95	0.380	1.8402	3.3862	1.114
4.5	2.228	0.100	0.506	88.53	0.373	1.5333	2.3511	1.121
3.5	2.332	0.104	0.400	90.02	0.366	1.2128	1.4710	1.127
2.5	2.443	0.111	0.288	90.86	0.363	0.8745	0.7647	1.130
1.5	2.558	0.114	0.174	91.47	0.361	0.5283	0.2791	1.133
0.5	2.673	0.115	0.058	91.82	0.359	0.1768	0.0312	1.134
-0.5	2.790	0.117						
-1.5	2.906	0.116						
-2.5	3.020	0.114			Slope	z_0'/cm	C_s'/cm	
-3.5	3.133	0.112		5.E-05	-0.00625	1.135	62.49	
-4.5	3.240	0.108						
-5.5	3.343	0.103						
-6.5	3.442	0.099						
-7.5	3.537	0.095						
-8.5	3.629	0.092						
-9.5	3.714	0.085						
-10.5	3.797	0.083						
-11.5	3.876	0.079						
-12.5	3.953	0.076						

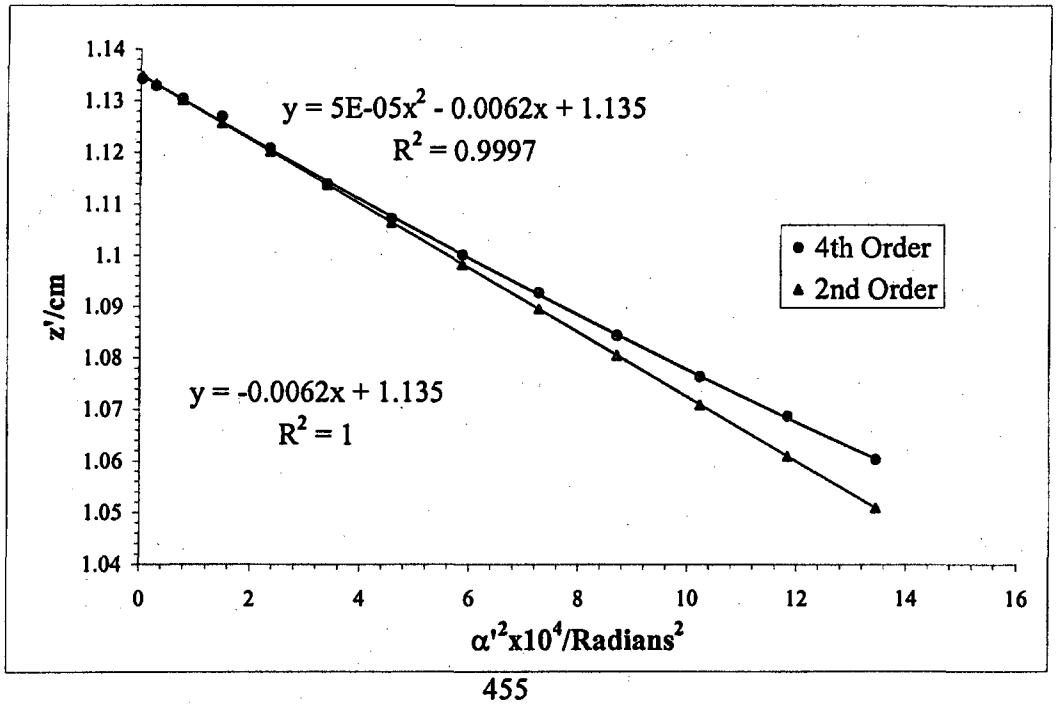

L4 Objective Lens — **Beam Voltage** 20 kV

Mesh/inch	V Ratio	Mesh	z/cm	e_1/cm	a/cm	z_{sp}/cm	z_0'/cm	C_s'/cm	$z_{sp}-z_o'$
600	0.90	Front	29.20	0.00423333	27.40	34.12	1.144	70.14	32.97

Bar location/ units	Shadow Reading X/cm	Spacing Δ/cm	E/cm	$\alpha \times 10^4$	$\alpha' \times 10^2$	$\alpha'^2 \times 10^4$	m	z'/cm	f/cm
9.5	1.510		1.310	14.680	3.959	15.673	0.0371	1.034	1.046
8.5	1.663	0.154	1.156	13.134	3.497	12.230	0.0376	1.058	1.059
7.5	1.811	0.148	1.008	11.589	3.051	9.311	0.0380	1.079	1.070
6.5	1.955	0.143	0.865	10.044	2.619	6.860	0.0383	1.096	1.079
5.5	2.094	0.139	0.726	8.499	2.198	4.833	0.0387	1.110	1.088
4.5	2.230	0.136	0.590	6.953	1.787	3.192	0.0389	1.122	1.095
3.5	2.363	0.133	0.456	5.408	1.382	1.911	0.0391	1.131	1.100
2.5	2.494	0.131	0.324	3.863	0.983	0.967	0.0393	1.137	1.104
1.5	2.625	0.130	0.194	2.318	0.589	0.346	0.0394	1.142	1.107
0.5	2.754	0.129	0.065	0.773	0.196	0.038	0.0394	1.144	1.108
-0.5	2.883	0.129							
-1.5	3.013	0.130							
-2.5	3.143	0.130							
-3.5	3.275	0.132							
-4.5	3.409	0.134							
-5.5	3.545	0.136							
-6.5	3.684	0.139							
-7.5	3.828	0.143							
-8.5	3.976	0.148							
-9.5	4.129	0.154							

g/cm	$(\rho/f_0)^2 = (m_0+1)^2\alpha'^2$
0.995	16.857
1.019	13.166
1.038	10.032
1.055	7.396
1.068	5.213
1.079	3.445
1.088	2.063
1.094	1.045
1.098	0.374
1.100	0.041

	Slope	m_o	μ_s
9.8E-07	-0.000166	0.03943885	-42.05

f vs $(\rho/f_o)^2$

$S_f = slope_f / f_0$

	$slope_f$	fo/cm	S_f
2.2E-05	-0.00407	1.108	-36.75

g vs $(\rho/f_o)^2$

$S_g = slope_g / f_0$

	$slope_g$	go/cm	S_g
-3.91E-06	-0.00616	1.100	-55.61

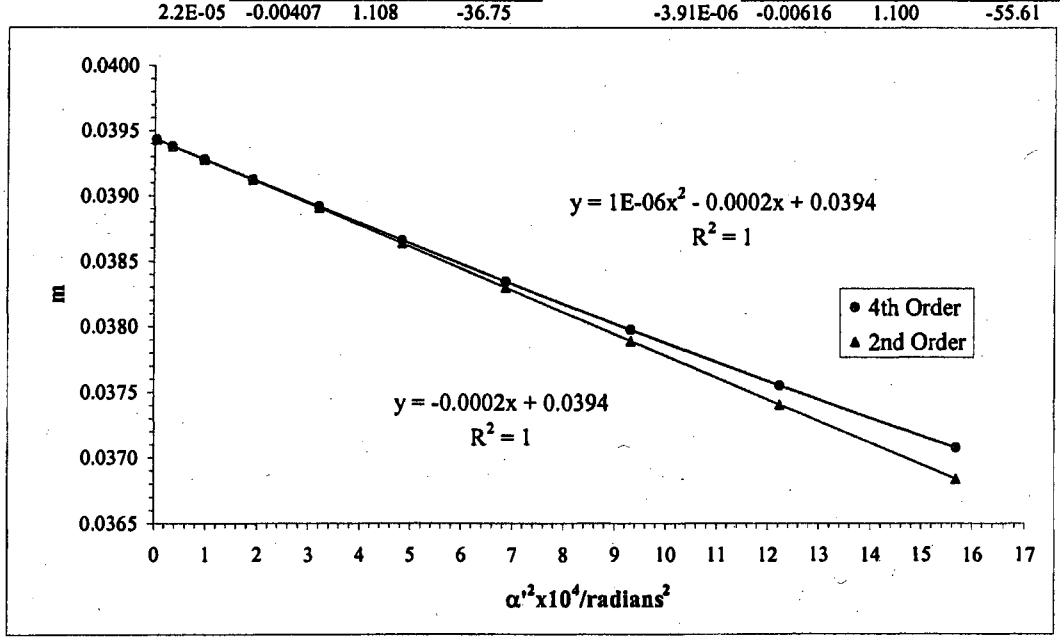

L4 Objective Lens — **Beam Voltage 20 kV**

Mesh/inch	V Ratio	Mesh	z/cm	e_1/cm	a/cm	z_{sp}/cm	z_0'/cm	C_s'/cm	$z_{sp}-z_0'$
600	0.70	Front	29.20	0.00423	27.40	34.12	1.144	70.14	32.97

Bar location/ units	Shadow Reading Y/cm	Spacing Δ/cm	E/cm	$\alpha \times 10^4$	$\alpha' \times 10^2$	$\alpha'^2 \times 10^4$	m	z'/cm	f/cm
13	0.800		1.889	20.088	5.689	32.361	0.03531	0.917	1.000
12	0.980	0.180	1.709	18.543	5.154	26.568	0.03597	0.958	1.017
11	1.151	0.171	1.539	16.997	4.645	21.579	0.03659	0.993	1.034
10	1.314	0.163	1.376	15.452	4.159	17.293	0.03716	1.023	1.049
9	1.470	0.156	1.221	13.907	3.691	13.626	0.03767	1.048	1.062
8	1.619	0.150	1.071	12.362	3.241	10.505	0.03814	1.070	1.075
7	1.764	0.144	0.927	10.816	2.806	7.872	0.03855	1.089	1.085
6	1.904	0.140	0.787	9.271	2.383	5.678	0.03891	1.104	1.095
5	2.040	0.136	0.650	7.726	1.970	3.882	0.03921	1.117	1.103
4	2.174	0.133	0.517	6.181	1.566	2.453	0.03946	1.127	1.110
3	2.305	0.131	0.386	4.636	1.169	1.367	0.03965	1.134	1.115
2	2.434	0.129	0.256	3.090	0.777	0.603	0.03979	1.140	1.119
1	2.563	0.128	0.128	1.545	0.388	0.150	0.03988	1.143	1.121
0	2.690	0.128							
-1	2.818	0.128					g/cm	$(\rho/f_0)^2 =$	
-2	2.946	0.128						$(m_0+1)^2\alpha'^2$	
-3	3.076	0.129					0.882	34.994	
-4	3.207	0.131					0.921	28.730	
-5	3.341	0.134					0.955	23.335	
-6	3.477	0.136					0.984	18.701	
-7	3.617	0.140					1.008	14.735	
-8	3.762	0.144					1.029	11.360	
-9	3.911	0.149					1.047	8.513	
-10	4.066	0.155		Slope	m_o	μ_s	1.062	6.140	
-11	4.229	0.162	1.15E-06	-0.00018	0.03989	-44.70	1.074	4.198	
-12	4.399	0.170					1.083	2.653	
-13	4.578	0.179					1.090	1.478	
			f vs $(\rho/f_o)^2$			g vs $(\rho/f_o)^2$	1.095	0.652	
		$S_f = slope_f / f_0$			$S_g = slope_g / f_0$		1.098	0.162	
		$slope_f$	fo/cm	S_f		$slope_g$	go/cm	S_g	
	2.7E-05	-0.00439	1.121	-39.19	-3E-06	-0.00613	1.099	-54.68	

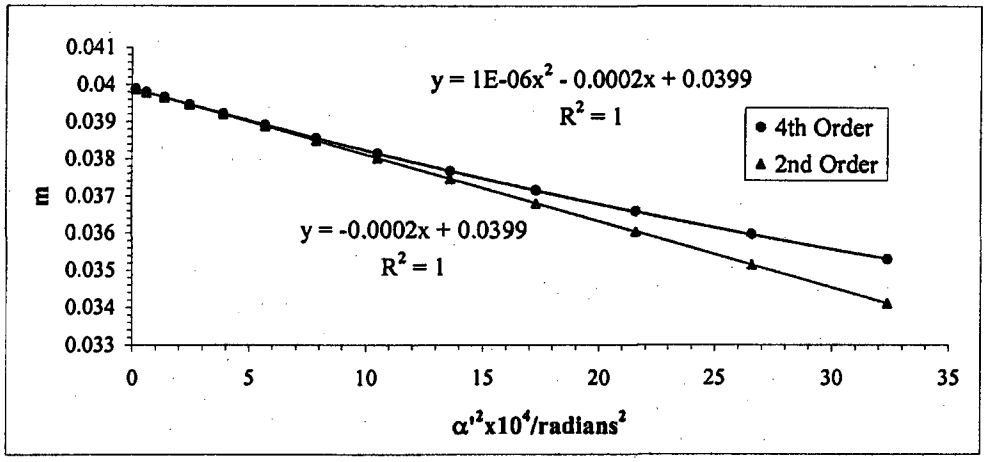

Beam Voltage	Volt Ratio	z/cm	z_0'/cm	C_s'/cm
20 kV	0.90	29.2	1.14	70.1

L4 Objective Lens

Average of m_o = 0.0397

Average of μ_s = -43.4

Paraxial properties :

f_o = 1.11 cm

g_o = 1.10 cm

S_f = -38.0

S_g = -55.1

Mesh/inch	V Ratio	Mesh	e'_1/cm	d/cm	b/cm		Beam	Voltage	20 kV
2000	0.95	Rear	0.00127	33.51	0.605	US			
								L4 Objective Lens	

Bar location/ units	Shadow Reading X/cm	Spacing Δ/cm	E'/cm	M'	c/cm	α' x 10^2	α'^2 x 10^4	z'/cm
9	0.972		1.195	-104.6	-0.317	3.6012	12.9689	0.922
8	1.147	0.174	1.028	-101.2	-0.328	3.0974	9.5940	0.933
7	1.301	0.155	0.876	-98.5	-0.337	2.6395	6.9669	0.941
6	1.444	0.142	0.736	-96.6	-0.343	2.2190	4.9238	0.948
5	1.578	0.134	0.604	-95.1	-0.349	1.8215	3.3179	0.953
4	1.705	0.127	0.478	-94.2	-0.352	1.4424	2.0805	0.957
3	1.831	0.125	0.355	-93.1	-0.356	1.0696	1.1440	0.961
2	1.951	0.120	0.235	-92.5	-0.358	0.7090	0.5027	0.963
1	2.069	0.119	0.117	-91.8	-0.361	0.3518	0.1238	0.965
0	2.185	0.116						
-1	2.303	0.117						
-2	2.421	0.118						
-3	2.540	0.119			Slope	z_o'/cm	C_s'/cm	
-4	2.662	0.122		1.03E-05	-0.00341	0.964	34.05	
-5	2.786	0.124						
-6	2.916	0.130						
-7	3.053	0.137						
-8	3.202	0.150						
-9	3.363	0.161						

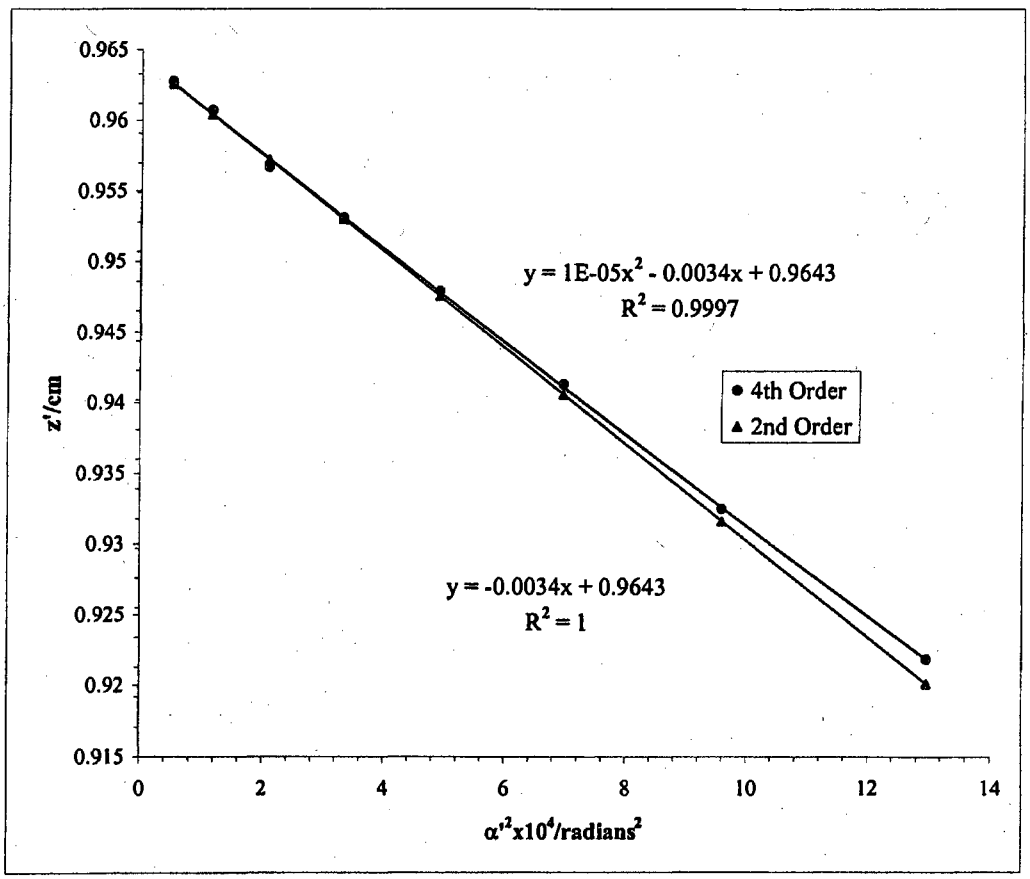

Mesh/inch	V Ratio	Mesh	e'_1/cm	d/cm	b/cm		Beam	Voltage	20 kV
2000	0.95	Rear	0.00127	33.51	0.605	US			
								L4 Objective Lens	

Bar location/ units	Shadow Reading Y/cm	Spacing Δ/cm	E'/cm	M'	c/cm	α' x 10^2	α'^{2} x 10^4	z'/cm
9.5	1.376		1.264	-104.8	-0.317	3.8072	14.4947	0.921
8.5	1.536	0.160	1.091	-101.0	-0.328	3.2870	10.8041	0.933
7.5	1.682	0.147	0.936	-98.3	-0.338	2.8217	7.9619	0.942
6.5	1.822	0.139	0.792	-96.0	-0.346	2.3886	5.7054	0.950
5.5	1.952	0.130	0.659	-94.3	-0.352	1.9859	3.9438	0.956
4.5	2.075	0.124	0.531	-92.9	-0.357	1.6013	2.5640	0.961
3.5	2.195	0.120	0.410	-92.1	-0.360	1.2352	1.5257	0.964
2.5	2.313	0.118	0.289	-91.2	-0.364	0.8731	0.7622	0.968
1.5	2.430	0.117	0.173	-90.6	-0.366	0.5209	0.2713	0.970
0.5	2.545	0.115	0.058	-91.5	-0.362	0.1752	0.0307	0.967
-0.5	2.662	0.116						
-1.5	2.776	0.114			Slope	z_o'/cm	C_s'/cm	
-2.5	2.892	0.116		3.05E-05	-0.00386	0.971	38.56	
-3.5	3.014	0.122						
-4.5	3.137	0.123						
-5.5	3.269	0.131						
-6.5	3.406	0.137						
-7.5	3.555	0.149						
-8.5	3.717	0.163						
-9.5	3.904	0.187						

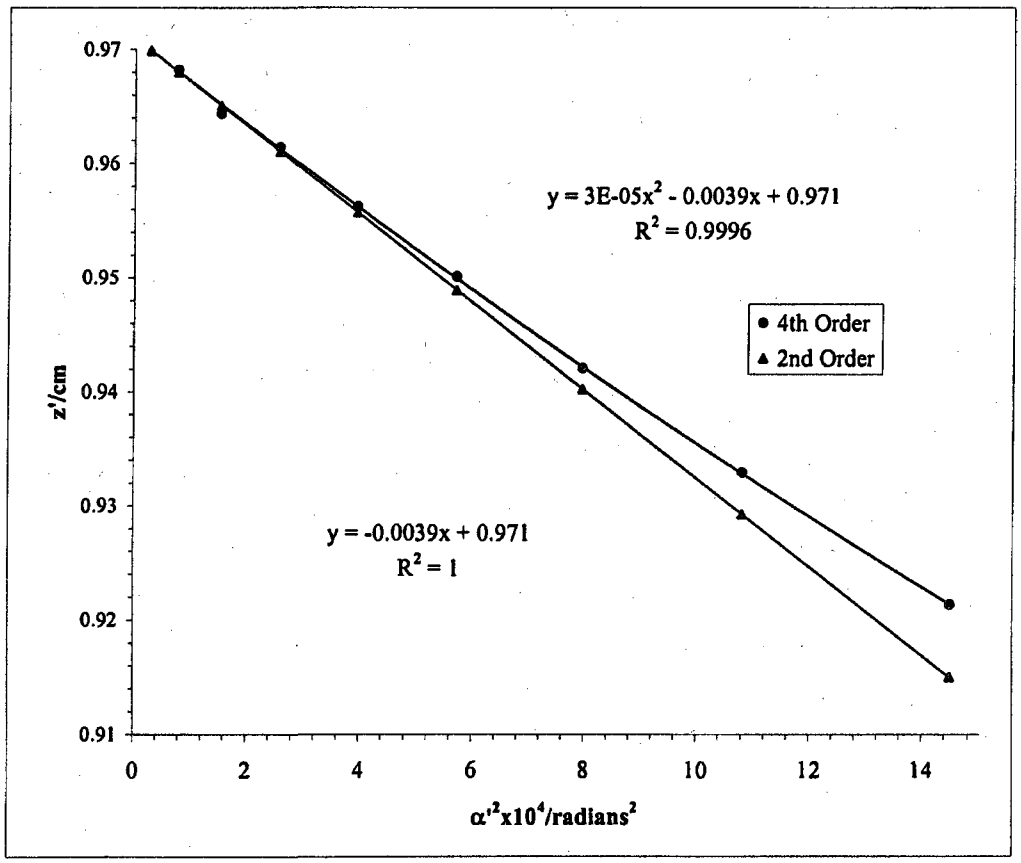

Mesh/inch	V Ratio	Mesh	e'_1/cm	d/cm	b/cm		Beam	Voltage	20 kV
2000	0.95	Rear	0.00127	33.01	1.113	DS			
								L4 Objective Lens	

Bar location/ units	Shadow Reading X/cm	Spacing Δ/cm	E'/cm	M'	c/cm	$\alpha' \times 10^2$	$\alpha'^2 \times 10^4$	z'/cm
7	1.4126		1.3546	152.37	0.2181	4.0770	16.6222	0.8945
6	1.5513	0.1387	1.2160	159.58	0.2081	3.6612	13.4042	0.9044
5	1.7033	0.1520	1.0645	167.64	0.1981	3.2060	10.2787	0.9145
4	1.8703	0.1670	0.8972	176.61	0.1880	2.7028	7.3053	0.9246
3	2.0584	0.1881	0.7085	185.96	0.1785	2.1350	4.5583	0.9341
2	2.2697	0.2113	0.4965	195.46	0.1697	1.4965	2.2394	0.9428
1	2.5084	0.2387	0.2583	203.36	0.1631	0.7786	0.6063	0.9494
0	2.7656	0.2572						
-1	3.0249	0.2593			Slope	z_0'/cm	C_s'/cm	
-2	3.2626	0.2377		2.99E-05	-0.00393	0.952	39.28	
-3	3.4754	0.2128						
-4	3.6647	0.1893						
-5	3.8324	0.1677						
-6	3.9834	0.1510						
-7	4.121747	0.1384						

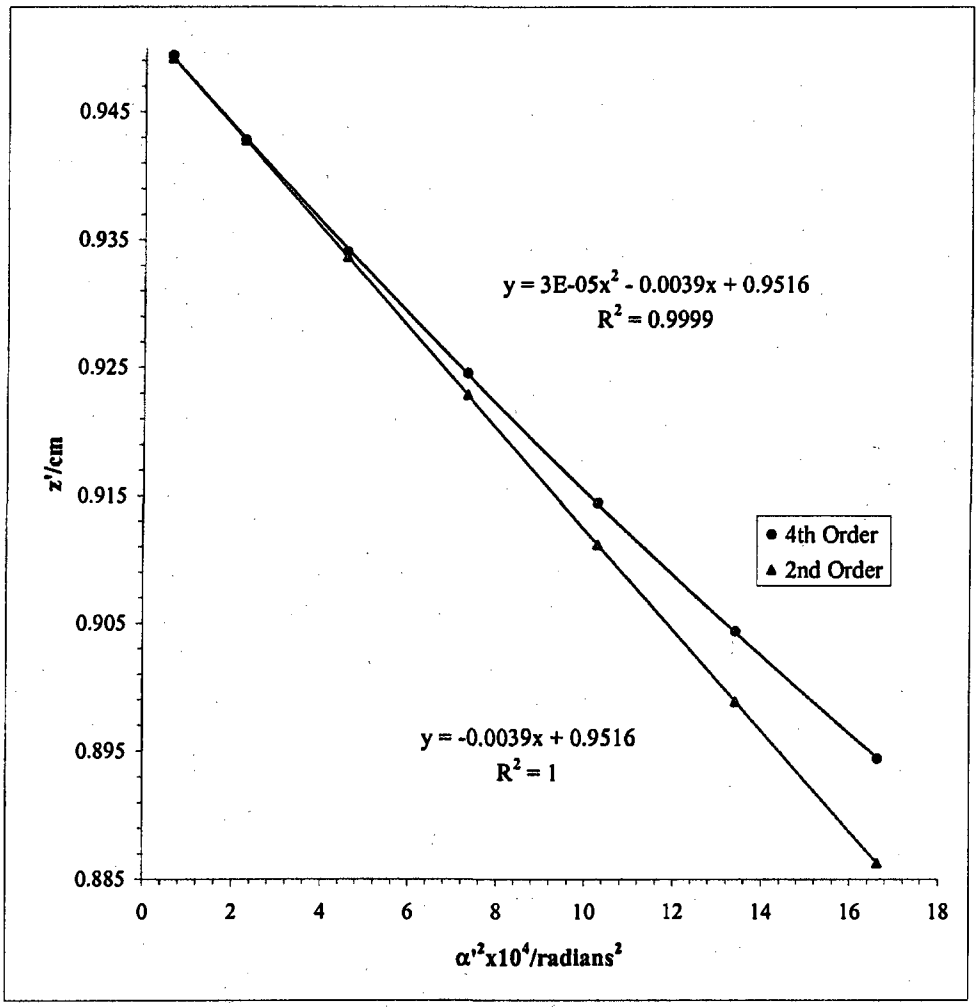

Mesh/inch	V Ratio	Mesh	e'_1/cm	d/cm	b/cm		Beam	Voltage	20 kV
2000	0.95	Rear	0.00127	33.01	1.113	DS			
								L4 Objective Lens	

Bar location/ units	Shadow Reading Y/cm	Spacing Δ/cm	E'/cm	M'	c/cm	α' x 10^2	α'^2 x 10^4	z'/cm
6.5	1.722		1.290	156.30	0.213	3.884	15.087	0.900
5.5	1.875	0.152	1.145	163.88	0.203	3.447	11.882	0.910
4.5	2.040	0.166	0.985	172.34	0.193	2.967	8.801	0.920
3.5	2.235	0.195	0.805	181.09	0.183	2.425	5.882	0.929
2.5	2.445	0.210	0.605	190.59	0.174	1.824	3.326	0.938
1.5	2.684	0.239	0.379	198.72	0.167	1.141	1.302	0.946
0.5	2.942	0.258	0.131	206.72	0.160	0.396	0.157	0.952
-0.5	3.204	0.263						
-1.5	3.441	0.237						
-2.5	3.655	0.214			Slope	z_o'/cm	C_s'/cm	
-3.5	3.845	0.190		4.17E-05	-0.00404	0.952	40.40	
-4.5	4.010	0.165						
-5.5	4.164	0.154						
-6.5	4.303	0.139						

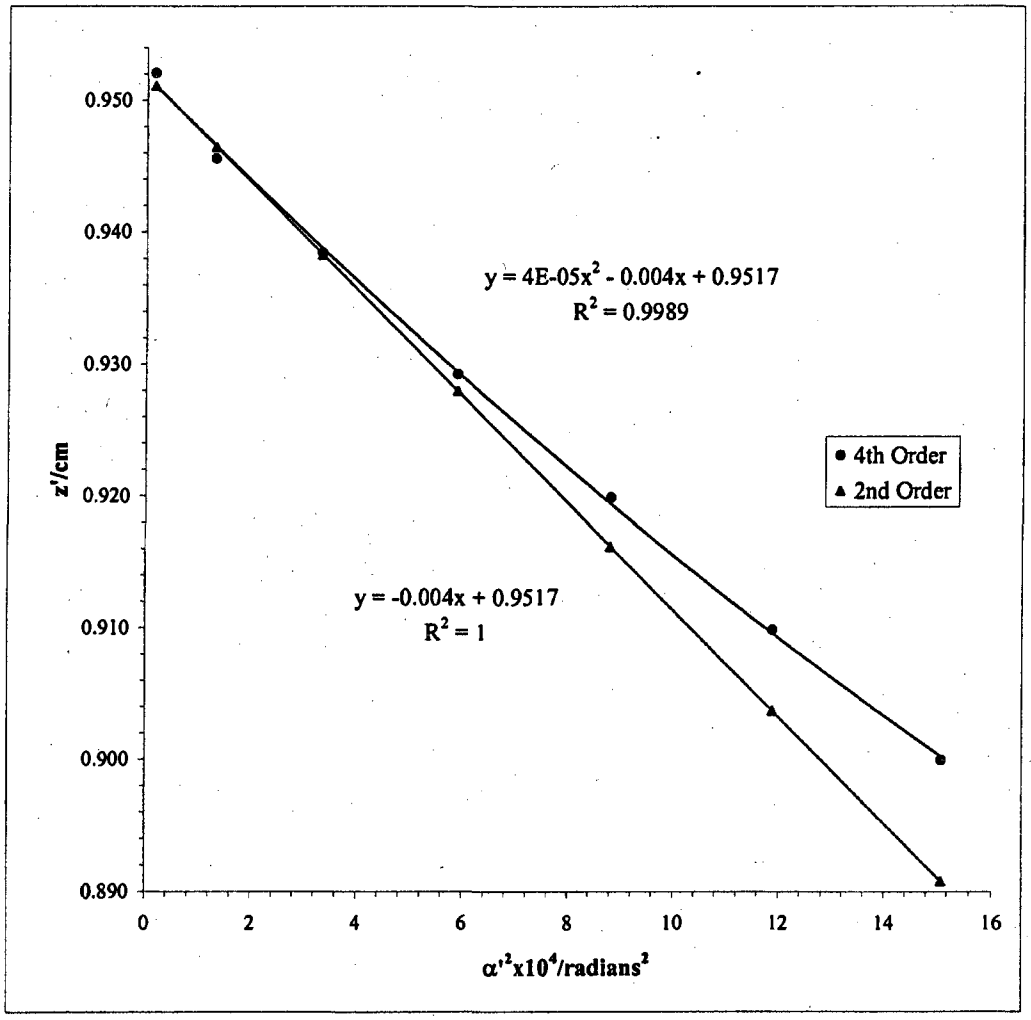

L4 Objective Lens — **Beam Voltage** **20 kV**

Mesh/inch	V Ratio	Mesh	z/cm	e_1/cm	a/cm	z_{sp}/cm	z_0'/cm	C_s'/cm	$z_{sp}-z_0'$
600	0.95	Front	29.20	0.004233	27.40	34.12	0.963	42.02	33.16

Bar location/ units	Shadow Reading X/cm	Spacing Δ/cm	E/cm	$\alpha \times 10^4$	$\alpha' \times 10^2$	$\alpha'^2 \times 10^4$	m	z'/cm	f/cm
10.5	1.119		1.763	16.225	5.299	28.081	0.0306	0.845	0.869
9.5	1.312	0.193	1.570	14.680	4.723	22.306	0.0311	0.869	0.882
8.5	1.497	0.185	1.386	13.134	4.170	17.387	0.0315	0.890	0.893
7.5	1.675	0.178	1.208	11.589	3.636	13.224	0.0319	0.908	0.903
6.5	1.847	0.172	1.036	10.044	3.120	9.734	0.0322	0.922	0.911
5.5	2.014	0.167	0.869	8.499	2.617	6.851	0.0325	0.934	0.919
4.5	2.177	0.163	0.705	6.953	2.127	4.522	0.0327	0.944	0.925
3.5	2.337	0.160	0.546	5.408	1.645	2.705	0.0329	0.952	0.930
2.5	2.495	0.158	0.388	3.863	1.170	1.369	0.0330	0.957	0.934
1.5	2.651	0.156	0.232	2.318	0.700	0.490	0.0331	0.961	0.936
0.5	2.806	0.155	0.077	0.773	0.233	0.054	0.0332	0.963	0.937
-0.5	2.960	0.155							
-1.5	3.115	0.155							
-2.5	3.271	0.156							
-3.5	3.428	0.158							
-4.5	3.588	0.160							
-5.5	3.751	0.163							
-6.5	3.918	0.167							
-7.5	4.090	0.172							
-8.5	4.268	0.178							
-9.5	4.452	0.185							
-10.5	4.645	0.193							

g/cm	$(\rho/f_0)^2 = (m_0+1)^2 \alpha'^2$
0.819	29.975
0.842	23.810
0.862	18.559
0.879	14.115
0.893	10.390
0.905	7.313
0.914	4.827
0.921	2.888
0.927	1.461
0.930	0.523
0.932	0.058

	Slope	m_o	μ_s
4.80E-07	-0.00010	0.03316	-31.36

f vs $(\rho/f_o)^2$

$S_f = slope_f / f_0$

	$slope_f$	fo/cm	S_f
1.16E-05	-0.00263	0.937	-28.05

g vs $(\rho/f_o)^2$

$S_g = slope_g / f_0$

	$slope_g$	go/cm	S_g
-9.5E-07	-0.0038	0.932	-40.09

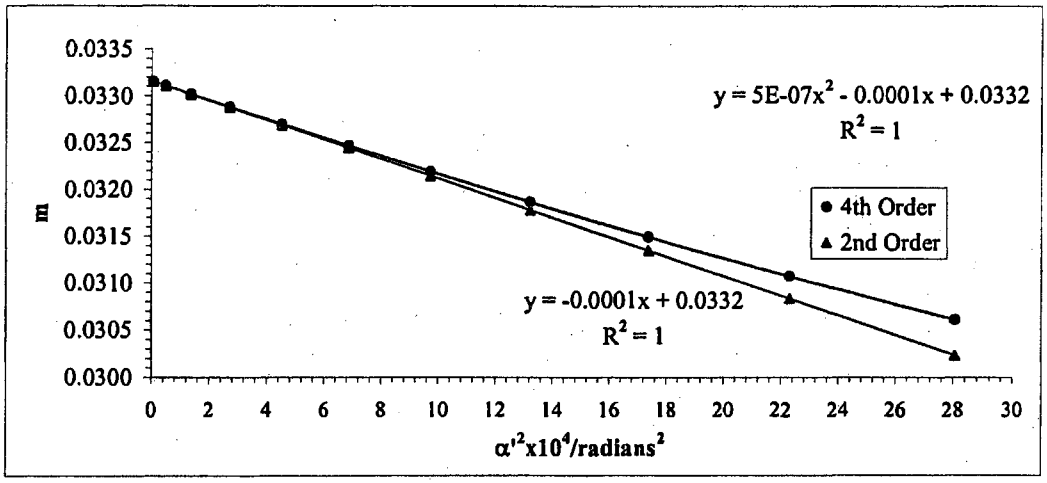

L4 Objective Lens — **Beam** — **Voltage** — **20 kV**

Mesh/inch	V Ratio	Mesh	z/cm	e_1/cm	a/cm	z_{sp}/cm	z_0'/cm	C_s'/cm	$z_{sp}-z_0'$
600	0.95	Front	29.20	0.00423	27.40	34.12	0.963	42.02	33.16

Bar location/ units	Shadow Reading Y/cm	Spacing Δ/cm	E/cm	$\alpha \times 10^4$	$\alpha' \times 10^2$	$\alpha'^2 \times 10^4$	m	z'/cm	f/cm
12	0.755		2.052	18.543	6.159	37.935	0.0301	0.804	0.856
11	0.962	0.206	1.846	16.997	5.547	30.770	0.0306	0.834	0.870
10	1.158	0.196	1.651	15.452	4.963	24.629	0.0311	0.860	0.883
9	1.345	0.187	1.463	13.907	4.403	19.383	0.0316	0.882	0.896
8	1.525	0.180	1.283	12.362	3.864	14.929	0.0320	0.900	0.906
7	1.698	0.173	1.110	10.816	3.343	11.177	0.0324	0.916	0.916
6	1.866	0.168	0.942	9.271	2.838	8.055	0.0327	0.929	0.925
5	2.029	0.163	0.778	7.726	2.346	5.503	0.0329	0.940	0.932
4	2.189	0.160	0.618	6.181	1.864	3.476	0.0332	0.949	0.938
3	2.346	0.157	0.461	4.636	1.391	1.935	0.0333	0.955	0.942
2	2.500	0.155	0.306	3.090	0.924	0.854	0.0334	0.960	0.946
1	2.654	0.153	0.153	1.545	0.461	0.213	0.0335	0.962	0.948
0	2.807	0.153							
-1	2.959	0.153							
-2	3.113	0.154							
-3	3.268	0.155							
-4	3.426	0.157							
-5	3.586	0.160							
-6	3.750	0.164							
-7	3.918	0.168							
-8	4.092	0.174							
-9	4.272	0.180							
-10	4.459	0.187							
-11	4.655	0.195							
-12	4.859	0.205							

	Slope	m_0	μ_s
5.58E-07	-0.00011	0.03353	-33.21

g/cm	$(\rho/f_0)^2 = (m_0+1)^2 \alpha'^2$
0.778	40.522
0.807	32.869
0.832	26.308
0.853	20.705
0.871	15.947
0.887	11.939
0.899	8.604
0.909	5.879
0.917	3.713
0.924	2.067
0.928	0.912
0.931	0.227

f vs $(\rho/f_0)^2$

$S_f = slope_f / f_0$

	$slope_f$	fo/cm	S_f
1.356E-05	-0.002823	0.948	-29.78

g vs $(\rho/f_0)^2$

$S_g = slope_g / f_0$

	$slope_g$	go/cm	S_g
-1.06672E-06	-0.003742	0.931	-39.47

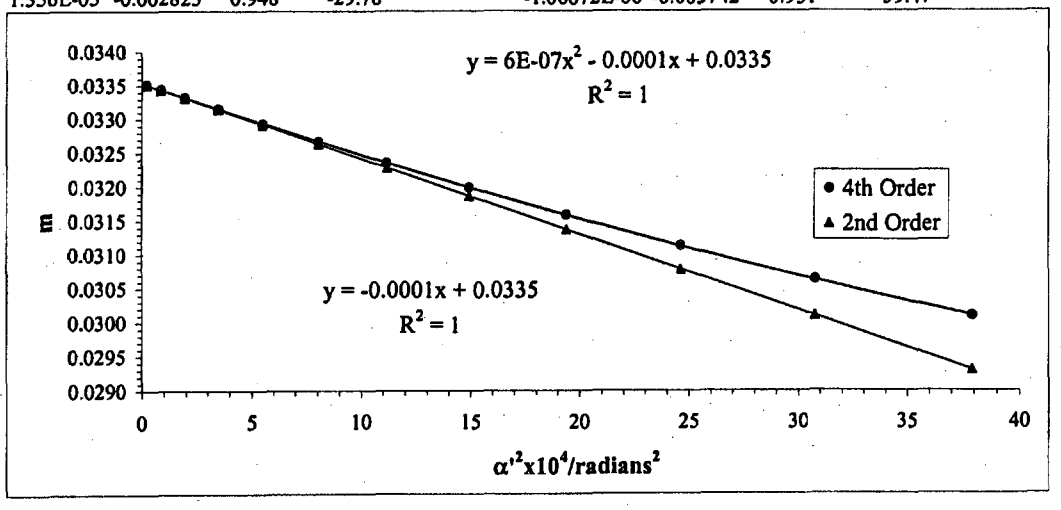

Beam Voltage	Volt Ratio	z/cm	z_0'/cm	C_s'/cm
20 kV	0.95	29.2	0.963	42.0

L4 Objective Lens

Average of m_0 = 0.0333

Average of μ_s = -32.3

Paraxial properties :

f_o = 0.943 cm

g_o = 0.932 cm

S_f = -28.9

S_g = -39.8

Mesh/inch	V Ratio	Mesh	e'_1/cm	d/cm	b/cm		Beam	Voltage	20 kV
2000	1.00	Rear	0.00127	33.64	0.478	US			
								L4 Objective Lens	

Bar location/ units	Shadow Reading X/cm	Spacing Δ/cm	E'/cm	M'	c/cm	α' x 10^2	α'^{2} x 10^4	z'/cm
13	0.693		2.011	-121.8	-0.274	6.0273	36.3289	0.751
12	0.948	0.255	1.756	-115.3	-0.289	5.2664	27.7351	0.767
11	1.160	0.212	1.546	-110.6	-0.301	4.6358	21.4904	0.779
10	1.345	0.185	1.361	-107.2	-0.311	4.0836	16.6760	0.789
9	1.514	0.169	1.192	-104.3	-0.319	3.5776	12.7995	0.797
8	1.669	0.155	1.037	-102.1	-0.326	3.1124	9.6873	0.804
7	1.814	0.145	0.892	-100.4	-0.332	2.6791	7.1775	0.809
6	1.952	0.138	0.754	-98.9	-0.337	2.2629	5.1205	0.814
5	2.084	0.132	0.622	-97.9	-0.340	1.8666	3.4842	0.818
4	2.213	0.129	0.493	-97.0	-0.343	1.4801	2.1908	0.821
3	2.338	0.125	0.368	-96.7	-0.345	1.1059	1.2231	0.822
2	2.462	0.124	0.244	-95.9	-0.347	0.7314	0.5350	0.825
1	2.586	0.124	0.122	-95.7	-0.348	0.3651	0.1333	0.825
0	2.707	0.121						
-1	2.829	0.122						
-2	2.949	0.120						
-3	3.074	0.125			Slope	z_o'/cm	Cs'/cm	
-4	3.198	0.124		8.50E-06	-0.00236	0.826	23.56	
-5	3.327	0.129						
-6	3.460	0.132						
-7	3.599	0.139						
-8	3.743	0.144						
-9	3.898	0.156						
-10	4.067	0.169						
-11	4.251	0.184						
-12	4.461	0.209						
-13	4.715	0.254						

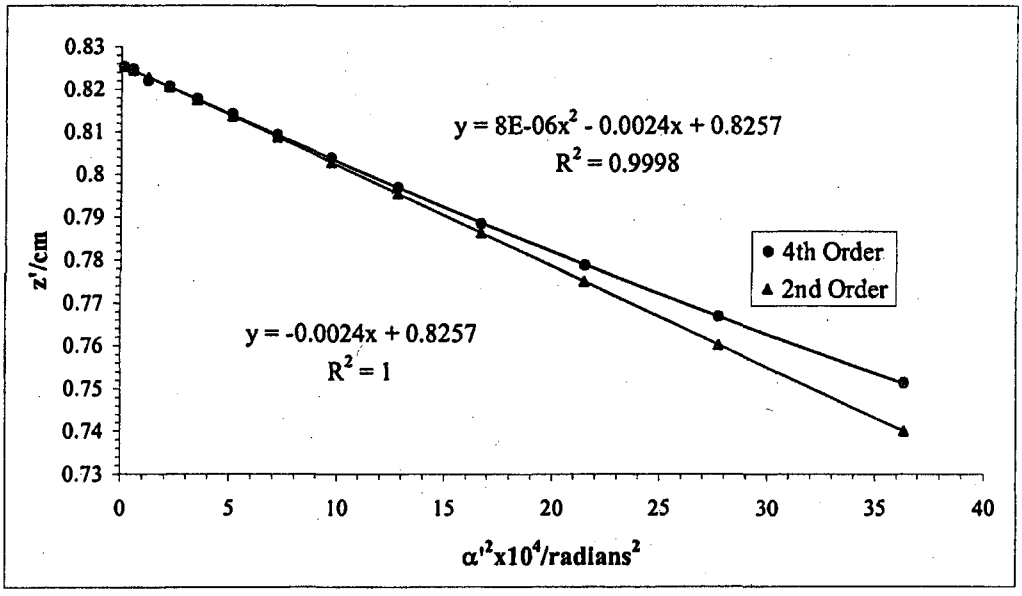

Mesh/inch	V Ratio	Mesh	e'_1/cm	d/cm	b/cm		Beam	Voltage	20 kV
2000	1.00	Rear	0.00127	33.64	0.478	US			
								L4 Objective Lens	

Bar location/ units	Shadow Reading Y/cm	Spacing Δ/cm	E'/cm	M'	c/cm	α' x 10^2	α'^2 x 10^4	z'/cm
13	0.594		2.062	-124.9	-0.2672	6.1795	38.1861	0.745
12	0.848	0.254	1.796	-117.9	-0.2830	5.3845	28.9924	0.761
11	1.062	0.214	1.575	-112.7	-0.2959	4.7218	22.2957	0.773
10	1.249	0.186	1.383	-108.9	-0.3061	4.1489	17.2135	0.784
9	1.416	0.168	1.212	-106.0	-0.3143	3.6364	13.2237	0.792
8	1.572	0.155	1.055	-103.8	-0.3210	3.1650	10.0170	0.799
7	1.718	0.146	0.907	-102.0	-0.3266	2.7220	7.4092	0.804
6	1.857	0.139	0.766	-100.5	-0.3313	2.2997	5.2887	0.809
5	1.991	0.134	0.631	-99.3	-0.3354	1.8933	3.5844	0.813
4	2.121	0.130	0.499	-98.3	-0.3388	1.4993	2.2480	0.816
3	2.248	0.127	0.371	-97.5	-0.3416	1.1154	1.2441	0.819
2	2.373	0.125	0.246	-96.9	-0.3436	0.7392	0.5464	0.821
1	2.496	0.123	0.123	-96.5	-0.3449	0.3682	0.1356	0.822
0	2.618	0.122						
-1	2.741	0.123						
-2	2.865	0.124			Slope	z_o'/cm	Cs'/cm	
-3	2.991	0.126		1.10E-05	-0.00244	0.822	24.42	
-4	3.120	0.129						
-5	3.252	0.132						
-6	3.389	0.137						
-7	3.531	0.142						
-8	3.681	0.149						
-9	3.840	0.160						
-10	4.0147	0.174						
-11	4.2112	0.196						
-12	4.4406	0.229						
-13	4.7187	0.278						

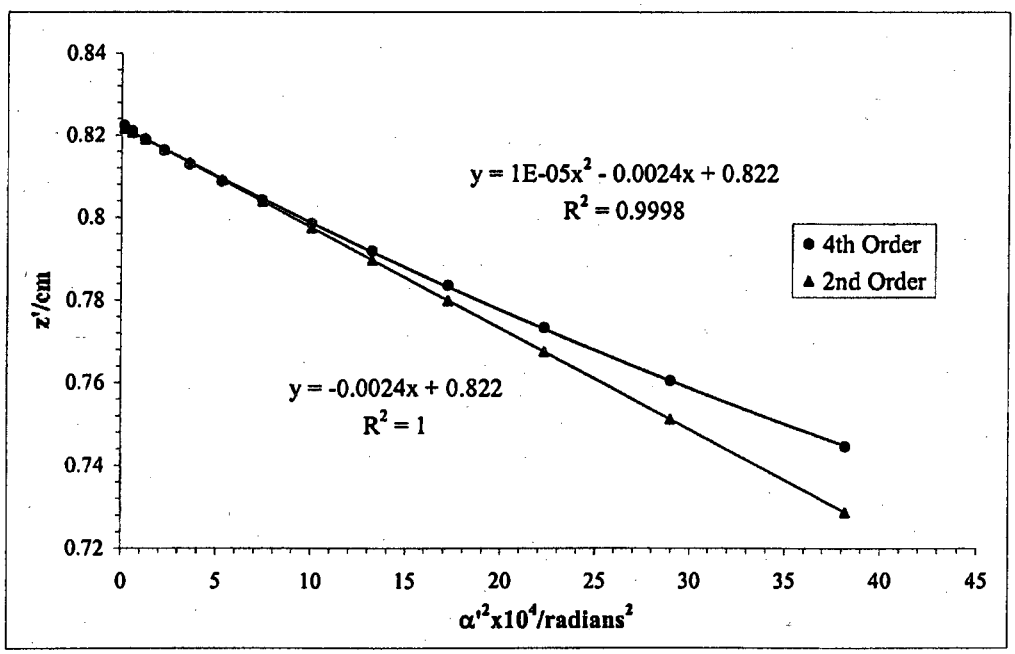

Mesh/inch	V Ratio	Mesh	e'_1/cm	d/cm	b/cm		Beam	Voltage	20 kV
2000	1.00	Rear	0.00127	33.01	1.113	DS			
								L4 Objective Lens	

Bar location/ units	Shadow Reading X/cm	Spacing Δ/cm	E'/cm	M'	c/cm	α' x 10^2	α'^{2} x 10^4	z'/cm
10	1.033		1.269	99.90	0.334	3.8056	14.4827	0.779
9	1.141	0.107	1.160	101.52	0.328	3.4811	12.1183	0.784
8	1.254	0.114	1.048	103.11	0.323	3.1433	9.8802	0.789
7	1.372	0.117	0.930	104.61	0.319	2.7906	7.7874	0.794
6	1.493	0.121	0.808	106.07	0.314	2.4258	5.8843	0.798
5	1.618	0.125	0.683	107.61	0.310	2.0511	4.2069	0.803
4	1.747	0.129	0.554	109.02	0.306	1.6626	2.7643	0.807
3	1.882	0.134	0.419	110.06	0.303	1.2589	1.5848	0.810
2	2.020	0.138	0.281	110.80	0.301	0.8450	0.7140	0.812
1	2.159	0.139	0.141	111.39	0.299	0.4247	0.1804	0.814
0	2.301	0.142						
-1	2.442	0.141						
-2	2.583	0.141						
-3	2.721	0.137						
-4	2.855	0.135			Slope	z_0'/cm	C_s'/cm	
-5	2.985	0.130		2.07E-05	-0.00273	0.81403	27.261	
-6	3.110	0.125						
-7	3.232	0.122						
-8	3.350	0.118						
-9	3.462	0.112						
-10	3.571	0.109						

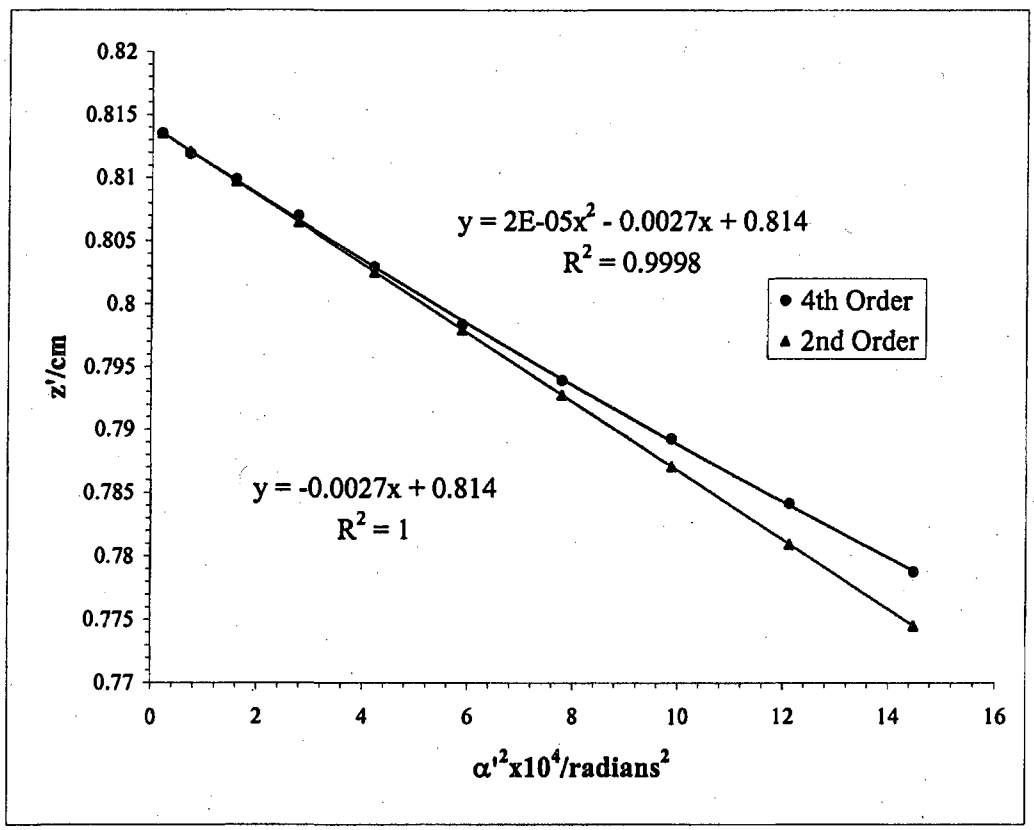

Mesh/inch	V Ratio	Mesh	e'_1/cm	d/cm	b/cm		Beam	Voltage	20 kV
2000	1.00	Rear	0.00127	33.01	1.113	DS			
								L4 Objective Lens	

Bar location/ units	Shadow Reading X/cm	Spacing Δ/cm	E'/cm	M'	c/cm	α' x 10^2	α'^{2} x 10^4	z'/cm
10	1.077		1.271	100.08	0.333	3.8124	14.5345	0.779
9	1.186	0.109	1.162	101.64	0.328	3.4852	12.1465	0.785
8	1.299	0.113	1.049	103.30	0.323	3.1489	9.9157	0.790
7	1.417	0.118	0.932	104.81	0.318	2.7961	7.8181	0.795
6	1.539	0.123	0.810	106.35	0.313	2.4321	5.9153	0.799
5	1.665	0.126	0.684	107.69	0.309	2.0526	4.2132	0.803
4	1.794	0.129	0.555	109.24	0.305	1.6660	2.7755	0.808
3	1.930	0.135	0.420	110.17	0.302	1.2602	1.5881	0.810
2	2.067	0.138	0.282	111.05	0.300	0.8469	0.7172	0.813
1	2.207	0.140	0.142	111.94	0.298	0.4269	0.1822	0.815
0	2.348	0.141						
-1	2.491	0.144						
-2	2.631	0.140						
-3	2.769	0.138			Slope	z_0'/cm	Cs'/cm	
-4	2.904	0.135		2.6E-05	-2.8E-03	0.81495	28.183	
-5	3.033	0.129						
-6	3.160	0.127						
-7	3.280	0.120						
-8	3.398	0.118						
-9	3.510	0.112						
-10	3.620	0.110						

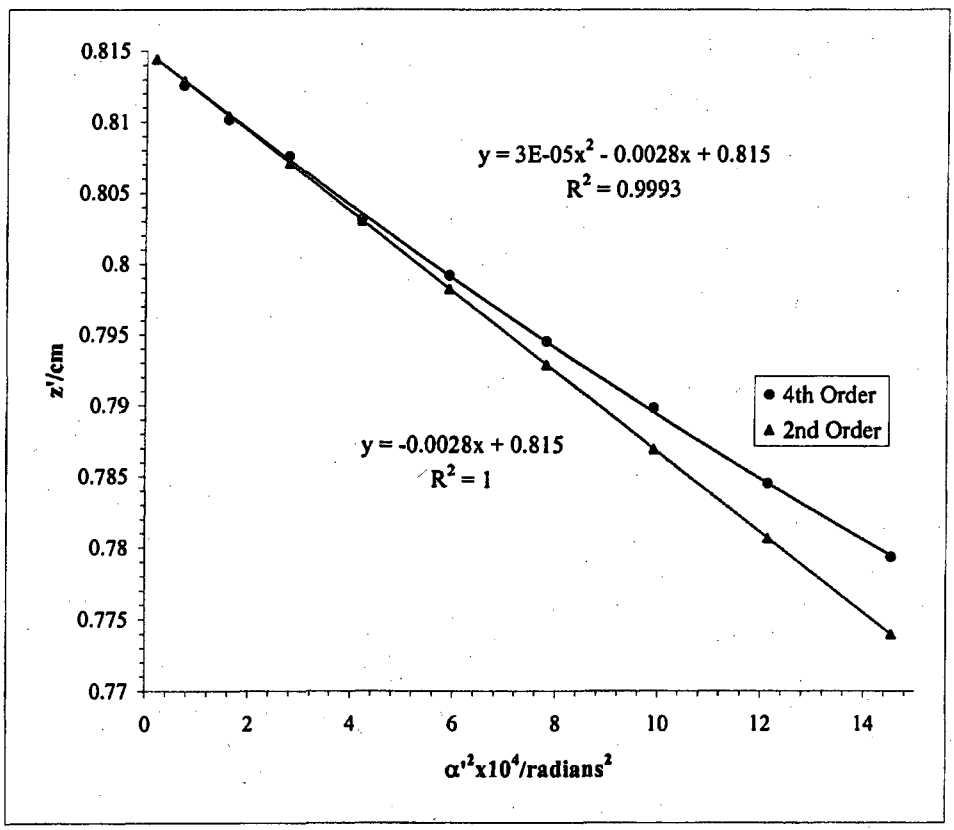

L4 Objective Lens							Beam	Voltage	20 kV
Mesh/inch	V Ratio	Mesh	z/cm	e_1/cm	a/cm	z_{sp}/cm	z_0'/cm	C_s'/cm	$z_{sp}-z_0'$
600	1.00	Front	29.20	0.004233	27.40	34.12	0.820	31.53	33.30

Bar location/ units	Shadow Reading X/cm	Spacing Δ/cm	E/cm	α x 10^4	α' x 10^2	α'² x 10^4	m	z'/cm	f/cm
10	0.880		1.918	15.452	5.741	32.964	0.02691	0.716	0.767
9	1.094	0.214	1.701	13.907	5.096	25.965	0.02729	0.738	0.777
8	1.306	0.212	1.490	12.362	4.468	19.959	0.02767	0.757	0.788
7	1.509	0.203	1.289	10.816	3.864	14.931	0.02799	0.773	0.796
6	1.702	0.193	1.094	9.271	3.281	10.765	0.02826	0.786	0.804
5	1.894	0.192	0.904	7.726	2.713	7.361	0.02848	0.797	0.810
4	2.080	0.185	0.719	6.181	2.158	4.657	0.02864	0.806	0.814
3	2.262	0.183	0.537	4.636	1.612	2.599	0.02876	0.812	0.817
2	2.442	0.179	0.358	3.090	1.074	1.153	0.02878	0.817	0.818
1	2.619	0.177	0.179	1.545	0.538	0.290	0.02870	0.819	0.815
0	2.798	0.179							
-1	2.977	0.179							
-2	3.157	0.180							
-3	3.336	0.179							
-4	3.517	0.181							
-5	3.702	0.185							
-6	3.890	0.187							
-7	4.086	0.196							
-8	4.287	0.201							
-9	4.496	0.209							
-10	4.716	0.220							

g/cm	$(\rho/f_0)^2 = (m_0+1)^2\alpha'^2$
0.696	34.900
0.717	27.489
0.735	21.131
0.751	15.808
0.764	11.397
0.774	7.793
0.782	4.930
0.789	2.751
0.793	1.221
0.796	0.307

	Slope	m_0	μ_s
1.18E-07	-0.00007	0.02894	-22.75

f vs $(\rho/f_o)^2$

$S_f = slope_f / f_0$

	$slope_f$	fo/cm	S_f
2.849E-06	-0.00168	0.822	-20.48

g vs $(\rho/f_o)^2$

$S_g = slope_g / f_0$

	$slope_g$	go/cm	S_g
-2.5E-07	-0.0029	0.796	-35.02

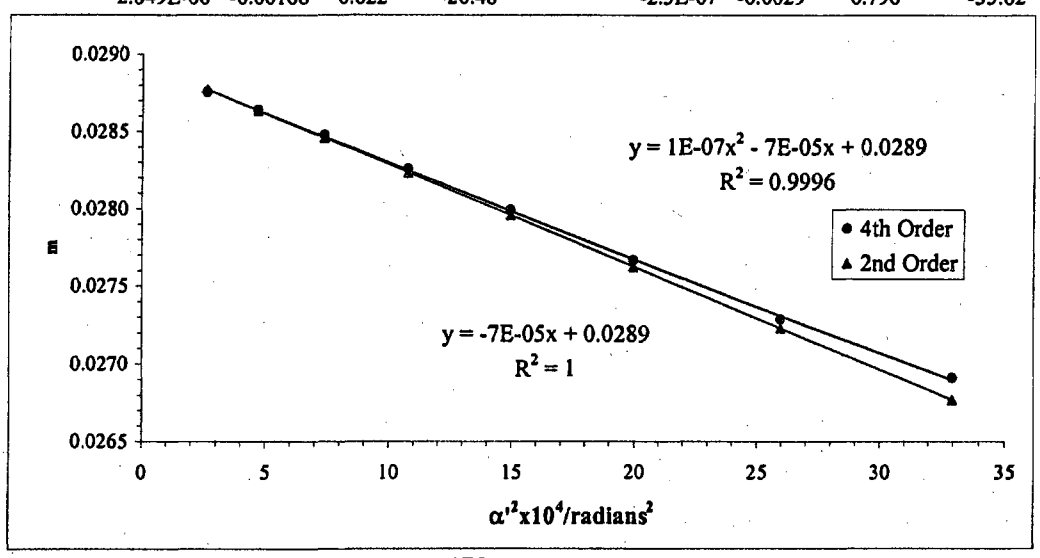

L4 Objective Lens — **Beam Voltage** 20 kV

Mesh/inch	V Ratio	Mesh	z/cm	e_1/cm	a/cm	z_{sp}/cm	z_0'/cm	C_s'/cm	$z_{sp}-z_0'$
600	1.00	Front	29.20	0.004233	27.40	34.12	0.8202	31.535	33.30

Bar location/ units	Shadow Reading Y/cm	Spacing Δ/cm	E/cm	$\alpha \times 10^4$	$\alpha' \times 10^2$	$\alpha'^2 \times 10^4$	m	z'/cm	f/cm
6.5	1.646		1.201	10.044	3.602	12.978	0.0279	0.779	0.793
5.5	1.840	0.194	1.007	8.499	3.022	9.132	0.0281	0.791	0.800
4.5	2.029	0.189	0.818	6.953	2.455	6.027	0.0283	0.801	0.805
3.5	2.215	0.186	0.632	5.408	1.899	3.605	0.0285	0.809	0.809
2.5	2.397	0.183	0.450	3.863	1.351	1.824	0.0286	0.814	0.813
1.5	2.578	0.181	0.269	2.318	0.808	0.653	0.0287	0.818	0.815
0.5	2.758	0.180	0.090	0.773	0.269	0.072	0.0287	0.820	0.816
-0.5	2.937	0.179							
-1.5	3.116	0.179							
-2.5	3.297	0.181							
-3.5	3.479	0.182							
-4.5	3.665	0.185							
-5.5	3.854	0.189							
-6.5	4.048	0.194							

g/cm	$(\rho/f)^2 = (m+1)^2 \alpha'^2$
0.757	13.734
0.769	9.664
0.778	6.378
0.786	3.815
0.791	1.930
0.795	0.691
0.797	0.077

Slope	m_o	μ_s
1.98E-07	-0.00007	0.02872	-23.55

f vs $(\rho/f_o)^2$

$S_f = slope_f / f_0$

$slope_f$	fo/cm	S_f
4.87E-06	-0.00173	0.816	-21.24

g vs $(\rho/f_o)^2$

$S_g = slope_g / f_0$

$slope_g$	go/cm	S_g
-3.83E-07	-0.00288	0.797	-35.27

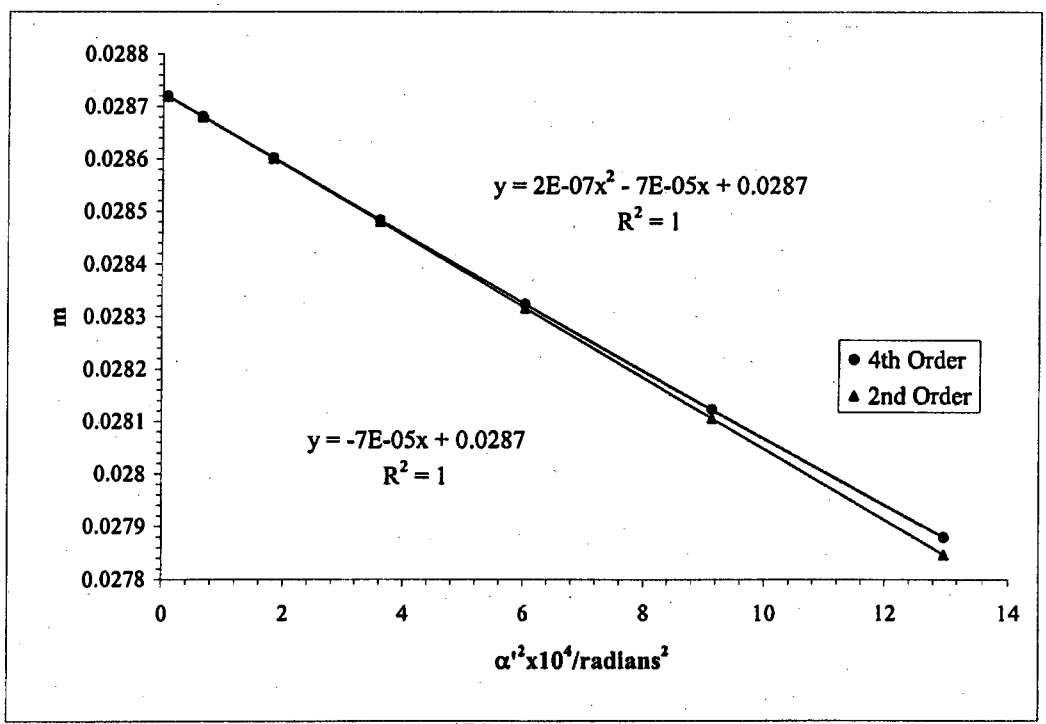

L4 Objective Lens

Beam Voltage	Volt Ratio	z/cm	z_0'/cm	C_s'/cm
20 kV	1.00	29.2	0.820	31.5

Average of m_o = 0.0288

Average of μ_s = -23.1

Paraxial properties :

f_o = 0.819 cm

g_o = 0.797 cm

S_f = -20.9

S_g = -35.1

Swept-back Electrostatic Interface Lens L_5 Data.

Mesh/inch	V Ratio	Mesh	e'_1/cm	d/cm	b/cm		Beam	Voltage	20 kV
2000	0.70	Rear	0.00127	31.73	1.661	US			

Bar location/ units	Shadow Reading X/cm	Spacing Δ/cm	E'/cm	M'	c/cm	L 5 α' x 10^2	Swept back Interface Lens α'^2 x 10^4	z'/cm
6.5	1.490		0.690	-83.57	-0.375	2.2003	4.841	2.036
5.5	1.646	0.155	0.541	-77.42	-0.405	1.7266	2.981	2.066
4.5	1.767	0.121	0.421	-73.75	-0.424	1.3464	1.813	2.086
3.5	1.872	0.105	0.318	-71.53	-0.437	1.0162	1.033	2.099
2.5	1.968	0.096	0.223	-70.13	-0.446	0.7118	0.507	2.107
1.5	2.059	0.091	0.132	-69.27	-0.452	0.4219	0.178	2.113
0.5	2.146	0.087	0.044	-69.19	-0.452	0.1405	0.020	2.113
-0.5	2.234	0.088						
-1.5	2.323	0.089						
-2.5	2.413	0.090						
-3.5	2.508	0.094			Slope	z_o'/cm	C_s'/cm	
-4.5	2.610	0.102		0.00013	-0.017084	2.116	170.84	
-5.5	2.727	0.117						
-6.5	2.870	0.143						

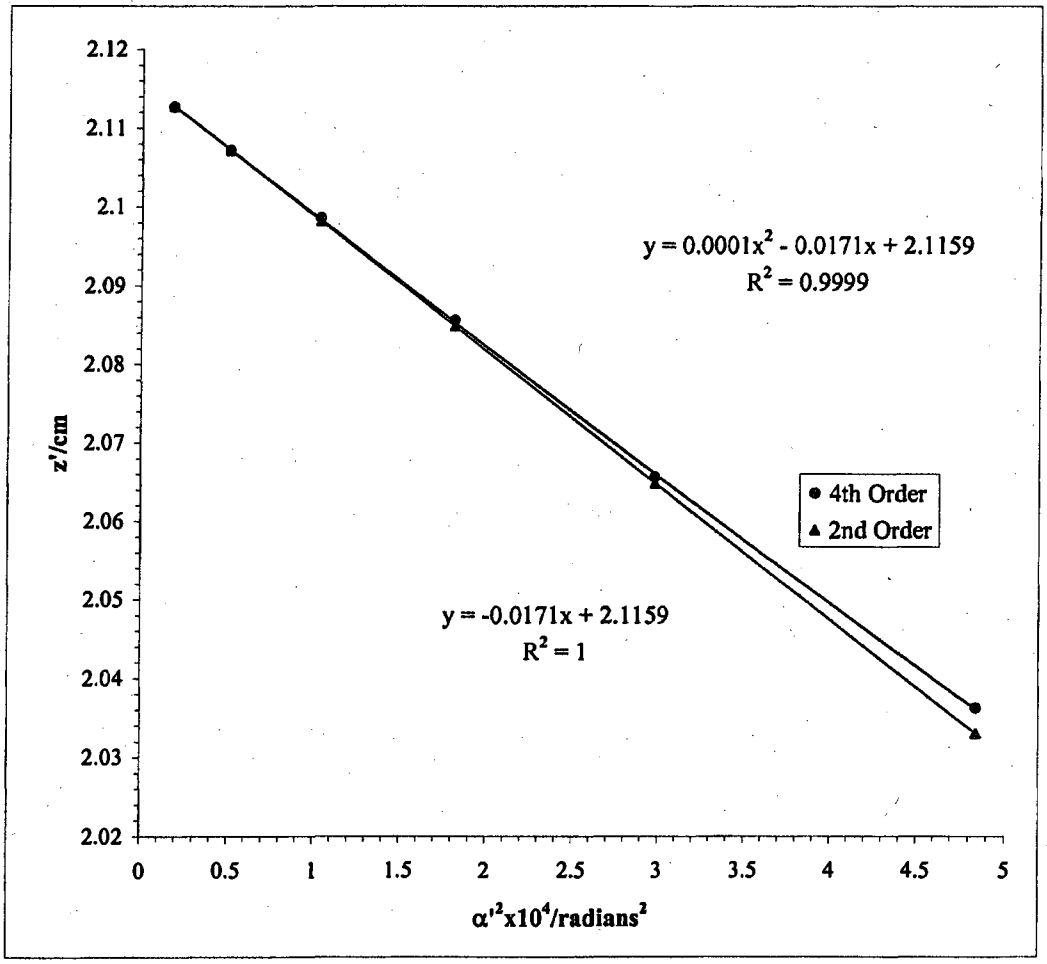

Mesh/inch	V Ratio	Mesh	e'_1/cm	d/cm	b/cm		Beam	Voltage	20 kV
2000	0.70	Rear	0.00127	31.73	1.66	US			

Bar location/ units	Shadow Reading Y/cm	Spacing Δ/cm	E'/cm	M'	c/cm	L 5 Swept back Interface Lens $\alpha' \times 10^2$	$\alpha'^2 \times 10^4$	z'/cm
6	1.428		0.627	-82.27	-0.381	1.9999	4.000	2.042
5	1.557	0.128	0.490	-77.14	-0.406	1.5639	2.446	2.067
4	1.664	0.108	0.377	-74.28	-0.421	1.2053	1.453	2.083
3	1.763	0.099	0.276	-72.46	-0.432	0.8822	0.778	2.093
2	1.858	0.095	0.180	-71.06	-0.440	0.5769	0.333	2.101
1	1.948	0.090	0.088	-69.51	-0.450	0.2823	0.080	2.111
0	2.036	0.088						
-1	2.125	0.089						
-2	2.219	0.094						
-3	2.315	0.096						
-4	2.419	0.104						
-5	2.536	0.117			Slope	z_0'/cm	C_s'/cm	
-6	2.682	0.146		0.0001	-0.0164	2.1064	164.48	

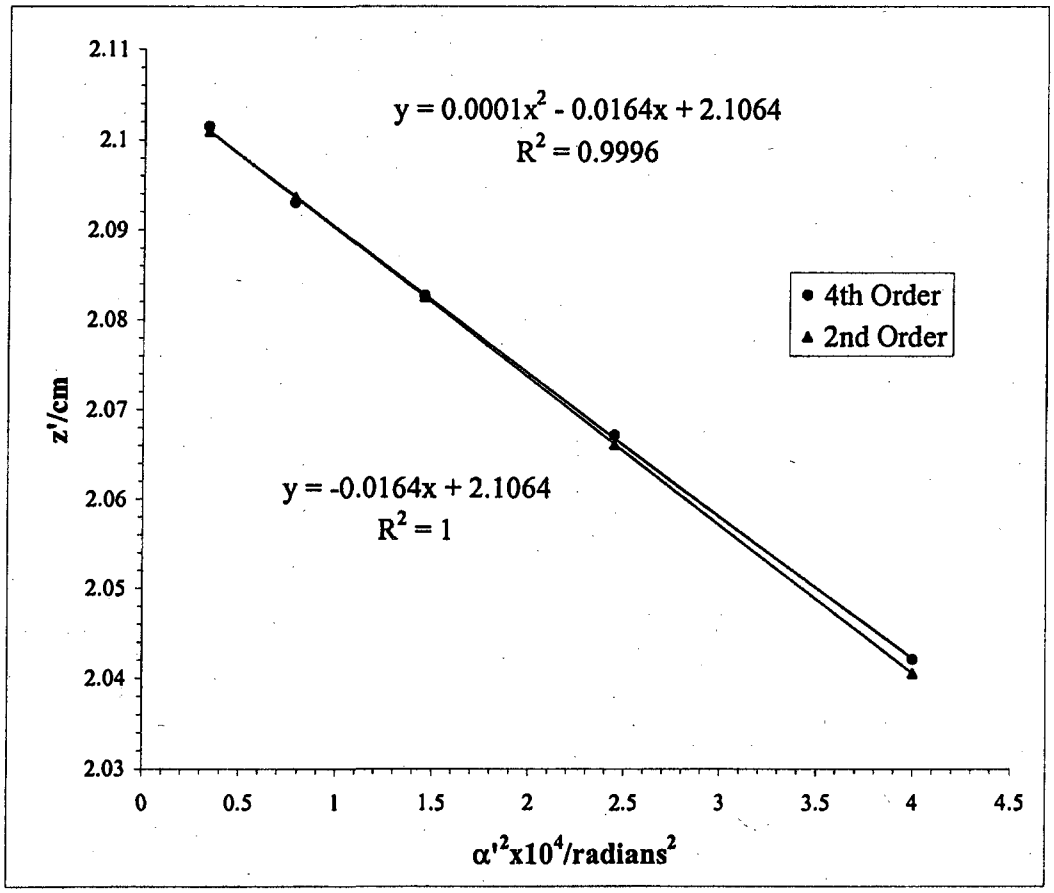

Mesh/inch	V Ratio	Mesh	e'_1/cm	d/cm	b/cm		Beam	Voltage	20 kV
2000	0.70	Rear	0.0013	31.14	2.25	DS			

Bar location/ units	Shadow Reading X/cm	Spacing Δ/cm	E'/cm	M'	c/cm	L 5 Swept back Interface Lens α' x 10^2	α'^2 x 10^4	z'/cm
8.5	1.390		0.781	72.32	0.4367	2.4720	6.1109	1.809
7.5	1.459	0.069	0.713	74.88	0.4215	2.2597	5.1061	1.824
6.5	1.531	0.072	0.641	77.65	0.4063	2.0317	4.1278	1.839
5.5	1.611	0.079	0.562	80.45	0.3920	1.7820	3.1756	1.853
4.5	1.698	0.087	0.477	83.50	0.3775	1.5140	2.2922	1.868
3.5	1.791	0.093	0.385	86.64	0.3637	1.2223	1.4939	1.882
2.5	1.892	0.101	0.284	89.37	0.3524	0.9009	0.8116	1.893
1.5	2.003	0.111	0.174	91.60	0.3438	0.5542	0.3071	1.902
0.5	2.119	0.116	0.059	93.17	0.3379	0.1879	0.0353	1.907
-0.5	2.238	0.118						
-1.5	2.352	0.115						
-2.5	2.460	0.108						
-3.5	2.561	0.101						
-4.5	2.652	0.091			Slope	z_o'/cm	C_s'/cm	
-5.5	2.735	0.083		2.80E-04	-0.0179	1.908	178.50	
-6.5	2.813	0.079						
-7.5	2.886	0.072						
-8.5	2.951	0.066						

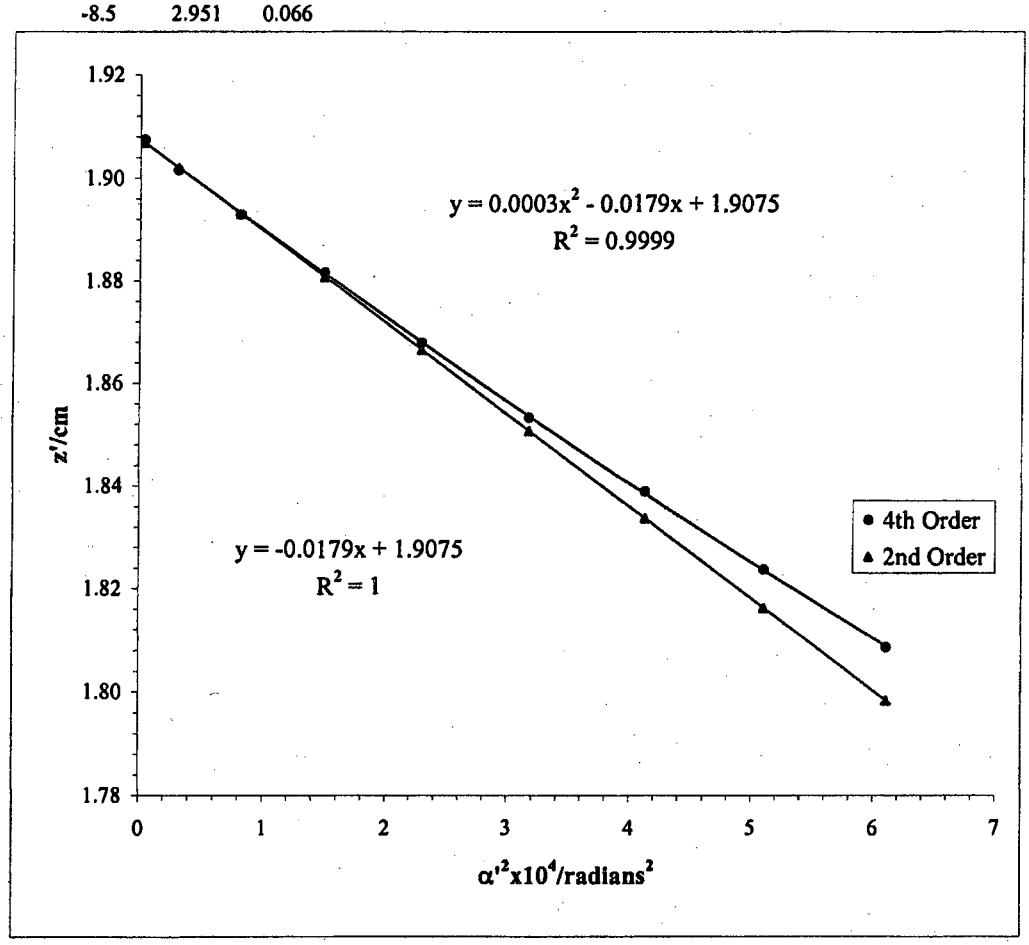

Mesh/inch	V Ratio	Mesh	e'_1/cm	d/cm	b/cm		Beam	Voltage	20 kV
2000	0.70	Rear	0.0013	31.14	2.25	DS			

Bar location/ units	Shadow Reading Y/cm	Spacing Δ/cm	E'/cm	M'	c/cm	L 5 Swept back Interface Lens α' x 10^2	α'^2 x 10^4	z'/cm
7	1.369		0.673	75.72	0.417	2.1329	4.5493	1.829
6	1.446	0.077	0.598	78.43	0.402	1.8946	3.5897	1.843
5	1.526	0.080	0.516	81.30	0.388	1.6373	2.6807	1.858
4	1.614	0.088	0.428	84.19	0.374	1.3570	1.8415	1.871
3	1.710	0.096	0.332	87.07	0.362	1.0530	1.1088	1.884
2	1.814	0.104	0.228	89.58	0.352	0.7225	0.5220	1.894
1	1.925	0.111	0.116	91.30	0.345	0.3682	0.1356	1.900
0	2.042	0.116						
-1	2.157	0.116						
-2	2.269	0.112						
-3	2.373	0.105						
-4	2.470	0.096						
-5	2.559	0.089						
-6	2.641	0.083			Slope	z_o'/cm	C_s'/cm	
-7	2.716	0.074		3.4E-04	-0.0179	1.903	178.71	

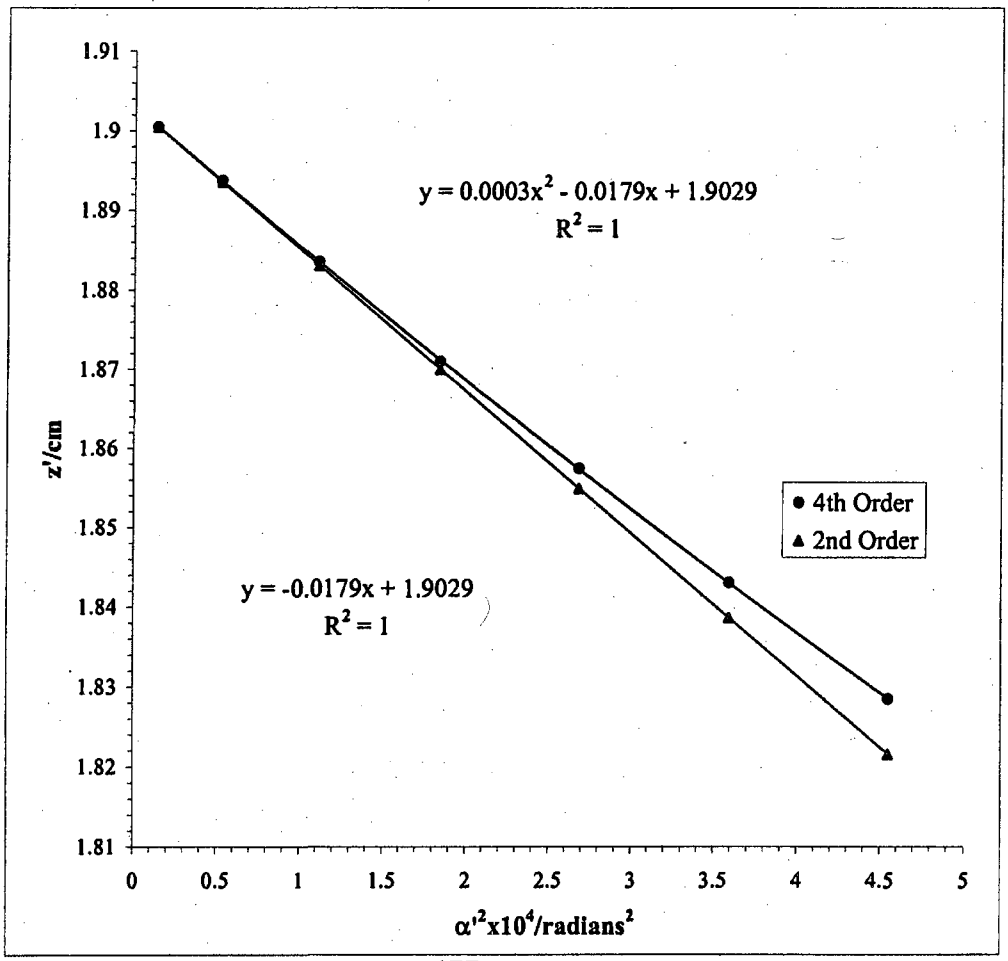

L 5	Swept back Interface Lens						Beam	Voltage	20 kV
Mesh/inch	V Ratio	Mesh	z/cm	e_1/cm	a/cm	z_{sp}/cm	z_0'/cm	C_s'/cm	$z_{sp}-z_o'$
600	0.70	Front	31.27	0.00423	26.42	33.39	2.008	173.13	31.38

Bar location/ units	Shadow Reading X/cm	Spacing Δ/cm	E/cm	$\alpha \times 10^4$	$\alpha' \times 10^2$	$\alpha'^2 \times 10^4$	m	z'/cm	f/cm
15	0.896		1.220	24.038	3.855	14.861	0.0624	1.751	1.848
14	0.993	0.096	1.123	22.436	3.555	12.636	0.0631	1.789	1.868
13	1.086	0.093	1.030	20.833	3.264	10.652	0.0638	1.824	1.887
12	1.176	0.090	0.940	19.231	2.981	8.887	0.0645	1.854	1.905
11	1.264	0.088	0.853	17.628	2.706	7.323	0.0651	1.881	1.922
10	1.349	0.085	0.768	16.026	2.438	5.945	0.0657	1.905	1.938
9	1.432	0.083	0.685	14.423	2.177	4.738	0.0663	1.926	1.953
8	1.513	0.081	0.604	12.821	1.921	3.690	0.0667	1.944	1.966
7	1.592	0.079	0.525	11.218	1.670	2.789	0.0672	1.960	1.978
6	1.670	0.078	0.447	9.615	1.423	2.026	0.0676	1.973	1.988
5	1.747	0.077	0.371	8.013	1.181	1.394	0.0679	1.984	1.997
4	1.822	0.076	0.295	6.410	0.941	0.885	0.0681	1.993	2.004
3	1.897	0.075	0.221	4.808	0.703	0.495	0.0683	2.000	2.010
2	1.971	0.074	0.147	3.205	0.468	0.219	0.0685	2.004	2.014
1	2.045	0.074	0.073	1.603	0.234	0.055	0.0686	2.007	2.016
0	2.118	0.073							
-1	2.191	0.073						g/cm	$(\rho/f_0)^2 =$
-2	2.265	0.073		Slope	m_o	μ_s			$(m_0+1)^2\alpha'^2$
-3	2.339	0.074	7E-06	-0.00052	0.068591	-76.25		1.636	16.970
-4	2.413	0.074						1.672	14.429
-5	2.488	0.075		f vs $(\rho/f_o)^2$				1.703	12.163
-6	2.565	0.076	$S_f = slope_f / f_0$					1.731	10.148
-7	2.642	0.077		$slope_f$	fo/cm	S_f		1.756	8.362
-8	2.721	0.079	0.00016	-0.01259	2.017	-62.41		1.778	6.789
-9	2.802	0.081						1.797	5.410
-10	2.884	0.083		g vs $(\rho/f_o)^2$				1.813	4.213
-11	2.969	0.085	$S_g = slope_g / f_0$					1.827	3.184
-12	3.056	0.087		$slope_g$	go/cm	S_g		1.839	2.314
-13	3.146	0.090	-2E-05	-0.01339	1.870	-66.40		1.849	1.591
-14	3.239	0.093						1.856	1.011
-15	3.336	0.096						1.862	0.565
								1.866	0.250
								1.869	0.062

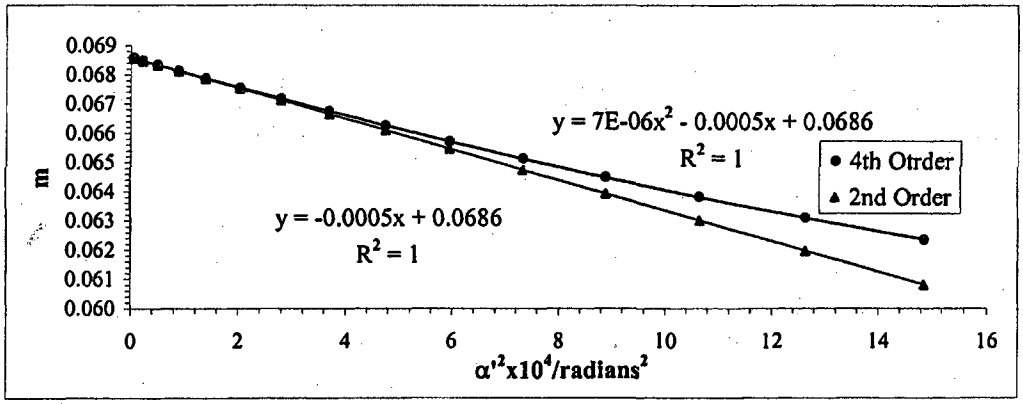

L 5	Swept back Interface Lens						Beam	Voltage	20 kV
Mesh/inch	V Ratio	Mesh	z/cm	e_1/cm	a/cm	z_{sp}/cm	z_0'/cm	C_s'/cm	$z_{sp}-z_0'$
600	0.70	Front	31.27	0.00423	26.42	33.39	2.008	173.13	31.38

Bar location/ units	Shadow Reading Y/cm	Spacing Δ/cm	E/cm	$\alpha \times 10^4$	$\alpha' \times 10^2$	$\alpha'^2 \times 10^4$	m	z'/cm	f/cm
13.5	1.284		1.110	21.635	3.512	12.336	0.0616	1.795	1.822
12.5	1.380	0.096	1.015	20.032	3.216	10.343	0.0623	1.829	1.841
11.5	1.473	0.093	0.923	18.429	2.928	8.575	0.0629	1.860	1.858
10.5	1.563	0.090	0.834	16.827	2.648	7.014	0.0635	1.887	1.874
9.5	1.651	0.087	0.748	15.224	2.375	5.643	0.0641	1.910	1.889
8.5	1.736	0.085	0.663	13.622	2.109	4.447	0.0646	1.931	1.903
7.5	1.819	0.083	0.581	12.019	1.848	3.414	0.0650	1.949	1.915
6.5	1.900	0.081	0.500	10.417	1.592	2.534	0.0654	1.964	1.926
5.5	1.980	0.080	0.421	8.814	1.340	1.795	0.0658	1.977	1.935
4.5	2.058	0.078	0.343	7.212	1.091	1.191	0.0661	1.988	1.943
3.5	2.135	0.077	0.266	5.609	0.846	0.716	0.0663	1.996	1.949
2.5	2.212	0.077	0.189	4.006	0.603	0.363	0.0665	2.002	1.954
1.5	2.288	0.076	0.113	2.404	0.361	0.130	0.0666	2.006	1.957
0.5	2.363	0.076	0.038	0.801	0.120	0.014	0.0667	2.008	1.959
-0.5	2.439	0.075							
-1.5	2.514	0.076						g/cm	$(\rho/f_0)^2 =$
-2.5	2.590	0.076		Slope	m_0	μ_s			$(m_0+1)^2\alpha$
-3.5	2.666	0.076	7E-06	-0.0005	0.06666	-73.99		1.682	12.324
-4.5	2.743	0.077						1.714	10.332
-5.5	2.821	0.078		f vs $(\rho/f_0)^2$				1.743	8.566
-6.5	2.900	0.079	$S_f = slope_f / f_0$					1.768	7.007
-7.5	2.981	0.080		$slope_f$	f_0/cm	S_f		1.789	5.637
-8.5	3.063	0.082	2E-04	-0.0135	1.959	-68.84		1.808	4.443
-9.5	3.146	0.084						1.824	3.411
-10.5	3.232	0.086		g vs $(\rho/f_0)^2$				1.838	2.531
-11.5	3.320	0.088	$S_g = slope_g / f_0$					1.850	1.793
-12.5	3.410	0.090		$slope_g$	g_0/cm	S_g		1.859	1.190
-13.5	3.503	0.093	-3E-05	-0.0155	1.878	-79.00		1.867	0.715
								1.872	0.363
								1.876	0.130
								1.877	0.014

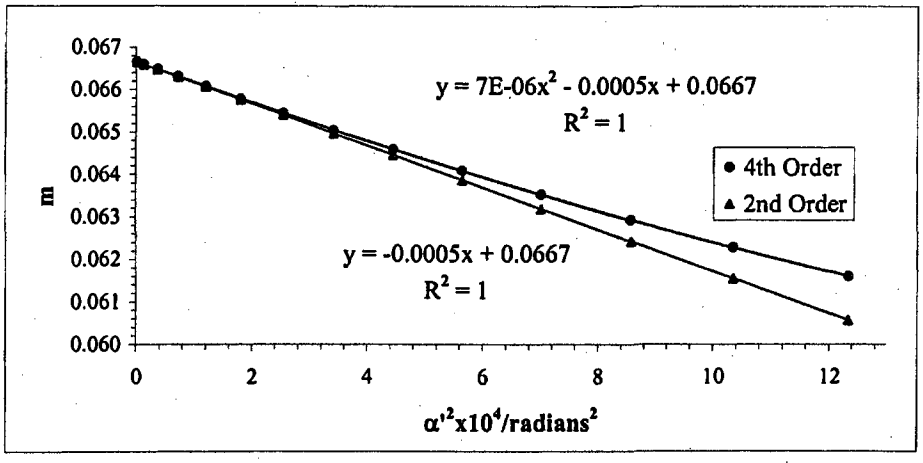

Beam Voltage	Volt Ratio	z/cm	L 5 z_0'/cm	Swept back Interface Lens C_s'/cm
20 kV	0.7	31.3	2.01	173

Average of m_o = 0.0676

Average of μ_s = -75.1

Paraxial properties :

f_o = 1.99 cm

g_o = 1.87 cm

S_f = -65.6

S_g = -72.7

Mesh/inch	V Ratio	Mesh	e'_1/cm	d/cm	b/cm		Beam	Voltage	20 kV
2000	0.80	Rear	0.00127	32.31	1.077	US			

Bar location/ units	Shadow Reading X/cm	Spacing Δ/cm	E'/cm	M'	c/cm	L 5 Swept back Interface Lens α' x 10^2	α'^2 x 10^4	z'/cm
8.5	1.799		1.396	-129.30	-0.248	4.3532	18.951	1.325
7.5	2.110	0.310	1.078	-113.14	-0.283	3.3647	11.321	1.360
6.5	2.315	0.205	0.874	-105.92	-0.302	2.7316	7.461	1.379
5.5	2.482	0.167	0.708	-101.40	-0.316	2.2137	4.901	1.392
4.5	2.630	0.148	0.561	-98.16	-0.326	1.7538	3.076	1.403
3.5	2.765	0.135	0.426	-95.91	-0.333	1.3331	1.777	1.410
2.5	2.892	0.127	0.300	-94.53	-0.338	0.9387	0.881	1.415
1.5	3.014	0.122	0.178	-93.49	-0.342	0.5571	0.310	1.419
0.5	3.133	0.119	0.059	-93.04	-0.344	0.1848	0.034	1.421
-0.5	3.251	0.118						
-1.5	3.370	0.119						
-2.5	3.492	0.122						
-3.5	3.617	0.125						
-4.5	3.752	0.134			Slope	z_o'/cm	C_s'/cm	
-5.5	3.898	0.147		4E-05	-0.00587	1.421	58.74	
-6.5	4.063	0.165						
-7.5	4.265	0.202						
-8.5	4.591	0.326						

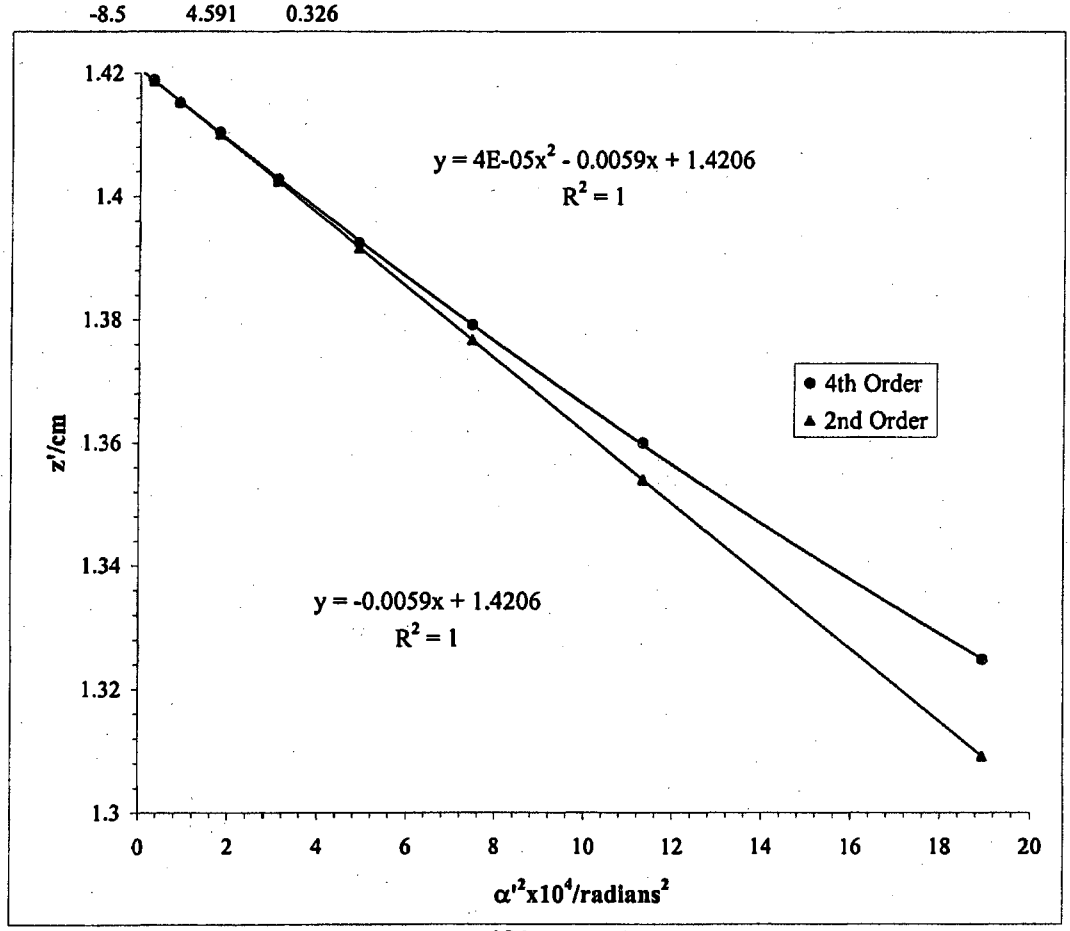

Mesh/inch	V Ratio	Mesh	e'_1/cm	d/cm	b/cm		Beam	Voltage	20 kV
2000	0.80	Rear	0.00127	31.73	1.66	DS			

Bar location/ units	Shadow Reading X/cm	Spacing Δ/cm	E'/cm	M'	c/cm	L 5 Swept back Interface Lens α' x 10^2	α'^2 x 10^4	z'/cm
9.5	1.791		1.282	106.30	0.301	4.0042	16.0335	1.360
8.5	1.887	0.096	1.187	109.96	0.291	3.7074	13.7448	1.370
7.5	1.989	0.103	1.085	113.96	0.281	3.3912	11.5002	1.380
6.5	2.099	0.110	0.975	118.16	0.271	3.0483	9.2922	1.390
5.5	2.216	0.117	0.856	122.61	0.261	2.6773	7.1682	1.400
4.5	2.344	0.127	0.728	127.39	0.251	2.2766	5.1831	1.410
3.5	2.482	0.138	0.588	132.18	0.242	1.8379	3.3779	1.419
2.5	2.633	0.151	0.434	136.78	0.234	1.3588	1.8463	1.427
1.5	2.797	0.164	0.267	140.41	0.228	0.8371	0.7007	1.434
0.5	2.972	0.175	0.091	142.59	0.224	0.2834	0.0803	1.437
-0.5	3.153	0.181						
-1.5	3.332	0.179						
-2.5	3.502	0.170						
-3.5	3.657	0.155						
-4.5	3.800	0.143						
-5.5	3.92924	0.129						
-6.5	4.049893	0.121						
-7.5	4.160314	0.110						
-8.5	4.260883	0.101						
-9.5	4.355462	0.095						

	Slope	z_0'/cm	C_s'/cm
3.7E-05	-0.005	1.44	54.15

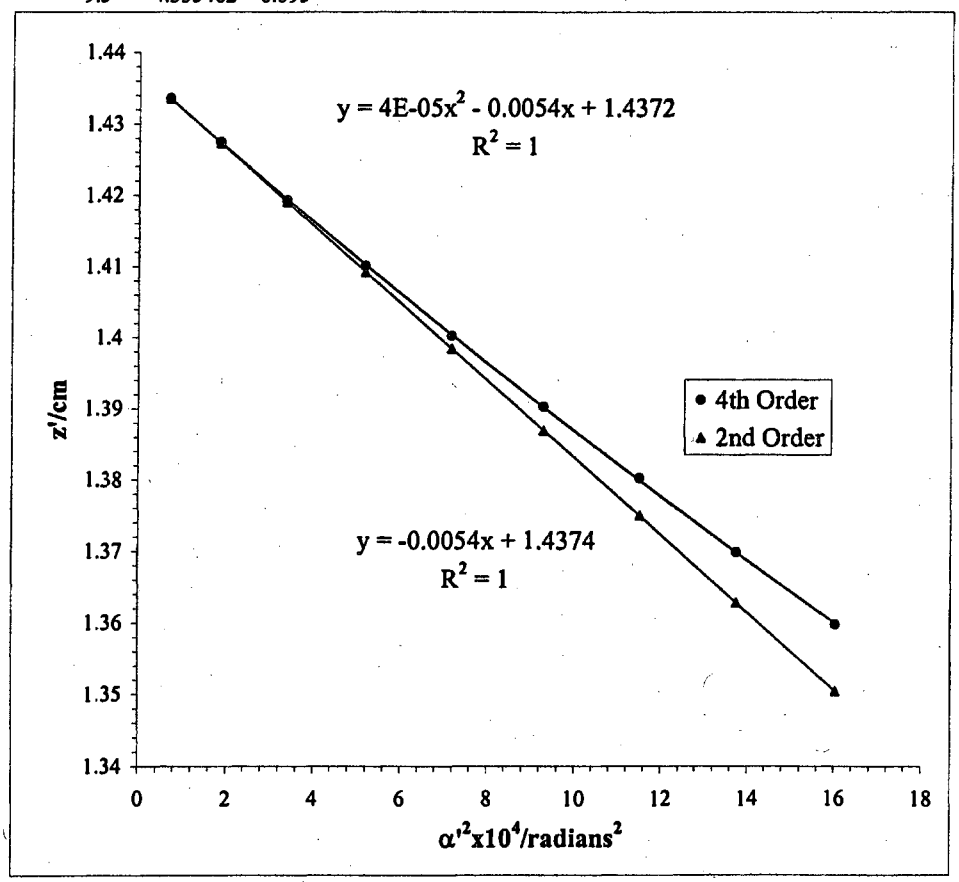

Mesh/inch	V Ratio	Mesh	e'_1/cm	d/cm	b/cm		Beam	Voltage	20 kV
2000	0.80	Rear	0.0013	31.73	1.66	DS			

Bar location/ units	Shadow Reading Y/cm	Spacing Δ/cm	E'/cm	M'	c/cm	L 5 Swept back Interface Lens α' x 10^2	α'^2 x 10^4	z'/cm
9	1.915		1.233	107.87	0.297	3.8500	14.8228	1.364
8	2.015	0.100	1.135	111.71	0.287	3.5451	12.5681	1.375
7	2.122	0.107	1.030	115.91	0.276	3.2198	10.3673	1.385
6	2.237	0.115	0.919	120.56	0.265	2.8715	8.2453	1.396
5	2.362	0.125	0.796	125.41	0.255	2.4900	6.2001	1.406
4	2.498	0.136	0.662	130.40	0.245	2.0720	4.2931	1.416
3	2.647	0.149	0.516	135.53	0.236	1.6155	2.6099	1.425
2	2.810	0.163	0.355	139.83	0.229	1.1114	1.2353	1.433
1	2.984	0.174	0.182	143.54	0.223	0.5706	0.3255	1.439
0	3.167	0.183						
-1	3.348	0.182						
-2	3.520	0.172			Slope	z_o'/cm	C_s'/cm	
-3	3.679	0.159		4E-05	-0.0057	1.440	57.50	
-4	3.823	0.143						
-5	3.954	0.132						
-6	4.074	0.120						
-7	4.183	0.109						
-8	4.285	0.102						
-9	4.381	0.096						

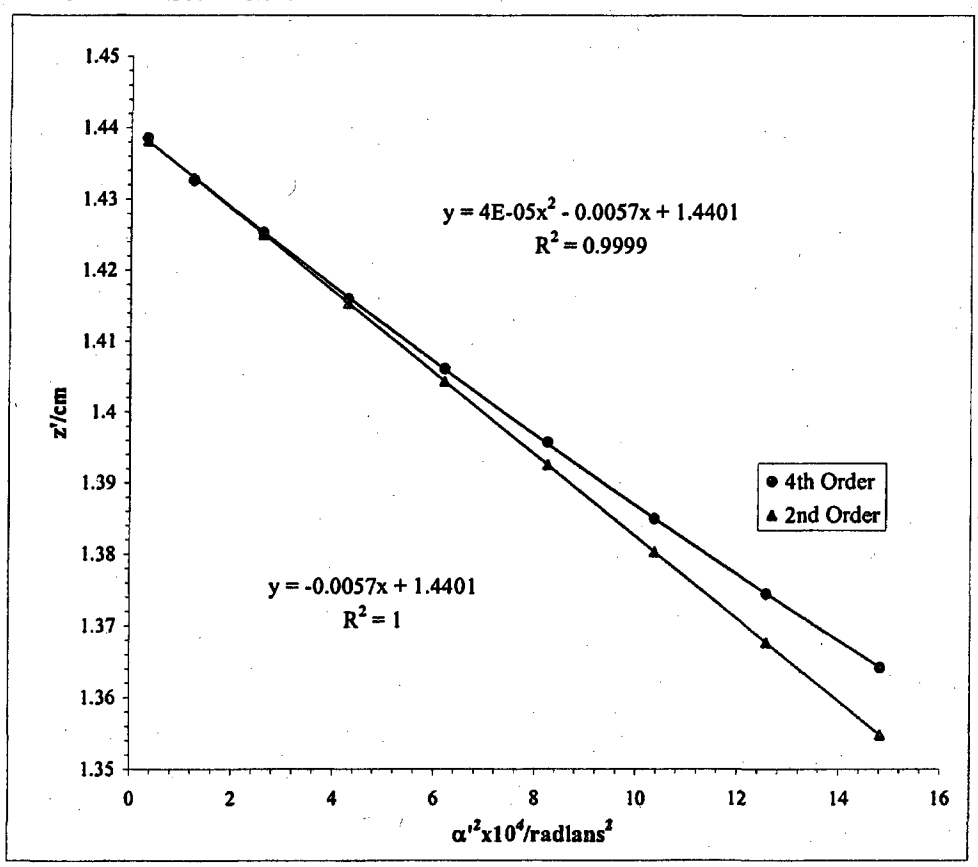

L 5	Swept back Interface Lens						Beam	Voltage	20 kV
Mesh/inch	V Ratio	Mesh	z/cm	e_i/cm	a/cm	z_{sp}/cm	z_0'/cm	C_s'/cm	$z_{sp}-z_o'$
600	0.80	Front	31.27	0.00423	26.42	33.39	1.430	58.12	31.96

Bar location/ units	Shadow Reading X/cm	Spacing Δ/cm	E/cm	$\alpha \times 10^4$	$\alpha' \times 10^2$	$\alpha'^2 \times 10^4$	m	z'/cm	f/cm
9.5	1.958		1.086	15.224	3.392	11.505	0.04488	1.363	1.345
8.5	2.081	0.123	0.964	13.622	3.010	9.060	0.04526	1.378	1.355
7.5	2.201	0.120	0.844	12.019	2.637	6.952	0.04559	1.390	1.365
6.5	2.319	0.118	0.726	10.417	2.271	5.156	0.04588	1.400	1.373
5.5	2.435	0.116	0.611	8.814	1.911	3.652	0.04612	1.409	1.380
4.5	2.549	0.114	0.498	7.212	1.556	2.423	0.04633	1.416	1.386
3.5	2.661	0.113	0.386	5.609	1.206	1.455	0.04650	1.422	1.391
2.5	2.773	0.111	0.275	4.006	0.859	0.738	0.04662	1.426	1.394
1.5	2.883	0.110	0.164	2.404	0.515	0.265	0.04671	1.429	1.397
0.5	2.993	0.110	0.055	0.801	0.171	0.029	0.04675	1.430	1.398
-0.5	3.103	0.110							
-1.5	3.212	0.110						g/cm	$(\rho/f_0)^2 = (m_0+1)^2\alpha'^2$
-2.5	3.322	0.110							
-3.5	3.433	0.111						1.303	12.606
-4.5	3.544	0.112						1.316	9.927
-5.5	3.657	0.113						1.328	7.617
-6.5	3.772	0.115						1.337	5.649
-7.5	3.889	0.117						1.345	4.001
-8.5	4.008	0.119						1.352	2.654
-9.5	4.131	0.123						1.357	1.594
								1.361	0.809
		Slope	m_o	μ_s				1.364	0.290
	1.2E-06	-0.0002	0.046753	-37.74				1.365	0.032

f vs $(\rho/f_o)^2$

$S_f = slope_f / f_0$

$slope_f$	fo/cm	S_f
2.99647E-05	-0.004588	1.398	-32.82

g vs $(\rho/f_o)^2$

$S_g = slope_g / f_0$

$slope_g$	go/cm	S_g
-3.4E-06	-0.00487	1.365	-34.80

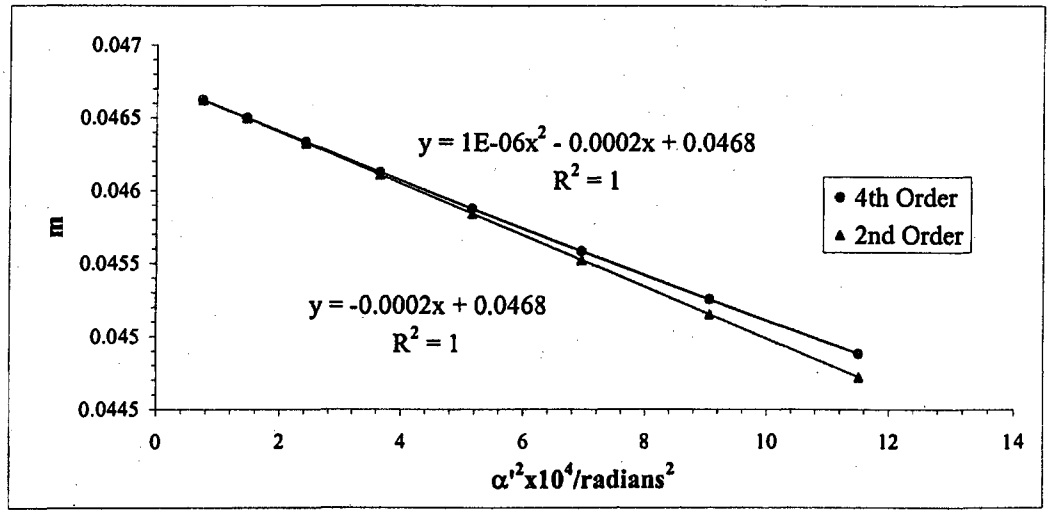

L 5	Swept back Interface Lens						Beam	Voltage	20 kV
Mesh/inch	V Ratio	Mesh	z/cm	e_1/cm	a/cm	z_{sp}/cm	z_0'/cm	C_s'/cm	$z_{sp}-z_o'$
600	0.80	Front	31.27	0.00423	26.42	33.39	1.430	58.12	31.96

Bar location/ units	Shadow Reading Y/cm	Spacing Δ/cm	E/cm	$\alpha \times 10^4$	$\alpha' \times 10^2$	$\alpha'^2 \times 10^4$	m	z'/cm	f/cm
10.5	2.107		1.236	16.827	3.856	14.866	0.0436	1.344	1.308
9.5	2.236	0.129	1.108	15.224	3.458	11.958	0.0440	1.361	1.319
8.5	2.362	0.126	0.983	13.622	3.069	9.421	0.0444	1.376	1.329
7.5	2.486	0.123	0.860	12.019	2.689	7.231	0.0447	1.388	1.338
6.5	2.606	0.121	0.741	10.417	2.316	5.363	0.0450	1.399	1.346
5.5	2.724	0.118	0.623	8.814	1.949	3.798	0.0452	1.408	1.353
4.5	2.841	0.116	0.507	7.212	1.587	2.519	0.0454	1.416	1.359
3.5	2.956	0.115	0.393	5.609	1.230	1.513	0.0456	1.422	1.364
2.5	3.069	0.114	0.280	4.006	0.876	0.768	0.0457	1.426	1.367
1.5	3.182	0.113	0.168	2.404	0.525	0.275	0.0458	1.429	1.370
0.5	3.294	0.112	0.056	0.801	0.175	0.031	0.0459	1.430	1.371
-0.5	3.406	0.112							
-1.5	3.517	0.112						g/cm	$(\rho/f_0)^2 = (m_0+1)^2 \alpha'^2$
-2.5	3.629	0.112							
-3.5	3.742	0.113						1.287	16.260
-4.5	3.856	0.114						1.303	13.080
-5.5	3.971	0.115						1.317	10.305
-6.5	4.088	0.117						1.328	7.909
-7.5	4.206	0.119						1.339	5.866
-8.5	4.328	0.121						1.347	4.154
-9.5	4.451	0.124						1.354	2.756
-10.5	4.578	0.127						1.359	1.655
								1.363	0.840
								1.366	0.301
								1.367	0.033

	Slope	m_0	μ_s
1.545E-06	-0.000172	0.04586	-37.50

f vs $(\rho/f_o)^2$

$S_f = slope_f / f_0$

	$slope_f$	fo/cm	S_f
3.817E-05	-0.004478	1.371	-32.66

g vs $(\rho/f_o)^2$

$S_g = slope_g / f_0$

	$slope_g$	go/cm	S_g
-4E-06	-0.00489	1.367	-35.69

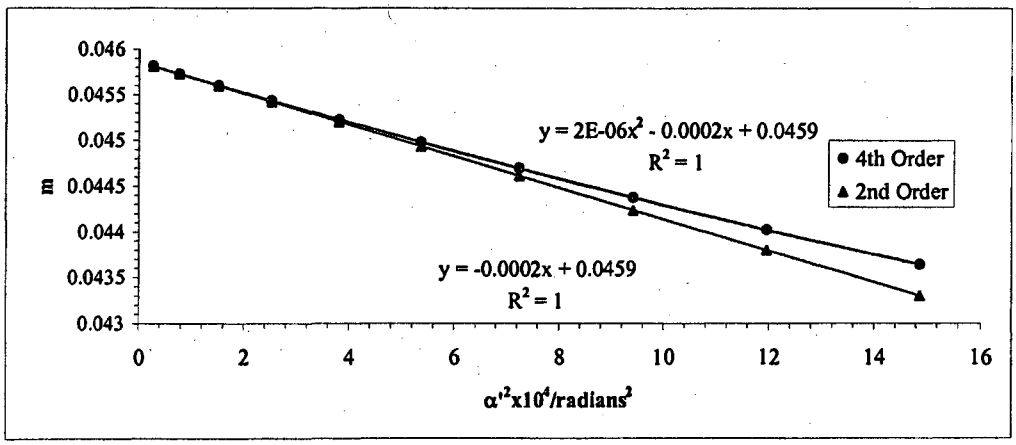

Beam Voltage	Volt Ratio	z/cm	L 5 z_0'/cm	Swept back Interface Lens C_s'/cm
20 kV	0.8	31.27	1.430	58.12

Average of m_0 = 0.0463

Average of μ_s = -37.62

Paraxial properties :

f_o = 1.38 cm

g_o = 1.37 cm

S_f = -32.74

S_g = -35.24

Mesh/inch	V Ratio	Mesh	e'_1/cm	d/cm	b/cm		Beam	Voltage	20 kV
2000	0.90	Rear	0.00127	32.62	0.772	US			

Bar location/ units	Shadow Reading X/cm	Spacing Δ/cm	E'/cm	M'	c/cm	L 5 Swept back Interface Lens $\alpha' \times 10^2$	$\alpha'^2 \times 10^4$	z'/cm
9	1.642		1.137	-99.48	-0.325	3.521	12.400	1.097
8	1.787	0.145	0.991	-97.54	-0.331	3.069	9.422	1.103
7	1.926	0.138	0.852	-95.87	-0.337	2.640	6.971	1.109
6	2.058	0.132	0.720	-94.49	-0.342	2.231	4.977	1.114
5	2.184	0.126	0.594	-93.50	-0.345	1.840	3.385	1.117
4	2.307	0.123	0.471	-92.64	-0.348	1.458	2.127	1.120
3	2.427	0.120	0.351	-92.03	-0.351	1.087	1.181	1.123
2	2.545	0.118	0.233	-91.61	-0.352	0.721	0.520	1.124
1	2.661	0.116	0.116	-91.50	-0.353	0.360	0.130	1.125
0	2.777	0.116						
-1	2.893	0.116			Slope	z_o'/cm	C_s'/cm	
-2	3.010	0.117		1.3E-05	-0.0025	1.126	25.02	
-3	3.128	0.118						
-4	3.248	0.120						
-5	3.371	0.123						
-6	3.498	0.127						
-7	3.630	0.133						
-8	3.769	0.139						
-9	3.916	0.147						

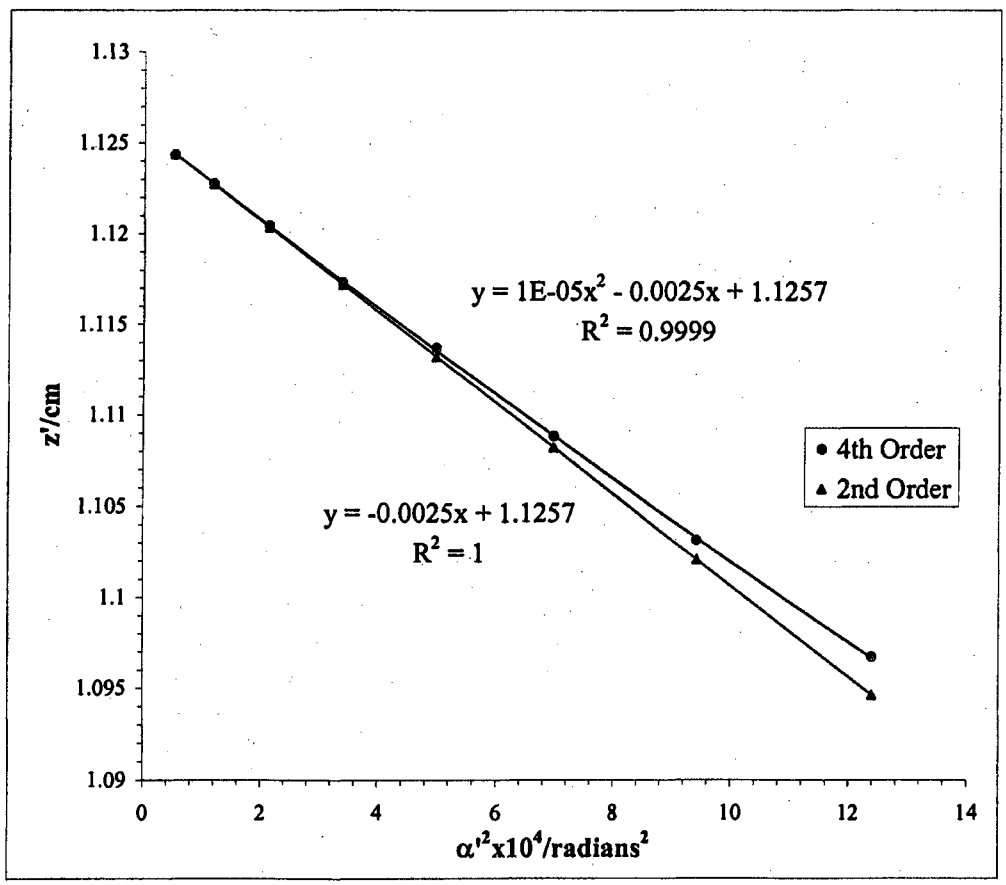

Mesh/inch	V Ratio	Mesh	e'_1/cm	d/cm	b/cm		Beam Voltage	20 kV
2000	0.90	Rear	0.00127	32.62	0.772	US		

Bar location/ units	Shadow Reading Y/cm	Spacing Δ/cm	E'/cm	M'	L 5 c/cm	Swept back Interface Lens α' x 10^2	α'^2 x 10^4	z'/cm
9	1.490		1.141	-99.87	-0.323	3.5348	12.495	1.096
8	1.637	0.147	0.994	-97.86	-0.330	3.0794	9.482	1.102
7	1.775	0.138	0.856	-96.23	-0.335	2.6502	7.024	1.108
6	1.907	0.132	0.724	-94.96	-0.340	2.2419	5.026	1.112
5	2.035	0.128	0.596	-93.83	-0.344	1.8462	3.408	1.116
4	2.159	0.124	0.472	-92.95	-0.347	1.4633	2.141	1.119
3	2.279	0.121	0.352	-92.33	-0.349	1.0902	1.189	1.122
2	2.397	0.118	0.234	-91.95	-0.351	0.7238	0.524	1.123
1	2.515	0.118	0.116	-91.37	-0.353	0.3597	0.129	1.125
0	2.632	0.116						
-1	2.747	0.116			Slope	z_o'/cm	C_s'/cm	
-2	2.865	0.117		3E-05	0.00	1.1250	26.79	
-3	2.983	0.118						
-4	3.103	0.120						
-5	3.226	0.123						
-6	3.354	0.128						
-7	3.486	0.132						
-8	3.625	0.139						
-9	3.772	0.147						

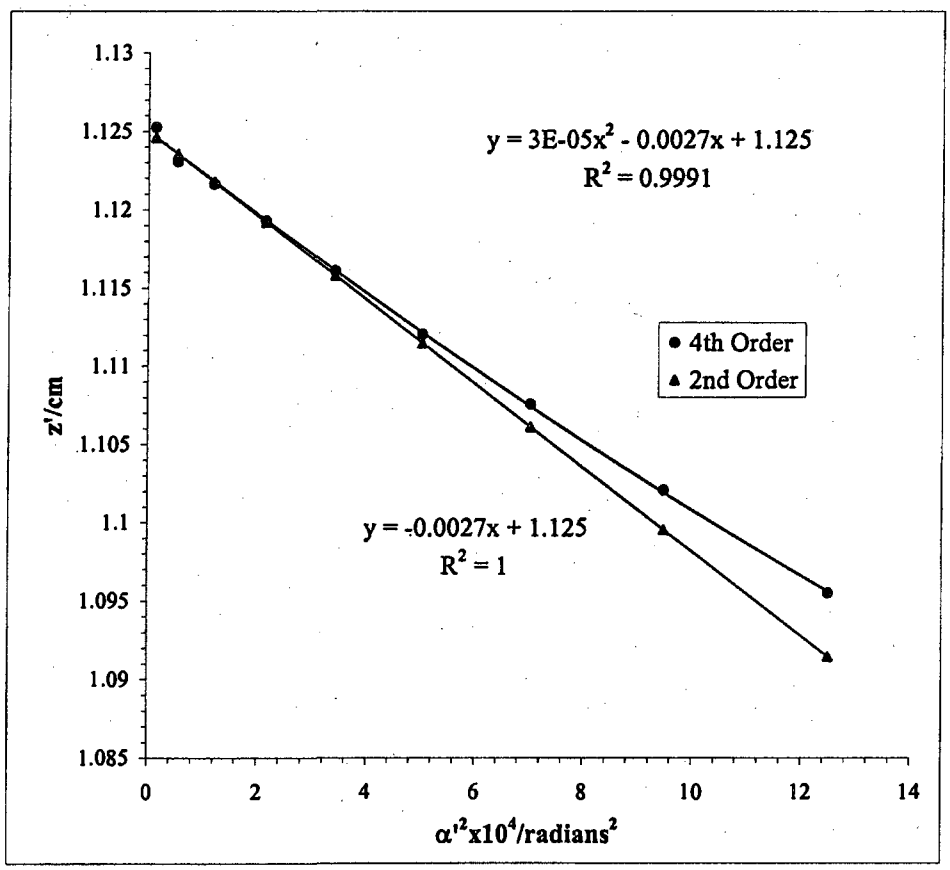

Mesh/inch	V Ratio	Mesh	e'_1/cm	d/cm	b/cm		Beam	Voltage	20 kV
2000	0.90	Rear	0.00127	32.29	1.10	DS			

Bar location/ units	Shadow Reading X/cm	Spacing Δ/cm	E'/cm	M'	c/cm	L 5 α' x 10^2	Swept back Interface Lens α'^2 x 10^4	z'/cm
4.5	1.572		1.171	204.88	0.158	3.609	13.025	0.944
3.5	1.783	0.211	0.968	217.66	0.149	2.983	8.898	0.953
2.5	2.027	0.244	0.731	230.31	0.141	2.255	5.085	0.962
1.5	2.303	0.276	0.465	243.92	0.133	1.433	2.054	0.969
0.5	2.615	0.312	0.160	251.50	0.129	0.493	0.243	0.973
-0.5	2.935	0.319						
-1.5	3.233	0.298						
-2.5	3.489	0.257			Slope	z_o'/cm	C_s'/cm	
-3.5	3.718	0.228		1E-05	-0.002	0.974	24.78	
-4.5	3.914	0.196						

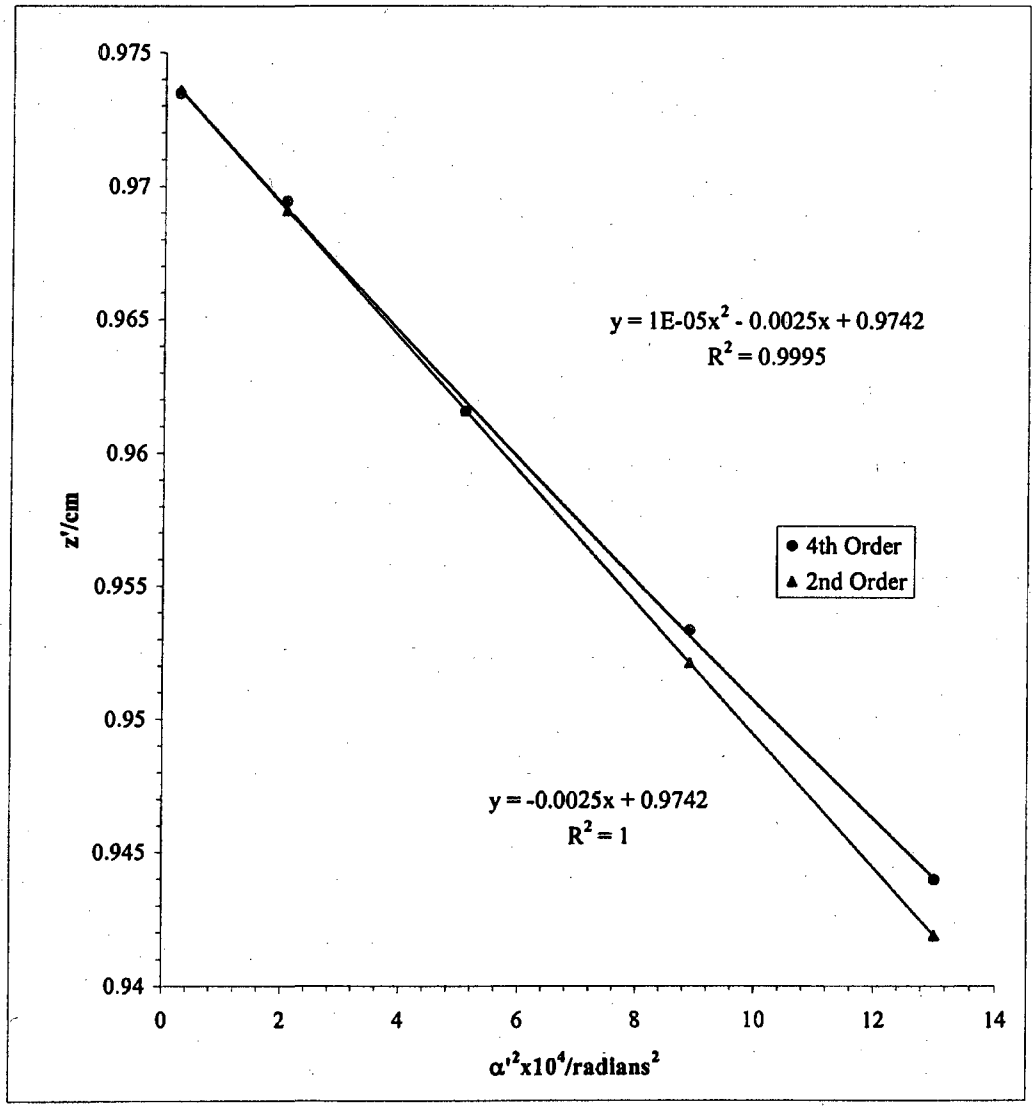

Mesh/inch	V Ratio	Mesh	e'_1/cm	d/cm	b/cm		Beam Voltage	20 kV
2000	0.90	Rear	0.00127	32.29	1.10	DS		

Bar location/ units	Shadow Reading Y/cm	Spacing Δ/cm	E'/cm	M'	c/cm	L 5 Swept back Interface Lens α' x 10^2	α'^2 x 10^4	z'/cm
5	1.878		1.252	197.23	0.165	3.859	14.8948	0.938
4	2.073	0.196	1.060	208.75	0.155	3.269	10.6850	0.947
3	2.296	0.223	0.844	221.58	0.146	2.603	6.7755	0.956
2	2.549	0.252	0.596	234.74	0.138	1.839	3.3816	0.964
1	2.840	0.292	0.312	245.96	0.132	0.964	0.9285	0.971
0	3.154	0.314						
-1	3.465	0.311			Slope	z_o'/cm	C_s'/cm	
-2	3.741	0.276		1.83E-05	-0.003	0.973	26.32	
-3	3.985	0.243						
-4	4.194	0.209						
-5	4.382	0.188						

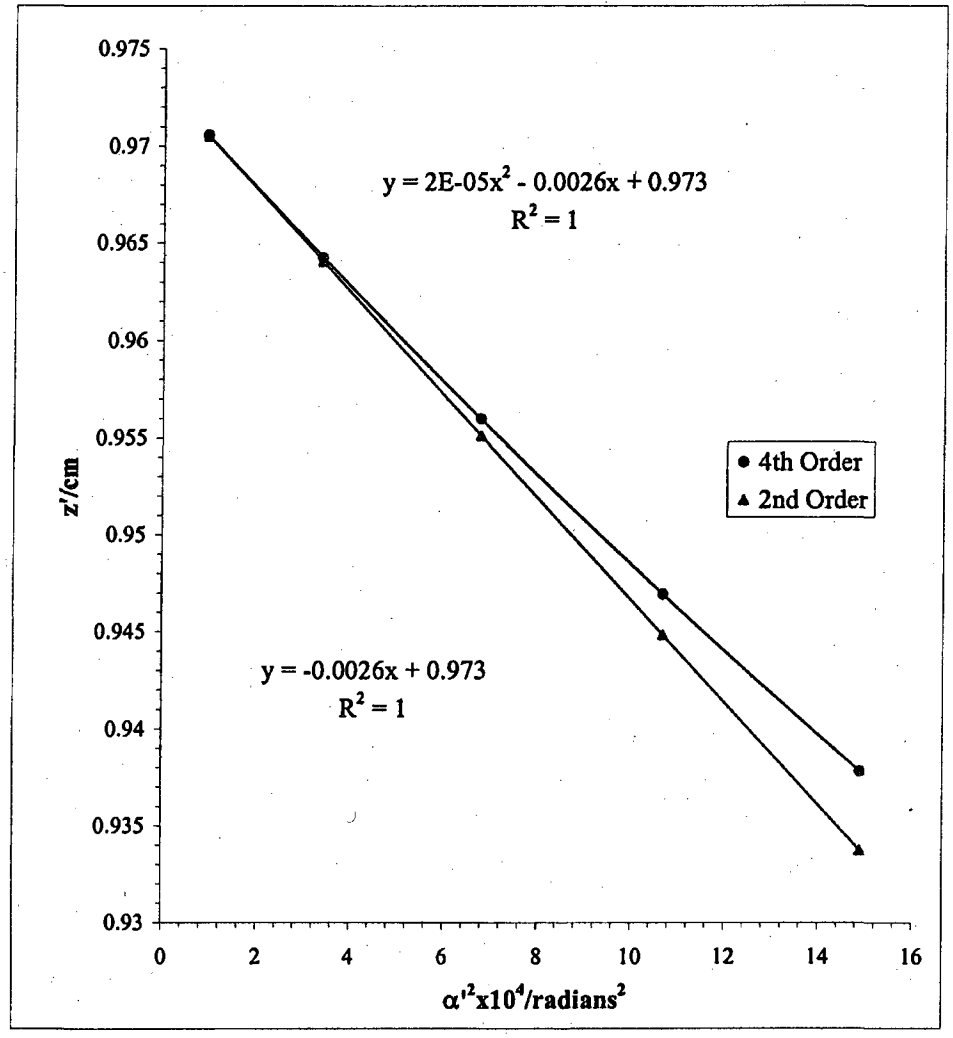

L 5	Swept back Interface Lens						Beam	Voltage	20 kV
Mesh/inch	V Ratio	Mesh	z/cm	e_1/cm	a/cm	z_{sp}/cm	z_0'/cm	C_s'/cm	$z_{sp}-z_o'$
600	0.90	Front	31.27	0.00423	26.42	33.39	0.966	21.30	32.42

Bar location/ units	Shadow Reading X/cm	Spacing Δ/cm	E/cm	$\alpha \times 10^4$	$\alpha' \times 10^2$	$\alpha'^2 \times 10^4$	m	z'/cm	f/cm
7	1.319		1.137	11.218	3.505	12.286	0.03200	0.940	0.972
6	1.488	0.170	0.969	9.615	2.987	8.923	0.03219	0.947	0.977
5	1.655	0.167	0.803	8.013	2.477	6.137	0.03235	0.953	0.982
4	1.820	0.165	0.640	6.410	1.974	3.897	0.03247	0.958	0.985
3	1.983	0.163	0.479	4.808	1.476	2.179	0.03257	0.962	0.988
2	2.144	0.161	0.318	3.205	0.982	0.964	0.03264	0.964	0.990
1	2.304	0.160	0.159	1.603	0.490	0.240	0.03269	0.966	0.991
0	2.463	0.159							
-1	2.622	0.159						g/cm	$(\rho/f_0)^2 = (m_0+1)^4 \alpha'^4$
-2	2.781	0.159							
-3	2.940	0.159						0.909	13.102
-4	3.101	0.160						0.916	9.516
-5	3.262	0.162						0.922	6.545
-6	3.426	0.164						0.926	4.156
-7	3.593	0.167						0.930	2.323
								0.932	1.028
		Slope	m_o	μ_s				0.933	0.256
	1.8E-07	-0.0001	0.03270	-17.95					

f vs $(\rho/f_o)^2$

$S_f = slope_f / f_0$

	$slope_f$	fo/cm	S_f
4.606E-06	-0.00161	0.992	-16.21

g vs $(\rho/f_o)^2$

$S_g = slope_g / f_0$

	$slope_g$	go/cm	S_g
-3.83E-07	-0.00189	0.934	-19.05

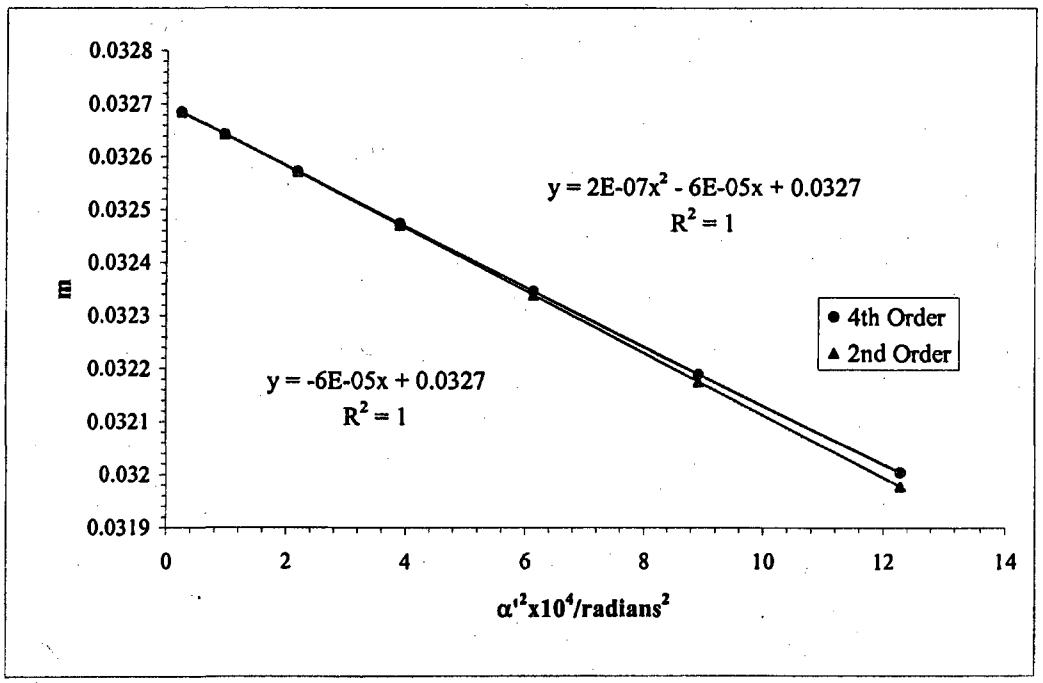

L 5 Swept back Interface Lens							Beam	Voltage	20 kV
Mesh/inch	V Ratio	Mesh	z/cm	e_1/cm	a/cm	z_{sp}/cm	z_0'/cm	C_s'/cm	$z_{sp}-z_o$'
600	0.90	Front	31.27	0.00423	26.42	33.39	0.966	21.30	32.42

Bar location/ units	Shadow Reading Y/cm	Spacing Δ/cm	E/cm	$\alpha \times 10^4$	$\alpha' \times 10^2$	$\alpha'^2 \times 10^4$	m	z'/cm	f/cm
7	3.002		1.156	11.218	3.563	12.694	0.0315	0.939	0.956
6	3.174	0.173	0.984	9.615	3.035	9.209	0.0317	0.947	0.962
5	3.344	0.169	0.816	8.013	2.516	6.329	0.0319	0.953	0.967
4	3.510	0.167	0.650	6.410	2.004	4.016	0.0320	0.958	0.970
3	3.674	0.164	0.486	4.808	1.498	2.245	0.0321	0.962	0.973
2	3.837	0.163	0.323	3.205	0.997	0.993	0.0322	0.964	0.976
1	3.999	0.162	0.161	1.603	0.498	0.248	0.0322	0.966	0.977
0	4.161	0.161							
-1	4.322	0.161						g/cm	$(\rho/f_0)^2 =$
-2	4.484	0.162							$(m_0 + 1)^2 \alpha'^2$
-3	4.646	0.163						0.909	13.506
-4	4.810	0.164						0.916	9.802
-5	4.976	0.166						0.922	6.738
-6	5.143	0.168						0.927	4.277
-7	5.314	0.171						0.930	2.391
								0.933	1.058
								0.934	0.264

	Slope	m_o	μ_s
3.6E-08	-0.0001	0.03	-18.09

f vs $(\rho/f_o)^2$

$S_f = slope_f / f_0$

	$slope_f$	fo/cm	S_f
6.96494E-07	-0.001598	0.977	-16.35

g vs $(\rho/f_o)^2$

$S_g = slope_g / f_0$

	$slope_g$	go/cm	S_g
-3.4E-07	-0.0019	0.935	-19.38

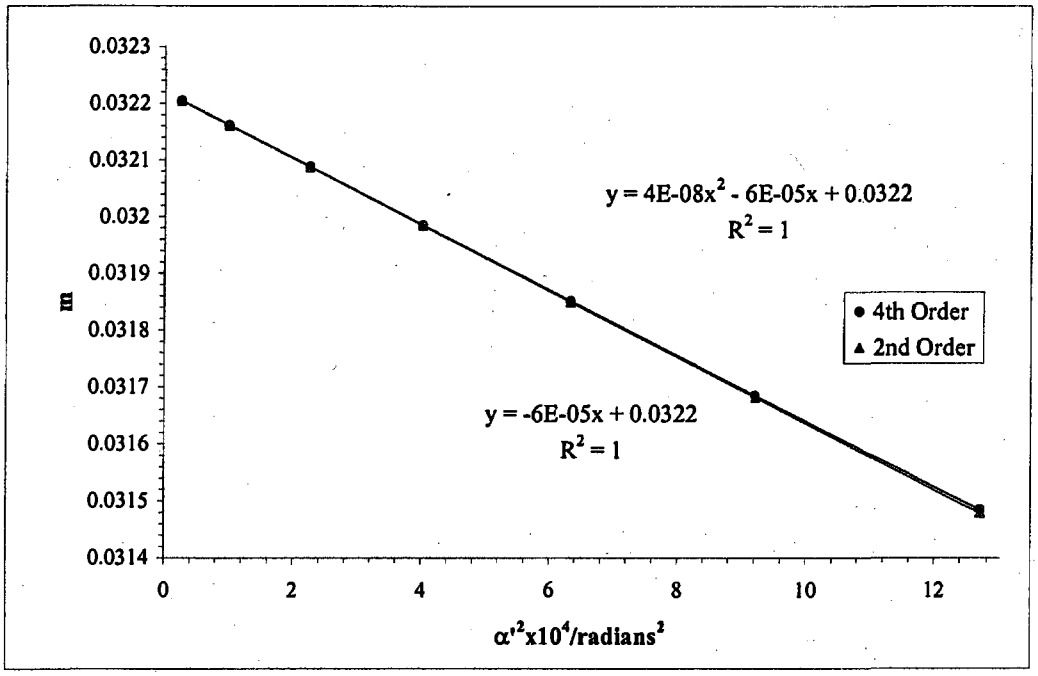

Beam Voltage	Volt Ratio	z/cm	L 5 z_0'/cm	Swept back Interface Lens C_s'/cm
20 kV	0.90	31.27	0.966	21.30

Average of m_o = 0.03246

Average of μ_s = -18.02

Paraxial properties :

f_o = 0.985 cm

g_o = 0.934 cm

S_f = -16.28

S_g = -19.22

Mesh/inch	V Ratio	Mesh	e'_1/cm	d/cm	b/cm		Beam	Voltage	20 kV
2000	0.95	Rear	0.00127	32.77	0.620	US			

Bar location/ units	Shadow Reading X/cm	Spacing Δ/cm	E'/cm	M'	c/cm	L 5 α' x 10^2	Swept back Interface Lens α'^2 x 10^4	z'/cm
4.5	2.671		1.278	-223.60	-0.146	3.9171	15.343	0.766
3.5	2.984	0.313	0.932	-209.57	-0.156	2.8563	8.158	0.775
2.5	3.260	0.276	0.640	-201.45	-0.162	1.9616	3.848	0.782
1.5	3.517	0.258	0.376	-197.19	-0.165	1.1522	1.328	0.785
0.5	3.767	0.250	0.124	-195.40	-0.167	0.3806	0.145	0.787
-0.5	4.015	0.248						
-1.5	4.268	0.254						
-2.5	4.539	0.270			Slope	z_o'/cm	C_s'/cm	
-3.5	4.847	0.308		1.8467E-06	-0.0014	0.787	14.15	
-4.5	5.226	0.380						

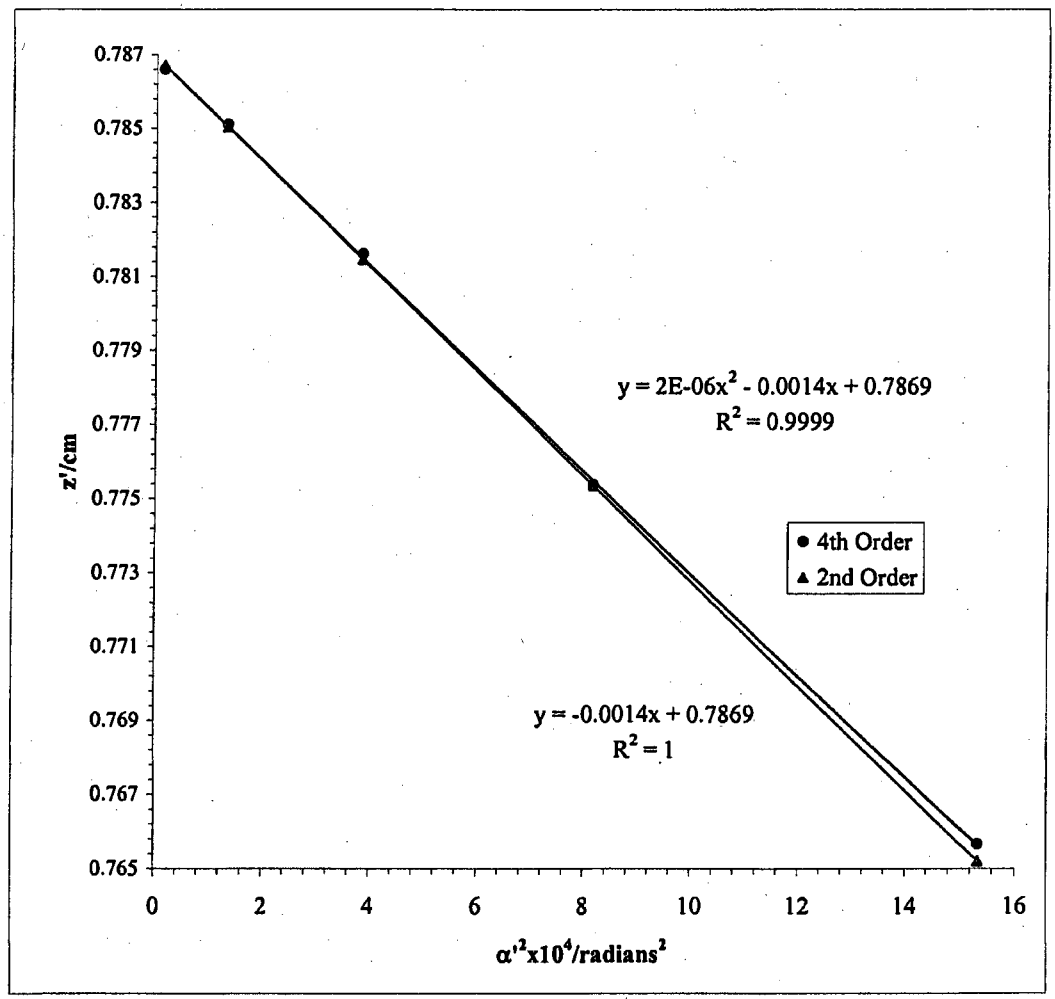

Mesh/inch	V Ratio	Mesh	e'_1/cm	d/cm	h/cm		Beam	Voltage	20 kV
2000	0.95	Rear	0.00127	32.77	0.62	US			

Bar location/ units	Shadow Reading Y/cm	Spacing Δ/cm	E'/cm	M'	c/cm	L 5 Swept back Interface Lens α' x 10^2	α'^2 x 10^4	z'/cm
4.5	1.591		1.265	-221.38	-0.147	3.8785	15.043	0.767
3.5	1.942	0.352	0.927	-208.66	-0.156	2.8440	8.088	0.776
2.5	2.238	0.295	0.639	-201.40	-0.162	1.9611	3.846	0.782
1.5	2.506	0.268	0.375	-196.75	-0.166	1.1496	1.322	0.785
0.5	2.758	0.252	0.124	-195.08	-0.167	0.3800	0.144	0.787
-0.5	3.006	0.248						
-1.5	3.255	0.250						
-2.5	3.516	0.261			Slope	z_o'/cm	C_s'/cm	
-3.5	3.797	0.281		6.52E-06	-0.0014	0.787	14.32	
-4.5	4.121	0.324						

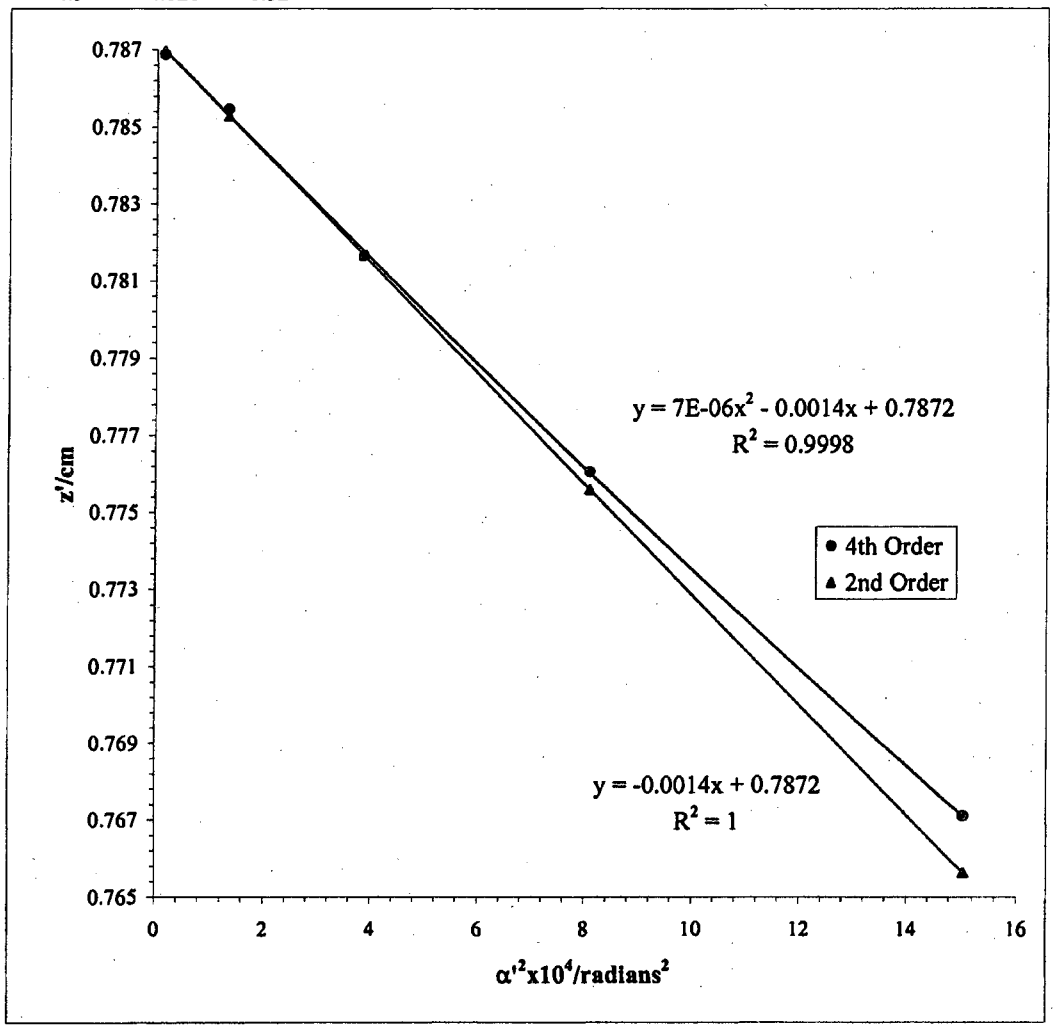

Mesh/inch	V Ratio	Mesh	e'_1/cm	d/cm	b/cm		Beam	Voltage	20 kV
2000	0.95	Rear	0.00127	32.49	0.90	DS			

Bar location/ units	Shadow Reading X/cm	Spacing Δ/cm	E'/cm	M'	c/cm	L 5 Swept back Interface Lens α' x 10^2	α'^2 x 10^4	z'/cm
3.5	1.729		1.202	270.33	0.121	3.6849	13.5785	0.779
2.5	2.016	0.288	0.912	287.13	0.114	2.7962	7.8187	0.786
1.5	2.347	0.330	0.579	303.83	0.107	1.7756	3.1529	0.792
0.5	2.722	0.375	0.200	315.12	0.103	0.6139	0.3769	0.796
-0.5	3.122	0.400						
-1.5	3.504	0.383						
-2.5	3.840	0.335						
-3.5	4.132	0.293						

	Slope	z_o'/cm	C_s'/cm
9.5E-06	-0.00144	0.796	14.37

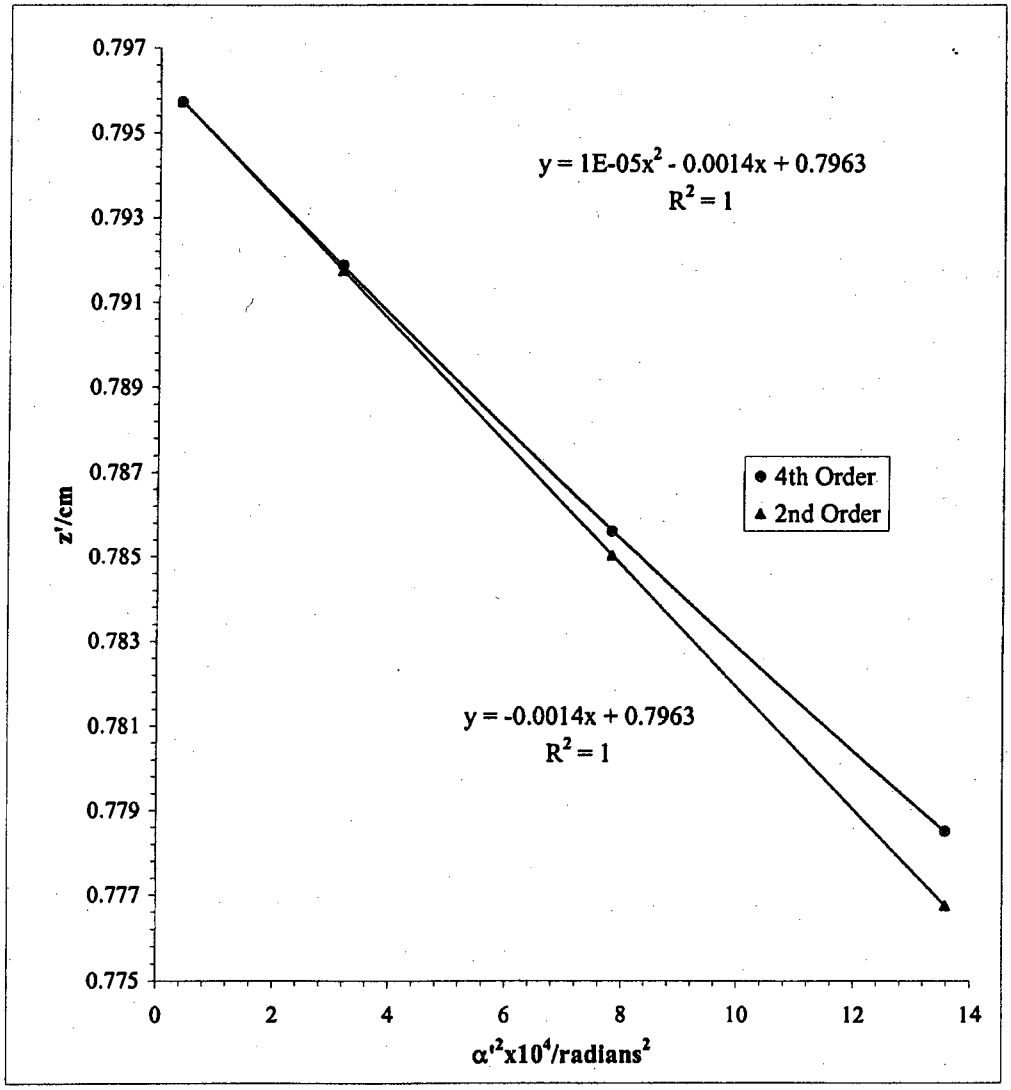

Mesh/inch	V Ratio	Mesh	e'_1/cm	d/cm	b/cm		Beam	Voltage	20 kV
2000	0.95	Rear	0.00127	32.49	0.90	DS			

Bar location/ units	Shadow Reading Y/cm	Spacing Δ/cm	E'/cm	M'	c/cm	L 5 Swept back Interface Lens α' x 10^3	α'^2 x 10^4	z'/cm
8.5	0.6398		2.2154	205.23	0.1591	6.7857	46.0458	0.7401
7.5	0.8139	0.1741	2.0469	214.90	0.1519	6.2709	39.3238	0.7473
6.5	0.9999	0.1860	1.8643	225.84	0.1445	5.7129	32.6377	0.7547
5.5	1.2017	0.2018	1.6650	238.36	0.1369	5.1031	26.0421	0.7623
4.5	1.4266	0.2249	1.4442	252.71	0.1291	4.4277	19.6042	0.7701
3.5	1.6751	0.2485	1.1945	268.72	0.1214	3.6628	13.4164	0.7778
2.5	1.9605	0.2854	0.9095	286.47	0.1138	2.7898	7.7827	0.7854
1.5	2.2902	0.3297	0.5776	303.19	0.1075	1.7719	3.1396	0.7916
0.5	2.6706	0.3804	0.1965	309.43	0.1053	0.6028	0.3634	0.7938
-0.5	3.0636	0.3930						
-1.5	3.4453	0.3818						
-2.5	3.7795	0.3342						
-3.5	4.0640	0.2845			Slope	z_o'/cm	C_1'/cm	
-4.5	4.3150	0.2510		4.05E-06	0.00	0.795964	13.99	
-5.5	4.5316	0.2166						
-6.5	4.7286	0.1969						
-7.5	4.9077	0.1791						
-8.5	5.0706	0.1630						

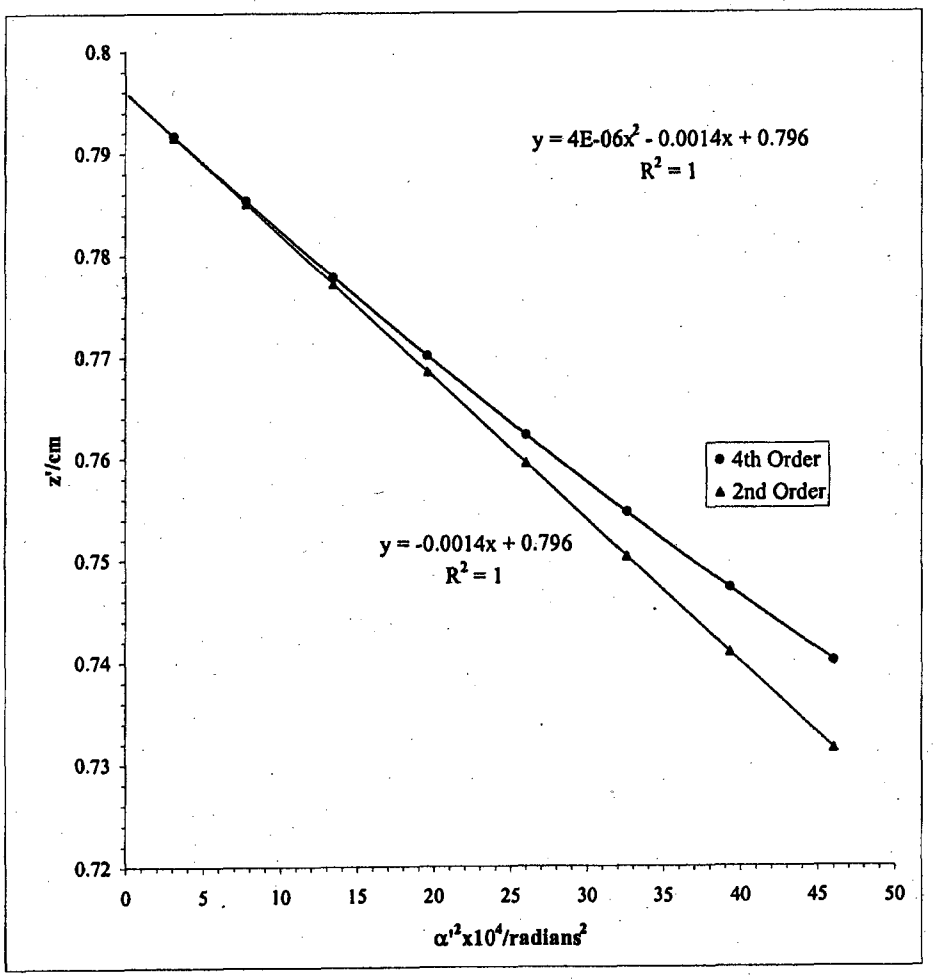

L 5	Swept back Interface Lens						Beam	Voltage	20 kV
Mesh/inch	V Ratio	Mesh	z/cm	e_1/cm	a/cm	z_{sp}/cm	z_0'/cm	C_s'/cm	$z_{sp}-z_o'$
600	0.95	Front	31.27	0.00423	26.42	33.39	0.792	14.21	32.60

Bar location/ units	Shadow Reading X/cm	Spacing Δ/cm	E/cm	$\alpha \times 10^4$	$\alpha' \times 10^2$	$\alpha'^2 \times 10^4$	m	z'/cm	f/cm
6.5	1.353		1.269	10.417	3.890	15.136	0.0268	0.770	0.817
5.5	1.554	0.201	1.068	8.814	3.273	10.715	0.0269	0.776	0.822
4.5	1.752	0.198	0.869	7.212	2.666	7.105	0.0271	0.781	0.825
3.5	1.948	0.196	0.673	5.609	2.065	4.266	0.0272	0.786	0.828
2.5	2.142	0.194	0.480	4.006	1.471	2.164	0.0272	0.789	0.831
1.5	2.335	0.193	0.287	2.404	0.881	0.776	0.0273	0.790	0.832
0.5	2.526	0.192	0.096	0.801	0.293	0.086	0.0273	0.791	0.833
-0.5	2.718	0.191							
-1.5	2.909	0.191						g/cm	$(\rho/f_0)^2 = (m_0+1)^4 \alpha'^4$
-2.5	3.101	0.192							
-3.5	3.295	0.194						0.748	15.974
-4.5	3.491	0.196						0.754	11.309
-5.5	3.689	0.198						0.759	7.499
-6.5	3.89105	0.202						0.763	4.502
		Slope	m_0	μ_4				0.766	2.284
	1.42E-07	-3.79E-05	0.02732	-13.88				0.768	0.819
								0.769	0.091

f vs $(\rho/f_o)^2$

$S_f = slope_f / f_0$

	$slope_f$	fo/cm	S_f
3.84E-06	-0.00106	0.833	-12.73

g vs $(\rho/f_o)^2$

$S_g = slope_g / f_0$

	$slope_g$	go/cm	S_g
-2.43E-07	-0.00129	0.769	-15.45

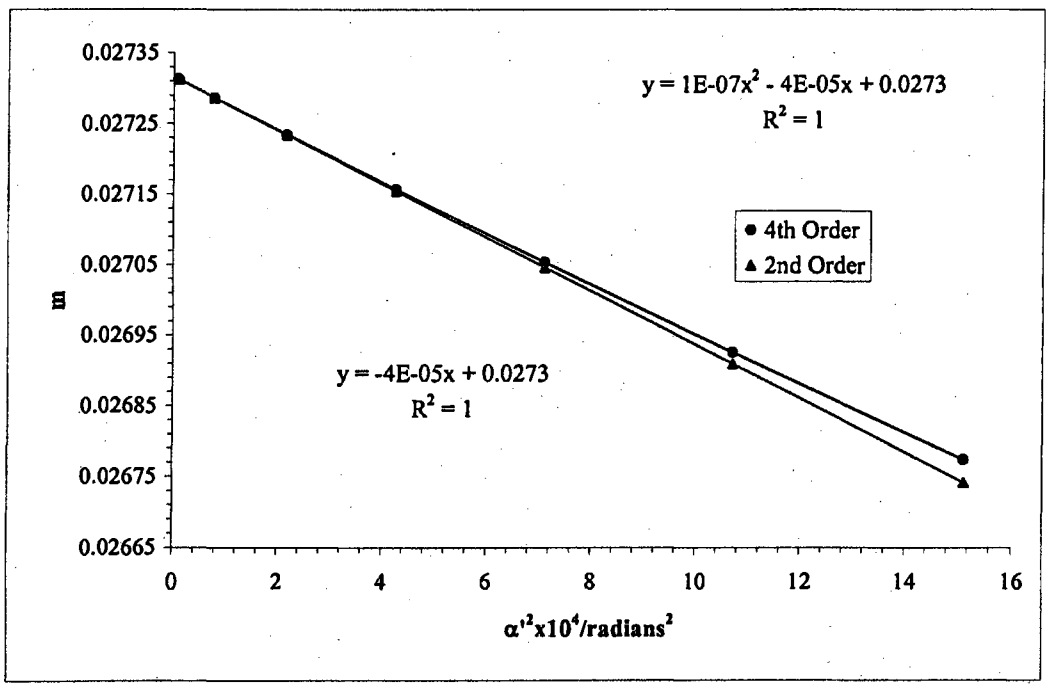

L 5	Swept back Interface Lens						Beam	Voltage	20 kV
Mesh/inch	V Ratio	Mesh	z/cm	e_1/cm	a/cm	z_{sp}/cm	z_0'/cm	C_s'/cm	$z_{sp}-z_o'$
600	0.95	Front	31.27	0.00423	26.42	33.39	0.792	14.21	32.60

Bar location/ units	Shadow Reading Y/cm	Spacing Δ/cm	E/cm	α x 10^4	α' x 10^2	α'^{2} x 10^4	m	z'/cm	f/cm
6.5	1.322		1.292	10.417	3.960	15.678	0.0263	0.769	0.803
5.5	1.526	0.205	1.087	8.814	3.333	11.106	0.0264	0.776	0.807
4.5	1.728	0.202	0.885	7.212	2.715	7.369	0.0266	0.781	0.810
3.5	1.927	0.199	0.686	5.609	2.104	4.426	0.0267	0.785	0.813
2.5	2.124	0.197	0.489	4.006	1.499	2.246	0.0267	0.788	0.815
1.5	2.320	0.196	0.293	2.404	0.898	0.806	0.0268	0.790	0.817
0.5	2.516	0.195	0.097	0.801	0.299	0.089	0.0268	0.791	0.818
-0.5	2.710	0.195							
-1.5	2.906	0.195						g/cm	$(\rho/f)^2 = (m+1)^2 \alpha'^2$
-2.5	3.102	0.196							
-3.5	3.299	0.197						0.748	16.514
-4.5	3.498	0.199						0.754	11.702
-5.5	3.700	0.202						0.760	7.766
-6.5	3.905	0.205						0.764	4.665
								0.767	2.368
		Slope	m_o	μ_s				0.769	0.849
	1.2E-07	-3.4E-05	0.026808	-12.60				0.770	0.094

f vs $(\rho/f_o)^2$

$S_f = slope_f / f_0$

	$slope_f$	fo/cm	S_f
3.2E-06	-0.0009	0.818	-11.52

g vs $(\rho/f_o)^2$

$S_g = slope_g / f_0$

	$slope_g$	go/cm	S_g
-2.7E-07	-0.0013	0.770	-15.85

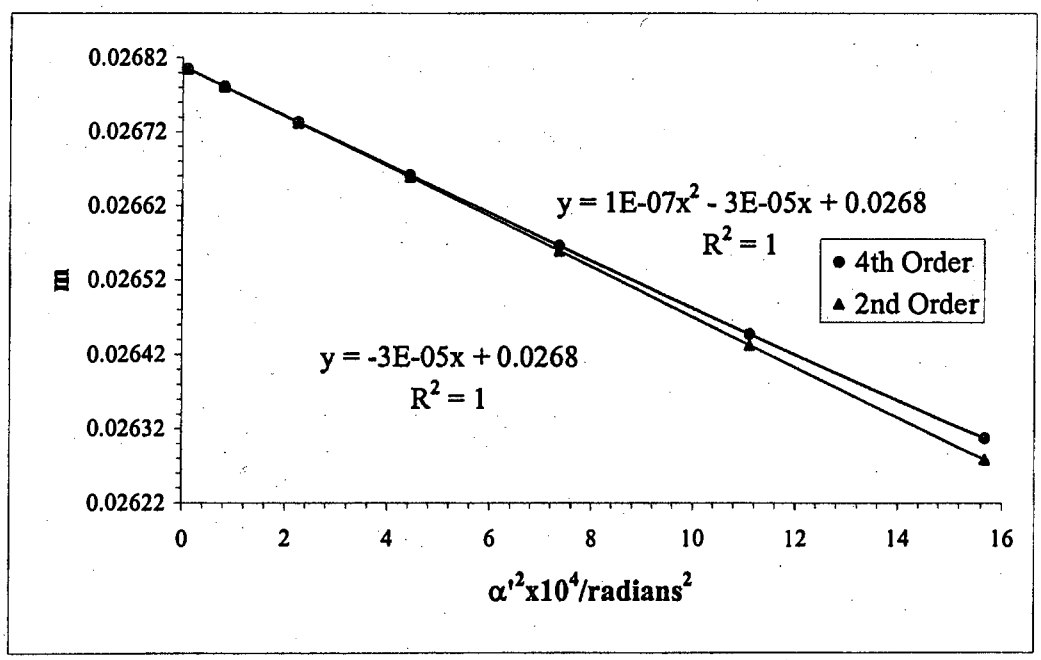

Beam Voltage	Volt Ratio	z/cm	L 5 z_0'/cm	Swept back Interface Lens C_s'/cm
20 kV	0.95	31.27	0.792	14.21

Average of m_o = 0.0271

Average of μ_s = -13.24

Paraxial properties :

f_o = 0.825 cm

g_o = 0.769 cm

S_f = -12.12

S_g = -15.65

Mesh/incl	V Ratio	Mesh	e'_1/cm	d/cm	b/cm		Beam	Voltage	20 kV
2000	1.00	Rear	0.0013	32.92	0.470	US			

Bar location/ units	Shadow Reading X/cm	Spacing Δ/cm	E'/cm	M'	c/cm	L 5 Swept back Interface Lens $\alpha' \times 10^2$	$\alpha'^2 \times 10^4$	z'/cm
5	1.929		1.239	-195.19	-0.168	3.7845	14.323	0.638
4	2.202	0.273	0.966	-190.12	-0.172	2.9493	8.699	0.642
3	2.458	0.256	0.708	-185.89	-0.176	2.1630	4.679	0.646
2	2.701	0.243	0.466	-183.45	-0.178	1.4232	2.026	0.648
1	2.935	0.234	0.232	-182.39	-0.180	0.7075	0.501	0.649
0	3.166	0.231						
-1	3.398	0.233						
-2	3.633	0.235						
-3	3.874	0.242						
-4	4.133	0.259						
-5	4.408	0.274						

Slope	z_o'/cm	C_s'/cm
9.1E-06	-0.001	0.650	10.26

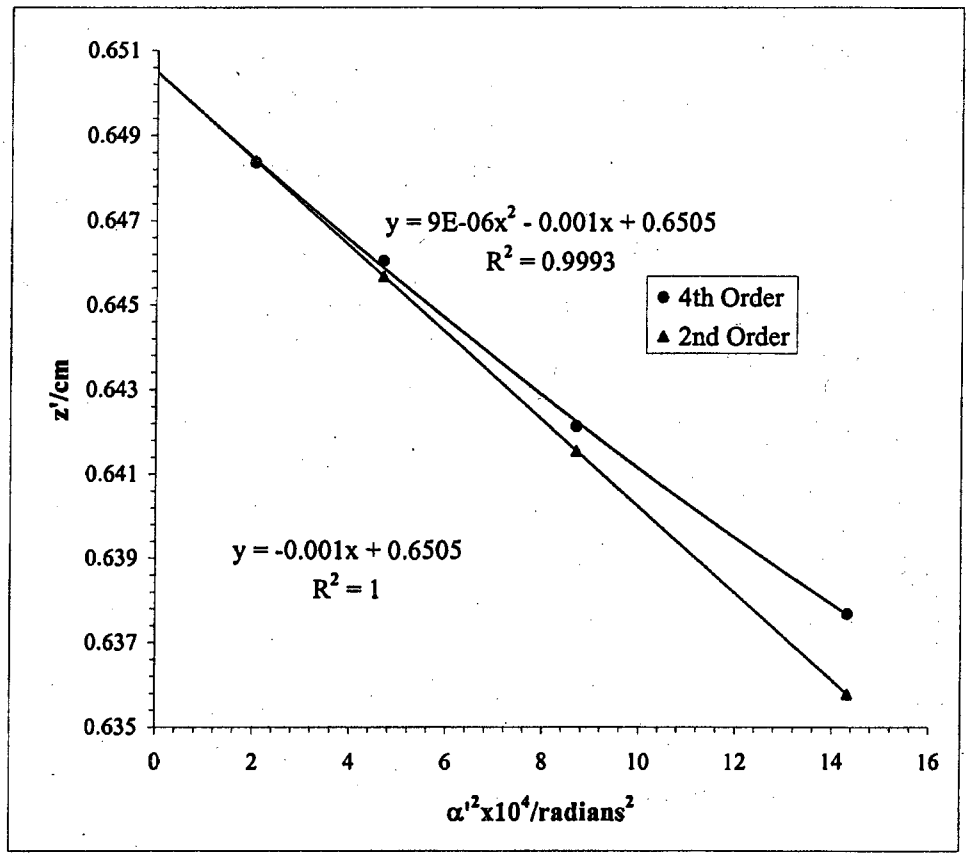

Mesh/inch	V Ratio	Mesh	e'_1/cm	d/cm	b/cm		Beam	Voltage	20 kV
2000	0.70	Rear	0.00127	32.92	0.47	US			

Bar location/ units	Shadow Reading Y/cm	Spacing Δ/cm	E'/cm	M'	c/cm	L 5 α' x 10^2	Swept back Interface Lens α'^2 x 10^4	z'/cm
7.5	0.622		2.141	-224.80	-0.146	6.5336	42.687	0.616
6.5	1.057	0.435	1.714	-207.65	-0.158	5.2323	27.377	0.628
5.5	1.392	0.335	1.380	-197.62	-0.166	4.2146	17.763	0.636
4.5	1.680	0.288	1.093	-191.28	-0.171	3.3382	11.144	0.641
3.5	1.941	0.261	0.832	-187.17	-0.175	2.5409	6.456	0.645
2.5	2.188	0.247	0.585	-184.20	-0.178	1.7862	3.191	0.648
1.5	2.428	0.240	0.345	-181.19	-0.181	1.0544	1.112	0.651
0.5	2.657	0.229	0.115	-181.85	-0.180	0.3527	0.124	0.650
-0.5	2.888	0.231						
-1.5	3.118	0.230						
-2.5	3.358	0.240						
-3.5	3.605	0.247						
-4.5	3.866	0.261						
-5.5	4.153	0.286				Slope	z_0'/cm	C_s'/cm
-6.5	4.485	0.333		1.92E-06	-9.074E-04	0.651	9.07	
-7.5	4.904	0.419						

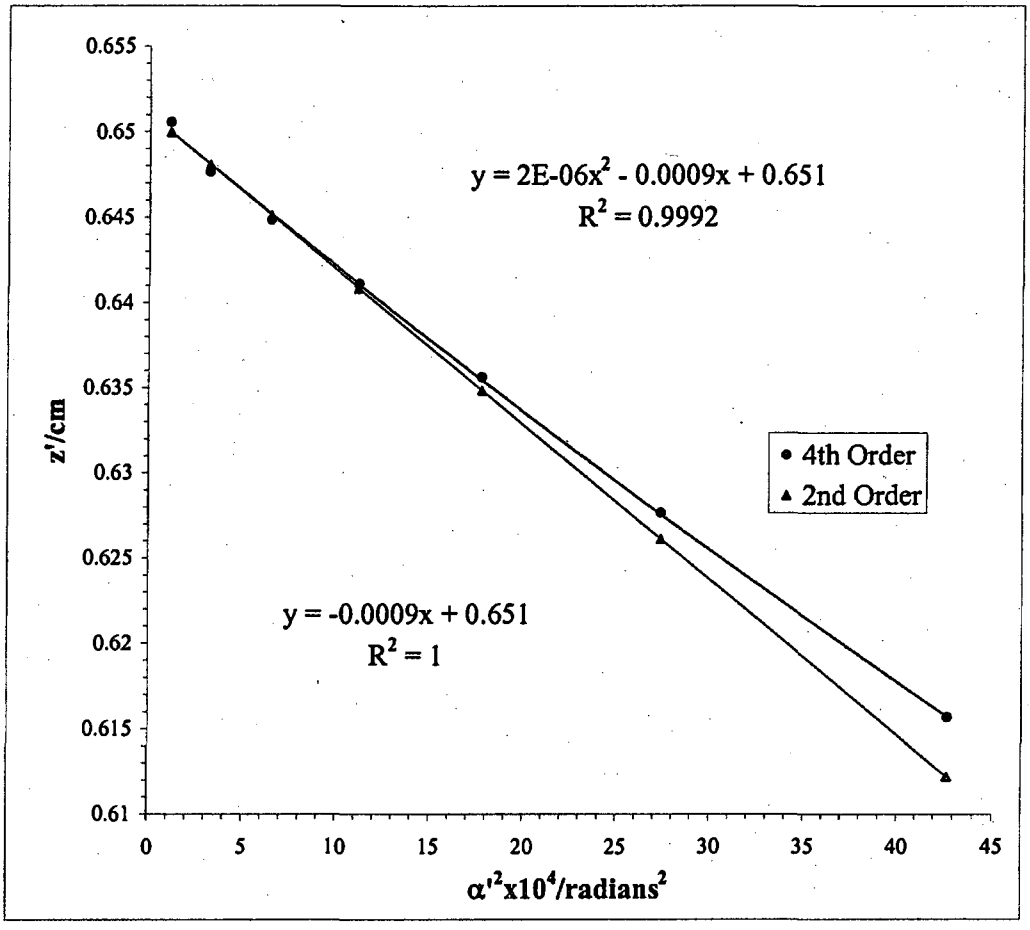

Mesh/inch	V Ratio	Mesh	e'_1/cm	d/cm	b/cm		Beam	Voltage	20 kV
2000	1.00	Rear	0.00127	32.62	0.77	DS			

Bar location/ units	Shadow Reading X/cm	Spacing Δ/cm	E'/cm	M'	c/cm	L 5 Swept back Interface Lens $\alpha' \times 10^2$	$\alpha'^2 \times 10^4$	z'/cm
6	0.6881		1.8372	241.10	0.1358	5.6094	31.4654	0.6363
5	0.9281	0.2400	1.6018	252.25	0.1298	4.8916	23.9279	0.6423
4	1.1948	0.2666	1.3405	263.88	0.1241	4.0944	16.7641	0.6481
3	1.4919	0.2972	1.0514	275.95	0.1186	3.2117	10.3152	0.6535
2	1.8190	0.3270	0.7290	287.01	0.1140	2.2274	4.9611	0.6581
1	2.1779	0.3590	0.3747	295.07	0.1109	1.1450	1.3111	0.6612
0	2.5559	0.3780						
-1	2.9274	0.3715						
-2	3.2770	0.3496						
-3	3.5947	0.3177			Slope	z_0'/cm	C_s'/cm	
-4	3.8758	0.2811		1.5E-06	-0.0009	0.662	8.77	
-5	4.13174	0.2559						
-6	4.36247	0.2307						

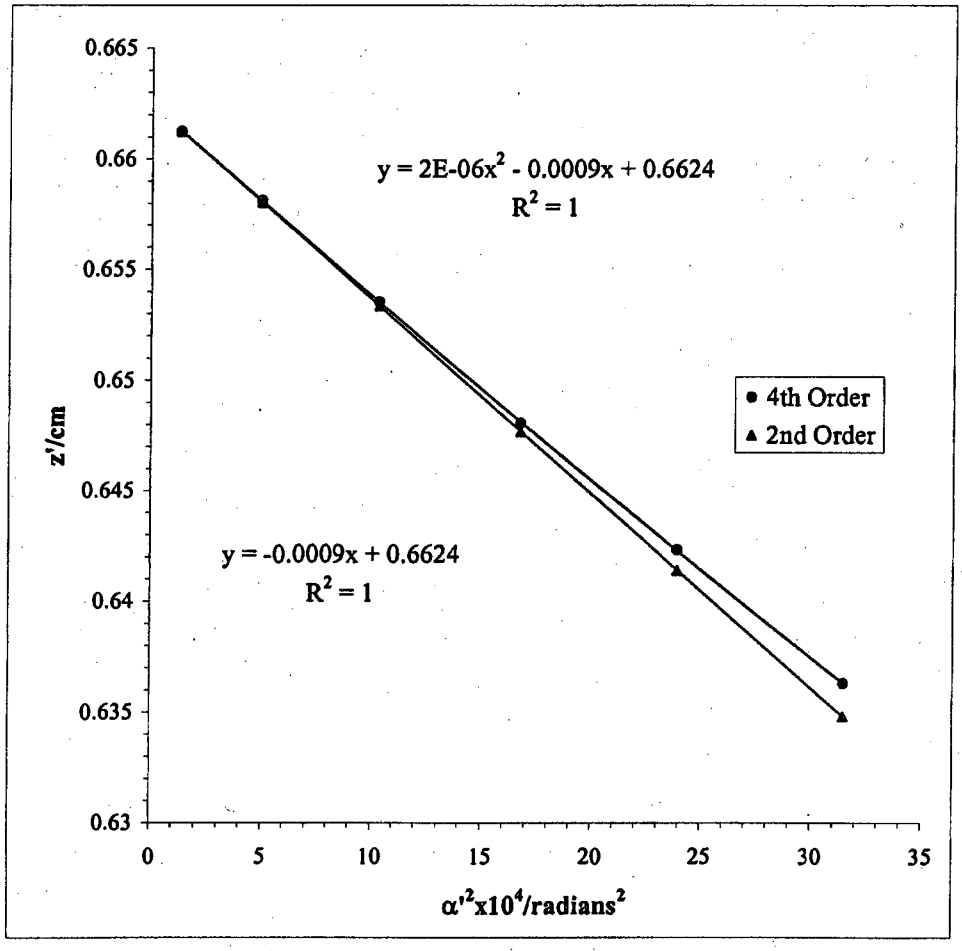

Mesh/inch	V Ratio	Mesh	e'_1/cm	d/cm	b/cm		Beam	Voltage	20 kV
2000	1.00	Rear	0.00127	32.62	0.77	DS			

Bar location/ units	Shadow Reading X/cm	Spacing Δ/cm	E'/cm	M'	c/cm	L 5 Swept back Interface Lens α' x 10^2	α'^2 x 10^4	z'/cm
8	0.921		2.2308	219.56	0.1492	6.8083	46.3525	0.6229
7	1.112	0.1911	2.0327	228.65	0.1433	6.2050	38.5020	0.6289
6	1.318	0.2060	1.8186	238.66	0.1372	5.5524	30.8288	0.6349
5	1.543	0.2250	1.5867	249.88	0.1311	4.8454	23.4783	0.6411
4	1.794	0.2511	1.3279	261.40	0.1253	4.0558	16.4491	0.6469
3	2.071	0.2775	1.0427	273.68	0.1196	3.1852	10.1458	0.6525
2	2.389	0.3180	0.7226	284.48	0.1151	2.2076	4.8736	0.6571
1	2.738	0.3481	0.3719	292.81	0.1118	1.1362	1.2910	0.6604
0	3.106	0.3681						
-1	3.481	0.3756			Slope	z_0'/cm	C_s'/cm	
-2	3.835	0.3534		1.8E-06	-0.000918	0.66	9.18	
-3	4.157	0.3223						
-4	4.450	0.2928						
-5	4.716	0.2666						
-6	4.955	0.2387						
-7	5.177	0.2223						
-8	5.382	0.2050						

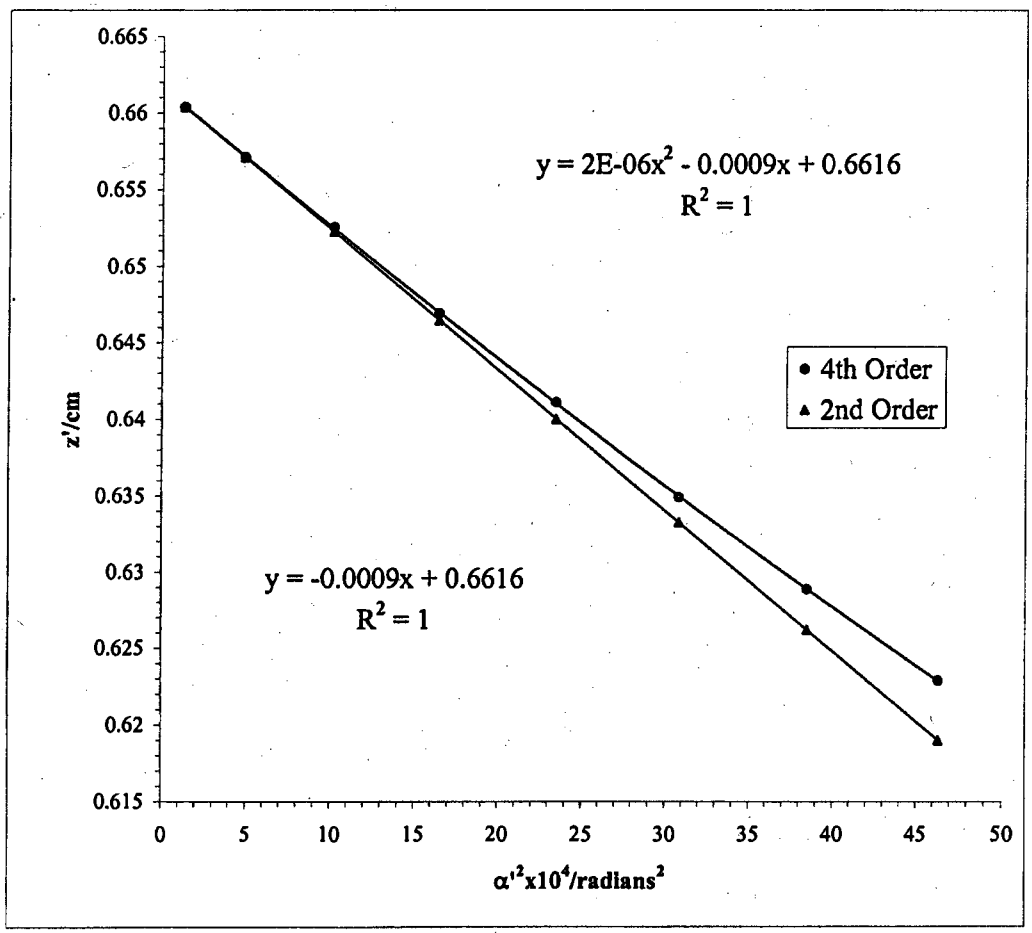

L 5	Swept back Interface Lens						Beam	Voltage	20 kV
Mesh/inch	V Ratio	Mesh	z/cm	e_1/cm	a/cm	z_{sp}/cm	z_0'/cm	C_s'/cm	$z_{sp}-z_o'$
600	1.00	Front	31.27	0.0042	26.42	33.39	0.656	9.32	32.73

Bar location/ units	Shadow Reading X/cm	Spacing Δ/cm	E/cm	$\alpha \times 10^4$	$\alpha' \times 10^2$	$\alpha'^2 \times 10^4$	m	z'/cm	f/cm
5	1.795		1.139	8.013	3.478	12.095	0.02304	0.645	0.706
4	2.024	0.229	0.906	6.410	2.769	7.666	0.02315	0.649	0.709
3	2.251	0.227	0.677	4.808	2.069	4.279	0.02324	0.652	0.712
2	2.476	0.225	0.450	3.205	1.375	1.892	0.02330	0.655	0.714
1	2.701	0.225	0.225	1.603	0.687	0.471	0.02334	0.656	0.715
0	2.925	0.224							
-1	3.150	0.225						g/cm	$(\rho/f_0)^2 = (m_0+1)^2 \alpha'^2$
-2	3.377	0.226							
-3	3.605	0.229						0.629	12.666
-4	3.837	0.232						0.633	8.028
-5	4.072	0.235						0.636	4.481
								0.638	1.981
		Slope	m_o	μ_s				0.639	0.494
	8.9E-08	-3E-05	0.02336	-11.63					

f vs $(\rho/f_o)^2$

$S_f = slope_f / f_0$

$slope_f$	fo/cm	S_f
2.47852E-06	-0.0008	0.715	-10.83

g vs $(\rho/f_o)^2$

$S_g = slope_g / f_0$

$slope_g$	go/cm	S_g
-1.338E-07	-0.00085	0.640	-11.93

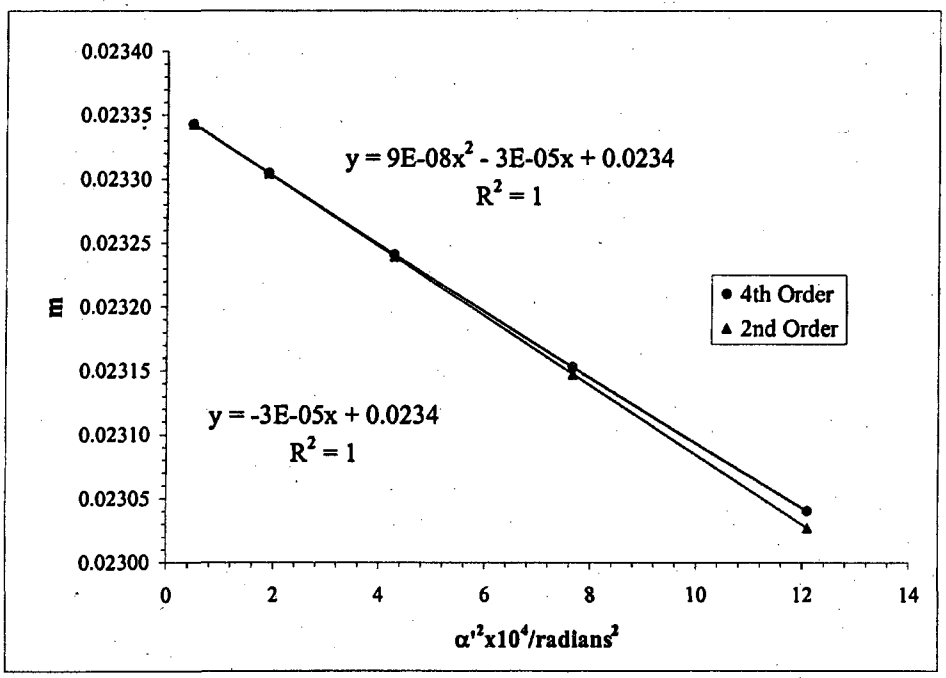

L 5	Swept back Interface Lens						Beam	Voltage	20 kV
Mesh/inch	V Ratio	Mesh	z/cm	e_1/cm	a/cm	z_{sp}/cm	z_0'/cm	C_s'/cm	$z_{sp}-z_o'$
600	1.00	Front	31.27	0.00423	26.42	33.39	0.656	9.32	32.73

Bar location/ units	Shadow Reading Y/cm	Spacing Δ/cm	E/cm	α x 10^4	α' x 10^3	α'^2 x 10^4	m	z'/cm	f/cm
5	1.664		1.156	8.013	3.532	12.474	0.02269	0.645	0.695
4	1.900	0.236	0.921	6.410	2.813	7.914	0.02279	0.649	0.698
3	2.133	0.233	0.688	4.808	2.103	4.422	0.02286	0.652	0.700
2	2.365	0.231	0.458	3.205	1.399	1.956	0.02292	0.655	0.702
1	2.594	0.229	0.229	1.603	0.698	0.488	0.02295	0.656	0.703
0	2.823	0.229							
-1	3.051	0.228						g/cm	$(\rho/f_0)^2 =$
-2	3.280	0.229							$(m_0+1)^2\alpha'^2$
-3	3.510	0.230						0.629	13.046
-4	3.742	0.232						0.633	8.279
-5	3.977	0.235						0.636	4.626
								0.638	2.047
		Slope	m_0	μ_x				0.640	0.510
	6.5E-08	0.0000	0.02296	-9.95					

f vs $(\rho/f_o)^2$

S_f = slope$_f$ / f_0

	slope$_f$	fo/cm	S_f
1.78391E-06	-0.00065	0.703	-9.23

g vs $(\rho/f_o)^2$

S_g = slope$_g$ / f_0

	slope$_g$	go/cm	S_g
-1.30891E-07	-0.00086	0.640	-12.23

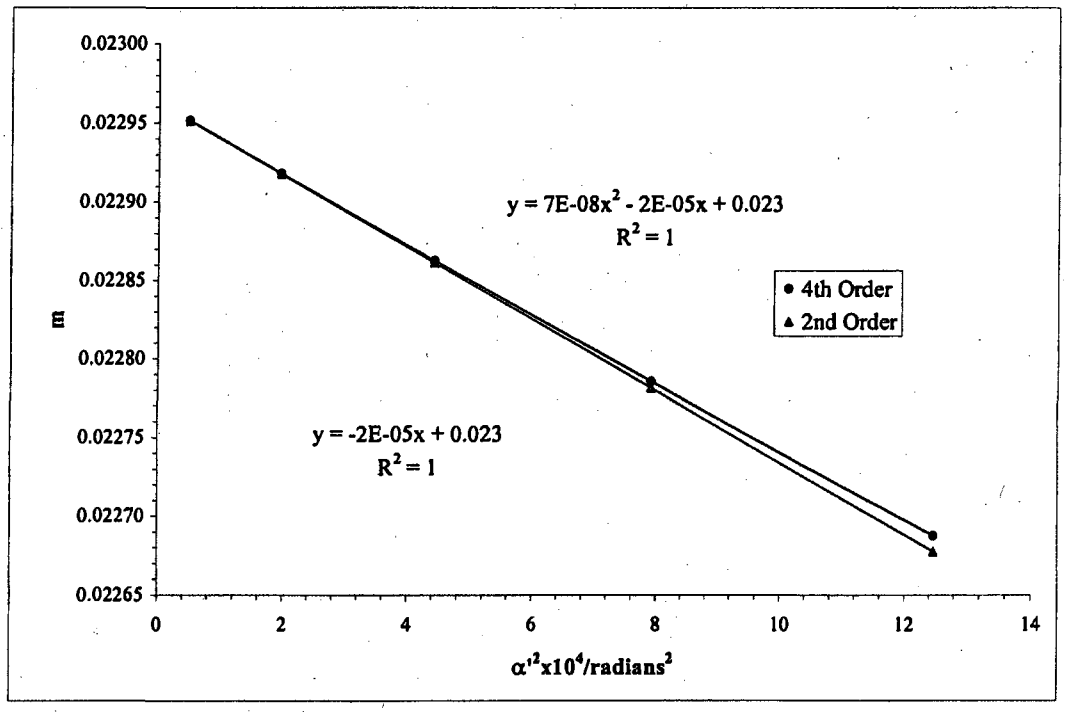

Beam Voltage	Volt Ratio	z/cm	L 5 z_0'/cm	Swept back Interface Lens C_s'/cm
20 kV	1.00	31.27	0.656	9.32

Average of m_0 = 0.0232

Average of μ_s = -10.79

Paraxial properties :

f_o = 0.709 cm

g_o = 0.640 cm

S_f = -10.03

S_g = -12.08

Appendix B. Derivation of the Magnetic Lenses Chromatic Aberration Coefficients C_f, C_g, μ_C, and C_C' from the Paraxial Model's Focal Length f_0, Focal Distance g_0 and Magnification m_0 Equations for the lenses L_1 and L_2.

Chromatic Coefficient C_f

Start with the paraxial focal length Eq.(9.7b) for the magnetic lens in Chapter 9

$$f_0 = \frac{1}{\tilde{\omega}\sin(\tilde{\omega}S)}. \tag{B.1}$$

The $\tilde{\omega}$ term $= \frac{\omega}{v}$ and v is the velocity of the electron equal to $\sqrt{\frac{2gV}{m}}$. Inverting Eq. (B.1) gives

$$\frac{1}{f_0} = \tilde{\omega}\sin(\tilde{\omega}S). \tag{B.2}$$

Taking the log on both sides of Eq. (B.2) gives

$$\begin{aligned} \ln\left(\frac{1}{f_0}\right) &= \ln\tilde{\omega} + \ln\left[\sin(\tilde{\omega}S)\right] \\ -\ln f_0 &= \ln\tilde{\omega} + \ln\left[\sin(\tilde{\omega}S)\right] \end{aligned} \tag{B.3}$$

Take the derivative of both sides of Eq. (B.3) gives

$$-\frac{\Delta f_0}{f_0} = \frac{\Delta\tilde{\omega}}{\tilde{\omega}} + \frac{\Delta\left[\sin(\tilde{\omega}S)\right]}{\sin(\tilde{\omega}S)} \tag{B.4}$$

The derivative of $\Delta(\tilde{\omega})$ is given by

$$\begin{aligned} \Delta(\tilde{\omega}) = \Delta\left(\frac{\omega}{v}\right) = \omega\Delta\left(v^{-1}\right) = -\omega v^{-2}\Delta v = -\frac{\omega}{v^2}\left[\frac{1}{2}\left(\frac{2eV}{m}\right)^{-1/2}\frac{2e}{m}\frac{\Delta V}{V}\right] \\ \Delta(\tilde{\omega}) = -\frac{\tilde{\omega}}{2}\frac{\Delta V}{V} \end{aligned} \tag{B.5}$$

Substituting Eq.(B.5) into Eq. (B.4) gives

$$-\frac{\Delta f_0}{f_0}=\frac{\Delta\tilde{\omega}}{\tilde{\omega}}+\frac{\Delta\left[\sin(\tilde{\omega}S)\right]}{\sin(\tilde{\omega}S)}=\frac{\Delta\tilde{\omega}}{\tilde{\omega}}+\frac{\cos(\tilde{\omega}S)}{\sin(\tilde{\omega}S)}S\Delta(\tilde{\omega})$$
$$-\frac{\Delta f_0}{f_0}=-\frac{\cancel{\tilde{\omega}}}{2\cancel{\tilde{\omega}}}\frac{\Delta V}{V}-\frac{\cos(\tilde{\omega}S)}{\sin(\tilde{\omega}S)}S\left(\frac{\tilde{\omega}}{2}\frac{\Delta V}{V}\right) \qquad \text{(B.6)}$$

Rearrange Eq. (B.6)

$$\frac{\Delta f_0}{f_0}=\frac{1}{2}\left[1+\frac{\tilde{\omega}S}{\tan(\tilde{\omega}S)}\right]\frac{\Delta V}{V}. \qquad \text{(B.7)}$$

Comparison with the definition of the chromatic aberration coefficient C_f in Eq. (3.24a) in Chapter 3 repeated below,

$$\frac{\Delta f_0}{f_0}=C_f\frac{\Delta V}{V} \qquad \text{(B.8)}$$

with Eq. (B.7) shows that the two equation are equivalent and that the C_f term can be expressed as

$$C_f=\frac{1}{2}\left(1+\frac{\tilde{\omega}S}{\tan(\tilde{\omega}S)}\right). \qquad \text{(B.9)}$$

This becomes the model equation for the aberration coefficient C_f for the magnetic lenses, L_1 and L_2, and is the same as Eq. (9.9a) in Chapter 9.

Coefficient C_g

The chromatic aberration C_g is found the same way the aberration coefficient C_f was found above. Start with the paraxial focal distance equation Eq.(9.7c) in Chapter 9 rewritten below

$$g_0 = \frac{S}{2} + \frac{1}{\tilde{\omega}\tan\tilde{\omega}S}. \tag{B.10}$$

Subtract $S/2$ from both sides and invert both sides of Eq. (B.10).

$$\left(g_0 - \frac{S}{2}\right)^{-1} = \tilde{\omega}\tan\left(\tilde{\omega}S\right) \tag{B.11}$$

Take the log on both sides of Eq. (B.11) giving

$$-\ln\left(g - \frac{S}{2}\right) = \ln\tilde{\omega} + \ln\tan\left(\tilde{\omega}S\right) \tag{B.12}$$

Take the derivative of both sides of Eq. (B.12)

$$\begin{aligned} -\Delta g_0\left(g_0 - \frac{S}{2}\right)^{-1} &= \frac{\Delta\tilde{\omega}}{\tilde{\omega}} + \frac{\Delta\tan\left(\tilde{\omega}S\right)}{\tan\left(\tilde{\omega}S\right)} \\ -\Delta g_0\left(g_0 - \frac{S}{2}\right)^{-1} &= \frac{\Delta\tilde{\omega}}{\tilde{\omega}} + \frac{\sec^2\left(\tilde{\omega}S\right)}{\tan\left(\tilde{\omega}S\right)} S\Delta\left(\tilde{\omega}\right) \end{aligned} \tag{B.13}$$

Substitute the derivative of $\Delta\tilde{\omega}$ given by Eq. (B.5), back into Eq.(B.13) and rearrange to give

$$\begin{aligned} -\Delta g_0\left(g_0 - \frac{S}{2}\right)^{-1} &= -\frac{\cancel{2}\tilde{\omega}}{2\cancel{\tilde{\omega}}}\frac{\Delta V}{V} + \frac{\sec^2\left(\tilde{\omega}S\right)}{\tan\left(\tilde{\omega}S\right)} S\left(-\frac{\tilde{\omega}}{2}\frac{\Delta V}{V}\right) \\ \Delta g_0\left(g_0 - \frac{S}{2}\right)^{-1} &= \frac{1}{2}\left[1 + \frac{\tilde{\omega}S}{\cos\left(\tilde{\omega}S\right)\sin\left(\tilde{\omega}S\right)}\right]\frac{\Delta V}{V} \end{aligned} \tag{B.14}$$

Multiply and divide both sides of Eq. (B.14) respectively by $\left(g_0 - \frac{S}{2}\right)^2$ and f_0 and rearrange to give

$$
\begin{aligned}
\frac{\Delta g_0}{f_0} &= \left(g_0 - \frac{S}{2}\right)\frac{1}{f_0}\frac{1}{2}\left[1 + \frac{\tilde{\omega}S}{\cos(\tilde{\omega}S)\sin(\tilde{\omega}S)}\right]\frac{\Delta V}{V} \\
\frac{\Delta g_0}{f_0} &= \frac{1}{\tilde{\omega}\tan(\tilde{\omega}S)}\frac{\tilde{\omega}\sin(\tilde{\omega}S)}{1}\frac{1}{2}\left[1 + \frac{\tilde{\omega}S}{\cos(\tilde{\omega}S)\sin(\tilde{\omega}S)}\right]\frac{\Delta V}{V} \\
\frac{\Delta g_0}{f_0} &= \cos(\tilde{\omega}S)\frac{1}{2}\left[1 + \frac{\tilde{\omega}S}{\cos(\tilde{\omega}S)\sin(\tilde{\omega}S)}\right]\frac{\Delta V}{V} \\
\frac{\Delta g_0}{f_0} &= \frac{1}{2}\left[\cos(\tilde{\omega}S) + \frac{\tilde{\omega}S}{\sin(\tilde{\omega}S)}\right]\frac{\Delta V}{V}
\end{aligned}
\tag{B.15}
$$

Comparing Eq. (3.24b) in Chapter 3, repeated below,

$$
\frac{\Delta g_0}{f_0} = C_g \frac{\Delta V}{V} \tag{B.16}
$$

with Eq. (B.15), shows the two equations are equivalent and the C_g term can be

expressed as

$$
C_g = \frac{1}{2}\left(\cos(\tilde{\omega}S) + \frac{\tilde{\omega}S}{\sin(\tilde{\omega}S)}\right). \tag{B.17}
$$

This is the same expression as Eq.(9.9b) in Chapter 9.

Coefficient μ_{c_1}

Start with the paraxial expression Eq. (2.2) from Chapter 2 given below and rearrange solving for m_0

$$z = g_0 + \frac{f_0}{m_0}$$
$$m_0 = \frac{f_0}{z - g_0} \tag{B.18}$$

where z is the object distance. Take the log and then derivative on both sides of Eq. (B.18) to get

$$\ln m_0 = \ln f_0 - \ln(z - g_0)$$
$$\frac{\Delta m_0}{m_0} = \frac{\Delta f_0}{f_0} - \frac{(-\Delta g_0)}{z - g_0} \tag{B.19}$$

Multiply top and bottom of the last term in Eq. (B.19) by f_0.

$$\frac{\Delta m_0}{m_0} = \frac{\Delta f_0}{f_0} + \frac{\Delta g_0}{f_0}\left(\frac{f_0}{z - g_0}\right) \tag{B.20}$$

Substituting Eq. (B.8) and (B.16) into Eq. (B.20) and rearrange to get

$$\frac{\Delta m_0}{m_0} = C_f \frac{\Delta V}{V} + C_g \frac{\Delta V}{V}\left(\frac{f_0}{z - g_0}\right)$$
$$\frac{\Delta m_0}{m_0} = \left[C_f + C_g\left(\frac{f_0}{z - g_0}\right)\right]\frac{\Delta V}{V} \tag{B.21}$$

From the definition of Eq. 3.18(b) in Chapter 3, rewritten below,

$$\frac{\Delta m_0}{m_0} = \mu_C \frac{\Delta V}{V} \tag{B.22}$$

we find

$$\mu_C = \left[C_f + C_g \left(\frac{f_0}{z - g_0} \right) \right] \tag{B.23}$$

Coefficient *Cc'*

Start with Eq. (3.12b)' from Chapter 3 rewritten below

$$z_0' = g_0 + f_0 m_0 . \tag{B.24}$$

Take the derivatives on both sides of Eq. (B.24).

$$\Delta z_0' = \Delta g_0 + m_0 \Delta f_0 + f_0 \Delta m_0 \tag{B.25}$$

Substitute the functions of $\Delta g_0, \Delta f_0$, and Δm_o from Eq. (B.16), (B.8), and (B.22) into Eq. (B.25) to get

$$\Delta z_0' = f_0 C_g \frac{\Delta V}{V} + m_0 f_0 C_f \frac{\Delta V}{V} + f_0 m_0 \mu_C \frac{\Delta V}{V} . \tag{B.26}$$

Collecting terms in Eq. (B.26) gives

$$\Delta z_0' = f_0 \left(C_g + m_0 \left(C_f + \mu_C \right) \right) \frac{\Delta V}{V} \tag{B.27}$$

From Eq. (3.17a) in Chapter 3, rewritten below,

$$\Delta z_0' = C_C' \frac{\Delta V}{V} \tag{B.28}$$

and comparing Eq. (B.27) with Eq. (B.28) we can write

$$C_C' = f_0 \left(C_g + m_0 \left(C_f + \mu_C \right) \right) . \tag{B.29}$$

Substituting Eq. (B.23) into Eq. (B.29) gives

$$C_C' = f_0\left(C_g + m_0\left(C_f + C_f + C_g\left(\frac{f_0}{z-g_0}\right)\right)\right)$$

$$C_C' = f_0\left(C_g + m_0\left(2C_f + C_g m_0\right)\right) \tag{B.30}$$

$$C_C' = f_0\left(C_g + m_0 2C_f + C_g m_0^2\right)$$

Rearranging Eq. (B.30) gives

$$C_C' = \left(\left(1+m_0^2\right)C_g + 2m_0 C_f\right)f_0 \tag{B.31}$$

which is Eq. (3.19) in Chapter 3.

Appendix C. The Derivation of the Radial r Motion and Transverse z Motion Equations of an Electron Entering and Moving through the Hyperbolic Field of the Lens Model

We assume the electrostatic lenses used in this study can be represented by a theoretical model of a rotational symmetric hyperbolic potential field in the middle with two electrodes on either side of the field. The model is symmetrical with respect to the center of the lens. The center electrode of the model is represented by an annular shape of an equipotential surface of a hyperbolic field, and the outer electrode are shaped as equipotential surfaces of a hyperbolic field, except for the two aperture openings on the axis shown in Figure C.1. The outer electrode apertures create a diverging lens affect on the electrons on entering and exiting the model lens that must be taken into consideration. The makeup of these outer lenses, with the hyperbolic field at the center, combine to form a three-lens system; a middle converging lens and a diverging lens on either end. The effects of the two diverging lens must be taken in consideration to properly describe the complete motion of the electrons through the electrostatic lens.

The simulated field is created by a model consisting of a center electrode that consists of an annular electrode at a potential of V_L that is negative relative to the outer electrodes or diverging lenses that are at an anode potential of V_A.

The actual shapes of the elements of the three electrostatic lenses in this study are not shaped like equipotential surfaces of a hyperbolic field. The different electrostatic lenses used in this investigation vary from each other in the size of the

openings and the separation the electrodes form each other. To make the model work on these electrostatic lenses, we assume that a relative small volume of the actual center of the lenses behaves like a hyperbolic field. Please refer to Chapter 7 for a detail description of the electrostatic lenses.

To find the equations of motion for an electron, start with the rotational symmetric hyperbolic potential field satisfying Laplace's equation

$$V(r,z) = V(0,z) - V''(0,z)\frac{r^2}{2^2} + V''''(0,z)\frac{r^4}{2^2 4^2} - \ldots\ldots \qquad \text{(C.1)}$$

where r and z are the radial and axial cylindrical coordinates. The above equation reduces to a hyperbolic potential field with V'' equal to a constant not equal to zero and with higher order derivatives becoming zero.

Integrating V'' with respect to z twice gives

$$V(0,z) = C_1\frac{z^2}{2} + C_2 z + C_3 \qquad \text{(C.2)}$$

By choosing the center of the hyperbolic field as the origin, the hyperbolic field equation becomes

$$V(r,z) - V_0 = C_1\frac{z^2}{2} - C_1\frac{r^2}{2^2} = k\left(z^2 - \frac{r^2}{2}\right) \qquad \text{(C.3)}$$

with V_0, the potential at the center. The center is chosen because the symmetry of the field in both r and z axis simplifies the equations of motion of the electrons.

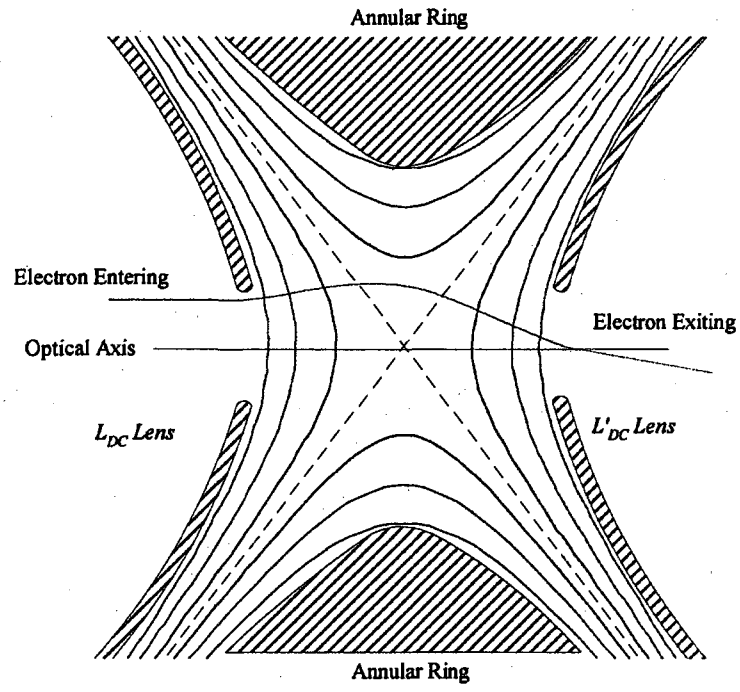

Figure C.1. Schematic of a hyperbolic lens and its field with electron entering and exiting the lens.

With reference to Fig C.1, the potential V in the hyperbolic field is given by

$$V - V_X = k\left(z^2 - \frac{r^2}{2}\right) \tag{C.4}$$

where V_0 has been replaced with V_X, the potential at the center, and the coefficient k is equal to $(V_A - V_X)/z_A^2$. $(V_A - V_X)$ represents the voltage difference between the outer diverging electrodes (lenses L_{DC} and L'_{DC}) and the center electrode lens with z_A being the distance from the center lens to either inside of the diverging lenses (L_{DC} and L'_{DC}). With reference to the center lens, the two diverging lenses, are usually at

ground potential V_A. With Equation (C.4) we can find the potential with reference to V_X for any point (r,z) in the hyperbolic field.

Effects of the Diverging Lens on the Motion of the Electron

We assume an electron approaching the electrostatic model lens from the left, parallel to the optical axis and at a height distance of r_i from the optical axis, Figure C.2.

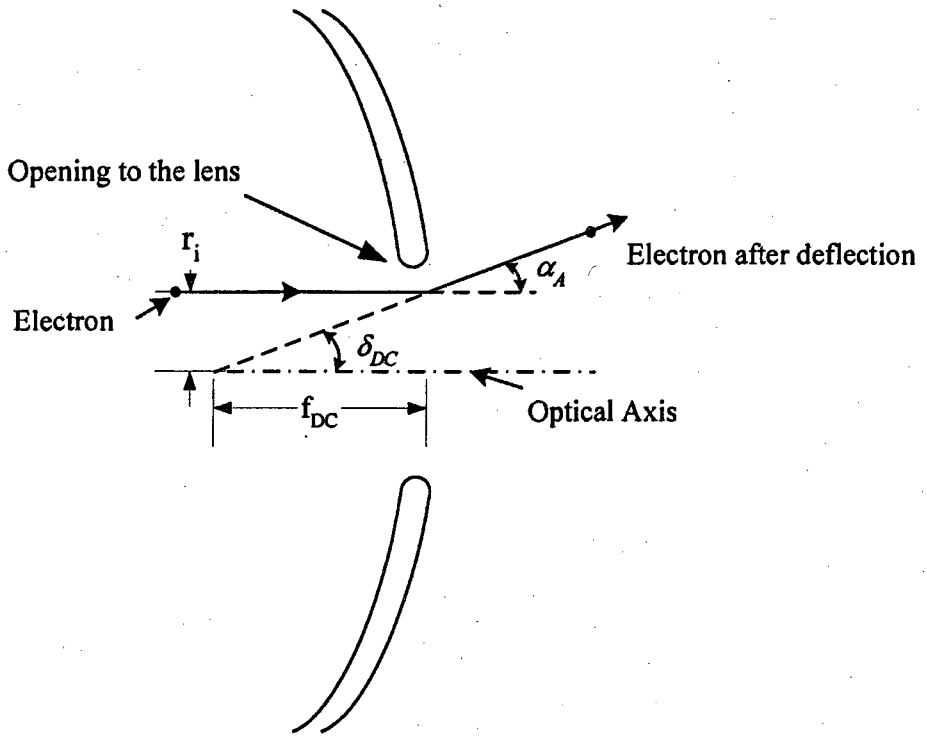

Figure C.2 Deflection of the electron at the diverging entrance of the electrostatic lens.

Outside, the lens, the electric field is minimal and does not influence the electron. On entering the lens, the electron is deflected by the diverging effects of the entrance aperture-lens L_{DC}. The path is deflected upward by an angle α_A and an equal angle

δ_{DC} with respect to the optical axis with no change in its initial speed v_i. The focal power f_{DC} of the L_{DC} lens is calculated by using the Davisson-Calbick (*D-C*) equation.

Aperture Lens Formula (*D-C*)

The focal length of an electrode having a circular aperture at the center can be found by the *D-C* formula Eq. (9.11) from Chapter 9

$$f_A = \frac{4V_B}{\left[\left(\frac{\partial V}{\partial z}\right)_2 - \left(\frac{\partial V}{\partial z}\right)_1\right]}. \tag{C.5}$$

The *D-C* formula gives the focal length of the surrounding field of the electrode in terms of the potential gradients at the two faces of the electrode. V_B is the beam voltage. The denominator is the difference between the potential gradients at the two faces of the electrodes. The subscript (1) is the potential gradient before entering the lens and subscript (2) is potential gradient on the other side of the entrance electrode. In cases where the variation in potential across the aperture is small compared with the beam voltage of the electrons, the *D-C* formula is a good approximation for weak lenses. The *D-C* formula applied for L_{DC} lens with $V_B = (V_A - V_C)$, $\left(\frac{\partial V}{\partial z}\right)_1 = 0$ and $\left(\frac{\partial V}{\partial z}\right)_2 = 2kz_A = \frac{2(V_A - V_X)}{z_A}$, gives

$$f_{DC} = \frac{4^{=2}(V_A - V_C)}{2kz_A} = \frac{2(V_A - V_C)z_A^2}{(V_A - V_X)z_A}$$

$$f_{DC} = \frac{2(V_A - V_C)z_A}{(V_A - V_X)} = \frac{2z_A}{\frac{(V_A - V_X)}{(V_A - V_C)}} \qquad \text{(C.6)}$$

$$f_{DC} = \frac{2z_A}{v_{XC}} \text{ where } v_{XC} = \frac{(V_A - V_X)}{(V_A - V_C)}$$

and z_A is the distance from the center electrode of the lens to the inside of L_{DC} lens. The sign convention is such that a distance measured from the left of the center is negative making the focal length of L_{DC} lens $f_{DC} = -\frac{2z_A}{v_{XC}}$.

Time and Coordinate System for the Model

The symmetry of the lens at the center helps to simplify the equations of motion by choosing the center of the lens as both the origin for the axial direction (z) and the time parameter (t). This is accomplished by introducing the symbol t_A to represent time markers. Time markers starting at the entrance of L_{DC} are marked as negative time left of the center of the lens to a positive time to the right of the center. Just before entering the exit lens L'_{DC} the time marker is t_f.

The use of the time term (t - t_A) will give the correct initial time of zero if $t = -t_A$ $\{(-t_A - (-t_A) = (-t_A + t_A) = 0\}$ for a particle entering the lens. The argument t represents the time marker $\{-t_A \rightarrow 0 \rightarrow +t_A\}$ of the electron as it goes through the gap of the lens. For example, let's say the electron takes four seconds to traverse from the entrance to the exit bores of the electrostatic lens. The time marker will start at t_A = -2

sec. and run thru $t_A = 0$ at the center to $t_A = +2$ sec. at the exit of the L'_{DC} lens. At the entrance the initial time is

$$\left(-2-(-2)\right) = 0.$$

Now lets say 1 second after entering into the gap, the electron is at the $t = -1$ second marker making the time $\left(-1-(-2)\right) = 1$ seconds spent in the lens. At the center, with the time marker at $t = 0$, the time marker gives $\left(0-(-2)\right) = 2$ seconds the electron has spent in the lens. After one second on passing the center of the lens, or three seconds after entering the time marker is $t = +1$ seconds, the time gives $\left(1-(-2)\right) = 3$ seconds. Finally on reaching the exit L'_{DC} lens but before exiting it, four seconds of flight time the electron has spent in the lens, the time marker is at $t = t_f = +2$ seconds giving $\left(t_f - t_A\right) = \left(2-(-2)\right) = 4$ seconds. This convention of representing the time will be used below staring with Equations (C.10).

The Radial Motion in the Hyperbolic Field

The radial force, as given by $F_r = -eE_r$, where $E_r = -\frac{\partial V}{\partial r}$, is given by

$$F_r = m\ddot{r} = -eE_r = -ekr \tag{C.7}$$

and the acceleration of the particle in the radial direction is given by

$$\ddot{r} = \frac{F_r}{m} = -\frac{ek}{m}r \tag{C.8}$$

Defining $\omega^2 = \frac{ek}{m}$, and inserting into Eq. (C.8) gives

$$\ddot{r} = -\omega^2 r$$
$$\ddot{r} + \omega^2 r = 0 \quad , \tag{C.9}$$

a second order differential equation with a solution of the form

$$r = A\sin\left(\omega\left(t - t_A\right)\right) + B\cos\left(\omega\left(t - t_A\right)\right) \tag{C.10}$$

and with the radial velocity given by

$$\dot{r} = \frac{dr}{dt} = A\omega\cos\left(\omega\left(t - t_A\right)\right) - B\omega\sin\left(\omega\left(t - t_A\right)\right). \tag{C.11}$$

With the boundary conditions $t = -t_A, r = r_A$ and $\dot{r} = \dot{r}_A$, the coefficients are found to be $A = \frac{\dot{r}_A}{\omega}$ and $B = r_A$ with Eq. (C.10) becoming

$$r = \frac{\dot{r}_A}{\omega}\sin\left(\omega\left(t - t_A\right)\right) + r_A\cos\left(\omega\left(t - t_A\right)\right). \tag{C.12}$$

$\dot{r}_A$ is the radial velocity the electron acquires on entering the L_{DC} lens and immersing in the hyperbolic field with an entrance height of r_A.

The diverging effect of entrance lens L_{DC} is introduced by a phase angle ϕ_{DC} as follows:

First write Eq.(C.12) as show below

$$r = \sqrt{A^2 + B^2}\left(\frac{\dot{r}_A/\omega}{\sqrt{A^2 + B^2}}\sin\left(\omega\left(t - t_A\right)\right) + \frac{r_A}{\sqrt{A^2 + B^2}}\cos\left(\omega\left(t - t_A\right)\right)\right) \tag{C.13}$$

and define the coefficients of the trigonometric functions above as

$$\frac{\dot{r}_A/\omega}{\sqrt{A^2 + B^2}} = \sin\phi_{DC} \qquad \frac{r_A}{\sqrt{A^2 + B^2}} = \cos\phi_{DC}.$$

Substitute these two functions into Eq. (C.13) giving

$$r = \sqrt{A^2 + B^2}\left(\sin(\phi_{DC})\sin\omega(t-t_A) + \cos(\phi_{DC})\cos\omega(t-t_A)\right). \qquad \text{(C.14)}$$

The identity $\cos(\omega(t-t_A))\cos(\phi_{DC}) + \sin(\omega(t-t_A))\sin(\phi_{DC}) = \cos(-\phi_{DC} + \omega(t-t_A))$

along with $\sqrt{A^2 + B^2} = \dfrac{r_A}{\cos\phi_{DC}}$ are substituted into Eq.(C.14) to give

$$r = \frac{r_A \cos(-\phi_{DC} + \omega(t-t_A))}{\cos\phi_{DC}} . \qquad \text{(C.15a)}$$

The derivative of Eq. (C.15a) with respect to t and not t_A gives the velocity

$$\dot{r} = -\frac{\omega r_A \sin(-\phi_{DC} + \omega(t-t_A))}{\cos\phi_{DC}} \qquad \text{(C.15b)}$$

These are the radial parametric equations of motion of an electron in the hyperbolic field with the effects of diverging lens L_{DC} represented by the phase angle ϕ_{DC}. These are the same as Eq. (9.15a) and (9.15b) in Chapter 9.

The value of the phase angle ϕ_{DC} is found from the ratio of Eq. (C.15b) to (C.15a) with the initial conditions of $r, \dot{r}$, and z at $t = -t_A$, being $r = r_i = r_A, \dot{r} = \dot{r}_A$ and $z = -z_A$

$$\frac{\dot{r}_A}{r_A} = \frac{-\dfrac{\omega r_A \sin(-\phi_{DC} + \omega(-t_A - (-t_A)))}{\cos\phi_{DC}}}{\dfrac{r_A \cos(-\phi_{DC} + \omega(-t_A - (-t_A)))}{\cos\phi_{DC}}} = -\omega\tan(-\phi_{DC}). \qquad \text{(C.15c)}$$

Looking at Figure C.2 the deflection of the electron by the L_{DC} lens can be characterized by the two angles that are equal, $\delta_{DC} = \alpha_A$. The δ_{DC} angle has the following relation

$$\tan\delta_{DC} \approx \delta_{DC} = \frac{r_A}{-f_{DC}}$$

and the α_{DC} angle

$$\sin\alpha_A \approx \alpha_A = \frac{\dot{r}_A}{v_A}.$$

with v_A the initial velocity of the electron has on entering the lens. Equating the two angles and use of Eq. (C.15c) gives

$$\delta_{DC} = \frac{r_A}{-f_{DC}} = \alpha_A = \frac{\dot{r}_A}{v_A} \Rightarrow \frac{\dot{r}_A}{r_A} = \frac{v_A}{-f_{DC}} = \omega\tan\phi_{DC}. \tag{C.15d}$$

The parameters of v_A, f_{DC}, and ω are defined in the following terms

$$v_A = \sqrt{\frac{2e(V_A - V_C)}{m}}$$

$$-f_{DC} = \frac{2z_A}{v_{XC}}$$

$$\omega = \sqrt{\frac{e}{m}k} = \sqrt{\frac{e}{m}\frac{(V_A - V_X)}{z_A^2}}$$

Substituting these parameters and the definition of $v_{XC} = \frac{(V_A - V_X)}{(V_A - V_C)}$ into Eq. (C.15d) gives

$$\tan\phi_{DC} = \frac{v_A}{\omega(-f_{DC})} = \sqrt{\frac{2e(V_A - V_C)}{m}\frac{mz_A^2}{e(V_A - V_X)}}\left(\frac{v_{XC}}{2z_A}\right)$$

$$\tan\phi_{DC} = \sqrt{\frac{2}{v_{XC}}\frac{(v_{XC})^2}{4}} = \sqrt{\frac{v_{XC}}{2}} \tag{C.15e}$$

The angle ϕ_{DC} in Equation (C.15e) is the amount of divergence the entrance lens L_{DC} provides that is subtracted from the cosine angle in Eq. (C.15a) and also changes the amplitude of the cosine curve from r_A to $\frac{r_A}{\cos\phi_{DC}}$.

The Axial Motion in the Hyperbolic Field

Starting with the axial force on the electron, $F_z = -eE_z$ with $E_z = -\frac{\partial V}{\partial z}$,

Newton's law gives

$$F_z = m\ddot{z} = -eE_z = e\frac{\partial V}{\partial z} = 2ekz \tag{C.16}$$

This produces a second order differential equation in z.

$$\begin{aligned} \ddot{z} &= \frac{2ek}{m}z \\ \ddot{z} - \frac{2ek}{m}z &= 0 \end{aligned} \tag{C.17}$$

Again substituting $\omega^2 = ek/m$ into Eq. (C.17) gives

$$\ddot{z} - 2\omega^2 z = 0 \tag{C.18}$$

and its solution in terms of hyperbolic functions is follows:

$$z = C\sinh(\sqrt{2}\omega t) + D\cosh(\sqrt{2}\omega t). \tag{C.19}$$

The t in the axial equations of motion represents the time markers only. The derivative of Eq. (C.19) gives the transverse velocity equation which together with Eq.(C.19) determine the coefficients C and D, with the initial conditions at the center of the lens of $t = 0, z = 0$, and $\dot{z} = \dot{z}(0)$. The coefficients found are

$$C = \frac{\dot{z}(0)}{\sqrt{2}\omega} \text{ and } D = 0$$

and substituting them into Eq.(C.19) gives the equation of motion in the axial direction

$$z = \frac{\dot{z}(0)}{\sqrt{2}\omega}\sinh(\sqrt{2}\omega t). \tag{C.20}$$

The derivative of Eq. (C.20) gives the axial velocity of the electron in the hyperbolic field

$$\dot{z} = \dot{z}(0)\cosh(\sqrt{2}\omega t) \tag{C.20a}$$

where $\dot{z}(0)$ is the axial velocity of the electron at the center of the lens. These equations are the same as (9.17a and b) from Chapter 9.

Eq. (C.15a) and (C.20) represent the equations of motion for an electron entering and moving through the hyperbolic field of the model lens right up to the exit aperture-lens L'_{DC} but not going through. Further motion for exiting and moving beyond L'_{DC} and the outside of the model lens, are completed back in Chapter 9 starting with Eq. (9.17c).

Appendix D. Derivation of the Electrostatic Lenses Chromatic Aberration Coefficients C_f and C_g from the Paraxial Focal Length Model f_0 and Focal Distance g_0 Equations for the lenses L_3, L_4, and L_5

Chromatic Coefficient C_f

Start with the paraxial focal length, Eq. (9.22b), from Chapter 9 shown below

$$f_0 = \frac{z_f \cos(-\phi_{DC})\cos(-\phi'_{DC})}{\sqrt{\frac{v_{XC}}{2}}\sin(-\phi_{DC}+\phi_{HF}-\phi'_{DC})}. \tag{D.1}$$

Take the log of both sides of the equation to give

$$\ln f_o = \ln\left[z_f \cos(-\phi_{DC})\cos(-\phi'_{DC})\left(\sqrt{\frac{v_{XC}}{2}}\sin(-\phi_{DC}+\phi_{HF}-\phi'_{DC})\right)^{-1}\right]. \tag{D.2}$$

Take the derivative on both sides of Eq. (D.2)

$$\frac{\Delta f_0}{f_0} = \frac{\Delta\cos(-\phi_{DC})}{\cos(-\phi_{DC})} + \frac{\Delta\cos(-\phi'_{DC})}{\cos(-\phi'_{DC})} - \frac{\Delta\sqrt{v_{XC}/2}}{v_{XC}/2} - \frac{\Delta\sin(-\phi_{DC}+\phi_{HF}-\phi'_{DC})}{\sin(-\phi_{DC}+\phi_{HF}-\phi'_{DC})}$$

$$\frac{\Delta f_0}{f_0} = -\tan(-\phi_{DC})\Delta(-\phi_{DC}) - \tan(-\phi'_{DC})\Delta(-\phi'_{DC}) - \frac{\Delta\sqrt{v_{XC}/2}}{v_{XC}/2} \tag{D.3}$$

$$-\cot(-\phi_{DC}+\phi_{HF}-\phi'_{DC})\Delta(-\phi_{DC}+\phi_{HF}-\phi'_{DC})$$

where the derivative for the constant z_f is zero.

The derivatives of $-\phi_{DC}$ and $-\phi'_{DC}$ give the same result since $(\phi_{DC} = \phi'_{DC})$.

With $\phi_{DC} = \phi'_{DC} = \tan^{-1}\left(\sqrt{\frac{v_{XC}}{2}}\right)$ we get

$$\Delta\phi_{DC} = \Delta\phi'_{DC} = \Delta\left[\tan^{-1}\left(\sqrt{\frac{v_{XC}}{2}}\right)\right] = \Delta\left(\sqrt{\frac{v_{XC}}{2}}\right) \div \left(1+\frac{v_{XC}}{2}\right) \tag{D.4}$$

The derivative of $\sqrt{\frac{v_{XC}}{2}}$ is

$$\Delta\left(\sqrt{\frac{v_{XC}}{2}}\right)=\left(\frac{1}{2}\sqrt{\frac{v_{XC}}{2}}\right)\frac{\Delta v_{XC}}{v_{XC}}, \tag{D.4a}$$

and substituting Eq. (D.4a) into Eq. (D.4) gives

$$\Delta\phi_{DC}=\Delta\phi'_{DC}=\left\{\left(\frac{1}{2}\sqrt{\frac{v_{XC}}{2}}\right)\div\left(1+\frac{v_{XC}}{2}\right)\right\}\frac{\Delta v_{XC}}{v_{XC}} \tag{D.5}$$

The derivative of ϕ_{HF} gives

$$\Delta\phi_{HF}=\Delta\left(\sqrt{2}\tanh^{-1}\left(\sqrt{v_{XC}}\right)\right)=\left\{\left(\sqrt{\frac{v_{XC}}{2}}\right)\div\left(1-v_{XC}\right)\right\}\frac{\Delta v_{XC}}{v_{XC}}. \tag{D.6}$$

Placing the derivatives, Eq. (D.5) and Eq. (D.6), into Eq.(D.3) and rearranging gives

$$\frac{\Delta f_0}{f_0}=-\left\{\frac{1}{2}+\left[\tan\phi+\frac{3}{2}\cot\left(-\phi_{DC}+\phi_{HF}-\phi'_{DC}\right)\left(\frac{v_{XC}}{1-v_{XC}}\right)\right]\left[\frac{\sqrt{\frac{v_{XC}}{2}}}{1+\frac{v_{XC}}{2}}\right]\right\}\frac{\Delta v_{XC}}{v_{XC}} \tag{D.7}$$

Note that the two *tan* functions in Eq. (D.3) were combined because $\left(\phi_{DC}=\phi'_{DC}\right)$ with the subscripts dropped in the *tan* function in Eq. (D.7). The parameters of the *cot* function in Eq. (D.7) were not combined to show the sequence of electrodes the electron encounters in its trajectory through the lens.

The v_{XC} term is equal to $\frac{V_A-V_X}{V_A-V_C}$ where V_A is the potential on the end electrodes of the electrostatic lenses and V_X represents the voltage of the asymptotic cones of the hyperbolic field created when a voltage is applied to the lens. In this

thesis, the end electrodes are at ground potential or zero volts. Therefore

$\frac{V_A - V_X}{V_A - V_C}$ reduces to $\frac{0 - V_X}{0 - V_C} = \frac{V_X}{V_C}$. The ratio $\frac{\Delta v_{XC}}{v_{XC}}$ can be written as $\frac{\Delta(V_X / V_C)}{V_X / V_C}$.

Taking the derivative of the above ratio gives

$$\frac{\Delta(V_X / V_C)}{V_X / V_C} = \Delta\left[(V_X)(V_C)^{-1}\right]\left(\frac{V_C}{V_X}\right)$$

$$\left\{(V_X)(-1)(V_C)^{-2}\Delta(V_C) + 0\right\}\left(\frac{V_C}{V_X}\right) \quad . \qquad \text{(D.7a)}$$

$$-\frac{(V_X)}{(V_C)^{2}}\frac{\Delta V_C}{1}\frac{(V_C)}{(V_X)} = -\frac{\Delta V_C}{V_C}$$

The variation of the cathode voltage V_C is the cause of the chromatic aberration in these derivations.

Eq. (D.7) is rewritten with the $\left(-\frac{\Delta V_C}{V_C}\right)$ ratio as follows:

$$\frac{\Delta f_0}{f_0} = \left\{\frac{1}{2} + \left[\tan\phi + \frac{3}{2}\cot\left(-\phi_{DC} + \phi_{HF} - \phi'_{DC}\right)\left(\frac{v_{XC}}{1 - v_{XC}}\right)\right]\left[\frac{\sqrt{\frac{v_{XC}}{2}}}{1 + \frac{v_{XC}}{2}}\right]\right\}\frac{\Delta V_C}{V_C} \qquad \text{(D.7b)}$$

From the definition of the chromatic aberration coefficient C_f, Eq.(7.8c) from Chapter 7 with the differences in energy of the beam electrons sufficiently small, the term involving ΔV_e can be dropped and Eq. (7.8d) rewritten below as

$$\frac{\Delta f_0}{f_0} = C_f \frac{\Delta V_C}{V_C} \, . \qquad \text{(D.7c)}$$

With equations, (D.7b) and (D.7c) having the same form, the terms in the {} brackets of Eq. (D.7b) are equivalent to the chromatic coefficient C_f of Eq. (D.7c). C_f is written

$$C_f = \frac{1}{2} + \left[\tan\phi + \frac{3}{2}\cot\left(-\phi_{DC} + \phi_{HF} - \phi'_{DC}\right)\left(\frac{v_{XC}}{1-v_{XC}}\right)\right]\left[\frac{\sqrt{\frac{v_{XC}}{2}}}{1+\frac{v_{XC}}{2}}\right]. \qquad \text{(D.8)}$$

This is the same as Eq. (9.27a) in Chapter 9 without the η and β factors.

Chromatic Coefficient C_g

For finding the chromatic coefficient Cg start with the paraxial focal distance equation shown below

$$g_0 = z_f + \frac{z_f}{\sqrt{\frac{v_{XC}}{2}}\left\{\tan\left(-\phi_{DC} + \phi_{HF}\right) + \tan\left(-\phi'_{DC}\right)\right\}} \qquad \text{(D.9)}$$

and take the log on both sides.

$$\ln g_0 = \ln\left[z_f + z_f\left(\sqrt{\frac{v_{XC}}{2}}\left\{\tan\left(-\phi_{DC} + \phi_{HF}\right) + \tan\left(-\phi'_{DC}\right)\right\}\right)^{-1}\right] \qquad \text{(D.10)}$$

Now take the derivative on both sides of the equation giving

$$\frac{\Delta g_0}{g_0} = \frac{\Delta\left[z_f + z_f\left(\sqrt{\frac{v_{XC}}{2}}\left\{\tan\left(-\phi_{DC} + \phi_{HF}\right) + \tan\left(-\phi'_{DC}\right)\right\}\right)^{-1}\right]}{g_0} \qquad \text{(D.11)}$$

Multiply both sides by g_0 and remembering that z_f is a constant gives

$$\Delta g_0 = z_f \Delta\left(\sqrt{\frac{v_{XC}}{2}}\left\{\tan\left(-\phi_{DC} + \phi_{HF}\right) + \tan\left(-\phi'_{DC}\right)\right\}\right)^{-1} \qquad \text{(D.12)}$$

where the term on the right has yet to be differentiated. Proceeding with the differentiation gives

$$\Delta g_0 = -z_f \left(\sqrt{\frac{v_{XC}}{2}} \left\{ \tan\left(-\phi_{DC} + \phi_{HF}\right) + \tan\left(-\phi'_{DC}\right) \right\} \right)^{-2} \times \left\{ \Delta\left[\sqrt{\frac{v_{XC}}{2}} \tan\left(-\phi_{DC} + \phi_{HF}\right) \right] + \Delta\left[\sqrt{\frac{v_{XC}}{2}} \tan\left(-\phi'_{DC}\right) \right] \right\} \tag{D.13}$$

Divide Eq. (D.13) by f_0, given by Eq. (9.22a) from Chapter 9, rewritten below.

$$f_0 = \frac{z_f \cos\left(-\phi_{DC}\right)}{\sqrt{\frac{v_{XC}}{2}} \left\{ \sin\left(-\phi_{DC} + \phi_{HF}\right) + \cos\left(-\phi_{DC} + \phi_{HF}\right) \tan\left(-\phi'_{DC}\right) \right\}}, \tag{D.14}$$

First modify Eq. (D.14) before dividing by factoring out the $\cos\left(-\phi_{DC} + \phi_{HF}\right)$ term in the denominator giving

$$f_0 = \frac{z_f \cos\left(-\phi_{DC}\right)}{\cos\left(-\phi_{DC} + \phi_{HF}\right) \sqrt{\frac{v_{XC}}{2}} \left\{ \tan\left(-\phi_{DC} + \phi_{HF}\right) + \tan\left(-\phi'_{DC}\right) \right\}}. \tag{D.15}$$

Now divide Eq. (D.15) into Eq. (D.13) giving

$$\frac{\Delta g_0}{f_0} = -\frac{\cos\left(-\phi_{DC} + \phi_{HF}\right)}{\cos\left(-\phi_{DC}\right) \left(\sqrt{\frac{v_{XC}}{2}} \left\{ \tan\left(-\phi_{DC} + \phi_{HF}\right) + \tan\left(-\phi'_{DC}\right) \right\} \right)} \times \left\{ \Delta\left[\sqrt{\frac{v_{XC}}{2}} \tan\left(-\phi_{DC} + \phi_{HF}\right) \right] + \Delta\left[\sqrt{\frac{v_{XC}}{2}} \tan\left(-\phi'_{DC}\right) \right] \right\} \tag{D.16}$$

Proceeding with the differentiation of Eq. (D.16) and using of the derivatives for $\sqrt{\frac{v_{XC}}{2}}$, ϕ_{DC}, and ϕ_{HF} given above by Eq. (D.4a), Eq. (D.5) and (D.6) respectively and collect terms gives

$$\frac{\Delta g_0}{f_0} = -\left\{\frac{1}{2}\left(\frac{\cos(-\phi_{DC}+\phi_{HF})}{\cos(-\phi_{DC})} + \sqrt{\frac{\mathcal{V}_{XC}}{2}}\left(\frac{\left(\frac{2+4\mathcal{V}_{XC}}{(1-\mathcal{V}_{XC})(2+\mathcal{V}_{XC})}\right) - \cos^2(-\phi_{DC}+\phi_{HF})}{\sin(-\phi_{DC}+\phi_{HF}-\phi'_{DC})}\right)\right)\right\}\frac{\Delta\mathcal{V}_{XC}}{\mathcal{V}_{XC}} \quad \text{(D.17)}$$

Replacing the ratio $\frac{\Delta\mathcal{V}_{XC}}{\mathcal{V}_{XC}}$ in Eq. (D.17) by Eq. (D.7a) gives

$$\frac{\Delta g_0}{f_0} = \left\{\frac{1}{2}\left(\frac{\cos(-\phi_{DC}+\phi_{HF})}{\cos(-\phi_{DC})} + \sqrt{\frac{\mathcal{V}_{XC}}{2}}\left(\frac{\left(\frac{2+4\mathcal{V}_{XC}}{(1-\mathcal{V}_{XC})(2+\mathcal{V}_{XC})}\right) - \cos^2(-\phi_{DC}+\phi_{HF})}{\sin(-\phi_{DC}+\phi_{HF}-\phi'_{DC})}\right)\right)\right\}\frac{\Delta V_C}{V_C} \quad \text{(D.17a)}$$

From the definition of the chromatic aberration coefficient C_g, Eq.(7.8d) from Chapter 7 with the differences in the energy of the electron beam sufficiently small, the term involving ΔV_e can be dropped from Eq. (7.8d) and rewritten below as

$$\frac{\Delta g_0}{f_0} = C'_g \frac{\Delta V_C}{V_C}. \quad \text{(D.17b)}$$

Equations, (D.17a) and (D.17b) have the same form and the terms in the {} bracket from Eq. (D.17a), represents the chromatic coefficient C_g of Eq. (D.17b). The C'_g term is then given as

$$C'_g = \frac{1}{2}\left(\frac{\cos(-\phi_{DC}+\phi_{HF})}{\cos(-\phi_{DC})} + \sqrt{\frac{\mathcal{V}_{XC}}{2}}\left(\frac{\left(\frac{2+4\mathcal{V}_{XC}}{(1-\mathcal{V}_{XC})(2+\mathcal{V}_{XC})}\right) - \cos^2(-\phi_{DC}+\phi_{HF})}{\sin(-\phi_{DC}+\phi_{HF}-\phi'_{DC})}\right)\right) \quad \text{(D.18)}$$

This term is the same as Eq. (9.27b) in Chapter 9 without η and β factors.

Appendix E. Derivation of the Image Aberrations C_c in terms of m_0, C_g, C_f, f_0 and C'_s in terms of m_0, S_g, S_f, f_0

Start with Newton's form of the lens equation Eq. (2.3) from Chapter 2 rewritten below

$$(z'-g)(z-g)=f^2. \tag{E.1}$$

Take the log of both sides of Eq. (E.1)

$$\ln(z'-g)+\ln(z-g)=2\ln f \tag{E.2}$$

and differentia both sides of the equation to give

$$\frac{\Delta(z'-g)}{(z'-g)}+\frac{\Delta(z-g)}{(z-g)}=\frac{2\Delta f}{f}$$
$$\frac{\Delta z'-\Delta g}{(z'-g)}+\frac{\Delta z^{=0}-\Delta g}{(z-g)}=\frac{2\Delta f}{f}$$

where z is a constant and therefore Δz equals zero. Multiply both sides by $(z'-g)$ and solve for $\Delta z'$.

$$\begin{aligned}\Delta z'-\Delta g-\frac{(z'-g)}{(z-g)}\Delta g&=2\frac{(z'-g)}{f}\Delta f\\ \Delta z'&=\left[\frac{(z'-g)}{(z-g)}+1\right]\Delta g+2\frac{(z'-g)}{f}\Delta f\end{aligned} \tag{E.3}$$

The magnification m from Newton's equations $z'-g=fm$ [Eq. (2.1)] and $\frac{z'-g}{z-g}=m^2$ [Eq. (2.4)] from Chapter 2 are substituted into Eq. (E.3) to give

$$\Delta z'=\left(m^2+1\right)\Delta g+2m\Delta f. \tag{E.4}$$

Rewriting the above equation in terms of the paraxial region, m becomes m_0 and z' becomes z'_0 and Eq. (E.4) becomes

$$\Delta z'_0 = \left(m_0^2 + 1\right)\Delta g + 2m_0\Delta f \,. \tag{E.5}$$

Image Aberration Coefficient C_c

From the definition of C_f and C_g given by equations (3.24a or 3.27a) and (3.24b or 3.27b) from Chapter 3, the voltages V and V_C refer to the same cathode voltage, these equations can be rewritten below as

$$\begin{aligned} \frac{\Delta f_0}{f_0} &= C_f \frac{\Delta V}{V} \\ \frac{\Delta g_0}{f_0} &= C_g \frac{\Delta V}{V} \end{aligned} \,. \tag{E.6a and b}$$

Now multiply both sides of Eq. (E.6a) and Eq. (E.6b) by f_0 giving

$$\begin{aligned} \Delta f_0 &= f_0 C_f \frac{\Delta V}{V} \\ \Delta g_0 &= f_0 C_g \frac{\Delta V}{V} \end{aligned} \,. \tag{E.7a and b}$$

Substitute the Eq. (E.7a) and (E.7b) into Eq. (E.5) and rearrange

$$\begin{aligned} \Delta z'_0 &= \left(m_0^2 + 1\right) f_0 C_g \frac{\Delta V}{V} + 2m_0 f_0 C_f \frac{\Delta V}{V} \\ \Delta z'_0 &= \left\{\left[\left(m_0^2 + 1\right)C_g + 2m_0 C_f\right] f_0\right\}\frac{\Delta V}{V} \end{aligned} \,. \tag{E.8}$$

From the definition of the longitudinal chromatic aberration coefficient, C'_C given by Eq. 3.7(c) from Chapter 3 rewritten below

$$\Delta z_0' = C_C' \frac{\Delta V}{V} \tag{E.9}$$

we equate the term C'_C of Eq. (E.9) to the bracketed {} terms on the right side of Eq. (E.8) and write

$$C_C' = \left[\left(m_0^2 + 1\right)C_g + 2m_0 C_f\right] f_0 . \tag{E.10}$$

This defines the C'_C in terms of the chromatic aberration coefficients C_f and C_g.

Image Aberration Coefficient C_s

The coefficient C_s, in terms of the spherical-aberration coefficients S_f, Eq. (3.20a) and S_g, Eq. (3.20b), from Chapter 3, is found by inserting Δf and Δg into Eq. (E.5). From Eq. (3.20a), rearranging in terms of Δf gives

$$\Delta f = f - f_0 = f_0 S_f \left(\frac{\rho}{f_0}\right)^2 \tag{E.11}$$

and rearrange Eq. (3.20b) in terms of Δg gives

$$\Delta g = g - g_0 = f_0 S_f \left(\frac{\rho}{f_0}\right)^2 . \tag{E.12}$$

Both $\left(\frac{\rho}{f_0}\right)$ terms in Eq. (E.11 and 12) to first order are equal to δ which is the deflection the electron experiences at the principal plane. From geometry, the angle of deflection δ equals the sum of the object and image ray angles, $\alpha + \alpha'$. Factoring out

α' from $(\alpha+\alpha')$ gives $\left(\frac{\alpha}{\alpha'}+1\right)\alpha'$. The fraction α/α' equals the magnification m_0.

Therefore, $\left(\frac{\rho}{f_0}\right)=\delta=(m_0+1)\alpha'$.

Squaring $(1+m_0)\alpha'$ and substituting into Eq. (E.11) and (E.12) gives

$$\begin{aligned}\Delta f &= f_0 S_f (1+m_0)^2 \alpha'^2 \\ \Delta g &= f_0 S_g (1+m_0)^2 \alpha'^2\end{aligned} \tag{E.13}$$

Substituting these two equations given by Eq. (E.13) into Eq. (E.5) and simplifying gives

$$\begin{aligned}\Delta z_0' &= (m_0^2+1) f_0 S_g (1+m_0)^2 \alpha'^2 + 2m_0 f_0 S_f (1+m_0)^2 \alpha'^2 \\ \Delta z_0' &= \left\{\left[(m_0^2+1)S_g + 2m_0 S_f\right] f_0 (1+m_0)^2\right\}\alpha'^2\end{aligned} \tag{E.15}$$

From the definition of C'_S given by Eq. (3.5) in Chapter 3, $z'-z_0'=\Delta z_0'=-C_S'\alpha'^2$, the bracket {} term in Eq. (E.15) is equated to C'_S and written as

$$C_S' = -\left[(m_0^2+1)S_g + 2m_0 S_f\right] f_0 (1+m_0)^2. \tag{E.16}$$

This gives C'_S in terms of the two spherical aberration coefficient S_f and S_g.